



HAL
open science

Integrative omics profiling reveals *Yersinia pestis* virulence determinants and host candidate biomarkers of plague

Pierre Lê-Bury

► **To cite this version:**

Pierre Lê-Bury. Integrative omics profiling reveals *Yersinia pestis* virulence determinants and host candidate biomarkers of plague. Microbiology and Parasitology. Université Paris Cité, 2023. English. NNT : 2023UNIP5043 . tel-04893583

HAL Id: tel-04893583

<https://theses.hal.science/tel-04893583v1>

Submitted on 17 Jan 2025

HAL is a multi-disciplinary open access archive for the deposit and dissemination of scientific research documents, whether they are published or not. The documents may come from teaching and research institutions in France or abroad, or from public or private research centers.

L'archive ouverte pluridisciplinaire **HAL**, est destinée au dépôt et à la diffusion de documents scientifiques de niveau recherche, publiés ou non, émanant des établissements d'enseignement et de recherche français ou étrangers, des laboratoires publics ou privés.

Université Paris Cité
Ecole doctorale Bio Sorbonne Paris Cité - ED562

Institut Pasteur, CNRS - UMR 6047
Unité de Recherche *Yersinia*

**Integrative omics profiling reveals
Yersinia pestis virulence determinants
and host candidate biomarkers of plague**

Par Pierre LÊ-BURY

Thèse de doctorat de Microbiologie

Dirigée par Olivier DUSSURGET
Soutenue publiquement le 22 juin 2023 à Paris

Devant un jury composé de :

Petra DERSCH, Rapportrice

Professeure, Institut d'Infectiologie, Université de Münster

Christophe JUNOT, Rapporteur

Directeur de Recherche, CEA, Université Paris Saclay

Francis IMPENS, Examineur

Professeur, Centre de Biotechnologie Médicale, Université de Gand

Friederike JÖNSSON, Examinatrice

Directrice de Recherche, CNRS, Institut Pasteur, Université Paris Cité, Sorbonne Université

Olivier DUSSURGET, Directeur de thèse

Professeur des Universités, Institut Pasteur, Université Paris Cité

Résumé

Une approche omique intégrative révèle des déterminants de virulence de *Yersinia pestis* et des candidats biomarqueurs de la peste

Yersinia pestis est le bacille hautement virulent responsable de la peste, une zoonose ré-émergente généralement transmise par les puces se nourrissant sur des mammifères bactériémiques. Les trois principales formes cliniques sont i) la peste bubonique, la forme la plus fréquente résultant de la piqûre par une puce infectée, ii) la peste pulmonaire transmise par voie aérienne entre individus et iii) la peste dite septicémique, la forme la plus foudroyante. Dans les trois formes, les bactéries atteignent la circulation sanguine et conduisent à la mort. Nous avons utilisé une approche intégrative de biologie des systèmes afin de découvrir les facteurs bactériens qui jouent un rôle critique dans la phase bactériémique de la peste, une étape nécessaire à sa transmission dans le réservoir animal et à la progression de la maladie chez l'homme.

Nous avons tout d'abord mis au point les conditions de culture de *Y. pestis* dans le plasma humain afin de générer un atlas protéique. Nous avons implémenté et optimisé une méthode d'extraction des protéines et validé son utilisation en environnement de sécurité de niveau 3. Un protocole original d'analyse protéomique après croissance des bactéries dans le sang a ensuite été mis au point afin de compléter les données plasmatiques. Nous avons obtenu le protéome de *Y. pestis* le plus complet à ce jour, couvrant plus de 2800 protéines. Parmi celles-ci, 1500 ont été détectées dans les bactéries associées aux monocytes et polynucléaires neutrophiles.

En parallèle, nous avons développé un site internet – Yersiniomics – afin d'analyser et visualiser ces données. Nous avons collecté les génomes complets ainsi que les expériences transcriptomiques et protéomiques publiées, représentant plus de 300 conditions biologiques *in vitro* et *in vivo* intégrées dans la base de données. Ce site unique permet d'accéder à la collection de données de l'espèce *Yersinia* la plus complète actuellement, grâce à un navigateur génomique interactif intégrant l'ensemble des expériences au niveau de chaque gène. Une visualisation des données de couverture de séquençage des ARNs ainsi que des plages de couleur représentant les données transcriptomiques et protéomiques ont été implémentées.

Nous avons ensuite sélectionné 47 protéines dont l'expression était modulée lors de la croissance bactérienne dans le plasma humain et/ou présentant un profil intéressant en utilisant Yersiniomics, puis nous avons inactivé les gènes correspondants. L'étude des souches mutantes nous a permis d'identifier plusieurs protéines impliquées dans l'homéostasie du cuivre, une subtilase, une protéase et des lipoprotéines nécessaires à la croissance de *Y. pestis* dans le sang humain et/ou à la virulence chez la souris.

Nous avons notamment démontré que la lipoprotéine SlyB joue un rôle critique pour la virulence dans les trois formes de peste et pour la croissance de *Y. pestis* dans le sérum et le sang. Un mutant de délétion *slyB* montre une sensibilité accrue aux composés de la réponse immunitaire innée, tels que le complément et les protéases et peptides anti-microbiens des polynucléaires neutrophiles, et montre une survie réduite dans des macrophages humains.

Ces phénotypes pourraient dériver d'une augmentation de l'instabilité et de la perméabilité de la membrane externe, et d'un dérèglement du protéome de l'enveloppe bactérienne.

Enfin, nous avons exploité nos modèles expérimentaux pour découvrir de nouveaux biomarqueurs de la peste. Nous souhaitons détecter les microARNs systémiques différentiellement exprimés lors de l'infection par *Y. pestis*, utilisables comme biomarqueurs pour le diagnostic précoce de la maladie. Nous avons criblé 179 microARNs à un stade précoce de la maladie dans un modèle de peste pulmonaire chez la souris et établi la preuve de concept de cette approche en identifiant trois candidats prometteurs. Nous développons maintenant une approche de criblage non biaisé basée sur le séquençage des microARNs totaux appliquée aux différents stades de la maladie.

Mots-clés

Yersinia pestis, peste, bactériémie, protéomique, base de données multi-omiques, facteurs de virulence, stress membranaire, immunité innée, microARNs, biomarqueurs précoces

Abstract

Integrative omics profiling reveals *Yersinia pestis* virulence determinants and host candidate biomarkers of plague

Yersinia pestis is the highly virulent etiological agent of plague, a reemerging zoonosis generally transmitted by fleas feeding on bacteremic mammals. The three clinical forms of the disease in humans are i) bubonic plague, the most frequent form resulting from the bite of an infected flea, ii) pneumonic plague, an airborne disease transmitted between individuals, and iii) septicemic plague, the most fulminant form. Bacteria reach the bloodstream in all three forms and spread to multiple organs ultimately leading to death. We used an integrative systems biology approach to investigate the poorly characterized bacteremic phase of plague, an essential stage for plague transmission in reservoirs and disease development in humans.

First, we set up culture conditions of *Y. pestis* in human plasma to generate a protein atlas. We implemented and optimized an acid-based protein extraction method and validated inactivation of bacteria in a biosafety level 3 environment. We further established an original protocol for proteome analysis of bacteria grown in whole blood to enrich data obtained in infected plasma. We detected more than 2,800 proteins, representing the most complete proteome of *Y. pestis* today. Interestingly, a pool of 1,500 proteins was detected in bacteria associated with monocytes and neutrophils.

In parallel, we developed an interactive website called Yersiniomics to help visualize and analyze these data. We gathered *Yersinia* genomic, transcriptomic and proteomic public data representing more than 300 *in vitro* and *in vivo* experiments, which were integrated in a unique database. Yersiniomics allows access to the most complete dataset collection of *Yersinia* species through an interactive genome browser displaying results of every experiment for each gene on *Yersinia* reference genomes. Visualization of RNA-Seq coverage and differential analysis heatmaps for transcriptomic- and proteomic-data were also implemented.

We then selected 47 proteins of *Y. pestis* based on Yersiniomics data and their expression profile during bacterial growth in human plasma and inactivated their corresponding genes. Phenotypic study of the mutants led to identification of several proteins involved in copper homeostasis, as well as a subtilase, a protease and lipoproteins of unknown function that were required for *Y. pestis* optimal growth in human blood and/or full virulence in a murine model of septicemic plague.

Notably, we demonstrated that the lipoprotein SlyB is critical for virulence in the three forms of plague in mice and for *Y. pestis* growth in human blood and serum. A *Y. pestis* *slyB* deletion mutant is characterized by an increased susceptibility to innate immunity components, such as complement, neutrophil proteases and antimicrobial peptides, as well as a reduced survival in human macrophages. These phenotypes possibly result from increased outer membrane instability and permeability and imbalance of the bacterial envelope proteome.

Lastly, our experimental models were exploited to discover new biomarkers of *Y. pestis*

infection. In a murine model of pneumonic plague, we aimed at detecting differentially expressed systemic microRNAs which could be used as early diagnostic biomarkers of the disease. We screened 179 microRNAs at an early stage of infection and could establish the proof of concept of this approach by identifying three promising candidates. We are now developing an unbiased screening approach based on microRNA sequencing applied at different stages of plague.

Keywords

Yersinia pestis, plague, bacteremia, proteomics, multi-omics database, virulence factors, membrane stress, innate immunity, microRNAs, early biomarkers

Remerciements

Je tiens à remercier tous les actuels et anciens membres de l'unité de recherche *Yersinia* aux côtés de qui j'ai passé de formidables années et eu de passionnantes discussions, plus ou moins scientifiques : la team des thésards, dont ma voisine pour la majorité de la thèse Clarisse (ainsi que David, chimiste considéré comme quasi occupant de notre bureau), les compagnons du P3 Guillem et Mara, les docteurs Jazmin et Océane, et futures docteurs Marion et Lou (courage pour la fin de la thèse!), ma nouvelle voisine (pour le dernier bout de thèse) Elena, ainsi que la dynamique team des stagiaires Josue, Jose, Zeyneb, Jeannie, et Emelyne qui a déjà réussi à apporter beaucoup de résultats à notre dernier projet. Merci à la team des techs, Julien et Rémi, qui m'ont bien aidé sur les expériences, les post-docs Hebert et Nadira ainsi que les permanents Anne-Sophie, Cyril, Anne, Christian et Pierre, dont j'ai tiré de précieux conseils tout au long de mon parcours, les membres du CNR Laura, Carine et Sylvie, toujours à l'écoute, et notre assistante Elisabeth, toujours prête à discuter. Je tiens tout particulièrement à remercier Javier et Olivier pour leur encadrement, la liberté que vous m'avez laissée pour explorer de nombreux projets dans l'unité et ouvrir sans cesse de nouvelles portes, et plus encore Olivier pour tous les aspects de la recherche, que ce soit discussion et réflexion scientifique, rédaction et gestion de projets, ou encadrement scientifique, qui ont pu créer le chercheur que je suis (ou crois être) aujourd'hui.

J'aimerais aussi remercier nos collaborateurs, notamment Mariette Matondo, Thibaut Douché et Quentin Gai Gianetto avec qui j'ai beaucoup interagi et qui m'ont énormément appris en protéomique, ainsi que Christophe Becavin et Pierre Lechat pour tous les conseils en informatique et qui nous ont permis de recréer et améliorer Yersiniomics, ainsi que la réception des produits biologiques pour tout le sang qu'ils sont allés chercher aux EFS pour mes expériences.

I would like to thank Friederike Jönsson and Petra Dersch for the discussions and advices as well as Christophe Junot and Francis Impens to have accepted to participate in my thesis jury. I would also like to thank Benoît Marteyn, Nienke Buddelmeijer, Frédéric Vernel-Pauillac and Melody Dazas for the various scientific or technical help.

J'aimerais remercier Jean-Nicolas Tournier et Roger Le Grand qui m'ont offert l'opportunité de continuer à travailler sur *Y. pestis* pour mon projet de post-doctorat, me permettant à la fois de finir sereinement les divers projets entamés dans l'unité de recherche *Yersinia* et de développer de nouveaux projets innovants dans leurs structures de recherche d'excellence en France, ainsi qu'Olivier Gorgé et Minoarisoa Rajerison qui nous ont permis d'obtenir le financement pour la suite des aventures.

J'aimerais finalement remercier mon entourage proche, notamment ma famille qui m'a apporté soutien (et logement) tout au long de ma thèse et en particulier ma soeur Gabrielle que j'ai copié en m'orientant vers l'étude des maladies infectieuses, ainsi que Cécile qui m'a épaulé et a réussi à me supporter ces trois dernières années (surtout pendant les confinements et l'écriture de la thèse).

Contents

I	Introduction	15
1	<i>Yersinia pestis</i> lifecycle	17
1.1	<i>Y. pestis</i> cycle in the environment	17
1.1.1	The vectorial transmission of plague	17
1.1.2	Maintenance of the plague enzootic cycle	19
1.2	<i>Y. pestis</i> cycle in the mammalian host	19
1.2.1	Bubonic plague	19
1.2.2	Septicemic plague	21
1.2.3	Pneumonic plague	22
1.2.4	Rare forms of plague	22
2	<i>Y. pestis</i> determinants of plague	23
2.1	Bacterial determinants of vectorial transmission	23
2.2	Virulence factors involved in plague	24
2.2.1	Virulence factors involved in bubonic plague	24
2.2.2	Virulence factors involved in pneumonic plague	24
2.2.3	Virulence factors involved in septicemic plague	25
2.3	The bacterial envelope at the interface with the immune system	25
2.3.1	The classical diderm envelope structure	26
	The lipopolysaccharide.	26
	Outer membrane proteins.	27
	Lipoproteins.	27
	The periplasmic content.	27
2.3.2	Role of the envelope stress responses in plague pathogenesis	28
	The CpxA/CpxR TCS.	28
	The σ^E response.	28
	The Psp response.	28
	The Rcs phosphorelay.	28
2.3.3	Role of environmental sensing in plague pathogenesis	29
	The PhoP/PhoQ TCS.	30
	The OmpR/EnvZ TCS.	30
2.3.4	Immune escape by LPS modifications	30
	Change in lipid A net charge.	30
	LPS tetra-acylation.	31
	Absence of O-antigen.	31
2.3.5	Structural integrity maintenance under stressed conditions	31
	Ail.	31
	Lpp.	31

3	Global approaches to study plague pathogenesis	32
3.1	Genomics	32
3.1.1	First <i>Yersinia</i> genome sequences	32
3.1.2	Second generation sequencing	32
3.1.3	Sequencing of ancient DNA	32
3.1.4	Third generation sequencing	33
3.2	Transcriptomics	33
3.2.1	Macro- and microarray-based transcriptomics	33
3.2.2	RNA-sequencing-based transcriptomics	33
3.3	Proteomics	35
3.4	Metabolomics	36
3.5	Interactomics	36
3.6	Transposon-based screening	36
3.7	Omics studies of host response	37
4	Innovation in plague diagnosis	38
4.1	Plague epidemiology and clinical presentation	38
4.2	<i>Yersinia pestis</i> infection diagnostics	39
4.2.1	Current diagnostic workflow	39
	Immunoassays - Rapid Diagnostic Test.	39
	Molecular biology assays.	40
	Bacteriological culture.	40
4.2.2	Limitations of current approaches	40
	RDT and bacteriological culture.	40
	Molecular biology assays.	41
	Early diagnosis.	41
4.3	New diagnosis approaches	41
4.3.1	Molecular biology-based approaches	41
4.3.2	LC-MS/MS identification	42
4.3.3	Plasma proteomics for circulating biomarkers	42
4.3.4	MicroRNA-based approaches	42
II	Objectives of the thesis	43
III	Results	47
5	Dual proteomic signature of blood infection by <i>Yersinia pestis</i>	49
5.1	Objectives and summary	49
5.2	Article	49
6	Yersiniomics, a multi-omics interactive database for <i>Yersinia</i> species	92
6.1	Objectives and summary	92
6.2	Article	92
7	<i>Yersinia pestis</i> lipoprotein SlyB promotes plague pathogenesis via envelope stress tolerance	116
7.1	Objectives and summary	116
7.2	Results	117
7.2.1	Identification of genes potentially involved in <i>Y. pestis</i> survival in human blood and in mice	117

	Characterization of <i>Y. pestis</i> early dissemination after intravenous injection of mice.	117
	Screen of <i>Y. pestis</i> mutants reveals several loci potentially involved in human blood survival.	118
7.2.2	Characterization of the $\Delta slyB$ mutant	119
	The <i>slyB</i> mutant shows a decreased survival in human blood and decreased virulence in mice.	119
	The <i>slyB</i> mutant is more sensitive to innate immunity killing mechanisms.	120
	The <i>slyB</i> mutant is more sensitive to membrane stress, cationic anti-microbial peptide and serine protease.	122
	The <i>slyB</i> deletion induces loss of periplasmic content.	123
	The <i>slyB</i> deletion induces mild envelope stress responses.	125
	The absence of SlyB rewires bacterial metabolism.	125
7.3	Discussion	129
7.3.1	SlyB in Gram-negative bacteria	129
7.3.2	SlyB, membrane integrity and virulence	129
7.3.3	SlyB, periplasmic homeostasis and stress response	130
7.4	Methods	131
7.4.1	Bacterial strains, culture media and blood	131
7.4.2	Mutagenesis and complementation	131
7.4.3	Mutant screening in human blood	132
7.4.4	Mice experiments	132
7.4.5	Neutrophil depletion from human whole blood	133
7.4.6	Macrophages intracellular survival	133
7.4.7	Stress assays	133
7.4.8	Mass spectrometry	134
	Sample preparation.	134
	Protein digestion and desalting.	134
	Peptide mixing and pre-fractionation	134
	LC-DIA-MS for DIA.	135
	Bioinformatic analyses.	135
	Statistical analysis.	135
7.4.9	Western blotting	136
7.5	Tables	137
8	MicroRNAs as biomarkers of plague	142
8.1	Objectives and summary	142
8.2	Results and discussion	142
8.2.1	Murine model of pneumonic plague	142
8.2.2	Blood sampling setup and optimization	143
8.2.3	Preliminary microRNAs RT-qPCR screen	144
	Sample quality controls.	144
	Circulating miRNAs differential expression.	145
	Biomarker analysis.	146
8.2.4	MicroRNAs screen during pneumonic plague	146
	Experimental procedure improvements.	146
	MicroRNA-sequencing.	147
	Pneumonic plague time course.	147
8.3	Methods	148
8.3.1	Mice experiments	148

8.3.2	Plasma collection, miRNA extraction and RT-qPCR screen	148
8.3.3	Data analysis	148
IV	Conclusion and perspectives	149
V	Bibliography	155
	Appendixes	172
A	Participation in other projects of the laboratory	174
A.1	Proteomics pipeline	174
A.2	Oxford Nanopore Technologies MinION sequencing	174
A.3	Mutant library annotation	174
A.4	The <i>Y. pestis</i> flagellin locus <i>fliC</i> contributes to virulence in the non-motile plague bacillus	175
A.5	Supervision of a Master student to study <i>pla</i> deletion in <i>Y. pestis</i>	175
A.6	Set up of a zebrafish model of infection by <i>Y. pestis</i>	175
B	Grant applications	176
B.1	Fundraising for a biotechnological startup	176
B.2	Post-doctoral fellowship	176
C	Minireview: Emerging evasion mechanisms of macrophage defenses by pathogenic bacteria	177
D	Review article: Bacterial determinants of bloodstream infections	187
E	Original article: Within-host evolution of <i>Yersinia enterocolitica</i> during a chronic human infection	245
F	Résumé substantiel en français	269

List of Figures

1.1	Phylogenetic reconstruction of the 26 <i>Yersinia</i> species	18
1.2	Scheme of <i>Y. pestis</i> cycle in the environment and evolution of clinical forms in humans	20
2.1	Structure of <i>Y. pestis</i> envelope	26
2.2	Lipopolysaccharide structure	27
2.3	<i>Y. pestis</i> virulence-associated envelope mechanisms	29
3.1	Number of <i>Yersinia</i> transcriptomes from 2005 to 2022	34
4.1	Worldwide distribution of plague cases	38
4.2	Global workflow for plague diagnostics	39
4.3	PCR workflow for plague diagnostics	40
7.1	<i>Y. pestis</i> dissemination in the mouse after intravenous injection	117
7.2	Screen of <i>Y. pestis</i> mutant survival in human blood and in mice	118
7.3	Survival in whole blood and virulence in mice of the $\Delta slyB$ strain	119
7.4	Growth of the $\Delta slyB$ strain in laboratory media and human serum	120
7.5	$\Delta slyB$ strain sensitivity towards neutrophils and macrophages	121
7.6	Resistance of the $\Delta slyB$ strain to membrane stresses and anti-microbial components	122
7.7	Periplasmic loss of the $\Delta slyB$ strain	124
7.8	Differentially regulated processes in the $\Delta slyB$ strain	126
7.9	Similarities in protein abundance between the $\Delta slyB$ strain and gene expression in other conditions	128
8.1	Progression of pneumonic plague in C57BL6/J mice	143
8.2	Quality control of the miRNAs screen	144
8.3	Up- and down-regulated circulating miRNAs during pneumonic plague	145
8.4	Comparison of two hemolysis assays after blood collection	147

List of Tables

7.1	Differential abundance for components of membrane complexes in the $\Delta slyB$ strain	137
7.2	Differential abundance of proteins involved in envelope stress response and two-component systems in the $\Delta slyB$ strain	139
7.3	LPS synthesis and modification proteins in the $\Delta slyB$ strain	139
7.4	KEGG pathways GSEA of the $\Delta slyB$ strain proteome	140
7.5	Similarities between the $\Delta slyB$ strain proteome and Δcrp strain transcriptome	140
8.1	Regulated miRNAs during pneumonic plague as compared to other respiratory infections	146

Abbreviations

ABC	ATP-binding cassette or Ammonium bicarbonate
ACN	Acetonitrile
Amf	Ammonium formate
AMP	Adenosine monophosphate
APC	Antigen-presenting cell
ATP	Adenosine triphosphate
BCA	Bicinchoninic acid
BPI	Bactericidal/permeability-increasing protein
C4BP	C4b-binding protein
CAA	Chloroacetamide
cAMP	cyclic AMP
CAMP	Cationic antimicrobial peptide
CFU	Colony forming unit
DDA	Data-dependent analysis
DIA	Data-independent analysis
dLN	Draining lymph node
ESR	Envelope stress response
FA	Formic acid
FASP	Filter-aided sample preparation
GO	Gene ontology
HBDM	Human blood derived monocytes
HIS	Human inactivated serum
ID	Intradermal
IN	Intranasal
IP	Intraperitoneal
IV	Intravenous
KEGG	Kyoto Encyclopedia of Genes and Genomes
LB	Lysogeny broth
LBH	Lysogeny broth + pork haemin
LC-MS/MS	Liquid chromatography + tandem mass spectrometry
LOS	Lipooligosaccharide
LPS	Lipopolysaccharide
MAC	Membrane attack complex
NE	Neutrophil elastase
NET	Neutrophil extracellular traps
NHS	Normal human serum
OD600	Optical density at 600nm
OM	Outer membrane
OMP	Outer membrane protein
PBS	Phosphate buffered saline
PVDF	Polyvinylidene difluoride

PES	Polyethersulfone
PCR	Polymerase chain reaction
PGF	Proteoglycophili
PMB	Polymyxin B
qPCR	Quantitative PCR
RDT	Rapid diagnostic test
RT-qPCR	Reverse transcription-qPCR
SDS	Sodium dodecyl sulfate
SPEED	Sample preparation by easy extraction and digestion
STRING	Search tool for the retrieval of interacting genes/proteins
T3SS	Type 3 secretion system
TCA	Trichloroacetic acid
TCEP	Tris(2-carboxyethyl)phosphine
TCS	Two-component system
TFA	Trifluoroacetic acid
TLR	Toll-like receptor

Part I

Introduction

Chapter 1

Yersinia pestis lifecycle

The newly defined *Yersiniaceae* family, originating from the split of the *Enterobacteriaceae* family in 2016 [1], encompasses the *Yersinia* type genus which includes 26 species [2]. Three of them are known human pathogens: *Yersinia pseudotuberculosis* and *Yersinia enterocolitica* cause self-limited enteritis [3] and *Yersinia pestis* is the etiological agent of plague [4]. Due to the presence of known virulence factors, the recently described *Yersinia wautersii* species is considered as a potential human pathogen [5]. The *Yersinia* genus also includes the fish pathogen *Yersinia ruckeri* [6], the insect pathogen *Yersinia entomophaga* [7] and 20 environmental species (Fig 1.1). *Y. pseudotuberculosis* and *Y. enterocolitica* are enteric pathogens transmitted by the oro-fecal route causing gastro-enteritis and possessing the ability to cross the intestinal barrier and colonize deeper organs in immunocompromised hosts. Interestingly, their virulence towards humans was parallelly acquired in different branches of the *Yersinia* genus [8]. On the other hand, *Y. pestis* is a clonal species recently emerged from *Y. pseudotuberculosis* around 6,000 years ago [9]. By a series of genetic gains and losses, *Y. pseudotuberculosis* turned from a pathogen causing a self-limited enteric disease into a highly virulent and deadly pathogen with a very different life cycle [8]. *Y. pestis* is known to be the cause of at least three pandemics: the Justinian plague from 541 to 750 common era (CE), the second pandemic from 1346 to 1772 CE which began with the infamous Black Death episode from 1346 to 1353 CE, and the third pandemic beginning in the middle of the 19th century, responsible for the current plague foci worldwide [10].

1.1 *Y. pestis* cycle in the environment

1.1.1 The vectorial transmission of plague

Plague is a zoonosis, primarily occurring in the environment. The first accurate description of *Y. pestis* was made by Alexandre Yersin, a Swiss-French physician and disciple of Louis Pasteur, during a plague outbreak in Hong Kong in 1894 [12]. In 1898, during another outbreak in Mumbai, the pasteurian Paul-Louis Simond performed the first experiment showing that fleas were a vector of the disease [13]. Although highly controversial at the time, this observation was confirmed in the following years [14–16]. It is now well admitted that plague is mainly transmitted between mammals by the fleas, such as the Oriental rat flea *Xenopsylla cheopis* or the ground squirrel flea *Oropsylla montana*, which are contaminated during a blood meal on a bacteremic mammalian host. During subsequent blood meals, the fleas can infect other animals, mainly rodents, which can develop the disease depending on their susceptibility. This is the main hypothesis of plague maintenance at low incidence in the environment, representing the enzootic cycle of the disease (Fig 1.2A). During outbreaks in a wild animal population, called epizootics, a spillover to human can occur and

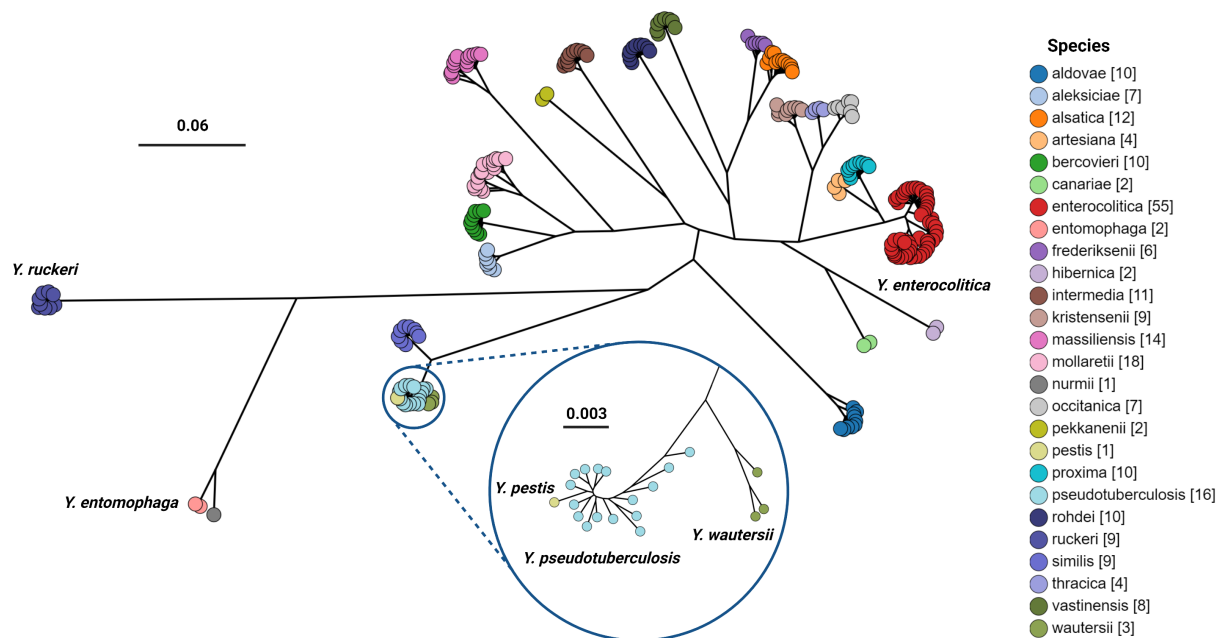


Figure 1.1. Phylogenetic reconstruction of the 26 *Yersinia* species based on the 500 genes of the *Yersinia* cgMLST [11]. Illustration adapted from [2].

cause sporadic cases or plague outbreaks (Fig 1.2B) [17]. Other ways of transmission can also occur depending on the ecological context, such as ingestion of rodents by carnivores, contacts between urban and rural rodents, aerosol contamination or infected flea carriage by domestic animals [4].

Simond's first mechanistic hypothesis for flea-mediated transmission was that bacteria were transmitted by flea feces on the skin, entering the body by the breach created upon feeding [13]. However, the English medical entomologist Arthur W. Bacot observed in 1914 bacteria-mediated blockage of the flea proventriculus which led to regurgitation of the bacilli during feeding [18, 19]. Three types of fleas regurgitation are now described: i) an early phase transmission, also called mass transmission, which occurs in the first days after flea infection and is poorly efficient, requiring many fleas to infect a new host, ii) a more efficient late-stage transmission caused by blockage of the flea proventriculus upon biofilm formation, which occurs later after infection of fleas that cannot feed anymore and iii) an intermediate partially blocked state in which fleas can feed but maturation of the biofilm already interferes with the proventriculus function [20]. A unified mode of transmission based on proventriculus colonization was proposed in which the kinetics of biofilm maturation is the main factor explaining the variability in transmission efficiency between early-phase and late-stage transmission [20]. Epidemiological models based on the rapid epizootic dynamics suggest the early-phase transmission to be responsible for the epizootics in wild rodent populations, but remain controversial due to the low efficiency of this type of transmission and the high variability in transmission efficiency depending on the flea and host species [20]. A recent report only partially supports a putative role of the early-phase transmission in epizootics depending on host susceptibility and blood characteristics, as previously reported [21, 22].

The vector mediating human plague outbreaks and particularly during the medieval Black Death is more controversial. Indeed, the presence of the eastern flea *X. cheopis* could not be proven in Europe, contrary to the human flea *Pulex irritans*, which however displays a very low transmission efficiency. Medieval and modern epidemiological data also suggest that direct transmission by pneumonic plague could hardly mediate the outbreak dynamics [23, 24]. Other vectors, such as the human lice *Pediculus humanus humanus*, have been

proposed to mediate human plague transmission [25]. As lice cannot regurgitate bacteria while feeding, it has been suggested that bacteria enter the body from lice feces on the skin upon self-scratching. However, this mechanism remains hypothetical [17].

1.1.2 Maintenance of the plague enzootic cycle

Independently of the vector species, the low efficacy of bacterial uptake and regurgitation from fleas requires a very high bacteremic level in the mammalian host, above 10^6 - 10^7 bacteria per milliliter of blood [26]. The infectivity period of the host is presumably quite short, as at this level of bacteremia, the mammalian host hardly survives more than a few days. This high mortality and short infectious time raise questions about the plague maintenance in the environment, as a subtle balance has to be found in infection to prevent either host or disease extinction. A widespread explanation is the presence of heterogeneous resistance of the main host reservoir population, allowing long-term maintenance of host population by renewing the pool of susceptible hosts [27–29]. Mechanisms of heterogeneity have been hypothesized such as immunisation by sublethal infection [22] or natural selection [28, 30]. Other hypotheses include telluric reservoirs, as *Y. pestis* can survive in soil, persistence of bacteria in fleas, or a transient stage in protozoa [17, 27]. A mechanism of maintenance in a fully susceptible species has also been proposed, highlighting the metapopulation spatial arrangement of some rodent species, where the disease spread from burrows to burrows by a percolation mechanism which could allow higher persistence through extinction-recolonization [28, 31–33]. In this model, some resistant species were also proposed as alternate host disseminating the disease between spatially distinct foci during epizootic episodes [32]. The metapopulation dynamics hypothesis remains however controversial, as empirical data only weakly support this model today [34].

1.2 *Y. pestis* cycle in the mammalian host

1.2.1 Bubonic plague

Y. pestis infection of the mammalian host often occurs after the bite of an infected flea into the dermis (Fig 1.2C). In a model of intradermal (ID) injection in the ear pinna of mice, bacteria are subjected to a strong bottleneck, where only a few of them migrate through lymphatic vessels to the draining lymph node (dLN). Bacteria can be detected as quickly as 10 minutes after injection, suggesting an extracellular way to reach the dLN following the lymph flow [35]. A strong neutrophil recruitment is observed at the site of injection, but occurs whether bacteria or sterile PBS is injected. After ID injection, bacteria are mainly associated with neutrophils and to a lesser extent to macrophages. Neither neutrophil depletion nor dendritic cells (DC) migration ablation affected bacterial transport to the dLN, supporting the hypothesis of extracellular transport via lymph [36]. In a natural model of infection by flea bite, neutrophil recruitment was only observed for bites of infected flea and its intensity correlated with the number of injected bacteria. Macrophages were recruited after the bite regardless of the presence of bacteria, and DCs showed a moderate recruitment driven by the infection. No specific associations or significant movement was observed between bacteria and these cell types at early time points [37]. These studies underline the importance of the infection model, where different outcomes are observed between artificial injection of bacteria grown in laboratory culture media and flea pre-conditioned bacteria injected by bites. Another study indeed showed upregulation of bacterial anti-phagocytic factors in the fleas [38], and fleas possibly inject effectors dampening inflammation during its blood meal. Despite their methodological differences, these studies suggest an extra-

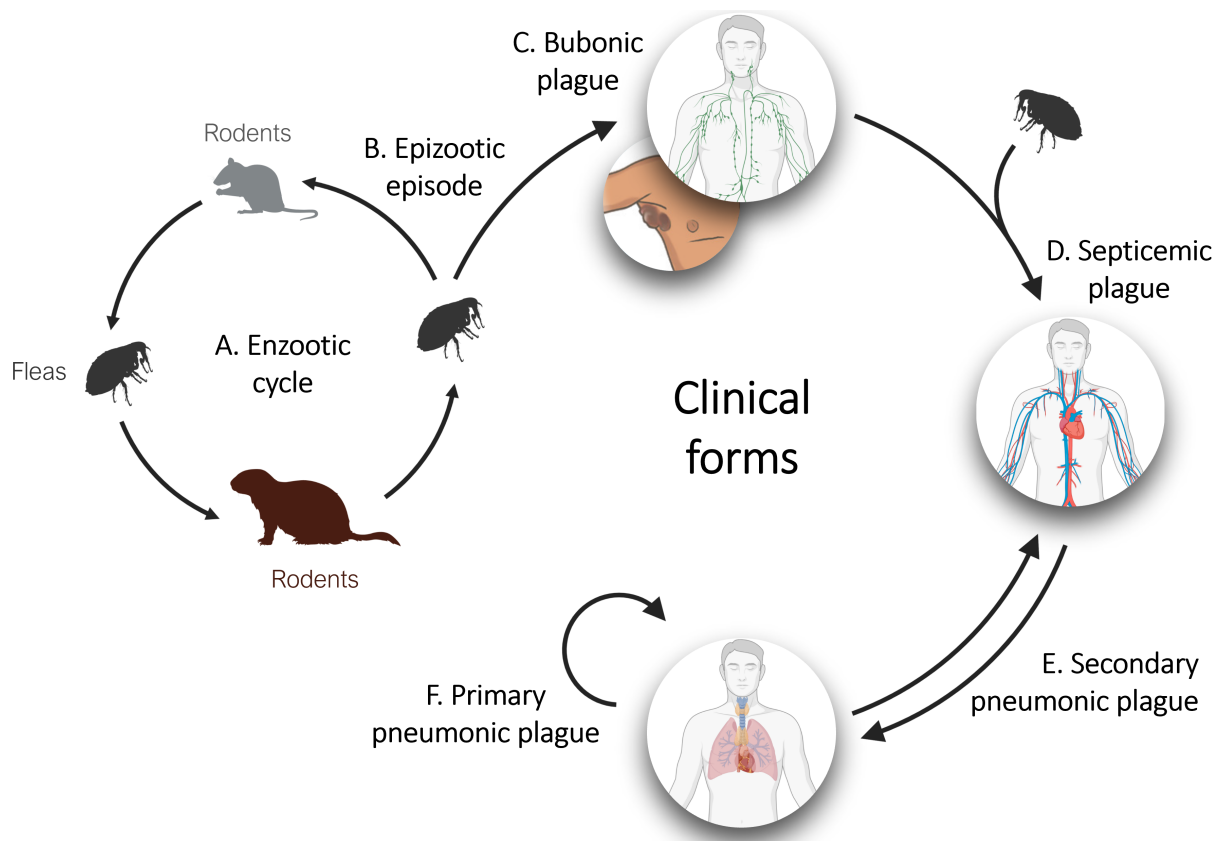


Figure 1.2. Simplified scheme of *Y. pestis* cycle in the environment and evolution of clinical forms in humans. (A) The enzootic cycle is maintained by the transmission of *Y. pestis* by fleas that are infected by feeding on bacteremic hosts. They can then infect more or less susceptible rodents during subsequent blood meals. (B) Epizootic episodes in the wild population can lead to spillover to the human population, causing epidemics. (C) After injection of *Y. pestis* in the dermis, bacteria reach the lymph node via the lymphatic vessels, where they replicate, triggering formation of swollen lymph node called bubo and causing bubonic plague. (D) If bacterial replication is not controlled in the lymph node, hematogeneous dissemination from the bubo can cause a secondary septicemic plague. Primary septicemic plague can also occur if bacteria are directly injected into the bloodstream by fleas. (E) During septicemia, bacteria can reach and colonize the lungs, causing secondary pneumonic plague. (F) Primary pneumonic plague is inter-individually transmitted by the cough or any exposure to contaminated fluids. Dissemination from the lungs also lead to secondary septicemic plague.

cellular route of migration from the injection site to the dLN. However, other studies, using injection into the hind paw or footpad, showed the importance of phagocytes and antigen-presenting cells (APC) receptors such as Langerin (CD207), CCR7, CCR2, sphingosine-1-phosphate (S1P) or CD209b for efficient bacterial dissemination [39–41]. These studies are supported by a recent work combining flow cytometry and single-cell RNA-Seq showing bacteria associated with migratory DCs into the dLN [42]. This result is mitigated by the use of subcutaneous injection, less representative of a natural flea infection than ID injection due to differences in dermis and subcutaneous immune composition [43]. Survival of *Y. pestis* inside macrophages and to a lesser extent in neutrophils has been demonstrated [44–46] and bacterial-mediated necroptosis of infected phagocytes is proposed as a mechanism of bacterial dispersal to the dLN and secondary lymph nodes [47]. This suggests complementary roles of early extracellular migration mediated by the lymph flow and subsequent and slower intracellular trafficking allowing optimal dissemination to the dLN, secondary lymph nodes and ultimately the whole organism.

In the lymph node, bacteria can replicate, provoking a disorganized neutrophil response which inefficiently control bacterial proliferation [48]. A massive influx of neutrophils, mediated by a strong cytokine induction such as CCL3 (coupled with neutrophil CCR1 receptor), is observed along macrophage and DC influx [39, 42]. *Y. pestis* subverts this immune response by neutrophil functional inactivation [42, 49] and cell apoptosis [50]. In mice, lymph nodes show necrosis in the first 24 hours [39], and late inflated lymph nodes appear necrotic, surrounded by a gelatinous and hemorrhagic capsule in a rat model of bubonic plague [48, 50]. The resulting swollen lymph node, named bubo, gave its name to the associated disease - bubonic plague.

1.2.2 Septicemic plague

In mice, these rapidly occurring hemorrhages have been recently suggested to come from a vasculature disruption by bacteria, opening tight junctions between endothelial cells, leading to dispersion from the bubo to the whole body via the bloodstream and causing secondary septicemic plague [51] (Fig 1.2D). Blood vessels disruption allows bacteria to colonize secondary organs from the bloodstream [51], in addition to a proposed intracellular-mediated way from the lymph node to the thoracic duct [39]. In the rat model, bacteria can be detected in blood and spleen as soon as 36 hours post infection, sign of hematogenous dissemination. Increased level of IFN- γ , TNF- α and IL-10 were detected in bacteremic rat sera. IFN- γ levels, along with thrombocytopenia and increased level of circulating neutrophils and macrophages, seem to correlate with the bacteremia level, consistent with human plague [50]. In mice, thrombocytopenia could be explained by an atypical disseminated intravascular coagulopathy characterized by a specific activation of the intrinsic pathway of coagulation, possibly due to opening of tight junctions of the endothelium by bacteria and contact of the subendothelial extracellular matrix with blood [52]. Circulating bacteria can be observed in the spleen vasculature, mostly aggregated around the white pulp. From the bloodstream, bacteria can also colonize other lymph nodes by disrupting the endothelium from the lumen [51]. After dissemination, bacteria multiply exponentially in colonized tissues [50], where they primarily target neutrophils and macrophages [53].

Primary septicemic plague can also occur if bacteria directly enter the bloodstream, via a wound, or when the flea directly injects bacteria into the bloodstream, which is thought to occur in up to 30% of human plague cases [54].

1.2.3 Pneumonic plague

Following hematogenous dissemination, bacteria can reach the lungs in which they replicate and induce a secondary pneumonic plague, characterized by pneumonia and cough (Fig 1.2E) [4]. Primary pneumonic plague can then be caused by airborne transmission of *Y. pestis* by coughing individuals, or by inhalation of infectious droplets from any contaminated sources (Fig 1.2F). Primary pneumonic plague exhibits a characteristic biphasic course, that has been studied in various animal models [55–58], beginning with a pre-inflammatory phase during which bacteria replicate in the lungs, followed by a pro-inflammatory phase causing lung damage, pneumonia and secondary septicemic plague after dissemination into the bloodstream [55]. During the pre-inflammatory phase in mice, *Y. pestis* directly targets alveolar macrophages and neutrophils [59]. During this phase, bacteria also prevent neutrophil recruitment by dampening production of chemoattractants, allowing early bacterial replication which would be impaired by neutrophil influx [60]. Bacteria activate pro-inflammatory IL-1 β and IL-18 shortly after entering the lungs, but a simultaneous activation of IL-1 receptor agonist promotes the pre-inflammatory phase [61]. Laser capture microdissection and RNA-Seq analysis of lung lesions in infected mice showed that *Y. pestis* also inhibits leukocyte migration and cell apoptosis [62], the latter being probably caused by degradation of Fas ligand [63]. It is thought that bacteria can then disseminate in the organism by hijacking APCs using host receptors such as CD205 [64]. Replicating bacteria along with an influx of neutrophils lead to a switch from the pre-inflammatory to the pro-inflammatory phase between 24 and 48 hours post infection. The necrotizing pneumonia characteristic of the pro-inflammatory phase is mainly caused by the massive influx and activation of neutrophils [59]. A recent study highlighted the complexity of this biphasic response by showing the importance of the myeloid differentiation primary response protein 88 (MyD88) to mediate primary pneumonic plague [65]. Deletion of murine MyD88 gene, involved in the signaling cascade of the inflammatory response, led to a reduced chemokine production and neutrophil influx at the early stage, 18 hours post infection, correlating with a higher bacterial burden in the lungs. However, MyD88 deficiency also led to reduced bacterial load in the lungs at 48 and 72 hours post infection, suggesting the necessity of a primary bacterial clearance to allow access of a subset of bacteria to a replicative niche. In addition, MyD88^{-/-} mice showed reduced lung lesions but were more susceptible to secondary septicemic plague, suggesting a tight balance between host damage and bacterial clearance in the different phases of the disease [65]. Importantly, instillation may lead to secondary septicemic plague with or without lung colonization depending on the experimental procedure [66].

1.2.4 Rare forms of plague

Consumption of raw or undercooked meat infected with *Y. pestis* can cause pharyngitis and invasion of the cervical lymph node, leading to pharyngeal plague [17]. Some rare complications of septicemia can also occur, such as meningitis, which has been observed mostly in young patients [67, 68]. Even rarer infections or complications include osteomyelitis [67, 69], myocarditis [67] or endophthalmitis [70, 71].

Chapter 2

Y. pestis determinants of plague

As a highly virulent pathogen, *Y. pestis* has been thoroughly studied to better understand its pathogenesis mechanisms [4, 9, 72]. In addition to the pCD1 plasmid-encoded type 3 secretion system (T3SS), shared by the three human pathogenic *Yersinia* [8], *Y. pestis* underwent several genetic events which led to its very specific lifestyle and virulence. Acquisition of virulence factors encoded by plasmids pMT1 and pPCP1, and loss of gene functions by pseudogenization leading to specialization are hallmarks of its specific adaptation.

2.1 Bacterial determinants of vectorial transmission

It was thought that *Y. pestis* first evolved to induce pulmonary infection by the acquisition of an ancestral allele of the plasminogen activator Pla [73]. However, one of the hallmarks of plague today is its vectorial transmission by the flea. To survive in the flea gut environment, the first evolution of *Y. pestis* from *Y. pseudotuberculosis* could have been acquisition of the *ymt* gene carried by the pMT1 plasmid, encoding *Yersinia* murine toxin, a phospholipase D allowing bacteria to better survive toxic compounds derived from blood digestion in the flea [74]. It was recently suggested that the importance of *ymt* to colonize the flea depends on the host blood status [75]. Ancestral virulent *Y. pestis* strains which lack Ymt could have survived in animal hosts with specific blood characteristics. Acquisition of *ymt* allowed bacteria to expand their host range to maintain the enzootic cycle [75]. *Y. pestis* also relies on lipopolysaccharide (LPS) modification enzymes and on the *oxyR* and *rovM* transcriptional regulators to resist antimicrobial peptides, reactive oxygen species and adapt to metabolic changes in the flea, respectively [20].

Additionally to factors allowing bacterial survival into the flea, *Y. pestis* also produces factors involved in biofilm formation to block the flea and better disseminate. Major biofilm factors are produced by the haemin storage locus *hms*, responsible for cyclic-di-GMP and extracellular matrix production, and repressed by the Rcs phosphorelay [20]. Importantly, pseudogenization of *rcaA* and a frameshift mutation in *Y. pestis rcsD* are important evolutionary steps allowing to fine-tune biofilm formation in the flea [74, 76]. Biofilm formation also depends on factors such as the two-component systems OmpR/EnvZ [77] and PhoP/PhoQ, the small RNA chaperone Hfq, and the cyclic adenosine monophosphate (cAMP) receptor protein (Crp).

Finally, loss of urease activity by mutating the *ureD* gene decreases *Y. pestis* virulence in flea and is necessary for flea colonization [78].

2.2 Virulence factors involved in plague

The best studied virulence factors, shared by the three human pathogenic *Yersinia* species, are the T3SS effectors encoded on the pYV plasmid (pCD1 in *Y. pestis*). This secretion system injects *Yersinia* outer proteins (Yops) in host immune cells such as macrophages and neutrophils [53], preventing phagocytosis, cell activation, and inducing cell death pathways [79, 80]. The T3SS activity is necessary for disease progression in any form of plague [51, 59, 81–83]. A *Y. pestis* strain cured of T3SS is highly attenuated in any form of plague, and is considered as a BSL-2 agent in France and other countries, in contrast to its parental fully virulent strain which requires manipulation in BSL-3 environment.

Determinants necessary for bacterial survival in the host or to induce the various forms of plague have been extensively reviewed [9, 72]. We will focus on the main factors in the following sections.

2.2.1 Virulence factors involved in bubonic plague

The plasminogen activator (Pla), encoded on the pPCP1 plasmid and specific to *Y. pestis* among the *Yersinia*, is required for bubonic but not septicemic plague [54]. Pla is a broad range protease cleaving plasminogen into plasmin, as well as a plethora of other substrates. Although the virulence of a strain deficient for Pla activity is highly reduced in bubonic plague, the function of Pla during infection remains mysterious. Its activity on coagulation and fibrinolysis *in vivo* suggests a role in fibrin clot dispersal, facilitating bacterial dissemination from the point of injection in the skin. However, a study suggests a role of Pla in bacterial multiplication in the bubo but not in dispersal from the site of injection since no difference was observed for a *pla* mutant strain [84]. Other authors have suggested that Pla could cleave *Y. pestis* own proteins allowing other functions, or cleave extracellular substrates to acquire nutrients [85].

Y. pestis encodes a chromosomal pigmentation locus (*pgm*) flanked by IS100 insertion sequences which can recombine at high frequency, leading its loss [86]. The *pgm* locus encompasses the *ripA* gene, required for intracellular survival in macrophages [87], and the high pathogenicity island (HPI), a mobile element encoding the yersiniabactin siderophore which is found in other bacteria [88]. Yersiniabactin has been shown to be required to induce bubonic plague when injected by peripheral route, by providing bacteria with the necessary iron sequestered by the host [81, 89].

The master regulator of virulence *rovA* is required for full virulence of both *Y. pseudotuberculosis* and *Y. pestis*. While RovA regulates the invasin in *Y. pseudotuberculosis*, it has a different regulatory role in *Y. pestis* which bears an inactive *inv* gene. *Y. pestis* RovA regulates the pH6 antigen PsaA, an antiphagocytic factor. The *rovA* and *psaA* mutants display similar virulence attenuation in bubonic plague by a mechanism that is still unknown [90].

The pMT1 plasmid encodes the Caf pseudocapsule, which is highly abundant in bacteria grown at 37°C and exhibits anti-phagocytic properties [46, 91]. While Caf has been reported to be required for full virulence of *Y. pestis* in a murine model of bubonic plague transmitted by flea bite [92], contradictory results for Caf requirement in bubonic and pneumonic plague models accumulated over the years [93, 94].

2.2.2 Virulence factors involved in pneumonic plague

Apart from the T3SS effectors required for the characteristic biphasic profile, few virulence factors contributing to pneumonic plague are known [59, 60, 83]. Although host microenvironments in lymph nodes and lungs are different, Pla plays a role in lung colonization and pneumonia [95], by degradation of the Fas ligand FasL, leading to decreased

apoptosis [63]. Pla is regulated by Crp, the central regulator of carbon catabolite repression allowing metabolism of lung carbon sources, which is itself regulated by the RNA chaperone Hfq. Both Crp and Hfq have been shown to be required for pneumonic plague [96]. Additionally, Pla and Caf could modulate *Y. pestis* resistance to lung antimicrobial peptides [97]. Pla, Ail and Psa play a role as adhesins allowing optimal injection of effectors by the T3SS [98–100]. A recent transposon screen identified new factors required for bacterial adhesion in the lungs, including YPO3903, which regulates PsaA fimbria and additional adhesins [101]. Finally, the bactericidal/permeability-increasing protein (BPI)-inducible protein BipA promotes *Y. pestis* resistance to neutrophil killing in the lungs during the early phase of primary pneumonic plague [102].

2.2.3 Virulence factors involved in septicemic plague

Y. pestis blood survival and dissemination have been less studied than bubonic and pneumonic of plague. The T3SS and Psa are required for full virulence of *Y. pestis* after intravenous (IV) injection, underlining the importance of immune cell neutralization during septicemia [53, 81, 82, 103], but neither Pla [54], the *pgm* locus [89], Caf [92] nor RovA [90] are essential for proficient septicemic plague.

The main factor required for resistance to complement is the adhesin Ail, a major component of the bacterial outer membrane (OM). Intriguingly, a Δail mutant becomes sensitive to bactericidal activity of a wide range of mammalian sera, but remains resistant to mouse serum [104]. Ail is required for all forms of plague in rat models but not for pneumonic plague in mice models, and contradictory results were found depending on the methodology used for septicemic plague models [105]. Ail displays pleiotropic activity on the complement system, by recruiting and binding the human Factor H, C4b-binding protein (C4BP) and vitronectin, inhibiting the principal, alternative and terminal pathways of the complement cascade, respectively [106]. In addition to complement resistance, Ail confers other properties such as adhesion, invasion and Yops delivery [106]. Interestingly, a recent study showed that sensitivity to human serum of a Δail strain is abrogated in the flea [107]. Although most of the literature on Ail-mediated serum resistance revolves around binding and inhibition of complement factors, recent findings suggest that most of Ail activity could originate from its envelope stabilization properties. Ail could indeed bind LPS, favorizing OM stability and integrity and mediating resistance to envelope stresses [108, 109]. In the next section, we will develop the maintenance of *Y. pestis* envelope integrity and its role during infection.

2.3 The bacterial envelope at the interface with the immune system

In addition to virulence factors mentioned above, *Y. pestis* and pathogenic bacteria in general evolved mechanisms to resist stresses encountered in the host. Among others, these stresses include pH changes, oxidative, nitrosative or osmotic stresses, exposure to cationic antimicrobial peptides (CAMP), proteases, or to the membrane attack complex (MAC) of the complement system. Many resistance mechanisms take place at the bacterial envelope, which will be the focus of the following section.

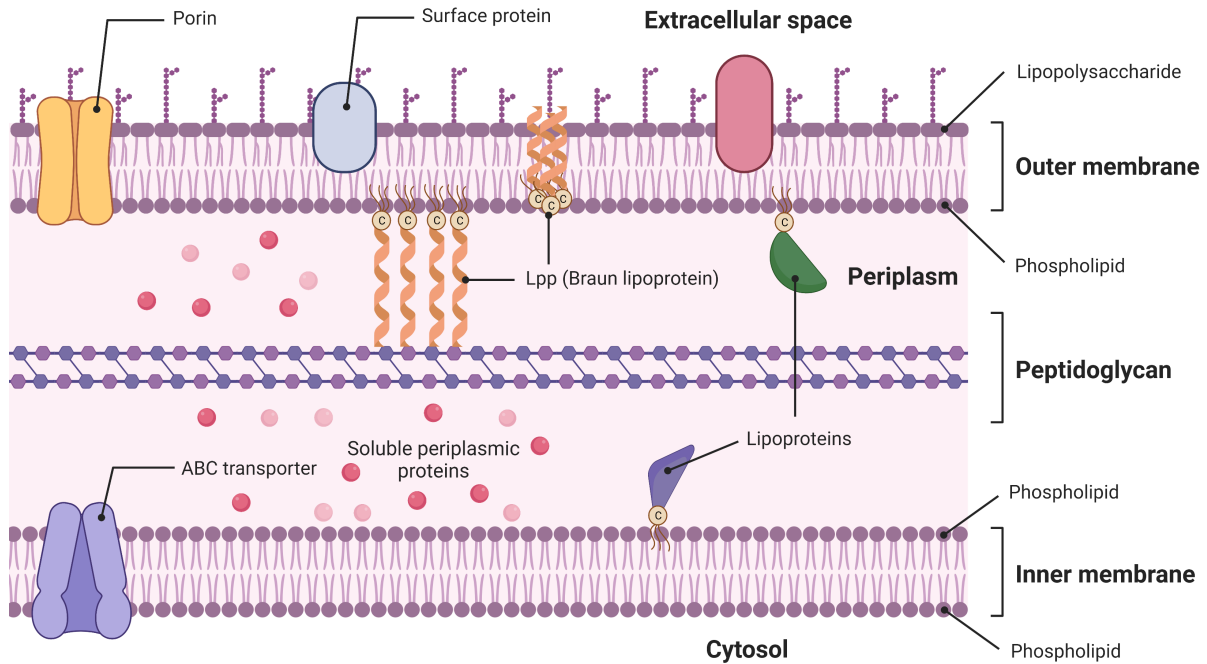


Figure 2.1. Structure of *Y. pestis* envelope. The inner membrane is composed of a symmetric phospholipid bilayer containing anchored lipoproteins or inserted transmembrane proteins such as ABC transporters. The outer membrane is composed of an asymmetric lipopolysaccharide-phospholipid bilayer, in which β -barrel outer membrane proteins such as porins, Ail or Pla are inserted, in addition to lipoprotein anchored in the phospholipid leaflet. Both membranes encompass the periplasm containing a thin peptidoglycan layer, covalently attached to the outer membrane by the Lpp Braun lipoprotein. The periplasm also contains soluble periplasmic proteins involved in various mechanisms such as nutrient transport or virulence.

2.3.1 The classical diderm envelope structure

Y. pestis is a Gram-negative bacterium, possessing a diderm envelope structure (Fig 2.1). The envelope is constituted from an inner membrane (IM), an outer membrane (OM) and a periplasm space (PP), containing a thin peptidoglycan (PG) layer. The IM is a symmetrical bilayer composed of phospholipids (PL), whereas the OM is constituted of PL in the inner leaflet and LPS on the outer leaflet [110]. Whereas the OM has long been thought to be a permeability barrier, its mechanical role to maintain cell integrity and compensate for the thin PG layer is now well accepted [111].

The lipopolysaccharide. The LPS is composed of lipid A, a core polysaccharide and an optional O-chain, or O-antigen (Fig 2.2). *Y. pestis* does not possess any O-antigen, thus the OM outer leaflet is alternatively called lipooligosaccharide (LOS) [112]. The classical lipid A structure characterized in *Escherichia coli* possesses 6 acyl chains leading to hexa-acylated LPS, but different levels of acylation can be observed depending on bacterial species and growth conditions. Due to several mutations, *Y. pestis* produces hexa-acylated LPS at room temperature but tetra-acylated LPS at 37°C, the mammalian host temperature [113–115]. The lipid A and the core contain negatively charged phosphate groups, and LPS molecules are compacted together thanks to divalent cations such as calcium or magnesium [116, 117], which give part of its mechanical properties to the OM [111]. The hydrophilic nature of sugars composing the LPS core and O-antigen, along with the hydrophobic nature of the lipid bilayer, offers an efficient permeability barrier to Gram-negative bacteria, which can however be destabilized in various ways [118].

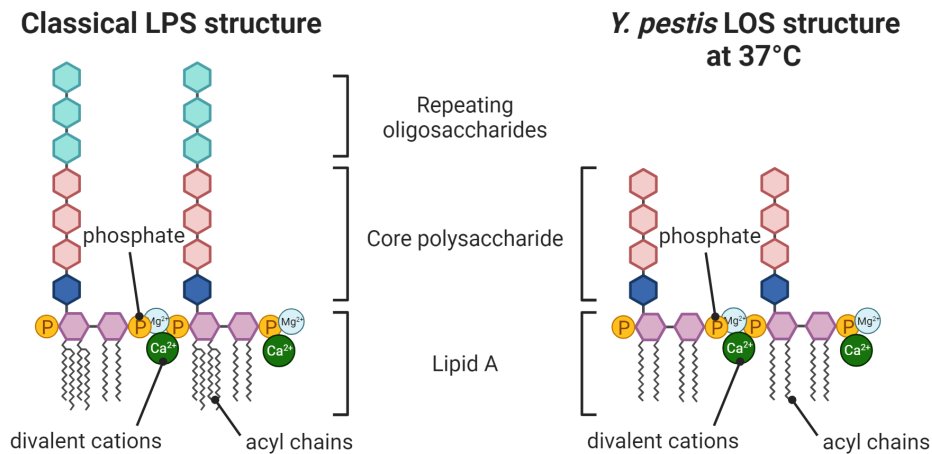


Figure 2.2. Classical lipopolysaccharide (LPS) structure of *E. coli*, constituted of a hexacylated lipid A attached to a core polysaccharide and finishing by a repeating oligosaccharide chain of various length (O-chain or O-antigen). *Y. pestis* lipooligosaccharide (LOS) does not contain any O-chain, and is characterized by a tetra-acylated lipid A when grown at 37°C. Divalent cations help to pack and stabilize the LPS by binding to negative phosphate groups of the lipid A.

Outer membrane proteins. Roughly 70% of the exposed area of the OM is composed of outer membrane proteins (OMPs) which are specific β -barrel proteins inserted into the OM thanks to the Bam machinery [111]. These OMPs can serve as porins allowing solutes and nutrients to cross the OM, or as virulence factor interacting with the external environment such as Pla or Ail in *Y. pestis*.

Lipoproteins. Lipoproteins are specific processed proteins that are anchored in the OM in majority but also in the IM. While most of lipoproteins face the periplasm, some cross the OM and can even be exposed to the surface [119]. It is the case of the first lipoprotein discovered, the Braun lipoprotein Lpp [120]. This protein is thought to be the most abundant protein in *E. coli* with 1 million copies per cell, representing 10% of its mRNA and 8% of the translation process load. About a third of the Lpp, called periplasmic or bound Lpp, is covalently linked to PG and participates in the integrity and sizing of the cell envelope. The remaining two-thirds, called free Lpp, is spanning through the OM, non-covalently linked to several OMPs and can be exposed to the surface [111, 120].

The periplasmic content. The PP also contains soluble periplasmic proteins that carry various functions, such as nutrient import, protein processing or pathogenesis. Some soluble periplasmic proteins such as MalE, TauA or OppA are linked to specific substrates (maltose, taurine and oligopeptides, respectively) that can be imported into the cytoplasm by specialized ATP-binding cassette (ABC) transporters, whose genes are often transcribed as operons along with genes of their periplasmic protein counterparts (MalEFG, TauABCD and OppABCDF, respectively) [121]. Other soluble periplasmic proteins allow to transport components between the membranes, such as LolA from the Lol pathway and LptA from the Lpt pathway, respectively exporting the lipoproteins and the LPS from the IM to the OM, or MlaC from the Mla pathway, transporting PL between membranes [121, 122].

Some periplasmic proteins are chaperones such as Skp or SurA, folding OMPs to present them to the Bam machinery, which will insert them in the OM [123], and others such as DsbA can add disulfide bonds for oxidative protein folding [124]. Finally, some proteins act as virulence factors such as the ecotin which binds to neutrophil elastase (NE), inhibits its protease

activity, and is required for full virulence of diverse bacteria such as *Y. pseudotuberculosis* [125–127].

2.3.2 Role of the envelope stress responses in plague pathogenesis

Diderms evolved several sensors in their envelope, allowing to sense abnormality in the assembly or integrity of this complex structure. These sensors and the mechanisms they trigger are called the envelope stress response (ESR, Fig 2.3A). These sensors often consist of two-component systems (TCS) or phosphorelays [128]. They have been associated to virulence in many infection models [129, 130].

The CpxA/CpxR TCS. The CpxA/CpxR TCS senses a range of envelope stresses such as defect in protein secretion across the IM, misfolded periplasmic proteins, or the NlpE OM lipoprotein mislocalization in the IM [131]. The TCS is activated by degradation of the periplasmic negative regulator CpxP, leading to autophosphorylation of CpxA and phosphorylation of the transcriptional regulator CpxR. A previous report initially involved CpxA in the T3SS function [132], however the Cpx response is not necessary for *Y. pestis* full virulence [133]. In contrast, it was later shown that CpxA inactivation led to accumulation of phosphorylated CpxR which downregulates the T3SS [134] and the global regulator RovA, regulating the Psa fimbriae among other virulence factors [90, 135–137]. Cpx is thus involved in complex regulatory loops and presumably plays a role in environmental survival to prevent costly production of envelope-associated virulence factors.

The σ^E response. The σ^E response involves several IM proteins such as the anti- σ^E factor RseA or the DegP protease, in coordination with periplasmic proteins, which can sense the specific C-terminus of misfolded OMPs in the periplasm. The σ^E response can be alternatively triggered by periplasmic LPS present in unusual quantity or shape. Activation of the σ^E response consists on a proteolytic cascade leading to the release of RpoE in the cytoplasm. The σ^E response is composed of two arms: i) a protein arm, where the RpoE regulator activates the expression of chaperones and proteases to remove misfolded OMP from the periplasm, and LPS biosynthesis and ii) an RNA arm, led by the RpoE-induced sRNAs which downregulate translation of OMPs and Lpp to allow the protein arm to restore envelope homeostasis [131, 138]. Although the σ^E response has been poorly studied in *Y. pestis*, it has been shown that RpoE over-expression leads to increase production of outer membrane vesicles (OMV) [139]. In *Y. pseudotuberculosis*, σ^E is required for growth in stress conditions [140] and regulates part of the T3SS [132, 141].

The Psp response. The Psp (phage shock proteins) response senses inner membrane defects. Although the exact signals are not clearly defined, Psp response is known to be activated by a change in proton motive force (PMF) or mislocalization of inner membrane proteins [131, 142]. Interestingly, the Psp has been well characterized in *Y. enterocolitica* and is known to be induced by T3SS expression and more precisely by the secretin. Mislocalization of the OM secretin to the IM could indeed change the PMF. Psp is required for *Y. enterocolitica* survival during expression of T3SS virulence factors [143].

The Rcs phosphorelay. The Rcs (Regulator of capsule synthesis) phosphorelay senses membrane integrity defect [144]. As mentioned previously, Rcs mutations lead to a change in regulation in *Y. pestis*. Some observations made in *Y. enterocolitica* such as T3SS regulation by Rcs remain to be characterized in *Y. pestis* [141]. However, the contribution of Rcs in biofilm formation in the flea is well documented [20, 74, 76].

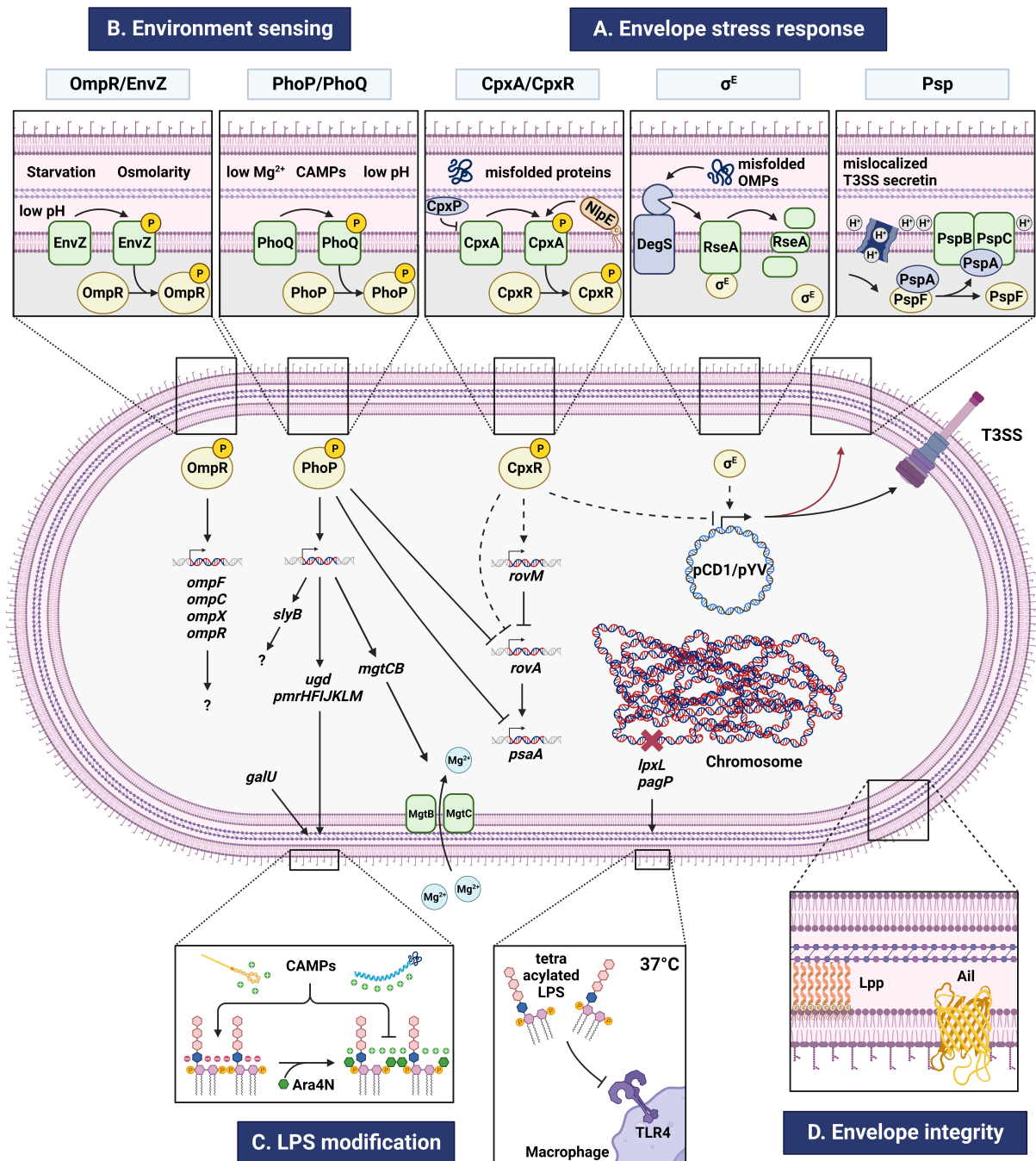


Figure 2.3. *Y. pestis* virulence-associated envelope mechanisms. (A) The CpxA/CpxR TCS negatively regulates virulence factors such as the RovA regulator or the T3SS, which is induced by the σ^E response and only viable in presence of an effective Psp response. (B) PhoP/PhoQ and OmpR/EnvZ TCS are essential for plague pathogenesis through LPS modification, intracellular survival and other unknown mechanisms. (C) LPS modification helps resist antimicrobial peptides and escape TLR4-mediated recognition by the host immune system. (D) Membrane integrity is maintained by abundant proteins such as the Braun lipoprotein Lpp and the outer membrane protein Ail. Full and blunted arrows respectively represent activation and repression. Dashed and red arrows are mechanism proven only in *Y. pseudotuberculosis* and *Y. enterocolitica* respectively. Adapted from [131, 138, 143].

2.3.3 Role of environmental sensing in plague pathogenesis

Other envelope sensors can sense environmental changes, such as Fe³⁺ and Al³⁺ levels for the PmrA/PmrB TCS [145] or low Mg²⁺ for the PhoP/PhoQ TCS [146], and regulate

transcription patterns in response to these stimuli. Several *Y. pestis* TCS confer resistance to neutrophil killing [147], and among them, PhoP/PhoQ and OmpR/EnvZ are required for bubonic, pneumonic and septicemic plague [133] (Fig 2.3B).

The PhoP/PhoQ TCS. The role of PhoP/PhoQ in *Y. pestis* pathogenicity is diverse and spans from innate immunity resistance to biofilm formation in the flea [146]. This TCS can sense low pH, low Mg²⁺ and CAMP, potentially encountered during intracellular life. PhoP/PhoQ is necessary to resist intracellular and extracellular macrophage and neutrophil killing [147, 148]. Intracellular low Mg²⁺ sensing induces the magnesium importers MgtB and MgtC, required for bacterial metabolism. PhoP could also negatively regulate RovA and the fimbriae PsaA [149], but this regulation was not observed by others [150]. The role of PhoP/PhoQ on LPS modification and its impact on pathogenicity is detailed in the next section.

Interestingly, PhoP/PhoQ is widely shared among pathogenic bacteria and the two most conserved members of its regulon are *phoP* itself and the OM lipoprotein gene *slyB* [150], which has been experimentally confirmed in *E. coli* [151], *Salmonella enterica* [152], *Shigella flexneri* [153], *Pseudomonas aeruginosa* [154] and *Y. pestis* [150]. It is thought that SlyB broad conservation is due to its activity as negative regulator of PhoP/PhoQ, which was demonstrated in *S. enterica* [150], but another study pointed out that it was not the case in *E. coli* and that the conserved negative regulation of PhoQ would rather come from the PhoP/PhoQ-regulated small peptide MgrB, which was shown in *E. coli*, *S. enterica* and *Y. pestis* [155]. Several studies pointed out the role of SlyB in membrane integrity maintenance [154, 156], but its mechanism and putative role in virulence remain to be elucidated.

The OmpR/EnvZ TCS. OmpR/EnvZ can detect osmolarity changes, low pH or nutrient deprivation in the environment [157]. In addition to be the only other TCS with PhoP/PhoQ known to be necessary to *Y. pestis* virulence, it promotes plague transmission by flea by sensing nutrient in the flea gut allowing metabolic adaptation of bacteria [77]. OmpR has been shown to upregulate OmpF, OmpC, OmpX and OmpR itself in *Y. pestis*, which differs from the regulation in *E. coli* [158]. The exact mechanism of OmpR/EnvZ requirement for full virulence remains to be deciphered.

2.3.4 Immune escape by LPS modifications

LPS is the major conserved Gram-negative bacterial component exposed to the surface. The host evolved mechanisms to detect LPS and trigger a protective immune response to bacterial infection. In a perpetual arm race, pathogens developed mechanisms to evade this immune response [159, 160] (Fig 2.3C).

Change in lipid A net charge. As described above, PhoP/PhoQ TCS is important for plague pathogenesis and more particularly to resist neutrophil and macrophages killing [147, 148]. O'Loughlin *et al.* showed that resistance to neutrophil granules can be partly explained by PhoP/PhoQ regulation of Ugd and PmrK, which mediate addition of 4-amino-4-deoxy-L-arabinose (Ara4N) to lipid A. This modification reduces the phosphate-dependent negative charge of LPS, conferring protection against CAMPs [161]. Ugd and PmrK have previously been identified as required for optimal survival of *Y. pestis* into macrophages [162]. A transposon screen also identified the *galU* gene as responsible for LPS core modification and Ara4N decoration, and its mutation reduced *Y. pestis* survival in macrophages and resistance to CAMP [163]. However, Ara4N addition and CAMP resistance tend to be greater at lower temperature rather than at 37°C, sign of adaptation for better fitness into the flea and

improved disease transmission [115, 164, 165]. Hexa-acylation of LPS at lower temperature was also thought to be necessary for flea transmission but this hypothesis was experimentally ruled out [166]. PhoP/PhoQ TCS also mediates LPS core modification, but its role in virulence is unknown [167].

LPS tetra-acylation. *Y. pestis* harbors a deletion in the *lpxL* gene, which transfers a secondary laurate chain to lipid A, along with a mutation in the outer membrane acyltransferase gene *pagP*, mediating the addition of palmitate to lipid A, allowing bacteria to maintain a tetra-acylated lipid A at 37°C. These mutations are thought to mediate immune evasion by reducing LPS recognition by Toll-like receptor 4 (TLR4), enhancing *Y. pestis* virulence [168–170]. However, reduced acylation could potentially lead to increased permeability of the outer membrane [171]. Additionally, PagP is thought to reduce PL load in the outer membrane when OM stress leads to loss of LPS, higher PL content in the outer leaflet and OM symmetrization. It has been recently shown that Ail interacts with LPS to counteract the side effects of these mutations, and helps to maintain its integrity at 37°C [108, 109].

Absence of O-antigen. Several mutations lead to loss of the O-antigen in *Y. pestis* [172]. This absence probably allows a better interaction with virulence factors such as Pla and their optimal activity towards big macromolecules which would be sterically hindered by the O-antigen [173, 174]. LOS core structure is also responsible for an optimal binding and activity of Ail [175].

2.3.5 Structural integrity maintenance under stressed conditions

Envelope integrity is required for bacterial survival, but some structural factors are more specifically associated to virulence (Fig 2.3D).

Ail. As described above, Ail was first described as a complement resistance factor and is thought to recruit Factor H, C4BP and vitronectin among other molecules. It is additionally an adhesin promoting T3SS function and Yop injection. However, recent studies pointed out the structural role of Ail to maintain LPS integrity, and particularly the tetra-acylated form produced at 37°C [106, 108, 109]. A Δail mutant had a decreased capacity to induce σ^E and the heat shock sigma factor SigH when grown at 37°C, leading to morphological changes and increased lysis when entering stationary phase. It has been hypothesized that Ail provides a local thickening and rigidity of the membrane, and that its deletion increases PL flow from the inner leaflet to the outer leaflet of the OM. The phospholipase A PldA, which removes over-abundant PL from the outer leaflet, could increase PL transport from the IM, leading to IM contraction and increased turgor pressure, ultimately leading to bacterial lysis [109].

Lpp. As one of the most abundant protein in *E. coli*, the role of Lpp in bacterial physiology has been extensively studied. It is known to be responsible for the right periplasmic sizing and signal transduction from the OM to the cytoplasm. Interestingly, the RNA regulatory arm of σ^E includes the *micL* sRNA which specifically targets the Lpp mRNA and reduces its translation during envelope stress, possibly to alleviate Lol or Bam pathways [120, 138]. Although an Δlpp mutant can grow normally in laboratory media, Lpp is required for *Y. pestis* pathogenesis thanks to its envelope integrity maintenance properties, which have been suggested to synergize with properties of the LPS modifying acyltransferase MsbB (LpxM) [176–178].

Chapter 3

Global approaches to study plague pathogenesis

In the last 30 years, advances in physics, nano-technologies and computer science allowed exponential growth of computational power and development of ever more precise and powerful technologies that could be applied to biological research. In this section we will briefly summarize recent technological advances and omics approaches which allowed a better understanding of *Yersinia* infections with a focus on the plague pathogen *Y. pestis* [179, 180].

3.1 Genomics

3.1.1 First *Yersinia* genome sequences

In 2001, the first whole genome of a *Yersinia* species, the genome of the *Y. pestis* CO92 strain, was sequenced using the Sanger technology [181]. Shortly afterwards, sequences from other *Y. pestis* strains [182, 183] and from its ancestor *Y. pseudotuberculosis* allowed comparative genomics analysis, shedding light on the evolutionary events that led a mildly virulent enteric bacteria to become a highly virulent vector-borne pathogen [184].

3.1.2 Second generation sequencing

The next-generation sequencing (NGS), also called second generation sequencing or massively parallel sequencing [185], widely represented by the Illumina technology, currently allows routine sequencing of clinical strains or genetically-modified laboratory strains. Growing genome sequencing projects coupled to new analytical tools led to refinement of the *Yersinia* species structure and description of new species [2, 11] and to a better understanding of *Y. pestis* worldwide spread in the last centuries [186].

3.1.3 Sequencing of ancient DNA

Recently, technological developments coupled with next-generation sequencing allowed to analyze ancient bacterial DNA retrieved from dental pulp of plague-deceased remains [10]. Ancient DNA analysis from the Neolithic, first and second pandemics refined our knowledge on *Y. pestis* evolution and spread for the last 5,000 years [187–190]. Additionally, this approach applied to human genetics recently revealed the selective pressure that Black

Death had on the human genome, leading to several immune disorders today [191]. Despite these new data, debates remain around the persistence or reintroduction of plague in Europe during the second pandemic [10, 192].

3.1.4 Third generation sequencing

The sequencing of single DNA molecules allows to perform the so-called long-read sequencing, also known as third generation sequencing [185]. Mainly represented by the PacBio technology at first, and now joined by the Oxford Nanopore technology, third generation sequencing allows to easily reconstruct high-quality complete genome when combined with second generation sequencing. As of the first trimester of 2023, 200 genome assemblies of *Yersinia* species were published at the complete or chromosomal level [193].

If third-generation sequencing is mostly used for complete genome sequencing, Nanopore sequencing recently allowed to characterize the multimerization of the pPCP1 plasmid in *Y. pestis* and was proposed as a bacterial identification and analysis tool [194]. Additionally, recent research in our laboratory unraveled the potential of long-read sequencing to tackle genetic questions such as genome rearrangement and plasmid identification in *Yersinia* species (see appendix A.2 and A.5)

3.2 Transcriptomics

With the first complete genome sequences from the beginning of the century, unbiased approaches to measure gene expression emerged, using first DNA-hybridization macro- and micro-arrays, then progressively replaced by NGS-based sequencing of cDNA or RNA, called RNA-sequencing or RNA-seq (Fig 3.1A). Various expression conditions representing environmental diversity, stresses, *in vivo* infection or mutations were analyzed over the years [193].

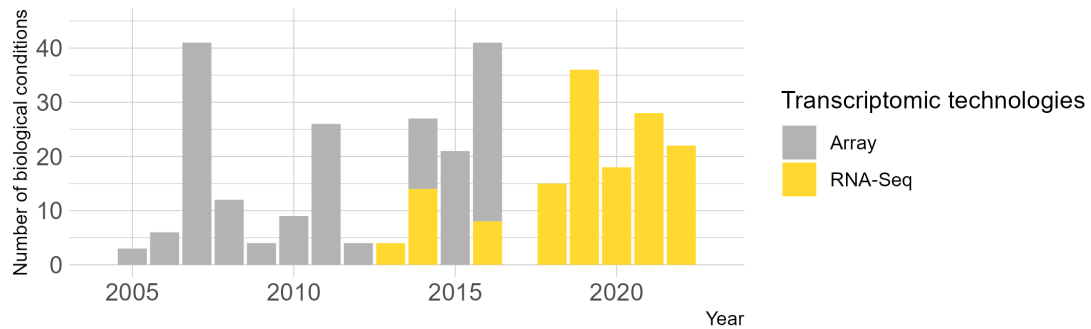
3.2.1 Macro- and microarray-based transcriptomics

The first applications of arrays to the study of plague were performed by several groups worldwide in parallel. The very first transcriptomes of *Y. pestis* were published by Motin *et al.* and Han *et al.* in 2004 [195, 196]. In the following years, the latter group massively used microarray to characterize expression profiles of a human-avirulent strain from the biovar *Microtus* in various stress conditions and the impact of several gene mutations [197]. The first transcriptome of *Y. pestis in vivo* was published by Lathem *et al.* in 2005 using a mouse model of pneumonic plague that unraveled important genes for lung colonization by *Y. pestis* [55]. Shortly after, Sebbane *et al.* published the bacterial transcriptome in a rat *bubo* [54]. Transcriptomic studies of bacteria grown in human plasma were then performed in France by Chauvaux *et al.* to study septicemic plague [198] and compare *Y. pestis* with *Y. pseudotuberculosis* [199]. To investigate *Y. pestis* natural cycle, the bacterial transcriptome in the flea was characterized [38]. Global regulators such as the PhoP/PhoQ TCS were studied *in vitro* and in the flea [150, 200, 201]. From 2004 to 2015, some microarrays experiment were performed on *Y. pseudotuberculosis* and *Y. enterocolitica* but the majority of studies focused on *Y. pestis* (Fig 3.1B).

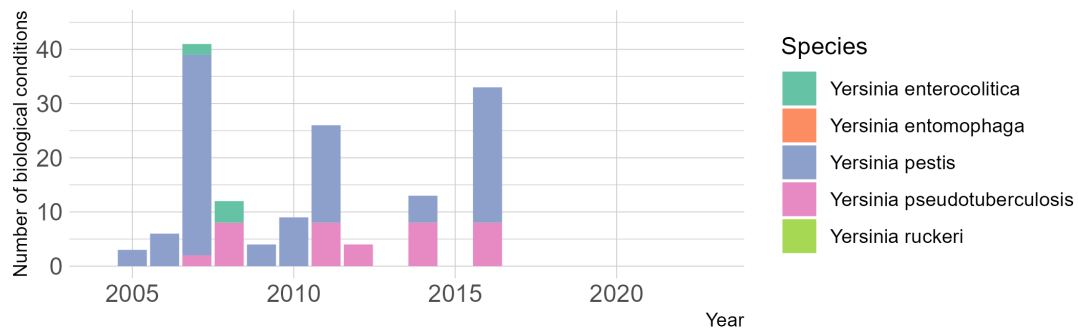
3.2.2 RNA-sequencing-based transcriptomics

From 2012, microarrays were progressively replaced by RNA-seq (Fig 3.1A). More experiments were performed on *Y. pseudotuberculosis* and *Y. enterocolitica* and expression

A. Transcriptomic experiments per technology



B. Array experiments per species



C. RNA-Seq experiments per species

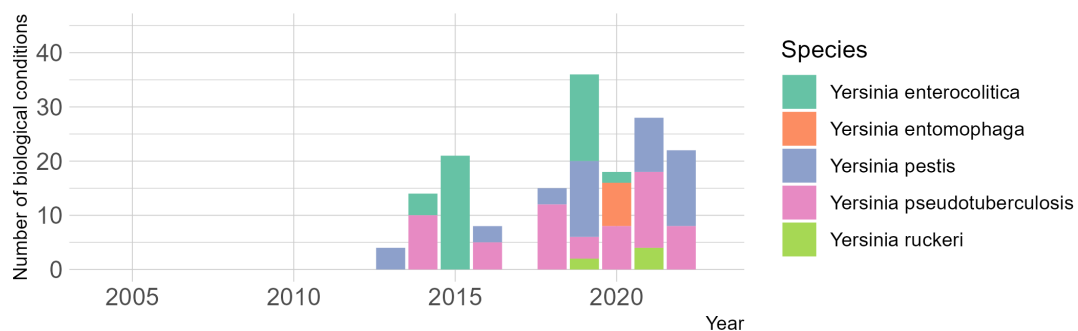


Figure 3.1. Number of *Yersinia* biological conditions analyzed by genome-wide transcriptomics from 2005 to 2022 collected on the Yersiniomics database [193]. (A) Number of biological conditions per technologies (arrays or RNA-seq) from 2005 to 2022. (B) Number of biological conditions per species analyzed by macro- or microarrays from 2005 to 2022. (C) Number of biological conditions per species analyzed by RNA-seq from 2005 to 2022.

data of the fish pathogen *Y. ruckeri* [202, 203] and the insect pathogen *Y. entomophaga* [204] were introduced (Fig 3.1C). A broad RNA-seq comparison of stresses applied to *Y. pseudotuberculosis* easily accessible online was recently published [193, 205].

Methodological advances led to the development of dual RNA-seq allowing analysis of both bacterial and host expression profiles during infection. First applied to *Y. pseudotuberculosis* [206, 207], recent dual RNA-seq studies were performed in lungs of mice infected with *Y. pestis* in a model of pneumonic plague [208] and in trunk kidney of channel catfish infected with *Y. ruckeri* [203].

Contrary to hybridization arrays, RNA-seq is not biased by gene annotation and only relies on genomic sequence. This allowed more efficient discovery of non-coding regulatory RNAs such as small RNAs [209–215] and riboswitches [206, 215] and to map transcriptional start sites (TSS) [206, 213, 215] in *Yersinia* species. RNA immunoprecipitation and cross-linking immunoprecipitation further allowed to decipher Hfq-mediated regulation in *Y. pestis* [216]. RNA-sequencing coverage of stranded experiments also allowed to discover anti-sense RNAs, one of which has been shown of importance in our laboratory (see appendix A.4).

3.3 Proteomics

To date, most of the *Yersinia* proteomics studies have been performed on *Y. pestis*. One of the first organism-wide experiment dates back to 2006 and consisted in identifying protein localization in soluble or insoluble fraction of bacteria as well as their differential abundance at several temperatures in culture medium with or without calcium [217]. This study used semiquantitative mass spectrometry (MS) based on Fourier-transform ion cyclotron resonance (FTICR-MS). Using spot intensities of proteins separated by 2D gel electrophoresis and identified by MS, a simultaneous study analyzed the temperature and calcium regulation of some proteins [218], and later studies focused on protein expression response to iron starvation, as well as the OM and periplasmic proteomes [219–221]. Advances in liquid chromatography - tandem mass spectrometry (LC-MS/MS) technologies, including the invention of the Orbitrap [222], allowed deeper proteome acquisition. Notably, the Pacific Northwest National Laboratory (PNNL) aggregated and processed many proteomes to create a tool that differentiates naturally occurring and laboratory strains of *Y. pestis* [223], encompassing data from different studies [224–226] as well as PNNL archives [227]. These data were generated using various shotgun LC-MS/MS technologies such as linear ion trap technologies and/or Orbitrap mass spectrometry for identification. Proteomes of natural isolates from Georgia were also characterized by LC-MS/MS, revealing differences in expression of several important factors such as the Caf pseudocapsule [228].

More recently, a proteomic study investigating *Y. pestis* Microtus strain 201 using Orbitrap LC-MS/MS technology (Thermo Fisher QExactive) was the first to characterize *Y. pestis* secretome. It led to identification of two novel secreted virulence factors [229], which function as E3 ligases during infection [230]. The same group used a multi-omic approach combining RNA-sequencing and LC-MS/MS to identify small open reading frame (sORF)-encoded peptides (SEP), refining *Y. pestis* genome annotation [231]. Proteogenomics and multi-omics approaches had already previously been used to correct *Y. pestis* annotation [224, 232]. Proteome profiling has also been recently used to compare *Y. pestis* strains of various antimicrobial susceptibilities [233].

3.4 Metabolomics

Most global metabolic studies of *Y. pestis* were addressed *in silico*, based on genomics validated by phenotyping [234, 235], or combined with transcriptomic or proteomic data [221, 236, 237]. Only one study used experimental metabolomics integrated in a multi-omic approach, revealing a specific glutamate metabolism possibly regulated at the post-translational level for a virulent *Y. pestis* strain at mammalian host temperature compared to lower temperature and avirulent strains [225].

3.5 Interactomics

The determination of protein-protein interaction (PPI) between bacterial proteins and other bacterial or host proteins allowed identification of mechanism for bacterial metabolism or virulence. First studies were performed by pull-down assays on individual proteins, followed by yeast two-hybrid (Y2H) screening allowing scale-up to hundreds of PPI identifications [238]. Despite the labor-intensive and time-consuming work required for Y2H assays, application of a high-throughput methodology allowed to screen hundreds of thousands of PPI for *Bacillus anthracis*, *Francisella tularensis* and *Y. pestis* proteins [239]. This study identified 4,059 protein-protein interactions between 1,218 *Y. pestis* proteins and 2,108 human proteins, leading to new mechanistic insights and characterization of proteins of unknown function.

3.6 Transposon-based screening

In addition to genome, gene transcription level and protein abundance comparisons, transposon-based mutational screen approaches have been used to study *Yersinia* pathogenesis. These approaches rely on a library of mutants generated by random transposition in the genome. This library can then be used to screen various phenotypes. The first signature-tagged mutagenesis (STM), developed in 1995, consisted in unique tags inserted into the transposon, depletion of specific mutants being revealed by hybridization arrays [240]. It was successfully applied to enteric *Yersinia* species in *in vivo* models of infection [241–243] and to *Y. pestis* in murine models of bubonic [244] and pneumonic [245] plague to reveal new virulence factors. To circumvent the small number of tagged transposons in STM, another technique called transposon site hybridization (TraSH) was developed, based on genomic DNA hybridization on microarray [246] and was applied to discover new *Y. pestis* genes involved in bacterial survival in macrophages [163]. Application of NGS to transposon screening opened new possibilities and led to the development of techniques such as transposon sequencing (Tn-seq) or transposon-directed insertion sequencing (TraDIS) [247]. These approaches were recently used to identify essential genes in *Y. pestis* [248–250] and *Y. pseudotuberculosis* during growth in laboratory media [251] or during antibiotic stress [252] and *Y. pestis* genes required for spleen colonization [248] and lung adherence [101]. New screening technologies based on clustered regularly interspaced short palindromic repeats interference (CRISPRi) coupled with NGS are now emerging with numerous advantages [253]. One of these techniques, called CRISPRi-seq, was recently successfully applied to streptococcal pulmonary infection [254, 255] and could be a useful tool to investigate *Y. pestis* pathogenesis.

3.7 Omics studies of host response

Omics technologies have also been used to study host response during *Y. pestis* infection. In 2001, an *ex vivo* setup analyzed the transcriptomic response of human whole blood neutrophils after incubation with avirulent and virulent *Y. pestis* strains [256]. It was later followed by a study of the proinflammatory response induced by *Y. pestis* in human monocytes [257]. The host proteomic response of infected cells was reported as soon as 2004 using 2D gel electrophoresis, comparing putative biomarkers of infection with the three pathogenic *Yersinia* species [258, 259]. A more recent RNA-seq experiment reported host immune modulation of a human macrophage cell line infected by *Y. pestis*, identifying the RIG-I-like receptor pathway as a response pathway to *Y. pestis* infection [260].

Host responses in *in vivo* infection models were also reported. A transcriptomic study of the bubo environment was performed using microarrays in 2010, showing the absence of immune response during bacterial proliferation [49]. Very recently, single-cell RNA-sequencing of infected bubos allowed to better understand the cell composition and dynamics during bubonic plague in mice [42]. The spleen transcriptional response had also been analyzed, after intraperitoneal injection of *Y. pestis* in mice [261]. The host response modulation during the course of pneumonic plague is also of interest due to its particular biphasic nature and transcriptome kinetics were recently studied in murine and non-human primate (NHP) models of infection [58, 208, 262, 263]. Multi-organ transcriptomic analysis revealed differences in lungs response compared to spleen and liver response in mice infected with virulent or avirulent strains [263, 264]. Expression analysis of infected NHP blood showed a very dynamic transcriptional rewiring of immune pathways during the first 24 hours of infection [58]. To complete the NHP transcriptome kinetic analysis, a plasma metabolomic study was also performed in this model, revealing an early inflammation and oxidative stress involving lipid pathways, an increased energy demand as well as a potential hepatic dysfunction [265].

Chapter 4

Innovation in plague diagnosis

4.1 Plague epidemiology and clinical presentation

Plague is a reemerging zoonotic disease which causes regular outbreaks in low-income countries such as Madagascar. It is endemic in many other countries all over the world, such as Democratic Republic of Congo (DRC), Peru, United States of America (USA) or central Asia (Fig 4.1) [17, 266].

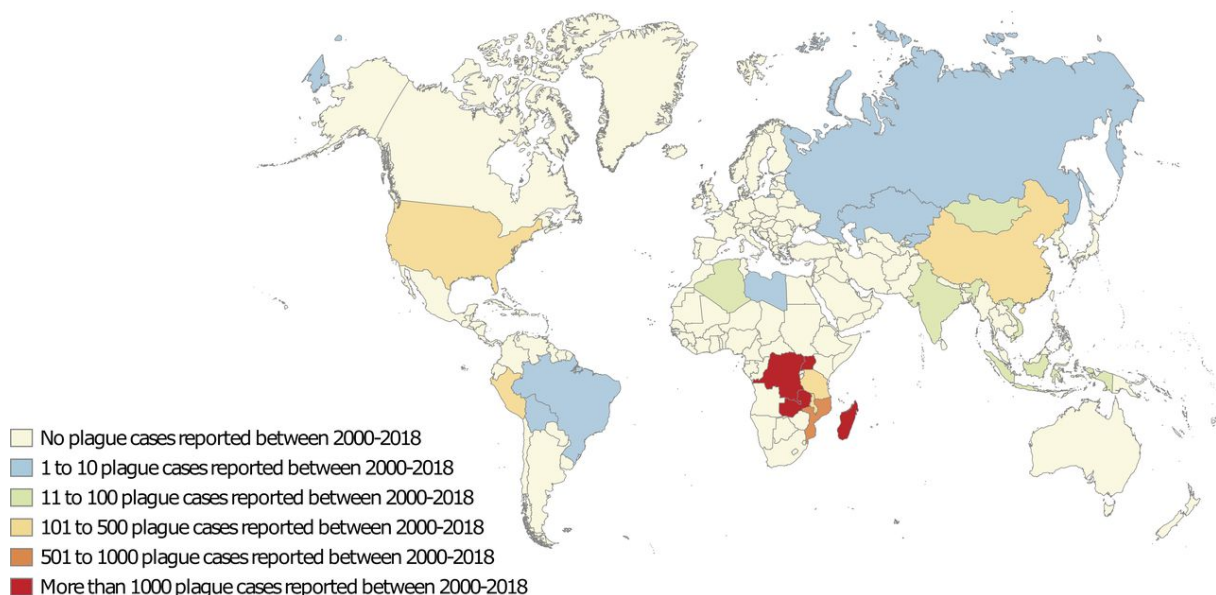


Figure 4.1. Worldwide distribution of plague cases reported by the World Health Organization (WHO) from 2000 to 2018. Illustration reprinted from [17].

The most frequent clinical form of the disease results from the bite of a *Y. pestis*-infected flea in the dermis, causing bubonic plague, leading to unspecific symptoms such as fever, headache and chills, and more characteristic painful swollen lymph nodes, called buboes. The incubation time range from 2 to 6 days and hematogenous dissemination leads to a fatality rate of 40 to 60%, mainly caused by septic shock if left untreated [4].

After dissemination in the organism and onset of secondary septicemic plague, bacteria can reach the lungs and cause a secondary pneumonic plague. Primary pneumonic plague can then be transmitted between individuals by the cough or inhalation of contaminated droplets. Primary pneumonic plague presents a short incubation time of 1 to 3 days and leads to 100% mortality if left untreated. Although rare (around 2% of the cases in the USA for instance), pneumonic plague is an extremely serious condition due to its unspecific flu-like symptoms and pneumonia followed by bloody sputum, quick progression of the disease

and high mortality [4, 9, 56].

Primary septicemic plague is defined as a positive blood culture without detectable bubo [4], and is thought to arise when the flea directly injects bacteria in the bloodstream, which occurs in 10% to 30% of cases [54, 267, 268] or any direct contact between blood and bacteria. Unspecific sepsis symptoms often lead physicians to apply general sepsis treatments targeting Gram-negative bacteria, however their lack of efficacy on *Y. pestis* leads to 30% to 50% mortality [4].

Although antibiotic treatment is efficient against plague if carried properly [269], it should be administered very early, especially for pneumonic or septicemic plague as death can occur only a few days after the onset of non-specific symptoms. These characteristics make early pneumonic plague diagnosis a major stake for clinicians in low-income countries but also for the military, *Y. pestis* being a potential bioweapon. *Y. pestis* is classified as a category A pathogen and Tier 1 Select Agent by the American Centers for Disease Control and Prevention. It is also one of the high-priority agents in the French government strategic axis on Emerging Infectious Disease - Chemical, Biological, Radiological and Nuclear Risk Mitigation.

4.2 *Yersinia pestis* infection diagnostics

4.2.1 Current diagnostic workflow

In addition to the clinical manifestations of the disease and the context of infection (e.g., recent travel in endemic areas, contact with wild or sick animals), clinicians can rely on different tools to diagnose plague [270, 271].

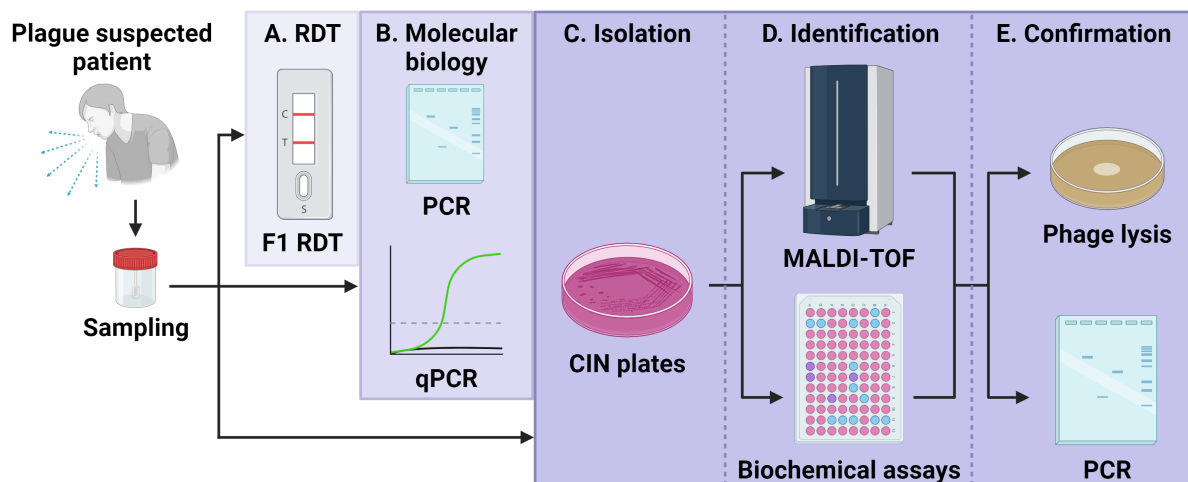


Figure 4.2. Current global workflow for plague diagnostics. (A) Suspected case of plague are rapidly screened at the point of care by RDT. (B) PCR and qPCR are performed in laboratories to confirm the cases. (C) Bacteriological isolation is performed on CIN plates in central laboratories, following by (D) identification by MALDI-TOF or biochemical assays and (E) confirmation by phage lysis or PCR. PCR: polymerase chain reaction. qPCR: quantitative PCR. RDT: rapid diagnostic test. CIN: cefsulodin–irgasan–novobiocin. MALDI-TOF: matrix assisted laser desorption ionization - time of flight. Illustration adapted from [9].

Immunoassays - Rapid Diagnostic Test. Plague rapid diagnostic tests (RDT) have been developed and used since the beginning of the 2000s. They are based on lateral flow assay and use antibodies to detect *Y. pestis* pseudocapsule protein F1 in clinical samples. They can be used at the point of care and give a result as quick as 15 minutes after sampling

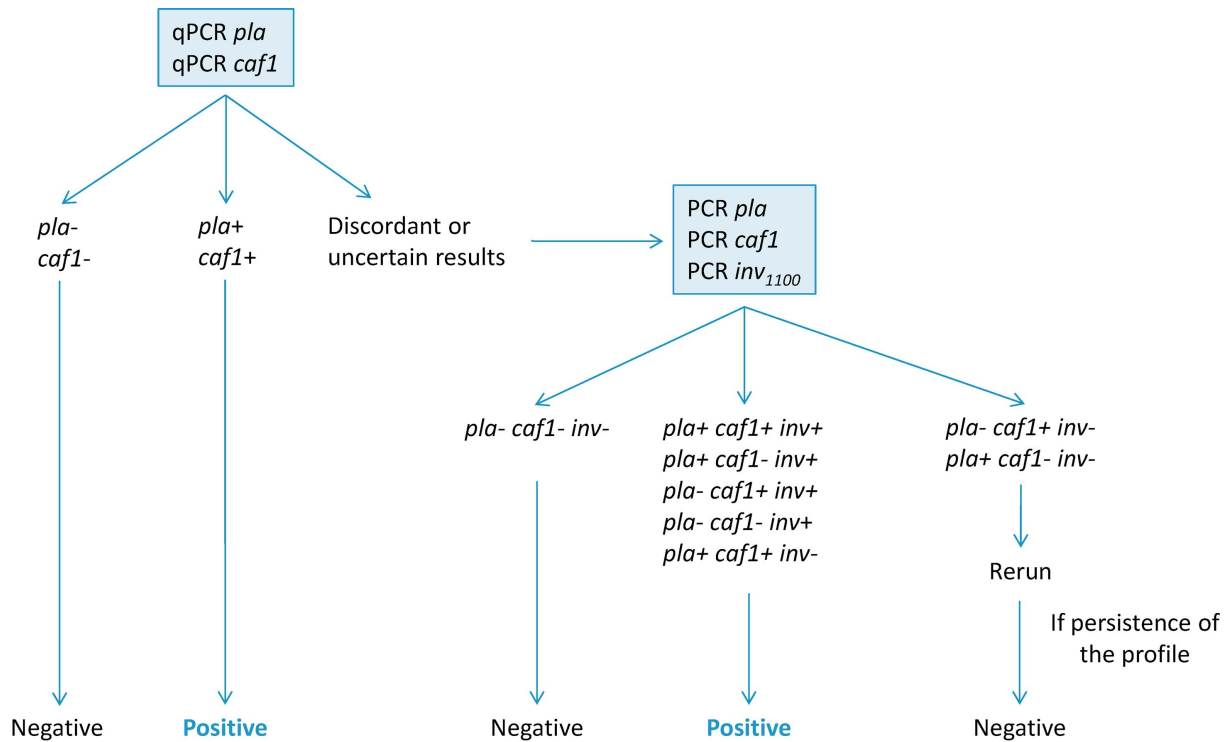


Figure 4.3. PCR workflow for plague diagnostic. A multiplexed qPCR is performed on the highly abundant but unspecific *pla* gene and on the less abundant but specific *caf1* gene. Discordant or uncertain results from the multiplexed qPCR is confirmed by standard PCR on the *pla*, *caf1* and *inv* genes, the size of the latest being specific to *Y. pestis*. More than 2 positive PCRs out of the three targets is considered as a positive result. Illustration reprinted from [274].

from bubo aspirate, sputum or blood (Fig 4.2A). They are used to quickly screen suspected plague cases [9, 272].

Molecular biology assays. From clinical samples, quantitative PCR (qPCR) and conventional PCR can be performed in a few hours to detect bacterial DNA (Fig 4.2B). The qPCR detects the *pla* gene, located on the pPCP1 (or pPla) plasmid present in around a hundred copies in *Y. pestis*, allowing a high sensitivity. However, the *pla* gene was recently identified in other bacteria [273]. Multiplexing with the specific *caf1* gene encoding *Y. pestis* pseudocapsule is thus necessary. If the qPCR shows uncertain or discordant results, a conventional PCR can be done on *pla*, *caf1* and the *inv* gene, whose amplification leads to a 400-base pairs product in *Y. pseudotuberculosis*, or a 1100-base pairs product in *Y. pestis*, which bears an insertion of an IS1541 element in the invasin gene (Fig 4.3) [9, 274].

Bacteriological culture. For a long time, bacteriological isolation remained the gold standard for plague diagnostics. Culture on cefsulodin–irgasan–novobiocin (CIN) plates allows to specifically isolate *Y. pestis* after 2 to 3 days of incubation (Fig 4.2C). Isolates can then be identified with biochemical assays and/or matrix assisted laser desorption ionization - time of flight (MALDI-TOF) mass spectrometry (Fig 4.2D). Confirmation of the identification is performed by phage lysis or PCR specific to *Y. pestis* (Fig 4.2E) [9].

4.2.2 Limitations of current approaches

RDT and bacteriological culture. Previous studies assessed RDT sensitivity and specificity relative to bacteriological culture [275]. However, these studies were biased by the very low sensitivity of the latter technique in sputum of patient suspected of pneumonic plague,

and by methodological flaws as culture was performed only when the RDT was positive in some studies. The 100% sensitivity [275] previously reported for RDT should thus be interpreted with caution. A recent modeling study indeed highlighted the limitations of currently used RDT during the 2017 plague outbreak in Madagascar, especially to diagnose pneumonic plague, for which sensitivity was estimated at 28% for RDT and 7% for the “gold standard” bacteriological culture [276]. The RDT specificity was evaluated at 82% to diagnose pneumonic plague, a suboptimal result for a low-incidence disease. In addition to its poor sensitivity, the 2 to 3 day-long bacteriological culture is inappropriate for the quick medical care required for a potentially fulminant disease. In addition, the RDT relies on presence of the F1 capsule and therefore cannot detect virulent strains of *Y. pestis* lacking the capsule-encoding *caf* operon described experimentally [277, 278] and observed in nature [279].

Finally, a recent analysis of the 2022 plague outbreak in DRC underlined the absence of an efficient and accessible pneumonic plague diagnostic tool [280].

Molecular biology assays. Molecular-based diagnostic methods such as qPCR perform better than RDT and culture (80% sensitivity and 100% specificity) but require more expensive equipment, trained personnel and are more difficult to perform at the point of care. Moreover, similar to all other techniques, they are limited by the amount of bacterial material (protein or DNA) found in the biological sample and thus can hardly be used shortly after infection during the pre-symptomatic stage.

Early diagnosis. In addition to the absence of a high-performance rapid test to diagnose symptomatic patients, there is a total lack of pre-symptomatic diagnosis method. In murine models, pneumonic plague is lethal in less than 72 hours after *Y. pestis* intranasal instillation. It is characterized by a long 36 hours pre-inflammatory phase followed by a pro-inflammatory phase [55]. In a non-human primate model, aerosolization of 200 bacteria can lead to death in 96 hours without apparent clinical sign [56]. The extremely quick course of the disease, the prolonged asymptomatic phase, and the risk of inter-human transmission during pneumonic plague require the setup of early diagnostic tools to identify the disease before bacterial systemic dissemination.

4.3 New diagnosis approaches

4.3.1 Molecular biology-based approaches

Various multiplexed PCR targeting the *Y. pestis* specific gene *YPO2088* were described [281, 282]. A loop-mediated isothermal amplification (LAMP) assay was also developed, abrogating the need for complex and expensive thermocycling machines [283], while others examined the convenience of portable conventional thermocycling machines [284] or new micro-cycling techniques [285]. Several approaches were proposed to detect bacteria from whole blood, such as a non-specific enrichment method to gain sensitivity when performing PCR [286] or an NGS-based pipeline [287]. Third generation sequencing is increasingly used to detect pathogens in environmental or biological samples, and application to *Y. pestis* detection or plague diagnostics has been considered [194, 288–290]. Recently, a MALDI-TOF misidentification of *Y. pseudotuberculosis* as *Y. pestis* in a blood culture was resolved by Nanopore sequencing [291]. CRISPR-based tools are also in development for sensitive detection of the plague agent, such as Cas12a-based platforms detecting specific sequences of *Y. pestis* [292, 293] or Cas13a-based detection tools set up for the detection of the *lcrV* gene [294].

4.3.2 LC-MS/MS identification

Mass spectrometry-based approaches were designed to detect peptides from the most abundant extracellular proteins of *Y. pestis* after immunocapture. It was applied to the Pla protease, the Ymt toxin or the receptor for the yersiniabactin siderophore Psn (also known as FyuA) on environmental samples [295] or with the tip of the T3SS protein LcrV and the Caf pseudocapsule on dried blood spots, which could be helpful for clinical sample preservation and transport from remote areas [296]. A non-specific enrichment method was also reported to identify *Y. pestis* proteins in whole blood with a high sensitivity by mass-spectrometry [286].

4.3.3 Plasma proteomics for circulating biomarkers

Plague diagnostic methods can be improved by using host biomarkers instead of bacterial protein or DNA to allow early diagnosis of the disease, when bacteria are present at low level in tissue compartments and before hematogenous spread and systemic dissemination. One strategy is to use host biomarkers as a diagnostic approach. For example, human plasma is increasingly being used to discover biomarkers of disease, despite the technical difficulties encountered when studying the highly complex plasma proteome. Mostly applied to the cancer research field, technological advances such as depletion of the most abundant proteins from plasma or extensive sample fractionation allowed to increase sensitivity [297], while high-throughput pipelines and fast microliter-based sampling and analysis were developed [298–300]. A recent study described usual cell contaminants to discriminate good from bad quality plasma samples, defining good practices for proteomic-based biomarker discoveries [301, 302]. While LC-MS/MS approaches have not been applied to plague diagnostic yet, the recent metabolomic study of plasma from plague-infected NHP measured hundreds of proteins during the course of infection using panels combined with the Luminex technology. Gautam *et al.* could identify 12 proteins at early time point and 11 proteins at late time point post-infection that were differentially regulated, including proteins involved in the coagulation cascade [265].

4.3.4 MicroRNA-based approaches

Another host biomarkers-oriented approach relies on the use of circulating microRNAs as an innovative tool for diagnostics [303]. MicroRNAs are key regulators of gene expression. They are often secreted, stabilized by protein complexes or in vesicles [304]. Their systemic dissemination and stability in biofluids [305, 306] allow their quantification in blood product (plasma or serum), urine or interstitial fluid. More than two thousand mature miRNAs have been identified in human [307], allowing identification of specific signatures of biological processes, including pre-symptomatic and symptomatic phases of infections such as malaria and tuberculosis [303, 308]. Development of miRNAs-based innovative diagnosis tools could be used for point-of-care diagnostics, using biofluid such as interstitial fluid [309–312], and new detection methods such as CRISPR/Cas13a-based [313] or fluorescent-based technologies [309].

Part II

Objectives of the thesis

Objectives of the thesis

My thesis has two distinct objectives, ranging from a better fundamental understanding of *Yersinia pestis* interaction with its host during infection to clinically applicable methods for a better plague diagnosis.

The first goal is to better characterize the crucial but understudied bacteremic phase of plague. By relying on advanced methods of high-throughput analysis and systems biology, we initially want to study protein expressions of host and bacteria in experimental setups representative of plague bacteremia. To do so, we need to implement methodological pipelines allowing the proteomic study of *Y. pestis* in complex samples such as human plasma or whole blood in the burdensome biosafety level 3 environment.

We then plan to implement a global online database of *Yersinia* omics data, which gathers published genomics, transcriptomics and proteomics experiments performed on *Yersinia* species and linked to other general annotation databases. This tool would allow to better analyze our own proteomics data and provide an accessible and user-friendly website to the whole *Yersinia* scientific community for studying bacterial systems biology.

Based on data retrieved from these pipelines and tools, we next intend to select several proteins of interest and delete their respective genes. We will study mutant strains in experimental setups representative of *Y. pestis* bacteremia to discover and characterize new factors involved in survival in blood and/or virulence.

The second goal is to develop new tools for the early diagnosis of plague, and more precisely the very fast-developing and deadly pneumonic plague. As current diagnostic tools relying on the detection of bacterial components in the host are not suitable for the early diagnosis of plague, we aim at discovering host biomarkers representative of early infection with *Y. pestis*.

To this end, we will set up a model of pneumonic plague and optimize blood sampling in mice. Using this model, we will then screen host circulating microRNAs in blood. A screen at early time points after pulmonary infection would allow to detect a new signature of pneumonic plague, which could be a first step in the development of a diagnostic tool.

Part III

Results

Chapter 5

Dual proteomic signature of blood infection by *Yersinia pestis*

5.1 Objectives and summary

To better understand the understudied *Yersinia pestis* bacteremia, we relied on recent technological improvement in mass-spectrometry and chose a global approach consisting in analyzing the bacterial proteomes after incubation in human plasma and whole blood. We first set up and bench-marked new sample preparation pipelines then chose and validated the most convenient one to use in a biosafety level 3 environment. *Y. pestis* incubation in human plasma revealed a major reshaping of bacterial protein landscape. We identified a metabolic shift towards important pathways such as methionine biosynthesis and iron acquisition, expanding previous transcriptomic results from our laboratory.

We then aimed at studying the bacterial and human proteomes of *Y. pestis* grown in whole blood to mimic more closely bacteremia and complete results obtained in plasma. However, dual proteomic study of microorganisms and their hosts in complex matrices remains challenging due to the very high protein dynamic range of samples. We thus constructed a dual proteomic pipeline of *Yersinia pestis* in human blood based on a bacterial pure culture used for library construction, an immune cell specific enrichment and a non-specific bacterial enrichment from blood. This provided the most complete *Y. pestis* proteome as of today. Remarkably, proteomic profiling in human blood highlights a greater *Yersinia* outer proteins intoxication of monocytes than neutrophils. Human proteome analysis confirmed the immunocapture-based specific cell enrichment. Our study unravels global expression changes and points to a specific pathogenic signature during infection, paving the way for future exploration of proteomes in the complex context of host-pathogen interactions.

5.2 Article

See next page.

Original article

1 **Dual proteomic signature of blood infection by *Yersinia pestis***

2 Running title: Dual proteomics of *Yersinia pestis* bacteremia

3 **Authors**

4 Pierre Lê-Bury¹, Thibaut Douché², Quentin Gai Gianetto^{2,3}, Mariette Matondo², Javier Pizarro-
5 Cerdá^{1,4}, Dussurget Olivier¹

6 **Affiliations**

7 ¹Institut Pasteur, Université Paris Cité, CNRS UMR6047, *Yersinia* Research Unit, Paris,
8 France

9 ²Institut Pasteur, Université Paris Cité, CNRS USR2000, Mass Spectrometry for Biology
10 Unit, Proteomic Platform, Paris, France

11 ³Institut Pasteur, Université Paris Cité, CNRS USR3756, Biostatistics and Bioinformatics
12 Hub, Paris, France

13 ⁴Institut Pasteur, Université Paris Cité, *Yersinia* National Reference Laboratory, WHO Col-
14 laborating Research and Reference Centre for Plague FRA-140, Paris, France

15 **Abstract**

16 Emerging and reemerging infectious diseases represent major public health concerns.
17 The urgent need for infection control measures requires deep understanding of molecular
18 pathogenesis. Global approaches to study biological systems such as mass-spectrometry
19 based proteomics benefited from groundbreaking physical and bioinformatical technologi-
20 cal developments over recent years. However, dual proteomic study of highly pathogenic
21 microorganisms and their hosts in complex matrices encountered during infection remains
22 challenging due to high protein dynamic range of samples and requirements imposed in
23 biosafety level 3 or 4 laboratories. Here, we constructed a dual proteomic pipeline of *Yersinia*
24 *pestis* in human plasma and blood, mirroring bacteremic phase of plague. We provide the
25 most complete *Y. pestis* proteome revealing a major reshaping of bacterial protein landscape
26 in human plasma. We identified a metabolic shift towards important pathways such as me-
27 thionine biosynthesis and iron acquisition. Remarkably, proteomic profiling in human blood
28 highlights a greater *Yersinia* outer proteins intoxication of monocytes than neutrophils. Our
29 study unravels global expression changes and points to a specific pathogenic signature dur-
30 ing infection, paving the way for future exploration of proteomes in the complex context of
31 host-pathogen interactions.

32 **Keywords**

33 Dual proteomics/human blood/monocytes/neutrophils/*Yersinia pestis*

34 **Subject Categories**

35 Microbiology, Virology and Host Pathogen Interaction, Proteomics

36 Introduction

37 Infectious diseases emerging and reemerging worldwide are major public health issues.
38 The understanding of microbial pathogenesis necessary for infection control immensely ben-
39 efits from technological progress. In particular, the current omics era shows spectacular
40 advances allowing affordable, fast and reliable genome sequencing and deep-coverage
41 of whole-genome transcriptomes. Simultaneously, whole-proteome exploration is quickly
42 gaining ground as the next step for functional studies in system biology. Classically, pro-
43 teomics pipeline includes 3 steps: sample preparation, followed by data acquisition in mass-
44 spectrometry and *in silico* data analysis. In the last decade, many breakthroughs focused on
45 sample preparation, leading to more efficient protein extraction protocols such as Filter Aided
46 Sample Preparation (FASP) (Wiśniewski, Zougman, et al. 2009), Single-Pot Solid-Phase-
47 Enhanced Sample Preparation (SP3) (Hughes et al. 2014), Suspension Trapping (STrap)
48 (Zougman et al. 2014) and detergent-free method known as Sample Preparation by Easy
49 Extraction and Digestion (SPEED) (Doellinger et al. 2020). Meanwhile, mass-spectrometry
50 and data management constantly improved, supported by development of the Orbitrap tech-
51 nology (Hu et al. 2005) and impressive growth of computational power, allowing deeper and
52 quicker acquisition of proteomic data. However, complex samples are still challenging to
53 tackle. Culture-independent bacterial identification by proteo-typing in complex matrices
54 such as blood or urine using tandem mass-spectrometry for clinical diagnosis is in its in-
55 fancy (Roux-Dalvai et al. 2019; Kondori et al. 2021), and very few dual-proteomics research
56 studies investigating complex host-pathogen interactions have been published (Geddes-
57 McAlister et al. 2021; Ball et al. 2020; Willems et al. 2021; Leseigneur et al. 2022; Masson
58 et al. 2021). Additionally, research on highly virulent microorganisms is restricted by regula-
59 tory requirements for safety purposes. Mandatory sample treatment steps generally include
60 pathogen inactivation and pathogen DNA and RNA elimination in biosafety level (BSL) -3 or
61 -4 laboratories.

62 *Yersinia pestis* is the highly virulent bacillus responsible for plague, a quickly fatal human
63 disease if left untreated. This reemerging disease whose epidemics had a considerable
64 death toll in human history generally manifests as bubonic plague following bites from fleas
65 infected with *Y. pestis*. Primary pulmonary plague is the second form of the disease, which
66 occurs by inhalation of infected respiratory droplets or aerosols usually emitted by an infected
67 patient. In some cases, injection of *Y. pestis* by fleas directly into the bloodstream leads to so-
68 called septicemic plague (Perry et al. 1997). In the three forms of the disease, bacteria reach
69 the blood resulting in systemic infection. While plague pathogenesis has been investigated

70 for decades, the bacteremic phase of the disease remains to be fully deciphered.

71 Here, we report the design of experimental pipelines allowing characterization of human
72 and bacterial proteomes in plasma and blood infected with *Y. pestis*. We first applied protein
73 extraction methods to *Y. pestis* comparing the SPEED method (Doellinger et al. 2020) based
74 on trifluoroacetic acid (TFA) lysis, the standard bead-beating lysis in urea followed by the
75 FASP method (Wiśniewski, Zougman, et al. 2009), and sonication in sodium dodecyl sulfate
76 (SDS) followed by buffer exchange and the FASP method (Wiśniewski, Zougman, et al.
77 2009). SPEED surpassed the other methods, allowing quick, efficient and safe sample
78 preparation in BSL-3 environment with fully virulent *Y. pestis*. It was thus further used to
79 conduct the first dual proteomic study of a bacterial species in human plasma and human
80 blood, revealing the pathogenic proteomic signature of *Y. pestis*.

81 Results

82 **Comparison of urea-, SDS- and TFA-based methods for *Y. pestis* proteomics.** To
83 study *Y. pestis* proteome, we first used the avirulent *Y. pestis* CO92 strain lacking pCD1 in a
84 BSL-2 environment. Bacteria were grown on lysogeny broth with 0.002% pork hemin (LBH)
85 agar plates at 37°C for 24 hours. We compared the three following protein extraction pro-
86 tocols: i) urea-based method: bacterial lysis by bead beating in 8M urea buffer, followed by
87 reduction-alkylation and digestion using the FASP method, ii) SDS-based method: bacterial
88 resuspension in 4% SDS buffer, heating at 95°C and lysis by sonication, followed by buffer
89 exchange with 8M urea, reduction-alkylation and digestion using the FASP method, and iii)
90 TFA-based SPEED method: bacterial lysis upon TFA acidification, followed by neutralization
91 with 10 volume of 2M Tris base, reduction-alkylation and digestion.

92 Three protein quantification methods were compared to assess their compatibility with
93 urea, SDS or TFA-Tris buffers. Bradford (Bradford 1976), BCA (Smith et al. 1985) and Qubit
94 assays were only compatible with one buffer each, and not with 10% TFA-2M Tris base buffer
95 (Table 1). Consequently, we implemented protein quantification by tryptophan fluorescence
96 spectroscopy (Wiśniewski and Gaugaz 2015) which was compatible with the three buffers
97 (Table 1, Fig EV1).

98 After data-dependent acquisition (DDA) analysis of triplicates using an Orbitrap mass-
99 spectrometer, we could detect a total of 1,587 proteins with at least one of the protocols,
100 1,390 bacterial proteins with the urea-based protocol, 1,444 proteins with the SDS-based
101 protocol and 1398 proteins with the TFA-based protocol (Fig 1, Table EV1). Overall 1,194

102 proteins were common to the three protocols, 30 proteins were only detected using the urea-
103 based protocol, 72 proteins were specifically detected using the SDS-based protocol and
104 34 proteins were exclusive to the TFA-based protocol (Fig 1). A total of 189 proteins were
105 detected using urea- or SDS-based protocols but not by using the TFA-based protocol. While
106 the three protocols led to similar *Y. pestis* proteomes, the TFA-based protocol surpassed
107 both bead-beating and sonication methods, which required a fastidious centrifugation step,
108 by its quick implementation, high-throughput potential and application to very small amount
109 of biomass, which is important when dealing with precious purified fractions from complex
110 samples. Moreover, the minimal number of steps of the SPEED method reduced the risk of
111 experimental errors and variability. These benefits led us to choose the SPEED method to
112 further investigate *Y. pestis* proteome in BSL-3 environment.

113 **Inactivation of virulent *Y. pestis* using the SPEED method in BSL-3 environment.**

114 Mass spectrometric analysis of virulent *Y. pestis* proteome performed in BSL-1 platform re-
115 quires bacterial inactivation according to French regulatory protocols from Agence Nationale
116 de la Sécurité du Médicament (ANSM). *Y. pestis* CO92 was grown on LBH agar plates at
117 37°C for 24 hours. Bacterial proteins were extracted using the SPEED method. To validate
118 absence of viable bacteria, lysogeny broth (LB) was inoculated with TFA lysates before and
119 after neutralization and incubated under agitation at 28°C for 72 hours. Absence of growth
120 measured by optical density at 600 nm certified inactivation of viable bacteria in both sam-
121 ples. To assess absence of bacteriostatic effect of the inactivating agent, the LB samples
122 were spiked with 1 to 2 bacteria and incubated 72 hours at 28°C. Growth measured at 600
123 nm revealed absence of bacteriostatic effect of the inactivating agent. *Y. pestis* specific
124 phage assay was used to assess the absence of contamination of the spiked sample (add
125 reference and/or in MM). To fulfill the French “Micro-Organismes et Toxines” (MOT) regu-
126 lation, bacterial DNA degradation was assessed by PCR on *Y. pestis* *caf*, *yopM*, and *pla*
127 genes after a 30-minutes dialysis to remove inhibiting salts. While amplicons correspond-
128 ing to the three genes were detected when PCR was performed on *Y. pestis* DNA used as
129 positive control, they could not be detected when PCR was performed on SPEED samples.
130 Together, our results indicate that the SPEED method allows bacterial inactivation and DNA
131 degradation directly after bacterial lysis and, consequently, that the following reduction, alky-
132 lation and digestion steps and mass spectrometry can be performed in a BSL-1 environment
133 (without MOT regulation).

134 **Proteomic reshaping of *Y. pestis* grown in human plasma.** To identify *Y. pestis* proteins
135 expressed in conditions mimicking human bacteremic phase of plague, we first compared
136 proteomes of bacteria grown in human plasma or in culture media. Proteomes of the fully
137 virulent *Y. pestis* CO92 strain were characterized in six BSL-3 culture conditions (Fig 2A): i)
138 inoculum grown overnight on LBH agar at 25°C (I25), ii) inoculum grown overnight on LBH
139 agar at 37°C (I37), iii) growth in chemically defined medium M9 at 37°C inoculated with I25
140 (I25-M9), iv) growth in M9 at 37°C inoculated with I37 (I37-M9), v) growth in human plasma
141 at 37°C inoculated with I25 (I25-Plasma) and vi) growth in human plasma at 37°C inoculated
142 with I37 (I37-Plasma). The two different inoculum temperatures reflect the origin of bacteria
143 entering the bloodstream: 25°C mimics direct transmission from fleas in primary septicemic
144 plague and 37°C mirrors hematogenous dissemination from the bubo or lungs in secondary
145 septicemic plague.

146 We identified 2,382 proteins across all samples, from a total of 3,915 coding sequences
147 and small open reading frame-encoded proteins (Table EV2) (Cao et al. 2021; Parkhill et
148 al. 2001). Optimization of Orbitrap-based mass-spectrometry in DDA mode led to a gain
149 in the number of proteins detected compared to our initial proteomic analysis, which iden-
150 tified 1,587 proteins (see above). From 2,025 to 2,205 proteins were identified in LBH and
151 M9 samples (Fig 2B). The number of protein identifications was reduced to 1,825-1,878 in
152 plasma samples, presumably due to presence of human proteins (Fig 2B). The most exten-
153 sive detection was achieved in the LBH sample grown at 25°C in which 2,205 proteins were
154 identified in the three replicates compared to the 2,033 proteins detected in LBH samples
155 grown at 37°C. Detection of proteins of lower abundance could have been prevented at 37°C
156 by the presence of highly produced proteins in the samples at that temperature, such as F1
157 pseudocapsule (Table 4) and type three secretion system (T3SS) (Demeure et al. 2019)
158 (Fig 4D).

159 Comparison of differential abundances of the proteins between samples revealed exten-
160 sive proteome reshaping across conditions (absolute fold change > 2 and adjusted p-value
161 < 0.01, Fig 2C). Expectedly, a shift in temperature and culture medium (I25 vs I25-M9, I25 vs
162 I25-Plasma) was associated with the highest number of differentially abundant proteins, with
163 439 and 444 proteins (taken into account only the proteins detected in both compared condi-
164 tions), respectively (Fig 2C). Temperature shift alone also induced major proteome changes
165 when I25 was compared to I37 (404 differentially abundant proteins). A change of culture
166 medium (I37 vs I37-M9, I37 vs I37-Plasma, I37-M9 vs I37-Plasma) led to slightly fewer differ-
167 entially abundant proteins with 375, 309, 247 proteins, respectively (Fig 2C). More modest

168 changes were observed when only shifting the inoculum temperature in M9 (117 proteins
169 for I25-M9 vs I37-M9) and in plasma (118 proteins for I25-Plasma vs I37-Plasma). A full de-
170 scription of numbers of differentially abundant proteins between each condition, as well as
171 numbers of proteins present in one condition but absent in another are indicated in Fig EV2.

172 To assess influence of donors on the proteome of *Y. pestis* grown in plasma, we com-
173 pared proteomes of bacteria grown in the plasma of four different donors inoculated with
174 I25 and I37 in triplicates. For each donor, we identified between 1,486 and 1,696 proteins
175 common to the three replicates (Fig EV3, Table EV3), slightly different numbers than in our
176 initial proteome analysis (see above, Fig 2B). Comparison of differentially abundant proteins
177 of samples derived from the four different donors identified approximately 100 proteins with
178 the 25°C inoculum, and 70 proteins with the 37°C inoculum, showing a good reproducibility
179 of proteomes when *Y. pestis* was grown in plasma of different donors.

180 Together, our results reveal a major expression remodeling upon growth in human plasma
181 at 37°C.

182 **Proteomic signature of *Y. pestis* grown in human plasma.** Gene set enrichment anal-
183 ysis (GSEA) was performed on the gene ontology (GO) biological process terms for the 9
184 comparisons. Most of the enriched terms between samples grown in different media were
185 related to metabolism, such as amino acid processes, purine synthetic processes such as
186 inosine monophosphate (IMP) biosynthesis (depleted in I37 compared to M9 and plasma),
187 tricarboxylic acid cycle (enriched in the I25 and I37 inoculi), carbohydrate transport (enriched
188 in the I25 derived cultures) (Fig 3, Table 2). In particular, methionine biosynthesis related
189 proteins such as MetE, MetR, MetF or MetAS were enriched in plasma compared to M9
190 (Fig 3, 4A), consistent with adaptation to nutrient composition of plasma and in line with
191 transcriptomic observations in murine models of plague (Sebbane et al. 2006; Lathem et al.
192 2005). In addition, iron transport was enriched in plasma samples compared to LBH or M9,
193 represented by the proteins involved in biosynthesis of the yersiniabactin siderophore and
194 other iron uptake systems such as YfeAB (Fig 3, 4B, Table 2), consistent with the low con-
195 centration of free iron in human plasma and extending transcriptomic data (Chauvaux et al.
196 2007). We also observed higher levels of proteins encoded by the virulence plasmid pCD1,
197 including T3SS effectors, in M9 compared to plasma and LBH (Fig 3, 4C, Table 3). Low
198 calcium is one of the stimuli inducing T3SS expression and secretion (Perry et al. 1997).
199 The low concentration of calcium in M9, i.e., 0.1 mM, compared to 1 mM of free ionized cal-
200 cium in human plasma (Bisello et al. 2008), even in the presence of the calcium ion chelator

201 acid-citrate-dextrose (ACD) serving as anti-coagulant, may thus be a trigger. Another signal
202 sensed by *Y. pestis* RNA thermometers to activate expression of the T3SS regulon is the
203 human host temperature of 37°C (Perry et al. 1997). Accordingly, when I25 and the other
204 proteomes derived from 37°C cultures were compared, T3SS effector proteins were pro-
205 duced more abundantly at 37°C than 25°C (Fig 3, 4D, Table 3). Similarly, the *caf* operon
206 encoding *Y. pestis* pseudocapsule is highly upregulated at 37°C (Demeure et al. 2019). Ex-
207 pectedly, we detected high levels of Caf1M, Caf1A, Caf1, and the regulator Caf1R when
208 *Y. pestis* was grown at 37°C (I37, I25-M9, I25-Plasma, I37-M9, I37-Plasma) but not at 25°C
209 (I25) (Table 4). In addition, pseudocapsule proteins were more abundant when cultures
210 were started with a 37°C inoculum (I37-M9 and I37-Plasma) than with a 25°C inoculum
211 (I25-M9 and I25-Plasma) (Table 4). Thus, *Y. pestis* growth in human plasma is character-
212 ized by a radical metabolic switch, induction of iron uptake machineries and calcium- and
213 temperature-dependent expression of important virulence determinants.

214 **Dual proteomics of *Y. pestis* in human blood.** To refine our model of bacteremia *ex vivo*,
215 we investigated *Y. pestis* grown in whole human blood. A proteotyping study used blood
216 cell lysis to deepen detection of bacterial peptides and identify *Staphylococcus aureus*, *Es-*
217 *cherichia coli* and *Candida albicans* for clinical diagnosis (Kondori et al. 2021). Although
218 this protocol enables proteomic analysis of bacteria in whole blood, it precludes identifica-
219 tion of human proteome, which is useful to understand host response to infection. Thus,
220 we set up an original pipeline allowing to analyze both bacterial and human proteomes in
221 whole blood. We first compared growth of *Y. pestis* in whole human blood using ethylenedi-
222 aminetetraacetic acid (EDTA), acid-citrate-dextrose (ACD) or heparin as anticoagulant. We
223 selected ACD, as *Y. pestis* grew the best in this blood compared to heparin- and EDTA-
224 anticoagulated blood, reaching 10⁸ bacteria/mL after an 8 hour-incubation (Fig EV4). Hu-
225 man blood is a highly complex biological fluid characterized by a high concentration of red
226 blood cells ($\approx 4.5\text{-}12.10^9$ cells/mL), and lower concentrations of platelets ($\approx 150\text{-}475.10^6$
227 cells/mL) and white blood cells ($\approx 5\text{-}10.10^6$ cells/mL). Neutrophils constitute the vast major-
228 ity of white blood cells (40-60%), followed by lymphocytes (20-40%) and monocytes (2-8%),
229 eosinophils ranging from 1 to 4% and basophils 0.5 to 1%. The high number of human cells
230 compared to bacteria in our sample (10⁸ bacteria/mL) and the vast dynamic range of hu-
231 man proteins abundance ($\approx 10^{13}$), makes characterization of dual proteomes a very difficult
232 challenge. We thus set up a pipeline to enrich *Y. pestis* associated to relevant immune cells,
233 neutrophils and monocytes (Arifuzzaman et al. 2018; Pujol et al. 2005; Spinner et al. 2014;

234 Dudte et al. 2017; Osei-Owusu et al. 2019). After 8-hour incubation of bacteria in ACD-
235 anticoagulated human blood, we purified these cells by immunomagnetic separation. Using
236 CD66b neutrophil-specific antibodies and CD14 monocyte-specific antibodies, $2 \cdot 10^5$ viable
237 neutrophils and $6 \cdot 10^4$ viable monocytes were recovered per milliliter of blood, which account
238 for around 10% of the total neutrophil and monocyte populations. Besides technical issues,
239 cell loss could be due to reduced lifespan of neutrophils *ex vivo* and *Y. pestis* capacity to
240 induce cell death (Marketon et al. 2005; Osei-Owusu et al. 2019). From 10^8 bacteria per
241 milliliter of whole blood, $4 \cdot 10^6$ bacteria were associated to the neutrophils fraction ($1/25^{\text{th}}$
242 of total bacteria), and $5 \cdot 10^5$ bacteria were associated to the monocyte fraction ($1/200^{\text{th}}$ of
243 total bacteria). This approach allowed to lower sample complexity and to switch from the
244 initial ratio of 10^8 bacteria to $5 \cdot 10^9$ human cells (1:50), to ratios of $4 \cdot 10^6$ bacteria to $2 \cdot 10^5$
245 neutrophils (20:1) and $5 \cdot 10^5$ bacteria to $6 \cdot 10^4$ monocytes (8:1). We then extracted proteins
246 using the SPEED method and analyzed samples by mass-spectrometry using a DIA mode.
247 To this end, we created two spectral libraries (Fig 5). The first library was constructed using
248 the antibody-mediated cell enrichments combined with a Nanotrap[®] enrichment, which had
249 previously been shown to concentrate *Y. pestis* bacteria from whole blood and bacterial pro-
250 teins from lysates (li et al. 2021). The second library was constructed from *Y. pestis* grown
251 in LB broth at 37°C to obtain the deepest peptide library. We identified 1,366 bacterial and
252 4,187 human proteins in the neutrophil fraction, and 877 bacterial and 3,969 human proteins
253 in the monocyte fraction (Table EV4). It is, to our knowledge, the first report of a pipeline
254 allowing semi-quantitative dual proteomics extracted from a complex matrix such as infected
255 whole blood, which could moreover be applied in a BSL-3 environment.

256 **Library depths and normalization strategies.** Nanotrap enrichment led to a good pep-
257 tide coverage of bacterial proteins that were very abundant in blood, such as MetE, MetF or
258 MetR, which were also enriched when *Y. pestis* was grown in human plasma (Fig 4A). Sim-
259 ilarly, T3SS proteins, such as YscX (Gurung et al. 2022; Day et al. 2000) and YopK, YopB,
260 YopD, YopT, YopH, whose secretion is induced in contact to host cells (Osei-Owusu et al.
261 2019) were identified. We could identify more than 2,800 bacterial proteins during the sec-
262 ondary library construction consisting in a DDA analysis of the fractionated pool of *Y. pestis*
263 grown in LB. To our knowledge, it is the most complete proteome of a *Yersinia* species. DIA
264 analysis led to identification of 1,366 bacterial proteins in the neutrophil fraction, 877 bac-
265 terial proteins in the monocyte fraction, 1,681 bacterial proteins in the Nanotrap enrichment
266 samples, and 2,335 bacterial proteins in *Y. pestis* grown in LB (Table 5). Hierarchical clus-

267 tering (Fig 6A) and principal component analysis (Fig 6B) based on MS peaks associated to
268 bacterial and human proteins showed an excellent clustering of the replicates as well as an
269 enrichment of bacterial and human proteins upon Nanotrap capture. The smaller number
270 of bacterial proteins identified in the monocyte fraction compared to the neutrophil fraction
271 (Table 5 and Fig 6A) are in line with the number of bacteria per cell, ranging from 8 bacteria
272 per cell in monocyte to 20 bacteria per cells for the neutrophils (see above).

273 We tested several normalization strategies to take into account the different ratio of bac-
274 teria per cell in both fractions. These strategies are detailed in Table 6. The differential anal-
275 ysis was performed taking into account either the proteins identified in at least one sample
276 (strategies A, H, Ya and Yc), which allows to identify proteins which are detected in one
277 condition but not the other, or in at least two samples per condition (strategies A2, H2, Ya2
278 and Yc2), which reduces the number of protein considered in the analysis but also reduces
279 the rate of false positive identification. Most of the differential analysis below will thus result
280 from this second set of strategies.

281 The A2 strategy consisted in normalizing the intensities of both human and bacterial
282 proteins by equalizing the medians of the human proteins in the samples across the two
283 conditions, and to perform a differential analysis on proteins which were detected in at least
284 2 replicates per condition. When using this strategy, the lower ratio of bacteria per cells in
285 the monocyte fraction compared to the neutrophil fraction was validated when analyzing the
286 differential abundance of the bacterial proteins. Indeed, a GSEA on biological processes GO
287 terms and KEGG pathways revealed an enrichment of translation and ribosomal processes
288 in the neutrophil fraction, considered here as house-keeping processes, and the associated
289 enriched protein $\log_2(\text{fold change})$ were centered around 2.5 (5.6 fold change) (Fig 7A and
290 B). This effect was also observed when we normalized only the bacterial proteins based on
291 the median of each conditions separately (strategy Yc2, Fig 7C), resulting in a "rotated" vol-
292 cano plot, where a large set of proteins mainly corresponding to ribosomal proteins seems
293 to be uniformly upregulated in the neutrophil fraction (Fig 7C). The calculated 5.6-fold ratio
294 based on ribosomal proteins was higher than the previous calculated ratio based on bac-
295 terial enumeration (8 viable bacteria per monocyte and 20 viable bacteria per neutrophil,
296 resulting in a 2.5-fold ratio) which could be explained by the lower intracellular survival of
297 *Y. pestis* in neutrophils compared to monocytes (Arifuzzaman et al. 2018; Pujol et al. 2005;
298 Spinner et al. 2014; Dudte et al. 2017; Osei-Owusu et al. 2019). When normalizing only
299 the bacterial proteins by equalizing the median of the samples from the two conditions taken
300 together (strategy Ya2), we observed a shift of the ribosomal proteins to the non differentially

301 abundant group when performing an enrichment analysis on non differentially abundant pro-
302 teins (Table 7). As the number of identified proteins in the monocyte was much lower than in
303 neutrophils, due to the lower number of bacteria per cell and subsequent reduced sensitivity,
304 most of the less abundant proteins in the monocyte fraction could presumably not be de-
305 tected. Only upregulated proteins in the monocyte fraction, identified in both the monocyte
306 and neutrophil fractions, could be measured and compared, resulting in a very asymmetrical
307 volcano plot (Fig 7D).

308 **Proteomic signature of *Y. pestis* in whole blood fractions.** Interestingly, using the Ya2
309 normalization strategy, most of the non-secreted pCD1 encoded proteins were not differen-
310 tially abundant, such as the T3S apparatus (T3SA) proteins YscL (cytoplasmic complex),
311 YscN (ATPase), YscJ (MS-ring forming proteins), YscC (outer membrane secretin), YscW
312 (pilotin), YscF (needle subunit), LcrV (needle tip), or regulators and chaperones such as
313 LcrG (negative cytosolic regulator), LcrH/SycD (YopBD chaperone), YscB (YopN chaper-
314 one), YPCD1.73c (chaperone), or YerA/SycE (YopE regulator) and YscE and YscG (putative
315 Yop translocation proteins) (Plano et al. 2013). On the other hand, secreted proteins of the
316 pCD1 plasmid such as the T3SS effectors (here, YopH, YopE, YopJ, YopK, YpkA/YopO and
317 YopM), the host-membrane pore-forming complex proteins YopB and YopD, the secreted
318 gatekeeper YopN, or the secreted protein YscX (Gurung et al. 2022; Day et al. 2000) were
319 more abundant in the monocyte fraction compared to neutrophil fraction. It was also the
320 case for the molecular ruler YscP, serving as a needle length control protein, and the inner
321 membrane platform protein LcrD/YscV, interacting with YscX, although both proteins were
322 never shown to be secreted in eukaryotic cells. To validate the hypothesis that monocytes
323 were more intoxicated with Yops than neutrophils, we used the A2 normalization strategy
324 and validated the higher abundance of Yops in the monocyte fraction when normalized by
325 human protein abundance (Table 8).

326 **Human proteome signature upon *Y. pestis* infection of whole blood fractions.** We
327 could identify 4,187 human proteins in at least one replicate of the neutrophil fraction and
328 3,969 human proteins in at least one replicate of the monocyte fraction (Table EV4). Among
329 the most abundant human proteins in monocytes based on PG quantities, we identified
330 the monocyte differentiation antigen CD14, annexin A2, interleukin-1 beta (induced in non-
331 intoxicated macrophages by YopJ-mediated inflammasome activation in neighboring intox-
332 icated cells (Orning et al. 2018)), the galectin-1 (shown to interact with YopJ/YopP to re-
333 duce nitric oxide production in macrophages (Jofre et al. 2021)), or the gamma-interferon-

334 inducible lysosomal thiol reductase (Table EV4). Among the most abundant human proteins
335 in neutrophils, we identified the carcinoembryonic antigen-related cell adhesion molecule
336 (CEACAM) 1, 6 and 8 (also respectively known as CD66a, CD66c and CD66b, specific for
337 granulocytes and neutrophils), the protein S100-A12, S100-A8 and S100-A9 (the most abun-
338 dant proteins in neutrophils (Tardif et al. 2015)), S100-P, annexin A3 (induced in neutrophils
339 during sepsis (Toufiq et al. 2020)) or galectin-10 (Fig 7B). The most abundant human pro-
340 teins in both fractions were the histone proteins (H2B type 1-O, H2A type 1-B, type 3, type
341 1-C, H4, H3.1, H1.3), cytoskeleton proteins (actin cytoplasmic 1 and 2, profilin), hemoglobin
342 and albumin, but most interestingly we could find almost all neutrophil cytoplasmic compo-
343 nents such as S100-A8 and S100-A9, and granule contents such as neutrophil defensin 3,
344 cathepsin G, neutrophil elastase, lactoferrin, azurocidin, lysozyme C or myeloperoxidase.

345 Using the H and H2 normalization strategies and performing a GSEA on biological pro-
346 cess GO term, we identified neutrophil-specific terms in the most enriched processes in the
347 neutrophil fraction, such as "neutrophil activation" or "leukocyte degranulation", as well as
348 terms related to actin cytoskeleton and motility, or carbohydrates metabolism (Fig 8A). On
349 the other hand, enriched terms in monocytes were mainly related to translation and metabolic
350 pathways linked to aerobic and mitochondrial respiration (Fig 8A). Among the protein only
351 identified in the neutrophil fraction, an enrichment of lipid metabolism-related proteins was
352 observed. The proteins only identified in the monocyte fraction were again related to transla-
353 tion and mitochondria, as well as major histocompatibility complex class II (MHC II) (Fig 8B).
354 These data are in line with the enrichment of the specific cell types we targeted. Indeed, in
355 addition to cell-specific terms such as neutrophil granule or the monocyte MHCII, neutrophils
356 are known to mainly rely on a glycolytic metabolism (Kumar et al. 2019; Injarabian, Devin,
357 et al. 2019; Jeon et al. 2020), which could explain the enrichment of aerobic metabolism in
358 the monocytes and a higher carbohydrate metabolism in the neutrophils.

Discussion

Dual proteomics to study bacterial host-interaction in *ex vivo* or *in vivo* conditions is challenging due to the high complexity of the host proteome and the high dynamic range between bacterial and host protein abundance. Moreover, application of protocols in a BSL-3 environment can be more difficult to implement and perform due to safety procedures and regulation.

Our pipeline, based on a non-specific enrichment from blood and a pure culture for the spectral library preparation and host cell purification for sample complexity reduction, and an efficient, safe and sample-economical TFA-based protein extraction, could overcome all these problematics. Using a *Y. pestis* model of bacteremia, this pipeline allowed us to work in a BSL3 environment, fulfilling the French regulation on MOT agents, and allowing the dual proteome study in a very high-complexity matrix, human whole blood. First, we benchmark then validated the TFA-based protein extraction method - SPEED - in a BSL-3 environment, confirming the bacterial inactivation when extracting the proteins, and allowing to compare bacterial proteins abundance after incubation in laboratory media or human plasma. We validated and expanded previous transcriptomic study (Chauvaux et al. 2007) by obtaining more sensitive and functionally relevant data. We then developed a new and affordable pipeline based on the SPEED extraction to study bacteria incubated in human whole blood and identified more than 5,500 proteins in the cellular fractions, composed of around 4/5 of human proteins and 1/4 of bacterial proteins, validating the possibility to use this pipeline for dual proteome studies. The cellular enrichment can be performed under a hood in a BSL-3 environment before the inactivation by protein extraction, eliminating the need for expensive cell-sorting instrument or fixation step. Differential analysis of bacterial protein abundances showed a higher injection of *Y. pestis* T3SS effectors in the monocytes than in the neutrophils, suggesting a higher affinity to target the monocyte, a better access to them in our experimental setup or a higher survival of bacteria in contact with the monocytes compared to the neutrophils, allowing a greater intoxication of the former cell type. The normalization method was validated by the fact that most of the translation-associated proteins such as the ribosomes, and metabolic pathway proteins, were not differentially abundant between both fractions. Human proteome analysis confirmed the good purification of CD14+ and CD66b+ cells, based on cell-specific GO terms and cell metabolic pathways, but a very high abundance of neutrophil components in both fractions was observed. This could imply a high degranulation of the neutrophils, followed by phagocytosis or macropinocytosis of the granules and/or dead neutrophils. Furthermore, it was recently shown that A100A8/A9 were

393 not released along with degranulation but upon formation of neutrophil extracellular traps
394 (NETs), suggesting activation of the NETosis in our infection model (Sprenkeler et al. 2022),
395 as S100-A8 and A9 were not only found abundantly in neutrophils but also in monocytes.

396 Based on our methodology, future studies could consist in comparing fraction proteomes
397 of infected and non-infected blood samples, to better understand the immune cell response
398 to bacterial infection in a relevant *ex vivo* environment, and to expand the fractionation to
399 other cell types such as platelets, T-cells or red blood cells, depending on the relevance for
400 the pathogen under study. This method, using few milliliters of blood, could also be applied
401 to the blood of bacteremic animals in *in vivo* conditions. Further improvement in sensitivity
402 could also be achieved by implementing hybrid spectral libraires based on DDA and DIA
403 runs (Willems et al. 2021), as well as using the sensitive bacterial proteome first obtained in
404 human plasma to enhance our spectral library used in whole blood.

405 Challenges remain to better characterize the bacteria in the bacteremic phase of dis-
406 eases. One of them is the comparison of the bacterial proteome between high-complexity
407 and low-complexity samples. We could indeed compare bacterial protein abundance be-
408 tween bacteria associated to neutrophils and monocytes as the host proteome background
409 was very similar. Similarly, we could compare the proteomes of bacteria incubated in LB
410 or human plasma, as a simple centrifugation and successive washes could separate the
411 bacteria from the plasma. However, it remains difficult to compare protein abundance of
412 cell-associated bacteria with that of a pure bacterial culture in laboratory media. One solu-
413 tion could be to add a host protein background during the protein extraction process to the
414 bacterial pure culture to mimic the sample complexity without altering protein expression.
415 Another challenge is the study of free bacteria not associated to cells in whole blood, as
416 our technique only applies to cell enrichment. A way to solve this issue could be to use
417 bacteria-specific antibodies coupled to magnetic beads, such as antibodies against the F1
418 pseudocapsule for *Y. pestis*, and enrich bacteria from the blood. However, this approach
419 would presumably also enrich cell-associated bacteria, and a second orthogonal separation
420 method such as differential centrifugation would be required to separate cell-free and cell-
421 associated bacteria. Moreover, the short life span of neutrophils once blood is drawn from
422 the host at 21 percents oxygen, greatly limits truly relevant models of bacteremia (Monceaux
423 et al. 2016; Injarabian, Skerniskyte, et al. 2021).

424 We believe that our methodological development successfully applied in challenging en-
425 vironments, such as BSL-3 laboratories, validates the proof of concept of studying host-
426 pathogen interactions of highly pathogenic bacteria in complex human samples.

427 **Methods**

428 **Strains, culture media and human material.** The avirulent *Y. pestis* CO92 pCD1- strain
429 was used for protein extraction setup in BSL2 environment. The fully virulent *Y. pestis* CO92
430 was used for validation in a BSL3 environment, and incubation in human plasma and whole
431 blood. Bacteria were routinely cultivated on LB agar plates supplemented with 0.002% pork
432 haemin, or in liquid LB under agitation at 180 rotations per minute (rpm), at 25°C or 37°C.
433 M9 was prepared by supplementation with 2 mM MgSO₄, 0.1 mM CaCl₂, 1% glucose, 1%
434 casamino acid and 1 mM Thiamine-HCl. Frozen human plasma and fresh anticoagulated
435 human blood (Citrate Dextrose) was ordered to Etablissement Français du Sang (EFS).
436 Whole blood inoculation were realized with a 25°C preculture on LBH plate. For bacterial
437 enumeration, bacteria were serial diluted in phosphate-buffered saline (PBS) and plated on
438 LBH agar plate, then incubated at 28°C for 48h. When enumerating bacteria after incubation
439 in human whole blood, 0.1% triton X100 was added in the first dilution to lyse eukaryotic cells.
440 Viable purified cells were counted in a Malassez chamber after addition of 0.1% Trypan blue
441 at a 1:1 ratio.

442 **Urea-based protein extraction.** The washed bacterial pellets were resuspended in 1 mL
443 of a urea lysis buffer composed of urea 8M, TrisHCl 100 mM, pH 8.5, vortexed, transferred
444 in a 2 mL tube with 0.1mm glass beads (Micro-organism lysing VK01, Bertin Corp), then
445 beaten in a Precellys24 in a cold chamber for 90 seconds at 5500rpm. The tubes were cen-
446 trifugated 5 minutes at 15 000g, then 500µL of supernatant were transferred in a Amicon®
447 Ultra tube 30kDa (Merck Millipore) and centrifugated at 14 000g for 20 minutes. The flow-
448 throughs were discarded, proteins were resuspended in 450µL urea 8M, TrisHCl 100mM, pH
449 8.5, before addition of 50µL of tris(2-carboxyethyl)phosphine (TCEP) 100 mM and chloroac-
450 etamide (CAA) 400 mM and incubation for 5 min at 95°C. The tubes were centrifugated at
451 14 000g for 10 minutes, then 300µL ammonium bicarbonate (ABC) 100 mM pH 8.0 was
452 added, following by centrifugation at 14000g for 10 minutes (3 times). The proteins were
453 resuspended in 350µL ABC 100 mM and quantified as explained below.

454 **SDS-based protein extraction.** The washed bacterial pellets were resuspended in 1mL
455 of a SDS lysis buffer composed of SDS 4%, TrisHCl 100mM, TCEP 10 mM, CAA 40 mM,
456 incubated for 5 minutes at 95°C and sonicated for 10 seconds. The tubes were centrifu-
457 gated at 16 000g for 5 minutes, the supernatants were transferred in a Amicon® Ultra tube
458 30kDa (Merck Millipore) and centrifugated at 14 000g for 20 minutes. The flow-throughs

459 were discarded, and 450µL urea 8M, TrisHCl 100 mM, pH 8.5 were added, following by
460 centrifugation at 14000g for 20 minutes (2 times). 100µL urea 8M, TrisHCl 100 mM, pH 8.5
461 were added, following by centrifugation at 14 000g for 15 minutes (3 times). Then 300µL
462 ABC were added, following by centrifugation at 14000g for 10 minutes (3 times). The pro-
463 teins were resuspended in 350µL ABC 100 mM, pH 8.0 and quantified as explained below.

464 **TFA-based protein extraction.** The washed bacterial or cell pellets were resuspended in
465 5 volumes of TFA compared to the pellet (for example 20 µl of TFA for a pellet of approxi-
466 mately 4 µL) for 10 minutes, then transferred in clean 1.5 mL protein low-binding tubes to
467 assure sample sterility in the tubes. 10 volumes, compared to the TFA volume (for example
468 200 µL) of Tris 2M were added, then 24 µL of TCEP 100mM, CAA 400 mM (for a final con-
469 centration of TCEP at 10 mM and CAA at 40 mM). The tubes were incubated at 95°C for
470 5 minutes, then the proteins were quantified as explained below, volumes were adjusted to
471 achieve the desired quantity of proteins to digest, and 5 volumes of water were added.

472 **Protein quantification.** Bradford, BCA and Qubit assays were performed as described by
473 the supplier. Bovine serum albumin (BSA) standard resuspended in Urea 8M, TrisHCl 100
474 mM, pH 8.5 or SDS 4%, TrisHcl 100 mM, pH 8.5 or TFA 10% - Tris 2M was used to assess
475 the buffer compatibility with the different assays. Tryptophan standard was performed using
476 pure L-tryptophan dissolved in distilled water. 50µL of samples were aliquoted in a black
477 96-well (or alternatively 384-well) plates and measured with a Xenius spectrophotometer
478 (or alternatively Synergy H1M microplate reader - BioTek) with an excitation wavelength of
479 280nm and an emission wavelength of 360nm.

480 **Protein digestion and desalting.** For the comparison of urea-based, SDS-based and
481 TFA-based protein extractions, proteins were digested using Sequencing Grade Modified
482 Trypsin (Promega - V5111) with a 1:50 ratio (enzyme:protein) at 37°C for 12h before stopping
483 the digestion by addition of TFA to reach a final pH less than 2. Then, digested peptides were
484 desalted on 50mg Sep-Pak C18 cartridge (Waters - WAT054955). The peptides were eluted
485 twice with a acetonitrile (ACN) 50%, formic acid (FA) 0.1% buffer and once with an ACN
486 80%, FA 0.1% buffer. Finally, the peptide solutions were speed-vac dried and resuspended
487 in ACN 2%, FA 0.1% buffer. For each sample, absorbance at 280 nm was performed with a
488 Nanodrop™ 2000 spectrophotometer (Thermo Scientific) to inject an equivalent of DO = 1.

489 For the *Y. pestis* incubation in human plasma and in human whole blood, digested pep-
490 tides were desalted using Stage-Tips method (Rappsilber et al. 2007) using C18 Empore

491 disc and eluted with ACN 80%, FA 0.1%. Finally, the peptide solutions were speed-vac
492 dried and resuspended in ACN 2%, FA 0.1% buffer. For each sample, absorbance at 280
493 nm was performed with a Nanodrop™ 2000 spectrophotometer (Thermo Scientific) to inject
494 an equivalent of DO = 1.

495 **Peptide mixing and pre-fractionation.** A pool of 100 µg of all SPEED digested samples
496 was used to obtain a spectral library for the DIA approach. To do this, an equivalent amount
497 of each digested sample was pooled together before proceeding to a peptide fractionation
498 using a manual workflow based on Stage-Tips or an automatic workflow with the AssayMAP
499 Bravo (Agilent).

500 Manual workflow was performed with a poly(styrene-divinylbenzene) reverse phase sul-
501 fonate (SDB-RPS) Stage-Tips method as described in (Rappsilber et al. 2007; Kulak et al.
502 2014). The pooled sample (20µg) was loaded into 3 SDB-RPS (Empore™, 66886-U) discs
503 stacked on a P200 tip and 8 serial elutions were applied as following: elution 1 (Ammonium
504 formate (AmF) 60mM, ACN 20%, FA 0.5%), elution 2 (AmF 80mM, ACN 30%, FA 0.5%),
505 elution 3 (AmF 95mM, ACN 40%, FA 0.5%) , elution 4 (AmF 110mM, ACN 50%, FA 0.5%),
506 elution 5 (AmF 130mM, ACN 60%, FA 0.5%), elution 6 (AmF 150mM, ACN 70%, FA 0.5%)
507 and elution 7 (ACN 80%, ammonium hydroxide 5%).

508 Automatic workflow was performed using the AssayMAP Bravo with the Fractionation
509 v1.1 protocol. The dried pooled sample (80 µg) was resuspended in 20 mM ammonium
510 formate, pH 10 before a high pH reverse phase fractionation. RPS cartridge (Agilent Tech-
511 nologies, 5 µL bead volume, G5496-60033) were primed with 100 µL ACN 80%, FA 0.1%
512 and equilibrated with 70 µL 20 mM AmF, pH 10. The samples were loaded at 5 µL/min
513 followed by an internal cartridge wash and cup wash with 50µL of 20 mM AmF, pH 10 at 5
514 µL/min. Step elution was performed with 60 µL of ACN 10%, 20%, 30%, 40%, 50%, and
515 80% in 20 mM AmF, pH 10 at 5 µL/min. A preexisting volume of 20 µL containing the same
516 elution buffer was present in the collection plates upon elution.

517 All fractions were speed-vac dried and resuspended with ACN 2%, FA 0.1% before injec-
518 tion. For all fractions, iRT peptides were spiked as recommended by Biognosys (Biognosys
519 - Ki-3002-1).

520 **LC-MS/MS for DDA and spectral libraries creation.** In all proteomic analyses, a nanochro-
521 matographic system (Proxeon EASY-nLC 1200 - Thermo Scientific) was coupled online with
522 a Q Exactive™ HF mass spectrometer (Thermo Scientific).

523 For the comparison of urea-based, SDS-based and TFA-based protein extractions, 1 µg

524 of peptides was injected into a reverse phase column (EASY-Spray™ - ES902 - Thermo
525 Scientific: 25cm x 75 µm ID, 2.0 µm particles, 100 Å pore size,) after an equilibration step
526 in 100% solvent A (H₂O, FA 0.1%).

527 For comparisons of *Y. pestis* protein abundances after growth in human plasma or labo-
528 ratory media and for the spectral library creation for the characterization of *Y. pestis* interac-
529 tion with its host after incubation in human whole blood, 1 µg of peptides was injected into a
530 reverse phase column (home-made column, 45cm x 75 µm ID, 1.9 µm particles, 100 Å pore
531 size, ReproSil-Pur Basic C18 - Dr. Maisch GmbH, Ammerbuch-Entringen, Germany) after
532 an equilibration step in 100% solvent A (H₂O, 0.1% FA).

533 Peptides were eluted with a multi-step gradient from 2 to 7% buffer B (ACN 80% / FA
534 0.1%) in 5 min, 7 to 23% buffer B in 70 min, 23 to 45% buffer B in 30 min and 45 to 95%
535 buffer B in 5 min at a flow rate of 250 nL/min for up to 132 min. Column temperature was
536 set to 60°C. Mass spectra were acquired using Xcalibur software using a data-dependent
537 Top 10 method with a survey scans (300-1700 m/z) at a resolution of 60,000 and MS/MS
538 scans (fixed first mass 100 m/z) at a resolution of 15,000. The AGC target and maximum
539 injection time for the survey scans and the MS/MS scans were set to 3.0×10^6 , 100ms and
540 1.0×10^5 , 45ms respectively. The isolation window was set to 1.6 m/z and normalized collision
541 energy fixed to 28 for HCD fragmentation. We used a minimum AGC target of 2.0×10^3 for
542 an intensity threshold of 4.4×10^4 . Unassigned precursor ion charge states as well as 1, 7,
543 8 and >8 charged states were rejected and peptide match was disable. Exclude isotopes
544 was enabled and selected ions were dynamically excluded for 45 seconds.

545 **LC-DIA-MS for DIA** For the *Y. pestis* incubation in human whole blood, two libraries for DIA
546 were constructed from i) CD14 and CD66b cell enrichments + Nanotrap®-enriched *Y. pestis*
547 and ii) pure culture in LB at 37°C. Mass spectra were acquired in DIA mode with the XCalibur
548 software using the same nanochromatographic system coupled on-line to a Q Exactive™
549 HF Mass Spectrometer. For each sample, 1 µg of peptides was injected into a reverse
550 phase column (home-made column, 45cm x 75 µm ID, 1.9 µm particles, 100 Å pore size,
551 ReproSil-Pur Basic C18 - Dr. Maisch GmbH, Ammerbuch-Entringen, Germany) after an
552 equilibration step in 100% solvent A (H₂O, 0.1% FA). Peptides were eluted using the same
553 multi-step gradient and temperature. MS data was acquired using the Xcalibur software with
554 a scan range from 295 to 1170 m/z. The DIA method consisted in a succession of one MS
555 scan at a resolution of 60,000 and 36 MS/MS scans of 1 Da overlapping windows (isolation
556 window = 25 m/z) at 30,000 resolution. The AGC (Automatic Gain Control) target and max-

imum injection time for MS and MS/MS scans were set to 3.0×10^6 , 60 ms and 5.0×10^5 , auto respectively. The normalized collision energy was set to 28 for HCD fragmentation.

Bioinformatic analyses MaxQuant analyses: DDA raw files were processed using MaxQuant software version 1.6.10.43 (Cox and Mann 2008) with Andromeda search engine (Cox, Neuhauser, et al. 2011). The MS/MS spectra were searched against a UniProt *Y. pestis* database (3,909 entries the 25/04/2019). Variable modifications (methionine oxidation and N-terminal acetylation) and fixed modification (cysteine carbamidomethylation) were set for the search and trypsin with a maximum of two missed cleavages was chosen for searching. The minimum peptide length was set to 7 amino acids and the false discovery rate (FDR) for peptide and protein identification was set to 0.01. The main search peptide tolerance was set to 4.5 ppm and to 20 ppm for the MS/MS match tolerance. Second peptides was enabled to identify co-fragmentation events. The “match between runs” feature was applied for samples having the same experimental condition with a maximal retention time window of 0.7 minute. One unique peptide to the protein group was required for the protein identification. Quantification was performed using the XIC-based LFQ algorithm with the Fast LFQ mode as described in Cox, Hein, et al. 2014. Unique and razor peptides included modified peptides, with at least 2 ratio count were accepted for quantification.

Spectral libraries generation: DDA raw data were directly loaded into Pulsar and spectral library generation was done using a personal *Y. pestis* CO92 database containing 3,991 entries, including 3,915 unique proteins from the initial CO92 Sanger sequencing (Parkhill et al. 2001), reannotated by RefSeq (Accession GCF_000009065.1_ASM906, accessed in 2020) and 76 small open frame (sORF) encoded peptides (SEP) recently identified (Cao et al. 2021) and the UniProt Homo sapiens database (20,361 entries the 03/03/2023). We applied the default BGS Factory Settings for both Pulsar Search and Library Generation. Briefly, full tryptic digestion allowing two missed cleavages, carbamidomethylation as a fixed modification on all cysteines, oxidation of methionines, and protein N-terminal acetylation as dynamic modifications were set. We used the search archive properties to create specific *Y. pestis* and human libraries as well as a combine library with a control of the FDR.

Spectronaut analyses: Spectronaut v. 16.0.220606 (Biognosys AG) (Bruderer et al. 2015) was used for DIA-MS data analyses. The data extraction was performed using the default BGS Factory Settings. Briefly, for identification, both precursor and protein FDR were controlled at 1%. For quantification, peptides were grouped based on stripped sequences and Qvalue was used for precursor filtering. MaxLFQ was used with no imputation and no

590 cross run normalization strategies.

591 **Statistical analysis.** Protocol comparison and plasma analysis: To find the proteins more
592 abundant in one condition than in another, the LFQ intensities quantified using MaxQuant
593 were compared. Only proteins identified with at least one peptide that is not common to
594 other proteins in the FASTA file used for the identification (at least one "unique" peptide)
595 were kept. Additionally, only proteins with at least two intensity values in one of the two com-
596 pared conditions were kept for further statistics. Proteins absent in a condition and present
597 in another are put aside. These proteins can directly be assumed differentially abundant
598 between the conditions. After this filtering, intensities of the remaining proteins were first
599 log-transformed (\log_2). Next, intensity values were normalized by median centering within
600 conditions (Quentin Gai Gianetto 2023). Missing values were imputed using the `impute.mle`
601 function of the R package `imp4p` (Q. Gai Gianetto et al. 2020). Statistical testing was con-
602 ducted using a `limma` t-test thanks to the R package `limma` (Ritchie et al. 2015). An adaptive
603 Benjamini-Hochberg procedure was applied on the resulting p-values thanks to the function
604 `adjust.p` of the `cp4p` R package (Quentin Gai Gianetto et al. 2016) using the robust method
605 described in Pounds et al. 2006 to estimate the proportion of true null hypotheses among
606 the set of statistical tests. The proteins associated to an adjusted p-value inferior to a FDR
607 (false discovery rate) level of 1% and an absolute $\log_2(\text{fold-change})$ superior to 1 have been
608 considered as significantly differentially abundant proteins. Finally, the proteins of interest
609 are therefore those which emerge from this statistical analysis supplemented by those which
610 are considered to be present from one condition and absent in another.

611 Whole blood analysis: To find the proteins more abundant in one condition than in an-
612 other, the intensities quantified using Spectronaut were compared. Only proteins identified
613 with at least one peptide that is not common to other proteins in the FASTA file used for the
614 identification (at least one "unique" peptide) were kept. Depending on the normalization and
615 differential analysis strategy used, only proteins with at least one intensity values in one of
616 the two compared conditions, or at least two intensity values in both compared conditions
617 were kept for further statistics. In the first case, proteins absent in a condition and present
618 in another are put aside. These proteins can directly be assumed differentially abundant
619 between the conditions. After this filtering, intensities of the remaining proteins were first
620 log-transformed (\log_2). Next, depending on the normalization strategy, intensity values only
621 for bacterial or human proteins were normalized either by median centering within condi-
622 tions or by median centering on all conditions (Quentin Gai Gianetto 2023). This method

623 consists in estimating the median of intensities in a sample j (med_j), to subtract this me-
624 dian to all the intensities x in the sample j and to add the average of median intensities
625 ($y = x - med_j + average(med_j)$). Missing values were imputed using the `impute.slsa`
626 function of the R package `imp4p` (Q. Gai Gianetto et al. 2020). Statistical testing was con-
627 ducted using a `limma` t-test thanks to the R package `limma` (Ritchie et al. 2015). An adaptive
628 Benjamini-Hochberg procedure was applied on the resulting p-values thanks to the function
629 `adjust.p` of the `cp4p` R package (Quentin Gai Gianetto et al. 2016) using the robust method
630 described in Pounds et al. 2006 to estimate the proportion of true null hypotheses among
631 the set of statistical tests. The proteins associated to an adjusted p-value inferior to a FDR
632 (false discovery rate) level of 1% and an absolute $\log_2(\text{fold-change})$ superior to 1 have been
633 considered as significantly differentially abundant proteins. Finally, the proteins of interest
634 are therefore those which emerge from this statistical analysis supplemented by those which
635 are considered to be present from one condition and absent in another.

636 We used the R package `clusterProfiler` v4.6.2 for enrichment and gene set enrichment
637 analysis (Wu et al. 2021). For the bacterial proteome in plasma, the `GSEA` function was used
638 based on UniProt accession number and mapped to a personal annotation file extracted
639 from the CO92 Gene Ontology terms downloaded from the QuickGo website accessed in
640 April 2023 (Binns et al. 2009). The `enrichKEGG` function was used with the online KEGG
641 dataset for the ype organism accessed in April 2023, based on the CO92 loci. Analysis were
642 performed with the detected proteins as statistical background. For the human proteome
643 analysis, the `gseGo` was used with the `org.Hs.eg.db` v3.16.0 as annotation database and
644 statistical background, and the `gseKEGG` was used with the online annotation for the `hsa`
645 organism accessed in April 2023 as annotation database and statistical background.

646 **Comparison of bacterial proteome after growth in human plasma or laboratory media.**

647 The fully virulent CO92 strain was cultivated overnight for 20h on LBH plate at 25°C or
648 37°C. Frozen human plasma (Donor A) was thawed, centrifugated at 8600g for 10 minutes
649 and filtrated on 0.22 μm filter to remove precipitates. Bacteria were resuspended in 3mL
650 PBS from overnight growth on LBH plates, and the optical density at 600nm (OD600) was
651 adjusted to 0.25 for the 25°C preculture and 0.67 for the 37°C preculture. 200 μL of each
652 inoculum were inoculated in 2mL of preheated human plasma or 2mL of preheated M9
653 media, then incubated at 37°C for 8h under agitation at 150rpm in 14mL polypropylene
654 tubes with round bottom, in 3 replicates. The inoculum and the 8h-growths were pelleted by
655 centrifugation and washes 3 times with cold PBS, following by centrifugation at 10000g for

656 10min at 4°C. Bacterial pellets were then lysed with 10µL TFA for the inoculum and the M9
657 growths, and 20µL TFA for the plasma growths, and processed as explained above in “TFA-
658 based protein extraction”. To assess reproducibility of protein expression between different
659 plasma donors, the same experiment was realized with Donor A and 3 other donors (B, C
660 and D).

661 **Comparison of monocyte- and neutrophil-associated bacterial proteome.** The fully
662 virulent CO92 strain was cultivated overnight for 20h on LBH plate at 25°C. Bacteria were
663 resuspended in 3mL PBS and the OD600 was adjusted to 0.25. 200µL of the inoculum were
664 inoculated in 2mL of preheated human blood at 37°C, and 2mL of preheated LB in 14mL
665 polypropylene tubes with round bottom, in 5 replicates. The tubes were incubated under
666 agitation at 37°C for 8h under agitation at 180rpm.

667 For the immune cell purifications, 1ml and 3mL of the blood incubations were aliquoted,
668 filtered on 30µm mesh to remove clogs and aggregates, in 5 replicates. StraightFrom®
669 Whole Blood kits (Miltenyi Biotec) were used to selectively enrich either monocytes (CD14
670 beads) or neutrophils (CD66b beads). 50µL of CD66b beads were added to the 1mL blood
671 and 150µL CD14 beads were added to the 3mL blood, incubated for 15 minutes at 4°C and
672 transfer in conditioned Whole Blood Columns (Miltenyi Biotec) following the kit instructions.
673 After 2 washes with PBS + 2mM EDTA, 0.5% BSA, the cells were eluted with 4mL Whole
674 Blood Column Elution Buffer (Miltenyi Biotec) and centrifugated at 500g for 10 minutes at
675 4°C. The supernatants were removed, the cells and associated bacteria were lysed with
676 80µL TFA and proteins were processed as explained above in “TFA-based protein extrac-
677 tion”.

678 For the first library construction, *Y. pestis* were enriched from whole blood with magnetic
679 Nanotrap® Microbiome A particles (Ceres Nanosciences, Inc) after the 8h-incubation, in 5
680 replicates. In 15-mL tubes, 1mL of Nanotrap® beads were added to 4mL of blood, shortly
681 vortexed, then incubated at room temperature for 30 min with regular quick vortexing. After
682 the addition of 6mL of PBS, the tubes were vortexed and put on a magnetic rack for 10
683 minutes. The supernatants were discarded, the tubes were removed from the magnetic
684 rack, 1mL PBS was added and the tubes were vortexed. The mix of beads and cells were
685 then transferred in 1.5mL protein low-binding tubes and pelleted on a magnetic rack for 10
686 minutes. The supernatants were discarded, and the pellets were washed a second time
687 with 1mL PBS. After a third magnetic pelleting, the cell pellets were lysed with 100µl TFA
688 and processed as explained above in “TFA-based protein extraction”.

689 For the second library construction, 4mL of the 8h-incubation in LB were pelleted by
690 centrifugation at 4000g for 15 minutes at 4°C and washed 3 times with 4mL cold PBS, in 5
691 replicates. The pellets were then lysed with 80µL TFA and processed as explained above
692 in “TFA-based protein extraction”.

693 **Data availability**

694 The mass spectrometry proteomics data have been deposited to the ProteomeXchange
695 Consortium via the PRIDE partner repository with the dataset identifier (Perez-Riverol et al.
696 2022).

697 **Acknowledgments**

698 We are grateful to all members of the *Yersinia* research unit and the *Yersinia* National
699 Reference Laboratory, WHO Collaborating Research and Reference Centre for Plague FRA-
700 140 for insightful discussions.

701 The project received funding from Institut Pasteur, Université Paris Cité, CNRS, LabEX
702 Integrative Biology of Emerging Infectious Diseases (ANR-10-LBX-62-IBEID), Agence de
703 l’Innovation de Défense (AID - DGA), Fondation pour la Recherche Médicale (FDT20220401-
704 5222) and the Inception program (Investissement d’Avenir grant ANR-16-CONV-0005). The
705 funders had no role in study design, data collection and interpretation, or the decision to
706 submit the work for publication.

707 Most of the figures were created with BioRender.

708 We declare no conflict of interest.

709 **Author contributions**

710 **Pierre Lê-Bury**: conceptualization ; investigation ; formal analysis ; visualization ; writing
711 – original draft ; **Thibaut Douché**: investigation ; formal analysis ; visualization ; **Quentin**
712 **Giai Gianetto**: investigation ; formal analysis ; visualization ; **Mariette Matondo**: formal
713 analysis ; writing – original draft ; funding acquisition ; **Javier Pizarro-Cerdá**: formal analysis
714 ; writing – original draft ; funding acquisition ; **Olivier Dussurget**: conceptualization ; formal
715 analysis ; writing – original draft ; funding acquisition. All the authors contributed to editing
716 the original manuscript before submission.

References

- 718 Arifuzzaman, Mohammad, W. X. Gladys Ang, Hae Woong Choi, Matthew L. Nilles, Ashley L. St John, and
719 Soman N. Abraham (Sept. 2018). "Necroptosis of infiltrated macrophages drives *Yersinia pestis* dispersal
720 within buboes". *JCI insight* 3.18.
- 721 Ball, Brianna, Arjun Sukumaran, and Jennifer Geddes-McAlister (Oct. 2020). "Label-free quantitative pro-
722 teomics workflow for discovery-driven host-pathogen interactions". *Journal of Visualized Experiments* 164.
- 723 Binns, David, Emily Dimmer, Rachael Huntley, Daniel Barrell, Claire O'Donovan, and Rolf Apweiler (Nov.
724 2009). "QuickGO: a web-based tool for Gene Ontology searching". *Bioinformatics* 25.22, 3045.
- 725 Bisello, Alessandro and Peter A. Friedman (Jan. 2008). "PTH and PTHrP actions on kidney and bone". *Prin-
726 ciples of Bone Biology, Two-Volume Set* 1, 665–712.
- 727 Bradford, Marion M. (May 1976). "A rapid and sensitive method for the quantitation of microgram quantities of
728 protein utilizing the principle of protein-dye binding". *Analytical Biochemistry* 72.1-2, 248–254.
- 729 Bruderer, Roland, Oliver M. Bernhardt, Tejas Gandhi, Saša M. Miladinović, Lin Yang Cheng, Simon Messner,
730 Tobias Ehrenberger, Vito Zanotelli, Yulia Butscheid, Claudia Escher, Olga Vitek, Oliver Rinner, and Lukas
731 Reiter (May 2015). "Extending the limits of quantitative proteome profiling with data-independent acquisi-
732 tion and application to acetaminophen-treated three-dimensional liver microtissues". *Molecular & cellular
733 proteomics* 14.5, 1400–1410.
- 734 Cao, Shiyang, Xinyue Liu, Yin Huang, Yanfeng Yan, Congli Zhou, Chen Shao, Ruifu Yang, Weimin Zhu, Zong-
735 min Du, and Chenxi Jia (Nov. 2021). "Proteogenomic discovery of sORF-encoded peptides associated
736 with bacterial virulence in *Yersinia pestis*". *Communications Biology* 2021 4:1 4.1, 1–12.
- 737 Chauvaux, S., M.-L. Rosso, L. Frangeul, C. Lacroix, L. Labarre, A. Schiavo, M. Marceau, M.-A. Dillies, J.
738 Foulon, J.-Y. Coppee, C. Medigue, M. Simonet, and E. Carniel (Sept. 2007). "Transcriptome analysis of
739 *Yersinia pestis* in human plasma: an approach for discovering bacterial genes involved in septicemic
740 plague". *Microbiology* 153.9, 3112–3124.
- 741 Cox, Jürgen, Marco Y. Hein, Christian A. Luber, Igor Paron, Nagarjuna Nagaraj, and Matthias Mann (Sept.
742 2014). "Accurate proteome-wide label-free quantification by delayed normalization and maximal peptide
743 ratio extraction, termed MaxLFQ". *Molecular & Cellular Proteomics* 13.9, 2513.
- 744 Cox, Jürgen and Matthias Mann (Dec. 2008). "MaxQuant enables high peptide identification rates, individ-
745 ualized p.p.b.-range mass accuracies and proteome-wide protein quantification". *Nature Biotechnology*
746 26.12, 1367–1372.
- 747 Cox, Jürgen, Nadin Neuhauser, Annette Michalski, Richard A. Scheltema, Jesper V. Olsen, and Matthias Mann
748 (Apr. 2011). "Andromeda: a peptide search engine integrated into the MaxQuant environment". *Journal of
749 Proteome Research* 10.4, 1794–1805.
- 750 Day, James B. and Gregory V. Plano (Apr. 2000). "The *Yersinia pestis* YscY protein directly binds YscX, a
751 secreted component of the type III secretion machinery". *Journal of Bacteriology* 182.7, 1834–1843.
- 752 Demeure, Christian E., Olivier Dussurget, Guillem Mas Fiol, Anne Sophie Le Guern, Cyril Savin, and Javier
753 Pizarro-Cerdá (2019). "*Yersinia pestis* and plague: an updated view on evolution, virulence determinants,
754 immune subversion, vaccination, and diagnostics". *Genes and Immunity* 20.5, 357–370.
- 755 Doellinger, Joerg, Andy Schneider, Marcell Hoeller, and Peter Lasch (Jan. 2020). "Sample preparation by easy
756 extraction and digestion (SPEED) - A universal, rapid, and detergent-free protocol for proteomics based
757 on acid extraction". *Molecular and Cellular Proteomics* 19.1, 209–222.
- 758 Dudte, Sophia C., B. Joseph Hinnebusch, and Jeffrey G. Shannon (Aug. 2017). "Characterization of *Yersinia
759 pestis* interactions with human neutrophils in vitro". *Frontiers in Cellular and Infection Microbiology* 7.AUG,
760 358.
- 761 Geddes-McAlister, J., A. Sukumaran, S.L. Vogt, J.L. Rowland, S.E. Woodward, B. Muselius, L. Gee, E.J.
762 Roach, C.M. Khursigara, B. Raupach, B.B. Finlay, and F. Meissner (Sept. 2021). "Dual perspective pro-
763 teomics infectome profiling discovers *Salmonella* type III secretion system effector functions in macro-
764 phages". *bioRxiv*, 2021.09.01.458519.
- 765 Giai Gianetto, Q., S. Wiecezorek, Y. Couté, and T. Burger (May 2020). "A peptide-level multiple imputation strat-
766 egy accounting for the different natures of missing values in proteomics data". *bioRxiv*, 2020.05.29.122770.
- 767 Giai Gianetto, Quentin (2023). "Statistical analysis of post-translational modifications quantified by label-free
768 proteomics across multiple biological conditions with R: illustration from SARS-CoV-2 infected cells". *Methods
769 in Molecular Biology* 2426, 267–302.
- 770 Giai Gianetto, Quentin, Florence Combes, Claire Ramus, Christophe Bruley, Yohann Couté, and Thomas
771 Burger (Jan. 2016). "Calibration plot for proteomics: a graphical tool to visually check the assumptions
772 underlying FDR control in quantitative experiments". *Proteomics* 16.1, 29–32.
- 773 Gurung, Jyoti M., Ayad A.A. Amer, Shiyun Chen, Andreas Diepold, and Matthew S. Francis (Apr. 2022). "Type
774 III secretion by *Yersinia pseudotuberculosis* is reliant upon an authentic N-terminal YscX secretor domain".
775 *Molecular Microbiology* 117.4, 886–906.
- 776 Hu, Qizhi, Robert J. Noll, Hongyan Li, Alexander Makarov, Mark Hardman, and R. Graham Cooks (Apr. 2005).
777 "The Orbitrap: a new mass spectrometer". *Journal of Mass Spectrometry* 40.4, 430–443.
- 778 Hughes, Christopher S, Sophia Foehr, David A Garfield, Eileen E Furlong, Lars M Steinmetz, and Jeroen
779 Krijgsveld (Oct. 2014). "Ultrasensitive proteome analysis using paramagnetic bead technology". *Molecular
780 Systems Biology* 10.10, 757.
- 781 li, Alexandra N., Shih Chao Lin, Benjamin Lepene, Weidong Zhou, Kylene Kehn-Hall, and Monique L. van Hoek
782 (Dec. 2021). "Use of magnetic nanotrapp particles in capturing *Yersinia pestis* virulence factors, nucleic
783 acids and bacteria". *Journal of Nanobiotechnology* 19.1, 1–17.
- 784 Injarabian, Louise, Anne Devin, Stéphane Ransac, and Benoit S. Marteyn (Dec. 2019). "Neutrophil metabolic
785 shift during their lifecycle: impact on their survival and activation". *International Journal of Molecular Sci-
786 ences* 21.1, 287.
- 787 Injarabian, Louise, Jurate Skerniskyte, Quentin Gai Gianetto, Véronique Witko-Sarsat, and Benoit S. Marteyn
788 (Aug. 2021). "Reducing neutrophil exposure to oxygen allows their basal state maintenance". *Immunology
789 and Cell Biology* 99.7, 782–789.

790 Jeon, Jae Han, Chang Won Hong, Eun Young Kim, and Jae Man Lee (Dec. 2020). "Current understanding on
791 the metabolism of neutrophils". *Immune Network* 20.6, 1–13.

792 Jofre, Brenda Lucila, Ricardo Javier Elicábe, Juan Eduardo Silva, Juan Manuel Pérez Sáez, María Daniela
793 Paez, Eduardo Callegari, Karina Valeria Mariño, María Silvia Di Genaro, Gabriel Adrián Rabinovich, and
794 Roberto Carlos Davicino (Nov. 2021). "Galectin-1 cooperates with *Yersinia* outer protein (Yop) P to thwart
795 protective immunity by repressing nitric oxide production". *Biomolecules* 11.11.

796 Kondori, Nahid, Amra Kurtovic, Beatriz Piñeiro-Iglesias, Francisco Salvà-Serra, Daniel Jaén-Luchoro, Björn
797 Andersson, Gelio Alves, Aleksey Ogurtsov, Annika Thorsell, Johannes Fuchs, Timur Tunovic, Nina Ka-
798 menska, Anders Karlsson, Yi Kuo Yu, Edward R.B. Moore, and Roger Karlsson (July 2021). "Mass spec-
799 trometry proteotyping-based detection and identification of *Staphylococcus aureus*, *Escherichia coli*, and
800 *Candida albicans* in blood". *Frontiers in Cellular and Infection Microbiology* 11.

801 Kulak, Nils A., Garwin Pichler, Igor Paron, Nagarjuna Nagaraj, and Matthias Mann (2014). "Minimal, encapsu-
802 lated proteomic-sample processing applied to copy-number estimation in eukaryotic cells". *Nature Methods*
803 11.3, 319–324.

804 Kumar, Sachin and Madhu Dikshit (Sept. 2019). "Metabolic insight of neutrophils in health and disease". *Fron-
805 tiers in Immunology* 10, 2099.

806 Lathem, Wyndham W., Seth D. Crosby, Virginia L. Miller, and William E. Goldman (Dec. 2005). "Progression of
807 primary pneumonic plague: A mouse model of infection, pathology, and bacterial transcriptional activity".
808 *Proceedings of the National Academy of Sciences of the United States of America* 102.49, 17786–17791.

809 Leseigneur, Clarisse, Laurent Boucnet, Magalie Duchateau, Javier Pizarro-Cerda, Mariette Matondo, Emma
810 Colucci-Guyon, and Olivier Dussurget (June 2022). "NAD kinase promotes *Staphylococcus aureus* patho-
811 genesis by supporting production of virulence factors and protective enzymes". *eLife* 11.

812 Marketon, Melanie M., R. William DePaolo, Kristin L. DeBord, Bana Jabri, and Olaf Schneewind (Sept. 2005).
813 "Plague bacteria target immune cells during infection". *Science* 309.5741, 1739–1741.

814 Masson, Florent, Samuel Rommelaere, Alice Marra, Fanny Schüpfer, and Bruno Lemaitre (Apr. 2021). "Dual
815 proteomics of *Drosophila melanogaster* hemolymph infected with the heritable endosymbiont *Spiroplasma*
816 *poulsonii*". *PLOS ONE* 16.4, e0250524.

817 Monceaux, Valérie, Clarisse Chiche-Lapierre, Catherine Chaput, Véronique Witko-Sarsat, Marie Christine Pre-
818 vost, Cormac T. Taylor, Marie Noelle Ungeheuer, Philippe J. Sansonetti, and Benoit S. Marteyn (Aug.
819 2016). "Anoxia and glucose supplementation preserve neutrophil viability and function". *Blood* 128.7, 993–
820 1002.

821 Orning, Pontus, Dan Weng, Kristian Starheim, Dmitry Ratner, Zachary Best, Bettina Lee, Alexandria Brooks,
822 Shiyu Xia, Hao Wu, Michelle A. Kelliher, Scott B. Berger, Peter J. Gough, John Bertin, Megan M. Proulx,
823 Jon D. Goguen, Nobuhiko Kayagaki, Katherine A. Fitzgerald, and Egil Lien (2018). "Pathogen blockade of
824 TAK1 triggers caspase-8–dependent cleavage of gasdermin D and cell death". *Science* 362.6418, 1064–
825 1069.

826 Osei-Owusu, Patrick, Thomas M. Charlton, Hwan Keun Kim, Dominique Missiakas, and Olaf Schneewind (Oct.
827 2019). "FPR1 is the plague receptor on host immune cells". *Nature* 574.7776, 57–62.

828 Parkhill, J., B. W. Wren, N. R. Thomson, R. W. Titball, M. T. G. Holden, M. B. Prentice, M. Sebahia, K. D. James,
829 C. Churcher, K. L. Mungall, S. Baker, D. Basham, S. D. Bentley, K. Brooks, A. M. Cerdeño-Tárraga, T.
830 Chillingworth, A. Cronin, R. M. Davies, P. Davis, G. Dougan, T. Feltwell, N. Hamlin, S. Holroyd, K. Jagels,
831 A. V. Karlyshev, S. Leather, S. Moule, P. C. F. Oyston, M. Quail, K. Rutherford, M. Simmonds, J. Skelton, K.
832 Stevens, S. Whitehead, and B. G. Barrell (Oct. 2001). "Genome sequence of *Yersinia pestis*, the causative
833 agent of plague". *Nature* 413.6855, 523–527.

834 Perez-Riverol, Yasset, Jingwen Bai, Chakradhar Bandla, David García-Seisdedos, Suresh Hewapathirana,
835 Selvakumar Kamatchinathan, Deepti J. Kundu, Ananth Prakash, Anika Frericks-Zipper, Martin Eisenacher,
836 Mathias Walzer, Shengbo Wang, Alvis Brazma, and Juan Antonio Vizcaíno (Jan. 2022). "The PRIDE
837 database resources in 2022: a hub for mass spectrometry-based proteomics evidences". *Nucleic Acids*
838 *Research* 50.D1, D543–D552.

839 Perry, R D and J D Fetherston (Jan. 1997). "*Yersinia pestis* - Etiologic agent of plague". *Clinical microbiology*
840 *reviews* 10.1, 35–66.

841 Plano, Gregory V. and Kurt Schesser (Dec. 2013). "The *Yersinia pestis* type III secretion system: expression,
842 assembly and role in the evasion of host defenses". *Immunologic Research* 57.1-3, 237–245.

843 Pounds, Stan and Cheng Cheng (Aug. 2006). "Robust estimation of the false discovery rate". *Bioinformatics*
844 22.16, 1979–1987.

845 Pujol, Céline, Jens P. Grabenstein, Robert D. Perry, and James B. Bliska (Sept. 2005). "Replication of *Yersinia*
846 *pestis* in interferon γ -activated macrophages requires ripA, a gene encoded in the pigmentation locus".
847 *Proceedings of the National Academy of Sciences of the United States of America* 102.36, 12909–12914.

848 Rappsilber, Juri, Matthias Mann, and Yasushi Ishihama (Aug. 2007). "Protocol for micro-purification, enrich-
849 ment, pre-fractionation and storage of peptides for proteomics using StageTips". *Nature Protocols* 2.8,
850 1896–1906.

851 Ritchie, Matthew E., Belinda Phipson, Di Wu, Yifang Hu, Charity W. Law, Wei Shi, and Gordon K. Smyth
852 (Apr. 2015). "*limma* powers differential expression analyses for RNA-sequencing and microarray studies".
853 *Nucleic Acids Research* 43.7, e47.

854 Roux-Dalvai, Florence, Clarisse Gotti, Mickaël Leclercq, Marie-Claude Hélie, Maurice Boissinot, Tabiawang
855 N Arrey, Claire Daully, Frédéric Fournier, Isabelle Kelly, Judith Marcoux, Julie Bestman-Smith, Michel G
856 Bergeron, and Arnaud Droit (2019). "Fast and accurate bacterial species identification in urine specimens
857 using LC-MS/MS mass spectrometry and machine learning". *Molecular & Cellular Proteomics* December,
858 mcp.TIR119.001559.

859 Sebbane, Florent, Clayton O Jarrett, Donald Gardner, Daniel Long, and B Joseph Hinnebusch (Apr. 2006).
860 "Role of the *Yersinia pestis* plasminogen activator in the incidence of distinct septicemic and bubonic forms
861 of flea-borne plague". *Proceedings of the National Academy of Sciences of the United States of America*
862 103.14, 5526–30.

863 Smith, P. K., R. I. Krohn, G. T. Hermanson, A. K. Mallia, F. H. Gartner, M. D. Provenzano, E. K. Fujimoto,
864 N. M. Goeke, B. J. Olson, and D. C. Klenk (Oct. 1985). "Measurement of protein using bicinchoninic acid".
865 *Analytical Biochemistry* 150.1, 76–85.

866 Spinner, Justin L., Seth Winfree, Tregel Starr, Jeffrey G. Shannon, Vinod Nair, Olivia Steele-Mortimer, and
867 B. Joseph Hinnebusch (Mar. 2014). "Yersinia pestis survival and replication within human neutrophil phago-
868 somes and uptake of infected neutrophils by macrophages". *Journal of Leukocyte Biology* 95.3, 389–398.

869 Sprenkeler, Evelien G.G., Judith Zandstra, Nadine D. van Kleef, Ines Goetschalckx, Bibian Verstegen, Cathelijn
870 E.M. Aarts, Hans Janssen, Anton T.J. Tool, Gerard van Mierlo, Robin van Bruggen, Ilse Jongerius, and
871 Taco W. Kuijpers (Jan. 2022). "S100A8/A9 is a marker for the release of neutrophil extracellular traps and
872 induces neutrophil activation". *Cells* 11.2.

873 Tardif, Mélanie R., Julie Andrea Chapeton-Montes, Alma Posvanzdic, Nathalie Pagé, Caroline Gilbert, and
874 Philippe A. Tessier (2015). "Secretion of S100A8, S100A9, and S100A12 by neutrophils involves reactive
875 oxygen species and potassium efflux". *Journal of Immunology Research* 2015.

876 Toufiq, Mohammed, Jessica Roelands, Mohamed Alfaki, Basirudeen Syed Ahamed Kabeer, Marwa Saadaoui,
877 Arun Prasath Lakshmanan, Dhinoth Kumar Bangarusamy, Selvasankar Murugesan, Davide Bedognetti,
878 Wouter Hendrickx, Souhaila Al Khodor, Annalisa Terranegra, Darawan Rinchai, Damien Chaussabel, and
879 Mathieu Garand (Dec. 2020). "Annexin A3 in sepsis: novel perspectives from an exploration of public
880 transcriptome data". *Immunology* 161.4, 291–302.

881 Willems, Patrick, Ursula Fels, An Staes, Kris Gevaert, and Petra Van Damme (Feb. 2021). "Use of hybrid data-
882 dependent and -independent acquisition spectral libraries empowers dual-proteome profiling". *Journal of*
883 *Proteome Research* 20.2, 1165–1177.

884 Wiśniewski, Jacek R. and Fabienne Z. Gaugaz (2015). "Fast and sensitive total protein and peptide assays for
885 proteomic analysis". *Analytical Chemistry* 87.8, 4110–4116.

886 Wiśniewski, Jacek R., Alexandre Zougman, Nagarjuna Nagaraj, and Matthias Mann (2009). "Universal sample
887 preparation method for proteome analysis". *Nature Methods* 6.5, 359–362.

888 Wu, Tianzhi, Erqiang Hu, Shuangbin Xu, Meijun Chen, Pingfan Guo, Zehan Dai, Tingze Feng, Lang Zhou,
889 Wenli Tang, Li Zhan, Xiaocong Fu, Shanshan Liu, Xiaochen Bo, and Guangchuang Yu (Aug. 2021). "clus-
890 terProfiler 4.0: A universal enrichment tool for interpreting omics data". *The Innovation* 2.3, 100141.

891 Zougman, Alexandre, Peter J. Selby, and Rosamonde E. Banks (May 2014). "Suspension trapping (STrap)
892 sample preparation method for bottom-up proteomics analysis". *Proteomics* 14.9, 1006–1000.

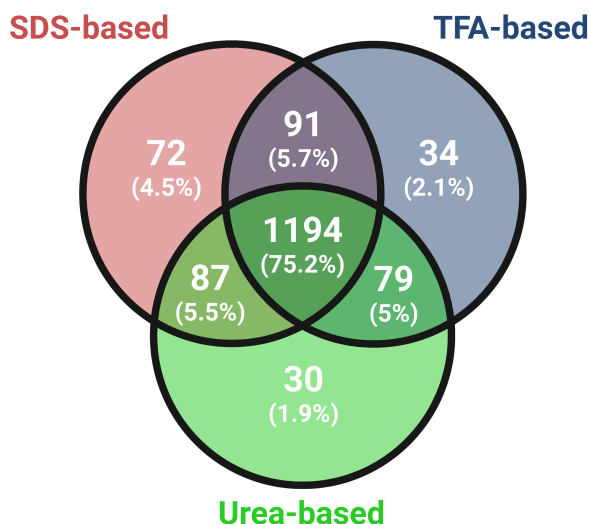


Figure 1. Venn diagram of identified proteins repartition between the urea-based, SDS-based and TFA-based protocols.

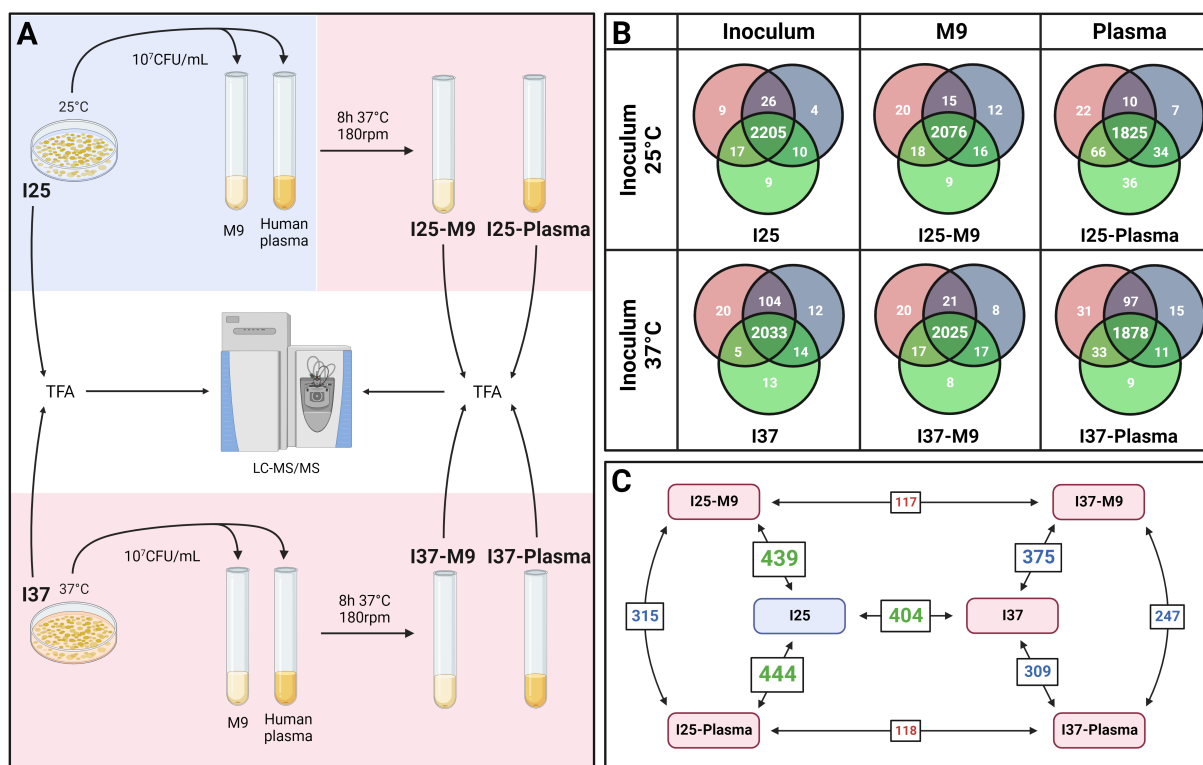


Figure 2. (A) Protocol comparing *Y. pestis* grown on LBH plate at 2 different temperatures and after growth in M9 or human plasma at 37°C. (B) Venn diagrams of the number of identified proteins across replicates in the same condition, for samples of *Y. pestis* grown on LBH, in M9 or human plasma at different temperatures. Each circle in the Venn diagrams corresponds to a replicate. (C) Number of differentially abundant proteins between samples after *Y. pestis* growth on LBH, in M9 or human plasma at different temperatures. These numbers only consider the proteins detected in both conditions. Condition in the blue rectangle is grown at 25°C and conditions in the red rectangles are grown at 37°C. Numbers in green are associated with change in temperature culture, numbers in blues are associated with a change in media grown at 37°C, and numbers in red are associated with a change in inoculum temperature in the same medium.

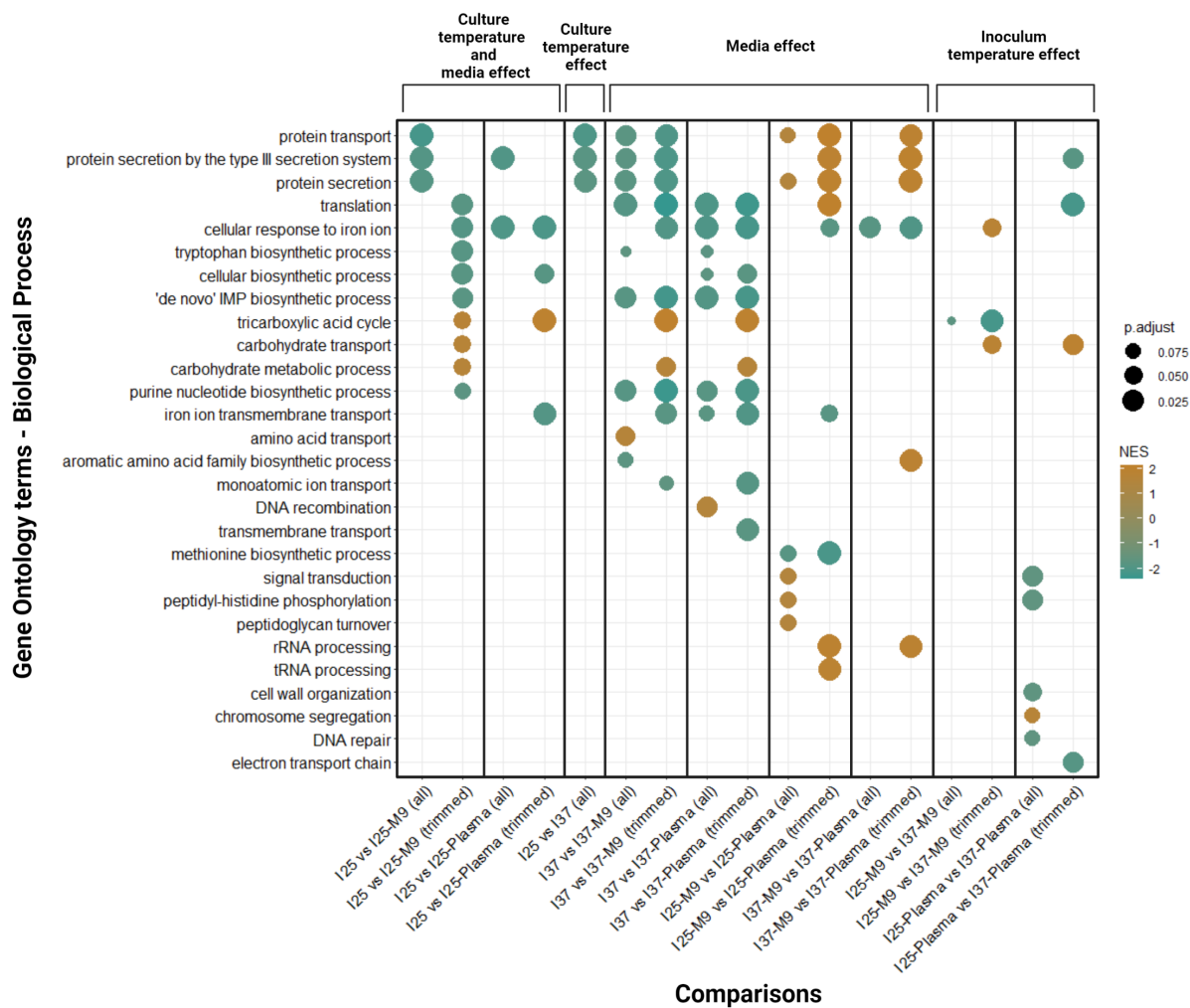


Figure 3. Dot plot representing the gene set enrichment analysis (GSEA) of the biological process terms from the gene ontology (GO) for the 9 proteomics comparisons. Each comparison is analyzed twice: i) with the whole data set comprising the proteins only present in one or the other conditions (marked "all") and ii) with the proteins detected only in both conditions (marked "trimmed"). The dot color represents the normalized enrichment score (NES) of the GO term in the GSEA. The dot size represents the adjusted p-value of the enriched GO term (control of the false discovery rate by the Benjamini-Hochberg correction).

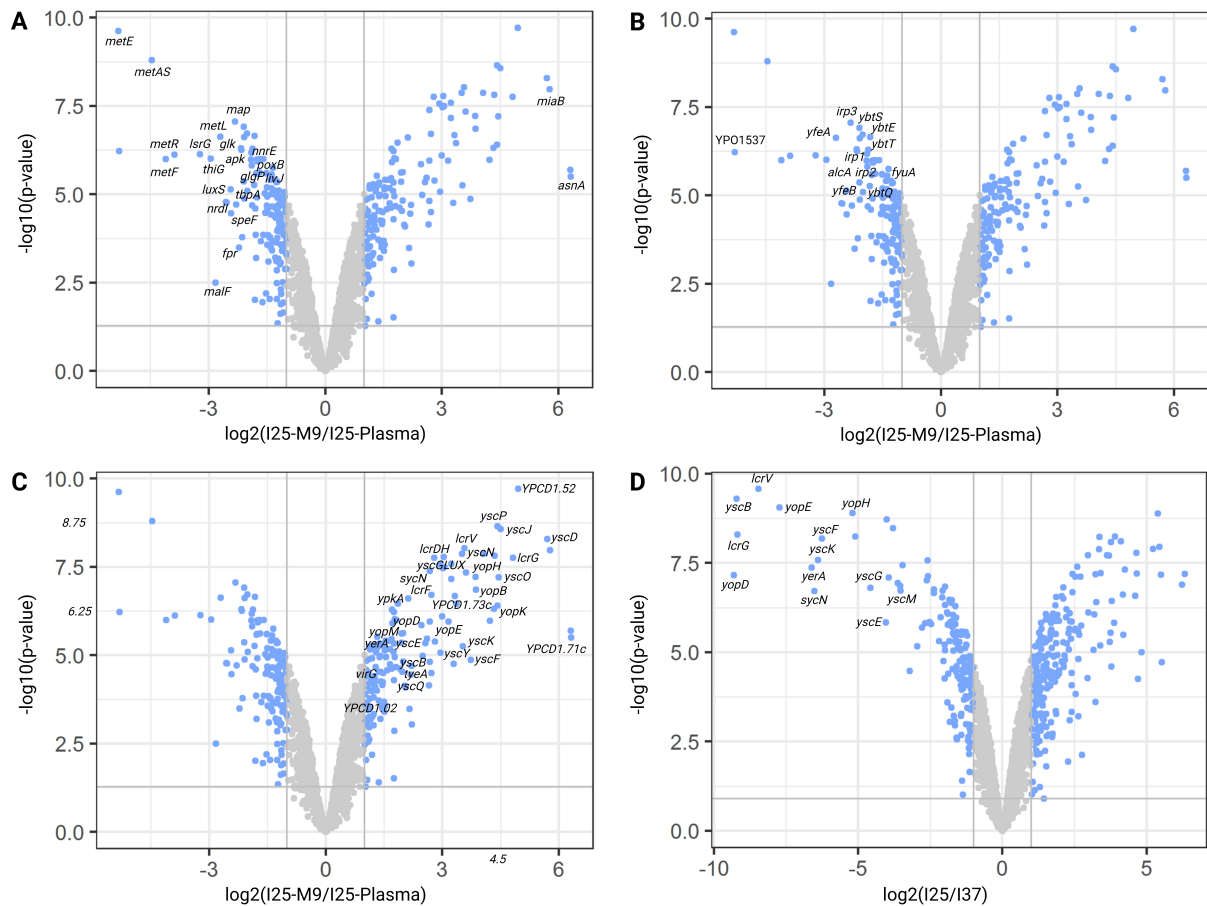


Figure 4. Volcano plots showing differentially abundant proteins between *Y. pestis* grown in different conditions. The displayed dots represent proteins detected in both condition of the comparison. In blue are the proteins which are significantly differentially expressed, considering a threshold of 1 for the absolute value of the $\log_2(\text{fold change})$, and a value of 1% for the unadjusted p-value. (A-C) M9 at 37°C with a 25°C inoculum (I25-M9) versus *Y. pestis* grown in human plasma at 37°C with a 25°C inoculum (I25-Plasma) with (A) a focus on regulated metabolism proteins and the corresponding annotated genes, (B) a focus on regulated iron acquisition proteins and the corresponding annotated genes and (C) a focus on T3SS regulated proteins and the corresponding annotated genes. (D) 25°C inoculum on LBH plate (I25) versus 37°C inoculum on LBH plate (I37), with a focus on T3SS regulated proteins and the corresponding annotated genes.

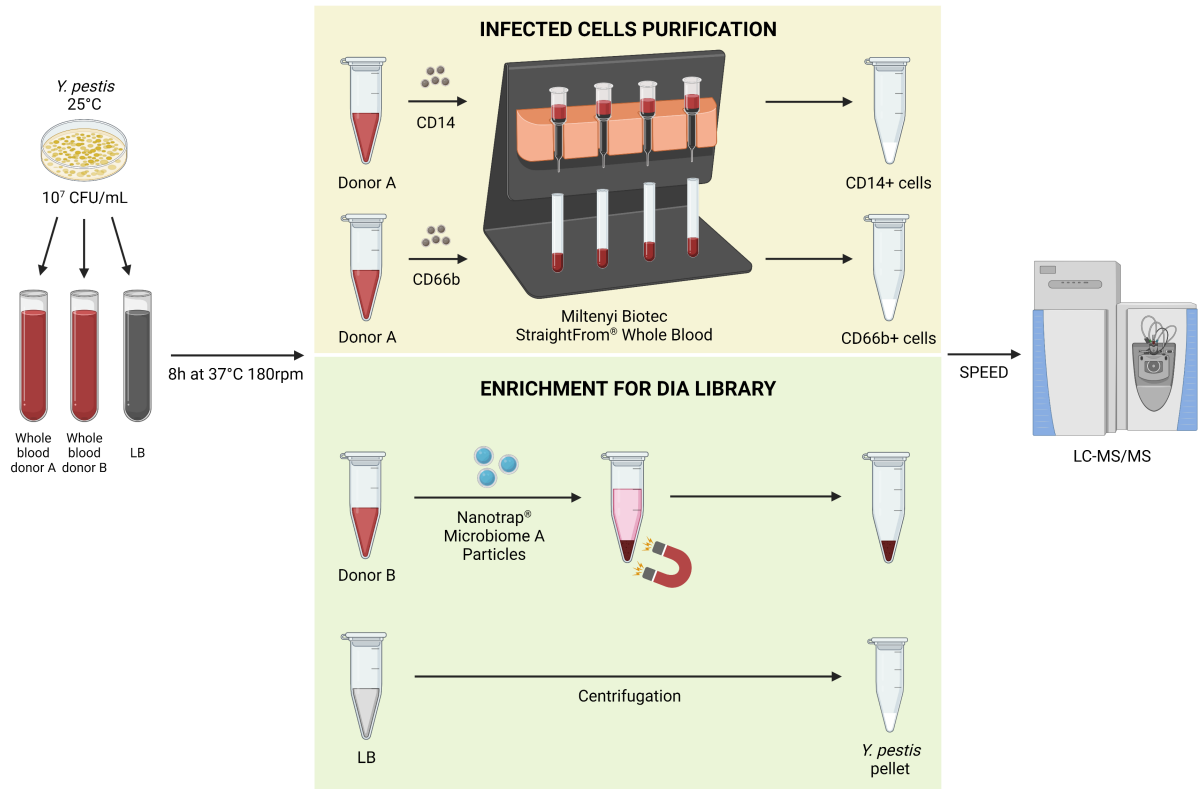


Figure 5. Workflow for enrichment of cell-associated *Y. pestis* from human whole blood, and library construction based on Nanotrap enrichment and pure culture in LB.

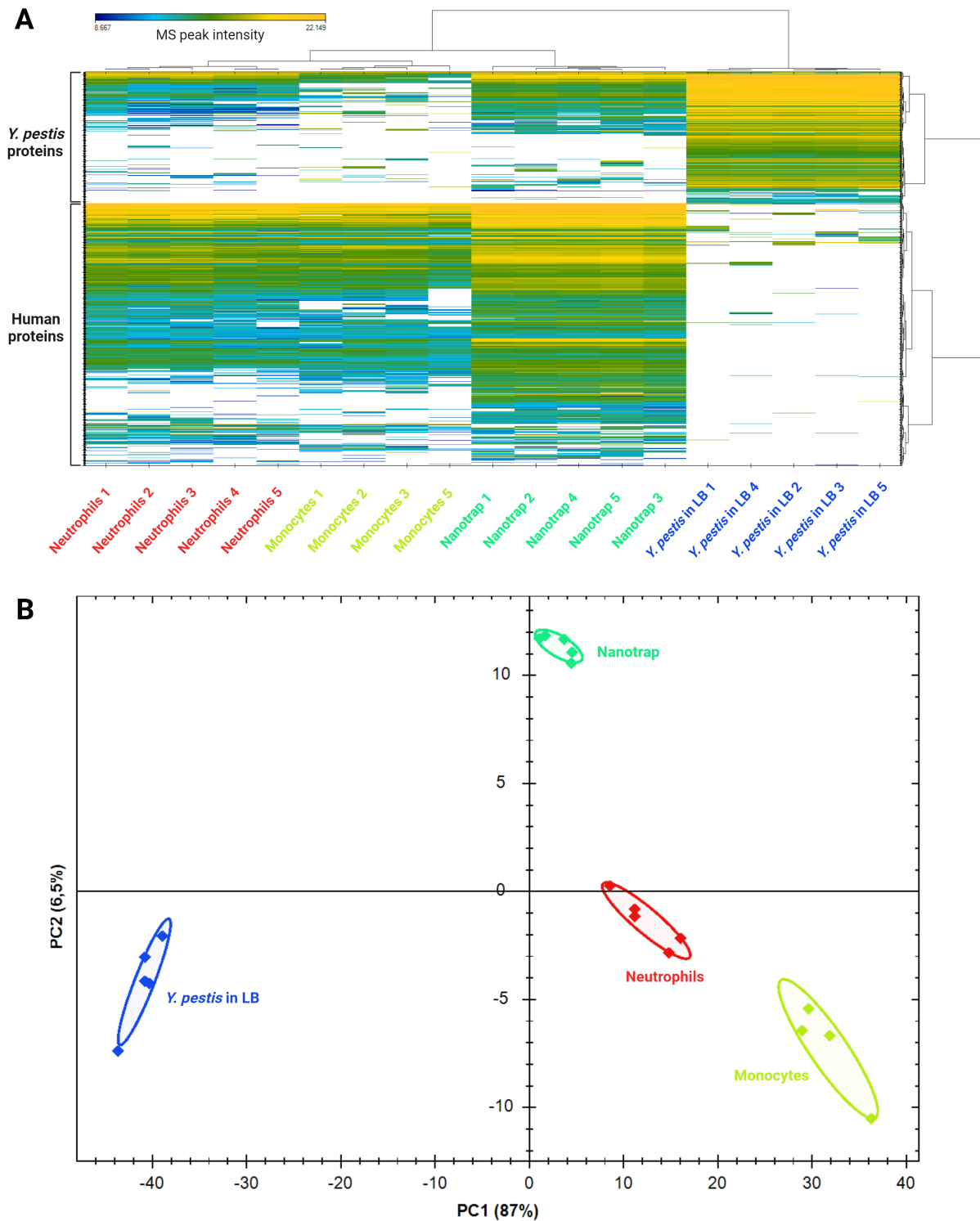


Figure 6. (A) Heatmap and (B) principal component analysis (PCA) based of the MS peak intensities for the bacterial and the human proteins on the neutrophil fraction, the monocyte fraction, the Nanotrap enrichment and the *Y. pestis* pure culture in LB. The replicate 4 of the monocyte fraction was removed due to a contamination with red blood cells during cell purification.

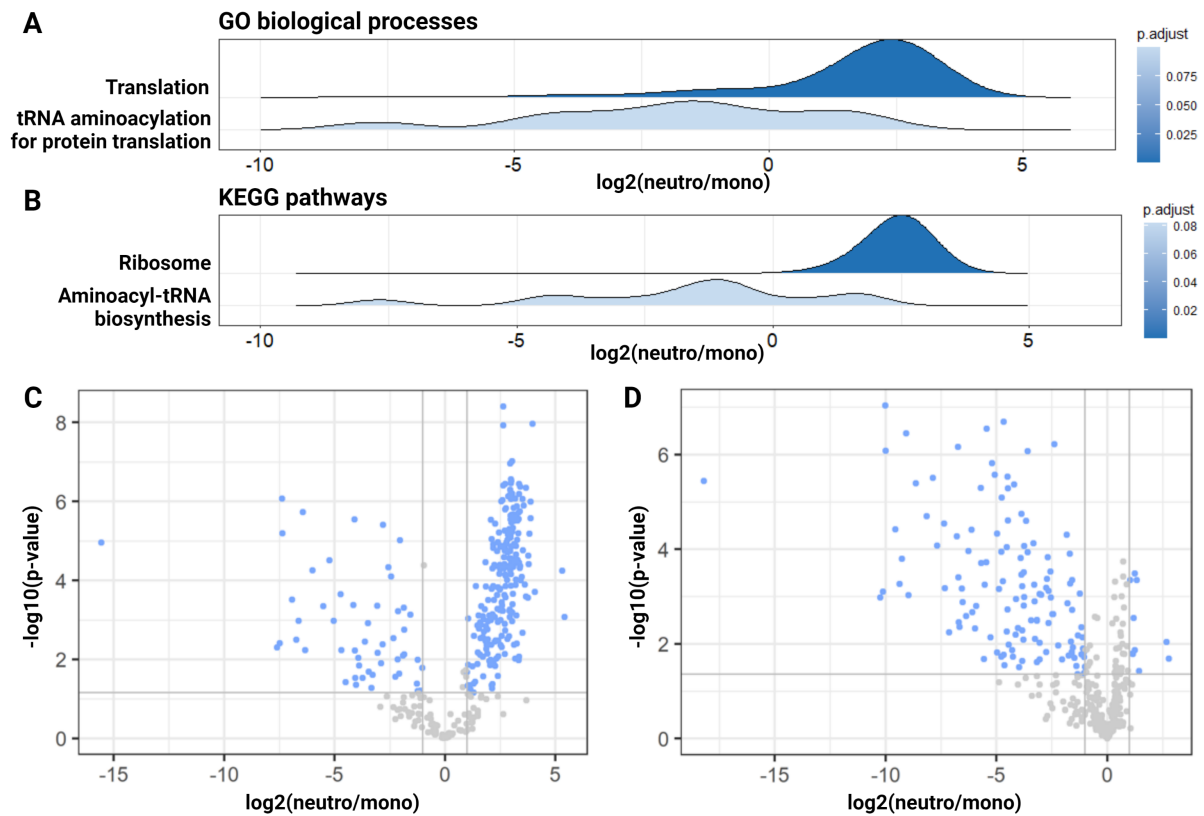


Figure 7. (A-B) Ridgeplots of enriched (A) GO biological processes or (B) KEGG pathways after performing a GSEA on *Y. pestis* protein differential abundances between the neutrophil and monocyte fractions using the A2 normalization strategy. The curve represent the density of proteins in the enriched terms depending on the fold change of these proteins. (C-D) Volcano plots showing differentially abundant *Y. pestis* protein between the neutrophil fraction and the monocyte fraction using (C) the Yc2 strategy and (D) the Ya2 strategy. In blue are the proteins which are significantly differentially expressed, considering a threshold of 1 for the absolute value of the $\log_2(\text{foldchange})$, and a value of 1% for the unadjusted p-value.

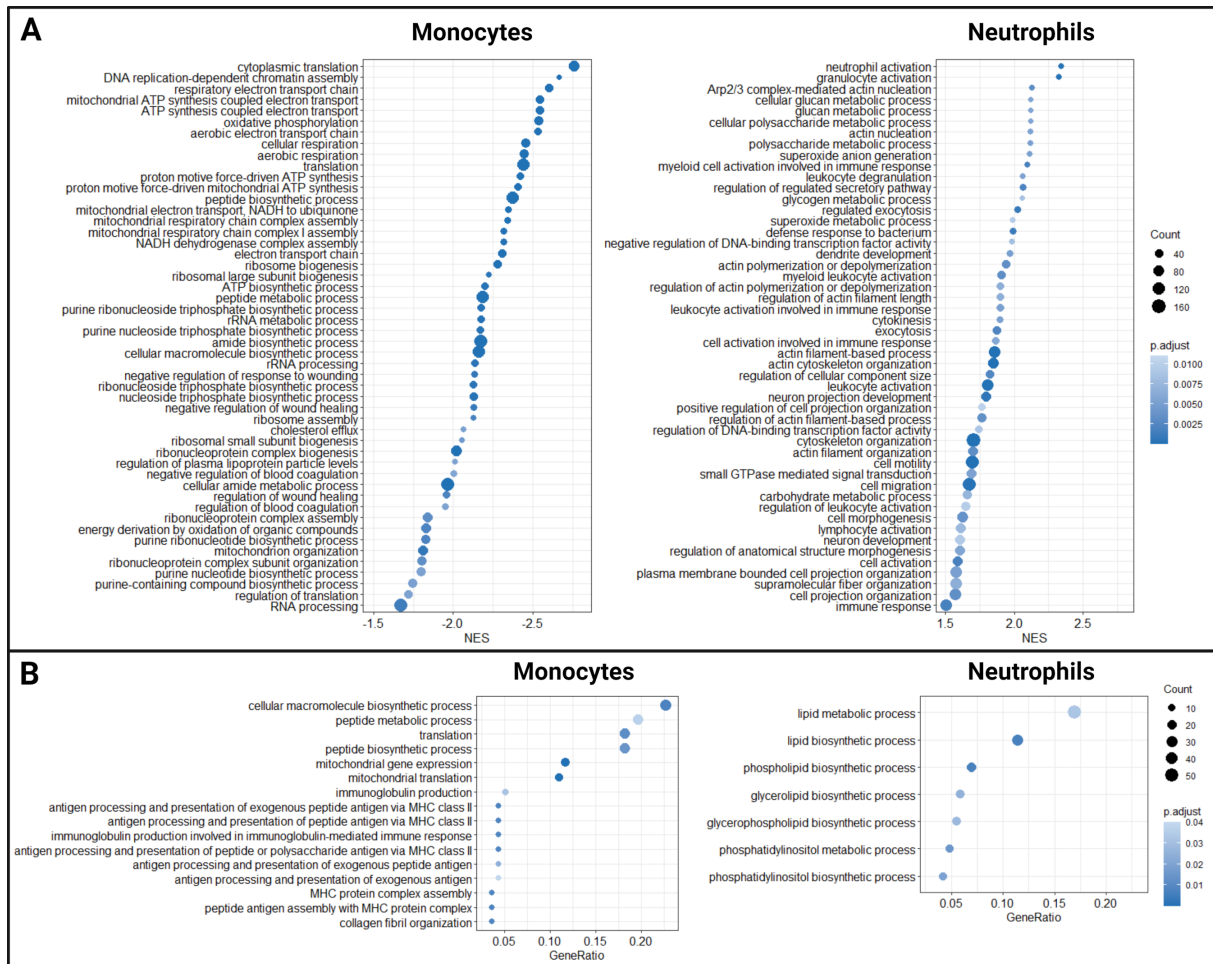
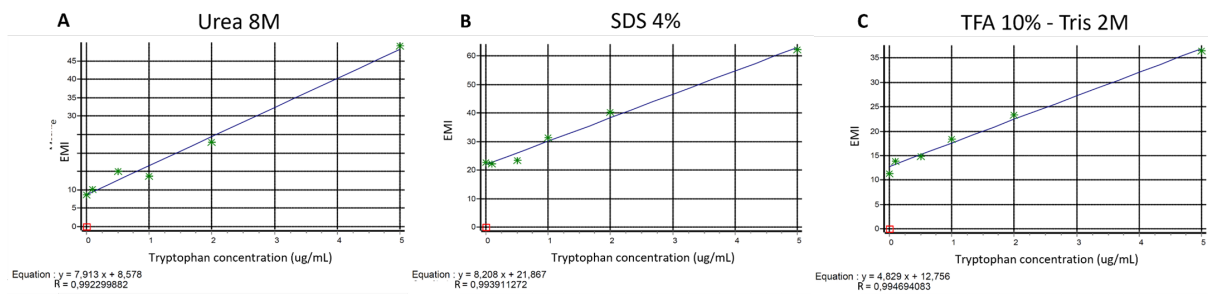


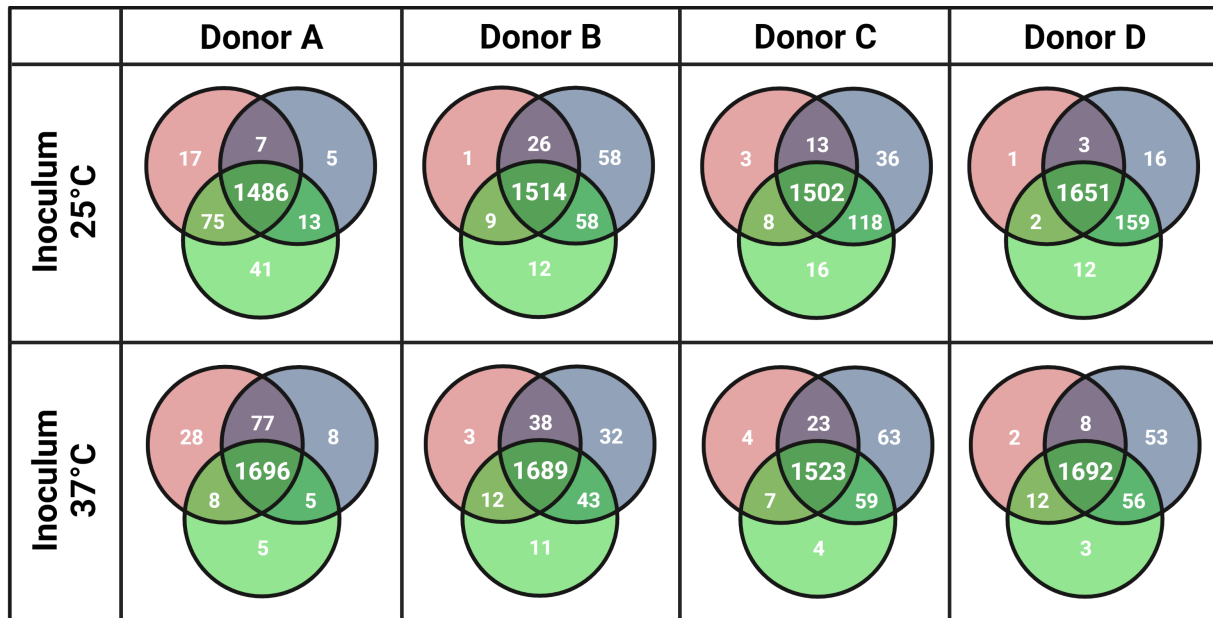
Figure 8. (A) Dotplots of enriched gene ontology (GO) biological processes after performing a gene set enrichment analysis (GSEA) on human protein differential abundances between the neutrophil and monocyte fractions using the H2 normalization strategy, with a focus on the 50 most enriched GO terms in monocytes (left) or in neutrophils (right). Data are ordered by normalized enrichment score (NES). (B) Dotplots of enriched GO biological processes after performing an enrichment analysis on human proteins only detected in monocytes (left) or in neutrophils (right) with the H normalization strategy. The dot size represents the number of proteins counted in this GO term. Terms are sorted by gene ratio. The dot color represents the adjusted p-value of the enriched GO term (control of the false discovery rate by the Benjamini-Hochberg correction).



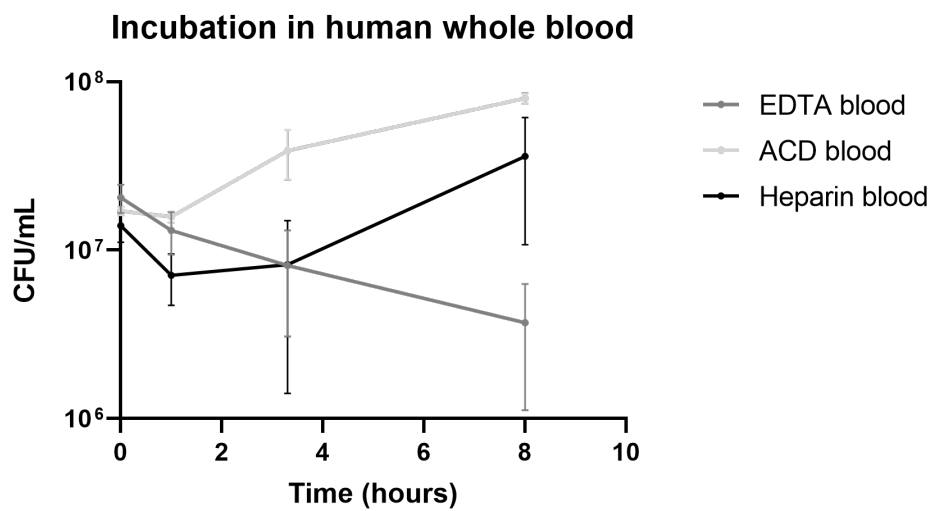
Expanded View Figure 1. Tryptophan standard measured by fluorescence (excitation: 280nm, emission: 360nm) in a plate reader for the three lysis buffer: (A) urea 8M, (B) SDS 4% and (C) TFA 10% - Tris 2M

A B	I25	I37	I25-M9	I37-M9	I25-Plasma	I37-Plasma
I25		86 175	94 166		63 182	
I37	194 229			63 154		37 123
I25-M9	246 273			38 46	40 150	
I37-M9		129 221	66 71			37 129
I25-Plasma	387 262		203 165			90 67
I37-Plasma		182 186		125 118	49 51	

Expanded View Figure 2. Differentially abundant protein and protein present and absent in the different comparisons. Each cell corresponds to the comparison A versus B (column versus row). In yellow are the number of proteins present in A and absent in B, in blue are the numbers of proteins present in both conditions and differentially more abundant in A versus B.



Expanded View Figure 3. Venn diagram of number of detected proteins in replicates after *Y. pestis* growth in different plasma donors.



Expanded View Figure 4. Incubation of *Y. pestis* CO92 in 2mL of whole blood anticoagulated with EDTA, ACD or heparin.

Tables

Table 1. Compatibility of Bradford, BCA, Qubit and tryptophan fluorescent assay with Urea 8M, SDS 4% and TFA 10% - Tris 2M lysis buffer for protein quantification.

		Extraction method		
		Urea 8M	SDS 4%	TFA 10% - Tris 2M
Measure method	Bradford	Compatible	Incompatible	Incompatible
	BCA	Incompatible	Compatible	Incompatible
	Qubit	Compatible	Incompatible	Incompatible
	Tryptophan fluorescence	Compatible	Compatible	Compatible

Table 2. Log₂(fold change) of protein abundance for proteins involved in metabolism and iron uptake. "15" states for proteins only detected in the first condition and "-15" for proteins only detected in the second condition. Protein in enriched terms are in bold.

Locus	Protein	Comparison				
		I25 vs I37	I37 vs I37-M9	I37 vs I37-Plasma	I25-M9 vs I25-Plasma	I37-M9 vs I37-Plasma
Purine biosynthesis						
YPO1636	PurB	0.8	-0.2	-0.5	0.4	-0.2
YPO1775	PurT	0.7	-1.3	-1.6	0.4	-0.2
YPO2387	PurR	0.1	-0.3	-0.5	0.3	-0.1
YPO2772	PurF	0.7	-1.2	-1.6	0.5	-0.3
YPO2828	PurM	1.3	-1.3	-1.3	0.4	0.0
YPO2829	PurN	0.9	-1.6	-1.0	0.8	0.6
YPO2870	GuaA	0.6	-0.1	-0.7	-0.2	-0.6
YPO2871	GuaB	0.7	-0.6	-0.6	-0.2	0.0
YPO2921	PurL	1.4	-1.9	-1.8	0.7	0.0
YPO3076	PurE	1.8	-2.5	-2.3	0.7	0.1
YPO3077	PurK	3.0	-4.3	-3.6	1.4	0.7
YPO3728	PurH	1.1	-1.6	-1.6	1.0	-0.1
YPO3729	PurD	0.9	-1.8	-1.5	1.0	0.2
Iron uptake and metabolism						
YPO0281	HmuT	2.3	-2.9	-3.3	0.0	-0.5
YPO0282	HmuS	0.7	-1.7	-1.1	0.6	0.6
YPO0283	HmuR	-0.9	-2.0	-2.3	-0.7	-0.3
YPO0955		1.9	-2.1	-2.2	1.4	-0.1
YPO0956		0.5	-1.8	-1.6	1.1	0.2
YPO1537		15.0	0.0	0.0	-5.3	0.0
YPO1753	FcuA	1.7	-2.1	-1.7	1.4	0.4
YPO1906	FyuA	-2.0	-0.7	-2.6	-1.3	-1.9
YPO1907	YbtE	-1.8	0.0	-2.2	-1.9	-2.1
YPO1908	YbtT	-1.6	-0.8	-3.0	-1.9	-2.2
YPO1909	YbtU	-1.7	0.2	-2.2	-2.1	-2.4
YPO1910	Irp1	-1.6	-0.2	-2.6	-1.8	-2.4
YPO1911	Irp2	-2.1	-0.2	-2.5	-1.8	-2.2
YPO1912	YbtA	0.0	0.0	-15.0	-1.1	-15.0
YPO1913	YbtP	-1.6	-0.8	-2.9	-1.2	-2.0
YPO1914	YbtQ	-3.0	-1.2	-3.4	-1.5	-2.3
YPO1916	YbtS	-2.6	0.3	-2.2	-2.0	-2.5
YPO1941		0.3	-0.5	-0.4	-0.1	0.1
YPO2439	YfeA	1.2	-1.0	-4.1	-2.7	-3.1
YPO2440	YfeB	0.5	-0.7	-2.6	-2.1	-1.9
YPO2650	NrdI	0.0	-2.2	-2.4	-2.3	-0.6
YPO2960	FbpC	0.3	-0.6	-0.5	-0.5	0.0
Tricarboxylic acid cycle						
YPO0348	AspA	-0.7	1.4	2.7	1.1	1.2
YPO0359		-1.6	0.9	1.5	0.0	0.6
YPO0897	SdhE	0.5	-0.9	0.0	0.6	0.9
YPO1108	GltA	-0.4	0.9	0.9	0.0	-0.1

YPO1109	SdhC	-1.2	15.0	15.0	0.0	0.0
YPO1110	SdhD	-0.3	15.0	15.0	0.0	0.0
YPO1111	SdhA	-0.7	0.9	1.6	1.1	0.7
YPO1113	SucA	-0.3	1.4	1.9	0.9	0.4
YPO1114	SucB	-0.3	0.9	1.1	0.7	0.2
YPO1115	SucC	0.1	0.8	1.2	0.8	0.4
YPO1116	SucD	-0.2	1.1	1.4	0.6	0.3
YPO1641	Icd	-0.1	0.9	0.5	0.1	-0.4
YPO2221	AcnA	-1.3	1.8	2.4	2.0	0.6
YPO2264	FumC	0.3	0.8	-0.3	-1.5	-1.0
YPO3415	AcnB	-0.3	1.1	1.7	1.1	0.6
YPO3418	AceF	0.2	-0.9	-0.1	0.7	0.8
YPO3419	AceE	-0.1	-0.7	0.1	0.6	0.7
YPO3724	AceK	1.7	2.3	6.2	-1.2	4.5
YPO3725	AceA	0.5	1.4	1.5	-0.8	0.1
YPO3726	AceB	1.1	1.7	0.9	-1.3	-0.8
Amino acid						
YPO0035	GltS	0.5	15.0	-0.8	0.0	0.0
YPO0584	SstT	0.8	15.0	-0.6	-0.1	-15.0
YPO1318	MetN2	1.2	15.0	15.0	0.0	0.0
YPO1321		0.5	15.0	-0.3	1.0	-15.0
YPO1846	TcyJ	-1.0	2.1	1.4	0.1	-0.6
YPO1853	PutP	0.7	15.0	15.0	0.0	0.0
YPO4110		-15.0	15.0	15.0	0.0	0.0
YPO4111		1.6	2.2	3.8	3.0	1.6
Methionine						
YPO0114	MetJ	-0.1	0.3	-0.9	0.3	-1.2
YPO0117	MetF	15.0	-15.0	-15.0	-4.1	-7.2
YPO0287		3.7	1.0	2.1	-0.7	1.1
YPO0681	MetC	0.6	0.6	0.0	-0.7	-0.5
YPO0931	MetK	0.5	0.1	-1.1	-0.4	-1.2
YPO1073	MetN	-0.2	-1.0	-1.7	-0.8	-0.7
YPO1522	MetG	0.2	0.4	0.1	0.2	-0.3
YPO3722	MetH	1.4	-0.1	1.9	0.6	2.0
YPO3727	MetA	0.3	-0.6	-5.1	-4.5	-4.5
YPO3788	MetE	-0.6	1.3	-2.0	-5.3	-3.3
YPO3789	MetR	0.0	0.0	-15.0	-3.9	-15.0
YPO3949	Asd	1.0	0.1	-0.6	-0.6	-0.7
Tryptophan						
YPO0157	TrpS	0.6	0.3	0.2	0.0	-0.1
YPO0169	PabA	1.2	-0.4	-2.1	0.0	-2.3
YPO0453	TrpR	-0.7	-1.9	-0.7	1.4	1.2
YPO1773	PabB	-0.3	-1.1	-0.5	1.0	0.6
YPO2203	TrpA	-0.2	-0.5	-0.1	0.9	0.5
YPO2204	TrpB	-0.4	-0.6	0.2	0.6	0.7
YPO2205	TrpCF	1.2	-2.5	-0.4	2.2	2.1
YPO2522	YbiB	0.5	0.7	-0.5	-0.5	-1.1

Table 3. Log₂(fold change) of protein abundance for proteins involved in the type 3 secretion system (T3SS). "15" states for proteins only detected in the first condition and "-15" for proteins only detected in the second condition.

Locus	Protein	Comparison				
		I25	I37	I37	I25-M9	I37-M9
		vs I37	vs I37-M9	vs I37-Plasma	vs I25-Plasma	vs I37-Plasma
YPCD1.05c	SycE	-6.6	-1.1	0.1	1.7	1.2
YPCD1.06	YopE	-7.7	-2.0	-0.1	2.8	1.9
YPCD1.19c	YopK	-15.0	-2.2	0.7	4.3	2.9
YPCD1.20	YopT	-15.0	-2.2	15.0	0.0	15.0
YPCD1.21	SycT	0.0	-15.0	0.0	0.0	15.0
YPCD1.26c	YopM	-15.0	-0.8	1.2	2.0	2.0
YPCD1.28c	YopD	-9.3	-1.3	0.8	2.5	2.2
YPCD1.29c	YopB	-15.0	-1.6	1.0	3.9	2.7
YPCD1.30c	LcrH	-15.0	-1.4	0.5	2.8	1.9
YPCD1.31c	LcrV	-8.5	-1.3	0.9	3.6	2.2
YPCD1.32c	LcrG	-9.2	-1.5	1.6	4.8	3.1
YPCD1.33c	LcrR	-15.0	-2.0	15.0	15.0	15.0
YPCD1.34c	LcrD	-15.0	-2.0	0.9	3.0	2.9
YPCD1.35c	YscY	-15.0	-1.7	1.4	3.0	3.1
YPCD1.36c	YscX	-15.0	-2.0	0.8	3.1	2.9
YPCD1.37c	SycN	-6.5	-2.5	0.0	2.7	2.5
YPCD1.38c	TyeA	-15.0	-1.6	0.3	2.7	1.9
YPCD1.39c	YopN	-15.0	-0.1	0.8	0.9	0.9
YPCD1.40	YscN	-15.0	-1.7	1.0	3.5	2.7
YPCD1.41	YscO	-15.0	-2.5	1.8	4.5	4.3
YPCD1.42	YscP	-15.0	-1.5	1.4	4.4	2.9
YPCD1.43	YscQ	-15.0	-0.9	1.3	2.7	2.2
YPCD1.44	YscR	0.0	-15.0	0.0	15.0	15.0
YPCD1.46	YscT	0.0	-15.0	0.0	15.0	15.0
YPCD1.47	YscU	-15.0	-2.2	1.0	3.2	3.2
YPCD1.48	YscW	-15.0	-0.8	-0.3	1.2	0.5
YPCD1.49	VirF	-15.0	-1.1	0.2	2.7	1.3
YPCD1.51	YscB	-9.2	-1.7	0.7	2.7	2.4
YPCD1.52	YscC	-15.0	-2.6	0.7	5.0	3.4
YPCD1.53	YscD	-15.0	-2.8	0.9	5.7	3.6
YPCD1.54	YscE	-4.0	-2.2	-0.2	2.6	2.0
YPCD1.55	YscF	-6.2	-2.5	0.3	3.7	2.8
YPCD1.56	YscG	-3.9	-2.3	-0.1	3.2	2.2
YPCD1.57	YopR	-15.0	-2.6	0.7	15.0	3.4
YPCD1.58	LcrO	-15.0	-3.7	1.6	15.0	5.1
YPCD1.59	YscJ	-15.0	-3.4	0.3	4.5	3.6
YPCD1.60	YscK	-6.4	-1.7	0.8	3.5	2.5
YPCD1.61	YscL	-15.0	-1.6	0.5	3.0	2.1
YPCD1.62	LcrQ	-3.5	-0.5	0.0	-1.4	0.5
YPCD1.67c	YopH	-5.2	-1.8	1.4	3.6	3.2
YPCD1.71c	YopJ	-15.0	-1.2	1.4	6.3	2.6
YPCD1.72c	YopO	-15.0	-0.6	1.0	2.1	1.5
YPCD1.95c	SycH	-1.5	1.0	0.5	-0.6	-0.5

Table 4. Value of \log_{10} (LFQ) for the *caf* operon encoding *Y. pestis* pseudocapsule. ND: Not Detected.

Protein	Sample					
	I25	I37	I25-M9	I25-Plasma	I37-M9	I37-Plasma
Caf1R	ND	8.52	ND	ND	7.69	8.35
Caf1M	ND	10.4	8.88	9.41	10.1	10.4
Caf1A	ND	9.66	8.14	8.41	9.43	9.70
Caf1	ND	10.1	8.98	9.26	10.5	10.0

Table 5. Number of bacterial proteins identified after the DIA analysis of the blood fractions, the Nanotrap enrichment and the pure culture in LB. The replicate 4 of the monocyte fraction was removed due to a contamination with red blood cells during cell purification.

	Sample				
	Neutrophils	Monocytes	Nanotrap	Pure culture	
Identified in	Replicate 1	944	440	1,215	2,280
	Replicate 2	992	532	1,223	2,270
	Replicate 3	939	483	1,146	2,275
	Replicate 4	844	N/A	1,162	2,270
	Replicate 5	784	277	1,306	2,279
	At least 1 replicate	1,366	877	1,681	2,335
	At least 2 replicates	1,011	446	1,346	2,326
	All replicates	575	148	857	2,176

Table 6. Normalization and differential analysis strategies for whole blood fraction analysis. The number of samples where the peptide were found (last column) was only taken into account during the differential analysis and not during normalization, which was based on all peptides. Yp: *Y. pestis*. Hsa: *Homo sapiens*. Spl: sample. Cond: biological condition (monocyte or neutrophil fraction).

Name	Description	Dataset	Median normalization	Normalized on	Protein found in at least
A	All	Hsa+Yp	on all spl	Hsa	1 spl
A2	All (2 spl)	Hsa+Yp	on all spl	Hsa	2 spl/cond
H	Hsa	Hsa	on all spl	Hsa	1 spl
H2	Hsa (2 spl)	Hsa	on all spl	Hsa	2 spl/cond
Ya	Yp all	Yp	on all spl	Yp	1 spl
Ya2	Yp all (2 spl)	Yp	on all spl	Yp	2 spl/cond
Yc	Yp by cond	Yp	by cond	Yp	1 spl
Yc2	Yp by cond (2 spl)	Yp	by cond	Yp	2 spl/cond

Table 7. Enrichment analysis of KEGG pathways for bacterial proteins with an absolute \log_2 (fold change) less than 1 between neutrophil and monocyte fraction after Ya or Ya2 normalization strategy.

KEGG ID	Description	Gene ratio	Background ratio	p-value	adjusted p-value
Ya normalization					
ype03010	Ribosome	47/142	54/557	7.3E ⁻²⁴	3.0E ⁻²²
ype01200	Carbon metabolism	26/142	65/557	4.5E ⁻³	6.3E ⁻²
ype00020	Citrate cycle	10/142	17/557	3.1E ⁻³	6.3E ⁻²
Ya2 normalization					
ype03010	Ribosome	46/121	50/229	3.4E ⁻¹¹	5.1E ⁻¹⁰

Table 8. Differential abundance of the pCD1 plasmid proteins between neutrophil and monocyte fractions, with Ya2 and A2 normalization strategies. \log_2 (fold change) less than -1 are represented in bold. T3SA: type 3 secretion apparatus.

Locus	Protein	Role	\log_2 (fold change) Norm. Ya2	\log_2 (fold change) Norm. A2
YPCD1.05c	YerA/SycE	regulator	-0.5	1.7
YPCD1.06	YopE	effector	-3.8	-1.6
YPCD1.19c	YopK	effector	-2.5	-0.3
YPCD1.26c	YopM	effector	-3.8	-1.6
YPCD1.28c	YopD	translocon	-4.1	-1.9
YPCD1.29c	YopB	translocon	-4.7	-2.5
YPCD1.30c	LcrH/SycD	chaperone	0.9	3.1
YPCD1.31c	LcrV	T3SA	0.9	3.1
YPCD1.32c	LcrG	regulator	0.2	2.4
YPCD1.34c	LcrD/YscV	T3SA	-9.3	-6.7
YPCD1.36c	YscX	secreted	-2.4	-0.3
YPCD1.39c	YopN	secreted regulator	-3.3	-1.1
YPCD1.40	YscN	T3SA	-0.1	1.9
YPCD1.42	YscP	T3SA	-9.0	-4.3
YPCD1.48	YscW	T3SA	-1.5	0.8
YPCD1.51	YscB	chaperone	-0.3	2.0
YPCD1.52	YscC	T3SA	0.4	2.6
YPCD1.54	YscE	T3SA	-0.4	1.8
YPCD1.55	YscF	T3SA	0.3	2.5
YPCD1.56	YscG	T3SA	-0.8	1.5
YPCD1.59	YscJ	T3SA	-0.7	1.2
YPCD1.61	YscL	T3SA	-0.9	1.2
YPCD1.67c	YopH	effector	-3.1	-0.9
YPCD1.71c	YopJ	effector	-4.5	-2.3
YPCD1.72c	YpkA/YopO	effector	-3.3	-1.1
YPCD1.73c		chaperone	-0.4	1.7

Chapter 6

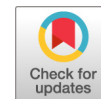
Yersiniomics, a multi-omics interactive database for *Yersinia* species

6.1 Objectives and summary

One of the main challenges emerging with the new omics technologies is the massive amount of data that are generated by different laboratories all over the world, as described in chapter 3. Worldwide repositories have been created to store experimental results, however most files are in a raw format, precluding research without bioinformatical knowledge to explore these data. The lack of a simple and centralized way to exploit these data led us to design Yersiniomics, a web-based platform allowing straightforward analysis of *Yersinia* omics data. Yersiniomics contains a curated multi-omics database at its core, gathering 200 genomic, 317 transcriptomic, and 62 proteomic data sets for *Yersinia* species. It integrates genomic, transcriptomic, and proteomic browsers, a genome viewer, and a heatmap viewer to navigate within genomes and experimental conditions. Based on previous publications, we designed an RNA-sequencing bioinformatical pipeline allowing a consistent analysis and display of all 26 public RNA-seq experiments encompassing 425 sequencing runs. For streamlined access to structural and functional properties, Yersiniomics directly links each gene to GenBank, the Kyoto Encyclopedia of Genes and Genomes (KEGG), UniProt, InterPro, IntAct, and the Search Tool for the Retrieval of Interacting Genes/Proteins (STRING), and each experiment to Gene Expression Omnibus (GEO), the European Nucleotide Archive (ENA), or the Proteomics Identifications Database (PRIDE). This platform also allowed us to explore and analyze data generated previously in our laboratory (chapter 5) in light of all the other published data sets.

6.2 Article

See next page.



Yersiniomics, a Multi-Omics Interactive Database for *Yersinia* Species

 Pierre Lê-Bury,^a Karen Druart,^b  Cyril Savin,^{a,e} Pierre Lechat,^c Guillem Mas Fiol,^a Mariette Matondo,^b Christophe Bécavin,^d  Olivier Dussurget,^a Javier Pizarro-Cerdá^{a,e}

^aInstitut Pasteur, Université Paris Cité, CNRS UMR6047, *Yersinia* Research Unit, Paris, France

^bInstitut Pasteur, Université Paris Cité, CNRS USR2000, Mass Spectrometry for Biology Unit, Proteomic Platform, Paris, France

^cInstitut Pasteur, Université Paris Cité, ALPS, Bioinformatic Hub, Paris, France

^dUniversité Côte d'Azur, CNRS, IPMC, Sophia-Antipolis, France

^eInstitut Pasteur, Université Paris Cité, *Yersinia* National Reference Laboratory, WHO Collaborating Research & Reference Centre for Plague FRA-140, Paris, France

ABSTRACT The genus *Yersinia* includes a large variety of nonpathogenic and life-threatening pathogenic bacteria, which cause a broad spectrum of diseases in humans and animals, such as plague, enteritis, Far East scarlet-like fever (FESLF), and enteric redmouth disease. Like most clinically relevant microorganisms, *Yersinia* spp. are currently subjected to intense multi-omics investigations whose numbers have increased extensively in recent years, generating massive amounts of data useful for diagnostic and therapeutic developments. The lack of a simple and centralized way to exploit these data led us to design Yersiniomics, a web-based platform allowing straightforward analysis of *Yersinia* omics data. Yersiniomics contains a curated multi-omics database at its core, gathering 200 genomic, 317 transcriptomic, and 62 proteomic data sets for *Yersinia* species. It integrates genomic, transcriptomic, and proteomic browsers, a genome viewer, and a heatmap viewer to navigate within genomes and experimental conditions. For streamlined access to structural and functional properties, it directly links each gene to GenBank, the Kyoto Encyclopedia of Genes and Genomes (KEGG), UniProt, InterPro, IntAct, and the Search Tool for the Retrieval of Interacting Genes/Proteins (STRING) and each experiment to Gene Expression Omnibus (GEO), the European Nucleotide Archive (ENA), or the Proteomics Identifications Database (PRIDE). Yersiniomics provides a powerful tool for microbiologists to assist with investigations ranging from specific gene studies to systems biology studies.

IMPORTANCE The expanding genus *Yersinia* is composed of multiple nonpathogenic species and a few pathogenic species, including the deadly etiologic agent of plague, *Yersinia pestis*. In 2 decades, the number of genomic, transcriptomic, and proteomic studies on *Yersinia* grew massively, delivering a wealth of data. We developed Yersiniomics, an interactive web-based platform, to centralize and analyze omics data sets on *Yersinia* species. The platform allows user-friendly navigation between genomic data, expression data, and experimental conditions. Yersiniomics will be a valuable tool to microbiologists.

KEYWORDS *Yersinia*, genome, transcriptome, proteome, database, RNA-Seq, mass spectrometry, microarray, multi-omics, synteny

The genus *Yersinia* comprises 26 Gram-negative bacterial species which belonged to the family *Enterobacteriaceae* until 2016 and which are now part of the new family *Yersiniaceae* (1). Although this genus includes mostly nonpathogenic environmental species, several important animal and human pathogens are also present in the group. *Yersinia enterocolitica* and *Yersinia pseudotuberculosis* are phylogenetically distant *Yersinia* species (2); however, the parallel acquisition of a diverse set of virulence factors (invasins, siderophores, and a type III secretion system) has endowed both species with the capacity

Editor Tino Polen, Forschungszentrum Jülich GmbH

Copyright © 2023 Lê-Bury et al. This is an open-access article distributed under the terms of the [Creative Commons Attribution 4.0 International license](https://creativecommons.org/licenses/by/4.0/).

Address correspondence to Javier Pizarro-Cerdá, javier.pizarro-cerda@pasteur.fr, or Olivier Dussurget, olivier.dussurget@pasteur.fr.

The authors declare no conflict of interest.

Received 17 October 2022

Accepted 26 January 2023

Published 27 February 2023

to invade the gastrointestinal tract of mammals and to cause enteritis, following an orofecal infectious cycle (3). Enteric yersiniosis is the third most reported bacterial foodborne zoonosis in Europe (4). In the United States, *Y. enterocolitica* is classified as a priority pathogen by the National Institutes of Health (NIH). In Africa, recent evidence indicates that *Y. enterocolitica* causes human digestive disorders with a frequency similar to that reported in other continents (5). *Yersinia pestis*, on the other hand, is a clone that recently emerged from *Y. pseudotuberculosis* (6) and acquired the capacity to infect fleas and to cause plague in humans through acquisition of novel virulence factors and massive gene inactivation (7). Plague is still endemic in the Americas, Africa, and Asia (8), and the major pneumonic plague outbreak in Madagascar in 2017 is a reminder that *Y. pestis* is a severe threat to human populations (9, 10). Two other animal pathogens, *Yersinia ruckeri* and *Yersinia entomophaga*, have the capacity to cause disease in fishes and insects, respectively (11, 12). *Y. ruckeri* is responsible for enteric redmouth disease, one of the most important disease of salmonids, which leads to significant economic losses (11). *Y. entomophaga* has a commercial interest for pest management, as it can infect and kill a wide range of insects (13).

Pathogenic *Yersinia* spp. have been instrumental models to understand the evolution and mechanisms of pathogenicity in the bacterial world. The invasin of *Y. pseudotuberculosis* was the first bacterial factor reported to promote bacterial internalization within mammalian nonphagocytic epithelial cells (14, 15). The subsequent identification of β 1 integrins as receptors for invasion (16) set the general basis to understand how bacterial surface effectors subvert mammalian cellular functions (phosphoinositide metabolism, Rho GTPase signaling, and actin polymerization) to invade host cells and tissues (17–20). The *Yersinia* type III secretion system was one of the first to be thoroughly characterized, making it possible to decipher the exquisite manipulation of phagocytic and immune functions by a bacterial pathogen through injection of bacterial effectors within the cytoplasm of host neutrophils, macrophages, and dendritic cells (21, 22).

Like several other important bacterial pathogens, members of the genus *Yersinia* have been investigated using omics approaches. In the last 2 decades, the ever-growing pace of technological innovation led to generation of a massive amount of data produced by omics methods, such as whole-genome sequencing combining short (such as Illumina sequencing) and long (such as PacBio or Nanopore sequencing) reads, DNA hybridization array (macro- and microarrays) for gene expression analysis, RNA sequencing (RNA-Seq), and semiquantitative mass spectrometry (Fourier-transform ion cyclotron resonance [FTICR-MS] and liquid chromatography-tandem mass spectrometry [LC-MS/MS]). Data type-specific databases allowing the deposition of these data have been created, e.g., GenBank (23) for genomes, Gene Expression Omnibus (24) and ArrayExpress (25) for microarrays, European Nucleotide Archive (26) and Sequence Read Archive (27) for RNA-Seq, and ProteomeXchange (28) for mass spectrometry. However, integration of these data in a genus- or species-dependent manner is currently restricted to a few model organisms (29–31), and pathogenic-microorganism-specific integrated data found in databases like PATRIC (32) have not been updated with recent experiments.

Here, we present a unique curated multi-omics database gathering 200 genomic, 317 transcriptomic, and 62 proteomic data sets originating from *Yersinia* spp. since the beginning of the omics revolution. This database was constructed using the Bacnet platform (33); we contributed to improvements of this platform. Indeed, with omics technologies evolving rapidly, new data formats, such as LC-MS/MS shotgun, which was absent from the first Bacnet-based website, were implemented (31). For several reference genomes, we implemented integrated views at the gene level of the Kyoto Encyclopedia of Genes and Genomes (KEGG) for biochemical pathways (34), UniProt for protein information (35), InterPro for protein domain signature (36), IntAct for molecular interactions (37) and the Search Tool for the Retrieval of Interacting Genes/Proteins (STRING) for protein interactions (38). Raw reads from 425 RNA-Seq runs were consistently processed and analyzed with our bioinformatic pipeline, and a quality control and differential analysis report is available for each experiment which

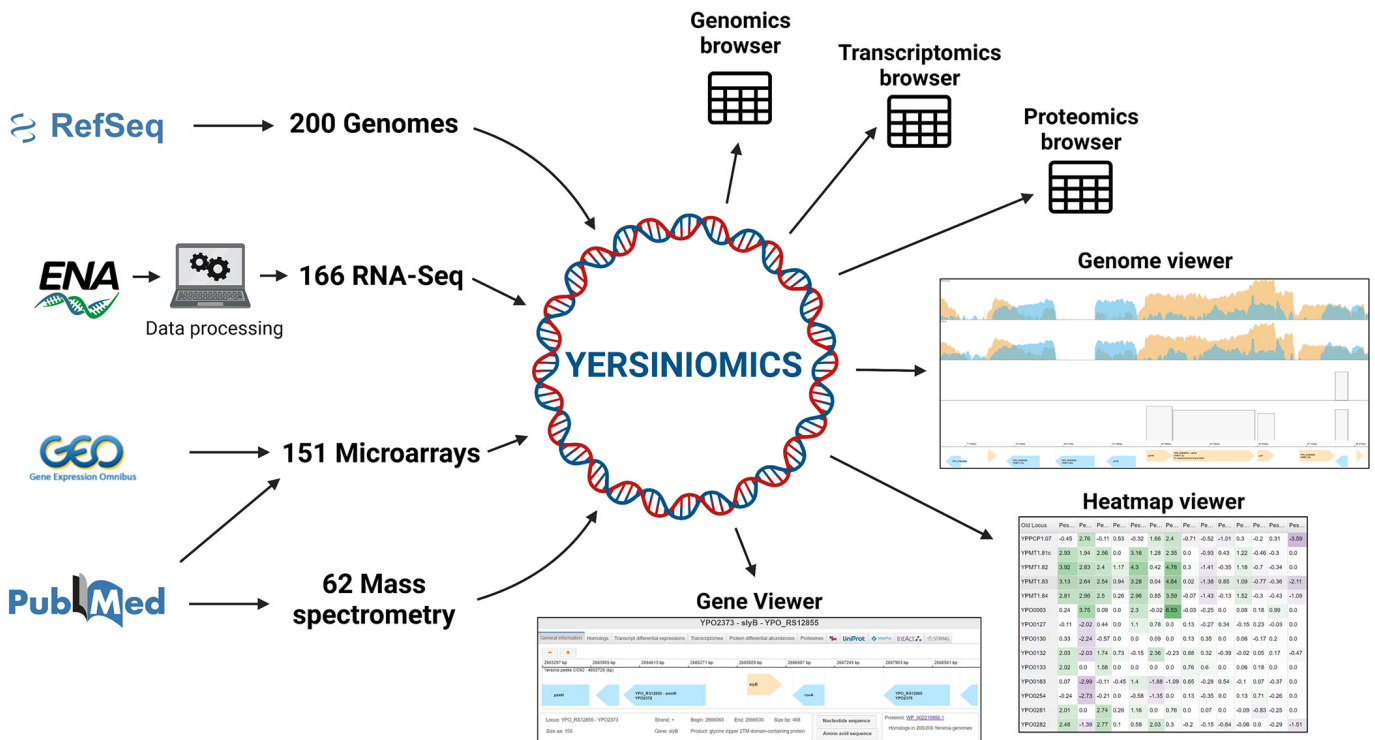


FIG 1 Yersiniomics database construction pipeline and tools. Genomes were collected on the RefSeq database (GenBank). RNA-Seq raw data (.fastq files) were collected on the ENA browser and then processed as read counts and fold change. Fold changes from microarray experiments were collected on GEO or from tables and supplemental tables in publications. Fold changes from proteomic experiments were collected from tables and supplemental tables in publications. Data sets were integrated into Yersiniomics and can be consulted via three omics browsers (genomics, transcriptomics, and proteomics) and three viewers (gene, genome, and heatmap).

encompassed replicates. Processed omics experiments are easily browsable, linked to their Gene Expression Omnibus (GEO) (24), European Nucleotide Archive (ENA) (26) or Proteomics Identifications Database (PRIDE) (39) repositories, and directly viewable at the gene level or according to experimental conditions on the dedicated Yersiniomics website that we have implemented (<https://yersiniomics.pasteur.fr/>).

RESULTS


From public databases, we collected genomic sequences, raw RNA-Seq data, microarray data, and mass spectrometry data that we processed and integrated into the Yersiniomics website (<https://yersiniomics.pasteur.fr/>). Yersiniomics relies on 6 principal tools (Fig. 1): (i) three omics browsers (“genomics,” “transcriptomics,” and “proteomics”) in a table format allowing navigation among the different genomes and biological conditions of the experiments implemented in the database; (ii) two omics data set viewers, called “genome viewer” and “heatmap viewer,” allowing navigation among transcriptomics and proteomics results; and (iii) a gene viewer allowing navigation among the genes of a specific genome, to quickly access associated entries in external databases and to browse associated omics data.

Database functionalities. (i) The omics data set browsers. From the Yersiniomics home page, three omics browsers are available: genomics, transcriptomics, and proteomics (Fig. 2, middle panel).

From the genomics browser, 200 complete *Yersinia* genomes are sorted according to their phylogenetic relatedness, based on the 500 genes of our recently proposed *Yersinia* core genome multilocus sequence typing (cgMLST) scheme (40) (Fig. 3). Displayed information related to genomes includes species name, the most recent assignment proposed by the French *Yersinia* National Reference Center and determined via our cgMLST, the number of chromosomes and plasmids, the chromosome and plasmid total size, the lineage and sublineage (when applicable) based on single nucleotide polymorphisms (SNP) analysis for

Downloaded from <https://journals.asm.org/journal/spectrum> on 13 April 2023 by 157.99.174.128.

Home



Yersiniomics integrates complete **genomes**, **transcriptomes** and **proteomes** published for *Yersinia* species.

Access **enriched information** about *Yersinia* species genes in complete genomes:
Annotation, gene conservation, synteny, transcript atlas, protein atlas, integration of external databases.

Use Yersiniomics to decipher **regulatory mechanisms** of your genome element of interest,
navigating among all these datasets with **enriched metadata** in a user-friendly format.

Gene viewersⁱ

<i>Y. pestis</i>			<i>Y. pseudotuberculosis</i>		<i>Y. enterocolitica</i>		<i>Y. ruckeri</i>	<i>Y. entomophaga</i>	
CO92	KIM	91001	YPIII	IP32953	8081	WA	SC09		
Pestoides F	EV76-CN		IP31758		Y1	Y11	QMA0440	MH96	

Omics browsersⁱ

Genomics browser Transcriptomics browser Proteomics browser

Data loadingⁱ

Load genome viewer Download processed data

Last update: January 2023

For more information on the website functionalities, please go to Lê-Bury et al.

If you use Yersiniomics, please cite our article

Contact us if you have a recently published "omics" dataset you want to be integrated to Yersiniomics:
yersiniomics@pasteur.fr

Credits
Yersinia Research Unit, Institut Pasteur, Paris




FIG 2 Yersiniomics home page. In the top panel, shortcuts to strain gene viewers of *Y. pestis*, *Y. pseudotuberculosis*, *Y. enterocolitica*, *Y. ruckeri*, and *Y. entomophaga* are implemented. In the middle panel, three buttons lead to the genomics, transcriptomics, and proteomics browsers. The bottom panel allows the user to load previously saved genome viewers and to download omics processed data.

Y. pestis (41, 42) and on our cgMLST (40) for the other *Yersinia* species, the biotype and serotype (when relevant), the isolation source, year and country, the number of genes, rRNAs, and tRNAs, and the assembly ID, linked to GenBank, and its FTP link. A specific genome can be opened in the gene viewer (see below) by double clicking on it, and several genomes can be selected to export a summary table. Genomes are highlighted in blue in the table when searched with the search box, and genomes selected in the table are highlighted in red on the phylogenetic tree displayed on the left, which can be exported in SVG format (Fig. 3).

The transcriptomics and proteomics browsers work in a similar way and summarize the biological conditions of transcriptomic and proteomic *Yersinia* experiments (Fig. 4). Biological condition names follow a nomenclature encompassing the main important information about each experiment: species name, strain name, whether it addresses a wild-type (WT) or a mutant strain (when applicable), culture temperature, culture medium/phase/time point (when applicable), other information relevant to comparisons (when applicable), the technology used, and the year of data deposition or publication. For example, "Pestis_KIM6+_WT_37C_HIB_pH6_NextSeq500_2021" refers to an

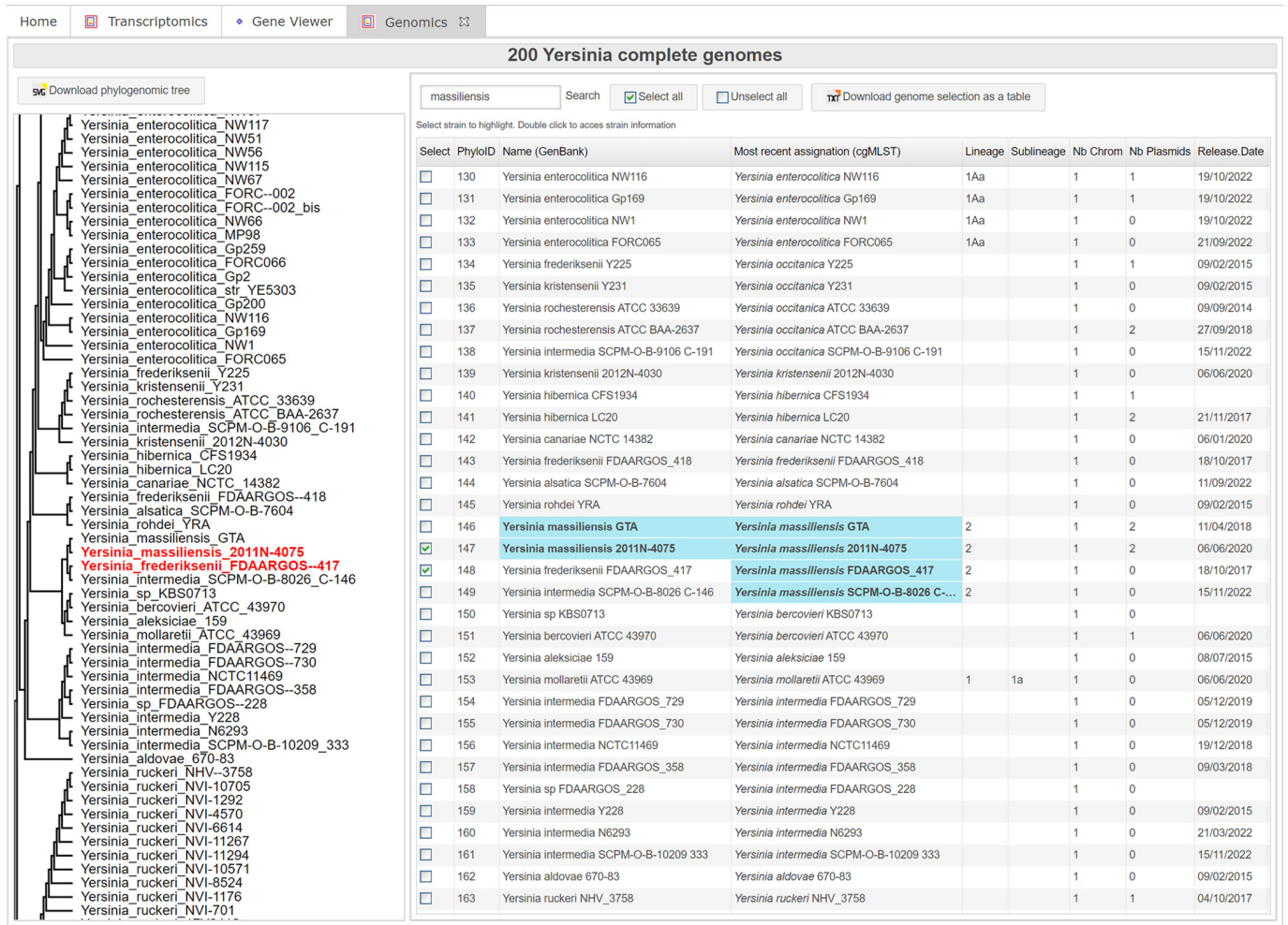


FIG 3 The genomics browser. A *Yersinia* phylogenetic tree is displayed on the left panel, and the strains information (name, lineage, isolate source, number of genes, etc.) is available on the right panel as a searchable table. Selected strains are automatically highlighted on the phylogenetic tree. An updated tree can be downloaded in SVG format.

RNA-Seq experiment using the Illumina NextSeq500 platform deposited in 2021 and measuring RNA levels of a *Y. pestis* KIM6+ strain grown at 37°C in heart infusion broth (HIB) at pH 6. “Pseudotuberculosis_YPIII_Mutant_rovA_25C_Log_Agilent_2014” refers to an experiment performed with an Agilent microarray in 2014 using a *Y. pseudotuberculosis* YPIII strain mutated at the *rovA* locus and grown at 25°C to logarithmic phase. Complementary information, such as details on the strain microarray, the genome on which the RNA-Seq experiment was mapped, the DESeq2 (43) differential analysis report for RNA-Seq data, the publication reference with a link to PubMed, and the link to the GEO (24), ENA (26), or PRIDE (39) entry, can be found in the table columns. A search bar can be used to explore the biological conditions of each experiment, and some filters are accessible, such as the reference genome used, the data type (“Gene Expression” for microarray experiments or “RNA-Seq”), as well as the selection of a specific mutant or growth phase. The proteomics browser also implements a “protein localization” column (i.e., supernatant, whole cell, or soluble or insoluble fraction), as well as the number of proteins detected in each experimental condition.

After selecting one or several biological conditions, their associated transcriptome or proteome values can be visualized in two ways: as a heatmap viewer or as a genome viewer. The heatmap viewer is a sortable table with each line corresponding to a gene in the genome and columns displaying expression comparisons of two biological conditions using a color code proportional to the fold change, facilitating tracking of highly differentially expressed genes. A log₂(fold change) cutoff, set to 1.5 by default,

Yersinia Transcriptomics Datasets

Select biological conditions and: Visualize their transcriptomics datasets with the Genome Viewer Visualize differently expressed genes and non-coding RNAs with the HeatMap Viewer

Select all Unselect all Download transcriptome selection as a table

Select	Data Name	Type	Date	Growth	TimePoint	Temp.	Mutant	Media
<input type="checkbox"/>	Enterocolitica_647176_Mutant_OAntigen_22C_Log_HiSeq2000_2015		04/03/2015	Logarithmic Phase		22	O-antigen-	LB
<input type="checkbox"/>	Enterocolitica_647176_Mutant_hfq_22C_Log_HiSeq2000_2015		04/03/2015	Logarithmic Phase		22	hfq-	LB
<input type="checkbox"/>	Enterocolitica_647176_Mutant_hfq_37C_Log_HiSeq2000_2015		04/03/2015	Logarithmic Phase		37	hfq-	LB
<input type="checkbox"/>	Enterocolitica_647176_Mutant_rfaH_22C_Log_HiSeq2000_2015		04/03/2015	Logarithmic Phase		22	rfaH-	LB
<input type="checkbox"/>	Enterocolitica_647176_Mutant_rfaH_37C_Log_HiSeq2000_2015		04/03/2015	Logarithmic Phase		37	rfaH-	LB
<input type="checkbox"/>	Enterocolitica_647176_Mutant_ybeY_22C_Log_HiSeq2000_2014		23/10/2014	Logarithmic Phase		22	ybeY-	LB
<input type="checkbox"/>	Enterocolitica_647176_Mutant_ybeY_37C_Log_HiSeq2000_2014		23/10/2014	Logarithmic Phase		37	ybeY-	LB
<input type="checkbox"/>	Enterocolitica_647176_WT_22C_Log_HiSeq2000_2015		04/03/2015	Logarithmic Phase		22		LB
<input type="checkbox"/>	Enterocolitica_647176_WT_37C_Log_HiSeq2000_2014		23/10/2014	Logarithmic Phase		37		LB
<input type="checkbox"/>	Enterocolitica_647176_WT_37C_Log_HiSeq2000_2015		04/03/2015	Logarithmic Phase		37		LB
<input type="checkbox"/>	Enterocolitica_8081_Mutant_yenR_26-37C_5h_SGUL_2008		17/11/2008		5h	26/37	yenR-	BHI-MOX
<input type="checkbox"/>	Enterocolitica_8081_Mutant_yenR_26C_8h_SGUL_2007		06/09/2007		8h	26	yenR-	LB
<input type="checkbox"/>	Enterocolitica_8081_Mutant_yenR_OverExpr_ytxR_26-37C_5h_SGUL_2008		17/11/2008		5h	26/37	yenR- ytxR+	BHI-MOX
<input type="checkbox"/>	Enterocolitica_8081_Mutant_yenR_rovA_26C_8h_SGUL_2007		06/09/2007		8h	26	yenR- rovA-	LB
<input type="checkbox"/>	Enterocolitica_8081_Mutant_yenR_ytxR_26C_SGUL_2008		17/11/2008		26	26	yenR- ytxR-	LB
<input type="checkbox"/>	Enterocolitica_8081_Mutant_yenR_ytxR_OverExpr_ytxR_26C_SGUL_2008		17/11/2008		26	26	yenR- ytxR- ytxR+	LB
<input type="checkbox"/>	Enterocolitica_8081_WT_25C_Log_LB_HiSeq2500_2019		17/03/2019	Logarithmic Phase		25		LB
<input type="checkbox"/>	Enterocolitica_8081_WT_25C_Stat_LB_HiSeq2500_2019		17/03/2019	Stationary Phase		25		LB
<input type="checkbox"/>	Enterocolitica_8081_WT_37C_Log_LB_HiSeq2500_2019		17/03/2019	Logarithmic Phase		37		LB
<input type="checkbox"/>	Enterocolitica_8081_WT_37C_Stat_LB_HiSeq2500_2019		17/03/2019	Stationary Phase		37		LB
<input type="checkbox"/>	Enterocolitica_8081_genome_Y1_WT_25C_Log_LB_HiSeq2500_2019		17/03/2019	Logarithmic Phase		25		LB
<input type="checkbox"/>	Enterocolitica_8081_genome_Y1_WT_25C_Stat_LB_HiSeq2500_2019		17/03/2019	Stationary Phase		25		LB
<input type="checkbox"/>	Enterocolitica_8081_genome_Y1_WT_37C_Log_LB_HiSeq2500_2019		17/03/2019	Logarithmic Phase		37		LB
<input type="checkbox"/>	Enterocolitica_8081_genome_Y1_WT_37C_Stat_LB_HiSeq2500_2019		17/03/2019	Stationary Phase		37		LB
<input type="checkbox"/>	Enterocolitica_ATCC23715_WT_26C_M63_Log_HiSeq2000_2020		03/06/2020	Logarithmic Phase		26	pYV-	M63
<input type="checkbox"/>	Enterocolitica_ATCC23715_mutant_rcsB_26C_M63_Log_HiSeq2000_2020		03/06/2020	Logarithmic Phase		26	pYV- rcsB-	M63
<input type="checkbox"/>	Enterocolitica_JB580v_WT_26C_120min_TYE_HiSeq2500_2015		20/04/2015		120min	26	pYV-	TYE
<input type="checkbox"/>	Enterocolitica_JB580v_WT_26C_240min_TYE_HiSeq2500_2015		20/04/2015		240min	26	pYV-	TYE
<input type="checkbox"/>	Enterocolitica_JB580v_WT_26C_30min_TYE_HiSeq2500_2015		20/04/2015		30min	26	pYV-	TYE
<input type="checkbox"/>	Enterocolitica_JB580v_WT_26C_60min_TYE_HiSeq2500_2015		20/04/2015		60min	26	pYV-	TYE
<input type="checkbox"/>	Enterocolitica_JB580v_WT_26C_Log_TYE_HiSeq2500_2015		20/04/2015	Log		26	pYV-	TYE

Gene expression array RNA-Seq and Ribo-Seq

FIG 4 The transcriptomics browser. Transcriptomics data sets are browsable in the main panel on the right and can be filtered through the search bar or with the preset filters on the left. Information on biological conditions, such as culture temperature, medium, growth stage, strain used, mutation, associated publication, and DESeq2 differential analysis report for RNA-Seq experiments, is accessible in the different columns of the table. After one or several lines are selected, the associated biological conditions can be viewed in the genome viewer or in the heatmap viewer by clicking on the buttons at the top.

can be set to any other value, or to 0 to display the whole genome. This view allows comparison of different results such as *Y. pestis* RNA abundance in infected C57BL/6 mouse lungs versus growth in brain heart infusion broth (BHI) (44), *Y. pestis* RNA abundance after growth in human plasma versus growth in lysogeny broth (LB) (45), and *Y. pestis* RNA abundance in infected brown Norway rat bubos versus growth in LB (46) (Fig. 5A).

The genome viewer (Fig. 5B and C) displays a value on the y axis (the number of mapped reads or the fold change in RNA or protein, for example) and corresponding genes on the x axis, allowing navigation of the genome. Depending on the data type, different information is plotted. For microarray experiments where only biological condition comparisons are available, fold change between two conditions is plotted as “relative expression data.” For RNA-Seq experiments, stranded or unstranded read coverage is plotted as “absolute expression data” (Fig. 5C) and fold changes can be plotted as “relative expression data.” For proteomics data, both relative and absolute (intensity; Fig. 5C) expression data can be plotted if available. A multi-omics view of different comparisons can be plotted this way, such as infected brown Norway rat bubos versus growth in LB (46), *Y. pestis* RNA abundance in infected C57BL/6 mouse lungs versus growth in BHI (44), and infected human plasma versus growth in LB (45) (Fig. 5B). A

A

Genome locus	Old Locus	Description	Pestis_CO92_WT_Lungs_...	Pestis_CO92_Plasma_...	Pestis_195P_WT_Rat_Bubo_...	Note	Begin	End	Length	Strand
YPO_RS10505	YPO1905		0.0	0.29	0.0	hypothetical protein	2139040	2139474	435	-
YPO_RS10510			0.0	0.0	0.0	hypothetical protein	2139617	2139967	351	-
YPO_RS10515	YPO1906	fyuA	1.21	1.31	7.49	siderophore yersiniabactin receptor FyuA	2140840	2142861	2022	-
YPO_RS10520	YPO1907	ybtE	1.47	1.02	7.37	yersiniabactin biosynthesis salicyl-AMP ligase YbtE	2142992	2144569	1578	-
YPO_RS10525	YPO1908	ybtT	1.43	1.57	7.51	yersiniabactin biosynthesis thioesterase YbtT	2144573	2145310	738	-
YPO_RS10530	YPO1909	ybtU	0.0	1.55	7.48	yersiniabactin biosynthesis oxidoreductase YbtU	2145373	2146473	1101	-
YPO_RS10535	YPO1910	irp1	1.4	0.37	15.0	yersiniabactin polyketide synthase HMWP1	2146470	2155961	9492	-
YPO_RS10540	YPO1911	irp2	1.09	2.83	7.62	yersiniabactin non-ribosomal peptide synthetase HMWP2	2156049	2162156	6108	-
YPO_RS10545	YPO1912	ybtA	0.0	0.53	4.59	yersiniabactin transcriptional regulator YbtA	2162347	2163306	960	-
YPO_RS10550	YPO1913	ybtP	1.74	2.01	15.0	yersiniabactin ABC transporter ATP-binding/permease protein YbtP	2163563	2165275	1713	+
YPO_RS10555	YPO1914	ybtQ	2.08	0.85	15.0	yersiniabactin ABC transporter ATP-binding/permease protein YbtQ	2165262	2167064	1803	+
YPO_RS10560	YPO1915	ybtX	1.64	1.52	6.61	yersiniabactin-associated zinc MFS transporter YbtX	2167057	2168337	1281	+
YPO_RS10565	YPO1916	ybtS	1.97	2.07	7.8	yersiniabactin biosynthesis salicylate synthase YbtS	2168365	2169669	1305	+
YPO_RS10570	YPO1917		0.0	0.0	-15.0	tyrosine-type recombinase/integrase	2169863	2171125	1263	-
YPO_RS10575			0.0	0.0	0.0					
YPO_RS10580	YPO1918		0.0	0.1	0.0	molecular chaperone	2171665	2172405	741	-
YPO_RS10585	YPO1919		0.0	0.41	0.0	fimbrial protein	2172402	2173751	1350	-
YPO_RS10590	YPO1920		0.0	-0.1	0.0	fimbrial biogenesis outer membrane usher protein	2173767	2176331	2565	-
YPO_RS10595	YPO1921		0.0	-0.68	0.0	molecular chaperone	2176407	2177051	645	-

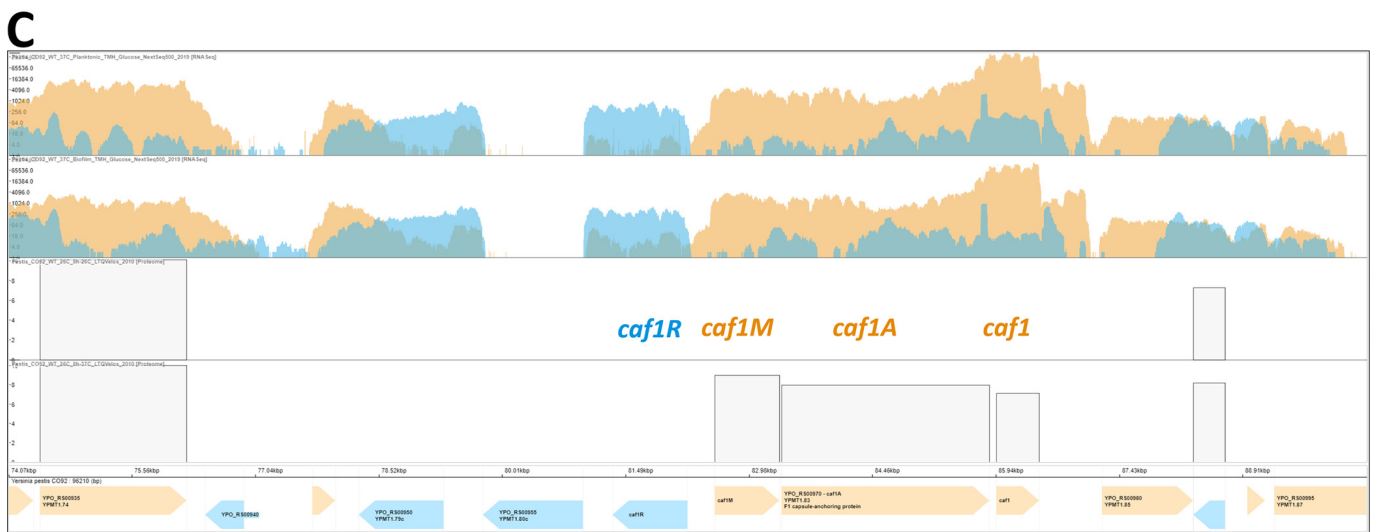
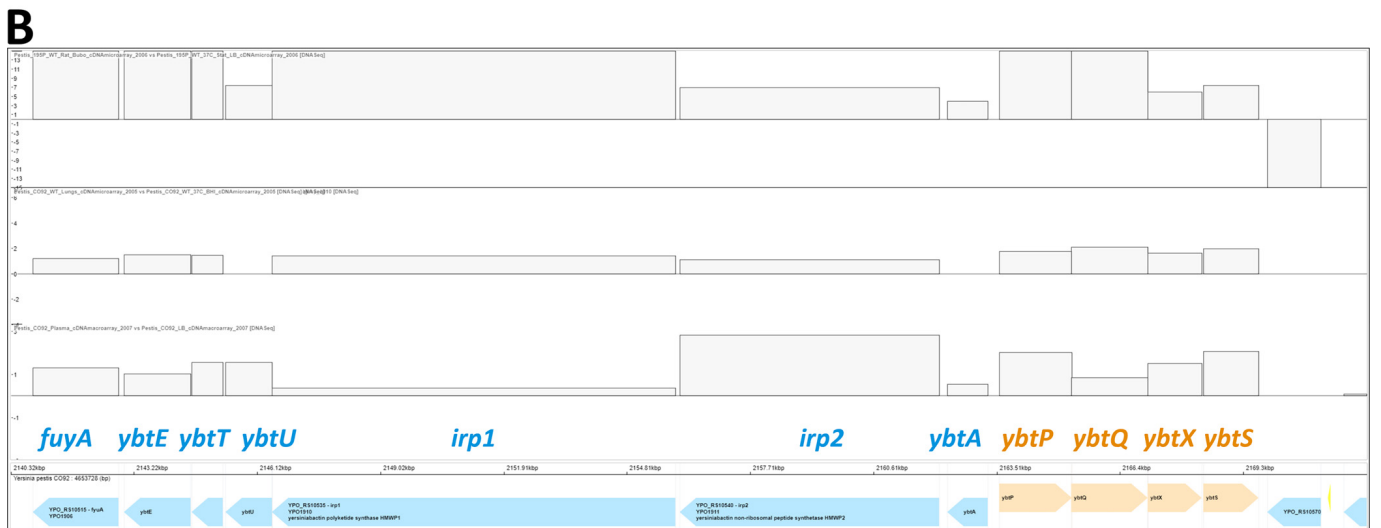


FIG 5 (A) Heatmap viewer. Heatmap view of the yersiniabactin siderophore *ybt* operon in the CO92 strain genome, displaying three *in vivo* and *ex vivo* experiments comparing (from left to right): *Y. pestis* RNA abundance in infected C57BL/6 mouse lungs versus growth in BHI (44), *Y. pestis* RNA abundance after growth in human plasma versus growth in LB (45), and *Y. pestis* RNA abundance in infected brown Norway rat bubos versus growth in LB (46). (B) Genome viewer. Multi-omics view showing the relative expression of the yersiniabactin siderophore *ybt* operon in the CO92 genome for the following (Continued on next page)

multi-omics view of absolute expression can also be plotted on this viewer, such as the two RNA-Seq stranded coverages, 37°C growth in planktonic and biofilm states in TMH medium supplemented with glucose (47), and LC-MS/MS data showing protein abundance after 8 h growth at 26°C or 37°C (48) (Fig. 5C). A specific view can be saved and downloaded in a .gview file with the “Save data selection” button. The .gview file can later be uploaded in a new session with the “Load data selection button” or from the home page.

For the 26 RNA-Seq experiments which included replicated samples, a quality control and differential analysis report is accessible from the transcriptomic browser in the “DESeq2 report” column. This column links to an interactive web page where different charts and tables make it possible to assess the overall quality of the experiment and bioinformatic pipeline. For example, the 36 *Y. pseudotuberculosis* YPIII samples generated by Avican et al. to create an RNA atlas of human pathogens exposed to different stresses can be examined (49). Mapped read counts are heterogenous between samples, but more than 2.5 million reads could be mapped for all runs except for the run [SRR11998801](#) (Fig. 6A). Based on the feature counts, hierarchical clustering and interactive three-dimensional (3D) principal-component analysis (Fig. 6B) showed a good clustering of sample replicates. Run [SRR11998801](#) differed from the two other replicates of the same condition. Interactive volcano plots allow rapid exploration of the up- and downregulated genes in every computed comparison within the same experiment, such as the bile acid stress condition versus untreated condition YPIII (Fig. 6C). Sortable tables, which can also be filtered by locus name or gene name, allow further exploration of regulations, and the processed data can be downloaded in CSV format. We recommend using Mozilla Firefox to benefit from all the functionalities implemented in the RNA-Seq reports.

(ii) The gene viewer. From the home page, a quick access to the gene viewer for reference strains is implemented (Fig. 2, top). In the gene viewer, each gene is accessible via a gene list or a graphical view after a specific *Yersinia* genome is selected (Fig. 7). A search bar makes it possible to quickly filter the list by gene name, gene locus, or any field present in the “General information” panel as described below.

For a specific open reading frame (ORF), information such as gene locus, name, product, position, strand, and size (in base pairs and amino acids) can be found under the “General information” panel. A link to the GenBank protein and the number of genomes presenting a homolog in the Yersiniomics database is also present, in addition to the graphical view presenting the genetic environment of the gene. Other general information extracted from the “features” field of the GenBank GFF file is also displayed. A synteny based on the SynTView software (50) was also implemented for some reference genomes: *Y. pestis* CO92 and KIM, *Y. pseudotuberculosis* IP32953 and YPIII, and *Y. enterocolitica* Y11 and 8081 (Table 1). As synteny data are heavy to download and the SynTView software requires a significant amount of memory and computational power, loading is optional and conditioned to the “Show synteny” button in the “General information” panel. After the loading of SynTView, the software displays the beginning of the genome. When clicking on or searching a gene in the Yersiniomics gene viewer panel, SynTView automatically centers on the corresponding gene. The software allows the user to browse the genetic environment and conservation of each gene among other closely related genomes present in Yersiniomics. SynTView allows the user to explore syntenic organization and dynamically zoom in on a position by genomic location or go directly to specific genes by name. The view is linked with dynamic interactions with other specialized views (circular view and dot plot).

FIG 5 Legend (Continued)

conditions (from top to bottom): infected brown Norway rat bubos versus growth in LB (46), *Y. pestis* RNA abundance in infected C57BL/6 mice lungs versus growth in BHI (44) and infected human plasma versus growth in LB (45). Induction of the yersiniabactin operon is observed both *in vivo* and *ex vivo*. (C) Genome viewer. Multi-omics view showing the absolute expression of the pseudocapsule *caf* operon in the CO92 pMT1 plasmid for the following conditions (from top to bottom): two RNA-Seq stranded coverages, growth at 37°C in planktonic and biofilm states in TMH medium supplemented with glucose (47), and LC-MS/MS data showing protein abundance after 8 h growth at 26°C or 37°C (48) where the *caf* operon is induced.

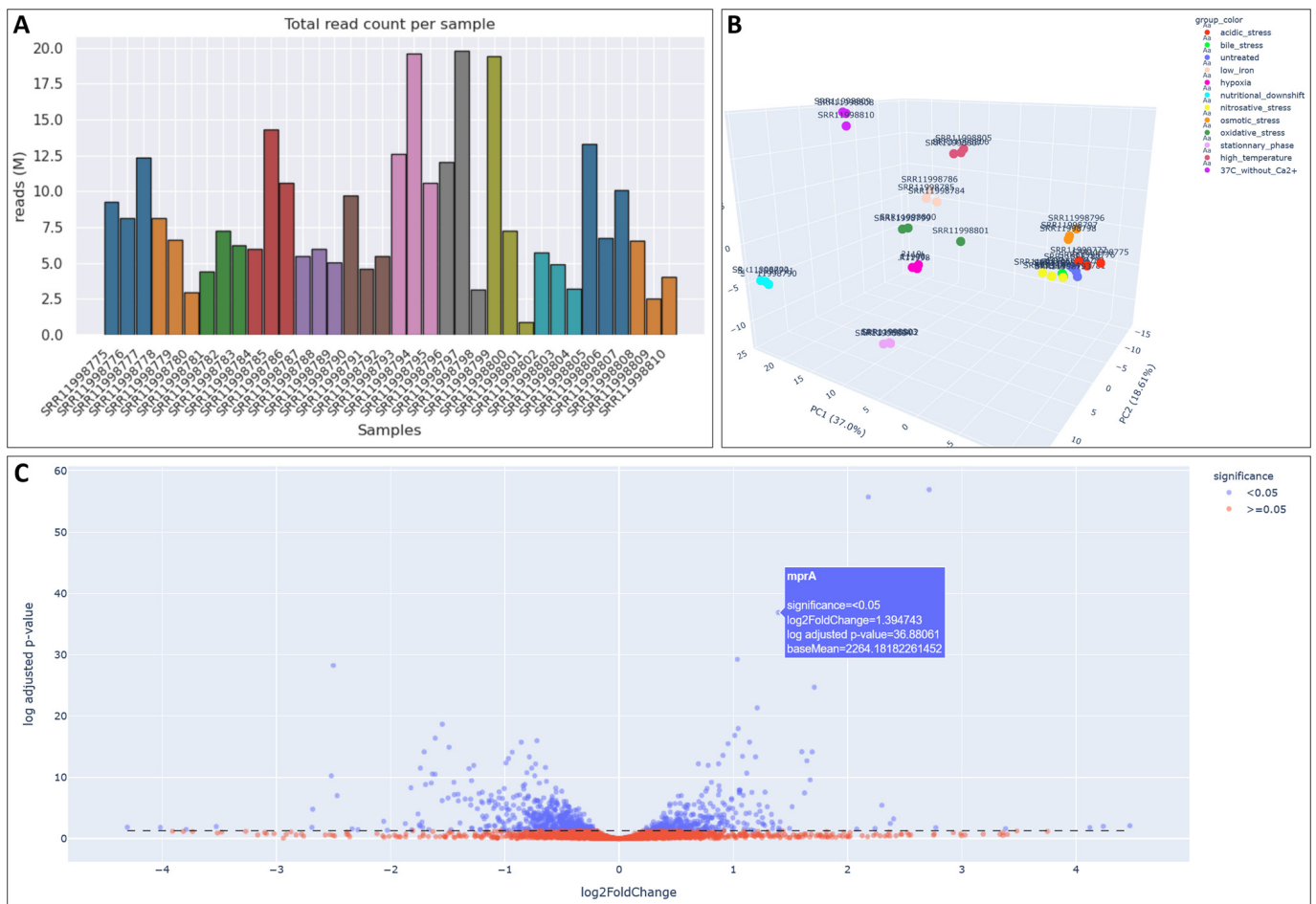


FIG 6 DESeq2 differential analysis report. (A) Mapped read counts of the 36 *Y. pseudotuberculosis* YPIII samples exposed to different stresses generated by Avican et al. (49). (B) Interactive 3D principal-component analysis based on mapped read counts showing good clustering between replicates among the 36 samples exposed to different stresses. (C) Interactive volcano plot of the bile acid stress condition versus untreated condition for the YPIII strain, allowing the user to rapidly explore the up- and downregulated genes.

The “Homologs” panel represents the 200 genomes present in the Yersiniomics database next to the phylogenetic tree (Fig. 8). For each genome, the homologous locus, old locus, and linked GenBank protein ID are displayed, next to the BLASTP results, such as the percentage of coverage and percentage of similarity on the covered region, or the BLAST E value and bit score. The “Bidirectional” column indicates if the best BLASTP hit of the homologous gene is reciprocal. Genomes are highlighted in blue in the table when searched with the search box, and genomes selected in the table are highlighted in red on the phylogenetic tree displayed on the left. The product of the percentage of coverage times the percentage of similarity is displayed alongside the gene locus in the phylogenetic tree, which can be exported in SVG format. The corresponding gene can be opened in its own gene viewer by double-clicking on its line in the homolog table, facilitating navigation between *Yersinia* homologs and access to their respective omics data.

For genomes presenting transcriptomic data sets such as microarray or RNA-Seq data, the panel “Transcript differential expressions” displays the fold change of the gene in each available transcriptome comparison (Fig. 9). These fold changes can be filtered with a cutoff to select over- or underexpressed genes over a certain threshold. A fold change of +15 or -15 corresponds to the absence of the transcript under one of the conditions. A fold change of exactly 0.0 indicates the absence of transcript under both conditions or that the information for this gene under these conditions could not be retrieved. For most of the RNA-Seq data, if replicates were measured, the *P* value

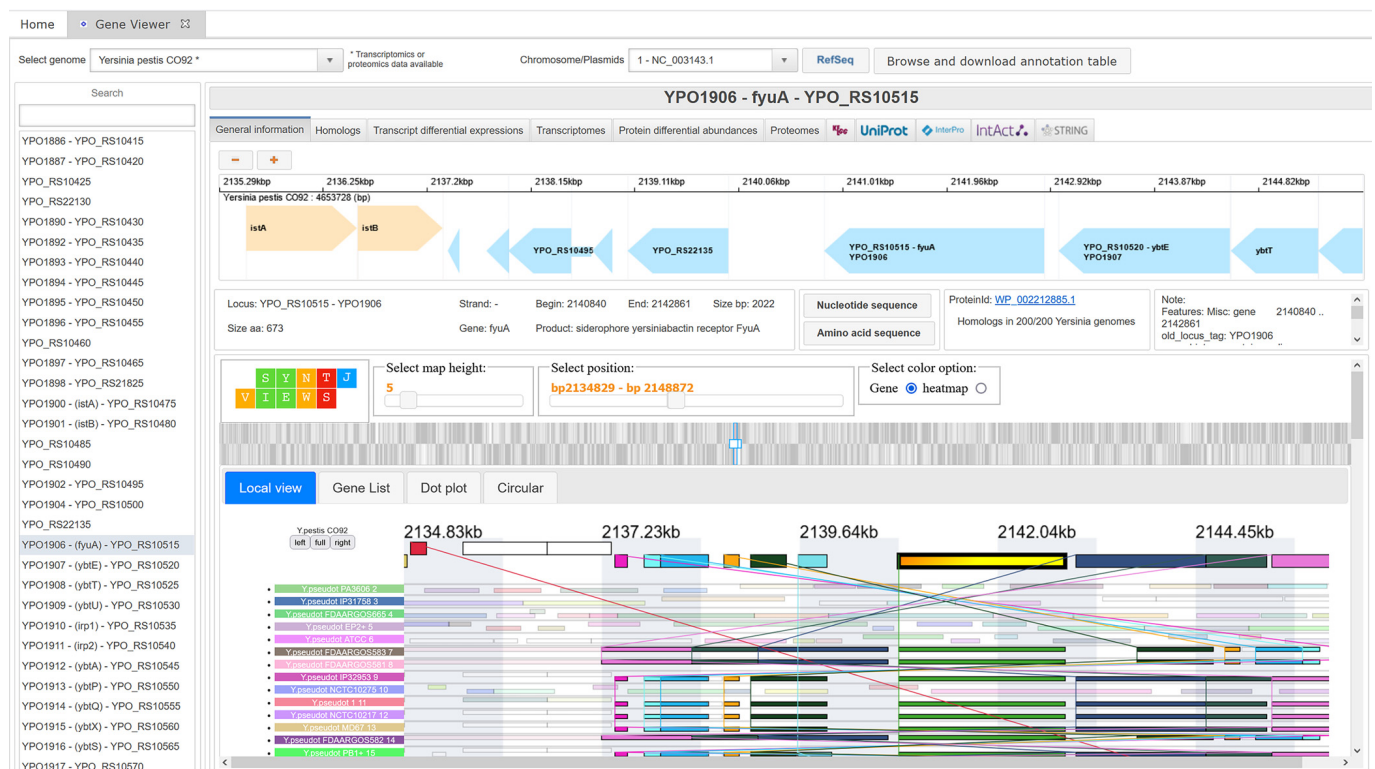


FIG 7 The gene viewer general information panel. Information about the *fyuA/psn* gene of *Yersinia pestis* CO92 (YPO1906) is displayed, such as the RefSeq new and old locus names, the length of the gene and protein, the gene position in the genome, and a graphical view of the surrounding genomic region. Nucleotide and amino acid sequences can be visualized and downloaded. A search bar to find other genes in the genome is available in the left column. A switch between the chromosome and the plasmids is available in the upper banner next to the “Chromosome/Plasmids” label. For several reference strains, synteny can be shown in the SynView software. Selection of a gene on the Yersiniomics gene viewer automatically searches for the corresponding gene in SynView. Genomes are aligned on the searched gene, which is shaded in yellow. Homologous genes are displayed with the same color. Genes of the reference genome can also be searched in the “Gene List” tab. Genome rearrangement between the reference and another genome can be visualized in the “Dot plot” tab. The “Circular” tab allows the user to map all the genomes on the reference genome on a circular plot.

and adjusted P value were computed and are displayed with the comparisons. The results can be filtered using a cutoff on the P value. For the microarray experiments and the RNA-Seq experiments without replicates, the P value and adjusted P value were set to 0.0 and the experiments cannot be filtered using the P value. Each comparison can be selected and displayed in two different ways, in the genome viewer or in the heatmap viewer, as detailed above. For RNA-Seq data, an additional panel called “Transcriptomes” displays the transcripts per million (TPM) normalized value (51) of the raw read counts mapped to the gene, allowing the user to assess whether the gene is highly transcribed.

For genomes presenting semiquantitative proteomic data, a similar panel called “Protein differential expressions” displays the fold change for the abundance of the gene-encoded protein in the available comparisons, very similarly to the “Transcript differential expressions” panel. The same customizable fold change cutoff is available, as well as the genome viewer and the heatmap viewer. A protein which is detected under one condition and not the other will also have a $\log_2(\text{fold change})$ set to +15 or –15. Experiments can also be filtered using the P value, and adjusted P values are shown next to the P value when present or set to 0.0 when they were not computed or not retrieved from publications. To assess for the presence of a protein in a semi-quantitative or nonquantitative proteomic experiment, the “Proteomes” panel displays the biological conditions in which the protein was detected, with its associated raw value (label-free quantitation [LFQ] or FTICR intensity) when available.

For several reference strains, dynamic access to KEGG, UniProt, InterPro, IntAct, and STRING was implemented at the gene level (Table 1). When a specific gene is selected, these tabs are automatically linked to the corresponding entries in each website. This

TABLE 1 Genomes with computed synteny and access to external databases^a

Strain	Synteny	KEGG, UniProt, InterPro	STRING
<i>Y. aldovae</i> 670-83		Yes	Yes
<i>Y. aleksiciae</i> 159		Yes	
<i>Y. alsatica</i> SCPM-O-B-7604		Yes	
<i>Y. canariae</i> NCTC 14382		Yes	
<i>Y. enterocolitica</i> 1055Rr		Yes	
<i>Y. enterocolitica</i> 2516-87		Yes	
<i>Y. enterocolitica</i> 8081	Yes	Yes	Yes
<i>Y. enterocolitica</i> FORC_002		Yes	
<i>Y. enterocolitica</i> WA		Yes	
<i>Y. enterocolitica</i> Y11	Yes	Yes	
<i>Y. enterocolitica</i> YE53/03		Yes	
<i>Y. entomophaga</i> MH96			Yes
<i>Y. hibernica</i> CFS1934		Yes	
<i>Y. hibernica</i> LC20		Yes	Yes
<i>Y. intermedia</i> Y228		Yes	Yes
<i>Y. massiliensis</i> GTA		Yes	Yes
<i>Y. mollaretii</i> ATCC 43969		Yes	Yes
<i>Y. occitanica</i> ATCC 33639			Yes
<i>Y. occitanica</i> Y225		Yes	
<i>Y. occitanica</i> Y231		Yes	
<i>Y. pestis</i> 91001		Yes	
<i>Y. pestis</i> A1122		Yes	
<i>Y. pestis</i> Angola		Yes	
<i>Y. pestis</i> Antiqua		Yes	
<i>Y. pestis</i> CO92	Yes	Yes	Yes
<i>Y. pestis</i> D106004		Yes	
<i>Y. pestis</i> D182038		Yes	
<i>Y. pestis</i> El Dorado		Yes	
<i>Y. pestis</i> Harbin 35		Yes	
<i>Y. pestis</i> Harbin 35bis		Yes	
<i>Y. pestis</i> KIM10+		Yes	Yes
<i>Y. pestis</i> KIM5	Yes	Yes	Yes
<i>Y. pestis</i> Nepal516		Yes	
<i>Y. pestis</i> PBM19		Yes	
<i>Y. pestis</i> Pestoides F		Yes	
<i>Y. pestis</i> Shasta		Yes	
<i>Y. pestis</i> Z176003		Yes	
<i>Y. pseudotuberculosis</i> 1		Yes	
<i>Y. pseudotuberculosis</i> ATCC 6904		Yes	Yes
<i>Y. pseudotuberculosis</i> EP2+		Yes	
<i>Y. pseudotuberculosis</i> IP31758		Yes	
<i>Y. pseudotuberculosis</i> IP32953	Yes	Yes	
<i>Y. pseudotuberculosis</i> IP32953bis		Yes	
<i>Y. pseudotuberculosis</i> MD67		Yes	
<i>Y. pseudotuberculosis</i> PA3606		Yes	
<i>Y. pseudotuberculosis</i> PB1+		Yes	
<i>Y. pseudotuberculosis</i> YPIII	Yes	Yes	
<i>Y. rohdei</i> YRA		Yes	Yes
<i>Y. ruckeri</i> Big Creek 74		Yes	
<i>Y. ruckeri</i> SC09			Yes
<i>Y. ruckeri</i> YRB		Yes	
<i>Y. similis</i> 228		Yes	

^aSpecies nomenclature proposed by the French *Yersinia* National Reference Center.

allows very quick access to diverse information, such as the implication in biological pathways in KEGG (Fig. 10A), the AlphaFold prediction structure in UniProt (Fig. 10C), the protein domains and Pfam families in InterPro, protein-interacting partners identified with methods such as a yeast two-hybrid screen against human proteins (52) accessible in IntAct (Fig. 10D), or other metalinks such as co-occurrence in abstract computed in the STRING database (Fig. 10B). A button allows the user to directly open the corresponding website in a new tab of the web browser. Due to cookie policies, we recommend using Mozilla Firefox to access the STRING tab embedded in Yersiniomics.

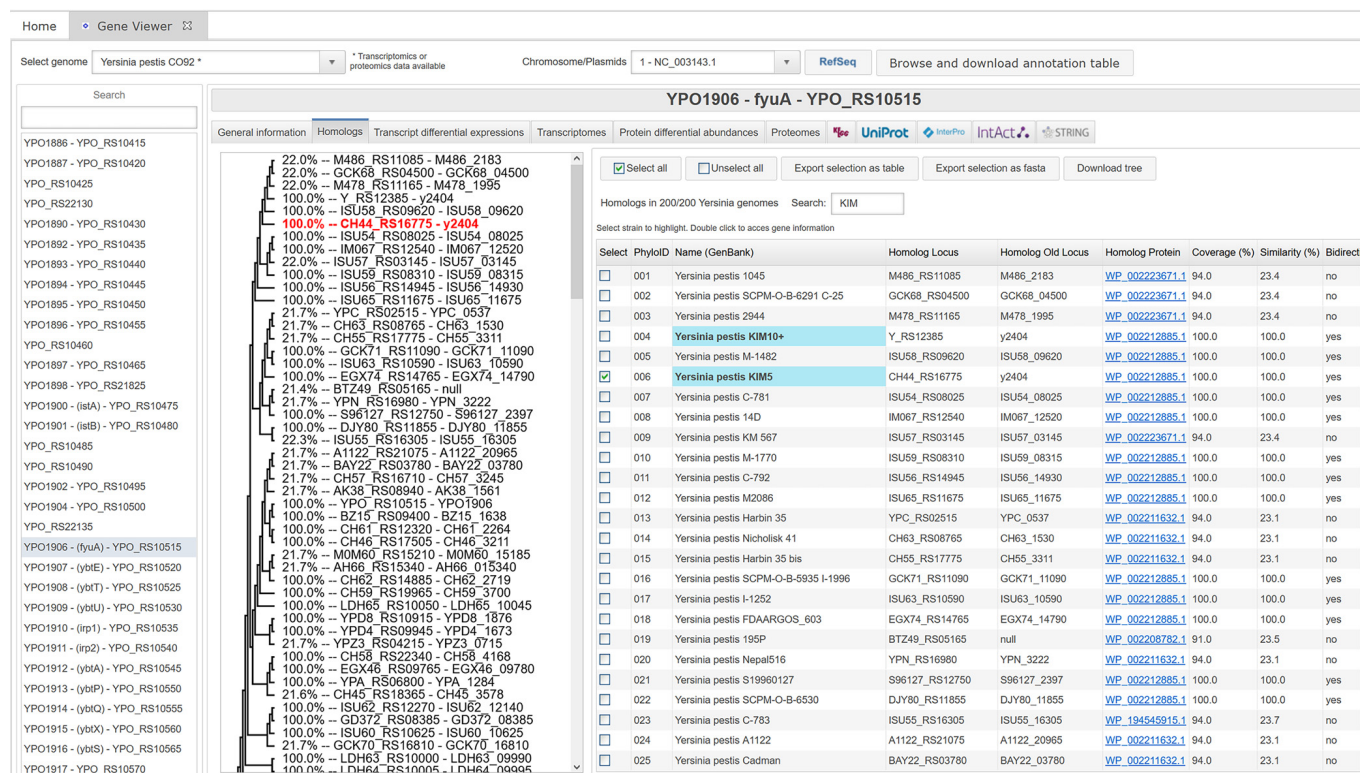


FIG 8 The gene viewer homolog panel. The table of the *fyuA* homologs in the Yersiniomics database is displayed on the right, with the gene locus, the BLASTP results (such as percent coverage and percent similarity on this coverage), the E value and bit score, and the name of the corresponding strain. The product of the percentage of similarity times the percent coverage, as well as the name of the homologous gene, are also displayed on the phylogenetic tree on the left and highlighted when selected. A multi-fasta protein file of the selected homologs can be downloaded.

Data loading. From the home page, two buttons allow the user to load a .gview file previously saved from the genome viewer and to download transcriptomics and proteomics processed data (Fig. 2, bottom panel). These data are sorted in the “Transcriptomes” and “Proteomes” directories, each one subdivided into strain-specific directories. Excel files showing genes in rows and biological conditions or comparisons of the selected strain in columns are available to download in each directory, i.e., \log_2 (fold change) table (Table_LOGFC_strain_name.excel), associated *P* value (Table_PVALUE_strain_name.excel), and associated adjusted *P* value (Table_PADJ_strain_name.excel) for the comparisons, TPM-normalized counts for RNA-Seq experiments (AllRNA-SeqTPM_strain_name.excel), and intensity values for proteomes (Table_Expr_strain_name.excel). The TPM-normalized count can then be used by each user to compare gene expression within the same sample or compute coexpression networks.

Genomic data set description. We collected 200 assemblies of *Yersinia* genomes, among which 10 were sequenced twice (annotated “bis”) by different laboratories with different technologies (such as Sanger or combination of Illumina and Nanopore or PacBio sequencing). Of the 190 unique genomes, we gathered 61 *Y. pestis*, 24 *Y. pseudotuberculosis*, and 37 *Y. enterocolitica* genomes. In addition, 37 strains of the fish pathogen *Y. ruckeri* were also collected, as well as one complete genome of the insect pathogen *Y. entomophaga* and 30 genomes of nonpathogenic *Yersinia* (Table 2).

In the genomics browser, the “Name (GenBank)” column refers to the GenBank taxonomic assignment, but particular attention should be drawn to the “Most recent assignment (cgMLST)” column, where 9 strains were reassigned by the cgMLST scheme developed in our laboratory (40).

Of note, the RefSeq-reannotated locus name, recognizable by its “..._RS...” pattern, was used to access the genes differing from the initial widely used locus name, such as “YPO...” for *Y. pestis* CO92 or “YPTB...” for *Y. pseudotuberculosis* IP32953. We added this previous name in a column named “Old Locus” in the heatmaps and this old

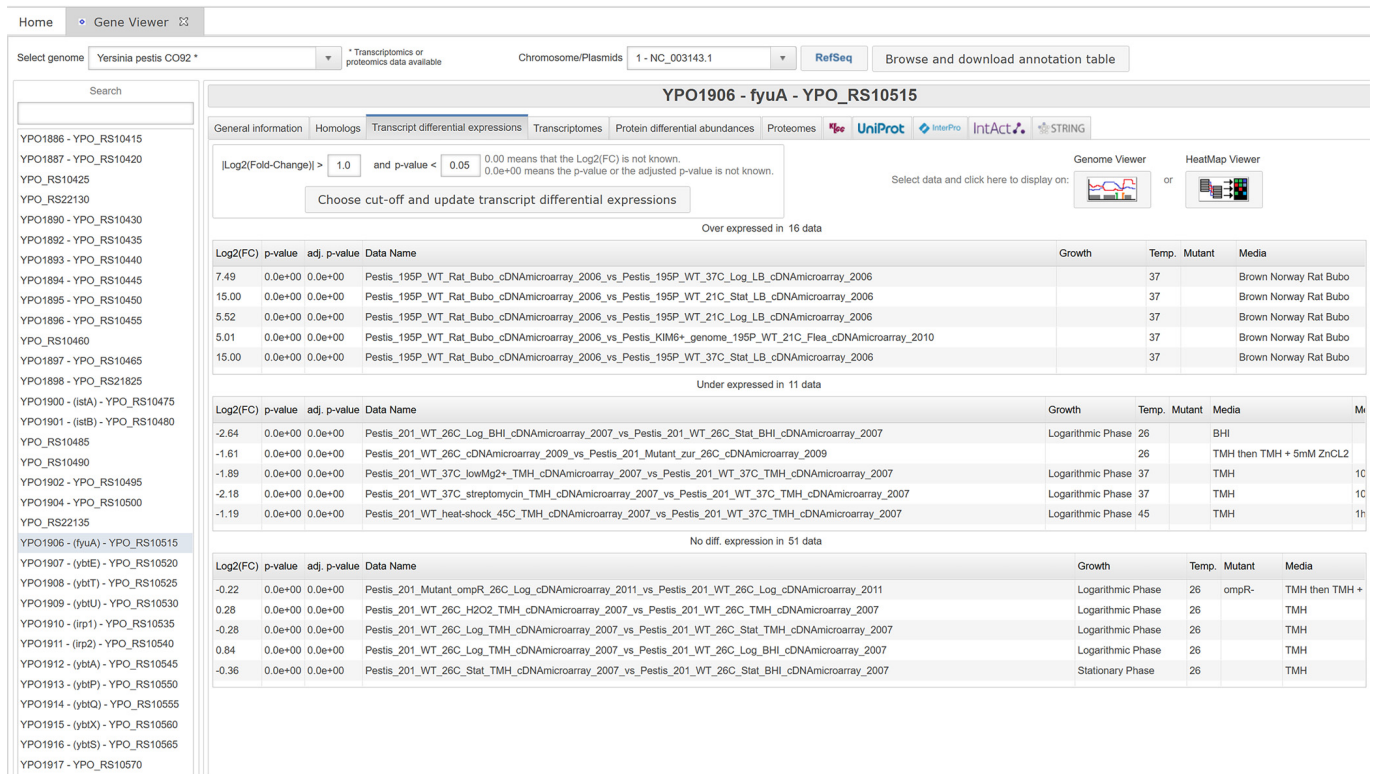


FIG 9 The gene viewer transcript differential expression panel. After selection of a log₂(fold change) cutoff, comparison of biological conditions is dispatched in three panels. For RNA-Seq experiments, results are also filtered by selecting a P value cutoff. The top panel shows upregulated conditions and corresponding fold change, P value, and adjusted P value. For example, *fyuA* expression is upregulated 180-fold in the rat compared to growth in LB at 37°C and upregulated 46-fold compared to growth in LB at 21°C. The middle panel shows downregulated conditions and the corresponding fold change. Expression of *fyuA* is decreased 6.2-fold in exponential phase compared to stationary phase in BHI at 26°C and decreased 4.5-fold in the presence of streptomycin at 37°C compared to the untreated condition. The lower panel displays condition comparisons in which fold change is below the selected cutoff and P value, when available. The conditions can be displayed with the genome viewer or the heatmap viewer via the two buttons on the top right.

locus is present after the RefSeq locus name in the gene list of a genome, separated by a dash, and followed by the gene name in parentheses. For example, the *mioC* gene in the CO92 genome can be found as “YPO_RS01005 - YPO0001 (mioC).”

The *Y. pestis* community widely uses the CO92 and KIM locus names to refer to genes, using the formats “YPO. . .” and “y. . .,” respectively. However, the KIM “y. . .” locus can be found only in the KIM10+ genome annotation in GenBank, a strain lacking several plasmids (pCD1/pYV and pPCP1/pPla) compared to its parental strain, KIM5. To map the RNA-Seq data to the most complete genome but conserve the known locus numbers widely used by the *Y. pestis* community, we reannotated the old locus of the KIM5 genome with the KIM10+ old locus using a systematic BLAST search between both genomes’ open reading frames.

Of note, the YPIII genome in GenBank lacks the pIB1 plasmid (the YPIII pYV virulence plasmid coding for a type III secretion system). Thus, this plasmid was not included in the database.

Transcriptomics data set description. Transcriptomic experiments were collected for *Yersinia* reference strains such as *Y. pestis* CO92, KIM, 91001, and Pestoides F, *Y. pseudotuberculosis* YPIII and IP32953, *Y. enterocolitica* 8081 and Y11, *Y. ruckeri* CSF007-82, and *Y. entomophaga* MH96 (Table 3). Of note, some strains’ data are mapped on genomes of other strains, such as *Y. pestis* 201 Microtus, whose microarray data were generated using CO92 microarray, or RNA-Seq data that were mapped to strain 91001 Microtus strain, as the strain 201 sequence is assembled only at the scaffold level. This is also the case for *Y. ruckeri* CSF007-82, whose complete assembled genomic sequence is not available, and RNA-Seq data were mapped to its genetically closest sequenced strain, QMA0440. We gathered 151 biological

TABLE 2 Numbers of complete *Yersinia* genomes^a

<i>Yersinia</i> species	No. of genomes	
	Unique complete	Sequenced twice
<i>Y. pestis</i>	61	6
<i>Y. enterocolitica</i>	37	1
<i>Y. ruckeri</i>	37	
<i>Y. pseudotuberculosis</i>	24	3
<i>Y. intermedia</i>	8	
<i>Y. occitanica</i>	5	
<i>Y. massiliensis</i>	4	
<i>Y. bercovieri</i>	2	
<i>Y. hibernica</i>	2	
<i>Y. aldovae</i>	1	
<i>Y. aleksiciae</i>	1	
<i>Y. alsatica</i>	1	
<i>Y. canariae</i>	1	
<i>Y. entomophaga</i>	1	
<i>Y. frederiksenii</i>	1	
<i>Y. kristensenii</i>	1	
<i>Y. mollaretii</i>	1	
<i>Y. rohdei</i>	1	
<i>Y. similis</i>	1	
Total	190	10

^aSpecies nomenclature proposed by the French *Yersinia* National Reference Center.

A summary of the 154 *Y. pestis* experiments can be found aggregated by culture temperature and strain (Table 4), culture medium and strain (Table 5), and genetic status and strain (Table 6).

Proteomic data set description. Many *Y. pestis* proteomes have been aggregated and processed by the Pacific Northwest National Laboratory (PNNL) to create a tool that differentiates naturally occurring and laboratory strains of *Y. pestis* (53), encompassing data from different studies (48, 54, 55) as well as PNNL archives (56). These processed intensity data sets were kindly shared by Eric D. Merkley. These data represent most of the 32 biological conditions which used whole-cell lysates of *Y. pestis* reference strain CO92 and were analyzed via shotgun LC-MS/MS using linear ion trap technologies and/or Orbitrap mass spectrometry for identification (Thermo Fisher LTQ XL/LTQ Velos). Proteomes also include 5 biological conditions from one study investigating *Y. pestis* Microtus strain 201 using Orbitrap LC-MS/MS technology (Thermo

TABLE 3 Number of omics biological conditions mapped to reference strains

Reference strain	No. of conditions		
	Microarray	RNA-Seq	Mass spectrometry
<i>Y. pestis</i> CO92	100	9	32
<i>Y. pestis</i> KIM	9	7	24
<i>Y. pestis</i> Microtus 91001		30	6
<i>Y. pestis</i> Pestoides F	8		
<i>Y. pestis</i> EV76		2	
<i>Y. pseudotuberculosis</i> YPIII	20	44	
<i>Y. pseudotuberculosis</i> IP32953		17	
<i>Y. pseudotuberculosis</i> PB1+	8		
<i>Y. enterocolitica</i> 8081	6	24	
<i>Y. enterocolitica</i> Y11		11	
<i>Y. enterocolitica</i> Y1		8	
<i>Y. ruckeri</i> SC09		4	
<i>Y. ruckeri</i> QMA0440		2	
<i>Y. entomophaga</i> MH96		8	
Total	151	166	62

TABLE 4 Number of *Y. pestis* transcriptomic experiments according to culture temperature and strain

Culture temp (°C)	<i>Y. pestis</i> strain used	No. of expts	
		Array	RNA-Seq
10	201	1	
21	195P	2	
	EV76		1
	KIM6+	5	
26	201	18	21
	CO92	4	
	Pestoides F	4	
28/37	CO92	4	
28	CO92	1	
	KIM5	4	
	KIM53	5	1
30	CO92	14	
37	195P	3	
	201	16	8
	CO92	18	9
	EV76		1
	GB	2	
	KIM53		4
	KIM6+		2
	Pestoides F	4	
45	201	1	
Multiple	201		1

Fisher QExact), the first and only study defining the *Y. pestis* secretome (57). In addition, 24 biological conditions from 2 studies focus on the *Y. pestis* strain KIM (12 in FTICR, 12 in 2D gel electrophoresis plus LC-MS/MS) and used cell fractionation to determine protein localization (58, 59) (Table 3).

Data set exploration and validation. One dual RNA-Seq experiment providing gene expression profiles in a murine pneumonic plague model did generate RNA-Seq raw data; however, gene content and differential expression were not analyzed. Our systematic processing pipeline allowed us to process and validate these data.

The *in vivo* experiment comparing transcripts of the *Y. pestis* KIM strain in OF1-infected mouse lungs versus HIB cultures confirmed most previous results described in the seminal microarray experiment in a pneumonic plague model that used the CO92 strain infecting C57BL/6 mice or grown in BHI (44): the methionine biosynthesis pathway genes *metA*, *metE*, *metF*, *metK*, and *metR* were among the most upregulated genes in the lungs in both studies. Similarly, the yersiniabactin operon (y2404 to y2394 in the KIM strain) was the most upregulated operon at 1 h, 24 h, and 48 h postinfection, highlighting the importance of metal acquisition by bacteria in their mammalian host. The pH 6 antigen *psaA* gene, encoding fimbriae required for virulence, was downregulated 48 h postinfection in both studies but was upregulated 1 h postinfection in the latter experiment. The cold shock-responsive gene *cspD* and genes involved in the detoxification of reactive oxygen species, such as *katA* and *katG* (*katY*), encoding catalases, and *sodB*, encoding superoxide dismutase, were downregulated in both studies, and nitric oxide-induced *hmpA* was even more upregulated in the experiment using the KIM strain than in the experiment based on the CO92 strain. However, the plasminogen activator *pla* was downregulated 24 h postinfection and not at 48 h postinfection in the study using the KIM strain, in contrast to the study using the CO92 strain. Similarly, *cspA1* and *cspA2* were upregulated in the lungs infected with the CO92 strain but downregulated in the study by Israeli et al. (60). Discrepancies between these results could be explained by differences in *Y. pestis* strains and mouse lines as well as culture conditions of bacteria *in vitro*.

TABLE 5 Number of *Y. pestis* transcriptomic experiments according to culture medium and strain

Culture medium ^a	<i>Y. pestis</i> strain used	No. of expts	
		Array	RNA-Seq
BAB broth	GB	2	
BHI	201	2	9
	CO92	7	1
Custom	CO92	8	
	Pestoides F	8	
DMEM	KIM5	1	
HIB	CO92	19	
	KIM53		2
	KIM6+		2
Human plasma	CO92	5	
LB	195P	4	
	201		2
	CO92	1	
	KIM6+	3	
Macrophages	CO92		2
	KIM5	3	
MHB	KIM53	5	
TMH	201	34	11
	CO92		6
<i>In vivo</i>	195P	1	
	201		2
	CO92	1	
	KIM53		3
Unknown	KIM6+	2	
	201		6
	EV76		2

^aBAB, blood agar base; DMEM, Dulbecco's modified Eagle medium; MHB, Mueller-Hinton broth.

DISCUSSION

Over the last 2 decades, the omics revolution has generated an impressive number of data sets which are often difficult to analyze in depth without any prior bioinformatic knowledge. In addition, only a fraction of generated and processed data is generally accessible and/or used in research articles. Here, we aimed at exploiting *Yersinia* omics data published over the last 20 years to make them accessible in a user-friendly way to biologists without familiarity with deep bioinformatics. We thus constructed and processed a database gathering 200 genomic, 317 transcriptomic, and 62 proteomic data sets of *Yersinia* species, which are browsable at the gene level and according to experimental conditions on the custom-made Yersiniomics website (<https://yersiniomics.pasteur.fr/>). Notably, three previous studies (60–62) did not measure differential gene expression under their biological conditions. These data were thus processed and included in Yersiniomics. One of these studies confirmed for the most part previous results obtained using a similar microarray approach. Other recent RNA-Seq studies did not make their raw sequencing data publicly available and could not be included in our database for now (63–66). To expand information on genes of interest, dynamic links to external databases were implemented for several reference strains, allowing the user to access KEGG pathways, UniProt annotation, InterPro domains, IntAct interactors and STRING networks at the gene level. These links also facilitate the access to other data, such as GO terms and AlphaFold structure predictions, implemented in UniProt.

As new data and data types continue to be published, we intend to update and upgrade the Yersiniomics database with newly published RNA-Seq and LC-MS/MS

TABLE 6 Number of *Y. pestis* transcriptomic experiment according to strain and genetic status

Strain used	Genetic status ^a	No. of expts	
		Array	RNA-Seq
195P	WT	5	
201	<i>cobB</i>		1
	<i>fur</i>	2	
	<i>fyuA</i>		2
	<i>fyuA</i> deletion GCA		2
	<i>hfq</i> pHfq		1
	<i>hfq</i> pHfq-FLAG		2
	<i>lcrG</i>	1	
	<i>ompR</i>	3	
	<i>oxyR</i>	1	
	pHfq-FLAG		1
	<i>phoP</i>	2	
	<i>rscB</i>		2
	<i>rscD</i> _{pestis} :: <i>rscD</i> _{pseudotb}		2
	WT pFLAG		3
	<i>yfiQ</i>		1
<i>zur</i>	1		
WT	26	13	
CO92	<i>crp</i> pCD1 ⁻		2
	pCD1 ⁻		4
	<i>pgm</i>	15	
	<i>pgm luxS</i>	2	
	<i>pgm ypeIR</i>	2	
	<i>pgm ypeIR yspIR</i>	1	
	<i>pgm ypeIR yspIR luxS</i>	2	
	<i>pgm yspl</i>	2	
	<i>pgm yspl ypeIR</i>	1	
	pPCP1 ⁻	8	
	WT	8	3
EV76-CN	WT		2
GB	<i>dam</i>	1	
	WT	1	
KIM5	WT	4	
KIM53	WT	5	5
KIM6+	pCD1 ⁻	5	
	<i>psaE</i>		1
	WT		1
Pestoides F	WT	8	

^aWT, wild-type strain; mutant strain (*mutated locus*).

data, with omics data generated in our laboratory, and with already available data types such as small RNAs (61–68), transcriptional start sites (TSS) (67–69), and riboswitches (67, 69). New analyses, such as gene ranking using TPM counts for each RNA-Seq experiments, will also be implemented. Ultimately, mutant phenotypes associated with specific gene locus could also be added based on signature-tagged mutagenesis screening (70–75), high-throughput transposon site hybridization procedure (76), or more recent next-generation sequencing using techniques such as transposon-insertion sequencing or transposon-directed insertion sequencing (77–81).

MATERIALS AND METHODS

Genomic data collection. Genomic data were browsed on the NCBI database with the keyword “*Yersinia*” (<https://www.ncbi.nlm.nih.gov/data-hub/genome>). Assemblies were filtered at the “chromosome” or “complete” level, and “chromosome” assemblies were manually curated to verify data completeness. The most recent RefSeq annotated assemblies were downloaded in December 2022.

Transcriptomic data collection. Microarray data were collected on Gene Expression Omnibus (<https://www.ncbi.nlm.nih.gov/geo/>), and the differential expressions calculated by data depositors were directly used when available. Alternatively, tables and supplemental tables were downloaded from articles and formatted. RNA-Seq data sets were browsed on the European Nucleotide Archive (<https://www.ebi.ac.uk/ena/>) using the keywords “*Yersinia*” and “transcriptome,” “RNA-Seq,” or “RNASeq” and on the Sequence Read Archive (<https://www.ncbi.nlm.nih.gov/sra/>) using the keyword “*Yersinia*” and selecting the “RNA” source. Raw data, consisting of sequencing reads in fastq format, were downloaded from the SRA FTP server <http://ftp.sra.ebi.ac.uk/vol1/> via the ENA website.

Proteomic data collection. As the treatment of LC-MS/MS raw data from the PRIDE repository is more complex and highly dependent on the mass spectrometry technology used, we directly retrieved the calculated differential expression from the tables and supplemental tables published in the literature when available. Alternatively, processed intensity data were kindly provided by their authors when data were not available online.

Genomic data processing. Genomes were directly processed through the Bacnet platform (33) and implemented in Yersiniomics. From the collected genomes, a phylogenetic tree was reconstructed using the 500 genes of our *Yersinia* cgMLST scheme recently developed in our laboratory (40). The 500 genes were concatenated and aligned using MAFFT v7.453 (82). Phylogenetic reconstruction was performed using IQTREE v2.0.6 (83), and the tree was rooted on *Yersinia entomophaga* MH96 (84), as it is the most ancestral branch of the genus *Yersinia* (40). The tree was drawn using Iroki (85). The taxonomic classification of the 66 *Y. pestis* genomes was based on the presence of SNPs defining the lineages, following the nomenclature developed in previous works (41, 42). *Y. pseudotuberculosis* IP32953 genome was also included in the analysis, to recover the ancestral genotypes. Briefly, either short-read sequencing data or contigs were mapped onto the *Y. pestis* CO92 reference genome (NC_003143) using the Snippy pipeline with default parameters (<https://github.com/tseemann/snippy>) to identify variants in the chromosome. Identified variants were inspected, and those falling within repetitive sequences (i.e., IS) were excluded, while variants associated with putative recombination events were identified using Gubbins v3.2.0 (86) and filtered out. The final set of variants ($n = 14,273$) was then used to reconstruct a maximum-likelihood phylogeny using IQ-TREE 2 (83) to classify the different *Y. pestis* genomes present in Yersiniomics into known evolutionary branches (0.PE2, 0.PE4, 0.PE3, 0.ANT, 1.ORI, 1.IN, 1.ANT, 2.ANT, 2.MED, and 4.ANT). For the other species, lineages were assessed from cgMLST.

Homolog database and synteny. A protein BLAST search was automatically performed for each gene of each genome against the other genomes to construct the homolog database, using the BLAST+ command-line tool v2.13.0 (87). Synteny was constructed using a best-hit bidirectional BLAST search and implemented in the SynTVView framework (50). The tool was reprogrammed from Flash to JavaScript with the HTML5 2d Canvas JavaScript library Konva (<https://konvajs.org/>), which enables high-performance animations. Drawing strategies were developed to ensure that graphical outputs remain below the technological limits of drawing more than 10,000 dynamic graphical objects, using a mix of static and dynamic objects. SynTVViewJS can be used on a public web application at <https://plechat.pages.pasteur.fr/syntviewjs/>. The code repository is at <https://gitlab.pasteur.fr/plechat/syntviewjs>.

Transcriptomic data processing. Downloaded microarray fold change tables were processed through the Bacnet platform. RNA-Seq raw data were processed using Sequana v0.14.6, Sequana-rnaseq v0.17.0, and Sequana-pipetools v0.10.0s (88), implementing the following software with default parameters: reads were trimmed using fastp v0.20.1 (89), processed reads were then aligned on the selected reference genome with Bowtie2 v2.4.4 (90), and strandedness was automatically identified by the Sequana pipeline. Mapped reads were then quantified using featureCounts (package subread v2.0.1) (91), and differential analysis was performed on raw read counts using DESeq2 v1.38.2 with R v4.2.1 with default parameters and Cook's cutoff enabled (43). *P* values and adjusted *P* values were calculated using default DESeq2 parameters consisting, respectively, of the Wald test and the Benjamini-Hochberg correction. Fold change and adjusted *P* value tables were extracted from DESeq2 results and processed using the Bacnet platform. BAM files generated by the Sequana pipeline were converted to strand-specific .wig files using the strand_cov function from the stranded-coverage package (<https://github.com/pmenzel/stranded-coverage.git>) and then processed using the Bacnet platform. Raw read counts from featureCounts were also normalized using the TPM method (51) to be displayed in the transcriptome panel of the gene viewer.

Proteomic data processing. For the differential analyses of one condition versus another, proteins identified in the reverse and contaminant databases and proteins “only identified by site” were first discarded from the list of identified proteins. Then, only proteins with at least three quantified intensities in a condition were kept. Differential expression was performed using LFQ when at least 1 unique peptide was detected and at least 2 peptides were quantified in a condition. A normalization was applied within the same condition centered on means of the medians (92). Remaining proteins without any intensity value in one of two conditions were considered quantitatively present in a condition and absent in another. They were therefore set aside and considered differentially abundant proteins. Missing values were imputed using the SLSA method thanks to the R package imp4p (93). Differential analysis was performed with a limma *t* test and an adaptive Benjamini-Hochberg correction to adjust the *P* values with the cp4P R package (94). Proteins with a fold change less than 2.0 were considered not significantly differentially abundant. Statistical testing of the remaining proteins (having a fold change greater than 2.0) was conducted using the limma *t* test (95).

These calculated fold changes were formatted and processed using the Bacnet platform, in parallel to fold change tables downloaded from published articles.

Yersiniomics website design. Yersiniomics was constructed with the Bacnet platform (33), based on Java and Eclipse e4 RCP/RAP API, and we contributed to its most recent update.

Links to external databases. The link to the KEGG database website uses the KEGG species identifier ("ype" for *Y. pestis* CO92) and the old locus name (for instance, "YPO0001" for the *miuC* gene of *Y. pestis* CO92), dynamically queried by URL in the form "<https://www.genome.jp/entry/ype:YPO0001>." UniProt accessions are dynamically retrieved and parsed with the KEGG species identifiers and the old locus name using KEGG REST Application Programming Interface (API), queried by URL in the form "<https://rest.kegg.jp/conv/uniprot/ype:YPO0001>." When a UniProt accession is retrieved ("A0A0H2W280" for the "YPO0001" old locus name of *Y. pestis* CO92), UniProt and InterPro are dynamically queried by URL in the forms "<https://www.uniprot.org/uniprotkb/A0A0H2W280>" and "<https://www.ebi.ac.uk/interpro/protein/UniProt/A0A0H2W280>," respectively. IntAct is dynamically accessed with the old locus name by URL in the form "<https://www.ebi.ac.uk/intact/search?query=YPO0001>" or "<https://www.ebi.ac.uk/intact/search?query=YPO0001%20A0A0H2W280>" if a UniProt accession was retrieved. A STRING URL is dynamically retrieved with the STRING species identifier ("214092" for *Y. pestis* CO92) and the old locus name, querying the STRING API in the form "<https://version-11-5.string-db.org/cgi/network?taskId=b10qgHbfGxqi&sessionId=b41GkPqd7zjt>." The retrieved URL is then accessed.

Data availability. The source code of the Yersiniomics website, based on the Bacnet platform, is available on the GitHub repository <https://github.com/becavin-lab/bacnet/>. All processed data can be directly downloaded from the Yersiniomics website.

ACKNOWLEDGMENTS

The project received funding from Institut Pasteur, Agence de l'Innovation de Défense (AID-DGA), Université Paris Cité, CNRS, LabEX Integrative Biology of Emerging Infectious Diseases (ANR-10-LBX-62-IBEID), Fondation pour la Recherche Médicale (FDT202204015222), and the Inception program (Investissement d'Avenir grant ANR-16-CONV-0005). The funders had no role in study design, data collection and interpretation, or the decision to submit the work for publication.

We thank Eric D. Merkley for sharing Pacific Northwest National Laboratory data sets. We are grateful to all members of the *Yersinia* research unit and the French national reference center for plague and other yersiniosis for insightful discussions.

We declare no conflict of interest.

REFERENCES

- Adeolu M, Alnajar S, Naushad S, Gupta RS. 2016. Genome-based phylogeny and taxonomy of the 'Enterobacteriales': proposal for *Enterobacteriales* ord. nov. divided into the families *Enterobacteriaceae*, *Erwiniaceae* fam. nov., *Pectobacteriaceae* fam. nov., *Yersiniaceae* fam. nov., *Hafniaceae* fam. nov., *Morganellaceae* fam. nov., and *Budviaceae* fam. nov. *Int J Syst Evol Microbiol* 66:5575–5599. <https://doi.org/10.1099/ijsem.0.001485>.
- Reuter S, Connor TR, Barquist L, Walker D, Feltwell T, Harris SR, Fookes M, Hall ME, Petty NK, Fuchs TM, Corander J, Dufour M, Ringwood T, Savin C, Bouchier C, Martin L, Miettinen M, Shubin M, Riehm JM, Laukkanen-Ninios R, Sihvonen LM, Siitonen A, Skurnik M, Falcão JP, Fukushima H, Scholz HC, Prentice MB, Wren BW, Parkhill J, Carniel E, Achtman M, McNally A, Thomson NR. 2014. Parallel independent evolution of pathogenicity within the genus *Yersinia*. *Proc Natl Acad Sci U S A* 111:6768–6773. <https://doi.org/10.1073/pnas.1317161111>.
- McNally A, Thomson NR, Reuter S, Wren BW. 2016. "Add, stir and reduce": *Yersinia* spp. as model bacteria for pathogen evolution. *Nat Rev Microbiol* 14:177–190. <https://doi.org/10.1038/nrmicro.2015.29>.
- European Centre for Disease Prevention and Control. 2022. Yersiniosis - annual epidemiological report for 2020.
- Saraka D, Savin C, Kouassi S, Cissé B, Koffi E, Cabanel N, Brémont S, Faye-Kette H, Dosso M, Carniel E. 2017. *Yersinia enterocolitica*, a neglected cause of human enteric infections in Côte d'Ivoire. *PLoS Negl Trop Dis* 11:e0005216. <https://doi.org/10.1371/journal.pntd.0005216>.
- Achtman M, Morelli G, Zhu P, Wirth T, Diehl I, Kusecek B, Vogler AJ, Wagner DM, Allender CJ, Easterday WR, Chenal-Francisque V, Worsham P, Thomson NR, Parkhill J, Lindler LE, Carniel E, Keim P. 2004. Microevolution and history of the plague bacillus, *Yersinia pestis*. *Proc Natl Acad Sci U S A* 101:17837–17842. <https://doi.org/10.1073/pnas.0408026101>.
- Demeure CE, Dussurget O, Mas Fiol G, le Guern AS, Savin C, Pizarro-Cerdá J. 2019. *Yersinia pestis* and plague: an updated view on evolution, virulence determinants, immune subversion, vaccination, and diagnostics. *Genes Immun* 20:357–370. <https://doi.org/10.1038/s41435-019-0065-0>.
- Bertherat E. 2019. Plague around the world in 2019/La peste dans le monde en 2019. *Wkly Epidemiol Rec* 94:289–293.
- Baril L, Vallès X, Stenseth NC, Rajerison M, Ratsitorahina M, Pizarro-Cerdá J, Demeure C, Belmain S, Scholz H, Girod R, Hinnebusch J, Vigan-Womas I, Bertherat E, Fontanet A, Yazadanpanah Y, Carrara G, Deuve J, D'Ortenzio E, Angulo JOC, Mead P, Horby PW. 2019. Can we make human plague history? A call to action. *BMJ Glob Health* 4:e001984. <https://doi.org/10.1136/bmjgh-2019-001984>.
- Vallès X, Stenseth NC, Demeure C, Horby P, Mead PS, Cabanillas O, Ratsitorahina M, Rajerison M, Andrianavoarimanana V, Ramasindrazana B, Pizarro-Cerdá J, Scholz HC, Girod R, Hinnebusch BJ, Vigan-Womas I, Fontanet A, Wagner DM, Telfer S, Yazdanpanah Y, Tortosa P, Carrara G, Deuve J, Belmain SR, D'Ortenzio E, Baril L. 2020. Human plague: an old scourge that needs new answers. *PLoS Negl Trop Dis* 14:e0008251. <https://doi.org/10.1371/journal.pntd.0008251>.
- Kumar G, Menanteau-Ledouble S, Saleh M, El-Matbouli M. 2015. *Yersinia ruckeri*, the causative agent of enteric redmouth disease in fish. *Vet Res* 46:e103. <https://doi.org/10.1186/s13567-015-0238-4>.
- Hurst MRH, Becher SA, Young SD, Nelson TL, Glare TR. 2011. *Yersinia entomophaga* sp. nov., isolated from the New Zealand grass grub *Costelytra zealandica*. *Int J Syst Evol Microbiol* 61:844–849. <https://doi.org/10.1099/ijvs.0.024406-0>.
- Glare TR, O'Callaghan M. 2019. Microbial biopesticides for control of invertebrates: progress from New Zealand. *J Invertebr Pathol* 165:82–88. <https://doi.org/10.1016/j.jip.2017.11.014>.
- Isberg RR, Falkow S. 1985. A single genetic locus encoded by *Yersinia pseudotuberculosis* permits invasion of cultured animal cells by *Escherichia coli* K-12. *Nature* 317:262–264. <https://doi.org/10.1038/317262a0>.
- Isberg RR, Voorhis DL, Falkow S. 1987. Identification of invasins: a protein that allows enteric bacteria to penetrate cultured mammalian cells. *Cell* 50:769–778. [https://doi.org/10.1016/0092-8674\(87\)90335-7](https://doi.org/10.1016/0092-8674(87)90335-7).
- Isberg RR, Leong JM. 1990. Multiple β 1 chain integrins are receptors for invasins, a protein that promotes bacterial penetration into mammalian cells. *Cell* 60:861–871. [https://doi.org/10.1016/0092-8674\(90\)90099-z](https://doi.org/10.1016/0092-8674(90)90099-z).
- Alrutz MA, Srivastava A, Wong KW, D'Souza-Schorey C, Tang M, Ch'Ng LE, Snapper SB, Isberg RR. 2001. Efficient uptake of *Yersinia pseudotuberculosis* via integrin receptors involves a Rac1-Arp 2/3 pathway that bypasses N-WASP function. *Mol Microbiol* 42:689–703.
- Wong KW, Isberg RR. 2003. Arf6 and phosphoinositol-4-phosphate-5-kinase activities permit bypass of the Rac1 requirement for β 1 integrin-

- mediated bacterial uptake. *J Exp Med* 198:603–614. <https://doi.org/10.1084/jem.20021363>.
19. Pizarro-Cerdá J, Cossart P. 2004. Subversion of phosphoinositide metabolism by intracellular bacterial pathogens. *Nat Cell Biol* 6:1026–1033. <https://doi.org/10.1038/ncb1104-1026>.
 20. Machner MP, Isberg RR. 2007. A bifunctional bacterial protein links GDI displacement to Rab1 activation. *Science* 318:974–977. <https://doi.org/10.1126/science.1149121>.
 21. Cornelis GR, Wolf-Watz H. 1997. The *Yersinia* Yop virulon: a bacterial system for subverting eukaryotic cells. *Mol Microbiol* 23:861–867. <https://doi.org/10.1046/j.1365-2958.1997.2731623.x>.
 22. Cornelis GR. 2002. The *Yersinia* Ysc–Yop “Type III” weaponry. *Nat Rev Mol Cell Biol* 3:742–752. <https://doi.org/10.1038/nrm932>.
 23. Sayers EW, Cavanaugh M, Clark K, Pruitt KD, Schoch CL, Sherry ST, Karsch-Mizrachi I. 2022. GenBank. *Nucleic Acids Res* 50:D161–D164. <https://doi.org/10.1093/nar/gkab1135>.
 24. Clough E, Barrett T. 2016. The Gene Expression Omnibus database. *Methods Mol Biol* 1418:93–110. https://doi.org/10.1007/978-1-4939-3578-9_5.
 25. Athar A, Füllgrabe A, George N, Iqbal H, Huerta L, Ali A, Snow C, Fonseca NA, Petryszak R, Papatheodorou I, Sarkans U, Brazma A. 2019. ArrayExpress update – from bulk to single-cell expression data. *Nucleic Acids Res* 47:D711–D715. <https://doi.org/10.1093/nar/gky964>.
 26. Cummins C, Ahamed A, Aslam R, Burgin J, Devraj R, Edbali O, Gupta D, Harrison PW, Haseeb M, Holt S, Ibrahim T, Ivanov E, Jayathilaka S, Kadhirvelu V, Kay S, Kumar M, Lathi A, Leinonen R, Madeira F, Madhusoodanan N, Mansurova M, O’Cathail C, Pearce M, Pesant S, Rahman N, Rajan J, Rinck G, Selvakumar S, Sokolov A, Suman S, Thorne R, Tootoo P, Vijayaraja S, Waheed Z, Zyoud A, Lopez R, Burdett T, Cochrane G. 2022. The European Nucleotide Archive in 2021. *Nucleic Acids Res* 50:D106–D110. <https://doi.org/10.1093/nar/gkab1051>.
 27. Katz K, Shutov O, Lapoint R, Kimelman M, Brister JR, O’Sullivan C. 2022. The Sequence Read Archive: a decade more of explosive growth. *Nucleic Acids Res* 50:D387–D390. <https://doi.org/10.1093/nar/gkab1053>.
 28. Deutsch EW, Bandeira N, Sharma V, Perez-Riverol Y, Carver JJ, Kundu DJ, Garcia-Seisdedos D, Jarnuczak AF, Hewapathirana S, Pullman BS, Wertz J, Sun Z, Kawano S, Okuda S, Watanabe Y, Hermjakob H, Maclean B, Maccoss MJ, Zhu Y, Ishihama Y, Vizcaino JA. 2020. The ProteomeXchange consortium in 2020: enabling ‘big data’ approaches in proteomics. *Nucleic Acids Res* 48:D1145–D1152. <https://doi.org/10.1093/nar/gkz984>.
 29. Keseler IM, Gama-Castro S, Mackie A, Billington R, Bonavides-Martínez C, Caspi R, Kothari A, Krummenacker M, Midford PE, Muñiz-Rascado L, Ong WK, Paley S, Santos-Zavaleta A, Subhraveti P, Tierrafraía VH, Wolfe AJ, Collado-Vides J, Paulsen IT, Karp PD. 2021. The EcoCyc Database in 2021. *Front Microbiol* 12:711077. <https://doi.org/10.3389/fmicb.2021.711077>.
 30. Cherry JM, Adler C, Ball C, Chervitz SA, Dwight SS, Hester ET, Jia Y, Juvik G, Roe T, Schroeder M, Weng S, Botstein D. 1998. SGD: *Saccharomyces* Genome Database. *Nucleic Acids Res* 26:73–79. <https://doi.org/10.1093/nar/26.1.73>.
 31. Bécavin C, Koutero M, Tchitchek N, Cerutti F, Lechat P, Maillet N, Hoede C, Chiapello H, Gaspin C, Cossart P. 2017. Listeriomics: an interactive web platform for systems biology of *Listeria*. *mSystems* 2:e00186-16. <https://doi.org/10.1128/mSystems.00186-16>.
 32. Davis JJ, Wattam AR, Aziz RK, Brettin T, Butler R, Butler RM, Chlenski P, Conrad N, Dickerman A, Dietrich EM, Gabbard JL, Gerdes S, Guard A, Kenyon RW, MacHi D, Mao C, Murphy-Olson D, Nguyen M, Nordberg EK, Olsen GJ, Olson RD, Overbeek JC, Overbeek R, Parrello B, Pusch GD, Shukla M, Thomas C, Vanoeffelen M, Vonstein V, Warren AS, Xia F, Xie D, Yoo H, Stevens R. 2020. The PATRIC Bioinformatics Resource Center: expanding data and analysis capabilities. *Nucleic Acids Res* 48:D606–D612. <https://doi.org/10.1093/nar/gkz943>.
 33. Danès L, Tchitchek N, Bécavin C. 2021. Bacnet: a user-friendly platform for building multi-omics websites. *Bioinformatics* 37:1335–1336. <https://doi.org/10.1093/bioinformatics/btaa828>.
 34. Kanehisa M, Furumichi M, Tanabe M, Sato Y, Morishima K. 2017. KEGG: new perspectives on genomes, pathways, diseases and drugs. *Nucleic Acids Res* 45:D353–D361. <https://doi.org/10.1093/nar/gkw1092>.
 35. UniProt Consortium, Bateman A, Martin M-J, Orchard S, Magrane M, Ahmad S, Alpi E, Bowler-Barnett EH, Britto R, Bye-A-Jee H, Cukura A, Denny P, Dogan T, Ebenezer T, Fan J, Garmiri P, da Costa Gonzales LJ, Hatton-Ellis E, Hussein A, Ignatchenko A, Insana G, Ishtiaq R, Joshi V, Jyothi D, Kandasaamy S, Lock A, Luciani A, Lugarcic M, Luo J, Lussi Y, MacDougall A, Madeira F, Mahmoudy M, Mishra A, Moulang K, Nightingale A, Pundir S, Qi G, Raj S, Raposo P, Rice DL, Saidi R, Santos R, Speretta E, Stephenson J, Tootoo P, Turner E, Tyagi N, Vasudev P, Warner K, Watkins X, Zaru R, Zellner H, Bridge AJ, Aimo L, Argoud-Puy G, Auchincloss AH, Axelsen KB, Bansal P, Baratin D, Batista Neto TM, Blatter M-C, Bolleman JT, Boutet E, Breuza L, Gil BC, Casals-Casas C, Echioukh KC, Coudert E, Cuhe B, de Castro E, Estreicher A, Famiglietti ML, Feuermann M, Gasteiger E, Gaudet P, Gehant S, Gerritsen V, Gos A, Gruaz N, Hulo C, Hyka-Nouspikel N, Jungo F, Kerhornou A, le Mercier P, Lieberherr D, Masson P, Morgat A, Muthukrishnan V, Paesano S, Pedruzzi I, Pilbout S, Pourcel L, Poux S, Pozzato M, Pruess M, Redaschi N, Rivoire C, Sigrist CJA, Sonesson K, Sundaram S, Wu CH, Arighi CN, Arminski L, Chen C, Chen Y, Huang H, Laiho K, McGarvey P, Natale DA, Ross K, Vinayaka CR, Wang Q, Wang Y, Zhang J. 2023. UniProt: the Universal Protein Knowledgebase in 2023. *Nucleic Acids Res* 51:D523–D531. <https://doi.org/10.1093/nar/gkac1052>.
 36. Blum M, Chang HY, Chuguransky S, Grego T, Kandasaamy S, Mitchell A, Nuka G, Paysan-Lafosse T, Qureshi M, Raj S, Richardson L, Salazar GA, Williams L, Bork P, Bridge A, Gough J, Haft DH, Letunic I, Marchler-Bauer A, Mi H, Natale DA, Necci M, Orengo CA, Pandurangan AP, Rivoire C, Sigrist CJA, Sillitoe I, Thanki N, Thomas PD, Tosatto SCE, Wu CH, Bateman A, Finn RD. 2021. The InterPro protein families and domains database: 20 years on. *Nucleic Acids Res* 49:D344–D354. <https://doi.org/10.1093/nar/gkaa977>.
 37. del Toro N, Shrivastava A, Ragueneau E, Meldal B, Combe C, Barrera E, Perfetto L, How K, Ratan P, Shirodkar G, Lu O, Mészáros B, Watkins X, Pundir S, Licata L, Iannuccelli M, Pellegrini M, Martin MJ, Panni S, Duesbury M, Vallet SD, Rappsilber J, Ricard-Blum S, Cesareni G, Salwinski L, Orchard S, Porras P, Panneerselvam K, Hermjakob H. 2022. The IntAct database: efficient access to fine-grained molecular interaction data. *Nucleic Acids Res* 50:D648–D653. <https://doi.org/10.1093/nar/gkab1006>.
 38. Szklarczyk D, Kirsch R, Koutrouli M, Nastou K, Mehryary F, Hachilif R, Gable AL, Fang T, Doncheva NT, Pyysalo S, Bork P, Jensen LJ, von Mering C. 2022. The STRING database in 2023: protein–protein association networks and functional enrichment analyses for any sequenced genome of interest. *Nucleic Acids Res* 51:D638–D646. <https://doi.org/10.1093/nar/gkac1000>.
 39. Perez-Riverol Y, Bai J, Bandla C, García-Seisdedos D, Hewapathirana S, Kamatchinathan S, Kundu DJ, Prakash A, Frericks-Zipper A, Eisenacher M, Walzer M, Wang S, Brazma A, Vizcaino JA. 2022. The PRIDE database resources in 2022: a hub for mass spectrometry-based proteomics evidences. *Nucleic Acids Res* 50:D543–D552. <https://doi.org/10.1093/nar/gkab1038>.
 40. Savin C, Crisculo A, Guglielmini J, le Guern AS, Carniel E, Pizarro-Cerdá J, Brisse S. 2019. Genus-wide *Yersinia* core-genome multilocus sequence typing for species identification and strain characterization. *Microb Genom* 5:e000301. <https://doi.org/10.1099/mgen.0.000301>.
 41. Morelli G, Song Y, Mazzoni CJ, Eppinger M, Roumagnac P, Wagner DM, Feldkamp M, Kusecek B, Vogler AJ, Li Y, Cui Y, Thomson NR, Jombart T, Leblois R, Lichtner P, Rahalison L, Petersen JM, Balloux F, Keim P, Wirth T, Ravel J, Yang R, Carniel E, Achtman M. 2010. *Yersinia pestis* genome sequencing identifies patterns of global phylogenetic diversity. *Nat Genet* 42:1140–1143. <https://doi.org/10.1038/ng.705>.
 42. Cui Y, Yu C, Yan Y, Li D, Li Y, Jombart T, Weinert LA, Wang Z, Guo Z, Xu L, Zhang Y, Zheng H, Qin N, Xiao X, Wu M, Wang X, Zhou D, Qi Z, Du Z, Wu H, Yang X, Cao H, Wang H, Wang J, Yao S, Rakin A, Li Y, Falush D, Balloux F, Achtman M, Song Y, Wang J, Yang R. 2013. Historical variations in mutation rate in an epidemic pathogen, *Yersinia pestis*. *Proc Natl Acad Sci U S A* 110:577–582. <https://doi.org/10.1073/pnas.1205750110>.
 43. Love MI, Huber W, Anders S. 2014. Moderated estimation of fold change and dispersion for RNA-seq data with DESeq2. *Genome Biol* 15:e550. <https://doi.org/10.1186/s13059-014-0550-8>.
 44. Latham WW, Crosby SD, Miller VL, Goldman WE. 2005. Progression of primary pneumonic plague: a mouse model of infection, pathology, and bacterial transcriptional activity. *Proc Natl Acad Sci U S A* 102:17786–17791. <https://doi.org/10.1073/pnas.0506840102>.
 45. Chauvaux S, Rosso M-L, Frangeul L, Lacroix C, Labarre L, Schiavo A, Marceau M, Dillies M-A, Foulon J, Coppee J-Y, Medigue C, Simonet M, Carniel E. 2007. Transcriptome analysis of *Yersinia pestis* in human plasma: an approach for discovering bacterial genes involved in septicemic plague. *Microbiology (Reading)* 153:3112–3124. <https://doi.org/10.1099/mic.0.2007/006213-0>.
 46. Sebbane F, Gardner D, Long D, Gowen BB, Hinnebusch BJ. 2005. Kinetics of disease progression and host response in a rat model of bubonic plague. *Am J Pathol* 166:1427–1439. [https://doi.org/10.1016/S0002-9440\(10\)62360-7](https://doi.org/10.1016/S0002-9440(10)62360-7).
 47. Ritzert JT, Minasov G, Embry R, Schipma MJ, Satchell KJF. 2019. The cyclic AMP receptor protein regulates quorum sensing and global gene expression in *Yersinia pestis* during planktonic growth and growth in biofilms. *mBio* 10:e02613-19. <https://doi.org/10.1128/mBio.02613-19>.

48. Schrimpe-Rutledge AC, Jones MB, Chauhan S, Purvine SO, Sanford JA, Monroe ME, Brewer HM, Payne SH, Ansong C, Frank BC, Smith RD, Peterson SN, Motin VL, Adkins JN. 2012. Comparative omics-driven genome annotation refinement: application across *Yersinia*. *PLoS One* 7: e33903. <https://doi.org/10.1371/journal.pone.0033903>.
49. Avican K, Aldahdooh J, Togninalli M, Mahmud AKMF, Tang J, Borgwardt KM, Rhen M, Fällman M. 2021. RNA atlas of human bacterial pathogens uncovers stress dynamics linked to infection. *Nat Commun* 12:e3282. <https://doi.org/10.1038/s41467-021-23588-w>.
50. Lechat P, Souche E, Moszer I. 2013. SynTVView - an interactive multi-view genome browser for next-generation comparative microorganism genomics. *BMC Bioinformatics* 14:e277. <https://doi.org/10.1186/1471-2105-14-277>.
51. Abrams ZB, Johnson TS, Huang K, Payne PRO, Coombes K. 2019. A protocol to evaluate RNA sequencing normalization methods. *BMC Bioinformatics* 20:679. <https://doi.org/10.1186/s12859-019-3247-x>.
52. Dyer MD, Nef C, Dufford M, Rivera CG, Shattuck D, Bassaganya-Riera J, Murali TM, Sobral BW. 2010. The human-bacterial pathogen protein interaction networks of *Bacillus anthracis*, *Francisella tularensis*, and *Yersinia pestis*. *PLoS One* 5:e0012089. <https://doi.org/10.1371/journal.pone.0012089>.
53. Merkley ED, Segó LH, Lin A, Leiser OP, Kaiser BL, Adkins JN, Keim PS, Wagner DM, Kreuzer HW. 2017. Protein abundances can distinguish between naturally-occurring and laboratory strains of *Yersinia pestis*, the causative agent of plague. *PLoS One* 12:e0183478. <https://doi.org/10.1371/journal.pone.0183478>.
54. Ansong C, Schrimpe-Rutledge AC, Mitchell HD, Chauhan S, Jones MB, Kim Y-M, McAteer K, Deatherage Kaiser BL, Dubois JL, Brewer HM, Frank BC, McDermott JE, Metz TO, Peterson SN, Smith RD, Motin VL, Adkins JN. 2013. A multi-omic systems approach to elucidating *Yersinia* virulence mechanisms. *Mol Biosyst* 9:44–54. <https://doi.org/10.1039/c2mb25287b>.
55. Lin A, Merkley ED, Clowers BH, Hutchison JR, Kreuzer HW. 2015. Effects of bacterial inactivation methods on downstream proteomic analysis. *J Microbiol Methods* 112:3–10. <https://doi.org/10.1016/j.mimet.2015.01.015>.
56. Payne SH, Monroe ME, Overall CC, Kiebel GR, Degan M, Gibbons BC, Fujimoto GM, Purvine SO, Adkins JN, Lipton MS, Smith RD. 2015. The Pacific Northwest National Laboratory library of bacterial and archaeal proteomic biodiversity. *Sci Data* 2:e150041. <https://doi.org/10.1038/sdata.2015.41>.
57. Cao S, Chen Y, Yan Y, Zhu S, Tan Y, Wang T, Song Y, Deng H, Yang R, Du Z. 2021. Secretome and comparative proteomics of *Yersinia pestis* identify two novel E3 ubiquitin ligases that contribute to plague virulence. *Mol Cell Proteomics* 20:e100066. <https://doi.org/10.1016/j.mcpro.2021.100066>.
58. Hixson KK, Adkins JN, Baker SE, Moore RJ, Chromy BA, Smith RD, McCutchen-Maloney SL, Lipton MS. 2006. Biomarker candidate identification in *Yersinia pestis* using organism-wide semiquantitative proteomics. *J Proteome Res* 5: 3008–3017. <https://doi.org/10.1021/pr060179y>.
59. Pieper R, Huang ST, Parmar PP, Clark DJ, Alami H, Fleischmann RD, Perry RD, Peterson SN. 2010. Proteomic analysis of iron acquisition, metabolic and regulatory responses of *Yersinia pestis* to iron starvation. *BMC Microbiol* 10:e30. <https://doi.org/10.1186/1471-2180-10-30>.
60. Israeli O, Cohen-Gihon I, Aftalion M, Gur D, Vagima Y, Zauberman A, Levy Y, Zvi A, Chitlaru T, Mamroud E, Tidhar A. 2021. Novel RNA extraction method for dual RNA-seq analysis of pathogen and host in the early stages of *Yersinia pestis* pulmonary infection. *Microorganisms* 9:e2166. <https://doi.org/10.3390/microorganisms9102166>.
61. Li N, Hennelly SP, Stubben CJ, Micheva-Viteva S, Hu B, Shou Y, Vuyisich M, Tung C-S, Chain PS, Sanbonmatsu KY, Hong-Geller E. 2016. Functional and structural analysis of a highly-expressed *Yersinia pestis* small RNA following infection of cultured macrophages. *PLoS One* 11:e0168915. <https://doi.org/10.1371/journal.pone.0168915>.
62. Yan Y, Su S, Meng X, Ji X, Qu Y, Liu Z, Wang X, Cui Y, Deng Z, Zhou D, Jiang W, Yang R, Han Y. 2013. Determination of sRNA expressions by RNA-seq in *Yersinia pestis* grown in vitro and during infection. *PLoS One* 8:e74495. <https://doi.org/10.1371/journal.pone.0074495>.
63. Koo JT, Alleyne TM, Schiano CA, Jafari N, Latham WW. 2011. Global discovery of small RNAs in *Yersinia pseudotuberculosis* identifies *Yersinia*-specific small, noncoding RNAs required for virulence. *Proc Natl Acad Sci U S A* 108:E709–E717. <https://doi.org/10.1073/pnas.1101655108>.
64. Beauregard A, Smith EA, Petrone BL, Singh N, Karch C, McDonough KA, Wade JT. 2013. Identification and characterization of small RNAs in *Yersinia pestis*. *RNA Biol* 10:397–405. <https://doi.org/10.4161/rna.23590>.
65. Schiano CA, Koo JT, Schipma MJ, Caulfield AJ, Jafari N, Latham WW. 2014. Genome-wide analysis of small RNAs expressed by *Yersinia pestis* identifies a regulator of the Yop-Ysc type III secretion system. *J Bacteriol* 196: 1659–1670. <https://doi.org/10.1128/JB.01456-13>.
66. Qu Y, Bi L, Ji X, Deng Z, Zhang H, Yan Y, Wang M, Li A, Huang X, Yang R, Han Y. 2012. Identification by cDNA cloning of abundant sRNAs in a human-avirulent *Yersinia pestis* strain grown under five different growth conditions. *Future Microbiol* 7:535–547. <https://doi.org/10.2217/fmb.12.13>.
67. Schmöhl C, Beckstette M, Heroven AK, Bunk B, Spröer C, McNally A, Overmann J, Dersch P. 2019. Comparative transcriptomic profiling of *Yersinia enterocolitica* O:3 and O:8 reveals major expression differences of fitness- and virulence-relevant genes indicating ecological separation. *mSystems* 4:e00239-18. <https://doi.org/10.1128/mSystems.00239-18>.
68. Nuss AM, Heroven AK, Waldmann B, Reinkensmeier J, Jarek M, Beckstette M, Dersch P. 2015. Transcriptomic profiling of *Yersinia pseudotuberculosis* reveals reprogramming of the Crp regulon by temperature and uncovers Crp as a master regulator of small RNAs. *PLoS Genet* 11:e1005087. <https://doi.org/10.1371/journal.pgen.1005087>.
69. Nuss AM, Beckstette M, Pimenova M, Schmöhl C, Opitz W, Pisano F, Heroven AK, Dersch P. 2017. Tissue dual RNA-seq allows fast discovery of infection-specific functions and riboregulators shaping host-pathogen transcriptomes. *Proc Natl Acad Sci U S A* 114:E791–E800. <https://doi.org/10.1073/pnas.1613405114>.
70. Karlyshev AV, Oyston PCF, Williams K, Clark GC, Titball RW, Winzeler EA, Wren BW. 2001. Application of high-density array-based signature-tagged mutagenesis to discover novel *Yersinia* virulence-associated genes. *Infect Immun* 69:7810–7819. <https://doi.org/10.1128/IAI.69.12.7810-7819.2001>.
71. Meccas J, Bilis I, Falkow S. 2001. Identification of attenuated *Yersinia pseudotuberculosis* strains and characterization of an orogastric infection in BALB/c mice on day 5 postinfection by signature-tagged mutagenesis. *Infect Immun* 69:2779–2787. <https://doi.org/10.1128/IAI.69.12.2779-2787.2001>.
72. Darwin AJ, Miller VL. 1999. Identification of *Yersinia enterocolitica* genes affecting survival in an animal host using signature-tagged transposon mutagenesis. *Mol Microbiol* 32:51–62. <https://doi.org/10.1046/j.1365-2958.1999.01324.x>.
73. Flashner Y, Mamroud E, Tidhar A, Ber R, Aftalion M, Gur D, Lazar S, Zvi A, Bino T, Ariel N, Velan B, Shafferman A, Cohen S. 2004. Generation of *Yersinia pestis* attenuated strains by signature-tagged mutagenesis in search of novel vaccine candidates. *Infect Immun* 72:908–915. <https://doi.org/10.1128/IAI.72.2.908-915.2004>.
74. Ponnusamy D, Fitts EC, Sha J, Erova TE, Kozlova EV., Kirtley ML, Tiner BL, Andersson JA, Chopra AK. 2015. High-throughput, signature-tagged mutagenic approach to identify novel virulence factors of *Yersinia pestis* CO92 in a mouse model of infection. *Infect Immun* 83:2065–2081. <https://doi.org/10.1128/IAI.02913-14>.
75. Leigh SA, Forman S, Perry RD, Straley SC. 2005. Unexpected results from the application of signature-tagged mutagenesis to identify *Yersinia pestis* genes required for adherence and invasion. *Microb Pathog* 38: 259–266. <https://doi.org/10.1016/j.micpath.2005.02.004>.
76. Klein KA, Fukuto HS, Pelletier M, Romanov G, Grabenstein JP, Palmer LE, Ernst R, Bliska JB. 2012. A transposon site hybridization screen identifies galU and wbcB as important for survival of *Yersinia pestis* in murine macrophages. *J Bacteriol* 194:653–662. <https://doi.org/10.1128/JB.06237-11>.
77. Willcocks S, Huse KK, Stabler R, Oyston PCF, Scott A, Atkins HS, Wren BW. 2019. Genome-wide assessment of antimicrobial tolerance in *Yersinia pseudotuberculosis* under ciprofloxacin stress. *Microb Genom* 5:e000304. <https://doi.org/10.1099/mgen.0.000304>.
78. Senior NJ, Sasidharan K, Saint RJ, Scott AE, Sarkar-Tyson M, Ireland PM, Bullifent HL, Rong Yang Z, Moore K, Oyston PCF, Atkins TP, Atkins HS, Soyer OS, Titball RW. 2017. An integrated computational-experimental approach reveals *Yersinia pestis* genes essential across a narrow or a broad range of environmental conditions. *BMC Microbiol* 17:e163. <https://doi.org/10.1186/s12866-017-1073-8>.
79. Willcocks SJ, Stabler RA, Atkins HS, Oyston PF, Wren BW. 2018. High-throughput analysis of *Yersinia pseudotuberculosis* gene essentiality in optimized in vitro conditions, and implications for the speciation of *Yersinia pestis*. *BMC Microbiol* 18:e46. <https://doi.org/10.1186/s12866-018-1189-5>.
80. Yang ZR, Bullifent HL, Moore K, Paszkiewicz K, Saint RJ, Southern SJ, Champion OL, Senior NJ, Sarkar-Tyson M, Oyston PCF, Atkins TP, Titball RW. 2017. A noise trimming and positional significance of transposon insertion system to identify essential genes in *Yersinia pestis*. *Sci Rep* 7: e41923. <https://doi.org/10.1038/srep41923>.
81. Eichelberger KR, Sepúlveda VE, Ford J, Selitsky SR, Mieczkowski PA, Parker JS, Goldman WE. 2020. Tn-Seq analysis identifies genes important for *Yersinia pestis* adherence during primary pneumonic plague. *mSphere* 5:e00715-20. <https://doi.org/10.1128/mSphere.00715-20>.

82. Katoh K, Standley DM. 2013. MAFFT multiple sequence alignment software version 7: improvements in performance and usability. *Mol Biol Evol* 30:772–780. <https://doi.org/10.1093/molbev/mst010>.
83. Minh BQ, Schmidt HA, Chernomor O, Schrempf D, Woodhams MD, von Haeseler A, Lanfear R, Teeling E. 2020. IQ-TREE 2: new models and efficient methods for phylogenetic inference in the genomic era. *Mol Biol Evol* 37:1530–1534. <https://doi.org/10.1093/molbev/msaa015>.
84. Hurst MRH, Beattie A, Altermann E, Moraga RM, Harper LA, Calder J, Laugraud A. 2016. The draft genome sequence of the *Yersinia entomophaga* entomopathogenic type strain MH96T. *Toxins* 8:e143. <https://doi.org/10.3390/toxins8050143>.
85. Moore RM, Harrison AO, McAllister SM, Polson SW, Eric Wommack K. 2020. Iroki: automatic customization and visualization of phylogenetic trees. *PeerJ* 8:e8584. <https://doi.org/10.7717/peerj.8584>.
86. Croucher NJ, Page AJ, Connor TR, Delaney AJ, Keane JA, Bentley SD, Parkhill J, Harris SR. 2015. Rapid phylogenetic analysis of large samples of recombinant bacterial whole genome sequences using Gubbins. *Nucleic Acids Res* 43:e15. <https://doi.org/10.1093/nar/gku1196>.
87. Camacho C, Coulouris G, Avagyan V, Ma N, Papadopoulos J, Bealer K, Madden TL. 2009. BLAST+: architecture and applications. *BMC Bioinformatics* 10:e421. <https://doi.org/10.1186/1471-2105-10-421>.
88. Cokelaer T, Desvillechabrol D, Legendre R, Cardon M. 2017. “Sequana”: a set of snakemake NGS pipelines. *J Open Source Softw* 2:e352. <https://doi.org/10.21105/joss.00352>.
89. Chen S, Zhou Y, Chen Y, Gu J. 2018. fastp: an ultra-fast all-in-one FASTQ preprocessor. *Bioinformatics* 34:i884–i890. <https://doi.org/10.1093/bioinformatics/bty560>.
90. Langmead B, Salzberg SL. 2012. Fast gapped-read alignment with Bowtie 2. *Nat Methods* 9:357–359. <https://doi.org/10.1038/nmeth.1923>.
91. Liao Y, Smyth GK, Shi W. 2014. featureCounts: an efficient general purpose program for assigning sequence reads to genomic features. *Bioinformatics* 30:923–930. <https://doi.org/10.1093/bioinformatics/btt656>.
92. Wieczorek S, Combes F, Lazar C, Giai Gianetto Q, Gatto L, Dorffer A, Hesse AM, Couté Y, Ferro M, Bruley C, Burger T. 2017. DAPAR & ProStaR: software to perform statistical analyses in quantitative discovery proteomics. *Bioinformatics* 33:135–136. <https://doi.org/10.1093/bioinformatics/btw580>.
93. Giai Gianetto Q, Wieczorek S, Couté Y, Burger T. 2020. A peptide-level multiple imputation strategy accounting for the different natures of missing values in proteomics data. *bioRxiv*. <https://doi.org/10.1101/2020.05.29.122770>.
94. Giai Gianetto Q, Combes F, Ramus C, Bruley C, Couté Y, Burger T. 2016. Calibration plot for proteomics: a graphical tool to visually check the assumptions underlying FDR control in quantitative experiments. *Proteomics* 16:29–32. <https://doi.org/10.1002/pmic.201500189>.
95. Smyth GK. 2005. limma: linear models for microarray data, p 397–420. *In* Gentleman R, Huber W, Carey VJ, Irizarry RA, Dudoit S (ed), *Bioinformatics and computational biology Solutions using R and Bioconductor*. Springer, Heidelberg, Germany.

Chapter 7

***Yersinia pestis* lipoprotein SlyB promotes plague pathogenesis via envelope stress tolerance**

7.1 Objectives and summary

Based on our plasma proteomics results (chapter 5) and the Yersiniomics database (chapter 6), we selected 47 *Y. pestis* proteins and deleted their corresponding genes in order to investigate their role in bacteremic phase of plague. The 47 mutants and the parental strain were compared for their capacity to survive in human blood and in a murine model of primary septicemic plague. Among mutants whose growth was defective in human blood and whose virulence was attenuated in mice, we identified the $\Delta slyB$ mutant. SlyB is well conserved in bacteria, including pathogenic bacteria [150], and suggested to be involved in maintenance of membrane integrity [154, 156]. We showed that a *Y. pestis* $\Delta slyB$ mutant displays decreased resistance to complement-mediated killing, intracellular survival in macrophages and resistance to neutrophil-mediated killing. Proteomic analysis of the mutant revealed a potential periplasmic leakage presumably resulting from weakening of the outer membrane and inducing a metabolic rewiring. Altogether, these defects led to an overall attenuation of virulence of *Y. pestis* in murine models of plague. To our knowledge, this is the first study uncovering the importance of SlyB in resistance to innate immunity and bacterial pathogenesis.

Of note, proteomic analysis combined with long-read Nanopore genome sequencing of the $\Delta slyB$ mutant strain very recently revealed a 70-kb duplication flanked by insertion sequences. This duplication could be reversible and/or present heterogeneously in the mutant population, as a clone derived from the *slyB* mutant for *slyB* complementation does not carry the duplication. Most importantly, results described in this chapter should be validated using a $\Delta slyB$ mutant lacking this duplication to assess its implication in the phenotypes observed.

7.2 Results

7.2.1 Identification of genes potentially involved in *Y. pestis* survival in human blood and in mice

Characterization of *Y. pestis* early dissemination after intravenous injection of mice.

As *in vivo* models of septicemic plague were less studied than models of bubonic or pneumonic plague, we first set up an infection model using the fully virulent *Y. pestis* CO92 strain and OF1 mice, which were inoculated intravenously with 10^5 to 10^6 bacteria. We observed that the bacteria progressively disappears from the bloodstream (Fig 7.1A) and that bacteria were mainly found in the liver and spleen 4 hours after injection (Fig 7.1B), as it was observed for other pathogenic bacteria inoculated in mice by the IV route that were trapped in the liver and killed by neutrophils [314]

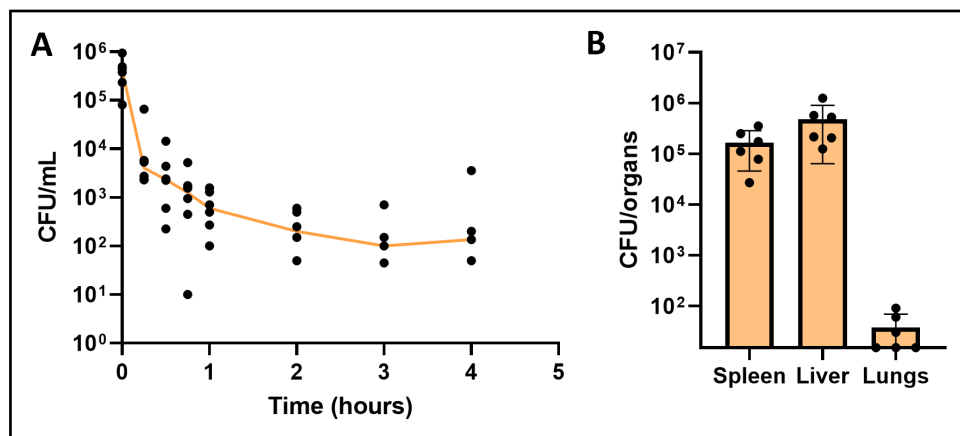


Figure 7.1. (A) *Y. pestis* CO92 burden in the blood after intravenous injection of 10^5 to 10^6 CFUs in OF1 mice. Each dot represents an individual mouse, followed over time. The orange line represent the median. (B) Bacterial burden in the spleen, liver and lungs 4 hours after intravenous injection of 10^5 to 10^6 CFUs in OF1 mice. Three lung samples were below the limit of detection of 30 bacteria. The means and standards deviation are represented for 6 different mice.

Screen of *Y. pestis* mutants reveals several loci potentially involved in human blood survival. Based on the proteome of *Y. pestis* grown in human plasma crossed with the omics data that we gathered on the Yersiniomics database, we selected and inactivated 35 loci encompassing 47 genes. We compared survival of the wild-type CO92 strain (WT) to that of these mutants after incubation for up to 24 hours in human blood (Fig 7.2 lower panel). Several mutants invalidated for factors such as YPO0337 (putative subtilase), YPO2373 (lipoprotein SlyB), YPO2531 (putative membrane protein ElaB), YPO2541 (protein of unknown function), YPO3276 (hypothetical copper oxido-reductase) or YPO3610 (hypothetical protein) had a survival decreased by more than 50% compared to that of the WT strain. Among them, the YPO2373 and YPO3276 mutants also showed a decreased virulence after intravenous injection in mice. (Fig 7.2 upper panel).

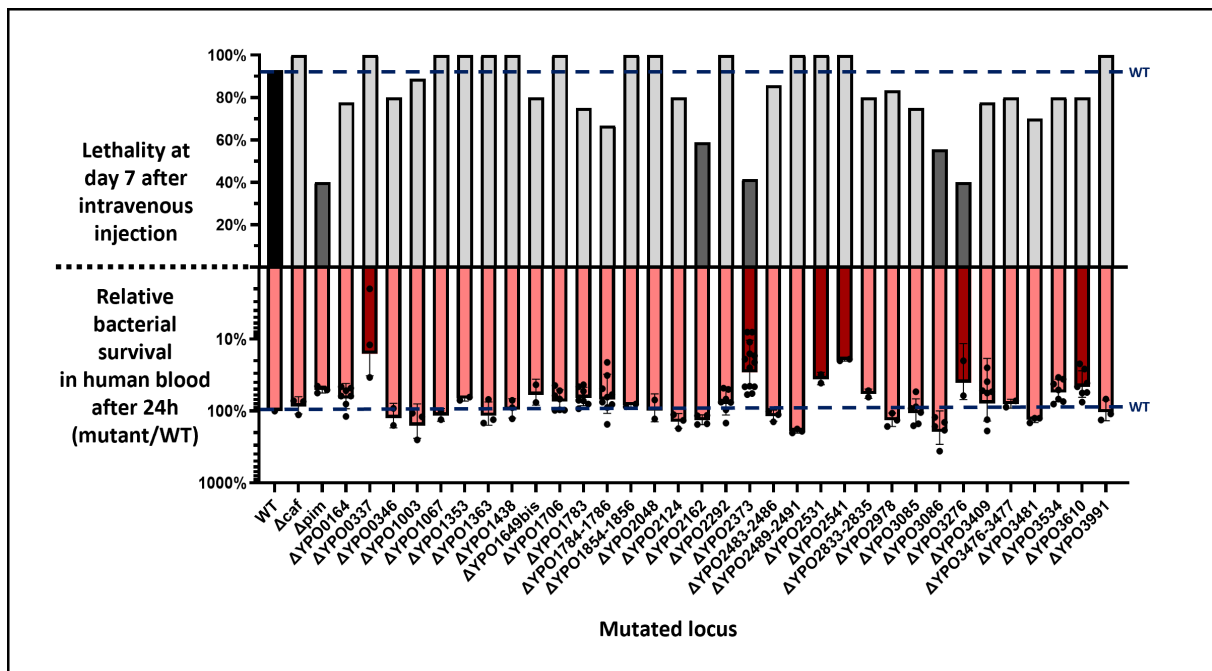


Figure 7.2. Screen of *Y. pestis* mutant survival in human blood and in mice. Mortality of OF1 mice 7 days after intravenous injection of 10-20 bacteria (upper panel). Dark grey bars represent the strains with less than 60% of lethality after intravenous injection in mice. Survival of *Y. pestis* CO92 (WT) and mutants after 24 hours of incubation in human blood, shown as the percentage of survival normalized by the CFUs of the WT (lower panel). A different blood donor was used for each replicate. The means and standard deviations are represented. Dark red bars represent mutants with less than 50% survival in human blood

7.2.2 Characterization of the $\Delta slyB$ mutant

The *slyB* mutant shows a decreased survival in human blood and decreased virulence in mice. Deletion of *slyB* led to a 5 to 10-fold decreased capacity of *Y. pestis* to survive in blood of 3 different donors (Fig 7.3A). We could consistently restore the WT level of survival in human blood by reintroducing the *slyB* gene in the mutant strain (Fig 7.3A). To assess if *slyB* was required for pathogenesis in the three main clinical forms of plague, we determined mice survival upon infection with WT, mutant and complemented strains using three infection methods reproducing the natural routes of infection in humans: intravenous injection in the tail vein, mimicking primary septicemic plague, intra-dermal injection in the ear pinna, mimicking the bite of a flea and causing bubonic plague, and intra-nasal instillation mimicking primary pneumonic plague. Virulence attenuation of the mutant after IV inoculation (Fig 7.3B) confirmed results obtained 7 days post-infection (Fig 7.2 upper panel). Deletion of SlyB also decreased *Y. pestis* virulence in models of bubonic and pneumonic plague. We could indeed observe a consistent reduction of virulence in all these forms of plague, restored by the complemented strain (Fig 7.3B). Complementation restored WT levels of virulence in the 3 murine models of plague (Fig 7.3B).

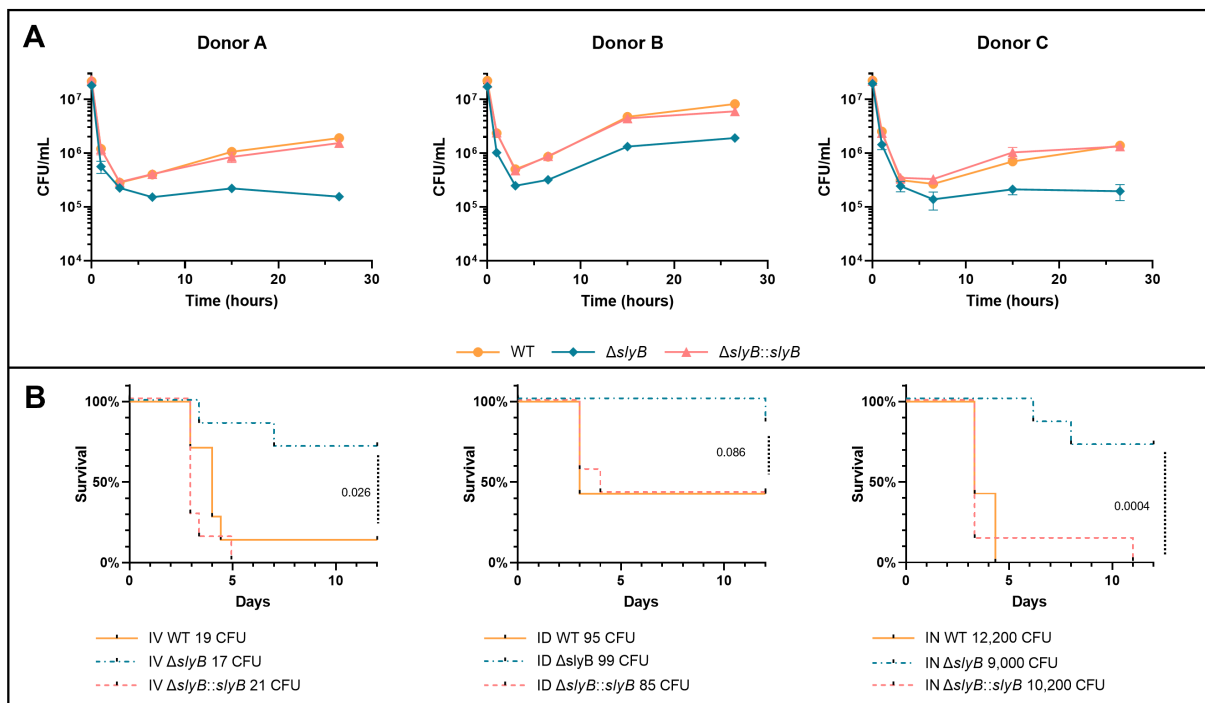


Figure 7.3. (A) Survival of the WT, $\Delta YPO2373$ ($\Delta slyB$) mutant and $\Delta slyB::slyB$ complemented strains for up to 26 hours and 30 minutes of incubation in blood of 3 different donors. The mean and standard deviation of 2 technical replicates are represented for the mutant and complemented strains. (B) Mice survival after intravenous injection of around 20 CFUs (left), intradermal injection of around 100 CFUs (middle) or intranasal instillation of around 10,000 CFUs (right) of the WT, $\Delta slyB$ mutant and $\Delta slyB::slyB$ complemented strains. Each group contains 7 mice. Infections were performed in triplicate and data shown are representative of the results. Displayed p-values are calculated between the WT and $\Delta slyB$ mutant using Mantel-Cox log-rank test.

The *slyB* mutant is more sensitive to innate immunity killing mechanisms. During the infectious process, *Y. pestis* encounters multiple host defenses, from soluble molecules such as the complement system to immune cells such as macrophages and neutrophils. To assess the role of the complement cascade on decreased survival of the *SlyB* mutant in human blood, we incubated the WT, mutant and complemented strains at 37°C in human normal serum, heat-inactivated serum and laboratory culture media supplemented with calcium as control. The *slyB* mutant grew at the same rate as the WT and complemented strains in LB broth and chemically defined M9 medium supplemented with calcium (Fig 7.4A and B). In contrast, growth of the mutant was slightly impaired in human serum after 7 hours of incubation (Fig 7.4C). It was restored to WT levels upon heat-inactivation of complement after 7 and 10 hours of incubation (Fig 7.4D). Of note, growth of the mutant was affected after 24 hours of incubation in de-complemented serum, suggesting that other compounds contribute to bactericidal activity of serum in addition to complement.

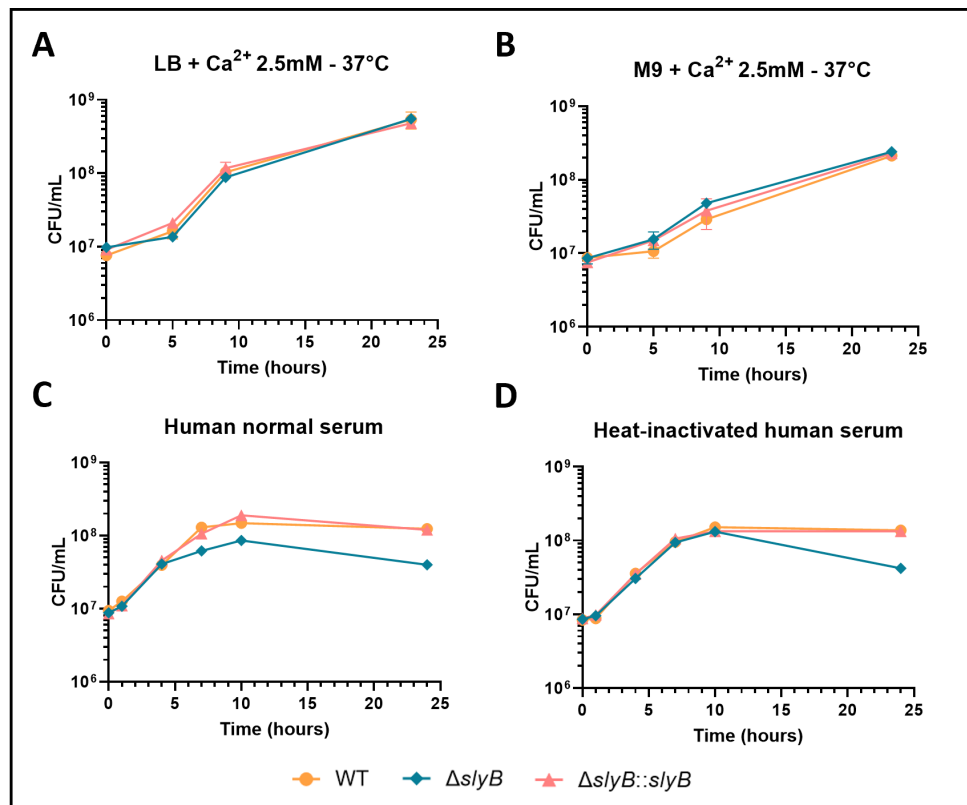


Figure 7.4. Growth of the WT, $\Delta slyB$ mutant and $\Delta slyB::slyB$ complemented strains at 37°C in: (A) lysogeny broth (LB) supplemented with 2.5 mM calcium chloride, (B) M9 minimal media supplemented with 2.5 mM calcium chloride, (C) human normal serum (one donor) and (D) heat-inactivated human serum (one donor). The means and standard deviation of 2 technical replicates are represented for growth in LB and M9.

Given that neutrophils and macrophages are primary lines of defense against bacterial infection in blood and in deep organs, and that *Y. pestis* quickly encounters these cells in the three major forms of plague, we assessed the susceptibility of the *slyB* mutant to killing by these cells. By selectively depleting neutrophils from human blood, we could abrogate the survival difference between the WT and *slyB* mutant strains for up to 15 hours (Fig 7.5A), suggesting a role of neutrophils in controlling the *slyB* mutant. To investigate further neutrophil killing mechanisms, we exposed the *slyB* mutant to neutrophil extracellular traps (NETs) and to the recently described proteoglycofili (PGF) [315], which are decorated with neutrophil granule components such as myeloperoxidase, lactoferrin, neutrophil elastase (NE) and cationic antimicrobial peptides (CAMP) such as the cathelicidin LL-37.

Contrary to incubation in PBS, we observed that *Y. pestis* could survive and grow in presence of NETs and PGF after 7 hours of incubation at 37°C (Fig 7.5B), which could possibly be due to acquisition of nutrients from degraded neutrophil products by bacterial proteases such as Pla [97]. Most importantly, we could observe a growth defect of the *slyB* mutant compared to the WT and the complemented strains treated with NETs and PGF. In addition to a reduced resistance against neutrophil killing, we also observed a reduced intracellular survival of the *slyB* mutant in human blood-derived macrophages (HBDM) after 5 hours of incubation (Fig 7.5C).

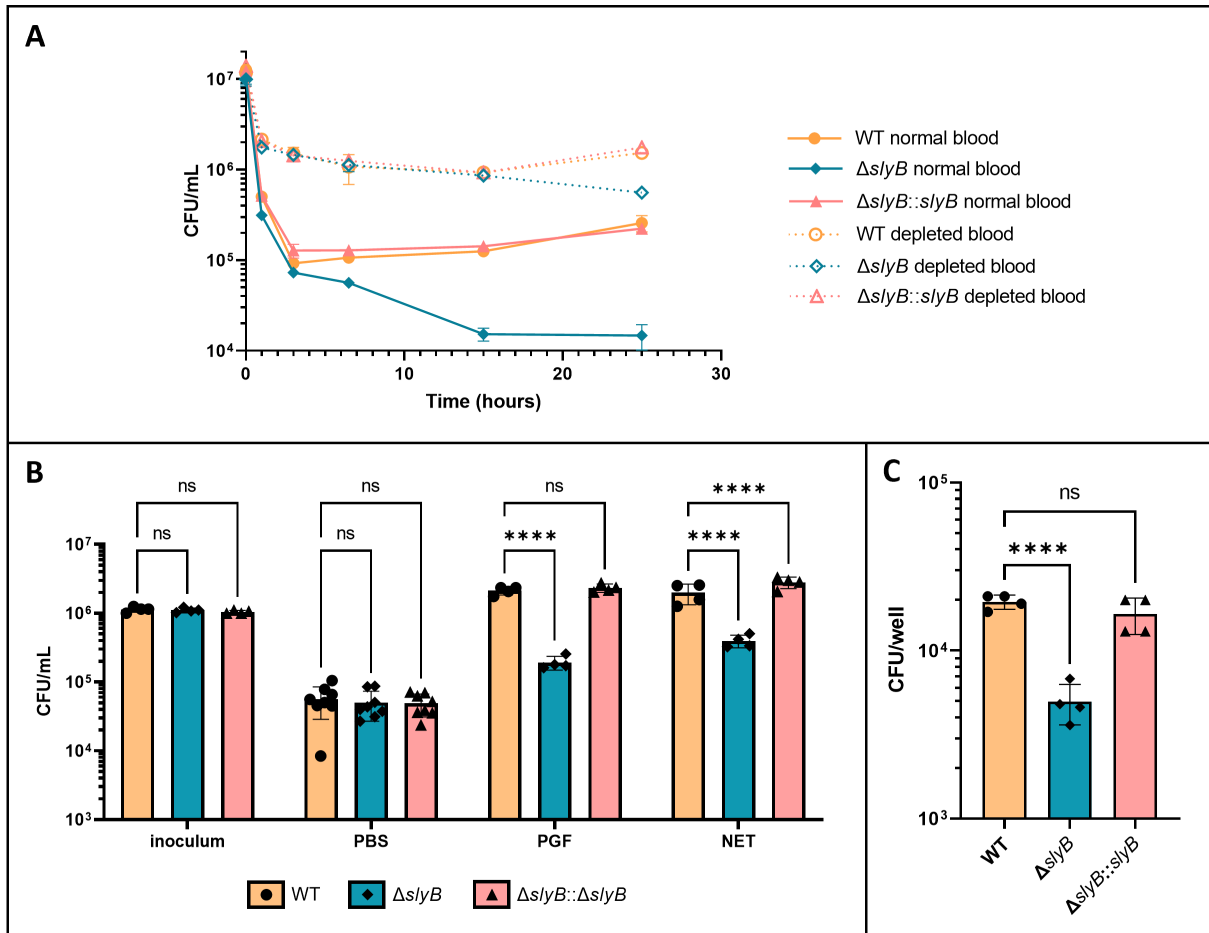


Figure 7.5. (A) Survival of the WT, $\Delta slyB$ mutant and $\Delta slyB::slyB$ complemented strains for up to 25 hours of incubation in human blood (one donor), with or without depletion of neutrophils. The means and standard deviations of 2 technical replicates are represented. (B) Survival of the WT, $\Delta slyB$ mutant and $\Delta slyB::slyB$ complemented strains after 9 hours of incubation in PBS (8 technical replicates), purified proteoglycophili (PGF, one donor, 4 technical replicates) or purified neutrophil extracellular traps (NETs, one donor, 4 technical replicates). Statistical testing was done using Tukey's multiple comparison test. ****: p-value < 0.0001. ns: non significant. The means and standard deviations are represented. (C) Intracellular survival of the WT, $\Delta slyB$ mutant and $\Delta slyB::slyB$ complemented strains in human blood derived macrophages (one donor, 4 replicates) at 5 hours post infection. Statistical testing was done using Dunnett's multiple comparison test. **** : p-value < 0.0001. ns: non significant. The means and standard deviations are represented.

The *slyB* mutant is more sensitive to membrane stress, cationic anti-microbial peptide and serine protease. Since phagocytes produce membrane-targeting compounds and SlyB had been involved in membrane stress tolerance *in vitro* [154, 156], we tested the effect of the detergent sodium dodecyl sulfate (SDS) and of the cationic antimicrobial peptide polymyxin B (PMB) on the *slyB* mutant incubated in M9 minimal medium. We observed an increased bactericidal effect of these membrane destabilizing compounds on the *slyB* mutant (Fig 7.6A) compared to the WT and complemented strains. To relate membrane stress susceptibility to neutrophil killing, we next tested the effect of specific neutrophil components on the *slyB* mutant. After exposing WT and mutant strains to increasing concentrations of purified NE, LL-37 and bactericidal/permeability-increasing protein (BPI), we observed a dose-dependent defect in survival of the mutant after treatment with NE and LL-37 (Fig 7.6B). No effect could be detected after exposure to BPI, which could be explained by the necessity of cofactors such as PLA₂ to induce bacterial killing [316], or by the specific mode of action of BPI through lipid A binding, compared to CAMP, LL-37 or the broad range protease NE.

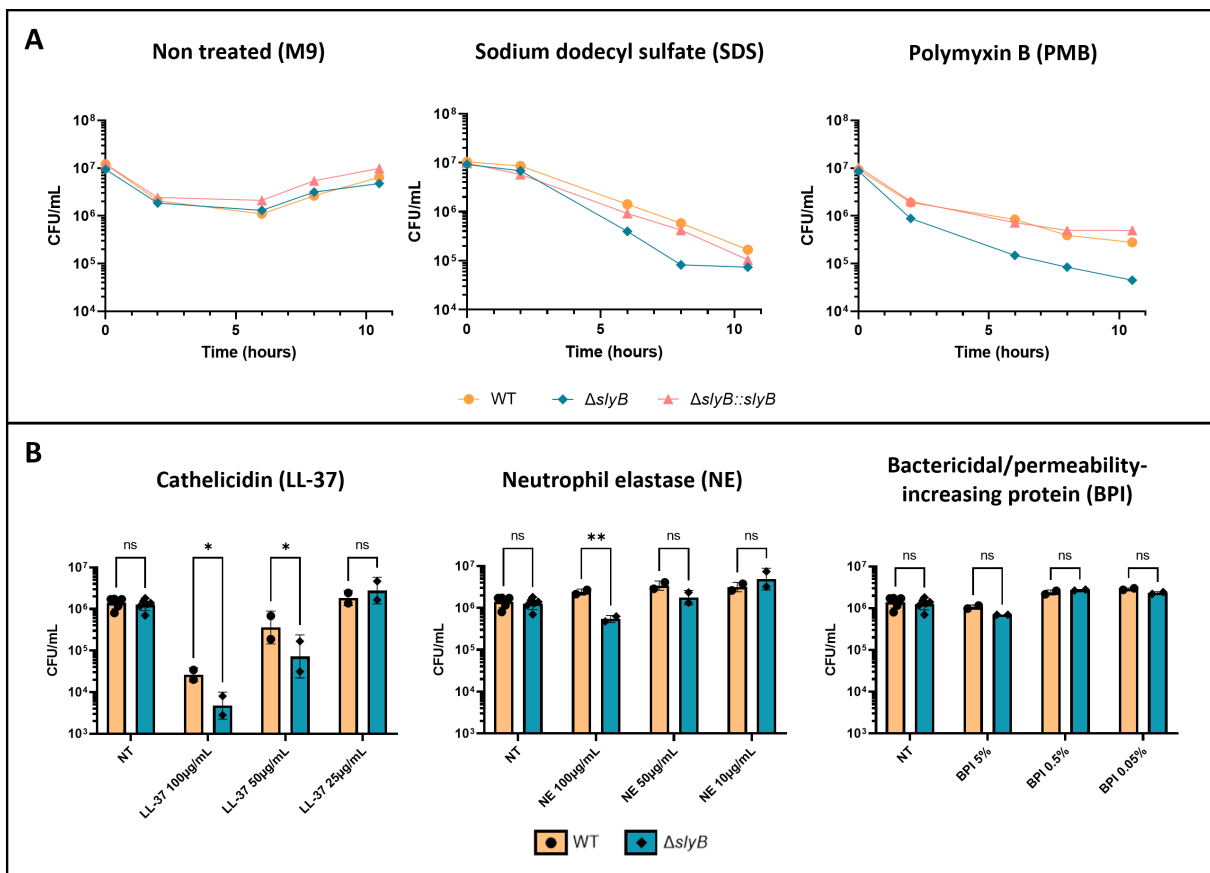


Figure 7.6. (A) Survival of the WT, $\Delta slyB$ mutant and $\Delta slyB::slyB$ complemented strains in M9 minimal medium (left panel), or in M9 supplemented with 0.01% sodium dodecyl sulfate (SDS, middle panel) or 10 μ g/mL polymyxin B (PMB, right panel). (B) Survival of the WT, $\Delta slyB$ mutant and $\Delta slyB::slyB$ complemented strains after 9 hours of incubation in M9 (non treated: NT, 6 technical replicates), or in M9 supplemented with purified cathelicidin (LL-37, 2 technical replicates per concentration, left panel), purified neutrophil elastase (NE, 2 technical replicates per concentration, middle panel) or purified bactericidal/permeability-increasing protein (BPI, 2 technical replicates per concentration, right panel). Values were log-transformed and statistical testing was done using Šidák's multiple comparison test. *: p-value < 0.05. **: p-value < 0.01. ns: non-significant. The means and standard deviations are represented.

The *slyB* deletion induces loss of periplasmic content. To better understand the role of SlyB in *Y. pestis* physiology, we analyzed the proteomes of whole cell lysate of the WT and mutant strains grown to mid-exponential phase (OD₆₀₀=0.6) at 37°C in LB broth (Supplementary Data S1). Without calcium or magnesium ions supplementation, we considered this condition as imposing a mild membrane stress to bacteria. When analyzing the cellular component Gene Ontology (GO) terms associated to the most differentially abundant proteins by gene set enrichment analysis (GSEA), we observed an enrichment in periplasmic proteins in the WT strain compared to the mutant strain (GO:0030288, outer membrane-bounded periplasmic space, normalized enrichment score = 1.78, adjusted p-value = 2.6×10^{-4} , Fig 7.7A). We looked in details at known envelope complexes including both from periplasmic and membrane components, and consistently observed a decrease in the periplasmic components compared to other proteins in the Δ *slyB* mutant, such as a decrease in LolA abundance compared to LolBCDE, LptA compared to LptBCDEFG, Skp and SurA compared to BamABCDD or soluble periplasmic binding proteins of different ATP binding cassette (ABC) transporters compared to their membrane-bound counterparts (Table 7.1 page 137). We hypothesized a stronger protein leakage in the mutant strain, possibly through a destabilized outer membrane, or formation of outer membrane vesicles releasing the periplasmic content into the medium. We could indeed detect higher levels of the periplasmic MalE protein in the supernatant of the mutant by Western blotting (Fig 7.7B).

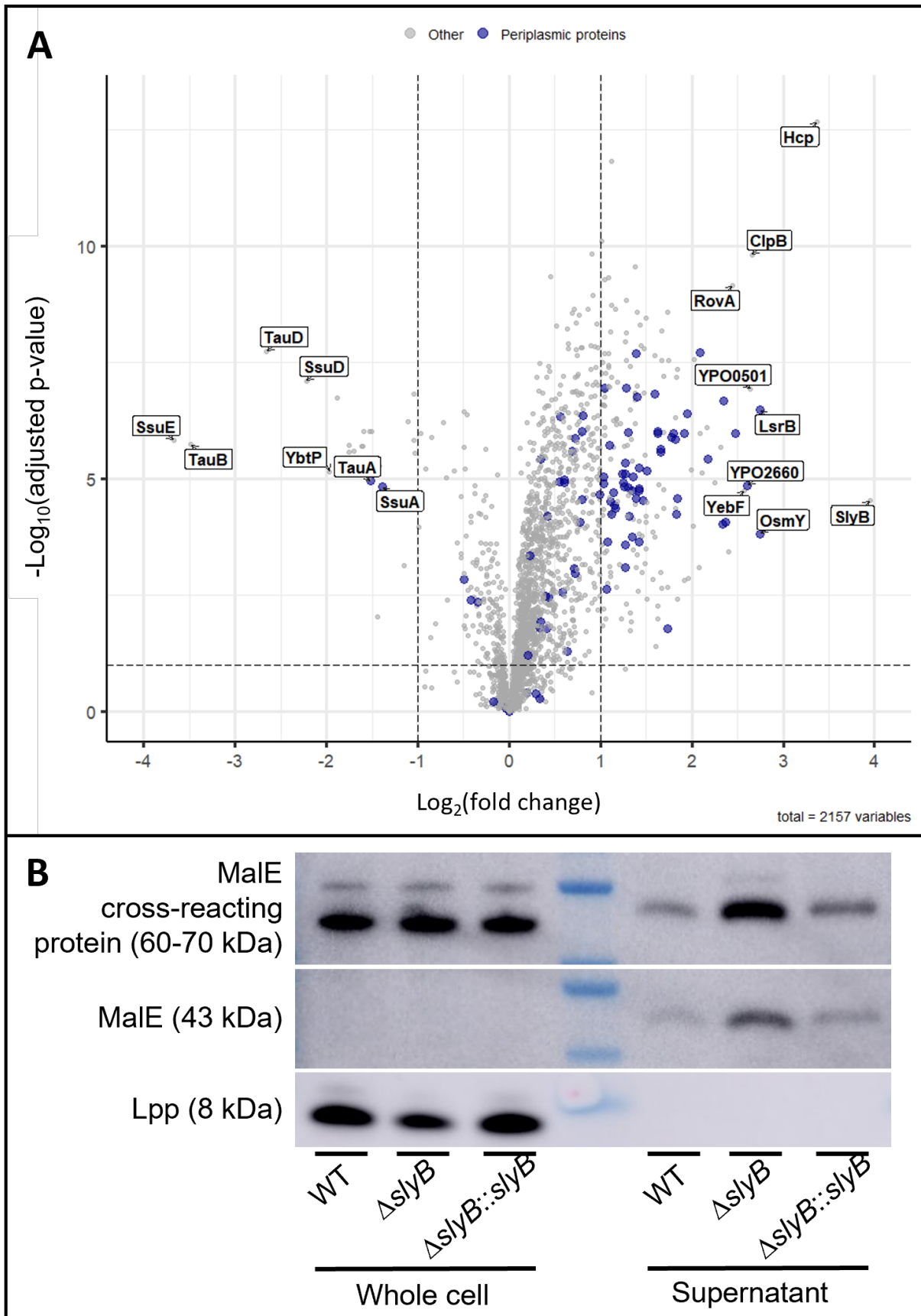


Figure 7.7. (A) Volcano plot of protein differential abundance for the WT versus Δ slyB strains. Proteins that are more abundant in the WT than in the Δ slyB mutant have a positive fold change. Soluble periplasmic proteins as annotated by Gene Ontology (GO) are highlighted in blue. The name of the most differentially abundant proteins are displayed. (B) Levels of MaIE and Lpp were analyzed by Western blot on whole cell extracts and supernatants from the WT, Δ slyB and complemented strains grown in LB broth at 37°C using specific antibodies

The *slyB* deletion induces mild envelope stress responses. To investigate if protein loss caused periplasmic stress in the mutant, we looked at abundance of proteins related to ESR such as σ E, Cpx, Rcs or Psp. We could not detect any major differences except for the Cpx operon proteins which were slightly more abundant in the Δ *slyB* strain and the Rcs response proteins which were slightly more abundant in the WT strain (Table 7.2 page 139). Importantly, pseudogenization of RcsA as well as a frameshift mutation in RcsD occurred during the emergence of *Y. pestis* from *Y. pseudotuberculosis*, modifying its regulatory function [76, 317].

Activation of these systems being rather mediated by phosphorylation and thus at the post-translational level, we then looked at the levels of proteins potentially regulated by these systems. We observed a 2-fold reduced abundance of the Braun lipoprotein Lpp in the mutant strain that was confirmed by Western blotting (Fig 7.7B). The protein was not detected in the supernatant, which excludes a leak of this massively abundant lipoprotein, anchored to the outer membrane and partly to the peptidoglycan. The lower level of Lpp could possibly involve the σ E response through induction of the transcription of the small RNA MicL which specifically targets the Lpp mRNA and represses Lpp synthesis [318]. As membrane stress often impacts LPS synthesis and/or modification, we analyzed LPS processing proteins. Most of the LPS biosynthesis proteins (Lpx) were not differentially abundant, except for the modifying enzymes LpxT and LpxP, which were slightly more abundant in the WT and Δ *slyB* strain, respectively (Table 7.3 page 139). LpxT is repressed by MicA [319] and LpxP is activated by RpoE [320] during the σ E response in *E. coli*, suggesting σ E response activation in the Δ *slyB* strain.

The absence of SlyB rewires bacterial metabolism. We next analyzed proteomic differences of metabolic pathways of the mutant. After removing periplasmic proteins from our dataset, we performed a gene set enrichment analysis (GSEA) on the Kyoto Encyclopedia of Genes and Genomes (KEGG) pathways, and observed an enrichment of sulfur metabolism components in the mutant caused by the higher abundance of the Tau, Ssu and Cys operon-encoded proteins (Table 7.4, Fig 7.8A). The yersiniabactin operon proteins, involved in siderophore synthesis required for *Yersinia* virulence, were more abundant in the mutant strain (Fig 7.8B). On the other hand, the Lsr operon proteins involved in autoinducer-2 import and quorum sensing was more abundant in the WT strain (Table 7.4, Fig 7.8C). In addition, proteins of the pCD1 encoded-type 3 secretion system (T3SS), major virulence factors of pathogenic *Yersinia*, were also more abundant in the WT strain. As pCD1-encoded proteins unrelated to T3SS such as replication and partitioning proteins were not differentially abundant, we expect the difference in T3SS abundance to come from differences in protein levels rather than in plasmid copy number (Table 7.4, Fig 7.8D).

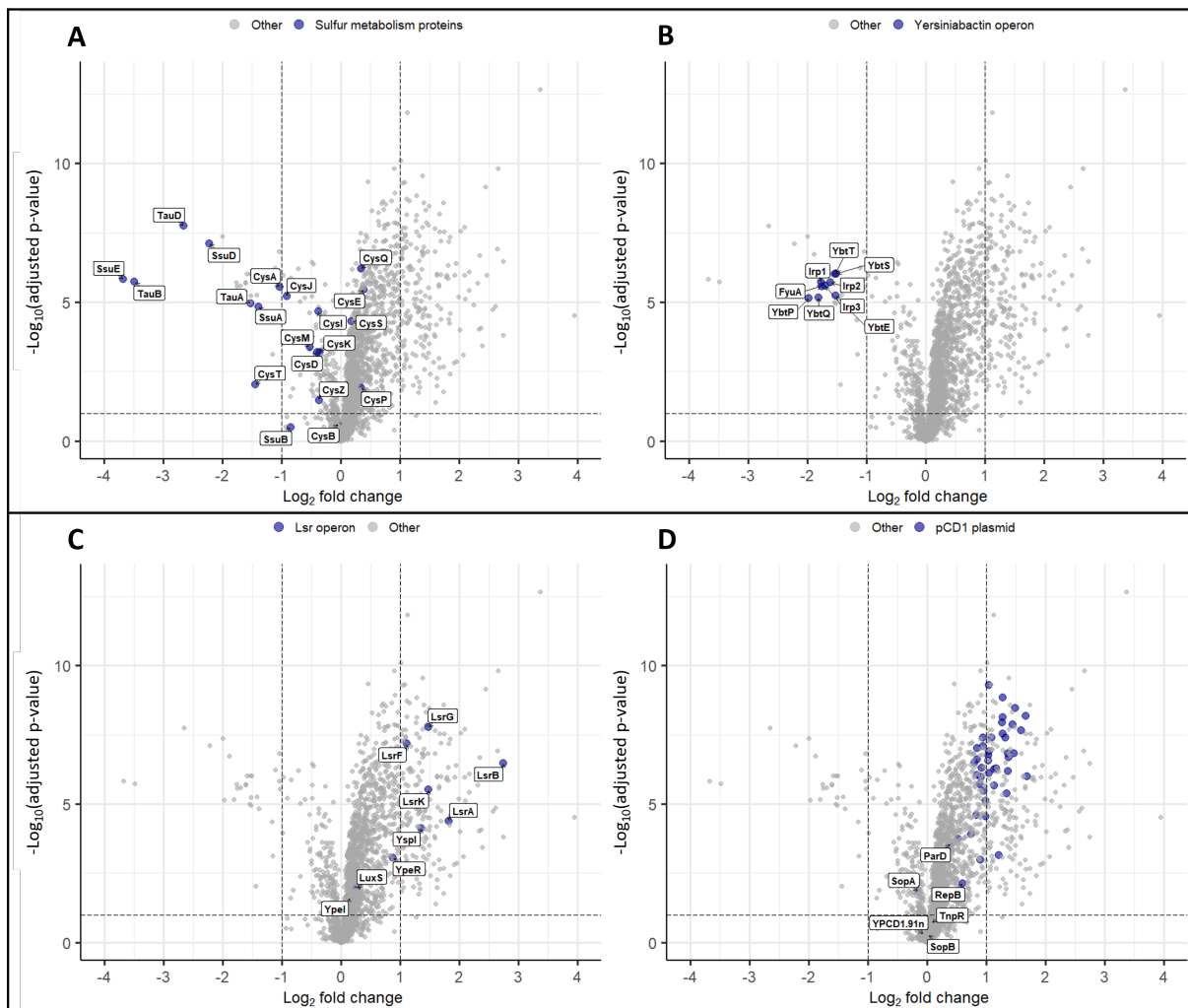


Figure 7.8. Volcano plot of protein differential abundance for the WT versus Δ *slxB* strains. Proteins that were more abundant in the WT than in the Δ *slxB* strain have a positive fold change. (A-B) Focus on more abundant proteins in the Δ *slxB* strain with: (A) proteins involved in sulfur metabolism such as the Tau, Ssu or Cys operon proteins highlighted in blue with their name displayed, and (B) proteins of the yersiniabactin operon highlighted in blue with their name displayed. (C-D) Focus on more abundant proteins in the WT strain with: (C) proteins of the Lsr operon, involved in autoinducer-2 import, highlighted in blue with their name displayed and (D) proteins of the pCD1 plasmid highlighted in blue. The names of the proteins not involved in the type three secretion system (T3SS) are displayed. All the other highlighted proteins without names are part of the T3SS.

To investigate further pathways regulated upon *slyB* deletion, we took advantage of the Yersiniomics database we previously constructed by gathering and processing omics experiments on *Yersinia* species [193]. We analyzed the correlation between protein fold changes of the *slyB* mutant and 202 transcriptomic comparison datasets from the *Y. pestis* strains CO92, KIM and 201, and the *Y. pseudotuberculosis* strains YPIII and IP32953 (Supplementary Data S2). Among the most correlated datasets, we found comparisons between stationary and exponential phase (Δ *slyB* strain being correlated with the exponential phase), comparisons between growth at high temperature, ranging from 37°C to 40°C, and growth at lower temperatures, ranging from 25°C to 30°C (the Δ *slyB* strain being correlated with the higher temperatures), but no specific patterns could be observed for the most differentially expressed gene (Fig 7.9A and B). Interestingly, the most correlated experiment was a comparison between a *crp* mutant and a WT strain of *Y. pestis* CO92 at 37°C, the *slyB* mutant correlating with the *crp* mutant condition (Fig 7.9C and D). CRP is a global regulator mediating carbon catabolite repression (CRP) together with its cofactor cyclic AMP (cAMP), allowing change in energy metabolism and carbon source during environmental changes and infection [321]. We indeed observed that most of the differentially abundant proteins or operons such as *RovA*, *Tau*, *Ssu*, *Ybt* or *Lsr* were differentially expressed in the same way in the *crp* mutant (Table 7.5 140). However, we did not detect any difference in the CRP protein level or in *CyaA*, the adenylate cyclase producing cAMP, neither a regulation of *Pla*, as it was previously described [322, 323].

To a lesser extent, a *fyuA* deletion mutant in the *Y. pestis* 201 strain [324] led to a profile similar to that of the *slyB* deletion mutant in *Y. pestis* CO92, in particular the *RovA*, *Tau*, *Ssu*, *Ybt* or T3SS proteins. However, the *Lsr* operon was also upregulated in the *fyuA* mutant, in contrast to the *slyB* mutant. These observations point towards of a metabolism rewiring upon *SlyB* deficiency, which could be partly mediated through CRP.

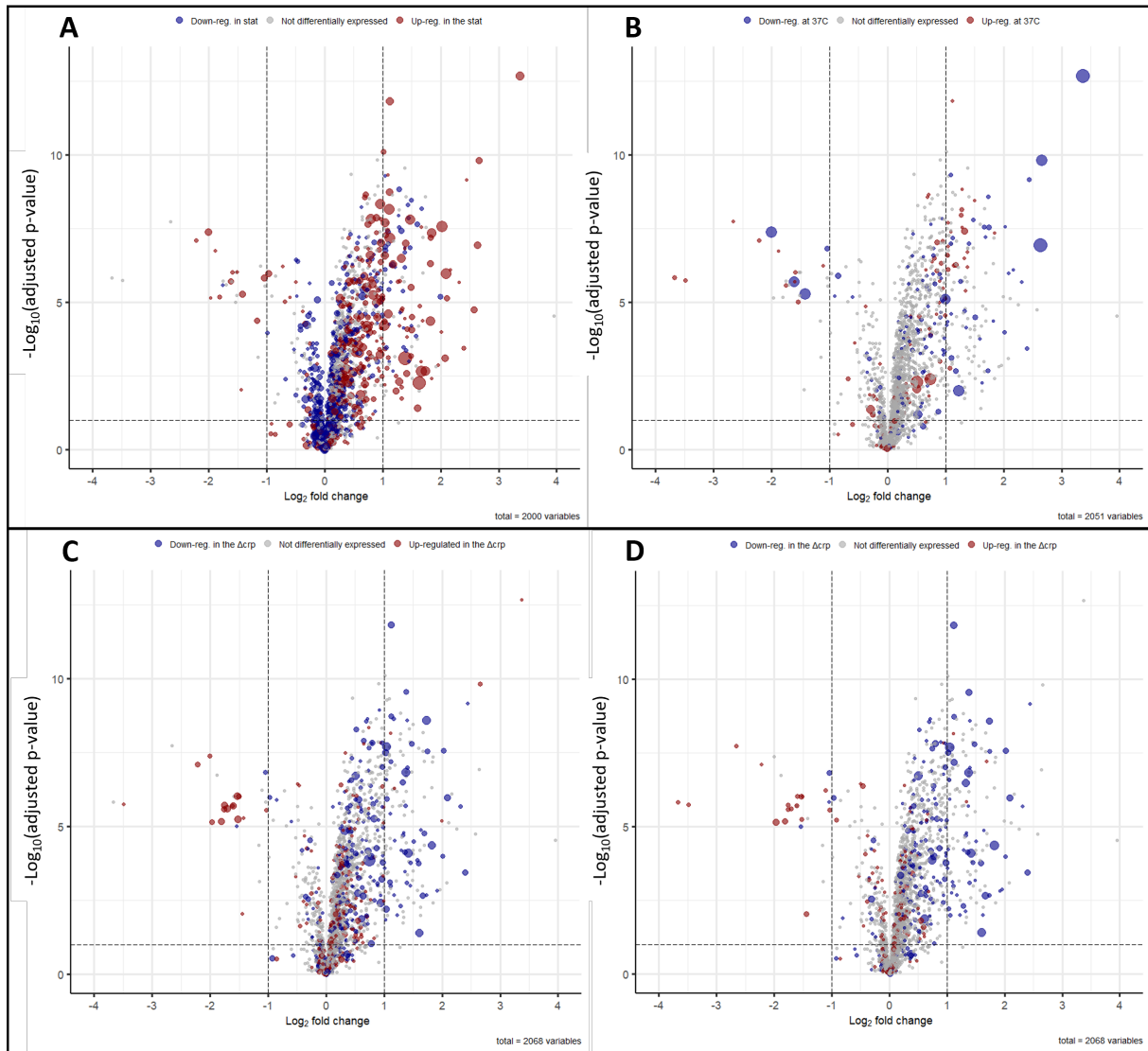


Figure 7.9. Volcano plot of protein differential abundance for the WT versus $\Delta slyB$ strains, compared to other published transcriptomics experiments. Proteins that are more abundant in the WT than in the $\Delta slyB$ strain have a positive fold change. The dot colors highlight proteins whose transcripts are more than 2 fold up-regulated (red) and 2 fold down-regulated (blue) in other transcriptomic experiments. The dot size represents the fold change for differentially expressed genes in these transcriptomic experiments. (A) *Y. pseudotuberculosis* IP32953 grown in LB broth at 28°C to OD600 3.59 (stationary phase) versus OD600 0.37 (exponential phase) [325]. (B) *Y. pestis* KIM53 grown in heart infusion broth (HIB) at 37°C versus 28°C [208]. (C-D) *Y. pestis* CO92 pCD1- grown in TMH media for a Δcrp strain versus WT strain in (C) planktonic and (D) biofilm state [323].

7.3 Discussion

7.3.1 SlyB in Gram-negative bacteria

The SlyB protein is an outer-membrane lipoprotein, described for the first time more than 30 years ago as a peptidoglycan-associated lipoprotein (PAL) cross-reacting protein and was first called PCP [326]. The associated gene name *pcp* can still be found in the literature or in some databases today. The SlyB name originates from the genetic proximity of its *slyB* encoding gene with the *slyA* gene [327], which was first erroneously identified as encoding a hemolysin in *Salmonella typhimurium*, hence called the salmolysin SlyA [328]. In reality, *slyA* (or *rovA* in *Yersinia* species [329]) encodes a transcriptional regulator which induces the hemolysin phenotype in *E. coli* but not in *S. typhimurium* [327]. The SlyA and SlyB names are still used in the literature today, despite its inaccurate initial annotation. SlyB function remains still unclear today. SlyB is well-conserved among different bacterial phyla. It has been established that SlyB is part of the core regulon of the PhoP/PhoQ two-component system in most species [150], and this has been confirmed experimentally in *E. coli* [151], *Salmonella enterica* [152], *Shigella flexneri* [153], *Pseudomonas aeruginosa* [154] and *Yersinia pestis* [150]. It is thought that SlyB broad conservation is due to its activity as negative regulator of PhoP/PhoQ, which was demonstrated in *S. enterica* [150]. However, another study pointed out that it was not the case in *E. coli* and that the conserved negative regulation of PhoQ would rather come from the PhoP/PhoQ-regulated small peptide MgrB, which was validated in *E. coli*, *S. enterica* and *Y. pestis* [155]. Other functions of SlyB can thus be hypothesized.

7.3.2 SlyB, membrane integrity and virulence

SlyB was previously identified in transposon screens as a factor involved in intracellular survival of *E. coli* in macrophages [330, 331]. Other studies showed a role of SlyB in membrane stress tolerance [154, 156], but the implication of SlyB in bacterial virulence and interaction with the host immune system has not been investigated so far. Using *in vitro*, *ex vivo* and *in vivo* approaches, we showed that *Y. pestis* SlyB contributes not only to membrane stress tolerance but also to pathogenesis in the three forms of plague in mice. Deletion of *slyB* had pleiotropic effects on bacterial interactions with host innate immune system, such as decreased resistance to complement, reduced intracellular survival in macrophages and a decreased resistance to neutrophil bactericidal compounds. This resulted in an overall virulence decrease *in vivo*, where bacteria encounter these host defenses in different environments such as the skin, lymph nodes, lungs, the blood, liver and spleen.

It has been shown that the PhoP/PhoQ TCS is important for plague pathogenesis [148] and more particularly for bacterial resistance to neutrophil killing [147]. O'Loughlin et al. showed that PhoP/PhoQ-dependent resistance to neutrophil granules can only be partly explained by regulation of *ugd* and *pmrK*, which mediate 4-amino-4-deoxy-L-arabinose (4-aminoarabinose) addition to lipid A, known to reduce the negative charge of LPS and protect against CAMPs [161]. We propose that SlyB is an additional PhoP/PhoQ-regulated factor providing increased resistance to the bactericidal activity of neutrophils.

Importantly, *Y. pestis* harbors a mutation in the *pagP* gene and a deletion in the *lpxL* gene, maintaining a tetra-acyl lipid A at 37°C. These evolutionary losses are thought to mediate immune evasion by reducing recognition by TLR4 [168–170]. However, reduced acylation could also lead to increased permeability of the outer membrane [171]. It has also been shown that Ail, a major OMP required for *Y. pestis* virulence, interacts with the LPS and helps to maintain its integrity at 37°C [108, 109]. One could hypothesize that SlyB contribute with Ail and other OMPs to maintain the OM integrity in *Y. pestis* grown at 37°C, by molecular

mechanisms that remain to be fully deciphered.

7.3.3 SlyB, periplasmic homeostasis and stress response

Consistent with a destabilization and permeabilization of the outer membrane, we observed a dramatic loss of periplasmic proteins in the $\Delta slyB$ mutant during growth in LB, which could be explained by leakage through the more permeable outer membrane, or by enhanced outer-membrane vesicle release. Among these less abundant soluble periplasmic proteins, we detected virulence-associated proteins such as the serine protease inhibitor ecotin, shown to inhibit NE activity [125], and contribute to serum resistance [127] and *Yersinia* virulence [126], or the DsbA protein required for stable expression of the T3SS [124].

Given the importance of the periplasm for nutrient import and cellular processes, it is not surprising that a decrease in periplasmic soluble proteins leads to an important metabolic rewiring. We could hypothesize that the WT strain could import specific carbon sources such as glucose easier and exhaust this source faster than the $\Delta slyB$ mutant, hence inducing a more efficient CRP response. Alternatively, a reduced import of quorum-sensing signal AI-2 in the $\Delta slyB$ mutant could modify bacterial metabolism, potentially explaining a proteomic profile resembling the exponential phase. Metabolic changes in response to the host environment are primordial for bacterial virulence [332] and the role of regulators such as CRP in virulence has been well described in *Yersinia* species [96, 143, 213, 322, 323, 333–336]. Metabolic dysregulation caused by an OM perturbation could therefore contribute to the virulence defect of the $\Delta slyB$ mutant. Further studies could define the cause of the metabolic changes by measuring intracellular cAMP or (p)ppGpp levels, AI-2 release or other metabolites which could point towards specific metabolic regulation. Importantly, proteins encoded by the *tau*, *ssu* and *cys* operons involved in sulfur metabolism, clustered together when analyzing a set of microarrays representative of various environmental conditions and/or mutations in *Y. pestis*. The cluster was associated to environmental stress, in line with a signature of enhanced stresses sensed by the SlyB mutant [197].

The Braun lipoprotein Lpp was less abundant in the $\Delta slyB$ mutant, whereas we could not detect it in the supernatant. Interestingly, Lpp was shown to be downregulated by the MicL sRNA induced by the σE response to OMP misfolding and periplasmic LPS [318], presumably to reduce the load of Lpp on the Lol pathway transporting lipoproteins through the periplasm, and on the Lpt pathways transporting the LPS but also some membrane-crossing lipoproteins such as Lpp or SlyB, as recently shown [337]. Lpp is one of the most abundant proteins in Gram-negative bacteria, linking the peptidoglycan to the outer membrane. Its absence has a major impact on virulence in *Y. pestis* [176, 177]. Reduction of its level could also be a hint of a σE response, that is corroborated by an induction of LpxP and a decrease in LpxT, LamB or OmpW abundances, all regulated by the σE response [319]. This would support the idea of an envelope default and particularly of an OMP insertion default into the OM upon deletion of *slyB*. However a drastic drop in OMPs was not observed, as we could expect from a classical σE response [319].

On the other hand SlyB was previously thought to be regulated by the σE stress response. In mucoid *Pseudomonas aeruginosa*, the PA3819 locus of the PAO1 reference strain was previously annotated as a *slyB* homolog (PA1053) but was later reannotated as YcfJ. Its mRNA was over-expressed upon RpoE (AlgU) induction [338], concordant with the putative RpoE binding site identified upstream of this gene [339]. Interestingly, this promoter region was also found at the 5' end of *Salmonella slyB* mRNA [339] but its function remains to be demonstrated [340]. Moreover, we could not detect any RpoE binding site in the 5' region of *Y. pestis slyB* locus. In contrast, the SlyB protein abundance dramatically increased along with OMPs such as OmpA and OmpW in an RpoE deficient *E. coli* 0157 strain at early

stationary phase [341], supporting an RpoE-mediated repression of SlyB in a mechanism similar to that discussed above for the control of *Y. pestis* Lpp levels. However, extensive studies of the RpoE regulon never identified *slyB* as a target. The parallel increase in SlyB and OMPs abundances point to a tight molecular association of SlyB with the OMPs that are known to be repressed by σ E [319]. Further characterization of the σ E response upon *slyB* deletion and of SlyB regulation by RpoE or small RNAs could shed light on feedback loops involved in the envelope quality control.

While virtually no other major ESR were detected, a mild abundance increase of the *cpx* operon proteins was observed in the Δ *slyB* mutant. This could explain the decreased abundance of the T3SS which is regulated by Cpx [134], but also the levels of the global virulence regulator RovA [90] which is repressed by Cpx [135–137], and regulated by the carbon storage regulator system Csr [333]. Altogether, these data link envelope stress response activated by the *slyB* deletion to virulence determinants, ultimately leading to reduced virulence of *Y. pestis*.

7.4 Methods

7.4.1 Bacterial strains, culture media and blood

The fully virulent *Y. pestis* CO92 strain was used in this study [181] Bacteria were routinely grown on LB agar plates supplemented with 0.002% pork haemin (LBH) at 25°C if not stated otherwise. Frozen human plasma (anticoagulated with acid-citrate-dextrose), frozen human serum, fresh human blood (anticoagulated with heparin) or buffy coats were provided by the Etablissement Français du Sang (EFS). For mutant screening, fresh blood was stored at 4°C and used less than 24 hours after collection from donors. For other experiments, fresh blood was stored at room temperature and used less than 6 hours after collection from donors. Bacterial growth curves were performed in 10 mL of LB at 28°C, or in 10 mL of human serum, modified M9 supplemented with 2.5 mM CaCl₂ or LB supplemented with 2.5 mM CaCl₂ at 37°C, at 180 rotations per minute (rpm) in 125 mL polycarbonate flasks. M9 modified media was prepared by supplementing M9 salts with 2 mM MgSO₄, 0.1 mM CaCl₂, 1% glucose, 1% casamino acid and 1 mM thiamine-HCl. Serum decomplexation was performed in a waterbath at 56°C for 30 minutes. For bacterial enumeration, bacteria were serially diluted 1/10 (20 μ l in 180 μ L) in phosphate-buffered saline (PBS) and plated on LBH agar plate. Colony-forming units (CFU) were enumerated after incubation at 28°C for 48 hours, or at room temperature for 3 to 4 days.

7.4.2 Mutagenesis and complementation

Gene deletion was performed as described before [342] Briefly, forward oligonucleotides were designed with around 50 nucleotides of homology with the beginning of the target genes and around 20 nucleotides of the beginning a kanamycin resistance cassette. The reverse oligonucleotides were designed with around 50 nucleotides of homology with the end of the target genes and around 20 nucleotides of the end of the kanamycin resistance cassette. PCR products were precipitated overnight in potassium acetate and ethanol at -20°C, centrifugated at 15,000 *g* for 30 minutes at 4°C, then 1 mL of 70% ethanol was added and centrifugated at 15,000 *g* for 15 minutes at 4°C. Supernatant was discarded and DNA pellets were dried for 15 minutes in a SpeedVac. The DNA pellets were resuspended in 5 μ L of milliQ water and dialyzed on 0.075 μ m filter for 30 minutes. Dialyzed DNAs were electroporated in electrocompetent *Y. pestis* CO92 strain harboring the pKOBEG-*sacB* plasmid. Recombinant clones harboring the resistance cassette were selected on LBH plates

containing 30 µg/mL kanamycin. Absence of the targeted genes was assessed by PCR using primers inside the target, and insertion of the cassette was assessed by PCR on the flanking region, using primers outside of the target and inside of the cassette. Curation of the pKOBEG-*sacB* plasmid was performed by growing clones on LBH plate without sodium chloride and with 10% of sucrose. Presence of the virulence plasmids was confirmed by PCR on the *yopM* (pCD1), *caf* (pMT1) and *pla* (pPCP1) genes.

The *slyB* mutant was complemented in *trans* by cloning the gene and its upstream and downstream regions in the pUC18R6K plasmid which does not replicate in *Y. pestis*, and harbors the miniTn7 transposon with a chloramphenicol resistance cassette. Electrocompetent cells of the Δ *slyB* strain were electroporated with 400 ng of pUC18R6K-miniTn7::*slyB* and 400 ng of pTNS2 harboring the transposase and which does not replicate in *Y. pestis* [343]. Selection for the insertion of the miniTn7 was done on LBH plates containing 25 µg/mL chloramphenicol. Verification of the presence of *slyB* was done by PCR with primers inside *slyB*, and insertion of the miniTn7 was verified with PCR on the flanking regions. Absence of the pUC18R6K-miniTn7::*slyB* and of the pTNS2 was assessed by streaking bacteria on LBH with 100 µg/mL carbenicillin and PCR on the *bla* resistance cassette. Strains genomes were analyzed by Nanopore MinION sequencing to validate the constructions.

7.4.3 Mutant screening in human blood

Parental CO92 and mutant strains were grown for 24 hours on LBH plate at 25°C. Bacteria were resuspended in 3 mL PBS, vortexed for 1 minute and the optical density at 600nm (OD600) was adjusted to 0.25 in 10 mL PBS to reach a concentration around 2×10^8 CFU/mL. Fresh blood was divided in 1 to 2 mL aliquots in 14 mL polypropylene tubes with round bottom, pre-warmed for 30 minutes at 37°C under agitation at 180 rpm, then inoculated with 1/10 (100 µL to 200 µL) of the prepared bacteria to reach a concentration of around 2×10^7 CFU/mL. Blood was incubated at 37°C under agitation at 180 rpm, and bacteria were enumeration at different time points from 0 to 24 hours post-inoculation. At each timepoint, blood was gently mixed by slowly pipetting with a P1000 pipette, and 20 µL were added to 180 µL PBS for bacterial enumeration. Because of the possible variability between donors, growth of the parental strain was studied in each blood, and growth of each mutant was assessed in the blood of 2 to 4 donors and compared to that of the parental strain in the blood of the same donor.

7.4.4 Mice experiments

All mice experiments were performed in a BSL-3 animal facility. 7 to 9-week-old OF1 mice were purchased from Charles River Laboratory. For intravenous and intradermal injection, bacteria were grown for 24 hours on LBH plates at 25°C. Bacteria were resuspended in 3 mL PBS, vortexed for 1 minute and the optical density at 600 nm (OD600) was adjusted to 0.25 in 10 mL PBS to reach a concentration around 2×10^8 CFU/mL. For intravenous injection, the suspension was serially diluted 1/10 6 times to reach around 20 bacteria in 100 µL. Mouse tails were heated with a paper soaked in warm water, and 100 µL of bacterial suspension were injected in the caudal vein with a 29G needle. The inoculum was verified by plating 100 µL of the suspension on LBH plates between each injection. For intradermal injection, the suspension was serially diluted to reach 5×10^4 CFU/mL (100 CFU in 2 µL) and the inoculum was verified by plating on LBH plates. Mice were anesthetized by intraperitoneal injection of xylazine and ketamine and 2 µL of the bacterial suspension were injected in the ear pinna with a NanoFil™ syringe (World Precision Instrument). For intranasal inoculation, strains were grown in BHI at 26°C under agitation at 250 rpm for 8 hours. OD600 was then adjusted to 0.05 in 9 mL BHI supplemented with 2.5 mM CaCl₂ and incubated at 37°C for

15 hours under agitation at 250 rpm to reach an OD600 between 2 and 4. Bacteria were diluted to reach a concentration of 5×10^5 CFU/mL (1×10^4 CFU in 20 μ L) and the inoculum was verified by plating on LBH plates. Mice were anesthetized by intraperitoneal injection of xylazine and ketamine and 20 μ L of the bacterial suspension were instilled intranasally by successive instillations of 5 μ L in each nostril. Survival of the mice was followed for 10 days.

7.4.5 Neutrophil depletion from human whole blood

Fresh heparinized blood was filtered on 30 μ m mesh to remove clumps and aggregates and separated in 2 aliquots of 4 mL. StraightFrom® Whole Blood CD66b kit (Miltenyi Biotec) was used to selectively deplete neutrophils. 200 μ L of CD66b beads (respectively 200 μ L of PBS as control) were added to 4 mL blood, incubated for 15 minutes at 4°C and transferred in conditioned Whole Blood Columns (Miltenyi Biotec) following the manufacturer's instructions. The first drops of eluted blood were discarded, and the first elution step was kept as neutrophil-depleted blood (CD66b beads) or control (PBS). Blood inoculation and bacterial enumeration were performed as described above for mutant screening.

7.4.6 Macrophages intracellular survival

Human blood derived macrophages were isolated and differentiated from buffy coats as previously described [191]. Briefly, blood mononuclear cells were isolated by density gradient centrifugation (Ficoll-Paque Premium, Sigma Aldrich, St. Louis, MI, USA). Monocytes were purified from peripheral blood mononuclear cells by positive selection with magnetic CD14 MicroBeads using LS columns (Miltenyi Biotec, Bergisch Gladbach, Germany). Monocytes were cultured for 7 days at 37°C and 5% CO₂ in RPMI-1640 supplemented with 10% heat-inactivated FBS, L-glutamine and M-CSF (20 ng/mL; R&D systems). Cells were fed every 2 days with complete medium supplemented with M-CSF. 96-well plates were seeded with 50 μ L containing 10^4 cells per well. Bacteria were grown in 10 mL LB at 28°C under agitation at 180 rpm to reach an OD600 of 0.4. Bacteria were serially diluted to reach 2×10^6 CFU/mL (10^5 CFU/ml in 50 μ L) in complete cell media. 50 μ L of bacterial suspension were added on cells at a multiplicity of infection of 10. Plates were centrifugated for 5 minutes at 400 *g* and incubated for 20 minutes at 37°C with 5% CO₂. Cells were washed three times with 150 μ L PBS, then fresh cell medium containing 10 μ g/mL gentamicin was added to cells to kill extracellular bacteria. Cells were incubated for 8 hours at 37°C with 5% CO₂. The medium was then removed and the cell lysed by addition of 100 μ L of Triton X100 0.1% for 10 minutes at room temperature. Lysates were serially diluted in PBS to enumerate intracellular bacteria.

7.4.7 Stress assays

Y. pestis strains were grown overnight on LBH agar plates at 25°C, resuspended in 3 mL PBS and vortexed for 1 minute. OD600 was adjusted to 0.25 in 10 mL PBS, then serially diluted to reach 2×10^6 CFU/mL. 2 μ L of bacterial suspension were aliquoted in sterile PCR plates. 2 μ L of stress agents or PBS were added on bacteria and gently mixed by pipetting. Wells were incubated at 37°C for 7 to 9 hours, then 66 μ L of PBS were added in the wells, mixed by pipetting and serially diluted for bacterial enumeration. PGFs and NETs were kindly provided by Dr. Benoît Marteyn.

7.4.8 Mass spectrometry

Sample preparation. *Y. pestis* WT CO92 strain and Δ *slyB* mutant were grown overnight on LBH agar plates at 25°C, resuspended in 3 mL PBS and vortexed for 1 minute. OD600 was adjusted to 0.25 in 10 mL PBS and 500 μ L were inoculated to 4.5 mL of preheated LB at 37°C in 14 mL polypropylene tubes in 5 replicates. Bacteria were incubated at 37°C under agitation at 180 rpm for 8 hours and 30 minutes to reach an OD600 of 0.6-0.7. Bacteria were pelleted by centrifugation at 4°C then washed three times with 1 mL of cold PBS. Proteins were extracted as described in chapter 5. Briefly, pellets were resuspended in 20 μ L trifluoroacetic acid (TFA) for 25 minutes, then neutralized by addition of 200 μ L of Tris 2M. Reduction and alkylation was performed by addition of 24 μ L of tris(2-carboxyethyl)phosphine (TCEP) 100 mM and chloroacetamide (CAA) 400 mM for a final concentration of TCEP 10 mM and CAA 40 mM, then incubation at 95°C for 5 minutes. Protein concentration was measured by spectrometry in a 384-well plate with an excitation wavelength of 280 nm and an emission wavelength of 360 nm. Tryptophan standard curve was performed using pure L-tryptophan dissolved in distilled water. Proteins were digested with mass-spectrometry grade trypsin (1:50 ratio) in a Thermomixer at 37°C, 600 rpm for 12 hours. Digestion was stopped by addition of 20 μ L of TFA. 16 μ g of each digested samples were pooled for further library preparation. Samples were stored at -80°C before further processing.

Protein digestion and desalting. Proteins were digested using Sequencing Grade Modified Trypsin (Promega - V5111) with a 1:50 ratio (enzyme:protein) at 37°C for 12h before stopping the digestion with 20 μ L of TFA. Then, digested peptides were desalted using C18 cartridge (Agilent Technologies, 5 μ L bead volume, 5190-6532) and eluted with acetonitrile (ACN) 80%, formic acid (FA) 0.1%. Finally, the peptide solutions were speed-vac dried and resuspended in ACN 2%, FA 0.1% buffer. For each sample, absorbance at 280 nm was performed with a NanodropTM 2000 spectrophotometer (Thermo Scientific) to inject an equivalent of DO = 1.

Peptide mixing and pre-fractionation A pool of all SPEED digested samples was used to obtain a spectral library for the DIA approach. To do this, an equivalent amount of each digested sample was pooled together before proceeding to a peptide fractionation using the Fractionation v1.1 protocol of the AssayMAP Bravo (Agilent). The dried pooled sample (80 μ g) was resuspended in 20 mM ammonium formate, pH 10 before a high pH reverse phase fractionation. RPS cartridge (Agilent Technologies, 5 μ L bead volume, G5496-60033) were primed with 100 μ L ACN 80%, FA 0.1% and equilibrated with 100 μ L 20 mM ammonium formate (AmF), pH 10. The samples were loaded at 5 μ L/min followed by an internal cartridge wash and cup wash with 50 μ L of 20 mM AmF, pH 10 at 5 μ L/min. Step elution was performed with 60 μ L of ACN 5%, 15%, 25%, 35%, 45%, and 80% in 20 mM AmF, pH 10 at 5 μ L/min. A preexisting volume of 20 μ L containing the same elution buffer was present in the collection plates upon elution. All fractions were speed-vac dried and resuspended with ACN 2%, FA 0.1% before injection. For all fractions and individual samples, iRT peptides were spiked as recommended by Biognosys (Biognosys - Ki-3002-1). LC-MS/MS for DDA and spectral libraries creation. A nanochromatographic system (Proxeon EASY-nLC 1200 - Thermo Scientific) was coupled online with an Orbitrap Fusion Lumos tribrid mass spectrometer (Thermo Scientific). 1 μ g of peptides was injected into a capillary column picotip silica emitter tip (home-made column, 42cm x 75 μ m ID, 1.9 μ m particles, 100 Å pore size, ReproSil-Pur Basic C18 - Dr. Maisch GmbH, Ammerbuch-Entringen, Germany) after an equilibration step in 100% solvent A (H₂O, 0.1% FA). Peptides were eluted with a multi-step gradient from 5 to 25% buffer B (ACN 80% / FA 0.1%) in 130 min, 25 to 40% buffer B in 20 min and 40 to 95% buffer B in 14 min at a flow rate of 250 nL/min for up to 178 min.

Column temperature was set to 60°C. Mass spectra were acquired using Xcalibur software using a data-dependent Top 2s method with a survey scans (300-1200 m/z) at a resolution of 60,000 and MS/MS scans (fixed first mass 110 m/z) at a resolution of 15,000. The AGC target and maximum injection time for the survey scans and the MS/MS scans were set to 4.0×10^5 , 50ms and 5.0×10^4 , 50ms respectively. The isolation window was set to 1.6 m/z and normalized collision energy fixed to 30 for HCD fragmentation. We used a minimum intensity threshold of 5×10^4 . Precursor ion charge states from 2 to 7 were accepted and advanced peak determination was enable. Exclude isotopes was enabled and selected ions were dynamically excluded for 45 seconds.

LC-DIA-MS for DIA. Mass spectra were acquired in DIA mode with the XCalibur software using the same nanochromatographic system coupled on-line to an Orbitrap Fusion Lumos tribrid Mass Spectrometer. For each sample, 1 µg of peptides was injected into the same capillary column picotip silica emitter tip after an equilibration step in 100% solvent A (H₂O, 0.1% FA). Peptides were eluted with a multi-step gradient from 5 to 25% buffer B (ACN 80% / FA 0.1%) in 95 min, 25 to 40% buffer B in 15 min and 40 to 95% buffer B in 10 min at a flow rate of 250 nL/min for up to 130 min. Column temperature was set to 60°C. MS data was acquired with a scan range from 300 to 1200 m/z. The DIA method consisted in a succession of one MS scan at a resolution of 60,000 and 36 MS/MS scans of 1 Da overlapping windows (isolation window = 25 m/z) at 30,000 resolution. The AGC (Automatic Gain Control) target and maximum injection time for MS and MS/MS scans were set to 4.0×10^5 , 50 ms and 5.0×10^5 , 54 ms respectively. The normalized collision energy was set to 30 for HCD fragmentation.

Bioinformatic analyses. MaxQuant analyses: DDA raw files were processed using MaxQuant software version 2.0.3.0 [344] with Andromeda search engine [345]. The MS/MS spectra were searched against a personal *Y. pestis* CO92 database containing 3,991 entries, including 3,915 unique proteins from the initial CO92 Sanger sequencing [181], re-annotated by RefSeq (Accession GCF_000009065.1_ASM906, accessed in 2020) and 76 small open frame (sORF) encoded peptides (SEP) recently identified [231]. Variable modifications (methionine oxidation and N-terminal acetylation) and fixed modification (cysteine carbamidomethylation) were set for the search and trypsin with a maximum of two missed cleavages was chosen for searching. The minimum peptide length was set to 5 amino acids and the false discovery rate (FDR) for peptide and protein identification was set to 0.01. The main search peptide tolerance was set to 4.5 ppm and to 20 ppm for the MS/MS match tolerance. Second peptides was enabled to identify co-fragmentation events.

Spectronaut analyses: Spectronaut 17.0.221202.55965 (Quasar) (Biognosys AG) was used for DIA-MS data analyses. The data extraction was performed using the default BGS Factory Settings. Briefly, for identification, both precursor and protein FDR were controlled at 1%. For quantification, Qvalue was used for precursor filtering and no imputation strategy was used; peptides were grouped based on stripped sequences. Cross Run Normalization was disabled.

Statistical analysis. To find the proteins more abundant in one condition than in another, the intensities quantified using Spectronaut were compared. Only proteins identified with at least one peptide that is not common to other proteins in the FASTA file used for the identification (at least one "unique" peptide) were kept. Additionally, only proteins with at least four intensity values in one of the two compared conditions were kept for further statistics. Proteins absent in a condition and present in another are put aside. These proteins can directly be assumed differentially abundant between the conditions. After this filtering, intensities of the remaining proteins were first log-transformed (log₂). Next, intensity values

were normalized by median centering within conditions (section 3.5 in [346]). Missing values were imputed using the `impute.slsa` function of the R package `imp4p` [347]. Statistical testing was conducted using a `limma` t-test thanks to the R package `limma` [348]. An adaptive Benjamini-Hochberg procedure was applied on the resulting p-values thanks to the function `adjust.p` of the `cp4p` R package [349] using the robust method described in [350] to estimate the proportion of true null hypotheses among the set of statistical tests. The proteins associated to an adjusted p-value inferior to a FDR (false discovery rate) level of 1% and an absolute $\log_2(\text{fold-change})$ superior to 1 have been considered as significantly differentially abundant proteins. Finally, the proteins of interest are therefore those which emerge from this statistical analysis supplemented by those which are considered to be present from one condition and absent in another ("ID table" in the S1 Dataset).

We used the R package `clusterProfiler` v4.6.2 for gene set enrichment analysis [351]. The `GSEA` function was used based on UniProt accession number and mapped to a personal annotation file extracted from the CO92 Gene Ontology terms downloaded from the QuickGo website accessed in April 2023 [352]. The `gseKEGG` function was used with the online KEGG dataset accessed in April 2023, based on the CO92 loci. All analysis were performed with the detected proteins as statistical background.

Yersinia transcriptomic data were downloaded from the Yersiniomics website and systematic protein BLAST were performed on the CO92 genome against the other strains genome to mapped homologous data, as previously described [193]. Correlations between the datasets were measured using the `cor` function of the "stats" R package.

7.4.9 Western blotting

Bacteria were grown in the same conditions as for mass spectrometry then cultivated in 50 mL LB in 125 mL polycarbonate flask at 37°C under agitation at 180 rpm for 7 hours, to an OD600 of 0.9-1. 1 mL of culture was pelleted by centrifugation at 10,000 *g* for 5 minutes. 45 mL of the culture was pelleted by centrifugation for 20 minutes at 4,600 *g*. The supernatant was carefully collected, filtered on 0.22 μm PES filter and aliquoted. 10 mL of supernatant were precipitated by addition of 2.5 mL trichloroacetic acid (TCA) at -20°C overnight. Precipitates were centrifugated at 21,000 *g* for 10 minutes, then washed two times with acetone. Bacterial pellets and supernatant precipitates were resuspended in Laemmli buffer+ β -mercaptoethanol, pH was adjusted by addition of 1.5 M Tris HCl pH 8.8, and heated at 95°C for 10 minutes. Samples were loaded and proteins separated on a 4-12% polyacrylamid gel (Invitrogen) and transferred on a PVDF membrane using the iBlot transfer device (Invitrogen). The gel was stained for 2 hours with PageBlue (Thermo Scientific) and destained overnight in water. The membrane was blocked with 5% milk overnight, then incubated with anti-Lpp and anti-MalE antibodies kindly provided by Dr. Nienke Budelmeijer.

7.5 Tables

Table 7.1. Differential abundance for components of membrane complexes. Periplasmic components are highlighted in red. FC is the $\log_2(\text{fold change}(\text{WT}/\Delta\text{sl}yB))$, so positive numbers denote more abundant proteins in the WT strain.

Complex	Substrate	Locus	Protein	Local.	FC	P-value	FDR
Lol	Lipoprotein	YPO1377	LoIA	PP	1.24	7.7E-6	3.4E-7
		YPO1626	LolC	IM	-0.02	6.2E-1	
		YPO1627	LolD	IM	0.04	3.8E-1	
		YPO1628	LolE	IM	-0.002	9.6E-1	
		YPO2015	LolB	OM	-0.06	2.2E-1	
Lpt	Lipo-polysaccharide	YPO0495	LptD	OM	-0.38	1.4E-5	
		YPO2609	LptE	OM	0.09	3.3E-1	
		YPO3439	LptG	IM	0.19	1.0E-1	
		YPO3440	LptF	IM	0.19	1.7E-2	
		YPO3579	LptC	IM	0.26	2.0E-2	
		YPO3580	LptA	PP	0.81	4.4E-7	
		YPO3581	LptB	IM	-0.02	7.4E-1	
Bam	Outer membrane protein	YPO0494	SurA	PP	0.72	1.4E-6	4.0E-7
		YPO1052	BamA	OM	0.22	8.9E-6	
		YPO1053	Skp	PP	1.04	9.0E-6	
		YPO1104	BamE	OM	0.04	8.7E-1	
		YPO2876	BamB	OM	-0.02	6.2E-1	
		YPO3061	BamC	OM	0.23	2.3E-5	
		YPO3278	BamD	OM	0.19	5.1E-4	
Tol-Pal		YPO1121	TolQ	IM	0.16	2.1E-2	
		YPO1122	TolR	IM	-0.13	4.6E-2	
		YPO1123	TolA	IM	0.24	2.4E-2	
		YPO1124	TolB	PP	0.69	2.6E-6	
		YPO1125	Pal	OM	0.21	1.2E-2	
Cys	Maltose	YPO3011	CysM	CP	-0.52	4.0E-4	1.4E-7
		YPO3012	CysA	IM	-1.03	2.8E-6	
		YPO3014	CysT	IM	-1.44	9.0E-3	
		YPO3015	CysP	PP	0.35	1.2E-2	
Liv	Leucine, isoleucine, valine	YPO3804	LivF	IM	0.04	9.5E-1	
		YPO3805	LivG	IM	0.49	5.8E-2	
		YPO3808	LivJ/K	PP	1.27	2.6E-4	
Lsr	Autoinducer-2	YPO0407	LsrG	CP	1.48	1.6E-8	3.2E-9
		YPO0408	LsrF	CP	1.12	6.7E-8	7.7E-9
		YPO0409	LsrB	PP	2.75	3.4E-7	2.6E-8
		YPO0412	LsrA	IM	1.83	4.3E-5	1.5E-6
		YPO0415	LsrK	CP	1.49	3.0E-6	1.5E-7
Mal	Maltose	YPO3710	MalM	PP	1.25	1.2E-5	5.1E-7
		YPO3712	MalK	IM	0.27	7.5E-2	1.4E-7
		YPO3714	MalE	PP	1.66	2.7E-6	
		YPO3715	MalF	IM	0.35	2.4E-2	
Mgl	Glucose, galactose	YPO1507	MglB	PP	1.42	1.6E-5	
		YPO1508	MglA	IM	0.32	1.4E-5	
		YPO1509	MglC	IM	0.77	9.2E-2	
Mla	Phospholipid	YPO3572	MlaC	PP	1.27	1.5E-5	

		YPO3573	MlaD	IM	0.16	1.4E-2	
		YPO3574	MlaE	IM	0.22	2.2E-1	
		YPO3575	MlaF	IM	0.11	9.6E-2	
Opp	Oligopeptide	YPO2182	OppA	PP	0.50	1.9E-3	
		YPO2183	OppB	IM	-1.10	8.0E-7	5.4E-8
		YPO2184	OppC	IM	-0.67	8.4E-5	
		YPO2185	OppD	IM	-0.96	5.1E-9	
		YPO2186	OppF	IM	-0.91	7.7E-9	
Pro	Glycine, betaine, proline	YPO2645	ProX	PP	2.35	2.1E-7	1.8E-8
		YPO2646	ProW	IM	1.34	1.4E-6	8.4E-8
		YPO2647	ProV	IM	1.16	2.3E-9	8.3E-10
Ssu	Sulfonate	YPO3623	SsuE	CP	-3.67	1.5E-6	8.8E-8
		YPO3624	SsuA	PP	-1.39	1.5E-5	6.0E-7
		YPO3625	SsuD	CP	-2.22	7.9E-8	8.8E-9
		YPO3627	SsuB	IM	-0.85	3.1E-1	
Tau	Taurine	YPO0182	TauA	PP	-1.52	1.1E-5	4.9E-7
		YPO0183	TauB	IM	-3.48	1.8E-6	1.0E-7
		YPO0184	TauC	IM	ND in WT		
		YPO0185	TauD	CP	-3.84	1.8E-8	3.4E-9
Znu	Zn ²⁺	YPO2060	ZnuC	IM	-0.13	7.3E-2	
		YPO2061	ZnuA	PP	1.12	5.7E-5	2.0E-6

Table 7.2. Differential abundance of proteins involved in envelope stress response and two-component systems.

Complex	Locus	Product	Local.	Log ₂ (WT/ Δ slyB)	P-value	FDR
Cpx	YPO0073	CpxA	IM	-0,47	1,7E-4	
	YPO0074	CpxR	CP	-0,26	2,5E-4	
	YPO0075	CpxP	PP	-0,50	1,4E-3	
	YPO1067	NlpE	OM	0,33	1,3E-4	
	YPO3382	DegP	PP	0,80	9,7E-7	
OmpR/EnvZ	YPO0136	OmpR	CP	0,06	2,5E-1	
	YPO0137	EnvZ	IM	0,07	9,9E-2	
PhoP/PhoQ	YPO1633	PhoQ	IM	0,06	1,1E-1	
	YPO1634	PhoP	CP	0,07	3,6E-1	
PmrA/PmrB	YPO3507	PmrA	CP	0,46	1,5E-01	
	YPO3508	PmrB	IM	0,19	2,6E-01	
Psp	YPO2349	PspC	IM	0,16	7,6E-03	
	YPO2350	PspB	IM	0,28	2,2E-02	
	YPO2351	PspA	CP	0,24	4,6E-05	
	YPO2352	PspF	CP	0,25	8,6E-03	
Rcs	YPO1070	RcsF	OM	0,46	2,7E-03	
	YPO1217	RcsC	IM	0,32	7,3E-03	
	YPO1218	RcsB	CP	0,98	1,0E-05	
	YPO1219	RcsD	IM	1,11	5,5E-05	1,9E-06
σ E	YPO1051	RseP	IM	-0,04	1,3E-01	
	YPO2711	RpoE	CP	0,13	1,7E-2	
	YPO2712	RseA	IM	0,06	7,3E-1	
	YPO2713	RseB	PP	0,42	6,4E-5	
	YPO3156	ClpX	CP	0,19	1,7E-4	
	YPO3157	ClpP	CP	0,22	6,6E-4	
	YPO3568	DegS	IM	0,17	1,9E-2	

Table 7.3. Differential abundance for LPS synthesis and modification proteins.

Complex	Locus	Product	Log ₂ (WT/ Δ slyB)	P-value	regulation
LPS	YPO0561	LpxC	0.04	7.5E-1	
	YPO1054	LpxD	0.04	6.8E-1	
	YPO1056	LpxA	0.03	2.7E-1	
	YPO1057	LpxB	-0.03	7.8E-1	
	YPO1276	LpxT	0.73	8.0E-4	σ E repressed
	YPO1396	LpxK	0.20	4.3E-2	
	YPO2063	LpxM	-0.05	2.9E-1	
	YPO3075	LpxH	0.11	2.5E-1	
	YPO3632	LpxP	-0.68	4.1E-3	σ E activated

Table 7.4. Gene set enrichment analysis (GSEA) results based on KEGG pathways and performed on the protein differential abundances between the WT and $\Delta slyB$ mutant strain. NES: normalized enrichment score.

KEGG ID	Description	gene set size	NES	adjusted p-value
ype00920	Sulfur metabolism	22	-2.6	1.4E-06
ype03070	Bacterial secretion system	33	1.9	3.1E-06
ype02024	Quorum sensing	37	1.7	9.9E-04

Table 7.5. Operons showing the same regulation pattern for $\Delta slyB$ mutant in proteomics and Δcrp mutant in transcriptomics. Differential expressions are $\text{Log}_2(\text{fold change})$.

Operon	Locus	Protein	WT/ $\Delta slyB$	Δcrp /WT (planktonic)	Δcrp /WT (biofilm)
Cys	YPO2991	CysK	-0.37	-0.78	0.71
	YPO2992	CysM	-0.36	0.33	1.88
	YPO3011	CysM	-0.52	0.37	0.83
	YPO3012	CysA	-1.03	1.96	2.27
	YPO3014	CysW	-1.44	2.31	2.88
	YPO3014	CysT	ND	1.64	2.83
	YPO3015	CysP	0.35	-0.77	2.00
Fad	YPO0589	FadH	0.77	-1.99	-3.04
	YPO2074	FadD	1.12	-2.97	-3.07
	YPO2744	FadL	0.42	-2.60	-3.12
	YPO2746	FadI	0.69	-2.17	-1.99
	YPO2747	FadJ	0.72	-1.23	-1.53
	YPO3244	FadE	1.04	-1.02	-1.78
	YPO3766	FadB	1.05	-5.27	-5.73
	YPO3767	FadA	1.13	-4.02	-4.16
	YPO3768	FadI	0.28	-0.10	0.70
Isc	YPO2894	IscA	0.74	-1.59	-0.96
	YPO2895	IscU	1.01	-0.54	-0.82
	YPO2896	IscS	0.59	-1.65	-1.20
	YPO2897	IscR	0.88	-1.19	-1.66
Lsr	YPO0407	LsrG	1.48	-2.83	-3.11
	YPO0408	LsrF	1.12	-2.50	-3.67
	YPO0409	LsrB	2.75	-3.93	-4.29
	YPO0410	LsrD	ND	-4.13	-3.89
	YPO0411	LsrC	ND	-3.73	-4.66
	YPO0412	LsrA	1.83	-4.74	-5.68
	YPO0415	LsrK	1.49	-0.31	0.30
	YPO3300	LuxS	0.27	0.70	1.13
Psa	YPO1301	PsaE	1,51	-2,01	-1,62
	YPO1302	PsaF	1,10	-2,95	-1,70
	YPO1303	PsaA	ND	-9,11	-2,22
	YPO1304	PsaB	ND	-7,78	-3,83
	YPO1305	PsaC	ND	-3,43	-0,55
Ssu	YPO2374	RovA	2,45	-1,62	-1,42
	YPO3623	SsuE	-3.67	0.03	1.73
	YPO3624	SsuA	-1.39	1.27	0.81
	YPO3625	SsuD	-2.22	2.70	1.53

	YPO3626	SsuC	ND	1.90	1.15
	YPO3627	SsuB	-0.85	2.26	1.27
Tau	YPO0182	TauA	-1.52	0.89	1.76
	YPO0183	TauB	-3.48	1.65	2.12
	YPO0184	TauC	ND in WT	2.47	2.57
	YPO0185	TauD	-3.84	0.78	1.86
Uvr	YPO1865	UvrY	0.86	-0.73	-0.36
	YPO1866	UvrC	0.76	-0.68	-0.26
Yersiniabactin	YPO1906	FyuA	-1.76	3.17	2.34
	YPO1907	YbtE	-1.52	4.17	2.37
	YPO1908	YbtT	-1.52	4.25	2.94
	YPO1909	YbtU	-1.70	4.24	2.49
	YPO1910	Irp1	-1.76	3.98	2.25
	YPO1911	Irp2	-1.61	3.96	2.52
	YPO1912	YbtA	ND	1.51	2.68
	YPO1913	YbtP	-1.97	3.02	3.64
	YPO1914	YbtQ	-1.81	3.69	3.43
	YPO1915	YbtX	ND	4.89	3.65
YPO1916	YbtS	-1.50	2.93	1.71	
Unknown	YPO0623		1,38	-2,83	-3,64
	YPO0624		1,59	-2,85	-3,14
	YPO0625		1,74	-5,07	-3,97
	YPO0627		1,03	-3,74	-3,23
	YPO0628		1,40	-1,63	-1,48
Unknown	YPO1241		ND	3,36	1,33
	YPO1242		-2,00	2,39	0,82
	YPO1243		-1,42	1,50	0,79
	YPO1244		-1,61	1,84	0,75
Unknown	YPO3048		1,41	-2,00	-1,36
	YPO3049		1,74	-1,36	-2,17
	YPO3050		2,09	-3,80	-3,98

Chapter 8

MicroRNAs as biomarkers of plague

8.1 Objectives and summary

Plague is a fulminant disease with a high-fatality rate and as such it requires efficient diagnostic tools to control outbreaks that periodically occur in low-income countries such as Madagascar or in case of biological warfare. In absence of such tools for early and reliable clinical diagnosis of plague, our aim is to discover early diagnostic biomarkers of pneumonic plague and extend their application to bubonic and septicemic forms of plague. Since plague, and particularly primary pneumonic plague, is a very fast-progressing disease with a pre-inflammatory and pre-symptomatic phase [55], current diagnostic tests for plague need to be substantially improved [276]. Past and present plague diagnosis relies on detection of proteins or DNA of *Y. pestis*, which compromises early disease identification and timely treatment.

Our working hypotheses are i) that early pre-symptomatic phase of pneumonic plague could be better identified by host response in biofluid rather than detection of bacterial components in infected tissues or sputum, and ii) that stable circulating host miRNAs signature could be a powerful tool to diagnose pneumonic plague with high specificity in host plasma. We thus propose to use host biomarkers, *i.e.*, stable circulating miRNAs, to diagnose early infection, when bacteria are present at low level in tissue compartments and before blood-stream spread and systemic dissemination.

To identify candidate miRNAs, we setup a murine model of pneumonic plague and screened 179 circulating miRNAs using RT-qPCR panels. We observed a robust 2-fold upregulation of 3 circulating miRNAs as early as 24 hours post infection. These miRNAs have not been described in other pneumonic infections before and could serve as putative early biomarkers of pneumonic plague. These encouraging preliminary results led us to optimize blood sampling and quality control of our experimental setup and to establish a miRNA-sequencing pipeline at various time points post infection to better characterize circulating biomarkers of pneumonic plague.

8.2 Results and discussion

8.2.1 Murine model of pneumonic plague

We first needed to set up a reproducible and well characterized murine model of primary pneumonic plague in our laboratory. Based on the literature, we chose the model from

Lathem *et al.* because it was the first to thoroughly describe the course of the disease [55] and was subsequently used in other studies from this laboratory. Host response to *Y. pestis* infection was thus studied in this model, which shows that upon intranasal instillation of 5,000 bacteria, pneumonic plague is characterized by a pre-inflammatory phase for the first 24 hours, during which the number of bacteria is multiplied by 100. After systemic dissemination around 36 hours post-infection (hpi), a switch to the pro-inflammatory phase of plague occurs 48 hpi, resulting in pneumonia, lung destruction and death 72 hpi [55]. Using the same *Y. pestis* CO92 strain and experimental setup, we determined the bacterial burden in lungs and spleen at various time points post infection, and could faithfully reproduce bacterial development in the lungs and the systemic dissemination previously described (Fig 8.1).

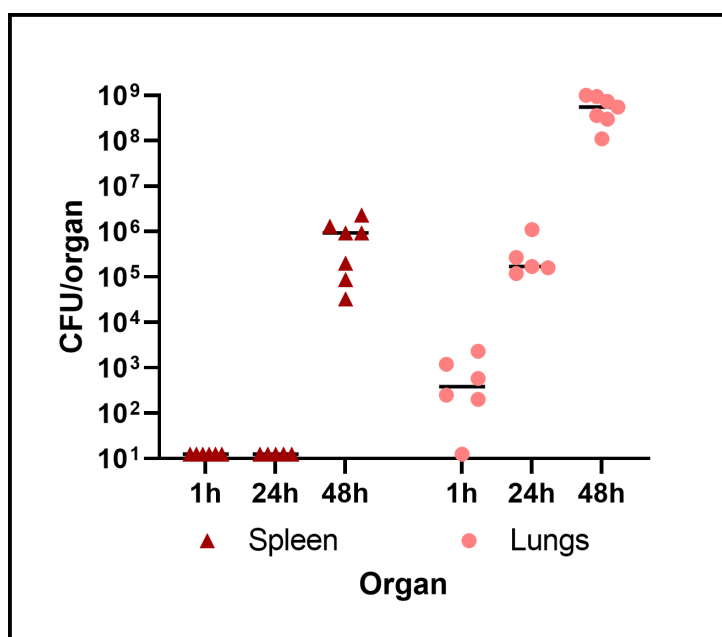


Figure 8.1. CFUs in the spleen (triangle) and the lungs (dot) at 1 hour, 24 hours and 48 hours after intranasal instillation of 5,000 *Y. pestis* CO92 in C57BL6/J mice. 10¹ CFUs is the limit of detection.

8.2.2 Blood sampling setup and optimization

As cell-free miRNAs circulate in low abundance in host blood, and the volume of plasma is less than half of the volume of whole blood, we needed to optimize blood sampling in mice to maximize the sampled volume. Cardiac puncture under terminal anesthesia was chosen because of the high sampling volume and the minimal contamination of blood with exogenous material which could occur from sub-mandibular sampling or drawing of blood in the chest or armpit cavity after vein sectioning. We reviewed screening studies comparing miRNAs detection from serum or plasma, and despite some contradictory results depending on sampling and screening methods [353–355], we chose to use plasma as it was shown to have a higher sensitivity than serum when using miRNA-sequencing. As recommended by the manufacturer of the miRNAs analysis kit, blood was sampled with EDTA as anticoagulant, as heparin inhibits reverse transcription and PCR steps. First samplings resulted in hemolysed blood, a major source of miRNA contamination in plasma. Therefore we tested several needle length and width to maximize the success rate of sampling with minimal hemolysis.

8.2.3 Preliminary microRNAs RT-qPCR screen

Sample quality controls. After optimization of our infection model, we aimed at establishing the proof of concept that circulating miRNAs could be differentially expressed shortly after infection. For this purpose, we screened 179 systemic microRNAs by RT-qPCR 24 hours post infection, during the preinflammatory phase of pneumonic plague, compared to uninfected mice. Each infected mouse was paired with an uninfected mouse all along the experiment and each paired samples were processed together, from infection to qPCR screen. Replicates were done on different dates, with a maximum of two replicates per day. We assessed quality of the various processing steps (Fig 8.2). Hemolysis derived from blood sampling was variable between samples. The $\Delta\text{Ct}(\text{miR-23a-3p}) - \text{Ct}(\text{miR-451a})$ indicator of hemolysis ranged between 3 and 6 (Fig 8.2A), an acceptable value being around 4 [356]. Spiked internal controls were consistent between samples and internally within a sample (Fig 8.2B), validating the different processing steps (total RNA extraction, miRNA-specific reverse transcription and miRNA-specific qPCR). The percentage of amplified miRNA targets below the Ct cutoff of 40 was consistent among the 20 samples (Fig 8.2C).

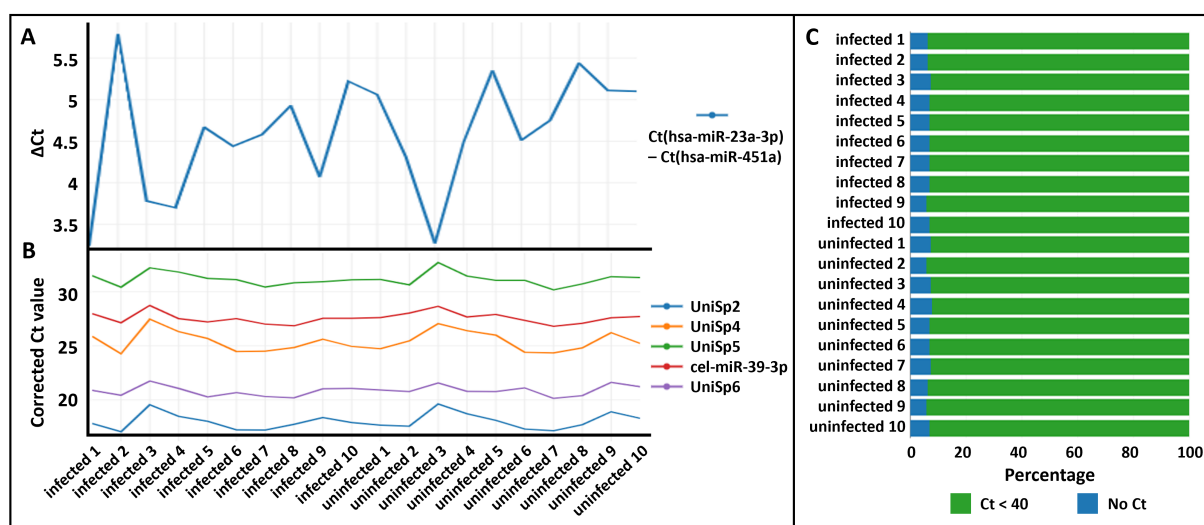


Figure 8.2. Quality control of the 20 samples used for the miRNAs screen. (A) Hemolysis plot showing the ΔCt of miR-23a-3p (hemolysis independent) minus miR-451a (hemolysis dependent). A lower score indicates a lower hemolysis. (B) Ct values for spiked control UniSp2, UniSp4 and UniSp5 (control for the RNA extraction) and cel-miR-39-3p and UniSp6 (control for the reverse transcription and qPCR). (C) Percentage of target miRNAs in the screen with a Ct lower than 40 (in green) or greater than 40 (no Ct, in blue)

Circulating miRNAs differential expression. Data clustering by principal component analysis or hierarchical clustering could not reveal any cluster pattern (data not shown), sign of a high variability between mice independently of the housing, infection status or date of the experiment. Removal of the most hemolysed samples from the analysis did not change this observation. However, a paired differential analysis based on all samples could identify three candidates with a fold change higher than 2 and a p-value below 0.05: miR-133a-3p, miR-133b and miR-1-3p (Fig 8.3). Interestingly, miR-1 and miR-133a are clustered on the human genome and coregulation of these 3 miRNAs have been previously observed in several experimental models [357–359].

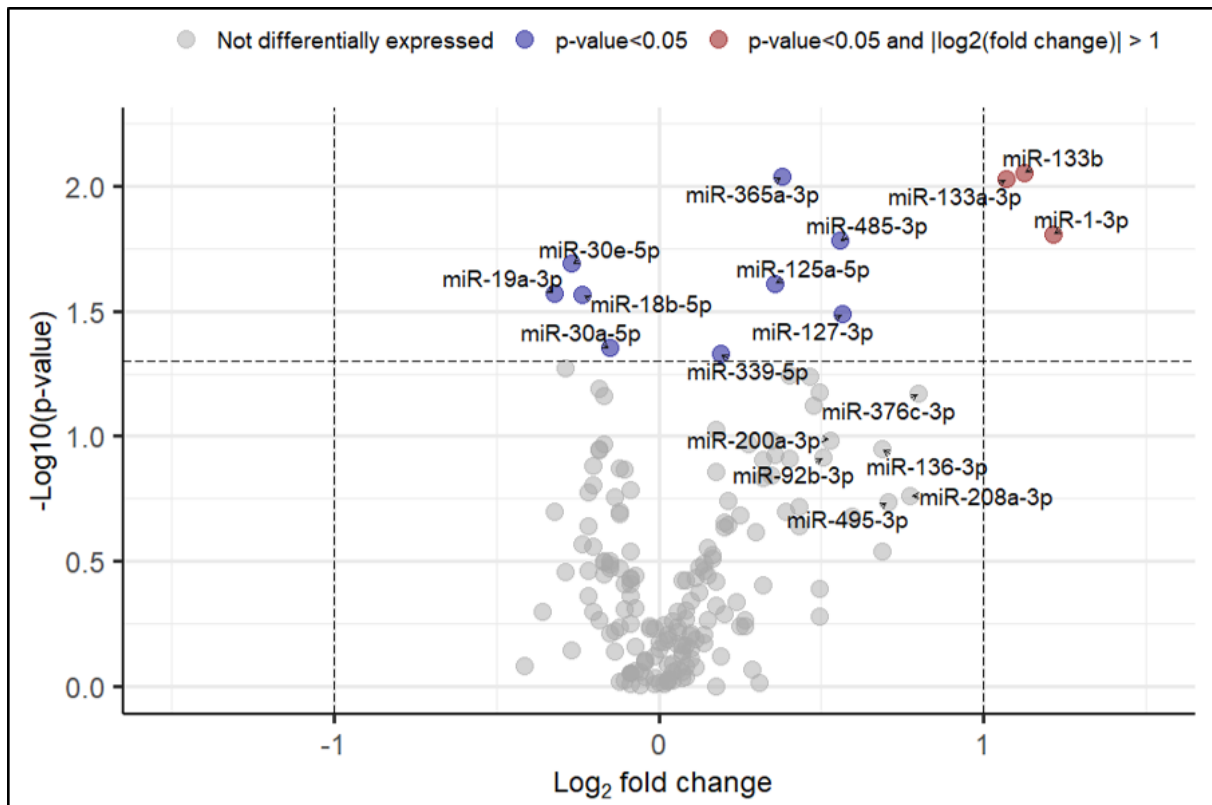


Figure 8.3. Volcano plot of up- and down-regulated circulating miRNAs expressed by infected or non-infected C57BL/6 mice (10 per group), 24 hours after intranasal inoculation of 5,000 *Y. pestis*.

Biomarker analysis. Strikingly, most of the upregulated miRNAs were not detected in other *in vitro*, *in vivo*, or clinical studies looking for biomarkers of other respiratory infections with pathogens such as *Mycobacterium tuberculosis* [360, 361], SARS-CoV-2 [362] and community acquired pneumonia (CAP)-mediating pathogens [360, 363]. Some miRNAs such as miR-136 or miR-376c were detected as up-regulated in both Influenza virus infection models [364] and pneumonic plague model (Table 8.1). miR-376c has also been identified as a circulating biomarker for various cancers such as breast cancer [365], colon cancer [366], gastric carcinomas [367], or glioma [368]. The three most differentially expressed miRNAs, miR-133a-3p, miR-133b and miR-1-3p, were not overexpressed in other model of pulmonary infections, but have been associated to cardiovascular diseases [369] such as myocardial infarction [370, 371] or coronary artery disease [372]. Interestingly, miR-133 was shown to be slightly downregulated during pulmonary disease such as tuberculosis or asthma in elderly patients [373]. In addition, miR-133a was shown to negatively regulate bronchial smooth muscle (BSM) contraction via RhoA, and miR-133a downregulation leads to BSM hyperresponsiveness [374]. Of note, RhoA is targeted by the *Yersinia* effector YopT [375] and YopE [9]. However the interaction between *Y. pestis* and BSM during pneumonic plague has not been reported.

These preliminary results reinforce our hypothesis that a specific signature of plague could be achieved through this methodological approach. However, we cannot exclude that the regulation of the 3 identified miRNAs is influenced by our experimental setting, *e.g.*, the presence in the inoculum of minute amount of BHI broth in which bacteria were grown. This potential flaw will be corrected in the following experiments.

Table 8.1. Differential expression of miRNAs in early infection using a pneumonic plague murine model as compared to influenza A and other respiratory infections. Mtb: *Mycobacterium tuberculosis*. CAP: community acquired pneumonia

miR	Pneumonic plague Log ₂ (inf/uninf)	p-value	Respiratory infections	Other
miR-1-3p	1.21	0.02		Up in heart diseases
miR-133b	1.12	0.01	Down in Mtb [373]	Up in heart diseases
miR-133a-3p	1.07	0.01	Down in Mtb [373]	Up in heart diseases
miR-376c-3p	0.80	0.07	Up H7N9 [364]	Up in various cancer
miR-208a-3p	0.77	0.17		
miR-495-3p	0.70	0.18		
miR-193a-5p	0.69	0.29	Up in CAP [363]	
miR-136-3p	0.69	0.11	Up in H5N1 [364]	
miR-136-5p	0.59	0.21	Up in H5N1 [364]	
miR-127-3p	0.57	0.03		
miR-485-3p	0.56	0.02		

8.2.4 MicroRNAs screen during pneumonic plague

Experimental procedure improvements. The first qPCR screen demonstrated the proof of concept that circulating miRNAs could be early biomarkers of infection during pneumonic plague. These results allowed me to obtain an Institut Pasteur Junior seed grant for PhD student to explore new approaches and evaluate innovative protocols. To improve our miRNAs screen, reduce its variability and apply it to a greater number of conditions such as

different time points of pneumonic plague progression, we refined blood sampling by performing intracardiac puncture after dissection. This improved drastically the success rate of sampling, reducing the number of mice necessary for the experiment, along with a reduction of hemolysis. We implemented a systematic Nanodrop measure for hemolysis [376] and switched from EDTA anticoagulant to sodium citrate, which allowed ever more limited hemolysis during sampling.

MicroRNA-sequencing. Previous reports showed that RT-qPCR had the highest sensitivity and was more cost-effective than miRNA-sequencing (miRNA-seq) [377]. However, recent improvements and drops in price of high-throughput sequencing led us to favor miRNA-Seq to screen biological fluids in an unbiased manner and to potentially discover new circulating miRNAs [378]. Coupling miRNA-Seq to RT-qPCR panel can even be done to achieve better sensitivity [378]. Comparisons of library protocols led us to chose QiaSeq miRNA kits (Qiagen) for library preparation and sequencing [379–382].

Pneumonic plague time course. We selected the 6 hours, 24 hours and 48 hours time points post infection, representative of very early and early pneumonic plague, during the pre-inflammatory phase, and of the switch to pro-inflammatory stage [55]. We could sample 2 mice per condition per time point and we repeated the experiment 4 different times. Nanodrop assessment for hemolysis was generally concordant with the $\Delta\text{Ct}(\text{miR-23a-3p}) - \text{Ct}(\text{miR-451a})$ value (Fig 8.4). During the first replicate experiment, most of the ΔCt values ranged between 0 and 1.5 (Fig 8.4), a far better score than during RT-qPCR screen (see above). Ct values for endogenous miRNAs (miR-103a-3p and miR-191-5p) and UniSp6 RT control were consistent with previous RT-qPCR screen experiments (data not shown). MiRNA-seq library preparation and sequencing are currently pending.

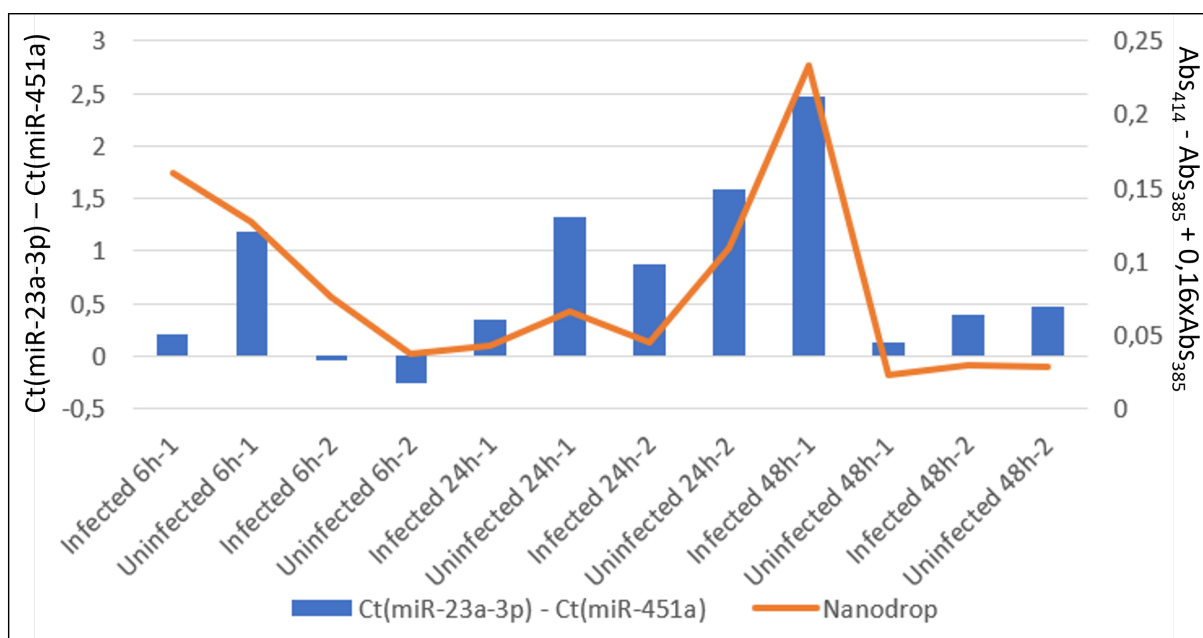


Figure 8.4. Comparison of two hemolysis assays of the first blood sampling replicate for the miRNA-seq (2 mice per condition per time points). A miRNA-specific RT-qPCR based method (blue bars), computing the $\Delta\text{Ct}(\text{miR-23a-3p}) - \text{Ct}(\text{miR-451a})$ and a Nanodrop-based approach (orange line), computing a lipemia-independent hemolysis score as follow: $A_{414\text{ nm}} - A_{385\text{ nm}} + 0.16 \cdot A_{385\text{ nm}}$ [376].

8.3 Methods

8.3.1 Mice experiments

All experiments were performed in a BSL-3 animal facility. 7-week-old C57BL6/J mice were purchased from Charles River Laboratory and were acclimated for at least one month in the animal facility. Experiments were performed on 10 to 12-week old mice for RT-qPCR screen and on 12 to 15-week-old mice for miRNA-seq. *Y. pestis* CO92 strain was grown in BHI broth at 26°C under agitation at 250 rpm for 8 hours. OD600 was then adjusted to 0.05 in 9 mL BHI supplemented with 2.5 mM CaCl₂ and incubated at 37°C for 15 hours under agitation at 250 rpm to reach an OD600 between 2 and 4. Bacteria were diluted to reach a concentration of 5x10⁵ CFU/mL (1x10⁴ CFU in 20 µL) and the inoculum was verified by plating on LBH plates. Mice were anesthetized by intraperitoneal injection of xylazine and ketamine and 20 µL of the bacterial suspension (or PBS for control mice) was instilled intranasally by successive instillation of 5 µL in each nostril. After terminal intraperitoneal injection of xylazine and ketamine at 6-, 24- or 48 hours post infection, 300 to 600 µL of whole blood was collected by intra-cardiac puncture with 60 µL of 50 mM EDTA as anticoagulant for the RT-qPCR screen, or after opening the chest and with 60 µL of 3.2% sodium citrate as anticoagulant for the miRNA-seq screen. For bacterial enumeration in organs, lungs and spleen were collected and lysed with 5 mL of PBS in gentleMACS M tubes using an Octo Dissociator (Miltenyi) with the RNA_2 program. Lysates were serially diluted in PBS, plated on LBH plates and allowed to grow for 48 hours at 28°C for bacterial enumeration.

8.3.2 Plasma collection, miRNA extraction and RT-qPCR screen

Plasma was collected in a BSL-3 laboratory by centrifugation of blood at 800 *g* for 10 minutes at room temperature, then filtrated by centrifugation at 5000 *g* for 5 minutes in SpinX 0.22 µm filter (Costar) to remove any bacteria and remaining platelets and other cells. For miRNA-seq experiment, absorbances at 385 nm and 414 nm were measured in 2 µL of plasma using a Nanodrop (Thermo), and the lipemia-independent hemolysis score was computed as follow: $A_{414\text{ nm}} - A_{385\text{ nm}} + 0.16 \cdot A_{385\text{ nm}}$ [376]. miRNAs were extracted from 150 to 200 µL of plasma with the miRNeasy kit (Qiagen). miRNAs-specific reverse transcription was performed with the miRCURY LNA RT Kit (Qiagen). cDNA levels were measured in a CFX384 Touch Real-Time PCR Detection System (BioRad) using the miRCURY LNA Serum/plasma miRNA Focus PCR Panel for human (Qiagen) in a 384-well plate format, which includes qPCR internal controls and 179 primers specific for circulating miRNAs in humans, from which 138 were also described in the mouse. The RNA Spike-In Kit For RT for miRCURY LNA miRNA PCR experiments (Qiagen) was used as a miRNA extraction and reverse transcription control, and UniSp6 from the miRCURY LNA RT Kit (Qiagen) as a reverse transcription control. Hemolysis was assessed using the Ct differences of miR-23a-3p (hemolysis independent) with miR-451a (hemolysis dependent).

8.3.3 Data analysis

Ct values were compiled and analyzed using the online tools provided by Qiagen on the GeneGlobe website (<https://geneglobe.qiagen.com/fr/analyze>). Data normalization was performed using the geNorm algorithm [383] on the miR-486-5p, miR-532-3p and miR-151a-5p reference miRNAs. The p-value was calculated using a paired two-tailed Student's t-test.

Part IV

Conclusion and perspectives

Conclusion and perspectives

This thesis gave me the opportunity to study *Y. pestis* infections from a number of different perspectives, spanning over various disciplines, techniques and methods. The two principal aspects, the fundamental study of bacteria-host interactions during plague bacteremia and the setup of a new plague diagnostic method, could further be subdivided in 4 distinct projects: i) a first part involving methodological and technological developments for dual proteomics analysis of complex samples in BSL-3 conditions, ii) a second bioinformatic and software engineering part which consisted in gathering, processing and displaying omics data on a user-friendly web application, iii) a third part based on an infection biology approaches, including bacterial genetics, animal experimentation in relevant infection models, and phenotypic characterization *in vitro*, and iv) a last part focused on applications of infection biology, consisting in methodological development for identification of molecular biomarkers of infection *in vivo*.

These diverse complementary research directions gave rise to important tools and results already published or prepared for submission, and revealed beneficial for many other projects of our laboratory (see appendix A page 174). Our study based on sophisticated approaches provides a wealth of information that will be useful for future investigations of bacterial pathogenesis and opens the door to the next generation of diagnostic tools.

Dual proteomics of blood infection by *Yersinia pestis*

Our dual proteomics methodological development applied in a BSL-3 environment, prepared for submission, opens two main perspectives.

First, we propose to apply our fractionation pipeline to other cell types, depending on the pathogen studied, and the development of cell sorting if available. The comparison of fraction proteomes of infected and non-infected blood samples would give an interesting insight into host response to infection. We also propose to expand our pipeline to *in vivo* studies with its application to blood of bacteremic animals. We could improve the DIA library by implementing hybrid spectral libraries based on DDA and DIA runs [384] and using the extensive proteome we obtained after bacterial growth in human plasma. To analyse the bacterial proteome in whole blood compared to laboratory culture, we propose to spike to the bacterial pure culture various amount of host protein background during the protein extraction process to mimic sample complexity without altering bacterial protein expression. Finally, bacterial enrichment by immunocapture could allow the proteomic study of free bacteria circulating in the blood.

Secondly, proteomic results obtained after growth of *Y. pestis* in plasma can be further analyzed. *Y. pestis* metabolic switch in the bloodstream has not been functionally studied so far, while it is known to play a role in virulence in other bacteria (see appendix D 187). Further mutagenesis and functional studies of mutants would thus be useful to perform based on our blood proteomics data.

The Yersiniomics database

Our multi-omic database was recently published [193] and was warmly welcomed by the *Yersinia* scientific community. It is now routinely used in our laboratory to study gene regulation, have a quick access to all gene annotations and analysis our most recent RNA-Seq and mass spectrometry data generated in the laboratory. We could also partially understand an unexplained phenotype we observed owing to systematic RNA-seq analysis performed on Yersiniomics (see appendix A.4 page 175).

However, maintenance of the software and the database in the long run will be necessary to keep an updated website with the latest published omics experiments. We will need to transfer this knowledge to permanent personnel of our institute. We also propose to add new data types such as recently published small RNAs, transcriptional start sites or genome-wide transposon-based screening data. A harder task will be to gather and cure all published *Yersinia* phenotypes associated to gene deletion or mutation and to implement this database in Yersiniomics. Our tool was also attractive to laboratories working on other bacteria inside and outside our institute. Our future aim will be to develop bacterial-specific websites in collaboration with other specialized laboratories and to transfer the structural maintenance, that we currently carry out in our laboratory, to the Institut Pasteur bioinformatic hub.

SlyB involvement in bacterial virulence

By studying *Y. pestis* plasma proteome and screening several deletion mutants, we could bring to light the role of SlyB lipoprotein during bacteremia and more generally during infection, by enhancing outer membrane resistance to innate immune response. Our study of SlyB function during infection is however clouded by the recently discovered 70-kb duplicated region inside the mutant strain. Our first priority is to recapitulate the observed phenotype with a mutant lacking this duplication in order to verify each result and ultimately publish our findings.

This new decisive role of SlyB during pathogenesis could have a major global impact on the study of Gram-negative infection, this protein being widely spread among phyla and belonging to the core regulon of the PhoP/PhoQ two-components system, known to be required in several pathogens to promote infection. If we can validate the observed phenotypes in *Y. pestis*, future research directions could consist in validating this phenotype in enteropathogenic *Y. pseudotuberculosis* and *Y. enterocolitica*, as well as in pathogenic *E. coli*, *Shigella*, *Salmonella* or *Pseudomonas* species. Structural and mechanistic roles of SlyB in the outer membrane remain to be deciphered and could be subjected to further studies in model bacteria such a *E. coli*.

Our mutant screen also revealed other poorly characterized loci, which seem to be required for full virulence of *Y. pestis*. Further research could focus on the characterization of these specific loci and their associated proteins.

MiRNAs as biomarkers of plague

In the last part of my thesis, we could identify 3 miRNAs especially upregulated 24 hours after intranasal instillation of *Y. pestis*. As minute amount of brain heart infusion (BHI) broth was inoculated in infected but not in uninfected mice, a first validation of these results will be to quantitate the levels of these miRNAs in experiments where control mice will be inoculated with the same traces of BHI as infected mice. With this setup, an unbiased miRNA-sequencing screen is currently ongoing at different time post infection and will draw a more

exhaustive map of miRNAs circulating during pneumonic plague progression.

To expand these results, we obtained funding (see appendix B.2 page 176) to establish a comprehensive host miRNAs signature during plague disease progression using different and complementary experimental settings: murine plague models of bubonic, septicemic and pneumonic plague, a non-human primate (NHP) model of pneumonic plague that we will setup in the Infectious Diseases Models for Innovative Therapies (IDMIT) laboratory of the Commissariat à l'énergie atomique et aux énergies alternatives (CEA), and clinical samples from healthy individuals and plague patients at the Institut Pasteur of Madagascar, in collaboration with the Institut de Recherche Biomédicale des Armées (IRBA) for the sequencing. The screen would allow the selection of several specific miRNAs which could be used to develop simple, robust and reliable tools for point-of-care diagnosis in the future. The secondary aim of this future project is to better understand miRNA-mediated host-pathogen interactions by studying the function of miRNA expressed during *Y. pestis* infection.

Part V

Bibliography

1. Adeolu, M., Alnajar, S., Naushad, S. & Gupta, R. S. Genome-based phylogeny and taxonomy of the 'Enterobacteriales': Proposal for *Enterobacterales* ord. nov. divided into the families *Enterobacteriaceae*, *Erwiniaceae* fam. nov., *Pectobacteriaceae* fam. nov., *Yersiniaceae* fam. nov., *Hafniaceae* fam. nov., *Morganellaceae* fam. nov., and *Budviciaceae* fam. nov. *International Journal of Systematic and Evolutionary Microbiology* **66**, 5575–5599 (Dec. 2016).
2. Le Guern, A.-S. *et al.* *Yersinia artesiana* sp. nov., *Yersinia proxima* sp. nov., *Yersinia alsatica* sp. nov., *Yersinia vastinensis* sp. nov., *Yersinia thracica* sp. nov. and *Yersinia occitanica* sp. nov., isolated from humans and animals. *International Journal of Systematic and Evolutionary Microbiology* **70**, 5363–5372 (Aug. 2020).
3. Reuter, S. *et al.* Parallel independent evolution of pathogenicity within the genus *Yersinia*. *Proceedings of the National Academy of Sciences of the United States of America* **111**, 6768–6773 (May 2014).
4. Perry, R. D. & Fetherston, J. D. *Yersinia pestis* - Etiologic agent of plague. *Clinical Microbiology Reviews* **10**, 35–66 (Jan. 1997).
5. Savin, C. *et al.* The *Yersinia pseudotuberculosis* complex: characterization and delineation of a new species, *Yersinia wautersii*. *International Journal of Medical Microbiology* **304**, 452–463 (May 2014).
6. Kumar, G., Menanteau-Ledouble, S., Saleh, M. & El-Matbouli, M. *Yersinia ruckeri*, the causative agent of enteric redmouth disease in fish. *Veterinary Research* **46**, e103 (Sept. 2015).
7. Hurst, M. R., Becher, S. A., Young, S. D., Nelson, T. L. & Glare, T. R. *Yersinia entomophaga* sp. nov., isolated from the New Zealand grass grub *Costelytra zealandica*. *International Journal of Systematic and Evolutionary Microbiology* **61**, 844–849 (Apr. 2011).
8. McNally, A., Thomson, N. R., Reuter, S. & Wren, B. W. 'Add, stir and reduce': *Yersinia* spp. as model bacteria for pathogen evolution. *Nature Reviews Microbiology* **14**, 177–190 (Feb. 2016).
9. Demeure, C. E. *et al.* *Yersinia pestis* and plague: an updated view on evolution, virulence determinants, immune subversion, vaccination, and diagnostics. *Genes and Immunity* **20**, 357–370 (2019).
10. Spyrou, M. A., Bos, K. I., Herbig, A. & Krause, J. Ancient pathogen genomics as an emerging tool for infectious disease research. *Nature Reviews Genetics* **20**, 323–340 (Apr. 2019).
11. Savin, C. *et al.* Genus-wide *Yersinia* core-genome multilocus sequence typing for species identification and strain characterization. *Microbial Genomics* **5**, e000301 (Oct. 2019).
12. Yersin, A. La peste bubonique à Hong Kong. *Annales de l'Institut Pasteur* **8**, 662–667 (1894).
13. Simond, P.-L. La propagation de la peste. *Annales de l'Institut Pasteur* **12**, 625–687 (1898).
14. Plague Research Commission. Experiments upon the transmission of plague by fleas. *The Journal of Hygiene* **6**, 425–482 (1906).
15. Plague Research Commission. Further observations on the transmission of plague by fleas, with special reference to the fate of the plague bacillus in the body of the rat flea (*P. cheopis*). *Epidemiology & Infection* **7**, 395–420 (1907).
16. Verjbitski, D. T. The part played by insects in the epidemiology of plague. *Epidemiology & Infection* **8**, 162–208 (1908).
17. Barbieri, R. *et al.* *Yersinia pestis*: the natural history of plague. *Clinical Microbiology Reviews* **34**, e00044–19 (2021).
18. Bacot, A. W. & Martin, C. J. Observations on the mechanism of the transmission of plague by fleas. *The Journal of Hygiene* **13**, 423–439 (Jan. 1914).
19. Bacot, A. W. Further notes on the mechanism of the transmission of plague by fleas. *The Journal of Hygiene* **14**, 774–776 (Jan. 1915).
20. Hinnebusch, B. J., Jarrett, C. O. & Bland, D. M. "Fleaing" the plague: adaptations of *Yersinia pestis* to its insect vector that lead to transmission. *Annual Review of Microbiology* **71**, 215–232 (Sept. 2017).
21. Bland, D. M., Jarrett, C. O., Bosio, C. F. & Hinnebusch, B. J. Infectious blood source alters early foregut infection and regurgitative transmission of *Yersinia pestis* by rodent fleas. *PLoS Pathogens* **14**, e1006859 (Jan. 2018).
22. Mitchell, C. L. *et al.* A role for early-phase transmission in the enzootic maintenance of plague. *PLoS Pathogens* **18**, e1010996 (Dec. 2022).
23. Earn, D. J., Ma, J., Poinar, H., Dushoff, J. & Bolker, B. M. Acceleration of plague outbreaks in the second pandemic. *Proceedings of the National Academy of Sciences of the United States of America* **117**, 27703–27711 (Nov. 2020).
24. Gani, R. & Leach, S. Epidemiologic determinants for modeling pneumonic plague outbreaks. *Emerging Infectious Diseases* **10**, 608–614 (2004).
25. Dean, K. R. *et al.* Human ectoparasites and the spread of plague in Europe during the Second Pandemic. *Proceedings of the National Academy of Sciences of the United States of America* **115**, 1304–1309 (Feb. 2018).
26. Lorange, E. A., Race, B. L., Sebbane, F. & Hinnebusch, B. J. Poor vector competence of fleas and the evolution of hypervirulence in *Yersinia pestis*. *Journal of Infectious Diseases* **191**, 1907–1912 (June 2005).

27. Eisen, R. J. & Gage, K. L. Adaptive strategies of *Yersinia pestis* to persist during inter-epizootic and epizootic periods. *Veterinary Research* **40**, 1 (Mar. 2009).
28. Gascuel, F., Choisy, M., Duplantier, J. M., Débarre, F. & Brouat, C. Host resistance, population structure and the long-term persistence of bubonic plague: contributions of a modelling approach in the Malagasy focus. *PLoS Computational Biology* **9**, e1003039 (2013).
29. Dubyanskiy, V. M. & Yeszhanov, A. B. Ecology of *Yersinia pestis* and the epidemiology of plague. *Advances in Experimental Medicine and Biology* **918**, 101–170 (Oct. 2016).
30. Nilsson, P. *et al.* Polygenic plague resistance in the great gerbil uncovered by population sequencing. *PNAS Nexus* **1**, 1–14 (Nov. 2022).
31. Davis, S., Trapman, P., Leirs, H., Begon, M. & Heesterbeek, J. A. The abundance threshold for plague as a critical percolation phenomenon. *Nature* **454**, 634–637 (July 2008).
32. Salkeld, D. J., Salathé, M., Stapp, P. & Jones, J. H. Plague outbreaks in prairie dog populations explained by percolation thresholds of alternate host abundance. *Proceedings of the National Academy of Sciences of the United States of America* **107**, 14247–14250 (Aug. 2010).
33. Zeppelini, C. G., de Almeida, A. M. P. & Cordeiro-Estrela, P. Zoonoses as ecological entities: a case review of plague. *PLoS Neglected Tropical Diseases* **10**, e0004949 (Oct. 2016).
34. Colman, R. E. *et al.* No evidence for enzootic plague within black-tailed prairie dog (*Cynomys ludovicianus*) populations. *Integrative Zoology* **16**, 834–851 (Nov. 2021).
35. Gonzalez, R. J., Lane, M. C., Wagner, N. J., Weening, E. H. & Miller, V. L. Dissemination of a highly virulent pathogen: tracking the early events that define infection. *PLoS Pathogens* **11**, e1004587 (2015).
36. Shannon, J. G. *et al.* *Yersinia pestis* subverts the dermal neutrophil response in a mouse model of bubonic plague. *mBio* **4**, e00170–13 (Aug. 2013).
37. Shannon, J. G., Bosio, C. F. & Hinnebusch, B. J. Dermal neutrophil, macrophage and dendritic cell responses to *Yersinia pestis* transmitted by fleas. *PLoS Pathogens* **11**, e1004734 (Mar. 2015).
38. Vadyvaloo, V., Jarrett, C., Sturdevant, D. E., Sebbane, F. & Hinnebusch, B. J. Transit through the flea vector induces a pretransmission innate immunity resistance phenotype in *Yersinia pestis*. *PLoS Pathogens* **6**, e1000783 (2010).
39. St. John, A. L. *et al.* S1P-dependent trafficking of intracellular *Yersinia pestis* through lymph nodes establishes buboes and systemic infection. *Immunity* **41**, 440–450 (Sept. 2014).
40. Yang, K. *et al.* Host Langerin (CD207) is a receptor for *Yersinia pestis* phagocytosis and promotes dissemination. *Immunology and Cell Biology* **93**, 815–824 (Oct. 2015).
41. Yang, K. *et al.* *Yersinia pestis* interacts with SIGNR1 (CD209b) for promoting host dissemination and infection. *Frontiers in Immunology* **10**, 96 (Mar. 2019).
42. Zhao, Y. *et al.* Single-cell transcriptomics of immune cells in lymph nodes reveals their composition and alterations in functional dynamics during the early stages of bubonic plague. *Science China Life Sciences* **66**, 110–126 (Jan. 2023).
43. Gonzalez, R. J., Weening, E. H., Lane, M. C. & Miller, V. L. Comparison of models for bubonic plague reveals unique pathogen adaptations to the dermis. *Infection and Immunity* **83**, 2855–2861 (July 2015).
44. Pujol, C. & Bliska, J. B. The ability to replicate in macrophages is conserved between *Yersinia pestis* and *Yersinia pseudotuberculosis*. *Infection and Immunity* **71**, 5892–5899 (Oct. 2003).
45. Spinner, J. L. *et al.* *Yersinia pestis* survival and replication within human neutrophil phagosomes and uptake of infected neutrophils by macrophages. *Journal of Leukocyte Biology* **95**, 389–398 (Mar. 2014).
46. Dudte, S. C., Hinnebusch, B. J. & Shannon, J. G. Characterization of *Yersinia pestis* interactions with human neutrophils in vitro. *Frontiers in Cellular and Infection Microbiology* **7**, 358 (Aug. 2017).
47. Arifuzzaman, M. *et al.* Necroptosis of infiltrated macrophages drives *Yersinia pestis* dispersal within buboes. *JCI insight* **3**, e122188 (Sept. 2018).
48. Guinet, F., Avé, P., Jones, L., Huerre, M. & Carniel, E. Defective innate cell response and lymph node infiltration specify *Yersinia pestis* infection. *PLoS One* **3**, e1688 (Feb. 2008).
49. Comer, J. E. *et al.* Transcriptomic and innate immune responses to *Yersinia pestis* in the lymph node during bubonic plague. *Infection and Immunity* **78**, 5086–5098 (Dec. 2010).
50. Sebbane, F., Gardner, D., Long, D., Gowen, B. B. & Hinnebusch, B. J. Kinetics of disease progression and host response in a rat model of bubonic plague. *American Journal of Pathology* **166**, 1427–1439 (2005).
51. Mikaty, G., Coullon, H., Fiette, L., Pizarro-Cerdá, J. & Carniel, E. The invasive pathogen *Yersinia pestis* disrupts host blood vasculature to spread and provoke hemorrhages. *PLoS Neglected Tropical Diseases* **15**, e0009832 (Oct. 2021).
52. Mikaty, G. *et al.* Atypical disseminated intravascular coagulopathy during bubonic plague. *Microbes and Infection* **25**, 105063 (Oct. 2022).
53. Marketon, M. M., DePaolo, R. W., DeBord, K. L., Jabri, B. & Schneewind, O. Plague bacteria target immune cells during infection. *Science* **309**, 1739–1741 (Sept. 2005).

54. Sebbane, F., Jarrett, C. O., Gardner, D., Long, D. & Hinnebusch, B. J. Role of the *Yersinia pestis* plasminogen activator in the incidence of distinct septicemic and bubonic forms of flea-borne plague. *Proceedings of the National Academy of Sciences of the United States of America* **103**, 5526–30 (Apr. 2006).
55. Lathem, W. W., Crosby, S. D., Miller, V. L. & Goldman, W. E. Progression of primary pneumonic plague: A mouse model of infection, pathology, and bacterial transcriptional activity. *Proceedings of the National Academy of Sciences of the United States of America* **102**, 17786–17791 (Dec. 2005).
56. Van Andel, R. *et al.* Clinical and pathologic features of cynomolgus macaques (*Macaca fascicularis*) infected with aerosolized *Yersinia pestis*. *Comparative Medicine* **58**, 68–75 (Feb. 2008).
57. Layton, R. C. *et al.* Primary pneumonic plague in the African green monkey as a model for treatment efficacy evaluation. *Journal of Medical Primatology* **40**, 6–17 (Feb. 2011).
58. Hammamieh, R. *et al.* Temporal progression of pneumonic plague in blood of nonhuman primate: a transcriptomic analysis. *PLoS One* **11**, e0151788 (Mar. 2016).
59. Pechous, R. D., Sivaraman, V., Price, P. A., Stasulli, N. M. & Goldman, W. E. Early host cell targets of *Yersinia pestis* during primary pneumonic plague. *PLoS Pathogens* **9**, e1003679 (Oct. 2013).
60. Vagima, Y. *et al.* Circumventing *Y. pestis* virulence by early recruitment of neutrophils to the lungs during pneumonic plague. *PLoS Pathogens* **11**, e1004893 (May 2015).
61. Sivaraman, V., Pechous, R. D., Stasulli, N. M., Miao, E. A. & Goldman, W. E. *Yersinia pestis* activates both IL-1 β and IL-1 receptor antagonist to modulate lung inflammation during pneumonic plague. *PLoS Pathogens* **11**, e1004688 (Mar. 2015).
62. Stasulli, N. M. *et al.* Spatially distinct neutrophil responses within the inflammatory lesions of pneumonic plague. *mBio* **6**, e01530–15 (Oct. 2015).
63. Caulfield, A. J., Walker, M. E., Giolda, L. M. & Lathem, W. W. The Pla protease of *Yersinia pestis* degrades Fas ligand to manipulate host cell death and inflammation. *Cell Host and Microbe* **15**, 424–434 (Apr. 2014).
64. Zhang, S. S. *et al.* Plasminogen activator Pla of *Yersinia pestis* utilizes murine DEC-205 (CD205) as a receptor to promote dissemination. *Journal of Biological Chemistry* **283**, 31511–31521 (Nov. 2008).
65. Olson, R. M., Dhariwala, M. O., Mitchell, W. J. & Anderson, D. M. *Yersinia pestis* exploits early activation of MyD88 for Growth in the lungs during pneumonic plague. *Infection and Immunity* **87**, e00757–18 (Apr. 2019).
66. Olson, R. M. & Anderson, D. M. Shift from primary pneumonic to secondary septicemic plague by decreasing the volume of intranasal challenge with *Yersinia pestis* in the murine model. *PLoS One* **14**, e0217440 (May 2019).
67. Becker, T. M. *et al.* Plague meningitis - a retrospective analysis of cases reported in the United States, 1970-1979. *Western Journal of Medicine* **147**, 554 (1987).
68. Cooley, K. M., Fleck-Derderian, S., McCormick, D. W. & Nelson, C. A. Plague meningitis: a systematic review of clinical course, antimicrobial treatment, and outcomes. *Health Security* **21**, 22–33 (Feb. 2023).
69. Padua, L. T. *et al.* Unique case of disseminated plague with multifocal osteomyelitis. *Journal of the Pediatric Infectious Diseases Society* **6**, e165–e168 (Sept. 2017).
70. Carter, D. B. & Ellis, P. P. *Yersinia pestis* endophthalmitis. *American Journal of Ophthalmology* **103**, 721–722 (May 1987).
71. Edmunds, D. R. *et al.* Ocular plague (*Yersinia pestis*) in mule deer (*Odocoileus hemionus*) from Wyoming and Oregon. *Journal of Wildlife Diseases* **44**, 983–987 (Oct. 2008).
72. Yang, R. *et al.* *Yersinia pestis* and plague: some knowns and unknowns. *Zoonoses* **3**, 5 (Jan. 2023).
73. Zimble, D. L., Schroeder, J. A., Eddy, J. L. & Lathem, W. W. Early emergence of *Yersinia pestis* as a severe respiratory pathogen. *Nature Communications* **6**, 7487 (June 2015).
74. Sun, Y. C., Jarrett, C. O., Bosio, C. F. & Hinnebusch, B. J. Retracing the evolutionary path that led to flea-borne transmission of *Yersinia pestis*. *Cell Host & Microbe* **15**, 578–586 (May 2014).
75. Bland, D. M., Miarijara, A., Bosio, C. F., Calarco, J. & Hinnebusch, B. J. Acquisition of *Yersinia* murine toxin enabled *Yersinia pestis* to expand the range of mammalian hosts that sustain flea-borne plague. *PLoS Pathogens* **17**, e1009995 (Oct. 2021).
76. Guo, X.-P. *et al.* A frameshift in *Yersinia pestis rcsD* alters canonical Rcs signalling to preserve flea-mammal plague transmission cycles. *eLife* **12**, 83946 (Apr. 2023).
77. Bontemps-Gallo, S. *et al.* Nutrient depletion may trigger the *Yersinia pestis* OmpR-EnvZ regulatory system to promote flea-borne plague transmission. *Molecular Microbiology* **112**, 1471–1482 (Nov. 2019).
78. Chouikha, I. & Hinnebusch, B. J. Silencing urease: a key evolutionary step that facilitated the adaptation of *Yersinia pestis* to the flea-borne transmission route. *Proceedings of the National Academy of Sciences of the United States of America* **111**, 18709–18714 (Dec. 2014).

79. Viboud, G. I. & Bliska, J. B. *Yersinia* outer proteins: role in modulation of host cell signaling responses and pathogenesis. *Annual Review of Microbiology* **59**, 69–89 (Oct. 2005).
80. Chen, K. W. & Brodsky, I. E. *Yersinia* interactions with regulated cell death pathways. *Current Opinion in Microbiology* **71**, 102256 (Feb. 2023).
81. Une, T. & Brubaker, R. R. *In vivo* comparison of avirulent Vwa- and Pgm- of Pst(r) phenotypes of *Yersinia*. *Infection and Immunity* **43**, 895–900 (1984).
82. Perry, R. D., Harmon, P. A., Bowmer, W. S. & Straley, S. C. A low-Ca²⁺ response operon encodes the V antigen of *Yersinia pestis*. *Infection and Immunity* **54**, 428–434 (1986).
83. Eichelberger, K. R., Jones, G. S. & Goldman, W. E. Inhibition of neutrophil primary granule release during *Yersinia pestis* pulmonary infection. *mBio* **10** (Nov. 2019).
84. Guinet, F. *et al.* Dissociation of tissue destruction and bacterial expansion during bubonic plague. *PLoS Pathogens* **11**, e1005222 (2015).
85. Sebbane, F., Uversky, V. N. & Anisimov, A. P. *Yersinia pestis* plasminogen activator. *Biomolecules* **10**, 1554 (Nov. 2020).
86. Buchrieser, C., Prentice, M. & Carniel, E. The 102-kilobase unstable region of *Yersinia pestis* comprises a high-pathogenicity island linked to a pigmentation segment which undergoes internal rearrangement. *Journal of Bacteriology* **180**, 2321–2329 (1998).
87. Pujol, C., Grabenstein, J. P., Perry, R. D. & Bliska, J. B. Replication of *Yersinia pestis* in interferon γ -activated macrophages requires *ripA*, a gene encoded in the pigmentation locus. *Proceedings of the National Academy of Sciences of the United States of America* **102**, 12909–12914 (Sept. 2005).
88. Carniel, E. The *Yersinia* high-pathogenicity island: an iron-uptake island. *Microbes and Infection* **3**, 561–569 (June 2001).
89. Sebbane, F., Jarrett, C., Gardner, D., Long, D. & Joseph Hinnebusch, B. Role of the *Yersinia pestis* yersiniabactin iron acquisition system in the incidence of flea-borne plague. *PLoS One* **5**, e14379 (2010).
90. Cathelyn, J. S., Crosby, S. D., Lathem, W. W., Goldman, W. E. & Miller, V. L. RovA, a global regulator of *Yersinia pestis*, specifically required for bubonic plague. *Proceedings of the National Academy of Sciences of the United States of America* **103**, 13514–13519 (Sept. 2006).
91. Du, Y., Rosqvist, R. & Forsberg, Å. Role of fraction 1 antigen of *Yersinia pestis* in inhibition of phagocytosis. *Infection and Immunity* **70**, 1453–1460 (2002).
92. Sebbane, F., Jarrett, C., Gardner, D., Long, D. & Hinnebusch, B. J. The *Yersinia pestis* *caf1M1A1* fimbrial capsule operon promotes transmission by flea bite in a mouse model of bubonic plague. *Infection and Immunity* **77**, 1222–1229 (2009).
93. Sha, J. *et al.* Characterization of an F1 deletion mutant of *Yersinia pestis* CO92, pathogenic role of F1 antigen in bubonic and pneumonic plague, and evaluation of sensitivity and specificity of F1 antigen capture-based dipsticks. *Journal of Clinical Microbiology* **49**, 1708–1715 (May 2011).
94. Weening, E. H. *et al.* The dependence of the *Yersinia pestis* capsule on pathogenesis is influenced by the mouse background. *Infection and Immunity* **79**, 644–652 (Feb. 2011).
95. Lathem, W. W., Price, P. A., Miller, V. L. & Goldman, W. E. A plasminogen-activating protease specifically controls the development of primary pneumonic plague. *Science* **315**, 509–513 (Jan. 2007).
96. Lathem, W. W. *et al.* Posttranscriptional regulation of the *Yersinia pestis* cyclic AMP receptor protein Crp and impact on virulence. *mBio* **5**, 1038–1051 (Feb. 2014).
97. Galván, E. M., Lasaro, M. A. & Schifferli, D. M. Capsular antigen fraction 1 and Pla modulate the susceptibility of *Yersinia pestis* to pulmonary antimicrobial peptides such as cathelicidin. *Infection and Immunity* **76**, 1456–1464 (Apr. 2008).
98. Galván, E. M., Chen, H. & Schifferli, D. M. The Psa fimbriae of *Yersinia pestis* interact with phosphatidylcholine on alveolar epithelial cells and pulmonary surfactant. *Infection and Immunity* **75**, 1272–1279 (Mar. 2007).
99. Felek, S. & Krukoni, E. S. The *Yersinia pestis* Ail protein mediates binding and Yop delivery to host cells required for plague virulence. *Infection and Immunity* **77**, 825–836 (Feb. 2009).
100. Felek, S., Tsang, T. M. & Krukoni, E. S. Three *Yersinia pestis* adhesins facilitate Yop delivery to eukaryotic cells and contribute to plague virulence. *Infection and Immunity* **78**, 4134–4150 (Oct. 2010).
101. Eichelberger, K. R. *et al.* Tn-Seq analysis identifies genes important for *Yersinia pestis* adherence during primary pneumonic plague. *mSphere* **5**, 00715–20 (Aug. 2020).
102. Crane, S. D. *et al.* The *Yersinia pestis* GTPase BipA promotes pathogenesis of primary pneumonic plague. *Infection and Immunity* **89**, e00673–20 (Feb. 2021).
103. Lindler, L. E., Klempner, M. S. & Straley, S. C. *Yersinia pestis* pH 6 antigen: genetic, biochemical, and virulence characterization of a protein involved in the pathogenesis of bubonic plague. *Infection and Immunity* **58**, 2569–2577 (1990).
104. Bartra, S. S. *et al.* Resistance of *Yersinia pestis* to complement-dependent killing is mediated by the Ail outer membrane protein. *Infection and Immunity* **76**, 612–622 (Feb. 2008).

105. Kolodziejek, A. M., Hovde, C. J. & Minnich, S. A. *Yersinia pestis* Ail: multiple roles of a single protein. *Frontiers in Cellular and Infection Microbiology* **2**, 103 (Aug. 2012).
106. Kolodziejek, A. M., Hovde, C. J. & Minnich, S. A. Contributions of *Yersinia pestis* outer membrane protein Ail to plague pathogenesis. *Current Opinion in Infectious Diseases* **35**, 188–195 (June 2022).
107. Kolodziejek, A. M. *et al.* *Yersinia pestis* Δ ail mutants are not susceptible to human complement bactericidal activity in the flea. *Applied and Environmental Microbiology* **89**, e01244–22 (Feb. 2023).
108. Singh, C. *et al.* Mutually constructive roles of Ail and LPS in *Yersinia pestis* serum survival. *Molecular Microbiology* **114**, 510–520 (Sept. 2020).
109. Kolodziejek, A. M., Hovde, C. J., Bohach, G. A. & Minnich, S. A. Deletion of *Yersinia pestis* ail causes temperature-sensitive pleiotropic effects, including cell lysis, that are suppressed by carbon source, cations, or loss of phospholipase A activity. *Journal of Bacteriology* **203**, e00361–21 (Nov. 2021).
110. Silhavy, T. J., Kahne, D. & Walker, S. The bacterial cell envelope. *Cold Spring Harbor Perspectives in Biology* **2**, a000414 (2010).
111. Sun, J., Rutherford, S. T., Silhavy, T. J. & Huang, K. C. Physical properties of the bacterial outer membrane. *Nature Reviews Microbiology* **20**, 236–248 (Nov. 2021).
112. Prior, J. L. *et al.* Characterization of the lipopolysaccharide of *Yersinia pestis*. *Microbial Pathogenesis* **30**, 49–57 (Feb. 2001).
113. Kawahara, K., Tsukano, H., Watanabe, H., Lindner, B. & Matsuura, M. Modification of the structure and activity of lipid A in *Yersinia pestis* lipopolysaccharide by growth temperature. *Infection and Immunity* **70**, 4092–4098 (2002).
114. Rebeil, R., Ernst, R. K., Gowen, B. B., Miller, S. I. & Hinnebusch, B. J. Variation in lipid A structure in the pathogenic *Yersiniae*. *Molecular Microbiology* **52**, 1363–1373 (June 2004).
115. Knirel, Y. A. *et al.* Lipopolysaccharide of the *Yersinia pseudotuberculosis* complex. *Biomolecules* **11**, 1410 (Sept. 2021).
116. Schneck, E. *et al.* Quantitative determination of ion distributions in bacterial lipopolysaccharide membranes by grazing-incidence X-ray fluorescence. *Proceedings of the National Academy of Sciences of the United States of America* **107**, 9147–9151 (May 2010).
117. Clifton, L. A. *et al.* Effect of divalent cation removal on the structure of Gram-negative bacterial outer membrane models. *Langmuir* **31**, 404–412 (Jan. 2015).
118. Vaara, M. Agents that increase the permeability of the outer membrane. *Microbiological Reviews* **56**, 395–411 (Sept. 1992).
119. Konovalova, A. & Silhavy, T. J. Outer membrane lipoprotein biogenesis: Lol is not the end. *Philosophical Transactions of the Royal Society B: Biological Sciences* **370**, 20150030 (Oct. 2015).
120. Asmar, A. T. & Collet, J. F. Lpp, the Braun lipoprotein, turns 50-major achievements and remaining issues. *FEMS Microbiology Letters* **365**, fny199 (Sept. 2018).
121. Moussatova, A., Kandt, C., O'Mara, M. L. & Tieleman, D. P. ATP-binding cassette transporters in *Escherichia coli*. *Biochimica et Biophysica Acta (BBA) - Biomembranes* **1778**, 1757–1771 (Sept. 2008).
122. Tang, X. *et al.* Structural insights into outer membrane asymmetry maintenance in Gram-negative bacteria by MlaFEDB. *Nature Structural & Molecular Biology* **28**, 81–91 (Nov. 2020).
123. Noinaj, N., Gumbart, J. C. & Buchanan, S. K. The β -barrel assembly machinery in motion. *Nature Reviews Microbiology* **15**, 197–204 (Apr. 2017).
124. Jackson, M. W. & Plano, G. V. DsbA is required for stable expression of outer membrane protein YscC and for efficient Yop secretion in *Yersinia pestis*. *Journal of Bacteriology* **181**, 5126–5130 (1999).
125. Eggers, C. T., Murray, I. A., Delmar, V. A., Day, A. G. & Craik, C. S. The periplasmic serine protease inhibitor ecotin protects bacteria against neutrophil elastase. *Biochemical Journal* **379**, 107–118 (Apr. 2004).
126. Clark, E. A. *et al.* Molecular recognition of chymotrypsin by the serine protease inhibitor ecotin from *Yersinia pestis*. *Journal of Biological Chemistry* **286**, 24015–24022 (July 2011).
127. Nagy, Z. A. *et al.* Ecotin, a microbial inhibitor of serine proteases, blocks multiple complement dependent and independent microbicidal activities of human serum. *PLoS Pathogens* **15**, e1008232 (2019).
128. Hoch, J. A. Two-component and phosphorelay signal transduction. *Current Opinion in Microbiology* **3**, 165–170 (Apr. 2000).
129. Flores-Kim, J. & Darwin, A. J. Regulation of bacterial virulence gene expression by cell envelope stress responses. *Virulence* **5**, 835 (2014).
130. Hews, C. L., Cho, T., Rowley, G. & Raivio, T. L. Maintaining integrity under stress: envelope stress response regulation of pathogenesis in Gram-negative bacteria. *Frontiers in Cellular and Infection Microbiology* **9**, 313 (Sept. 2019).
131. Mitchell, A. M. & Silhavy, T. J. Envelope stress responses: balancing damage repair and toxicity. *Nature Reviews Microbiology* **17**, 417–428 (May 2019).

132. Carlsson, K. E., Liu, J., Edqvist, P. J. & Francis, M. S. Extracytoplasmic-stress-responsive pathways modulate type III secretion in *Yersinia pseudotuberculosis*. *Infection and Immunity* **75**, 3913–3924 (Aug. 2007).
133. Reboul, A. *et al.* *Yersinia pestis* requires the 2-component regulatory system OmpR-EnvZ to resist innate immunity during the early and late stages of plague. *The Journal of Infectious Diseases* **210**, 1367–1375 (Nov. 2014).
134. Liu, J., Thanikkal, E. J., Obi, I. R. & Francis, M. S. Elevated CpxR-P levels repress the Ysc–Yop type III secretion system of *Yersinia pseudotuberculosis*. *Research in Microbiology* **163**, 518–530 (Sept. 2012).
135. Carlsson, K. E., Liu, J., Edqvist, P. J. & Francis, M. S. Influence of the Cpx extracytoplasmic-stress-responsive pathway on *Yersinia* sp.-eukaryotic cell contact. *Infection and Immunity* **75**, 4386–4399 (Sept. 2007).
136. Liu, J., Obi, I. R., Thanikkal, E. J., Kieselbach, T. & Francis, M. S. Phosphorylated CpxR restricts production of the RovA global regulator in *Yersinia pseudotuberculosis*. *PLoS One* **6** (2011).
137. Thanikkal, E. J. *et al.* The *Yersinia pseudotuberculosis* Cpx envelope stress system contributes to transcriptional activation of *rovM*. *Virulence* **10**, 37–57 (Jan. 2019).
138. Grabowicz, M. & Silhavy, T. J. Envelope stress responses: An interconnected safety net. *Trends in Biochemical Sciences* **42**, 232–242 (Mar. 2017).
139. Eddy, J. L., Gielda, L. M., Caulfield, A. J., Rangel, S. M. & Lathem, W. W. Production of outer membrane vesicles by the plague pathogen *Yersinia pestis*. *PLoS One* **9**, e107002 (Sept. 2014).
140. Palonen, E., Lindström, M., Somervuo, P. & Korkeala, H. Alternative sigma factor σE has an important role in stress tolerance of *Yersinia pseudotuberculosis* IP32953. *Applied and Environmental Microbiology* **79**, 5970–5977 (2013).
141. Flores-Kim, J. & Darwin, A. J. Links between type III secretion and extracytoplasmic stress responses in *Yersinia*. *Frontiers in Cellular and Infection Microbiology* **2**, 125 (Oct. 2012).
142. Flores-Kim, J. & Darwin, A. J. The phage shock protein response. *Annual Review of Microbiology* **70**, 83–101 (Sept. 2016).
143. Chen, S., Thompson, K. M. & Francis, M. S. Environmental regulation of *Yersinia* pathophysiology. *Frontiers in Cellular and Infection Microbiology* **6**, 25 (Mar. 2016).
144. Meng, J., Young, G. & Chen, J. The Rcs system in *Enterobacteriaceae*: envelope stress responses and virulence regulation. *Frontiers in Microbiology* **12**, 163 (Feb. 2021).
145. Chen, H. D. & Groisman, E. A. The biology of the PmrA/PmrB two-component system: the major regulator of lipopolysaccharide modifications. *Annual Review of Microbiology* **67**, 83–112 (Sept. 2013).
146. Fukuto, H. S., Viboud, G. I. & Vadyvaloo, V. The diverse roles of the global transcriptional regulator PhoP in the lifecycle of *Yersinia pestis*. *Pathogens* **9**, 1039 (Dec. 2020).
147. O’Loughlin, J. L., Spinner, J. L., Minnich, S. A. & Kobayashi, S. D. *Yersinia pestis* two-component gene regulatory systems promote survival in human neutrophils. *Infection and Immunity* **78**, 733–782 (Feb. 2010).
148. Oyston, P. C. *et al.* The response regulator PhoP is important for survival under conditions of macrophage-induced stress and virulence in *Yersinia pestis*. *Infection and Immunity* **68**, 3419–3425 (June 2000).
149. Zhang, Y. *et al.* Reciprocal regulation of pH 6 antigen gene loci by PhoP and RovA in *Yersinia pestis* biovar Microtus. *Future Microbiology* **8**, 271–280 (Feb. 2013).
150. Perez, J. C. *et al.* Evolution of a bacterial regulon controlling virulence and Mg²⁺ homeostasis. *PLoS Genetics* **5**, e1000428 (Mar. 2009).
151. Minagawa, S. *et al.* Identification and molecular characterization of the Mg²⁺ stimulon of *Escherichia coli*. *Journal of Bacteriology* **185**, 3696–3702 (July 2003).
152. Lejona, S., Aguirre, A., Cabeza, M. L., García Vescovi, E. & Soncini, F. C. Molecular Characterization of the Mg²⁺-Responsive PhoP-PhoQ Regulon in *Salmonella enterica*. *Journal of Bacteriology* **185**, 6287–6294 (Nov. 2003).
153. Lin, Z. *et al.* Virulence and stress responses of *Shigella flexneri* regulated by PhoP/PhoQ. *Frontiers in microbiology* **8**, 2689 (Jan. 2018).
154. Yang, B. *et al.* Identification of novel PhoP-PhoQ regulated genes that contribute to polymyxin B tolerance in *Pseudomonas aeruginosa*. *Microorganisms* **9**, 344 (Feb. 2021).
155. Lippa, A. M. & Goulian, M. Feedback inhibition in the PhoQ/PhoP signaling system by a membrane peptide. *PLoS Genetics* **5**, e1000788 (Dec. 2009).
156. Plesa, M., Hernalsteens, J. P., Vandenbussche, G., Ruyschaert, J. M. & Cornelis, P. The SlyB outer membrane lipoprotein of *Burkholderia multivorans* contributes to membrane integrity. *Research in Microbiology* **157**, 582–592 (July 2006).
157. Chakraborty, S. & Kenney, L. J. A new role of OmpR in acid and osmotic stress in *Salmonella* and *E. coli*. *Frontiers in Microbiology* **9**, 2656 (Nov. 2018).

158. Gao, H. *et al.* Phenotypic and transcriptional analysis of the osmotic regulator OmpR in *Yersinia pestis*. *BMC Microbiology* **11**, 1–11 (Feb. 2011).
159. Rosadini, C. V. & Kagan, J. C. Early innate immune responses to bacterial LPS. *Current Opinion in Immunology* **44**, 14–19 (Feb. 2017).
160. Rathinam, V. A., Zhao, Y. & Shao, F. Innate immunity to intracellular LPS. *Nature Immunology* **20**, 527–533 (Apr. 2019).
161. Winfield, M. D., Latifi, T. & Groisman, E. A. Transcriptional regulation of the 4-amino-4-deoxy-L-arabinose biosynthetic genes in *Yersinia pestis*. *Journal of Biological Chemistry* **280**, 14765–14772 (Apr. 2005).
162. Grabenstein, J. P., Fukuto, H. S., Palmer, L. E. & Bliska, J. B. Characterization of phagosome trafficking and identification of PhoP-regulated genes important for survival of *Yersinia pestis* in macrophages. *Infection and Immunity* **74**, 3727 (July 2006).
163. Klein, K. A. *et al.* A transposon site hybridization screen identifies *galU* and *wecBC* as important for survival of *Yersinia pestis* in murine macrophages. *Journal of Bacteriology* **194**, 653 (Feb. 2012).
164. Aoyagi, K. L. *et al.* LPS modification promotes maintenance of *Yersinia pestis* in fleas. *Microbiology* **161**, 628–638 (Mar. 2015).
165. Mathew, B., Aoyagi, K. L. & Fisher, M. A. *Yersinia pestis* lipopolysaccharide remodeling confers resistance to a *Xenopsylla cheopis* cecropin. *ACS Infectious Diseases* **7**, 2536–2545 (Aug. 2021).
166. Rebeil, R. *et al.* Characterization of late acyltransferase genes of *Yersinia pestis* and their role in temperature-dependent lipid A variation. *Journal of Bacteriology* **188**, 1381–1388 (Feb. 2006).
167. Hitchen, P. G. *et al.* Structural characterization of lipo-oligosaccharide (LOS) from *Yersinia pestis*: regulation of LOS structure by the PhoPQ system. *Molecular Microbiology* **44**, 1637–1650 (June 2002).
168. Sun, W. *et al.* Pathogenicity of *Yersinia pestis* synthesis of 1-dephosphorylated lipid A. *Infection and Immunity* **81**, 1172–1185 (Apr. 2013).
169. Montminy, S. W. *et al.* Virulence factors of *Yersinia pestis* are overcome by a strong lipopolysaccharide response. *Nature Immunology* **7**, 1066–1073 (Oct. 2006).
170. Chandler, C. E. *et al.* Early evolutionary loss of the lipid A modifying enzyme PagP resulting in innate immune evasion in *Yersinia pestis*. *Proceedings of the National Academy of Sciences of the United States of America* **117**, 22984–22991 (Sept. 2020).
171. Li, Y., Wang, Z., Chen, J., Ernst, R. K. & Wang, X. Influence of lipid A acylation pattern on membrane permeability and innate immune stimulation. *Marine Drugs* **2013** **11**, 3197–3208 (Aug. 2013).
172. Prior, J. L. *et al.* The failure of different strains of *Yersinia pestis* to produce lipopolysaccharide O-antigen under different growth conditions is due to mutations in the O-antigen gene cluster. *FEMS Microbiology Letters* **197**, 229–233 (Apr. 2001).
173. Kukkonen, M. *et al.* Lack of O-antigen is essential for plasminogen activation by *Yersinia pestis* and *Salmonella enterica*. *Molecular Microbiology* **51**, 215–225 (Jan. 2004).
174. Suomalainen, M. *et al.* Temperature-induced changes in the lipopolysaccharide of *Yersinia pestis* affect plasminogen activation by the Pla surface protease. *Infection and Immunity* **78**, 2644–2652 (June 2010).
175. Kolodziejek, A. M. *et al.* Outer membrane protein X (Ail) contributes to *Yersinia pestis* virulence in pneumonic plague and its activity is dependent on the lipopolysaccharide core length. *Infection and Immunity* **78**, 5233–5243 (Dec. 2010).
176. Sha, J. *et al.* Braun lipoprotein (Lpp) contributes to virulence of yersiniae: potential role of Lpp in inducing bubonic and pneumonic plague. *Infection and Immunity* **76**, 1390–1409 (Apr. 2008).
177. Liu, T., Agar, S. L., Sha, J. & Chopra, A. K. Deletion of Braun lipoprotein gene (*lpp*) attenuates *Yersinia pestis* KIM/D27 strain: role of Lpp in modulating host immune response, NF- κ B activation and cell death. *Microbial Pathogenesis* **48**, 42–52 (Jan. 2010).
178. Sha, J. *et al.* Deletion of the Braun lipoprotein-encoding gene and altering the function of lipopolysaccharide attenuate the plague bacterium. *Infection and Immunity* **81**, 815–828 (Mar. 2013).
179. Yang, R. *et al.* Omics strategies for revealing *Yersinia pestis* virulence. *Frontiers in Cellular and Infection Microbiology* **2**, 157 (2012).
180. Yang, R. & Motin, V. L. *Yersinia pestis* in the Age of Big Data. *Advances in Experimental Medicine and Biology* **918**, 257–272 (2016).
181. Parkhill, J. *et al.* Genome sequence of *Yersinia pestis*, the causative agent of plague. *Nature* **413**, 523–527 (Oct. 2001).
182. Deng, W. *et al.* Genome sequence of *Yersinia pestis* KIM. *Journal of Bacteriology* **184**, 4601 (2002).
183. Song, Y. *et al.* Complete genome sequence of *Yersinia pestis* strain 91001, an isolate avirulent to humans. *DNA Research* **11**, 179–197 (Jan. 2004).
184. Chain, P. S. *et al.* Insights into the evolution of *Yersinia pestis* through whole-genome comparison with *Yersinia pseudotuberculosis*. *Proceedings of the National Academy of Sciences of the United States of America* **101**, 13826–13831 (Sept. 2004).

185. Slatko, B. E., Gardner, A. F. & Ausubel, F. M. Overview of next-generation sequencing technologies. *Current Protocols in Molecular Biology* **122**, e59 (Apr. 2018).
186. Morelli, G. *et al.* *Yersinia pestis* genome sequencing identifies patterns of global phylogenetic diversity. *Nature Genetics* **42**, 1140–1143 (Oct. 2010).
187. Rascovan, N. *et al.* Emergence and spread of basal lineages of *Yersinia pestis* during the Neolithic decline. *Cell* **176**, 295–305 (Jan. 2019).
188. Keller, M. *et al.* Ancient *Yersinia pestis* genomes from across Western Europe reveal early diversification during the First Pandemic (541–750). *Proceedings of the National Academy of Sciences of the United States of America* **116**, 12363–12372 (June 2019).
189. Spyrou, M. A. *et al.* The source of the Black Death in fourteenth-century central Eurasia. *Nature* **606**, 718–724 (June 2022).
190. Valtueña, A. A. *et al.* Stone Age *Yersinia pestis* genomes shed light on the early evolution, diversity, and ecology of plague. *Proceedings of the National Academy of Sciences of the United States of America* **119**, e2116722119 (Apr. 2022).
191. Klunk, J. *et al.* Evolution of immune genes is associated with the Black Death. *Nature* **611**, 312–319 (Oct. 2022).
192. Bramanti, B., Wu, Y., Yang, R., Cui, Y. & Stenseth, N. C. Assessing the origins of the European plagues following the Black Death: a synthesis of genomic, historical, and ecological information. *Proceedings of the National Academy of Sciences of the United States of America* **118**, e2101940118 (Sept. 2021).
193. Lê-Bury, P. *et al.* Yersiniomics, a multi-omics interactive database for *Yersinia* species. *Microbiology Spectrum* **11**, e0382622 (Feb. 2023).
194. Gargis, A. S., Cherney, B., Conley, A. B., McLaughlin, H. P. & Sue, D. Rapid detection of genetic engineering, structural variation, and antimicrobial resistance markers in bacterial biothreat pathogens by Nanopore sequencing. *Scientific Reports* **9**, 1–14 (Sept. 2019).
195. Motin, V. L. *et al.* Temporal global changes in gene expression during temperature transition in *Yersinia pestis*. *Journal of Bacteriology* **186**, 6298–6305 (Sept. 2004).
196. Han, Y. *et al.* Microarray analysis of temperature-induced transcriptome of *Yersinia pestis*. *Microbiology and Immunology* **48**, 791–805 (Nov. 2004).
197. Han, Y. *et al.* Comparative transcriptomics in *Yersinia pestis*: a global view of environmental modulation of gene expression. *BMC Microbiology* **7**, 1–16 (Oct. 2007).
198. Chauvaux, S. *et al.* Transcriptome analysis of *Yersinia pestis* in human plasma: an approach for discovering bacterial genes involved in septicemic plague. *Microbiology* **153**, 3112–3124 (Sept. 2007).
199. Rosso, M. L. *et al.* Growth of *Yersinia pseudotuberculosis* in human plasma: impacts on virulence and metabolic gene expression. *BMC Microbiology* **8**, 211 (2008).
200. Li, Y. *et al.* Identification and characterization of PhoP regulon members in *Yersinia pestis* biovar *Microtus*. *BMC Genomics* **9**, 143 (Mar. 2008).
201. Vadyvaloo, V. *et al.* Role of the Phop-PhoQ gene regulatory system in adaptation of *Yersinia pestis* to environmental stress in the flea digestive tract. *Microbiology* **161**, 1198–1210 (July 2015).
202. Jozwick, A. K., LaPatra, S. E., Graf, J. & Welch, T. J. Flagellar regulation mediated by the Rcs pathway is required for virulence in the fish pathogen *Yersinia ruckeri*. *Fish & Shellfish Immunology* **91**, 306–314 (Aug. 2019).
203. Yang, Y. *et al.* Dual RNA-seq of trunk kidneys extracted from channel catfish infected with *Yersinia ruckeri* reveals novel insights into host-pathogen interactions. *Frontiers in Immunology* **12**, 775708 (Dec. 2021).
204. Paulson, A. R., O'Callaghan, M., Zhang, X. X., Rainey, P. B. & Hurst, M. R. *In vivo* transcriptome analysis provides insights into host-dependent expression of virulence factors by *Yersinia entomophaga* MH96, during infection of *Galleria mellonella*. *G3* **11**, jkaa024 (Jan. 2021).
205. Avican, K. *et al.* RNA atlas of human bacterial pathogens uncovers stress dynamics linked to infection. *Nature Communications* **12**, e3282 (Dec. 2021).
206. Nuss, A. M. *et al.* Tissue dual RNA-seq allows fast discovery of infection-specific functions and riboregulators shaping host-pathogen transcriptomes. *Proceedings of the National Academy of Sciences of the United States of America* **114**, 791–800 (Jan. 2017).
207. Kusmierek, M., Heroven, A. K., Beckstette, M., Nuss, A. M. & Dersch, P. Discovering *Yersinia*–host interactions by tissue dual RNA-seq. *Methods in Molecular Biology* **2010**, 99–116 (2019).
208. Israeli, O. *et al.* Novel RNA extraction method for dual RNA-seq analysis of pathogen and host in the early stages of *Yersinia pestis* pulmonary infection. *Microorganisms* **9**, e2166 (Oct. 2021).
209. Koo, J. T., Alleyne, T. M., Schiano, C. A., Jafari, N. & Latham, W. W. Global discovery of small RNAs in *Yersinia pseudotuberculosis* identifies *Yersinia*-specific small, noncoding RNAs required for virulence. *Proceedings of the National Academy of Sciences of the United States of America* **108**, E709–E717 (Sept. 2011).

210. Beauregard, A. *et al.* Identification and characterization of small RNAs in *Yersinia pestis*. *RNA Biology* **10**, 397–405 (2013).
211. Yan, Y. *et al.* Determination of sRNA expressions by RNA-seq in *Yersinia pestis* grown *in vitro* and during infection. *PLoS One* **8**, e74495 (2013).
212. Schiano, C. A. *et al.* Genome-wide analysis of small RNAs expressed by *Yersinia pestis* identifies a regulator of the Yop-Ysc type III secretion system. *Journal of Bacteriology* **196**, 1659–1670 (2014).
213. Nuss, A. M. *et al.* Transcriptomic profiling of *Yersinia pseudotuberculosis* reveals reprogramming of the Crp regulon by temperature and uncovers Crp as a master regulator of small RNAs. *PLoS Genetics* **11**, e1005087 (Mar. 2015).
214. Li, N. *et al.* Functional and structural analysis of a highly-expressed *Yersinia pestis* small RNA following infection of cultured macrophages. *PLoS One* **11**, e0168915 (Dec. 2016).
215. Schmühl, C. *et al.* Comparative transcriptomic profiling of *Yersinia enterocolitica* O:3 and O:8 reveals major expression differences of fitness- and virulence-relevant genes indicating ecological separation. *mSystems* **4**, 00239–18 (Apr. 2019).
216. Han, Y. *et al.* Hfq globally binds and destabilizes sRNAs and mRNAs in *Yersinia pestis*. *mSystems* **4** (Aug. 2019).
217. Hixson, K. K. *et al.* Biomarker candidate identification in *Yersinia pestis* using organism-wide semi-quantitative proteomics. *Journal of Proteome Research* **5**, 3008–3017 (2006).
218. Chromy, B. A. *et al.* Proteomic characterization of *Yersinia pestis* virulence. *Journal of Bacteriology* **187**, 8172–8180 (Dec. 2005).
219. Pieper, R. *et al.* Characterizing the dynamic nature of the *Yersinia pestis* periplasmic proteome in response to nutrient exhaustion and temperature change. *Proteomics* **8**, 1442–1458 (Apr. 2008).
220. Pieper, R. *et al.* Temperature and growth phase influence the outer-membrane proteome and the expression of a type VI secretion system in *Yersinia pestis*. *Microbiology* **155**, 498–512 (Feb. 2009).
221. Pieper, R. *et al.* Proteomic analysis of iron acquisition, metabolic and regulatory responses of *Yersinia pestis* to iron starvation. *BMC Microbiology* **10**, e30 (Jan. 2010).
222. Hu, Q. *et al.* The Orbitrap: a new mass spectrometer. *Journal of Mass Spectrometry* **40**, 430–443 (Apr. 2005).
223. Merkley, E. D. *et al.* Protein abundances can distinguish between naturally-occurring and laboratory strains of *Yersinia pestis*, the causative agent of plague. *PLoS One* **12**, e0183478 (Aug. 2017).
224. Schrimpe-Rutledge, A. C. *et al.* Comparative omics-driven genome annotation refinement: application across *Yersinia*. *PLoS One* **7**, e33903 (Mar. 2012).
225. Ansong, C. *et al.* A multi-omic systems approach to elucidating *Yersinia* virulence mechanisms. *Molecular BioSystems* **9**, 44–54 (Nov. 2013).
226. Lin, A., Merkley, E. D., Clowers, B. H., Hutchison, J. R. & Kreuzer, H. W. Effects of bacterial inactivation methods on downstream proteomic analysis. *Journal of Microbiological Methods* **112**, 3–10 (May 2015).
227. Payne, S. H. *et al.* The Pacific Northwest National Laboratory library of bacterial and archaeal proteomic biodiversity. *Scientific Data* **2**, e150041 (Aug. 2015).
228. Nozadze, M. *et al.* Comparative proteomic studies of *Yersinia pestis* strains isolated from natural foci in the Republic of Georgia. *Frontiers in Public Health* **3**, 239 (Oct. 2015).
229. Cao, S. *et al.* Secretome and comparative proteomics of *Yersinia pestis* identify two novel E3 ubiquitin ligases that contribute to plague virulence. *Molecular & Cellular Proteomics* **20**, e100066 (2021).
230. Cao, S. *et al.* Subversion of GBP-mediated host defense by E3 ligases acquired during *Yersinia pestis* evolution. *Nature Communications* **13**, 1–17 (Aug. 2022).
231. Cao, S. *et al.* Proteogenomic discovery of sORF-encoded peptides associated with bacterial virulence in *Yersinia pestis*. *Communications Biology* **4**, 1–12 (Nov. 2021).
232. Payne, S. H., Huang, S.-T. & Pieper, R. A proteogenomic update to *Yersinia*: enhancing genome annotation. *BMC Genomics* **11**, 460 (Aug. 2010).
233. Deatherage Kaiser, B. L. *et al.* Proteomic signatures of antimicrobial resistance in *Yersinia pestis* and *Francisella tularensis*. *Frontiers in Medicine* **9**, 108 (Feb. 2022).
234. Navid, A. & Almaas, E. Genome-scale reconstruction of the metabolic network in *Yersinia pestis*, strain 91001. *Molecular BioSystems* **5**, 368–375 (Mar. 2009).
235. Charusanti, P. *et al.* An experimentally-supported genome-scale metabolic network reconstruction for *Yersinia pestis* CO92. *BMC Systems Biology* **5**, 1–13 (Oct. 2011).
236. Navid, A. & Almaas, E. Genome-level transcription data of *Yersinia pestis* analyzed with a new metabolic constraint-based approach. *BMC Systems Biology* **6**, 1–18 (Dec. 2012).
237. Ansong, C. *et al.* Studying *Salmonellae* and *Yersinia* host–pathogen interactions using integrated ‘omics and modeling. *Current Topics in Microbiology and Immunology* **363**, 21–41 (2012).

238. Yang, H. *et al.* Insight into bacterial virulence mechanisms against host immune response via the *Yersinia pestis*-human protein-protein interaction network. *Infection and Immunity* **79**, 4413–4424 (Nov. 2011).
239. Dyer, M. D. *et al.* The human-bacterial pathogen protein interaction networks of *Bacillus anthracis*, *Francisella tularensis*, and *Yersinia pestis*. *PLoS One* **5**, e0012089 (2010).
240. Hensel, M. *et al.* Simultaneous identification of bacterial virulence genes by negative selection. *Science* **269**, 400–3 (July 1995).
241. Darwin, A. J. & Miller, V. L. Identification of *Yersinia enterocolitica* genes affecting survival in an animal host using signature-tagged transposon mutagenesis. *Molecular Microbiology* **32**, 51–62 (Apr. 1999).
242. Karlyshev, A. V. *et al.* Application of high-density array-based signature-tagged mutagenesis to discover novel *Yersinia* virulence-associated genes. *Infection and Immunity* **69**, 7810–7819 (2001).
243. Meccas, J., Bilis, I. & Falkow, S. Identification of attenuated *Yersinia pseudotuberculosis* strains and characterization of an orogastric infection in BALB/c mice on day 5 postinfection by signature-tagged mutagenesis. *Infection and Immunity* **69**, 2779–2787 (2001).
244. Flashner, Y. *et al.* Generation of *Yersinia pestis* attenuated strains by signature-tagged mutagenesis in search of novel vaccine candidates. *Infection and Immunity* **72**, 908–915 (Feb. 2004).
245. Ponnusamy, D. *et al.* High-throughput, signature-tagged mutagenic approach to identify novel virulence factors of *Yersinia pestis* CO92 in a mouse model of infection. *Infection and Immunity* **83**, 2065–2081 (2015).
246. Sasseti, C. M., Boyd, D. H. & Rubin, E. J. Comprehensive identification of conditionally essential genes in *Mycobacteria*. *Proceedings of the National Academy of Sciences of the United States of America* **98**, 12712 (Oct. 2001).
247. Van Opijnen, T. & Camilli, A. Transposon insertion sequencing: a new tool for systems-level analysis of microorganisms. *Nature Reviews Microbiology* **11**, 435–442 (May 2013).
248. Palace, S. G., Proulx, M. K., Lu, S., Baker, R. E. & Goguen, J. D. Genome-wide mutant fitness profiling identifies nutritional requirements for optimal growth of *Yersinia pestis* in deep tissue. *mBio* **5**, e01385–14 (Aug. 2014).
249. Yang, Z. R. *et al.* A noise trimming and positional significance of transposon insertion system to identify essential genes in *Yersinia pestis*. *Scientific Reports* **7**, e41923 (Feb. 2017).
250. Senior, N. J. *et al.* An integrated computational-experimental approach reveals *Yersinia pestis* genes essential across a narrow or a broad range of environmental conditions. *BMC Microbiology* **17**, e163 (July 2017).
251. Willcocks, S. J., Stabler, R. A., Atkins, H. S., Oyston, P. F. & Wren, B. W. High-throughput analysis of *Yersinia pseudotuberculosis* gene essentiality in optimised in vitro conditions, and implications for the speciation of *Yersinia pestis*. *BMC Microbiology* **18**, e46 (May 2018).
252. Willcocks, S. *et al.* Genome-wide assessment of antimicrobial tolerance in *Yersinia pseudotuberculosis* under ciprofloxacin stress. *Microbial Genomics* **5**, e000304 (2019).
253. Rousset, F. & Bikard, D. CRISPR screens in the era of microbiomes. *Current Opinion in Microbiology* **57**, 70–77 (Oct. 2020).
254. Liu, X. *et al.* Exploration of bacterial bottlenecks and *Streptococcus pneumoniae* pathogenesis by CRISPRi-seq. *Cell Host & Microbe* **29**, 107–120 (Jan. 2021).
255. De Bakker, V., Liu, X., Bravo, A. M. & Veening, J. W. CRISPRi-seq for genome-wide fitness quantification in bacteria. *Nature Protocols* **17**, 252–281 (Jan. 2022).
256. Subrahmanyam, Y. V. *et al.* RNA expression patterns change dramatically in human neutrophils exposed to bacteria. *Blood* **97**, 2457–2468 (Apr. 2001).
257. Das, R. *et al.* Study of proinflammatory responses induced by *Yersinia pestis* in human monocytes using cDNA arrays. *Genes & Immunity* **8**, 308–319 (Apr. 2007).
258. Chromy, B. A. *et al.* Proteomic characterization of host response to *Yersinia pestis* and near neighbors. *Biochemical and Biophysical Research Communications* **320**, 474–479 (July 2004).
259. Zhang, C. G. *et al.* Subcellular proteomic analysis of host-pathogen interactions using human monocytes exposed to *Yersinia pestis* and *Yersinia pseudotuberculosis*. *Proteomics* **5**, 1877–1888 (May 2005).
260. Du, Z. *et al.* Transcriptomic response to *Yersinia pestis*: RIG-I like receptor signaling response is detrimental to the host against plague. *Journal of Genetics and Genomics* **41**, 379–396 (July 2014).
261. Rogers, J. V. *et al.* Transcriptional responses in spleens from mice exposed to *Yersinia pestis* CO92. *Microbial Pathogenesis* **43**, 67–77 (Aug. 2007).
262. Liu, H. *et al.* Transcriptional profiling of a mice plague model: insights into interaction between *Yersinia pestis* and its host. *Journal of Basic Microbiology* **49**, 92–99 (Feb. 2009).
263. Yang, H. *et al.* Host transcriptomic responses to pneumonic plague reveal that *Yersinia pestis* inhibits both the initial adaptive and innate immune responses in mice. *International Journal of Medical Microbiology* **307**, 64–74 (Jan. 2017).

264. Galindo, C. L. *et al.* Comparative analyses of transcriptional profiles in mouse organs using a pneumonic plague model after infection with wild-type *Yersinia pestis* CO92 and its Braun lipoprotein mutant. *Comparative and Functional Genomics* (2009).
265. Gautam, A. *et al.* Metabolomic analyses reveal lipid abnormalities and hepatic dysfunction in non-human primate model for *Yersinia pestis*. *Metabolomics* **15**, 1–19 (Jan. 2019).
266. Bertherat, E. Plague around the world in 2019/La peste dans le monde en 2019. *Weekly Epidemiological Record* **94**, 289–293 (June 2019).
267. Steele, J. H. CRC handbook series in zoonoses. Section A : Bacterial, rickettsial, and mycotic diseases (1979).
268. Hull, H. F., Montes, J. M. & Mann, J. M. Septicemic plague in New Mexico. *The Journal of Infectious Diseases* **155**, 113–118 (Jan. 1987).
269. Kugeler, K. J., Mead, P. S., Campbell, S. B. & Nelson, C. A. Antimicrobial treatment patterns and illness outcome among United States patients with plague, 1942-2018. *Clinical Infectious Diseases* **70**, S20–S26 (2020).
270. World Health Organization. *Plague outbreak toolbox*
271. Nikiforov, V. V., Gao, H., Zhou, L. & Anisimov, A. Plague: clinics, diagnosis and treatment. *Advances in Experimental Medicine and Biology* **918**, 293–312 (2016).
272. Chanteau, S. *et al.* Development and testing of a rapid diagnostic test for bubonic and pneumonic plague. *The Lancet* **361**, 211–216 (Jan. 2003).
273. Hänisch, S. *et al.* The *pla* gene, encoding plasminogen activator, is not specific to *Yersinia pestis*. *BMC Research Notes* **8**, 1–3 (Oct. 2015).
274. D'Ortenzio, E. *et al.* Plague: bridging gaps towards better disease control. *Médecine et Maladies Infectieuses* **48**, 307–317 (Aug. 2018).
275. Jullien, S., Dissanayake, H. A. & Chaplin, M. Rapid diagnostic tests for plague. *Cochrane Database of Systematic Reviews* **2020**, CD013459 (2020).
276. Ten Bosch, Q. *et al.* Analytical framework to evaluate and optimize the use of imperfect diagnostics to inform outbreak response: Application to the 2017 plague epidemic in Madagascar. *PLoS Biology* **20**, e3001736 (Aug. 2022).
277. Derbise, A. *et al.* An encapsulated *Yersinia pseudotuberculosis* is a highly efficient vaccine against pneumonic plague. *PLoS Neglected Tropical Diseases* **6**, e1528 (Feb. 2012).
278. Derbise, A., Hanada, Y., Khalifé, M., Carniel, E. & Demeure, C. E. Complete protection against pneumonic and bubonic plague after a single oral vaccination. *PLoS Neglected Tropical Diseases* **9**, e00041–62 (Oct. 2015).
279. Winter, C. C., Cherry, W. B. & Moody, M. D. An unusual strain of *Pasteurella pestis* isolated from a fatal human case of plague. *Bulletin of the World Health Organization* **23**, 408 (1960).
280. Sah, R., Reda, A., Mehta, R., Mohapatra, R. K. & Dhama, K. A situation analysis of the current plague outbreak in the Democratic Republic of Congo and counteracting strategies. *International Journal of Surgery* **105**, 106885 (Sept. 2022).
281. Matero, P. *et al.* Real-time multiplex PCR assay for detection of *Yersinia pestis* and *Yersinia pseudotuberculosis*. *APMIS* **117**, 34–44 (Jan. 2009).
282. Nguyen, S. T., Dinh, H. T. T. & Nghiem, M. N. A hexaplex PCR assay developed for simultaneous detection of *Bacillus anthracis* and *Yersinia pestis* and distinguish their virulence levels tested on Vietnamese samples. *SN Comprehensive Clinical Medicine* **1**, 510–516 (May 2019).
283. Feng, N. *et al.* *Yersinia pestis* detection by loop-mediated isothermal amplification combined with magnetic bead capture of DNA. *Brazilian Journal of Microbiology* **49**, 128–137 (Jan. 2018).
284. Mölsä, M. *et al.* Monitoring biothreat agents (*Francisella tularensis*, *Bacillus anthracis* and *Yersinia pestis*) with a portable real-time PCR instrument. *Journal of Microbiological Methods* **115**, 89–93 (Aug. 2015).
285. Müller, K. *et al.* Pulse-Controlled Amplification—A new powerful tool for on-site diagnostics under resource limited conditions. *PLoS Neglected Tropical Diseases* **15**, e0009114 (2021).
286. Li, A. N. *et al.* Use of magnetic nanotrapp particles in capturing *Yersinia pestis* virulence factors, nucleic acids and bacteria. *Journal of Nanobiotechnology* **19**, 186 (Dec. 2021).
287. Israeli, O. *et al.* A rapid high-throughput sequencing-based approach for the identification of unknown bacterial pathogens in whole blood. *Future Science OA* **6**, FSO476 (July 2020).
288. Hewitt, F. C., Guertin, S. L., Ternus, K. L., Schulte, K. & Kadavy, D. R. Toward rapid sequenced-based detection and characterization of causative agents of bacteremia. *bioRxiv*, 162735 (July 2017).
289. Wołkiewicz, T. The utility and perspectives of NGS-based methods in BSL-3 and BSL-4 laboratory – sequencing and analysis strategies. *Briefings in Functional Genomics* **17**, 471–476 (Nov. 2018).
290. Player, R. *et al.* Comparison of the performance of an amplicon sequencing assay based on Oxford Nanopore technology to real-time PCR assays for detecting bacterial biodefense pathogens. *BMC Genomics* **21**, 166 (Feb. 2020).

291. Sim, E. M. *et al.* Case report: a genomics-guided reclassification of a blood culture isolate misassigned by MALDI-TOF as *Yersinia pestis*. *Access Microbiology* **4**, 000422 (Oct. 2022).
292. Chen, G. *et al.* Obtaining specific sequence tags for *Yersinia pestis* and visually detecting them using the CRISPR-Cas12a system. *Pathogens* **10**, 562 (May 2021).
293. You, Y. *et al.* Highly specific and sensitive detection of *Yersinia pestis* by portable Cas12a-UPTLFA platform. *Frontiers in Microbiology* **12**, 1702 (July 2021).
294. Schultzhaut, Z., Wang, Z. & Stenger, D. Systematic analysis, identification, and use of CRISPR/Cas13a-associated crRNAs for sensitive and specific detection of the *lcrV* gene of *Yersinia pestis*. *Diagnostic Microbiology and Infectious Disease* **99**, 115275 (Mar. 2021).
295. Chenau, J. *et al.* Detection of *Yersinia pestis* in environmental and food samples by intact cell immunocapture and liquid chromatography-tandem mass spectrometry. *Analytical Chemistry* **86**, 6144–6152 (2014).
296. Rifflet, A. *et al.* Quantification of low abundance *Yersinia pestis* markers in dried blood spots by immuno-capture and quantitative high-resolution targeted mass spectrometry. *European Journal of Mass Spectrometry* **25**, 268–277 (2019).
297. Geyer, P. E., Holdt, L. M., Teupser, D. & Mann, M. Revisiting biomarker discovery by plasma proteomics. *Molecular Systems Biology* **13**, 942 (2017).
298. Geyer, P. E. *et al.* Plasma proteome profiling to assess human health and disease. *Cell Systems* **2**, 185–195 (Mar. 2016).
299. Xue, L. *et al.* Mixed-mode ion exchange-based integrated proteomics technology for fast and deep plasma proteome profiling. *Journal of Chromatography A* **1564**, 76–84 (Aug. 2018).
300. Woo, J. & Zhang, Q. A streamlined high-throughput plasma proteomics platform for clinical proteomics with improved proteome coverage, reproducibility, and robustness. *Journal of the American Society for Mass Spectrometry* **34**, 754–762 (2023).
301. Geyer, P. E. *et al.* Plasma proteome profiling to detect and avoid sample-related biases in biomarker studies. *EMBO Molecular Medicine* **11**, e10427 (2019).
302. Ignjatovic, V. *et al.* Mass spectrometry-based plasma proteomics: considerations from sample collection to achieving translational data. *Journal of Proteome Research* **18**, 4085–4097 (Oct. 2019).
303. Correia, C. N. *et al.* Circulating microRNAs as potential biomarkers of infectious disease. *Frontiers in Immunology* **8**, 118 (Feb. 2017).
304. Sohail, M. H. Extracellular/circulating microRNAs: release mechanisms, functions and challenges. *Achievements in the Life Sciences* **10**, 175–186 (Dec. 2016).
305. Glinge, C. *et al.* Stability of circulating blood-based microRNAs – pre-analytic methodological considerations. *PLoS One* **12**, e0167969 (Feb. 2017).
306. Weber, J. A. *et al.* The microRNA spectrum in 12 body fluids. *Clinical chemistry* **56**, 1733 (Nov. 2010).
307. Kozomara, A., Birgaoanu, M. & Griffiths-Jones, S. miRBase: from microRNA sequences to function. *Nucleic Acids Research* **47**, D155–D162 (Jan. 2019).
308. Verma, P., Pandey, R. K., Prajapati, P. & Prajapati, V. K. Circulating microRNAs: potential and emerging biomarkers for diagnosis of human infectious diseases. *Frontiers in Microbiology* **7**, 1274 (Aug. 2016).
309. Li, J. *et al.* Interstitial fluid biomarkers' minimally invasive monitoring using microneedle sensor arrays. *Analytical Chemistry* **94**, 968–974 (Jan. 2022).
310. He, R. *et al.* A hydrogel microneedle patch for point-of-care testing based on skin interstitial fluid. *Advanced Healthcare Materials* **9**, 1901201 (Feb. 2020).
311. Xue, P. *et al.* Blood sampling using microneedles as a minimally invasive platform for biomedical diagnostics. *Applied Materials Today* **13**, 144–157 (Dec. 2018).
312. Babity, S. *et al.* Advances in the design of transdermal microneedles for diagnostic and monitoring applications. *Small* **14**, 1803186 (Dec. 2018).
313. Bruch, R. *et al.* CRISPR/Cas13a-powered electrochemical microfluidic biosensor for nucleic acid amplification-free miRNA diagnostics. *Advanced Materials* **31**, 1905311 (Dec. 2019).
314. Gregory, S. H., Sagnimeni, A. J. & Wing, E. J. Bacteria in the bloodstream are trapped in the liver and killed by immigrating neutrophils. *The Journal of Immunology* **157**, 2514–2520 (Sept. 1996).
315. André, A. C. *et al.* Neutrophils degranulate GAG-containing proteoglycans, which block *Shigella* growth and degrade virulence factors. *bioRxiv*, 2022.02.08.479570 (Feb. 2022).
316. Weiss, J., Inada, M., Elsbach, P. & Crowl, R. M. Structural determinants of the action against *Escherichia coli* of a human inflammatory fluid phospholipase A2 in concert with polymorphonuclear leukocytes. *Journal of Biological Chemistry* **269**, 26331–26337 (Oct. 1994).
317. Sun, Y. C., Hinnebusch, B. J. & Darby, C. Experimental evidence for negative selection in the evolution of a *Yersinia pestis* pseudogene. *Proceedings of the National Academy of Sciences of the United States of America* **105**, 8097–8101 (June 2008).
318. Guo, M. S. *et al.* MicL, a new σ E-dependent sRNA, combats envelope stress by repressing synthesis of Lpp, the major outer membrane lipoprotein. *Genes & Development* **28**, 1620–1634 (July 2014).

319. Gogol, E. B., Rhodius, V. A., Papenfort, K., Vogel, J. & Gross, C. A. Small RNAs endow a transcriptional activator with essential repressor functions for single-tier control of a global stress regulon. *Proceedings of the National Academy of Sciences of the United States of America* **108**, 12875–12880 (Aug. 2011).
320. Rezuchova, B., Miticka, H., Homerova, D., Roberts, M. & Kormanec, J. New members of the *Escherichia coli* σ E regulon identified by a two-plasmid system. *FEMS Microbiology Letters* **225**, 1–7 (Aug. 2003).
321. Deutscher, J., Francke, C. & Postma, P. W. How phosphotransferase system-related protein phosphorylation regulates carbohydrate metabolism in bacteria. *Microbiology and Molecular Biology Reviews* **70**, 939–1031 (Dec. 2006).
322. Kim, T. J. *et al.* Direct transcriptional control of the plasminogen activator gene of *Yersinia pestis* by the cyclic AMP receptor protein. *Journal of Bacteriology* **189**, 8890–8900 (Dec. 2007).
323. Ritzert, J. T., Minasov, G., Embry, R., Schipma, M. J. & Satchell, K. J. The cyclic AMP receptor protein regulates quorum sensing and global gene expression in *Yersinia pestis* during planktonic growth and growth in biofilms. *mBio* **10**, e02613–19 (Nov. 2019).
324. Chen, Y. *et al.* Attenuation of *Yersinia pestis* *fyuA* mutants caused by iron uptake inhibition and decreased survivability in macrophages. *Frontiers in Cellular and Infection Microbiology* **12**, 527 (May 2022).
325. Virtanen, J. P., Keto-Timonen, R., Jaakkola, K., Salin, N. & Korkeala, H. Changes in transcriptome of *Yersinia pseudotuberculosis* IP32953 grown at 3 and 28°C detected by RNA sequencing shed light on cold adaptation. *Frontiers in Cellular and Infection Microbiology* **8**, 416 (Nov. 2018).
326. Deich, R. A., Metcalf, B. J., Finn, C. W., Farley, J. E. & Green, B. A. Cloning of genes encoding a 15,000-dalton peptidoglycan-associated outer membrane lipoprotein and an antigenically related 15,000-dalton protein from *Haemophilus influenzae*. *Journal of Bacteriology* **170**, 489–498 (1988).
327. Ludwig, A. *et al.* SlyA, a regulatory protein from *Salmonella typhimurium*, induces a haemolytic and pore-forming protein in *Escherichia coli*. *Molecular and General Genetics MGG 1995 249:5* **249**, 474–486 (1995).
328. Libby, S. J. *et al.* A cytolysin encoded by *Salmonella* is required for survival within macrophages. *Proceedings of the National Academy of Sciences* **91**, 489–493 (Jan. 1994).
329. Will, W. R. *et al.* The evolution of SlyA/RovA transcription factors from repressors to countersilencers in *Enterobacteriaceae*. *mBio* **10**, e00009–19 (2019).
330. Bringer, M. A., Barnich, N., Glasser, A. L., Bardot, O. & Darfeuille-Michaud, A. HtrA stress protein is involved in intramacrophagic replication of adherent and invasive *Escherichia coli* strain LF82 isolated from a patient with Crohn's disease. *Infection and Immunity* **73**, 712–721 (Feb. 2005).
331. Prudent, V. *et al.* The Crohn's disease-related bacterial strain LF82 assembles biofilm-like communities to protect itself from phagolysosomal attack. *Communications Biology* **4**, 627 (May 2021).
332. Olive, A. J. & Sasseti, C. M. Metabolic crosstalk between host and pathogen: sensing, adapting and competing. *Nature Reviews Microbiology* **14**, 221–234 (Mar. 2016).
333. Heroven, A. K., Böhme, K., Rohde, M. & Dersch, P. A Csr-type regulatory system, including small non-coding RNAs, regulates the global virulence regulator RovA of *Yersinia pseudotuberculosis* through RovM. *Molecular Microbiology* **68**, 1179–1195 (June 2008).
334. Zhang, Y. *et al.* Autoregulation of PhoP/PhoQ and positive regulation of the cyclic AMP receptor protein-cyclic AMP complex by PhoP in *Yersinia pestis*. *Journal of Bacteriology* **195**, 1022–1030 (Mar. 2013).
335. Zhang, Y. *et al.* CRP Acts as a transcriptional repressor of the YPO1635-phoPQ-YPO1632 operon in *Yersinia pestis*. *Current Microbiology* **70**, 398–403 (Nov. 2014).
336. Bücker, R., Heroven, A. K., Becker, J., Dersch, P. & Wittmann, C. The pyruvate-tricarboxylic acid cycle node: a focal point of virulence control in the enteric pathogen *Yersinia pseudotuberculosis*. *Journal of Biological Chemistry* **289**, 30114–30132 (Oct. 2014).
337. Luo, Q. *et al.* Lipoprotein sorting to the cell surface via a crosstalk between the Lpt and Lol pathways during outer membrane biogenesis. *bioRxiv*, 2022.12.25.521893 (Dec. 2022).
338. Firoved, A. M. & Deretic, V. Microarray analysis of global gene expression in mucoid *Pseudomonas aeruginosa*. *Journal of Bacteriology* **185**, 1071–1081 (Feb. 2003).
339. Firoved, A. M., Boucher, J. C. & Deretic, V. Global genomic analysis of AlgU (σ _E)-dependent promoters (Sigmulon) in *Pseudomonas aeruginosa* and implications for inflammatory processes in cystic fibrosis. *Journal of Bacteriology* **184**, 1057–1064 (2002).
340. Lewis, C. Extracytoplasmic stress response systems in *S. typhimurium*. *Doctoral dissertation*, University of Glasgow (2008).
341. Vidovic, S. *et al.* Importance of the RpoE regulon in maintaining the lipid bilayer during antimicrobial treatment with the polycationic agent, chlorhexidine. *Proteomics* **18**, e1700285 (Feb. 2018).
342. Derbise, A., Lesic, B., Dacheux, D., Ghigo, J. M. & Carniel, E. A rapid and simple method for inactivating chromosomal genes in *Yersinia*. *FEMS Immunology & Medical Microbiology* **38**, 113–116 (Sept. 2003).

343. Choi, K. H. *et al.* A Tn7-based broad-range bacterial cloning and expression system. *Nature Methods* **2**, 443–448 (May 2005).
344. Tyanova, S., Temu, T. & Cox, J. The MaxQuant computational platform for mass spectrometry-based shotgun proteomics. *Nature Protocols* **11**, 2301–2319 (Oct. 2016).
345. Cox, J. *et al.* Andromeda: a peptide search engine integrated into the MaxQuant environment. *Journal of Proteome Research* **10**, 1794–1805 (Apr. 2011).
346. Giai Gianetto, Q. Statistical analysis of post-translational modifications quantified by label-free proteomics across multiple biological conditions with R: illustration from SARS-CoV-2 infected cells. *Methods in Molecular Biology* **2426**, 267–302 (2023).
347. Giai Gianetto, Q., Wieczorek, S., Couté, Y. & Burger, T. A peptide-level multiple imputation strategy accounting for the different natures of missing values in proteomics data. *bioRxiv*, 2020.05.29.122770 (May 2020).
348. Ritchie, M. E. *et al.* *limma* powers differential expression analyses for RNA-sequencing and microarray studies. *Nucleic Acids Research* **43**, e47 (Apr. 2015).
349. Giai Gianetto, Q. *et al.* Calibration plot for proteomics: a graphical tool to visually check the assumptions underlying FDR control in quantitative experiments. *PROTEOMICS* **16**, 29–32 (Jan. 2016).
350. Pounds, S. & Cheng, C. Robust estimation of the false discovery rate. *Bioinformatics* **22**, 1979–1987 (Aug. 2006).
351. Wu, T. *et al.* clusterProfiler 4.0: A universal enrichment tool for interpreting omics data. *The Innovation* **2**, 100141 (Aug. 2021).
352. Binns, D. *et al.* QuickGO: a web-based tool for Gene Ontology searching. *Bioinformatics* **25**, 3045 (Nov. 2009).
353. Wang, K. *et al.* Comparing the microRNA spectrum between serum and plasma. *PLoS One* **7**, 41561 (July 2012).
354. Dufourd, T. *et al.* Plasma or serum? A qualitative study on rodents and humans using high-throughput microRNA sequencing for circulating biomarkers. *Biology Methods & Protocols* **4**, bpz006 (Dec. 2019).
355. Mompeón, A. *et al.* Disparate miRNA expression in serum and plasma of patients with acute myocardial infarction: a systematic and paired comparative analysis. *Scientific Reports* **10**, 1–11 (Dec. 2020).
356. Blondal, T. *et al.* Assessing sample and miRNA profile quality in serum and plasma or other biofluids. *Methods* **59**, S1–S6 (Jan. 2013).
357. Koutsoulidou, A., Mastroiannopoulos, N. P., Furling, D., Uney, J. B. & Phylactou, L. A. Expression of miR-1, miR-133a, miR-133b and miR-206 increases during development of human skeletal muscle. *BMC Developmental Biology* **11**, 34 (June 2011).
358. Li, N., Zhou, H. & Tang, Q. MiR-133: a suppressor of cardiac remodeling? *Frontiers in Pharmacology* **9**, 903 (Aug. 2018).
359. Asai, S. *et al.* Impact of miR-1/miR-133 clustered miRNAs: PFN2 facilitates malignant phenotypes in head and neck squamous cell carcinoma. *Biomedicines* **10**, 663 (Mar. 2022).
360. Abd-El-Fattah, A. A., Sadik, N. A. H., Shaker, O. G. & Aboulftouh, M. L. Differential microRNAs expression in serum of patients with lung cancer, pulmonary tuberculosis, and pneumonia. *Cell Biochemistry and Biophysics* **67**, 875–884 (Dec. 2013).
361. Qi, Y. *et al.* Altered serum microRNAs as biomarkers for the early diagnosis of pulmonary tuberculosis infection. *BMC Infectious Diseases* **12**, 384 (Dec. 2012).
362. Visacri, M. B. *et al.* Role of miRNAs as biomarkers of COVID-19: a scoping review of the status and future directions for research in this field. *Biomarkers in Medicine* **15**, 1785–1795 (Dec. 2021).
363. Hermann, S. *et al.* Diagnostic potential of circulating cell-free microRNAs for community-acquired pneumonia and pneumonia-related sepsis. *Journal of Cellular and Molecular Medicine* **24**, 12054–12064 (Oct. 2020).
364. Keshavarz, M. *et al.* MiRNA-based strategy for modulation of influenza A virus infection. *Epigenomics* **10**, 829–844 (June 2018).
365. Hamam, R. *et al.* Circulating microRNAs in breast cancer: novel diagnostic and prognostic biomarkers. *Cell Death & Disease* **2017 8:9** **8**, e3045 (Sept. 2017).
366. Vychytilova-Faltejskova, P. *et al.* Serum-based microRNA signatures in early diagnosis and prognosis prediction of colon cancer. *Carcinogenesis* **37**, 941–950 (Oct. 2016).
367. Hung, P. S. *et al.* miR-376c promotes carcinogenesis and serves as a plasma marker for gastric carcinoma. *PLoS One* **12**, e0177346 (May 2017).
368. Huang, Q. *et al.* Serum microRNA-376 family as diagnostic and prognostic markers in human gliomas. *Cancer Biomarkers* **19**, 137–144 (Jan. 2017).
369. McManus, D. D. & Ambros, V. Circulating microRNAs in cardiovascular disease. *Circulation* **124**, 1908–1910 (Nov. 2011).
370. D'Alessandra, Y. *et al.* Circulating microRNAs are new and sensitive biomarkers of myocardial infarction. *European Heart Journal* **31**, 2765–2773 (Nov. 2010).

371. Wang, R., Li, N., Zhang, Y., Ran, Y. & Pu, J. Circulating microRNAs are promising novel biomarkers of acute myocardial infarction. *Internal Medicine* **50**, 1789–1795 (2011).
372. Al-Muhtareh, H. A., Salem, A. H. & Al-Kafaji, G. Upregulation of circulating cardiomyocyte-enriched miR-1 and miR-133 associate with the risk of coronary artery disease in type 2 diabetes patients and serve as potential biomarkers. *Journal of Cardiovascular Translational Research* **12**, 347–357 (Aug. 2019).
373. Qaisar, R., Karim, A., Muhammad, T. & Shah, I. Circulating biomarkers of accelerated sarcopenia in respiratory diseases. *Biology* **9**, 322 (Oct. 2020).
374. Chiba, Y. & Misawa, M. MicroRNAs and their therapeutic potential for human diseases: miR-133a and bronchial smooth muscle hyperresponsiveness in asthma. *Journal of Pharmacological Sciences* **114**, 264–268 (2010).
375. Sorg, I., Goehring, U. M., Aktories, K. & Schmidt, G. Recombinant *Yersinia* YopT leads to uncoupling of RhoA-effector interaction. *Infection and immunity* **69**, 7535–7543 (2001).
376. Appierto, V. *et al.* A lipemia-independent NanoDrop®-based score to identify hemolysis in plasma and serum samples. *Bioanalysis* **6**, 1215–1226 (June 2014).
377. Pritchard, C. C., Cheng, H. H. & Tewari, M. MicroRNA profiling: approaches and considerations. *Nature Reviews Genetics* **13**, 358–369 (May 2012).
378. Hong, L. Z. *et al.* Systematic evaluation of multiple qPCR platforms, NanoString and miRNA-Seq for microRNA biomarker discovery in human biofluids. *Scientific Reports* **11**, 1–11 (Feb. 2021).
379. Wong, R. K., MacMahon, M., Woodside, J. V. & Simpson, D. A. A comparison of RNA extraction and sequencing protocols for detection of small RNAs in plasma. *BMC Genomics* **20**, 446 (June 2019).
380. Grieco, G. E. *et al.* Protocol to analyze circulating small non-coding RNAs by high-throughput RNA sequencing from human plasma samples. *STAR Protocols* **2**, 100606 (Sept. 2021).
381. Androvic, P., Benesova, S., Rohlova, E., Kubista, M. & Valihrach, L. Small RNA-sequencing for analysis of circulating miRNAs: benchmark study. *bioRxiv*, 2021.03.27.437345 (Mar. 2021).
382. Benesova, S., Kubista, M. & Valihrach, L. Small RNA-sequencing: approaches and considerations for miRNA analysis. *Diagnostics* **11**, 964 (May 2021).
383. Vandesompele, J. *et al.* Accurate normalization of real-time quantitative RT-PCR data by geometric averaging of multiple internal control genes. *Genome Biology* **3**, research0034.1 (June 2002).
384. Willems, P., Fels, U., Staes, A., Gevaert, K. & Van Damme, P. Use of hybrid data-dependent and -independent acquisition spectral libraries empowers dual-proteome profiling. *Journal of Proteome Research* **20**, 1165–1177 (Feb. 2021).
385. Susat, J. *et al.* *Yersinia pestis* strains from Latvia show depletion of the *pla* virulence gene at the end of the second plague pandemic. *Scientific Reports* **10**, 1–10 (Sept. 2020).

Appendixes

Appendix summary

In these appendices, we will summarize other projects and studies we took part to during my thesis in the *Yersinia* research unit. My participation in other projects of the laboratory are listed in the appendix A (page 174) and includes the application of the proteomics pipeline developed in chapter 5 (appendix A.1); the setup of long-read Oxford Nanopore sequencing with a recently acquired MinION device (appendix A.2); the writing of an R pipeline allowing the annotation of an ordered mutant library constructed in the laboratory (appendix A.3); the use of omics studies to understand the role of the *fliC* locus in plague pathogenesis (appendix A.4); the mechanism of a recombination event involving a virulence factor of *Y. pestis* (appendix A.5) and the set up of a zebrafish model of plague infection (appendix A.6).

A second appendix describes my participation in different grant applications (appendix B page 176), notably the participation to raise funds for a biotechnological startup hosted in Paris hospital laboratories (appendix B.1) and the post-doctoral fellowship I obtained from the Agence nationale de recherches sur le SIDA et les hépatites virales - maladies infectieuses émergentes (ANRS-MIE) (appendix B.2).

The next appendices include a published minireview on macrophage subversion by pathogens (appendix C page 177), a review in preparation on bloodstream infections (appendix D page 187) and an original article submitted for publication on a clinical case of *Y. enterocolitica* within-host evolution (appendix E page 245).

The last appendix is an expanded summary of my thesis project in French (appendix E page 245).

Appendix A

Participation in other projects of the laboratory

A.1 Proteomics pipeline

Thanks to the benchmark performed for sample preparation for proteomics (chapter 5), we designed an efficient and quick pipeline based on the SPEED method using trifluoroacetic acid. In addition to my personal thesis project to study *Y. pestis* in blood and the *slyB* mutant I constructed, we could easily apply this pipeline to other projects of the laboratory on an extensive number of samples. In particular, I helped other members of the laboratory to prepare and study the proteomes of 50 samples from different *Y. enterocolitica* genotypes, 30 samples of various genotypes and mutated strains of *Y. pseudotuberculosis*, 20 samples of *Y. enterocolitica* clinical strains (see appendix E) and applied our extraction methodology to study a *Y. pestis* mutated at the *fliC* locus (see appendix A.4).

A.2 Oxford Nanopore Technologies MinION sequencing

Due to the French regulation on "Micro-Organismes et Toxines" (MOT), sequencing of *Y. pestis* nucleic acids in platforms external to the laboratory can be complex. To circumvent this problem, we purchased a MinION device from Oxford Nanopore Technologies (ONT) to routinely sequence strains and plasmids in the laboratory. As a first user, I had to study and select the different kits proposed by ONT, implement the protocols and set up the bioinformatical tools to treat the raw data. A positive unexpected side effect of this long-read sequencing technology is the possibility to describe genome rearrangement based on insertion sequences (see chapter 7 and appendix A.5), to verify transposon insertion (see appendix A.3) or to assemble and describe complete plasmids identified in clinical strains by the national reference center (NRC) hosted in our laboratory.

A.3 Mutant library annotation

One of the project of the laboratory is to construct an ordered library of mutants based on random transposon insertion. To do so, thousands of random clones were isolated, a PCR was performed to amplify the transposon insertion region and these small products were sequenced by Sanger technologies. To automatized the annotation of the transposon insertion site in the genome, we took advantage of my bioinformatic skills acquired during my thesis to set up an in-house bioinformatical pipeline in R language. This script takes se-

quencing files as input and generate tables describing the entire library such as the position of each mutated genes in the library, the quality of sequencing and confidence in the annotation. This library, still expanding, is now used for phenotypic screening, and the previously described Nanopore sequencing is now used to verify transposon insertion in the genome and its genomic position.

A.4 The *Y. pestis* flagellin locus *fliC* contributes to virulence in the non-motile plague bacillus

The development of the Yersiniomics database and the systematic processing of RNA-sequencing experiments allowed to explore RNA-seq read mapping on the whole genome. In addition to give a good visual insight into several experiments on 3'- and 5'- untranslated regions (UTR), we also detected an interesting anti-sense RNA, which could explain a phenotype observed in the laboratory. During my thesis, another PhD student was working on the *fliC* locus of *Y. pestis*, whose deletion decreases virulence during bubonic plague despite the absence of flagella expression in this bacteria. The failure to detect the FliC protein and the discovery of an anti-sense RNA in the mutated locus led us to consider a regulation role of this anti-sense RNA.

In addition, we took advantage of the proteomics pipeline developed in chapter 5 to study the proteome of the *fliC* mutant strain, revealing decreased abundance of virulence associated factors such as the pseudocapsule F1, highlighting other potential regulatory effects of the anti-sense RNA or of putative small peptides encoded at the *fliC* locus.

A.5 Supervision of a Master student to study *pla* deletion in *Y. pestis*

Previous reports highlighted the loss of the virulence factor encoding gene *pla* in ancient DNA sequenced from the second pandemic [192, 385]. By analyzing the sequences of the *pla* deletion region, I identified particular genetic features which could potentially lead to this deletion. By long-read sequencing of strains from our collection, using the Oxford Nanopore technology described earlier, I observed a specific recombination event which could drive *pla* deletion.

These observations led us to recruit a Master 2 student I supervised to study the molecular mechanism of the *pla* deletion in an *E. coli* model and in *Y. pestis*. Promising results obtained during the student's internship, combined with other previous works from the laboratory on this topic, will presumably lead to several publications.

A.6 Set up of a zebrafish model of infection by *Y. pestis*

Driven by a recent publication from collaborators with members of the laboratory [191], we wanted to set up new animal models to study specific host genes. In collaboration with another laboratory from our institute, we chose a zebrafish model of intravenous injection with *Y. pestis* in our BSL-3 laboratory. We could successfully inject fluorescent bacteria into zebrafish larvae and observe neutrophil expansion during infection. Further development of this vertebrate model could be instrumental to decipher the role of host factors in plague susceptibility.

Appendix B

Grant applications

B.1 Fundraising for a biotechnological startup

During the first lockdown due to the COVID-19 pandemic in March 2020, I was contacted by Altevax, a biotechnological startup working on a therapeutic vaccine adjuvant to treat glioblastoma, to help them raise funding from the French national research agency (ANR), the French public investment bank (BPI) or venture capitalists. During the two following years, I had the opportunity to coordinate the administrative part of the writing and submission of collaborative projects to the ANR. I also participated in the setup of an extensive collaborative project submitted to a hospital-university research program (RHU) for clinical trials of cancer vaccine candidates. I greatly benefited from this experience, as it allowed me to write other grant applications and obtain a post-doctoral fellowship.

B.2 Post-doctoral fellowship

Following the first encouraging results from the RT-qPCR miRNA screen (chapter 8), we submitted and obtained a short-term grant from the Institut Pasteur directed towards PhD students and post-doctoral fellows working on emerging infectious diseases, to fund the miRNA-seq setup.

We also submitted a grant application to continue our study on discovery of early biomarkers of plague and obtained funding from the Agence nationale de recherches sur le SIDA et les hépatites virales - maladies infectieuses émergentes (ANRS-MIE), which opened a call for studies on emerging infectious diseases in collaboration with low- and middle-income countries. For this project, we created a consortium including the Plague Unit at the Institut Pasteur de Madagascar (IPM), the Infectious Diseases Models for Innovative Therapies (IDMIT) laboratory at the Commissariat à l'Énergie Atomique et aux Énergies Alternatives (CEA) and the Bacteriological Unit in the Institut de Recherche Biomédicale des Armées (IRBA). While a PhD student will work under my supervision on murine models of bubonic, pneumonic and septicemic plague in the *Yersinia* Research Unit at the Institut Pasteur de Paris (IPP), I will set up a model of pneumonic plague in non-human primates at IDMIT. IPM will collect blood samples from human plague cases, while IRBA will be in charge of miRNA sequencing. IPP, IDMIT and IRBA will test the specificity of the candidate biomarkers in other pulmonary infection models, and the PhD student in IPP will work on the understanding of the role of miRNA in host-pathogen interactions.

Appendix C

Minireview: Emerging evasion mechanisms of macrophage defenses by pathogenic bacteria

In this minireview published in *Frontiers in Cellular and Infection Microbiology* in 2020, we took advantages of our expertise on pathogenic bacteria studied in our laboratory, namely *Listeria monocytogenes*, *Staphylococcus aureus* and *Yersinia* species, to analyze the latest discoveries related to macrophage subversion by these bacteria. My personal contribution concerned the section on *Yersinia* and the illustrations.



Emerging Evasion Mechanisms of Macrophage Defenses by Pathogenic Bacteria

Clarisse Leseigneur^{1,2}, Pierre Lê-Bury^{1,2}, Javier Pizarro-Cerdá^{1,3,4} and Olivier Dussurget^{1,2*}

¹ Unité de Recherche Yersinia, Institut Pasteur, Paris, France, ² Université de Paris, Sorbonne Paris Cité, Paris, France, ³ National Reference Laboratory Plague & Other Yersiniosis, Institut Pasteur, Paris, France, ⁴ WHO Collaborative Research & Reference Centre for Yersinia, Institut Pasteur, Paris, France

OPEN ACCESS

Edited by:

Manisha Yadav,
University of Delhi, India

Reviewed by:

Yuan He,
Wayne State University, United States
Leandro J. Carreno,
University of Chile, Chile

*Correspondence:

Olivier Dussurget
olivier.dussurget@pasteur.fr

Specialty section:

This article was submitted to
Microbes and Innate Immunity,
a section of the journal
Frontiers in Cellular and Infection
Microbiology

Received: 29 June 2020

Accepted: 26 August 2020

Published: 25 September 2020

Citation:

Leseigneur C, Lê-Bury P,
Pizarro-Cerdá J and Dussurget O
(2020) Emerging Evasion Mechanisms
of Macrophage Defenses by
Pathogenic Bacteria.
Front. Cell. Infect. Microbiol. 10:577559.
doi: 10.3389/fcimb.2020.577559

Macrophages participate to the first line of defense against infectious agents. Microbial pathogens evolved sophisticated mechanisms to escape macrophage killing. Here, we review recent discoveries and emerging concepts on bacterial molecular strategies to subvert macrophage immune responses. We focus on the expanding number of fascinating subversive tools developed by *Listeria monocytogenes*, *Staphylococcus aureus*, and pathogenic *Yersinia* spp., illustrating diversity and commonality in mechanisms used by microorganisms with different pathogenic lifestyles.

Keywords: phagocyte, immune escape, virulence, listeriosis, staphylococcal infection, plague, yersiniosis

INTRODUCTION

As professional phagocytes, macrophages are key components of host first line of defense against infection. Upon sensing local microenvironmental signals, macrophages display a continuous spectrum of functional characteristics, known as macrophage polarization, leading to microbicidal M1 or M2 macrophages associated with tissue repair and inflammation resolution (Locati et al., 2020). Macrophages detect pathogenic microorganisms by expressing pattern recognition receptors (PRRs), which interact with conserved microbe-associated molecular patterns (MAMPs). Among PRRs, Toll-like receptors (TLRs) play a major role in triggering immune responses as they recognize specifically a wide range of MAMPs, such as lipoproteins, lipopolysaccharide, flagellin, DNA, and RNA (Fitzgerald and Kagan, 2020). PRRs/MAMPs interactions activate signaling pathways, ultimately leading to cytokine production and/or phagocytosis (Figure 1). Once internalized, microorganisms are located in phagosomes, which mature and fuse with lysosomes, creating phagolysosomes. These acidic vesicles contain multiple antimicrobial molecules such as proteases, reactive oxygen species (ROS), reactive nitrogen species (RNS), and antimicrobial peptides, which contribute to degradation of pathogens (Levin et al., 2016). Macrophages also use nutritional immunity to actively sequester nutrients, thus preventing bacteria to acquire essential factors such as iron and manganese (Sheldon and Skaar, 2019). In addition, macrophages have been shown to produce macrophage extracellular traps that immobilize and kill pathogens (Doster et al., 2018).

Despite this powerful arsenal, macrophages fail to eliminate a wide variety of pathogens, which evolved complex strategies to counter and evade host immune system (Baxt et al., 2013). Some microorganisms prevent immune recognition by modulating their surface components, secrete immunomodulators to inhibit macrophage activation, hide in host cells or kill immune cells directly through toxin secretion and/or indirectly by inducing apoptosis (Kaufmann and Dorhoi, 2016). Others are able to evade phagocytosis and antigen presentation and hijack host cell pathways to acquire nutrients and ensure their survival (Hmama et al., 2015; Kaufmann and Dorhoi, 2016; Mitchell et al., 2016). While pathogens share multiple mechanisms, they developed specific evasion strategies depending on their pathogenic lifestyle. In this minireview, we will present recent advances in our understanding of macrophage subversion by important pathogenic bacteria characterized by specific life cycles: *Listeria monocytogenes*, *Staphylococcus aureus* and *Yersinia* spp.

LISTERIA MONOCYTOGENES

Listeria monocytogenes is the etiologic agent of listeriosis, a foodborne infection whose clinical manifestations range from self-limiting enteritis in immunocompetent individuals to life-threatening sepsis and meningitis-encephalitis in the elderly and newborns. Three decades of research established this facultative intracellular bacterium as a model to study cellular and infection microbiology (Impens and Dussurget, 2020; Lecuit, 2020). *L. monocytogenes* fascinating life cycle in macrophages, i.e., entry, phagosomal escape, replication, actin-based movement and spread, was first described by Tilney and Portnoy (Tilney and Portnoy, 1989). This seminal study paved the way for identification of the major factors required to bypass cellular defenses and promote bacterial replication, including the pore-forming toxin listeriolysin O (LLO), PlcA and PlcB phospholipases, the ActA surface protein necessary for actin-based motility and their transcriptional activator PrfA (Radoshevich and Cossart, 2018).

PrfA is the master regulator of virulence in *L. monocytogenes*. New facets of its properties have recently been revealed (Figure 2). PrfA was shown to induce secretion of the chaperone PrsA2 and the chaperone/protease HtrA, whose protein folding and stabilizing functions promote bacterial fitness and survival during infection of macrophages (Ahmed and Freitag, 2016). In addition, PrfA function has been reported to depend on the balance between activating and inhibitory oligopeptides imported by the Opp permease (Kryptou et al., 2019). Cysteine-containing peptides provides cysteine necessary for synthesis of glutathione, the PrfA activator, contributing to *L. monocytogenes* survival in macrophages. This study uncovers a new mechanism of regulation of PrfA by controlling the oligopeptide composition of the environment. It also reinforces the link between metabolism and virulence previously underscored by the demonstration of PrfA activation by the global nutritional regulator CodY (Lobel et al., 2015). Along the same lines, L-glutamine imported by the GlnPQ ABC transporter, has been

shown to be an indicator of intracellular localization and an inducer of *L. monocytogenes* virulence genes (Haber et al., 2017).

One of the most important virulence factors positively regulated by PrfA is LLO. This cholesterol-dependent cytolysin forms pores in the phagosomal membrane, resulting in vacuolar rupture and bacterial escape to the cytosol. However, it is expressed at all stages of the intracellular cycle and could be cytotoxic if active outside of the phagosome. The N-terminal PEST-like sequence of LLO is essential to restrict its cytosolic activity and prevent cell killing (Decatur and Portnoy, 2000). The adaptor-related protein complex 2 Ap2a2, a subunit of the AP-2 endocytic machinery, has recently been shown to interact with the PEST-like region of LLO, revealing how cytotoxicity is controlled (Chen et al., 2018). Recognition of LLO by AP-2 triggers its endocytic removal from plasma membrane and its degradation, possibly through autophagosomal or multivesicular body-mediated pathways. The acidic content of the phagosome is known to be optimal for LLO, which contributes to the compartmentalization of its activity. The transient exposure of *L. monocytogenes* to the low pH of the phagosome imposes mechanisms of adaptation. The ethanolamine permease EutH is required for ethanolamine uptake and promotes bacterial growth at low pH *in vitro*. Anderson et al. broadened this concept by showing that EutH is important for *L. monocytogenes* survival in the phagosome (Anderson et al., 2018).

Additional new genes involved in the intracellular life cycle of *L. monocytogenes* have been identified by the Portnoy's lab using an elegant strategy relying on screening a library of *himar1* transposon mutants constructed in a Cre/Lox-based suicide strain that failed to replicate in macrophages upon activation of ActA (Reniere et al., 2016). The *spxA1* gene encoding a putative disulfide stress transcriptional regulator and the *ohrA* gene encoding a peroxiredoxin domain-containing protein of the organic hydroperoxide resistance subfamily, were required for *L. monocytogenes* survival in the phagosome and optimal replication in bone marrow-derived macrophages. The *yjbH* gene encoding a putative thioredoxin and the *arpJ* gene encoding an amino-acid permease were required for *L. monocytogenes* spread from cell-to-cell. This study confirmed the contribution of the PplA lipoprotein to *L. monocytogenes* intracellular life cycle. Processing of PplA leads to secretion of a peptide, which has been previously shown to be required for vacuolar escape (Xayarath et al., 2015). *L. monocytogenes* glutathione synthase gene *gshF* was expectedly identified in the screen, as glutathione is an allosteric activator of PrfA (Reniere et al., 2015). Overall, these findings point to an important role of redox metabolism during *L. monocytogenes*/macrophages interactions.

After rupture of the phagosomal membrane, bacteria replicate in the cytosol. Our understanding of the mechanisms by which *L. monocytogenes* evades cell defenses and survives intracellularly has significantly improved in the last 5 years. Besides its spectacular role in actin-based propulsion of bacteria, ActA has long been known to play a key role in escape from autophagic recognition by recruitment of the Arp2/3 complex and Ena/VASP at the bacterial surface (Birmingham et al., 2007; Yoshikawa et al., 2009). Several studies confirmed the importance of ActA and the role of PlcA and PlcB in escape from autophagy (Tattoli

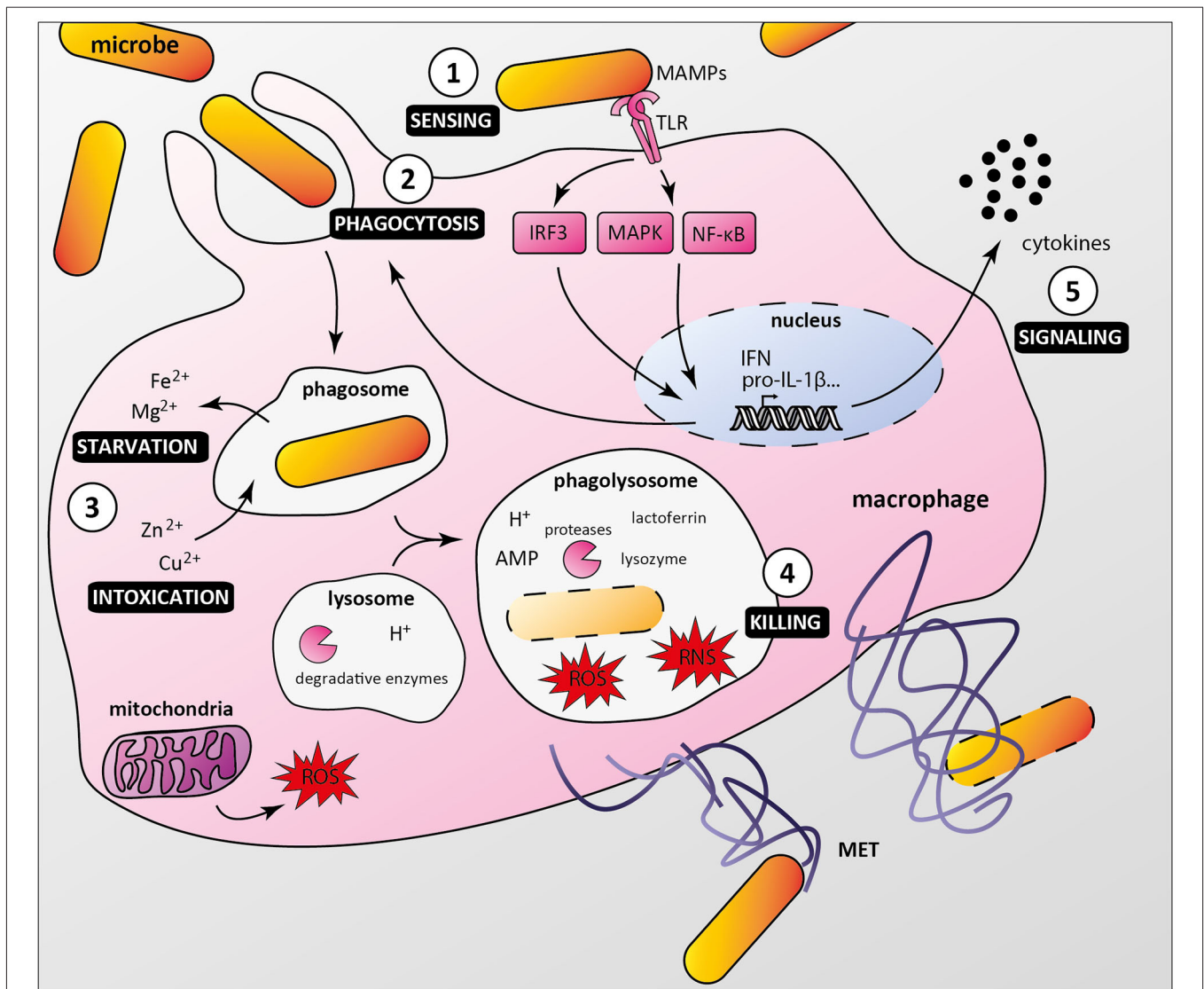


FIGURE 1 | Macrophage anti-microbial mechanisms. **(1)** Bacteria are recognized by macrophage pattern recognition receptors (PRRs) such as Toll-like receptors (TLR), which bind conserved microbe-associated molecular patterns (MAMPs). **(2)** MAMP/PRR interaction triggers signaling cascades (e.g., IRF3, MAPKs, NF- κ B) leading to macrophage responses, including formation of the phagocytic cup. **(3)** Internalized bacteria reside in phagosomes, from which nutrients and essential factors such as iron and magnesium are transported to the cytoplasm, restricting their supply to bacteria. Macrophages combine this starvation strategy with a poisoning mechanism involving phagosomal import of toxic amount of zinc and copper. **(4)** Phagosome maturation and fusion with lysosomes lead to acidification of the compartment lumen and activation of digestive enzymes such as proteases, which along with antimicrobial peptides (AMP), reactive oxygen and nitrogen species (ROS and RNS), lysozyme and lactoferrin contribute to bacterial killing. Macrophages can also undergo ETosis to release macrophage extracellular traps (MET) that immobilize and kill extracellular bacteria. **(5)** Additionally, infected macrophages secrete multiple cytokines to attract and activate other cells, which contribute to an effective immune response.

et al., 2013; Mitchell et al., 2015, 2018). In addition to their contribution to vacuolar rupture, phospholipases are required for bacterial multiplication in infected cells by subverting the autophagic process, possibly by blocking LC3 lipidation. *Listeria monocytogenes* also escapes innate immune response by inducing mitophagy in macrophages (Zhang et al., 2019). Secretion of LLO triggers oligomerization of the mitophagy receptor NLRX1, resulting in increased mitophagy, lower levels of mitochondrial ROS and increased bacterial survival. Another mechanism

evolved by *L. monocytogenes* to evade macrophage oxidative defenses is secretion of the nucleomodulin OrfX (Prokop et al., 2017). This PrfA-regulated virulence factor has been shown to inhibit ROS and NO production in infected macrophages. OrfX is targeted to the nucleus and interacts with RybP, a regulatory protein that controls infection. OrfX decreases RybP levels, thereby promoting bacterial survival.

Listeria monocytogenes also subverts cellular processes by producing extracellular vesicles. Coelho et al. demonstrated

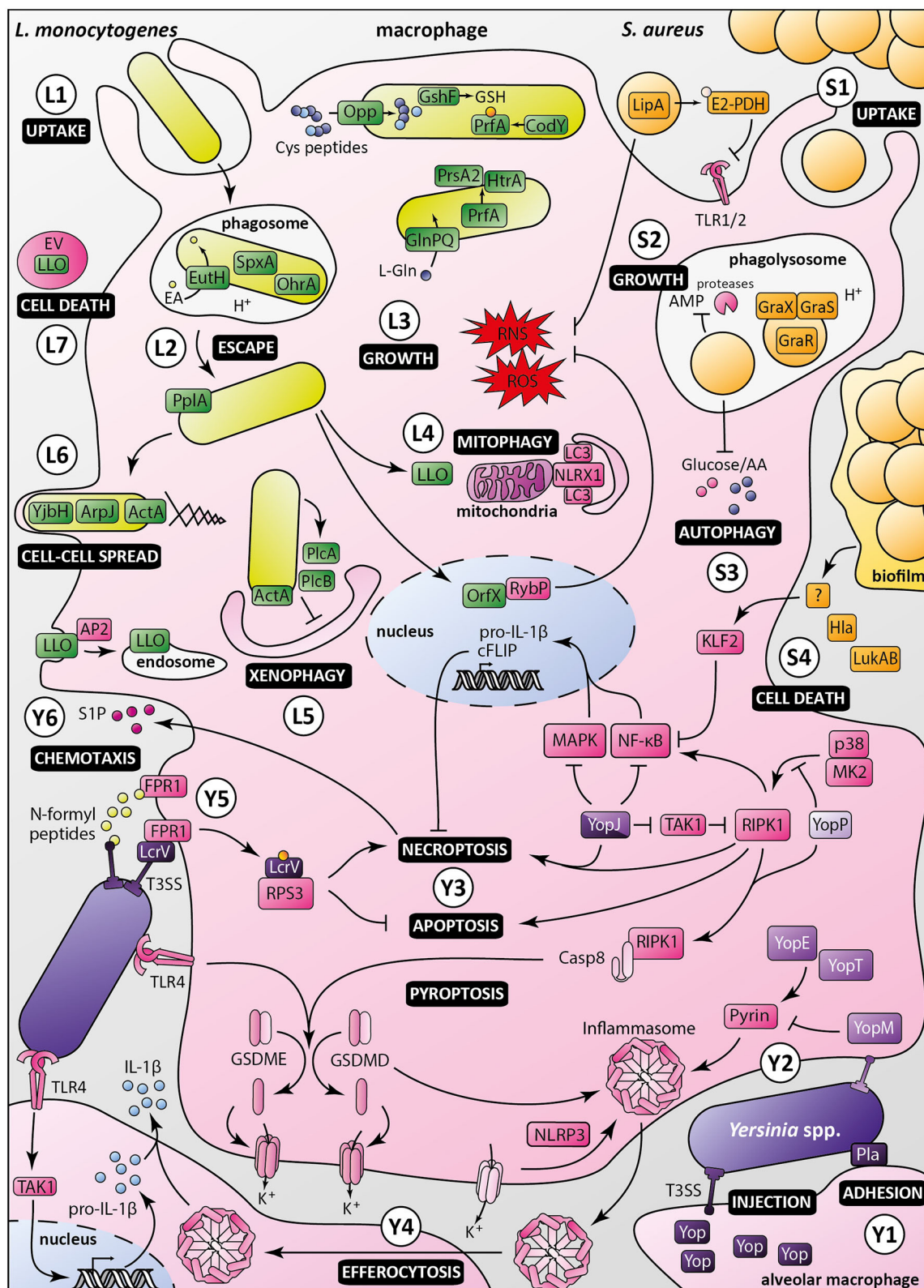


FIGURE 2 | Macrophage evasion mechanisms by *Listeria monocytogenes*, *Staphylococcus aureus* and pathogenic *Yersinia*. *Listeria monocytogenes*: (L1) Upon uptake by the macrophage, *Listeria monocytogenes* is engulfed in a phagosome, in which ethanolamine uptake through EutH permease and activation of redox-responsive *spxA1* and *ohrA* are required for its survival. (L2) In addition to secretion of LLO and phospholipases, processing of the PpIA lipoprotein is required (Continued)

FIGURE 2 | for phagosomal escape. **(L3)** Once in the cytosol, bacterial growth and virulence are mediated by the master regulator PrfA, which is activated by CodY and glutathione (GSH). The Opp permease ensures importation of cysteine-containing oligopeptides to allow glutathione synthesis by GshF. Full expression of *Listeria* virulence genes requires appropriate amounts of L-glutamine imported by the high-affinity ABC transporter GlnPQ. PrfA triggers secretion of PrsA2 chaperone and HtrA chaperone/protease, whose functions are required for invasion and intracellular growth. **(L4)** *Listeria* induces mitophagy through the oligomerization of NLRX1 receptor by LLO, lowering ROS levels, and promoting bacterial survival. *Listeria* also controls ROS levels by secretion of the nucleomodulin OrfX, which interacts with the regulator RybP. **(L5)** ActA inhibits xenophagy along with PlcA and PlcB, which block LC3 lipidation. *Listeria* intracellular survival also depends on Ap2a2-mediated control of LLO cytotoxicity by restricting its cytosolic activity. **(L6)** Besides ActA, YjbH, and ArpJ are required for efficient bacterial spread from cell to cell. **(L7)** *Listeria* produces extracellular vesicles (EV) containing many virulence factors, including LLO, to promote macrophage death and control innate immunity response.

Staphylococcus aureus: **(S1)** *Staphylococcus aureus* is phagocytosed by macrophages. The moonlighting metabolic protein pyruvate dehydrogenase, once lipoylated by LipA, suppresses macrophage activation by lipopeptides through binding to TLR1/2. LipA also decreases RONS production. **(S2)** Staphylococci reside and multiply in mature phagosomes, through sensing of acidification by GraXRS and activation of several genes allowing bacterial replication and resistance to antimicrobial peptides (AMP). **(S3)** *S. aureus* also modulates metabolic fluxes to induce a starvation-like state of macrophages, triggering autophagy. **(S4)** Secretion of alpha-toxin Hla and leukocidin AB (LukAB), besides having a direct cytotoxic effect, inhibits macrophage phagocytosis and promotes biofilm formation. Through a yet unknown intermediate, biofilm conditioned medium attenuates NF- κ B activation by increasing KLF2 expression. Pathogenic *Yersinia*, i.e., *Y. enterocolitica* (light purple), *Y. pseudotuberculosis* (purple), and *Y. pestis* (dark purple): **(Y1)** In the lungs, *Yersinia* adheres to alveolar macrophages through Pla, which shows immunosuppressive properties. **(Y2)** Injection of Yops, virulence effectors, in macrophages through the T3SS allows manipulation of host cell pathways. In absence of YopM, YopE, and YopT activate the inflammasome by dephosphorylating pyrin. **(Y3)** Once translocated into the host cell, LcrV is glutathionylated, promoting binding to RPS3, suppressing apoptosis and increasing necroptosis. YopJ inhibition of TAK1 leads to activation of RIPK1 and induction of necroptosis or apoptosis of targeted macrophage. YopJ also inhibits MAPK and NF- κ B pathways, inhibiting pro-IL-1 β production and limiting pro-inflammatory response. YopP inhibits RIPK1 phosphorylation by p38^{MAPK}/MK2, triggering macrophage apoptosis and activation of cell death effectors gasdermin D and E. **(Y4)** Macrophages intoxicated with low levels of YopJ can release IL-1 β upon uptake of inflammasome from highly intoxicated dead cells, possibly by efferocytosis. **(Y5)** N-formylpeptides released by *Y. pestis* are recognized by host receptor FPR1, promoting immune cell chemotaxis toward bacteria. Adhesion of bacteria to macrophage is mediated by FPR1/LcrV interaction, which allows the assembly of type three secretion system. **(Y6)** Sphingosine-1-phosphate released from dead cells attracts new phagocytes, which in turn are targeted by *Yersinia* released from necroptotic cells, ultimately promoting infection.

that *L. monocytogenes* secretes vesicles that contain many virulence factors, including LLO and PlcA (Coelho et al., 2019). These vesicles mediate LLO-dependent macrophage toxicity, consolidating the emerging concept of extracellular vesicles as prominent weapons in host-pathogen interactions.

STAPHYLOCOCCUS AUREUS

Staphylococcus aureus is a highly successful facultative intracellular opportunistic pathogen, which has developed many mechanisms to counter host immune defenses. This arsenal allows bacteria to infect virtually any human tissue, leading to diverse clinical manifestations, ranging from mild to severe skin and soft tissue infections to life-threatening endocarditis, necrotizing pneumonia or septicemia (Tong et al., 2015). *S. aureus* secretes several toxins that can directly and specifically interfere with cellular functions, trigger cell death or damage immune cells (Spaan et al., 2017). This pathogen is also able to withstand phagocyte-mediated killing. Though most studies on *S. aureus*/phagocyte interactions focused on neutrophils (de Jong et al., 2019), macrophages also gained attention as they may be “Trojan horses” used by bacteria to disseminate throughout the body. Accordingly, *S. aureus* can resist phagocytic oxidative and nitrosative killing, antimicrobial peptides and nutritional immunity (Flannagan et al., 2015). Here, we present recent findings uncovering novel mechanisms developed by *S. aureus* to evade macrophage-mediated killing (Figure 2).

Contrary to *L. monocytogenes*, which quickly escapes phagosomes and replicates in the cytosol, *S. aureus* resides and multiplies in mature phagolysosomes in murine and human macrophages (Flannagan et al., 2016). Bacteria divide in mature phagolysosomes and trigger macrophage death by apoptosis or necroptosis rather than membrane disruption. Acidification

of the phagolysosome, usually a bactericidal mechanism, is sensed by *S. aureus* through the GraXRS regulatory system (Flannagan et al., 2018). It triggers transcription of genes involved in adaptation to the phagolysosome hostile environment such as resistance to antimicrobial peptides. This adaptation is independent of toxin production, as mutants of the Agr quorum sensing system or SaeR, two major regulators of toxin production, and alpha phenol soluble modulins mutants can still replicate in macrophages. Interestingly, this seems in contradiction with previous reports showing that *agr* expression was induced in THP1 macrophages and by acidic pH (Tranchemontagne et al., 2015). Strains, cell lines and methodological differences could explain discrepancies between these studies, as discussed by Flannagan et al. (2018). Multiplication of *S. aureus* in mature phagolysosomes, ultimately leading to cell death and bacterial dissemination, is compatible with the “Trojan horse” hypothesis.

The link between metabolism, immunity and virulence has recently gained attention. Once inside macrophages, *S. aureus* exploits host cell metabolism to ensure its own proliferation. Methicillin-resistant *S. aureus* infection of HeLa cells and bone marrow derived macrophages from BALB/c mice has been shown to modulate cellular metabolic fluxes, depleting notably glucose and amino acid pools (Bravo-Santano et al., 2018). These changes induce a starvation-like state of infected cells, activating AMPK and ERK pathways and triggering autophagy. Inhibition of autophagy blocked *S. aureus* replication, suggesting that metabolic activation of autophagy is essential for intracellular bacterial proliferation. Proteins involved in bacterial metabolism may also play a role in immune evasion, as revealed by the study of moonlighting proteins (Wang et al., 2014). These multifunctional proteins are highly conserved in bacteria. In addition to their cytoplasmic role in metabolism and stress response, some of them are released outside of bacteria

where they contribute to virulence properties such as tissue adhesion and immune escape. For instance, *S. aureus* can blunt macrophage activation by modification and secretion of the moonlighting protein pyruvate dehydrogenase (PDH) (Grayczyk et al., 2017). The authors showed in this study that bacterial lipoyl synthetase LipA adds a lipoyl acid on the E2 subunit of the PDH complex, yielding lipoyl-E2-PDH whose role in the cytoplasm is to convert pyruvate to acetyl-CoA. The lipoyl-E2-PDH is excreted by bacteria and suppresses macrophage activation through specific binding and inhibition of TLR1/2 heterodimer activation. The same group also showed that LipA decreases production of ROS and reactive nitrogen species (RNS) by NADPH oxidase and iNOS, respectively, both *in vitro* and in a mouse model of *S. aureus* infection (Grayczyk and Alonzo, 2019). Together, these studies support the concept that specific cytoplasmic proteins moonlight outside bacteria and link metabolism and virulence.

Staphylococcus aureus capacity to form biofilms is important for successful immune escape. A biofilm matrix surrounding bacteria prevents recognition and phagocytosis by immune cells. In addition, biofilms may directly dampen immune response by polarizing macrophages toward an anti-inflammatory phenotype (Thurlow et al., 2011). More recently, it was shown that *S. aureus* growing in biofilms subverts immune responses through active secretion of virulence factors (Scherr et al., 2015). The authors demonstrated that alpha-toxin Hla and leukocidin LukAB have a synergistic action resulting in inhibition of macrophage phagocytosis and induction of cytotoxicity, promoting biofilm formation in a murine model of *S. aureus* orthopedic implant infection. Another group showed that biofilm-conditioned medium was responsible for attenuated NF- κ B activation due to increased expression of the anti-inflammatory transcription factor Kruppel-like factor 2 in RAW264.7 macrophages (Alboslemy et al., 2019). While bacterial molecule(s) responsible for KLF2 induction remain(s) to be identified, these findings confirm the importance of virulence factor secretion to suppress macrophage functions in addition to the role of biofilms as a physical barrier.

YERSINIA

The *Yersinia* genus includes three human pathogenic species: the two enteropathogens *Yersinia enterocolitica* and *Yersinia pseudotuberculosis*, as well as *Yersinia pestis*, the etiological agent of plague. The three species harbor the pCD1 plasmid coding for a type three secretion system (T3SS) and *Yersinia* outer proteins Yops, potent virulence effectors that are injected in target cells. In contrast to *L. monocytogenes* and *S. aureus*, pathogenic *Yersinia* are well-equipped to manipulate host cells from the outside, by mechanisms recently reviewed (Pinaud et al., 2018; Demeure et al., 2019). Translocation of Yops into host immune cells modulates pyroptosis/apoptosis. Apoptosis is triggered via caspase-8 activation by YopP/J, while YopM and YpkA activate caspase-3. Pyroptosis can be regulated by Yops acting on caspase-4/5, pyrin, NLRP3, ASC, RhoGTP or

caspase-8. YopP/J and YopE also interfere with MAPK and NF- κ B signaling. Depending on the phase of the disease, *Yersinia* spp. trigger pro- or anti-inflammatory responses. Yops can also prevent phagocytosis: YopH, YopT, YopE, and YpkA/YopO can block phagocytosis signaling and modulate GTPases or actin. In addition to Yops, capsular antigen fraction 1 (F1) and Psa fimbria (pH 6 antigen) prevent macrophage adhesion and phagocytosis. Psa and Ail outer-membrane protein enhance Yops delivery, and Ail and Pla outer-membrane protein promote cell attachment and invasion.

Recent studies refined our understanding of *Yersinia* interactions with macrophages, in particular subversion of cell death processes (Figure 2). *Y. enterocolitica* YopP has been shown to inhibit phosphorylation of the master regulator of cell fate RIPK1 by p38^{MAPK}/MK2 (Menon et al., 2017). Upon suppression of MK2 activity, RIPK1 autophosphorylates and triggers macrophage apoptosis to promote infection. Along the same lines, in a murine model of bubonic plague, *Y. pestis* YopJ induced RIPK1-dependent necroptotic cell death causing bubo necrosis. Necroptosis was delayed by pro-survival factors such as FLIP, allowing *Y. pestis* to replicate inside macrophages before cell death. Sphingosine-1-phosphate secreted by dying cells attracted new phagocytes, which could be infected by bacilli released from necroptotic cells, ultimately enhancing spread of *Y. pestis* (Arifuzzaman et al., 2018). Gasdermin D (GSDMD) and gasdermin E (GSDME) are cell death effectors triggering cell membrane permeabilization and potassium efflux upon cleavage by caspase-1/4/11 and caspase-3/7, respectively. Two studies recently reported an additional pathway controlling gasdermin processing. In murine macrophages infected with *Y. pseudotuberculosis*, YopJ induced cell death by inhibiting TAK1 and by RIPK1/caspase-8-dependent cleavage of gasdermin D (GSDMD) and gasdermin E (GSDME) downstream of TLR4-TRIF activation (Orning et al., 2018; Sarhan et al., 2018). Orning et al. suggest that *Yersinia* spp. inhibition of TAK1 results in cell death with features of both apoptosis and pyroptosis and in GSDMD-dependent activation of the NLRP3 inflammasome leading to IL-1 β release. Sarhan et al. hypothesized that IL-1 β production requires a heterogeneous population of infected macrophages. Macrophages with levels of YopJ too low to block MAPK signaling retain their capacity to produce pro-IL-1 β which is then possibly matured by efferocytosis of dead cells, or uptake of ASC/NLRP3 inflammasomes released from dead cells that were heavily intoxicated. Interestingly, human macrophages are resistant to cell death induced by TAK1 inhibition and produced little if any IL-1 β (Sarhan et al., 2018). This resistance and TLR4 hypo-responsiveness to *Y. pestis* tetra-acylated LPS presumably contribute to the initially silent preinflammatory phase of plague. Macrophage infection with *Yersinia* spp. can trigger activation of the NLRP3 inflammasome but also caspase-1 inflammasome assembled upon RhoA-sensitive pyrin activation (Orning et al., 2018; Medici et al., 2019). RhoA-targeting YopE and YopT trigger inflammasome assembly, in absence of YopM that inactivates pyrin. In *Y. pseudotuberculosis*, YopE and, to a lower extent YopT, were recently shown to induce dephosphorylation of pyrin Ser205, thereby activating the inflammasome (Medici et al.,

2019). This study reveals that RhoA specificity of Yops affects pyrin activation.

Selective destruction of immune cells by *Y. pestis* is a landmark of plague, allowing bacterial multiplication and systemic spread. The plague receptor on human immune cells has recently been identified by the Schneewind's group (Osei-Owusu et al., 2019). A CRISPR-Cas9 screen in U937 macrophages linked *Y. pestis* T3SS-mediated killing to N-formylpeptide receptor FPR1, a member of the GPCR family that triggers immune cells chemotaxis and cytokine production upon sensing N-formylpeptides released by bacteria. Binding of the T3SS cap protein LcrV to FPR1 was necessary for assembly of the translocon and injection of effectors, which subvert signaling pathways and trigger cell death. Of note, FPR1 is not essential for *Y. pestis* effector translocation in mouse macrophages. Importantly, this study identified human *FRP1 R190W* as a potential plague resistance allele. The same group discovered that *Y. pestis* LcrV was glutathionylated at Cys273 with host-derived glutathione, a posttranslational modification required for successful infection in mice and rats (Mitchell et al., 2017). Macrophage ribosomal protein S3 (RPS3) was identified as a ligand of LcrV. RPS3 is a component of ribosomal 40S subunit and a regulator of apoptosis, DNA repair and innate immune response. Glutathionylation of LcrV promoted RPS3 binding, reduced the rate of effector injection, suppressing apoptosis, increasing necroptosis and IL-1 β and IL-18 release, triggering an inflammatory response correlated with increased virulence.

An early preinflammatory phase is critical for *Y. pestis* proliferation in lungs and progression of pneumonic plague. While importance of Yops in this early phase has long been known, a recent report refined the role of the plasminogen activator protease Pla in the progression of primary pneumonic plague (Banerjee et al., 2019). Using human precision-cut lung slices, human primary alveolar macrophages and a murine intranasal infection model, the authors showed that Pla was required for bacterial adherence and optimal effector secretion into alveolar macrophages, the primary host cells targeted by *Y. pestis* in the early phase of pneumonic plague. They further showed that Pla contributes to dampen inflammatory cytokine production in the human lung model, establishing its immunosuppressive properties and supporting its role in the preinflammatory phase of pneumonic plague.

REFERENCES

- Ahmed, J. K., and Freitag, N. E. (2016). Secretion chaperones PrsA2 and HtrA are required for *Listeria monocytogenes* replication following intracellular induction of virulence factor secretion. *Infect. Immun.* 84, 3034–3046. doi: 10.1128/IAI.00312-16
- Alboslemy, T., Yu, B., Rogers, T., and Kima, M. H. (2019). *Staphylococcus aureus* biofilm-conditioned medium impairs macrophage-mediated antibiofilm immune response by upregulating KLF2 expression. *Infect. Immun.* 87:e00643–e00618. doi: 10.1128/IAI.00643-18
- Anderson, C. J., Satkovich, J., Köseoglu, V. K., Agaisse, H., and Kendall, M. M. (2018). The ethanolamine permease EutH promotes vacuole adaptation of *Salmonella enterica* and *Listeria monocytogenes* during macrophage infection. *Infect. Immun.* 86:e00172–e00118. doi: 10.1128/IAI.00172-18
- Arifuzzaman, M., Ang, W. X. G., Choi, H. W., Nilles, M. L., St John, A. L., and Abraham, S. N. (2018). Necroptosis of infiltrated macrophages drives *Yersinia pestis* dispersal within buboes. *JCI Insight.* 3:122188. doi: 10.1172/jci.insight.122188
- Banerjee, S. K., Huckuntod, S. D., Mills, S. D., Kurten, R. C., and Pechous, R. D. (2019). Modeling pneumonic plague in human precision-cut lung slices highlights a role for the plasminogen activator protease in facilitating type 3 secretion. *Infect. Immun.* 87, e00175–e00119. doi: 10.1128/IAI.00175-19
- Baxt, L. A., Garza-Mayers, A. C., and Goldberg, M. B. (2013). Bacterial subversion of host innate immune pathways. *Science* 340, 697–701. doi: 10.1126/science.1235771

PERSPECTIVES

L. monocytogenes, *S. aureus*, and *Yersinia* spp. have been powerful model organisms to decipher the molecular mechanisms of interactions between pathogenic bacteria and macrophages. While the universe of bacterial subversion strategies has recently expanded, our understanding of macrophage biology has also immensely progressed (Ginhoux and Guillems, 2016; Gao et al., 2017; Gordon and Plüddemann, 2019; Guillems et al., 2020) and pathogenomics data showing within-species heterogeneity skyrocketed (Bosi et al., 2016; Maury et al., 2016; Seif et al., 2018; Savin et al., 2019; Oyas et al., 2020), uncovering an unforeseen complexity. Future studies of the dialogue between bacteria and these cells will thus be more challenging than ever and will undoubtedly rely on technological developments, in particular in imaging and systems biology. In parallel, refinement of cellular, tissular and *in vivo* infection models will be required in order to discover relevant new concepts. In particular, heterogeneity of bacterial and macrophage populations, spatiotemporal dynamics of interactions and multiplicity of microenvironmental cues can hardly be recapitulated in standard assays using cell lines. This calls for appropriate *in vivo* infection models, which frequently reveals unexpected findings that were not or could not be observed *in vitro* (Blériot et al., 2015; Jones and D'Orazio, 2017; Gluschko et al., 2018; Paudel et al., 2020) and which are instrumental to development of innovative therapeutic strategies (Dickey et al., 2017; Kaufmann et al., 2018; Morrison, 2020).

AUTHOR CONTRIBUTIONS

All authors listed have made a substantial, direct and intellectual contribution to the work, and approved it for publication.

FUNDING

Work on this topic was supported by Institut Pasteur, Université de Paris, Direction Générale de l'Armement, Agence Innovation Défense and Agence Nationale de la Recherche (ANR-17-CE18-0011-02). The *Yersinia* Research Unit is a member of the Laboratory of Excellence Integrative Biology of Emerging Infectious Diseases (ANR LBX-62-IBEID).

- Birmingham, C. L., Canadien, V., Gouin, E., Troy, E. B., Yoshimori, T., Cossart, P., et al. (2007). *Listeria monocytogenes* evades killing by autophagy during colonization of host cells. *Autophagy* 3, 442–451. doi: 10.4161/autof.4450
- Blériot, C., Dupuis, T., Jouvion, G., Eberl, G., Disson, O., and Lecuit, M. (2015). Liver-resident macrophage necroptosis orchestrates type 1 microbicidal inflammation and type-2-mediated tissue repair during bacterial infection. *Immunity* 42, 145–158. doi: 10.1016/j.immuni.2014.12.020
- Bosi, E., Monk, J. M., Aziz, R. K., Fondi, M., Nizet, V., and Palsson, B. O. (2016). Comparative genome-scale modelling of *Staphylococcus aureus* strains identifies strain-specific metabolic capabilities linked to pathogenicity. *Proc. Natl. Acad. Sci. U.S.A.* 113, 3801–3809. doi: 10.1073/pnas.1523199113
- Bravo-Santano, N., Ellis, J. K., Mateos, L. M., Calle, Y., Keun, H. C., Behrends, V., et al. (2018). Intracellular *Staphylococcus aureus* modulates host central carbon metabolism to activate autophagy. *mSphere* 3, e00374–e00318. doi: 10.1128/mSphere.00374-18
- Chen, C., Nguyen, B. N., Mitchell, G., Margolis, S. R., Ma, D., and Portnoy, D. A. (2018). The listeriolysin O PEST-like sequence co-opts AP-2-mediated endocytosis to prevent plasma membrane damage during *Listeria* infection. *Cell Host Microbe* 23, 786–795.e5. doi: 10.1016/j.chom.2018.05.006
- Coelho, C., Brown, L., Maryam, M., Vij, R., Smith, D. F. Q., Burnet, M. C., et al. (2019). *Listeria monocytogenes* virulence factors, including listeriolysin O, are secreted in biologically active extracellular vesicles. *J. Biol. Chem.* 294, 1202–1217. doi: 10.1074/jbc.RA118.006472
- de Jong, N. W. M., van Kessel, K. P. M., and van Strijp, J. A. G. (2019). Immune evasion by *Staphylococcus aureus*. *Microbiol. Spectr.* 7, 618–639. doi: 10.1128/9781683670131.ch39
- Decatur, A. L., and Portnoy, D. A. (2000). A PEST-like sequence in listeriolysin O essential for *Listeria monocytogenes* pathogenicity. *Science* 290, 992–995. doi: 10.1126/science.290.5493.992
- Demeure, C. E., Dussurget, O., Mas Fiol, G., Le Guern, A. S., Savin, C., and Pizarro-Cerdá, J. (2019). *Yersinia pestis* and plague: an updated view on evolution, virulence determinants, immune subversion, vaccination, and diagnostics. *Genes Immun.* 20, 357–370. doi: 10.1038/s41435-019-0065-0
- Dickey, S. W., Cheung, G. Y. C., and Otto, M. (2017). Different drugs for bad bugs: antivirulence strategies in the age of antibiotic resistance. *Nat. Rev. Drug Discov.* 16, 457–471. doi: 10.1038/nrd.2017.23
- Doster, R. S., Rogers, L. M., Gaddy, J. A., and Aronoff, D. M. (2018). Macrophage extracellular traps: a scoping review. *J. Innate Immun.* 10, 3–13. doi: 10.1159/000480373
- Fitzgerald, K. A., and Kagan, J. C. (2020). Toll-like receptors and the control of immunity. *Cell* 180, 1044–1066. doi: 10.1016/j.cell.2020.02.041
- Flannagan, R. S., Heit, B., and Heinrichs, D. E. (2015). Antimicrobial mechanisms of macrophages and the immune evasion strategies of *Staphylococcus aureus*. *Pathogens* 4, 826–868. doi: 10.3390/pathogens4040826
- Flannagan, R. S., Heit, B., and Heinrichs, D. E. (2016). Intracellular replication of *Staphylococcus aureus* in mature phagolysosomes in macrophages precedes host cell death, and bacterial escape and dissemination. *Cell. Microbiol.* 18:514–535. doi: 10.1111/cmi.12527
- Flannagan, R. S., Kuiack, R. C., McGavin, M. J., and Heinrichs, D. E. (2018). *Staphylococcus aureus* uses the GraXRS regulatory system to sense and adapt to the acidified phagolysosome in macrophages. *mBio* 9:e01143-18. doi: 10.1128/mBio.01143-18
- Gao, Y., Chen, Y., Zhan, S., Zhang, W., Xiong, F., and Ge, W. (2017). Comprehensive proteome analysis of lysosomes reveals the diverse function of macrophages in immune responses. *Oncotarget* 8, 7420–7440. doi: 10.18632/oncotarget.14558
- Ginhoux, F., and Williams, M. (2016). Tissue-resident macrophage ontogeny and homeostasis. *Immunity* 44, 439–449. doi: 10.1016/j.immuni.2016.02.024
- Gluscho, A., Herb, M., Wiegmann, K., Krut, O., Neiss, W. F., Utermöhlen, O., et al. (2018). The $\beta 2$ integrin Mac-1 induces protective LC3-associated phagocytosis of *Listeria monocytogenes*. *Cell Host Microbe* 23, 324–337.e5. doi: 10.1016/j.chom.2018.01.018
- Gordon, S., and Plüddemann, A. (2019). The mononuclear phagocytic system. Generation of diversity. *Front. Immunol.* 10:1893. doi: 10.3389/fimmu.2019.01893
- Graczyk, J. P., and Alonzo, F. (2019). *Staphylococcus aureus* lipolic acid synthesis limits macrophage reactive oxygen and nitrogen species production to promote survival during infection. *Infect. Immun.* 87, e00344–e00319. doi: 10.1128/IAI.00344-19
- Graczyk, J. P., Harvey, C. J., Laczkovich, I., and Alonzo, F. (2017). A lipoylated metabolic protein released by *Staphylococcus aureus* suppresses macrophage activation. *Cell Host Microbe* 22, 678–687. doi: 10.1016/j.chom.2017.09.004
- Guilliams, M., Thierry, G. R., Bonnardel, J., and Bajenoff, M. (2020). Establishment and maintenance of the macrophage niche. *Immunity* 52, 434–451. doi: 10.1016/j.immuni.2020.02.015
- Haber, A., Friedman, S., Lobel, L., Burg-Golani, T., Sigal, N., Rose, J., et al. (2017). L-glutamine induces expression of *Listeria monocytogenes* virulence genes. *PLoS Pathog.* 13:e1006161. doi: 10.1371/journal.ppat.1006161
- Hmama, Z., Pena-Diaz, S., Joseph, S., and Av-Gay, Y. (2015). Immuno-evasion and immunosuppression of the macrophage by *Mycobacterium tuberculosis*. *Immunol. Rev.* 264, 220–232. doi: 10.1111/imr.12268
- Impens, F., and Dussurget, O. (2020). Three decades of listeriology through the prism of technological advances. *Cell. Microbiol.* 22:e13183. doi: 10.1111/cmi.13183
- Jones, G. S., and D’Orazio, S. E. (2017). Monocytes are the predominant cell type associated with *Listeria monocytogenes* in the gut, but they do not serve as an intracellular growth niche. *J. Immunol.* 198, 2796–2804. doi: 10.4049/jimmunol.1602076
- Kaufmann, S. H. E., and Dorhoi, A. (2016). Molecular determinants in phagocyte-bacteria interactions. *Immunity* 44, 476–491. doi: 10.1016/j.immuni.2016.02.014
- Kaufmann, S. H. E., Dorhoi, A., Hotchkiss, R. S., and Bartenschlager, R. (2018). Host-directed therapies for bacterial and viral infections. *Nat. Rev. Drug Discov.* 17, 35–56. doi: 10.1038/nrd.2017.162
- Kryptou, E., Scortti, M., Grundström, C., Oelker, M., Luisi, B. F., Sauer-Eriksson, A. E., et al. (2019). Control of bacterial virulence through the peptide signature of the habitat. *Cell Rep.* 26, 1815.e5–1827.e5. doi: 10.1016/j.celrep.2019.01.073
- Lecuit, M. (2020). *Listeria monocytogenes*, a model in infection biology. *Cell. Microbiol.* 22:e13186. doi: 10.1111/cmi.13186
- Levin, R., Grinstein, S., and Canton, J. (2016). The life cycle of phagosomes: formation, maturation, and resolution. *Immunol. Rev.* 273, 156–179. doi: 10.1111/imr.12439
- Lobel, L., Sigal, N., Borovok, I., Belitsky, B. R., Sonenshein, A. L., and Herskovits, A. A. (2015). The metabolic regulator CodY links *Listeria monocytogenes* metabolism to virulence by directly activating the virulence regulatory gene *prfA*. *Mol. Microbiol.* 95, 624–644. doi: 10.1111/mmi.12890
- Locati, M., Curtale, G., and Mantovani, A. (2020). Diversity, mechanisms, and significance of macrophage plasticity. *Annu. Rev. Pathol.* 15, 123–147. doi: 10.1146/annurev-pathmechdis-012418-012718
- Maury, M. M., Tsai, Y. H., Charlier, C., Touchon, M., Chenal-Francisque, V., Leclercq, A., et al. (2016). Uncovering *Listeria monocytogenes* hypervirulence by harnessing its biodiversity. *Nat. Genet.* 48, 308–313. doi: 10.1038/ng.3501
- Medici, N. P., Rashid, M., and Bliska, J. B. (2019). Characterization of pyrin dephosphorylation and inflammasome activation in macrophages as triggered by the *Yersinia* effectors YopE and YopT. *Infect. Immun.* 87, e00822–e00818. doi: 10.1128/IAI.00822-18
- Menon, M. B., Gropengießer, J., Fischer, J., Novikova, L., Deuretzbacher, A., Lafera, J., et al. (2017). p38(MAPK)/MK2-dependent phosphorylation controls cytotoxic RIPK1 signalling in inflammation and infection. *Nat. Cell Biol.* 19, 1248–1259. doi: 10.1038/ncb3614
- Mitchell, A., Tam, C., Elli, D., Charlton, T., Osei-Owusu, P., Fazlollahi, F., et al. (2017). Glutathionylation of *Yersinia pestis* LcrV and its effects on plague pathogenesis. *mBio* 8, e00646–e00617. doi: 10.1128/mBio.00646-17
- Mitchell, G., Chen, C., and Portnoy, D. A. (2016). Strategies used by bacteria to grow in macrophages. *Microbiol. Spectr.* 4:MCHD-0012-2015. doi: 10.1128/microbiolspec.MCHD-0012-2015
- Mitchell, G., Cheng, M. I., Chen, C., Nguyen, B. N., Whiteley, A. T., Kianian, S., et al. (2018). *Listeria monocytogenes* triggers noncanonical autophagy upon phagocytosis, but avoids subsequent growth-restricting xenophagy. *Proc. Natl. Acad. Sci. U.S.A.* 115, E210–E217. doi: 10.1073/pnas.1716055115
- Mitchell, G., Ge, L., Huang, Q., Chen, C., Kianian, S., Roberts, M. F., et al. (2015). Avoidance of autophagy mediated by PlcA or ActA is required for *Listeria monocytogenes* growth in macrophages. *Infect. Immun.* 83, 2175–2184. doi: 10.1128/IAI.00110-15

- Morrison, C. (2020). Industry shows increased appetite for macrophage biology. *Nat. Rev. Drug Discov.* 19, 295–297. doi: 10.1038/d41573-020-00075-3
- Orning, P., Weng, D., Starheim, K., Ratner, D., Best, Z., Lee, B., et al. (2018). Pathogen blockade of TAK1 triggers caspase-8-dependent cleavage of gasdermin D and cell death. *Science* 362, 1064–1069. doi: 10.1126/science.aau2818
- Osei-Owusu, P., Charlton, T. M., Kim, H. K., Missiakas, D., and Schneewind, O. (2019). FPR1 is the plague receptor on host immune cells. *Nature* 574, 57–62. doi: 10.1038/s41586-019-1570-z
- Oyas, O., Borrell, S., Trauner, A., Zimmermann, M., Feldmann, J., Liphardt, T., et al. (2020). Model-based integration of genomics and metabolomics reveals SNP functionality in *Mycobacterium tuberculosis*. *Proc. Natl. Acad. Sci. U.S.A.* 117, 8494–8502. doi: 10.1073/pnas.1915551117
- Paudel, A., Hamamoto, H., Panthee, S., Matsumoto, Y., and Sekimizu, K. (2020). Large-scale screening and identification of novel pathogenic *Staphylococcus aureus* genes using a silkworm infection model. *J. Infect. Dis.* 221, 1795–1804. doi: 10.1093/infdis/jiaa004
- Pinaud, L., Sansonetti, P. J., and Phalipon, A. (2018). Host cell targeting by enteropathogenic bacteria T3SS effectors. *Trends Microbiol.* 26, 266–283. doi: 10.1016/j.tim.2018.01.010
- Prokop, A., Gouin, E., Villiers, V., Nahori, M. A., Vincentelli, R., Duval, M., et al. (2017). OrfX, a nucleomodulin required for *Listeria monocytogenes* virulence. *mBio*. 8, e01550–e01517. doi: 10.1128/mBio.01550-17
- Radoshevich, L., and Cossart, P. (2018). *Listeria monocytogenes*: towards a complete picture of its physiology and pathogenesis. *Nat. Rev. Microbiol.* 16, 32–46. doi: 10.1038/nrmicro.2017.126
- Reniere, M. L., Whiteley, A. T., Hamilton, K. L., John, S. M., Lauer, P., Brennan, R. G., et al. (2015). Glutathione activates virulence gene expression of an intracellular pathogen. *Nature* 517, 170–173. doi: 10.1038/nature14029
- Reniere, M. L., Whiteley, A. T., and Portnoy, D. A. (2016). An *in vivo* selection identifies *Listeria monocytogenes* genes required to sense the intracellular environment and activate virulence factor expression. *PLoS Pathog.* 12:e1005741. doi: 10.1371/journal.ppat.1005741
- Sarhan, J., Liu, B. C., Muendlein, H. I., Li, P., Nilson, R., Tang, A. Y., et al. (2018). Caspase-8 induces cleavage of gasdermin D to elicit pyroptosis during *Yersinia* infection. *Proc. Natl. Acad. Sci. U.S.A.* 115, 10888–10897. doi: 10.1073/pnas.1809548115
- Savin, C., Criscuolo, A., Guglielmini, J., Le Guern, A.-S., Carniel, E., Pizarro-Cerda, J., et al. (2019). Genus-wide *Yersinia*-core genome multilocus sequence typing for species identification and strain characterization. *Microb. Genom.* 5:e000301. doi: 10.1099/mgen.0.000301
- Scherr, T. D., Hanke, M. L., Huang, O., James, D. B., Horswill, A. R., Bayles, K. W., et al. (2015). *Staphylococcus aureus* biofilms induce macrophage dysfunction through leukocidin AB and alpha-toxin. *mBio* 6:e01021–e01015. doi: 10.1128/mBio.01021-15
- Seif, Y., Kavvas, E., Lachance, J.-C., Yurkovich, J. T., Nuccio, S.-P., Fang, X., et al. (2018). Genome-scale metabolic reconstructions of multiple *Salmonella* strains reveal serovar-specific metabolic traits. *Nat. Commun.* 9:3771. doi: 10.1038/s41467-018-06112-5
- Sheldon, J. R., and Skaar, E. P. (2019). Metals as phagocyte antimicrobial effectors. *Curr. Opin. Immunol.* 60, 1–9. doi: 10.1016/j.coi.2019.04.002
- Spaan, A. N., Van Strijp, J. A. G., and Torres, V. J. (2017). Leukocidins: staphylococcal bi-component pore-forming toxins find their receptors. *Nat. Rev. Microbiol.* 15, 435–447. doi: 10.1038/nrmicro.2017.27
- Tattoli, I., Sorbara, M. T., Yang, C., Tooze, S. A., Philpott, D. J., and Girardin, S. E. (2013). *Listeria* phospholipases subvert host autophagic defenses by stalling pre-autophagosomal structures. *EMBO J.* 32, 3066–3078. doi: 10.1038/emboj.2013.234
- Thurlow, L. R., Hanke, M. L., Fritz, T., Angle, A., Aldrich, A., Williams, S. H., et al. (2011). *Staphylococcus aureus* biofilms prevent macrophage phagocytosis and attenuate inflammation *in vivo*. *J. Immunol.* 186, 6585–6596. doi: 10.4049/jimmunol.1002794
- Tilney, L. G., and Portnoy, D. A. (1989). Actin filaments and the growth, movement, and spread of the intracellular bacterial parasite, *Listeria monocytogenes*. *J. Cell Biol.* 109, 1597–1608. doi: 10.1083/jcb.109.4.1597
- Tong, S. Y. C., Davis, J. S., Eichenberger, E., Holland, T. L., and Fowler, V. G. (2015). *Staphylococcus aureus* infections: epidemiology, pathophysiology, clinical manifestations, and management. *Clin. Microbiol. Rev.* 28, 603–661. doi: 10.1128/CMR.00134-14
- Tranchemontagne, Z. R., Camire, R. B., O'Donnell, V. J., Baugh, J., and Burkholder, K. M. (2015). *Staphylococcus aureus* strain USA300 perturbs acquisition of lysosomal enzymes and requires phagosomal acidification for survival inside macrophages. *Infect. Immun.* 84, 241–253. doi: 10.1128/IAI.00704-15
- Wang, G., Xia, Y., Cui, J., Gu, Z., Song, Y., Chen, Y. Q., et al. (2014). The roles of moonlighting proteins in bacteria. *Curr. Issues Mol. Biol.* 16, 15–22. doi: 10.21775/cimb.016.015
- Xayarath, B., Alonzo, F., and Freitag, N. E. (2015). Identification of a peptide-pheromone that enhances *Listeria monocytogenes* escape from host cell vacuoles. *PLoS Pathog.* 11:e1004707. doi: 10.1371/journal.ppat.1004707
- Yoshikawa, Y., Ogawa, M., Hain, T., Yoshida, M., Fukumatsu, M., Kim, M., et al. (2009). *Listeria monocytogenes* ActA-mediated escape from autophagic recognition. *Nat. Cell Biol.* 11, 1233–1240. doi: 10.1038/ncb1967
- Zhang, Y., Yao, Y., Qiu, X., Wang, G., Hu, Z., Chen, S., et al. (2019). *Listeria* hijacks host mitophagy through a novel mitophagy receptor to evade killing. *Nat. Immunol.* 20, 433–446. doi: 10.1038/s41590-019-0324-2

Conflict of Interest: The authors declare that the research was conducted in the absence of any commercial or financial relationships that could be construed as a potential conflict of interest.

Copyright © 2020 Leseigneur, Lè-Bury, Pizarro-Cerdá and Dussurget. This is an open-access article distributed under the terms of the Creative Commons Attribution License (CC BY). The use, distribution or reproduction in other forums is permitted, provided the original author(s) and the copyright owner(s) are credited and that the original publication in this journal is cited, in accordance with accepted academic practice. No use, distribution or reproduction is permitted which does not comply with these terms.

Appendix D

Review article: Bacterial determinants of bloodstream infections

In this review, we present a comprehensive overview of molecular mechanisms evolved by pathogenic bacteria to survive and replicate in blood. After a focus on complement subversion that I personally reviewed, we also discuss cellular subversion, metabolic determinants as well as regulatory components playing a critical role in bacteremia, specifically reviewed by Hebert Echenique-Rivera.

Review article

Bacterial determinants of bloodstream infection

Authors

Pierre Lê-Bury¹, Hebert Echenique-Rivera¹, Javier Pizarro-Cerdá^{1,2}, Dussurget Olivier¹

Affiliations

¹Institut Pasteur, Université Paris Cité, CNRS UMR6047, Yersinia Research Unit, F-75015 Paris, France

²Institut Pasteur, Université Paris Cité, Yersinia National Reference Laboratory, WHO Collaborating Research & Reference Centre for Plague FRA-140, Paris, France

Abstract

Bloodstream infection is a major public health concern associated with high mortality and high healthcare cost worldwide. Bacteremia can trigger fatal sepsis whose prevention, diagnosis and management have been recognized as a global health priority by the World Health Organization. In addition, infection control is increasingly threatened by antimicrobial resistance which is the focus of global action plans to generate a One Health response. In-depth knowledge of the infection process is needed to develop efficient preventive and therapeutic measures. Pathogenesis of bloodstream infection is a dynamic process resulting from invasion of the vascular system by bacteria, which finely regulate their metabolic pathways and virulence factors to overcome blood immune defenses and survive. In this review, we highlight our current understanding of bacterial factors involved in pathogenesis of bloodstream infection and discuss their interactions with molecular and cellular components of blood.

Keywords

Bacteremia, bacteria, infection, pathogenesis, blood, virulence factors, immunity

1 Introduction

Bacteremia is the presence of viable bacteria in the bloodstream. It sometimes results from activities such as toothbrushing, dental extraction or other minor medical procedures, leading generally to transient and asymptomatic colonization of blood before bacterial elimination by the immune system [1]. On the other hand, it can constitute a *bona fide* step of bacterial pathogenesis. Bacteria can enter the bloodstream directly from a breach in the vascular system upon catheterization, surgery, intravenous drug injection, arthropod bite or injuries such as accidents, falls and cuts. Blood can also be colonized as a complication of a primary infection site, *e.g.*, following pneumonia, meningitis, peritonitis, or skin, soft tissue, bone, joints, biliary and urinary tract infections. Bacteria can then colonize other organs by hematogenous spread triggering secondary infections such as infectious endocarditis or osteomyelitis. Uncontrolled bloodstream infections ultimately lead to sepsis, septic shock and death [2].

Bloodstream infection is a major public health issue worldwide. Sepsis is estimated to affect 31.5 million individuals leading to 5.3 million deaths annually, and its control has been declared a health priority by WHO [2–4]. The incidence rate of bloodstream infections has been estimated to range from 113 to 204 per 100,000 person-years in North America and Europe [5]. In the same population, short-term fatality rates and mortality rates were 13-20% and 20-37 per 100,000 person-years, respectively [5]. Bacteria most frequently isolated from blood are *Staphylococcus aureus* and *Escherichia coli*. A worldwide sentinel study from 1997 to 2016 highlights inverse frequency trends with *S. aureus* decreasing from 22 to 18%, while *E. coli* rising from 18 to 24% [6]. Urinary tract infection is the leading source of *E. coli* bloodstream infection. A recent systematic review of the literature indicates an estimated incidence rate of *E. coli* bacteremia reaching 48 per 100,000 person-years in high income countries [7]. This rate increases over 100 in 55-to-75-year-olds and over 300 in 75-to-85-year-olds. The average estimated case fatality rate of *E. coli* bacteremia is 12% [7]. Skin infection is the most common cause of *S. aureus* bloodstream infection, which is associated with high morbidity and mortality [8, 9]. Far less frequent bacteria responsible for bloodstream infections are *Klebsiella pneumoniae*, *Pseudomonas aeruginosa*, *Enterococcus faecalis*, *Staphylococcus epidermidis*, *Enterobacter cloacae*, *Streptococcus pneumoniae*, *Enterococcus faecium* and *Acinetobacter baumannii*, representing 2 to 7% [6]. In low-resource regions, *Salmonella enterica* is a major cause of bloodstream infections [10, 11].

Bloodstream infections are associated with high mortality, long hospital stays and high healthcare costs, in particular those acquired by critically ill patients in intensive care units [12–14]. Emergence and spread of multi-drug resistant clones are additional concerns limiting therapeutic options and increasing the economic burden of bacteremia management. Prevalence of antibiotic-resistant enterobacteria isolated from bloodstream infections more than doubled in 20 years, reaching 15.8% in 2016 [6]. In contrast, global prevalence of oxacilline-resistant *S. aureus* slightly decreased among both hospital- and community-acquired isolates [6]. Although bloodstream infections due to antibiotic-resistant bacteria currently represent a minority of cases, they can cause a higher fatality and mortality risks and a heavier economic burden per infection than susceptible isolates [8, 15–17]. Beyond the high hospital costs associated with bloodstream infection care, long term disabilities following severe sepsis have major socioeconomic impacts [18].

Bloodstream infection pathogenesis is a complex and dynamic process. In broad outline, it can be divided in several steps starting with vascular system invasion by bacteria possibly upon dissemination from a primary site infection, followed by interactions with blood immune components potentially triggering sepsis, and in some cases, metastatic spread to secondary sites of infection. Successful bloodstream infection relies on the capacity of bac-

teria to overcome host immune defenses based on tissular barriers, immune cells, soluble messengers and antibacterial factors. Invading bacteria face phagocytosis by neutrophils, monocytes and macrophages. Killing occurs by generation of toxic levels of reactive oxygen and nitrogen species, fine tuning of nutrient metal homeostasis and production of antimicrobial peptides and proteases [19, 20]. In blood, complement kills bacteria directly by formation of the lytic membrane attack complex and indirectly by mediating macrophage ospono-phagocytosis [21]. Other blood antibacterial defense components include platelet microbicidal proteins (PMPs) and kinocidins released by alpha-granules, interleukin-26, defensins and nutritional immunity proteins such as transferrin, hemopexin and haptoglobin [22–24].

Here, we review the molecular mechanisms evolved by bacteria to counteract host defenses and survive in the bloodstream. We focus on bacterial determinants identified in genomics studies based on cutting-edge technologies and whose function in blood has been investigated *ex vivo* and in animal models.

2 Complement inhibitors

2.1 The complement system

The complement system is one of the most important component of innate immune response. It has been extensively reviewed elsewhere [25]. Briefly, the complement cascade can be activated by three different pathways: the Classical Pathway (CP), the Lectin Pathway (LP) and the Alternative Pathway (AP) (Figure 1). The three pathways lead to the activation of the Terminal Pathway (TP). In a nutshell, the CP is activated by binding of the C1 complex, composed of the C1q sub-units scaffold and the C1s and C1r proteases, to immunoglobulins (Ig) bound to an antigen. The LP is activated by Mannose-Binding-Lectin (MBL) or ficolin, complexed with MASP1 and MASP2 proteases, and bound to specific target carbohydrates. Both complexes will then recruit and cleave C4 and C2 components into C2a, C2b, C4a and C4b components. C2b and C4b subsequently form the C3 convertase C4b2b (formerly known as C4b2a), cleaving C3 in C3a and C3b, when C4b is not degraded by the coordinated action of C4b-binding protein (C4BP) and the Factor I protease.

The AP is first activated by C3b and factor B deposition on bacterial surface. The deposited C3b is a product of the soluble C3 convertase, composed of C3 bound to H₂O and factor B, or of C3 convertases from the other pathways, the AP also serving as an amplification loop. C3b bound to factor B and stabilized by properdin (Factor P) forms a C3 convertase, C3bBb (or C3bBbP). Factor I can cleave C3b in inactive C3b (iC3b), an opsonin binding to Complement receptor 3 (CR3). Factor D activates the AP by cleaving factor B, generating C3(H₂O)Bb and C3bBb. Factor H and factor I prevent activation of AP.

C3 convertases cleave C3 in C3a and C3b. C3a is a multifunctional peptide required for chemotaxis, which binds C3a receptor (C3aR), and activates immune cells. C3b is an opsonin binding to complement receptor 1 (CR1), and is essential for propagation of the complement cascade. C3b binds to all C3 convertases forming C5 convertases C4b2b3b (CP/LP) and C3bBbC3b (AP), which cleave C5 in C5a and C5b. C5a is a chemoattractant for immune cells. Upon membrane binding, it triggers the TP. C5b deposition recruits C6, C7, C8 and C9 that insert and polymerize in the bacterial membrane, forming the membrane-attack complex (MAC), a pore forming complex resulting in bacterial lysis. MAC assembly can be negatively regulated by vitronectin (mediated by heparin), clusterin, CD59 or the cartilage oligomeric matrix protein (COMP).

Many components of the complement cascade can be targeted by pathogenic bacteria. Hundreds of factors have been shown to interact with complement components. Factors

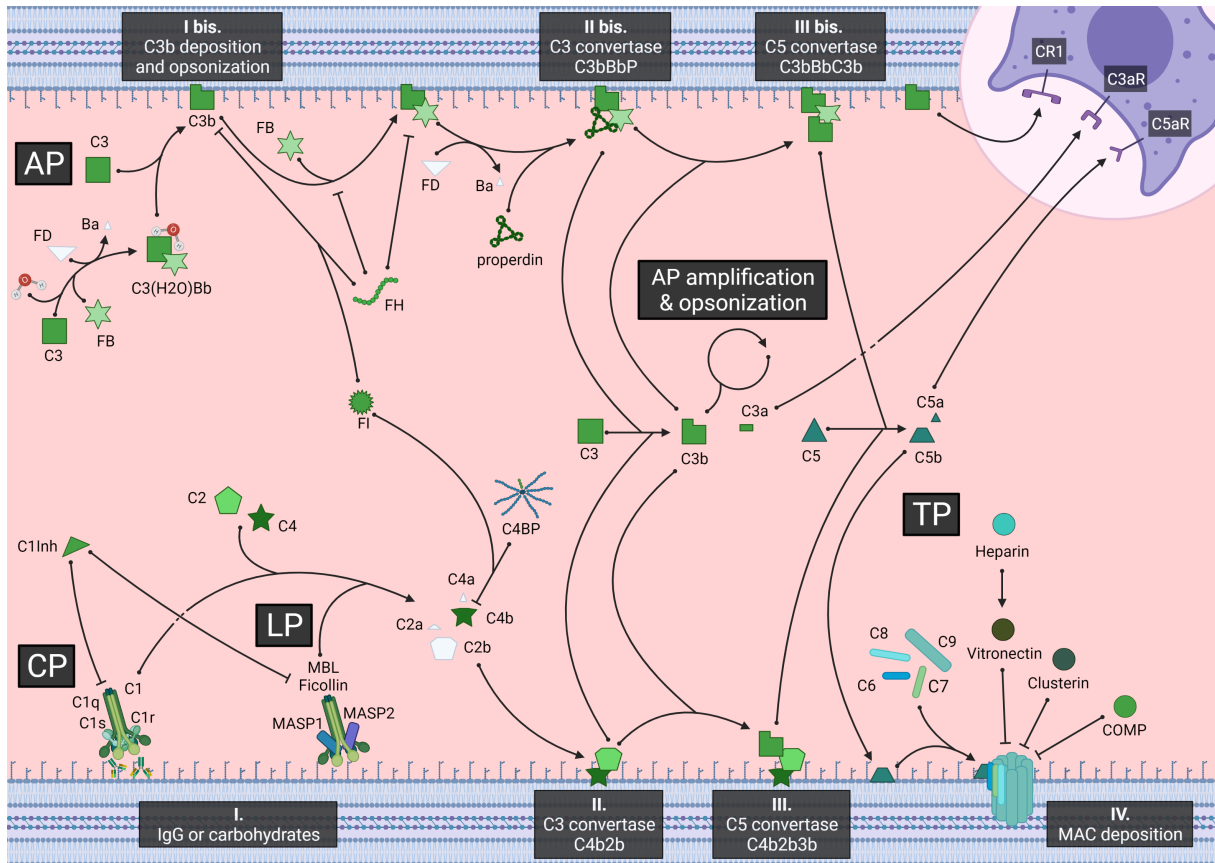


Figure 1. The complement pathways

specific to *S. aureus* [26], *E. coli* [27, 28], *K. pneumoniae* [29], *Haemophilus* [30], *Borrelia* [31], *Leptospira* [32], *Streptococcus* [33, 34], *Salmonella* [35] or *Neisseria* [36, 37] and general evasion mechanisms [38–41] have been extensively reviewed. The following section gives an overview of the main factors from clinically relevant pathogenic bacteria involved in complement resistance (Figure 2, Table 1)

2.2 Bacterial factors targeting components of the classical and lectin pathways

The CP is activated by binding of C1 complex (C1q, C1r and C1s) to Ig bound to bacterial surface. Some bacteria have evolved strategies to prevent this activation, such as inhibition of Ig interaction with C1q mediated by Sbi [42] or SpA proteins [43] in *S. aureus*. SpA also suppresses B cells response during bloodstream infection [44]. Importantly, surface components such as capsule or lipopolysaccharide (LPS) are crucial in CP/LP evasion. Capsules are major determinants of bacterial pathogenesis, involved in several steps of infectious processes, such as adhesion and escape from immune responses, in particular in the bloodstream. Polysaccharidic capsules contribute to resistance to complement-mediated killing and inhibition of phagocytosis. Physical and chemical properties of capsules, as well as other surface polysaccharides such as exopolysaccharides (EPS), promote complement evasion by decreasing IgA, IgG or IgM binding to the surface, thereby reducing CP activation. Capsules have been shown to reduce Ig binding and promote serum resistance in *N. meningitidis* [45, 46] and *Streptococcus* [47]. In *Kingella kingae*, the *pamABCDE* operon involved in galactan EPS synthesis is important for virulence in a rat infection model and to resist the complement CP but only when the *csaA* capsule gene was also mutated, resulting in an EPS and capsule double mutant [48]. Other functions of capsules in complement evasion are de-

veloped in sections below. LPS is a complex molecule specific to Gram-negative bacteria that consists of a lipid A membrane anchor, an oligosaccharidic core and chains of carbohydrates, the O antigen. Core LPS have been shown to interact with mannose-binding lectin (MBL) in *Neisseria gonorrhoeae* and *Salmonella enterica*. LPS structure is suggested to be the determinant of MBL binding level, which is reduced by O-Antigen and sialic acid [49]. Lipooligosaccharide (LOS) structure, a particular type of LPS found in *Haemophilus* spp and *Neisseria* spp, is also crucial for complement evasion. *H. influenzae* prevents binding of IgM by changing LOS structure through expression of galactose-containing oligosaccharide, reducing complement activation and killing by neutrophils [50]. Furthermore, phase-variable LOS biosynthesis gene *IgtC* is required to minimize C4b deposition on *H. influenzae* surface [51]. *N. gonorrhoeae* also reduces C4b deposition upon PorB binding which is enhanced by lipid A phosphoethanolamine [52]. Like capsules, LPS acts on several other components of the complement system that are developed in following sections.

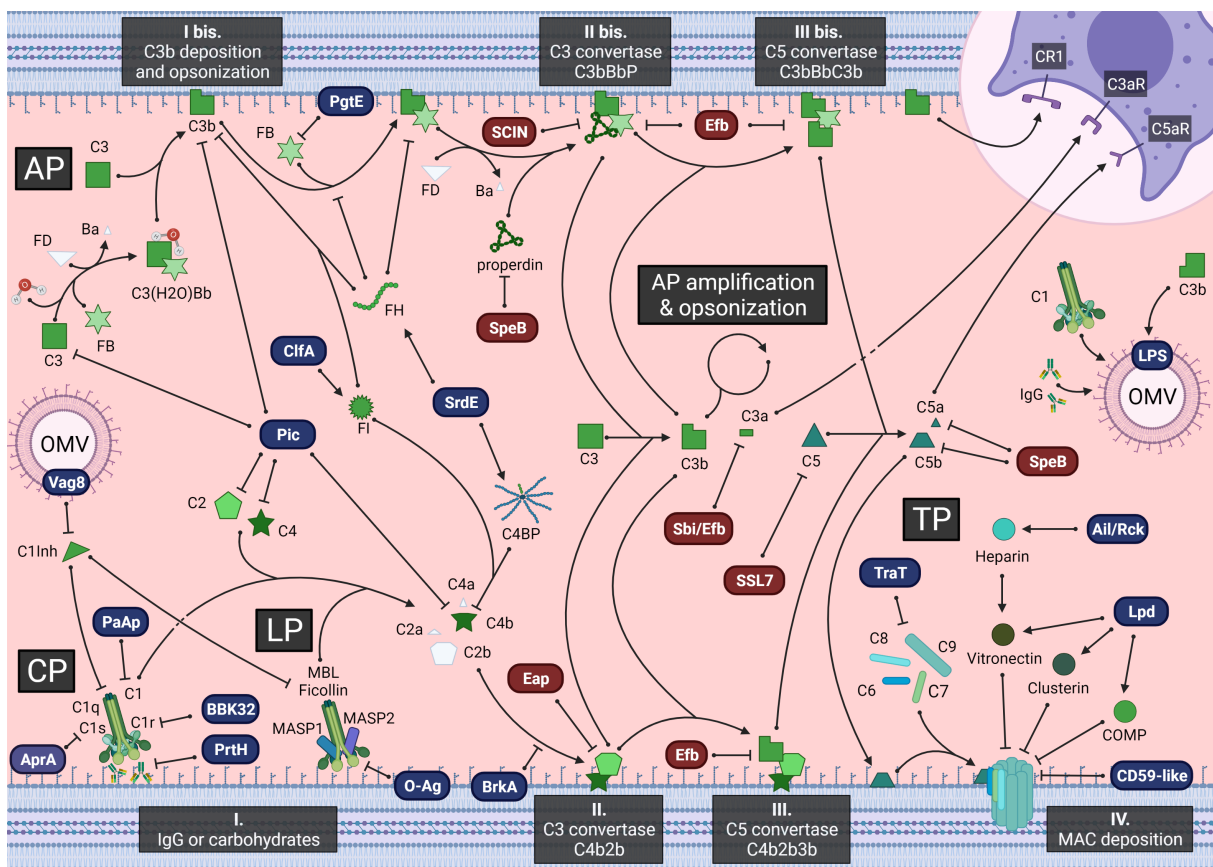


Figure 2. Examples of bacterial factors targeting the complement components and regulators. Targeted complement components are in green, membrane associated bacterial factors are in blue and secreted bacterial factors are in red.

Other components of the CP and LP are targeted by bacteria: *Pseudomonas aeruginosa* produces proteases such as AprA degrading C1s protease and C2 (and also C5a) [53] or PaAP and PaE that degrade C1q and C3 [54]. *Borrelia burgdorferi* encodes the BBK32 lipoprotein which binds C1r and promotes bloodstream survival [55, 56]. Polyfunctional factors such as the Pic autotransporter of *E. coli* can cleave C2, C3, C3b, C4 and C4b [57]. Analysis of *B. burgdorferi* transcriptome upon temperature shift and growth in human blood identified the adhesin OspC gene as one of the top upregulated genes [58]. The role of OspC in bacterial survival in blood was demonstrated in a later study showing its binding to C2 and C4b [59]. *Bordetella pertussis* encodes the surface autotransporter BrkA that has the ability to decrease C4 deposition, reducing serum killing activity [60].

S. aureus has been shown to target all C3 and C5 convertases, including those of CP/LP, by expressing the staphylococcal complement inhibitor protein SCIN inhibiting C4b2b [61, 62] or the extracellular complement-binding protein Ecb and the extracellular fibrinogen-binding protein Efb targeting C4b2bC3b [62], thereby promoting bloodstream infection in a murine infection model [63]. Other pathogens can cleave or bind C1-Inh, a serine protease inhibitor that negatively regulates C1r and C1s (CP) or MASP-1 and MASP-2 (LP). *B. pertussis* encodes Vag8 expressed on Outer Membrane Vesicles (OMV), that degrades C1-Inh at a distance from bacteria, activating the CP and the LP away from the bacterial surface [64]. *E. coli* StcE metalloprotease can cleave and also recruits C1-Inh on host cells, protecting adherent bacteria from complement [65].

Most importantly, a majority of bacteria involved in bloodstream infections produce factors interacting with the main negative regulator of CP and LP pathways, the C4-binding protein (C4BP), to prevent complement activation. Among others, *Streptococcus* encodes the protein H [66] and the M capsule [67], *E. coli* interacts with C4BP through Nlpl [68] and OmpA [69] proteins, and *N. meningitidis* expresses the porins PorB1 [70] and PorA [71] to resist serum killing.

2.3 Bacterial factors targeting components of the alternative pathway

As for C4BP, most invasive bacteria evolved one or several factors targeting the main negative regulators of the AP, factor H (FH), factor H-like (FHL-1) and factor H-related protein (FHR-1) [72]. FH degrades C3b owing to proteolytic activity of factor I, and prevents C3b and factor B association. Many bacterial membrane proteins have been shown to recruit FH and promote survival in serum or blood, such as *Acinetobacter baumannii* OmpA [73], *Aggregatibacter actinomycetemcomitans* Omp100 [74], *E. coli* OmpW [75] or *N. meningitidis* factor-H binding protein fHBP [76]. Expression of the NspA protein initially shown to be increased in a microarray analysis of *N. meningitidis* incubated in human blood [77], was later demonstrated to interact with Factor H, like sialylated LOS, promoting serum resistance in *Neisseria* spp. [78–80]. The numerous bacterial factors interacting with FH are listed in the table 1.

Other components of the AP can also be targeted. For instance, the factor B is degraded by *Salmonella* spp PgtE protease [81], the C3 convertase C3bBbP is inhibited by *S. aureus* SCIN [61, 62], Efb and Ecb [62], like the CP/LP C3 convertase. Efb and Ecb can also interact with the AP C5 convertase C3bBbC3b [62], promoting bloodstream infection in mice [63]. In *P. aeruginosa*, the lytic polysaccharide monoxygenase (LPMO) encoded by *cbpD* promotes survival of the bacterium in human blood and virulence in mice by lowering the activity of AP C5 convertase C3b2Bb, thereby attenuating MAC assembly [82]. C3 convertase can also be targeted indirectly. *Streptococcus* SpeB protease has been shown to cleave properdin (factor P), which stabilizes C3 convertase [83]. Lastly, other factors target the AP by unknown mechanisms, e.g., type-II O-antigen from *Burkholderia pseudomallei* LPS is required for AP resistance and virulence in three animal models of melioidosis [84].

2.4 Bacterial factors targeting general components of the system

C3 is a central component of complement cascades, common to the three activation pathways. Some pathogenic bacteria have evolved factors degrading C3, such as the thermolysin protease of *Leptospira interrogans* [85, 86] or the NalP protease of *N. meningitidis* [87]. Other proteins such as *S. pneumoniae* exoglycosidases NanA, BgaA and StrH act on human glycoconjugates on bacterial surface to reduce C3 deposition [88]. Degradation of C3b is often due to binding of plasminogen (PLG) and/or plasmin by bacterial factors such

as moonlighting elongation factor EF-Tu in *A. baumannii* [89], *P. aeruginosa* [90], or *B. anthracis* [91], *Salmonella* spp protease PgtE [92] or *S. aureus* staphylokinase [93]. Some bacterial factors binding plasmin/PLG also target C4BP, Factor H or vitronectin (see Table 1).

Capsules, in addition to prevent Ig binding, can also reduce C3 deposition and opsonization, thereby reducing phagocytosis and promoting survival in mice, as it has been observed with the Vi capsule of *Salmonella enterica* Typhi [94, 95]. Examples of capsule-mediated inhibition of C3/C3b deposition resulting in serum resistance exist in numerous pathogens such as *H. influenzae* [96], *K. pneumoniae* [97], *B. anthracis* [98], *Streptococcus* [47] and *B. pseudomallei* [99]. Other surface polysaccharides such as *P. aeruginosa* EPS also mediate resistance to complement by decreasing C3 binding [100]. LPS and more specifically the O-antigen has been shown to reduce C3 binding in *Francisella tularensis* and convert rapidly C3b to iC3b [101]. The O-antigen is thought to efficiently bind C3 away from bacterial surface, thereby reducing complement-mediated lysis.

Another complement general protein targeted by pathogenic bacteria is factor I, the protease responsible for degradation of C4b via C4BP (CP and LP) and degradation of C3b via FH (AP). Factor I is recruited by clumping factor ClfA of *S. aureus*, increasing C3b cleavage [102]. Agonists of C5 have been described, such as the *S. aureus* superantigen like protein 7 (SSL7), preventing its cleavage in C5a and C5b [103]. Degradation of C3a, C3 and C3b, plasmin binding by *S. aureus* Sbi and Efb result in reduced chemotaxis [104] and inhibition of C5a by *S. aureus* CHIPS impairs neutrophil recruitment in a mouse peritonitis model [105].

In *A. baumannii* genomic analysis of a hypervirulent clinical isolate identified a spontaneous transposon insertion in the *gtr6* gene encoding a glycosyltransferase that modifies acetylation of the capsule. Absence of capsule modification by Gtr6 protects bacteria from C3b deposition, phagocytosis and clearance from blood, resulting in lethal infection in mice [106].

2.5 Bacterial factors targeting components of the terminal pathway

Deposition of C5b on bacterial membrane leads to insertion and assembly of the MAC through the recruitment of C6, C7, C8 and C9. C5b can be degraded by *Streptococcus* SpeB protease [107]. C5b-C6 interaction is inhibited by *E. coli* TraT protein [108], promoting serum survival. *Borrelia* factors BGA66 and BGA71 bind C7, C8 or C9, preventing MAC assembly [109], as *Streptococcus* phosphoglycerate kinase Pgc does with C5, C7 and C9, reducing hemolytic activities of human serum [110]. Gram-positive bacteria naturally resist to the TP owing to their thick peptidoglycan wall preventing MAC insertion. Gram-negative bacteria evolved strategies reducing MAC efficacy on their outer membrane such as synthesis of the capsule in *Neisseria* [36], and production of LPS bearing anionic polysaccharide repeat units (A-LPS) by *Porphyromonas gingivalis* [111]. As described above, LPS and O-antigen have a central role in complement resistance, possibly due to reduction of membrane fluidity affecting MAC insertion [112] or to the deposition of complement components and MAC away from bacterial outer membrane, as it has been shown in *Salmonella* spp [113, 114] and *K. pneumoniae* by electronic microscopy [115].

Inhibitors of MAC assembly such as heparin-regulated vitronectin, clusterin, COMP or CD-59, can be recruited or mimicked. *H. influenzae* proteins F and H have been shown to interact with vitronectin and promote bacterial survival in serum [116, 117]. The Ldp moonlighting protein of *P. aeruginosa* can bind both clusterin and vitronectin to inhibit the TP and promote bacteria survival in serum [118]. Ubiquitous surface protein A2 of *Moraxella catarrhalis*, UspA2, can bind COMP, inhibiting MAC activity in serum and phagocytic killing by neutrophils [119]. Lastly, *Borrelia* spp express a CD-59 like molecule binding C9 and reducing bactericidal activity of serum [120].

2.6 Bacterial factors targeting multiple components of different complement pathways

Some bacterial factors are Swiss-knives able to interact with multiple components of the different complement pathways, allowing protection at different levels of the activation cascades. For example, *Streptococcus* protease SpeB cleaves C1-INH, C2, C3, C3b, C4, C5a, C6, C7, C8, C9 and degrades properdin, assuring inactivation of complement at all stage of the cascade [83, 121, 122]. Streptococcal C5a peptidase ScpA can also cleave C3 and C3a [123].

Salmonella encodes a surface protease, PgtE, that cleaves C3b through plasminogen activation, C4b, C5, [92], factor B and factor H [81], promoting serum survival. Intriguingly, PgtE is a homolog of *Yersinia pestis* Pla virulence factor that has been shown to activate plasminogen but does not affect bacterial survival in serum or during bloodstream infection [124, 125].

Other bacterial factors can inhibit CP, LP and AP by simultaneously binding to C4BP and FH. It is the case for *S. aureus* SrdE/Bbp [126] or *Leptospira interrogans* LigAB [127]. Other factors can even bind vitronectin in addition to C4BP and FH, inhibiting the TP. This is the case of *Streptococcus* PspC [128–133], *L. interrogans* moonlighting enolase [134] and *Yersinia enterocolitica* adhesin YadA [135–137]. In addition *Yersinia* and *Salmonella* encode Ail and Rck, respectively, homologous proteases shown to bind FH, C4BP and heparin, recruit vitronectin and inhibit MAC formation by blocking its insertion and C9 polymerization, enhancing serum resistance in *Salmonella* spp [138–140], *Y. pestis* [141–145], *Y. enterocolitica* [135, 137, 146] and *Yersinia pseudotuberculosis* [147].

2.7 Complement exhaustion

As mentioned above, *B. pertussis* Vag8 expressed on OMVs degrades C1-INH and activates complement away from bacterial surface [64]. Similar observations have been reported with *Neisseria* OMVs exhausting complement components and allowing bacterial serum survival [148], LPS expressed on *P. gingivalis* OMVs [149], *Vibrio cholerae* OMVs expressing OmpU recognized by natural human IgG [150], and *A. actinomycetemcomitans* OMVs contributing to serum resistance [151]. Furthermore, streptococcal NanA neuraminidase removes sialic acid from platelets and host cells (see the following section), important for FH binding, thereby activating and exhausting complement on host cells [152].

2.8 Bacterial factors involved in complement resistance by unknown mechanisms

Phenotypic observations of bacterial isolates or experimental approaches using screens such as Tn-Seq TraDIS, TraSH, INSeq identified factors required for complement resistance by hypothetical mechanisms. This is the case for the capsule and LPS-mediated resistance phenotype that has been observed for more than 40 years in *E. coli*, *P. aeruginosa*, *Salmonella* spp or *K. pneumoniae*. Although the main mechanisms of resistance described above have been deciphered in some bacteria, it remains to be studied in others. For instance, the increased complement fixation on unencapsulated *E. coli* remains to be fully characterized [153]. It has been shown that an *E. coli* K1 capsule-negative mutant in the *neuC* gene encoding the UDP *N*-acetylglucosamine 2-epimerase, which catalyzes formation of *N*-acetylmannosamine, has a decreased resistance to complement, deficient growth in human serum and in a model of infection of neonatal rats [154]. Polysialic acid capsular K1 polysaccharide which is strongly expressed in blood by *E. coli* could possibly bind FH and prevent complement activation [28]. Similarly, the LPS has long been shown to be

important for complement resistance in *E. coli* [154–157] but its precise mechanism is still being investigated. In a UPEC strain, a point mutation in the gene *wzy* encoding the O-antigen polymerase has been identified by genomic analysis and affects serum resistance [156]. More recent studies using a TraDIS approach in *E. coli* screening growth of mutants in human serum identified the gene *waaW* involved in LPS biosynthesis as a candidate necessary for survival in serum. The *waaW* gene encodes a UDP-galactose:(galactosyl) LPS alpha 1,2-galactosyltransferase, which is involved in the synthesis of the R1 and R4 LPS core oligosaccharides. Inactivation of this gene prevents attachment of O-antigen side chains to the core oligosaccharide of LPS. Growth of the *waaW* mutant is defective in human serum and in a model of infection of neonatal rats [154]. In *Salmonella*, the O-antigen can contribute to serum resistance owing to decreased MAC efficacy or MBL binding (see previous sections). Newly discovered mechanisms are still being unraveled. It has been reported that O-antigen glucosylation mediated by glycosyltransferase activity of the *gtr* operons provides resistance to serum killing [158]. However, the exact molecular cause for this resistance is currently unknown. Another role of the O-antigen in *K. pneumoniae* is the protection to the complement mediated killing. Deletion of the *wbbO* gene encoding the galactosyltransferase necessary for O-antigen synthesis did not affect C3 binding nor resistance to serum or blood mediated killing. In contrast, *wbbO* deletion affected the capacity of *K. pneumoniae* to cause bacteremia in a mouse model [159].

O-antigen and capsular polysaccharide variability between strains are also factors that influence serum and whole blood susceptibility. By mutating the capsule gene *kpsD* and the O antigen gene *waaL* in three different types of O-antigens in uropathogenic *E. coli*, it was shown that O1, O6 and O18 antigens were required for survival in human serum. The role of the capsule was less clear and linked to O-antigen type in serum, but both K1 and K2 capsular antigens promoted survival in whole blood [160]. The molecular mechanisms remain to be identified.

In *Vibrio vulnificus*, Tad pili have been reported to contribute to resistance to AP-mediated lysis, favoring invasion and septicemia in a murine infection model [161] by an unknown mechanism. A transposon screen of ExPEC mutants affected in growth in swine serum identified colanic acid biosynthesis gene *wcaF*, O-antigen biosynthesis genes *rmICD*, lipid A-core biosynthesis genes *waaBGIP* and enterobacterial common antigen (ECA) biosynthesis genes *wceAD*, suggesting their role in evasion from the complement system. Mutations in *rmID*, *waaG* or *wecD* decreased bacterial load in blood in a murine infection model of infection [162]. Importantly, some phenotypic heterogeneity was observed in a UPEC strain after exposure to serum and to the complement system. Subpopulations of serum-resistant and serum-sensitive strains subsequently appeared but the mechanism is unknown [163].

3 Bacterial factors subverting blood cell defenses

3.1 Phagocytes

Complement activation plays an important role in phagocytosis through opsonization of bacteria by complement components (C3b and iC3b), facilitating their uptake by macrophage, monocyte and neutrophils. This phenomenon called opsonophagocytosis is widely counteracted by bacterial factors described in previous sections. Capsule protection from opsonin and Ig deposition is the main mechanism protecting bacteria from this phenomenon. Non capsulated *E. coli* are more susceptible to opsonophagocytosis by neutrophils and monocytes [153]. In *S. aureus*, capsule reduces opsonin deposition and macrophage phagocytosis, promoting pathogenesis *in vivo* [164]. It has also been suggested that C3 on the cell wall beneath the capsule layer is less accessible by phagocyte receptors [165].

C3/C3b deposition and neutrophil uptake are decreased by the capsule in *B. anthracis* [98], *K. pneumoniae* [97] or *Streptococcus* spp [47, 166]. C3/C3b deposition and macrophage uptake are also decreased by *H. influenzae* capsule [96] and *Salmonella* Vi capsule [94, 95]. Additionally, the capsule can hide pathogen-associated molecular patterns (PAMPs) such as lipoteichoic acid (LTA) or peptidoglycan (PG) from pattern recognition receptors (PRRs), dampening immune responses. It is the case for *E. faecalis* capsule that hides C3 bound to the surface and prevents LTA recognition by macrophages, thereby decreasing opsonophagocytosis and macrophage activation [167]. Enterococcal polysaccharide (EPA) decorations have also been shown to reduce phagocytosis and are critical for virulence in models of zebrafish bloodstream infection [168] and mouse peritonitis [169]. Other bacterial factors also decrease opsonophagocytosis, such as the exoglycosidases NanA neuraminidase, BgaA and StrH in *S. pneumoniae*. These proteins act on human glycoconjugates on the surface of bacteria to reduce C3 deposition and prevent opsonophagocytosis. [88]. C3 and IgG cleavage by the PrtH protease of *P. gingivalis* also decreases opsonization and subsequent neutrophils uptake [170]. The enterococcal surface protein ElrA reduces adherence to macrophage and internalization, and promotes infection in a mouse peritonitis model [171]. In *N. meningitidis*, a comparative proteomic analysis from bacteria isolated from different niches after infection using a murine model identified NMC0101, a putative membrane protein without functional assignment, as potentially important for blood survival [172]. A NMC0101 mutant strain is more resistant to phagocytosis compared to the wild-type strain. The same study shows that a *guaB* mutant, lacking a putative inosine-50-monophosphate dehydrogenase involved in purine nucleotide biosynthesis protected bacteria from macrophage-mediated bacterial clearance [172]. In *S. pyogenes*, M-related protein Mrp4 interacts with human fibrinogen, reducing C3b deposition and subsequent opsonophagocytosis [173].

S. aureus lacking the structural gene encoding sortase A *srtA* reduce their capacity to prevent phagocytic clearance in blood. Sortase A anchors important virulence factors to the cell wall such as ClfA, which interferes with complement and coagulation activation (see the following section) and the adenosine synthase A AdsA, an enzyme that converts adenosine monophosphate to adenosine. Abscess formation was dependent on AdsA and could be rescued by exogenous supply of adenosine, suggesting that *S. aureus* exploits the immunomodulatory attributes of adenosine to escape host immune responses [174]. Another phagocytic evasion mechanism developed by *E. coli* and *N. meningitidis* is erythrocyte binding via CR1, protecting bacteria from uptake and oxidative burst [175]. In *S. mutans* a proteomic analysis in plasma led to identification of the autolysin AltA which binds fibronectin and contributes to resistance to phagocytosis by neutrophils and survival in the bloodstream in a rat infection model [176]. In *P. aeruginosa* exotoxin A (ETA) has been shown to be important for bacteremia and virulence in a model of leukopenic mice after oral administration of bacteria [177]. Pathogenic bacteria can also directly attack phagocytes to prevent immune response. In *B. anthracis* the lethal toxin LT is required to impair neutrophil functions and preventing killing of the vegetative bacteria [178, 179]. In *S. aureus* expression of leukocidins such as HlgAB, HlgCB and LukAB, is upregulated in human blood but single mutants of these factors show little virulence defect *in vivo*, presumably due to leukocidin redundancy [180, 181]. It has been further shown that the leukocidin LukED is essential in murine bloodstream infection by targeting neutrophils [182]. *S. aureus* SaeP and SaeQ accessory proteins of the two-components system (TCS) SaeSR, are important in the interactions with human neutrophils. Mutations in *saeP* increase cytotoxicity against neutrophils *ex vivo* and increase bacterial survival. In contrast, deletion of *saeQ* does not affect interaction with neutrophils but is required to cause bacteremia [183]. SaeP increases secretion of extracellular proteins causing significantly more damage to the plasma membrane of human neutrophils. The enhanced cytotoxicity of *saeP* mutant towards human neutrophils correlated with an

increased expression of bi-component leukocidins known to target these cells. The double mutant *saePQ* shows a significant increase in survival following neutrophil phagocytosis similar to that of a Δ *saeP* single mutant and increases the virulence in a model of murine bacteremia. These data provide evidence that SaeP modulates the Sae-mediated response of *S. aureus* against human neutrophils and suggest that *saeP* and *saeQ* modulate pathogenesis *in vivo* by mechanisms that need further investigation [183]. In *S. agalactiae*, the β -hemolysin/cytolysin (β H/C) encoded by *cylE* is important for survival in human blood and reduces clearance in the bloodstream of mice, due to the induction of cytolysis and apoptosis of phagocytes [184]. In *S. suis*, the muramidase-released protein MRP has been shown to interact with human fibrinogen, triggering aggregation and exhaustion of neutrophils via an α X β 2 integrin-dependent mechanism and promoting bacteria survival in blood [185]. In *S. mutans*, the glucan binding protein C GbpC has been shown to be important in bacteremia. The mutant of GbpC survived better in blood of infected rats, since the mutants are less susceptible to phagocytosis by neutrophils [186]. Another *S. mutans* factor playing a role in the interaction with phagocytes is the protein antigen c PAc. A PAc mutant is less susceptible to phagocytosis in human polymorphonuclear leukocytes and more virulent in a rat model of bacteremia. PAc is important for phagocytosis susceptibility to human neutrophils and the lack of this protein in some clinical isolates could potentially increase the risk to develop bacteremia [187].

Some pathogenic bacteria that do not escape phagocytosis encode factors allowing intracellular survival. Streptococcal β H/C is necessary for expression of a carotenoid pigment preventing oxidative damage and enhancing survival inside phagocytes [184]. In *S. pneumoniae* a mutant deficient for an Id-carboxypeptidase, the DacB lipoprotein, has a decreased intracellular survival in murine macrophages and a decreased spread into the bloodstream in a mouse infectious model [188]. More recently, the *S. pneumoniae* aquaporin mutant *aqpC*, which acts as an oxygen porin, was reported to play a role in virulence. The mutant has a decreased resistance to H₂O₂ and NO and affects pneumolysin release, thereby markedly reducing damage to macrophages, affecting its survival in macrophages, and significantly reducing mice lethality [189]. *S. aureus* antioxidant staphyloxanthin (STX) is an important virulence factor promoting intracellular survival in phagocytes, presumably through resistance to reactive oxygen species (ROS) produced by the phagosomal NADPH oxidase. STX contributes to *S. aureus* resistance to hydrogen peroxide (H₂O₂) and survival in human blood [190]. A microarray analysis in *N. meningitidis* identified an operon controlled by the iron uptake regulator Fur. Deletion of one of the gene of this operon encoding NMB1436–38, a protein of unknown function, increases sensitivity to hydrogen peroxide increasing susceptibility to neutrophil killing and impairing the capacity of bacteria to survive in blood in a murine infection model [191].

In addition to phagocytosis, neutrophils can trigger NETosis, a specific cell death program that promotes formation of neutrophils extracellular traps (NET) by releasing a net made of DNA, histones, granular proteins and antimicrobial peptides, trapping and degrading pathogenic microbes [192]. Some bacteria encode endonucleases or DNAses to evade NETs, increasing their survival in blood, such as for *S. pyogenes* Sda1 DNase [193]. In *S. suis* the *ypzA* gene encodes a cell wall anchored LPXTG protein of unknown function whose expression is upregulated in blood during infection in a mouse model and which is required to prevent phagocytosis by macrophage and for full virulence in infected mice [194].

3.2 Platelets and coagulation factors

Circulating platelets have important functions in thrombosis and in modulating immune and inflammatory responses. Several pathogenic bacteria subvert the coagulation cascade and platelet functions. *Y. pestis* T3SS effector YopM has been shown to inhibit thrombin

and ristocetin-induced platelet aggregation. YopM could thus prevent platelet functions and be important for initial stages of infection [195]. It has been further proven *in vitro* that *Y. pestis* T3SS and the plasminogen activator Pla are important for thrombi destabilization and NET escape [196]. However, Pla is not necessary in a septicemic plague model [124]. *S. aureus* can also inhibit coagulation. In addition to interacting with IgG and C1q [197], staphylococcal superantigen-like protein 10, SSL10, binds prothrombin and factor Xa. The γ -carboxyglutamic acid (Gla) domains of these proteins are important for binding and inhibition of coagulation by SSL10 [198]. Efb contributes to *S. aureus* survival in the bloodstream through interaction with fibrinogen and complement factors inhibiting phagocytosis [199]. Additionally, two coagulases, Coa and von Willebrand factor binding protein vWbp, activate prothrombin to cleave fibrinogen, and ClfA allows staphylococci to associate with the resulting fibrin cables, promoting agglutination and infection severity in a mouse model of sepsis [200]. ClfA binding to fibrinogen further improves its antiphagocytic effect [201]. SSL5 interacts with GPIIb α , resulting in activation of platelets. SSL5 enhanced platelet aggregation in a plasma-free, reconstituted blood model suggesting that this mechanism can contribute to *S. aureus*-induced thrombocytopenia [202]. A similar activation of human platelets has been reported for other Gram-positive bacteria, such as Fc-gammaRII and complement-mediated platelet activation by *B. anthracis* peptidoglycan [203]. Peptidoglycan also contributes to disseminated intravascular coagulation (DIC), important in the pathogenesis of *B. anthracis* infection [204]. In *S. pneumoniae*, neuraminidases targeting surface sialic acids are critical for FH-mediated complement regulation on cells, including platelets. The NanA neuraminidase catalyzes release of sialic acids from platelets in an *ex vivo* model. Removal of sialic acid residues by NanA increases complement activity in blood, while absence of NanA blocked complement triggering and hemolytic activity indicating that NanA subverts activation of innate immune response [152]. Furthermore, the *S. pyogenes* M1 protein is able to form a complex in plasma with fibrinogen, Ig and complement components. These complexes bind the surface of platelets, enhancing their phagocytosis by monocyte, contributing to thrombocytopenia [205]. In addition to its complement inhibition *S. pyogenes* secreted streptococcal inhibitor of complement protein SIC has also been shown to interfere with the contact system of the coagulation cascade, promoting growth in plasma and dissemination in a mouse model of sepsis [206]. Moreover, a more recent study showed that SIC interacts with plasminogen, reduces fibrinolysis and protects against killing within fibrin clots [207]. Among Gram-positive bacteria, *S. agalactiae* is remarkably resistant to platelet killing. *S. agalactiae* possesses a capsule polysaccharide (CPS) with terminal α 2,3-linked sialic acid (Sia) residues that mimic a common epitope present on human cell surface glycoalkalix. Bacteria engage inhibitory Sia-recognizing Ig superfamily lectins (Siglecs) expressed on platelet surface to suppress their activation. A *S. agalactiae* mutant deficient in CPS Sia is more sensitive to killing by human platelets, thrombin-activated platelet releasate and synthetic platelet-associated antimicrobial peptides [208].

4 Bacterial metabolic factors and nutritional immunity

4.1 Energy source and carbon source

Nutritional requirements needed by the different pathogenic bacteria during the blood phase of infection can be divided between nutrients obtained from the media and bacterial metabolic pathways that are needed during the infectious process. Also the pathways necessary for the generation of energy for biological functions during this phase are described.

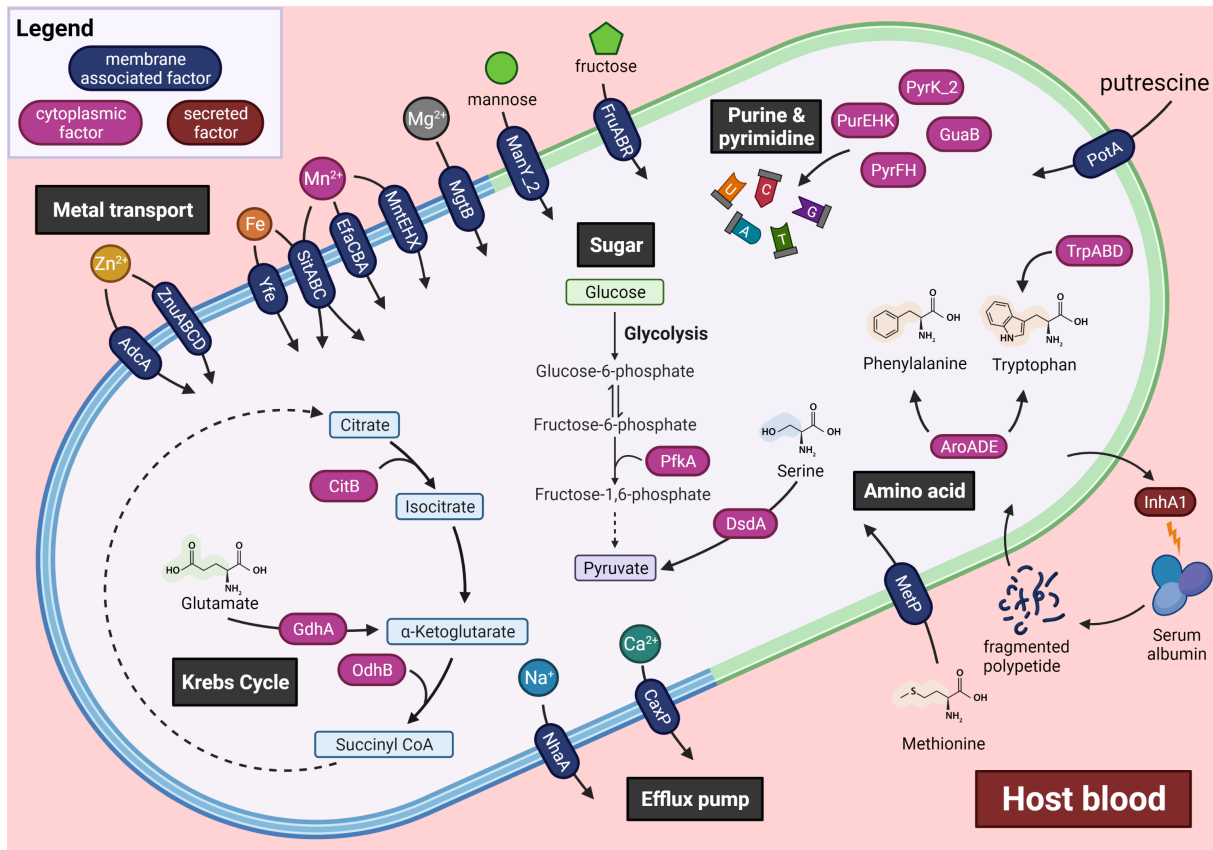


Figure 3. Metabolic factors and nutritional immunity

4.1.1 Energy Source

Tricarboxylic acid cycle. In *S. pyogenes* a TRASH screening identified 2 genes involved in energy production and conversion, *acoB* and *citF*. Growth of mutants for these 2 genes was attenuated in human blood [209]. In *S. aureus* a STM screening identified mutations in *odhB* encoding a subunit of the oxoglutarate dehydrogenase complex and the aconitase gene *citB* which convert alpha-ketoglutarate into succinate and citrate into isocitrate, respectively. Virulence of both mutants was impaired in a murine model of bacteremia [210].

4.1.2 Carbon source: transport of sugars

Glucose. Phosphoenolpyruvate-phosphotransferase system (PTS) is a global regulatory network connecting sugar uptake with signal transduction. This system is found only in bacteria, where it catalyzes transport and phosphorylation of numerous monosaccharides, disaccharides, amino sugars, polyols, and other sugar derivatives. To carry out its catalytic function in sugar transport and phosphorylation, a PTS uses phosphoenolpyruvate (PEP) as an energy source and phosphoryl as donor. PTS is the main system used by bacteria for the uptake of sugars and sugar derivatives as well as for signal transduction. PTS is made up of distinct proteins, including two cytosolic components, enzyme I (EI) (*ptsI*) and phosphocarrier protein Hpr (*ptsH*), and several membrane-bound sugar-specific enzyme IIs (EIIs). Each EII is composed of two cytosolic components (EIIA-B), an integral membrane domain (EIIC) and in some cases a fourth component (EIID). The second system for transport of glucose is a non-PTS transport based on permeases that are driven by proton motive forces. By using an IVET screen in *E. coli*, the mutant in the gene *bgIG* encoding a β -glucoside-metabolizing enzyme involved in the PTS system was shown to be attenuated in a competitive infection model of septicemia [211] but the clear role of this gene in bacteremia needs further investigation. Also, in *N. meningitidis* one component of the PTS system involved in transport

of glucose was identified to play a role in blood survival. The PTS system is incomplete in *N. meningitidis*, but the HPr encoded by *ptsH* is present. A *ptsH* mutant is more sensitive to complement killing, has a defective growth in human serum and in infected mice, including in mouse blood. The factor for which the mutant elicits a higher sensitivity to complement still needs to be identified and the role of *ptsH* seems to be related to stress resistance [212]. In *S. pyogenes* a TRASH screen in human blood allowed to identify a sugar metabolism related gene, *fruA*, coding for a fructose-specific component of the PTS system, which contributes to growth in human blood [209]. Later, another study in *S. pyogenes* identified mutations in the genes *fruR* and *fruB*, components of the canonical PTS_{fructose} (fructose) impairing survival in human blood, neutrophils and monocytes [213]. The *fruB* gene encoded the enzyme 1-phosphofructokinase while FruR is the fructose-responsive regulator. Interestingly, the phenotypes of the mutants were not reproduced in murine blood or in a mouse model of infection, suggesting that FruR and FruB could be important for *S. pyogenes* survival in a human-specific environment [213]. In *E. faecium*, the combination of RNA-seq and Tn-seq screening in human serum of a vancomycin resistant clinical isolate allowed to identify a gene encoding a component of the PTS system important for virulence. The gene corresponds to the phosphotransferase system subunit ManY₂ and is predicted to form the IIA component of a permease system. Deletion of this gene led to decreased growth of the mutant in human serum and virulence attenuation in a zebrafish infection model [214]. The *S. pyogenes* metabolism heavily depends on glucose. Deletion of the glukokinase gene *nagC* involved in PTS-independent glucose import blocks utilization of glucose. The study defined that this PTS-independent system is the primary player in glucose transport, survival in human blood and in lesions at the local site of infection in a skin infection model in mice pathogenesis. [215].

Carbon. In *N. meningitidis* the utilization of carbon sources was shown to be essential during the bloodstream infection phase. This was demonstrated by linking the activity of the LctP lactate permease, involved in the central carbon metabolism, and the sialic acid biosynthesis pathway in modulating the response to complement-mediated killing [216]. Another example is given by an INSeq analysis in a murine model of bloodstream infection by *Serratia marcescens*, which identified the gene *pgm*, encoding a phosphoglucomutase that converts glucose into pyruvate with a capsule-deficient phenotype and is linked to the central glucose metabolism. A glycolytic mutant of *pfkA* encoding a phosphofructokinase also exhibited reduced replication in human serum and in a mouse infection model [217].

In swine *E. coli* (ExPEC) a transcriptomic analysis of bacteria in blood from infected animals identified important pathways for generation of energy. The mutation of $\Delta rbsDACB \Delta citCEFXG$ involved in ribose and citrate pathways showed reduced fitness in host blood and reduced virulence in infected mice [218]. Deletion of $\Delta hybABCD \Delta hycEFG$ encoding NiFe hydrogenases 2 and 3 involved in anaerobic respiratory chains, impairs growth in swine blood and in mice [218]. D-serine degradation by *Proteus mirabilis* mediated by the DsdA protein using this mechanism as carbon-source was also shown to be essential for bloodstream infection *in vivo* [219].

In *S. pyogenes* a TRASH screen in human blood identified the gene *spy1794* involved in transport and carbohydrate metabolism as required for survival in blood [209]. In *S. pneumoniae* mutation of the *ldh* gene encoding the lactate dehydrogenase had defective glucose metabolism and decreased virulence in mice infected by the IV or intranasal routes [220]. *S. pneumoniae* lacks the respiratory electron transport chain and a complete tricarboxylic acid (TCA) cycle. To generate energy, it relies on the fermentation process to generate energy for survival and replication. *S. pneumoniae* can metabolize different types of carbohydrates and complex glycans. In the bloodstream, it can metabolize free glucose to generate energy. Alterations of energy metabolism have been demonstrated for some genes involved

in pathways described above. Loss of Ldh promotes bacteremia in mice but the loss of *spxB*, *pdhC* and *pfl2* affects catabolism of sugars leading to a decrease of acetyl-CoA and capsule production. This translates into a decreased survival in blood and an increased host survival in a mouse model [221]. This clearly shows the versatility of *S. pneumoniae* to change its metabolism and adapt to different niches depending on the carbon source available.

Size variation of *S. aureus* colonies after growth in human blood has been studied. Small-colony variants (SCV) do not produce leukocidins, hemolysins and staphyloxanthin and lack a functional electron transport chain compared to wild type colonies. Despite this impairment in virulence factors, small colonies were more resistant to human blood and to purified neutrophils. Supplementation of the culture medium of the heme-auxotrophic small-colony variants with heme restored hemolysin and staphyloxanthin production and sensitivity to oxidative burst. This observation was completed in *E. faecalis* that is a natural auxotroph for heme. The restoration of the electron transport chain affected the survival in blood of *E. faecalis*. This suggested that the lack of a functional electron transport chain in *S. aureus* SCV and *E. faecalis* reduced the growth rate generating an advantage to resist host immune defenses [222].

Nitrogen. Another element important for bacterial metabolism is nitrogen. In *P. mirabilis*, a Tn-Seq approach in heat-inactivated (HI) naive serum and HI acute phase serum allowed to identify a role for a twin arginine translocation (TatAC) system in motility, translocation of virulence factors and fitness in the bloodstream. This study suggests an interplay between two nitrogen assimilation pathways in the bloodstream, providing evidence that the GS-GOGAT (*glnA/gltB*) system may be preferentially utilized [223].

4.2 Biosynthetic pathways

4.2.1 Amino acids and protein synthesis

A particular mechanism used by *B. anthracis* is to proteolyze human hemoglobin to liberate essential amino acids which enhance its growth. This process is mediated by *InhA1*, a secreted metalloprotease [224]. The authors also suggested that this could extend to at least three other serum proteins, including serum albumin [224]. However microarray analysis of *B. anthracis* transcriptome did not show any differential expression of *inhA1* [225].

Arginine. The Gram-negative bacterium *P. mirabilis* is a common cause of catheter-associated urinary tract infections (CAUTI), which can progress to secondary bacteremia. A Tn-seq approach *in vivo* and *ex vivo* identified the dual function of the arginine decarboxylase *SpeA* to be important for fitness within the bloodstream due to its role in putrescine biosynthesis rather than its contribution to maintenance of membrane potential [223]. In *S. pneumoniae*, the ABC transporter *PotA* involved in spermidine/putrescine transport contributes to virulence in a septicemia mouse model [226].

Tryptophan and aromatic compounds. In the bloodstream of a host, aromatic compounds are not freely available. An INSEQ screening in *K. pneumoniae* identified the *aroE* gene as important for colonization of the lungs. The *aroE* gene, which encodes a shikimate dehydrogenase is required for aromatic amino acid synthesis and the mutation in this gene decreases the *K. pneumoniae* fitness in a mouse model of competitive infection. The *aroE* mutant does have a moderate defect in serum survival and seems to be required to evade complement-mediated serum killing [227]. In *S. enterica* Typhimurium *aroA* and *AroD* mutants are also attenuated *in vivo* and are susceptible to serum killing in addition to their

auxotrophy and also sensitivity to complement killing [228]. An *rfaC* mutant was approximately five times more sensitive to complement killing. In Gram-positive bacteria, an example is *S. agalactiae*, in which the shikimate pathway was functionally demonstrated to play a role in survival in blood and serum by using the deletion mutant of the *aroA* gene [229]. In *S. aureus* an STM screening allowed identification of the genes *trpA*, *trpB* and *trpD*. These genes encode enzymes of the tryptophan biosynthetic pathway and have been shown to be attenuated in a murine model of bacteremia [210]. A *S. typhimurium*, deletion mutant of *aroB* encoding a dehydroquinate synthase involved in the synthesis of chorismate which is a precursor of aromatic amino acids, is attenuated when injected intravenously in a mouse model [230].

Glutamate. Glutamate uptake from the host is critical for *N. meningitidis* survival because it is an essential precursor for the *de novo* biosynthesis of several essential amino acids, and enhanced expression of GdhA glutamate dehydrogenase was detected in hyper-virulent clinical strains. Furthermore, GdhA is also involved in the biogenesis of glutathione, which plays a pivotal role in protecting bacteria against oxidative stress in the host. A *gdhA* mutant displayed attenuated survival and virulence in murine infection model [172]. In *N. meningitidis* the gene NMB1966, encoding an ABC transporter, and annotated to be involved in glutamate metabolism/transport was inactivated. The mutant had a reduced survival in human blood and in mice infected by intraperitoneal injection associated with remodeling of the outer membrane and surface structures [231].

Aspartate, lysine, threonine and methionine. Screening of *S. aureus* transposon mutants in calf serum allowed to identify a gene, *asd*, encoding aspartate semialdehyde dehydrogenase, involved in survival in CS. Asd is an essential enzyme for the biosynthesis of lysine, methionine, and threonine from aspartate, suggesting that lysine and threonine biosynthesis are essential for growth in calf serum. Mutants in *metE*, *thrC*, *lysA* and *asd* showed reduced growth in mouse serum and were attenuated in a mouse model of bacteremia [232].

Methionine. In *S. agalactiae* the methionine transporter MetP was identified to be important for growth in both human blood and plasma [229]. This gene was identified using a TRaDIS screening in human blood.

4.2.2 Purines and Pyrimidines synthesis

The *de novo* synthesis pathways of purines and pyrimidines have been shown to be essential for successful proliferation of some pathogens in the bloodstream during bacteremia. In Gram-negative bacteria, the role of purines in *Salmonella* bacteremia was addressed a long time ago. For these studies *Salmonella* expressing the Vi antigen, *Salmonella dublin*, and purine-auxotrophic mutants were compared. Mutants in different genes such as *aroA* (aromatic dependent) and *purA* (adenine dependent) were avirulent in a mouse model after IP injection. Mutants in *purF*, *purG*, *purC* or *purJHD* operon also showed reduced virulence and mutants of *guaA* and *guaB* showing guanine requirement were also attenuated *in vivo*. Importantly, these findings were confirmed in *S. typhimurium* [233].

A screening of mutants of *E. coli* identified essential genes required for growth in human serum to be involved in purine and pyrimidines biosynthesis. Some genes such as *carA*, *pyrE*, *purA*, *purE* and *guaB* were shown to be required for survival in human serum confirming their role [234]. This observation was extended to *S. typhimurium* and *B. anthracis*. Interestingly, although sensitivity to human serum and mouse serum was observed for two

mutants in purine pathway such as *purE* and *purK*, only *purE* was essential for bacteremia. This suggests that some mutants can scavenge intermediates that promote proliferation and that *de novo* nucleotide biosynthesis is a critical function for bacterial growth in human serum [234]. In another *E. coli* strain causing sepsis in pigs a transposon mutagenesis screening identified important genes for serum survival in swine serum. The identified genes were related to the *de novo* synthesis pathway of purines (*purA*, *purE* and *purF*) and pyrimidines (*carAB*, *pyrD* and *pyrF*) [162]. Deletion mutants showed a significant growth deficiency compared with that of wild-type strain in swine serum, suggesting that *de novo* nucleotide biosynthesis pathways are necessary for ExPEC growth in porcine bloodstream. The mutation of *purE* and *pyrF* also affected the virulence in a mouse infection model [162]. For *V. vulnificus* by using the IVIAT (in vivo-induced antigen technology) approach, the *de novo* nucleotides biosynthesis genes *pyrH* and *purH*, were identified and shown to be important for survival in a mouse model [235]. In the case of *Y. pestis* the *de novo* synthesis of purines has also been implicated in virulence using a guinea pig model in a pioneering study of nutritional virulence [236]. A transcriptomic analysis of *Y. pestis* in human serum confirmed the role of purines and pyrimidines, showing upregulation of these pathways in a condition mimicking septicemic plague [237]. In *N. meningitidis*, a comparative proteomic analysis of bacteria isolated from different niches after infection using a mouse disease model highlighted increased levels of the inosine-50-monophosphate dehydrogenase encoded by the *guaB* gene involved in purine nucleotide biosynthesis in the CSF compared to bacteria isolated from the nasal fluid [172]. In this particular case, the *guaB* deletion confers a growth advantage in human serum. As stated previously, this mutation also protected bacteria from macrophage-mediated bacterial clearance [172]. This represents the unique example of deletion of a gene involved in purine biosynthesis promoting virulence.

The *de novo* biosynthetic pathway of purines has been shown to be essential in virulence of *B. anthracis*. The *purH* mutant was characterized in a guinea pig infection model [238] and was attenuated in the blood, in concordance to the phenotype of other mutants of the same pathway (see above) [234]. Random mutagenesis and functional genomics have provided a major contribution in the identification of *de novo* nucleotide synthesis genes required during bacteremia. By performing a dual approach of RNA-seq analysis and Tn-seq screening of *E. faecium* growth in human serum pyrimidine metabolism genes *pyrK_2* and *pyrF* and purine metabolism genes *purD* and *purH* were shown to be important for growth in serum, using a vancomycin resistance clinical isolate [214]. The *pyrK_2* deletion mutant was shown to be attenuated in an intravenous zebrafish infection model [214]. The *S. pneumoniae* gene *purK* involved in purine biosynthesis identified by STM is important for virulence in a septicemic mouse model [226]. In *S. pyogenes* a TRASH screening identified *guaB* whose mutant growth is attenuated in human blood [209]. In *S. aureus*, a screening of mutants in human serum identified *purA* and *purB* purine biosynthesis genes and showed their importance for growth and in a zebrafish model of infection. The precursor of pyrimidines PabA also contributes to survival in human blood and zebrafish [239]. These multiple examples points to the importance of *de novo* nucleotide biosynthesis for survival of bacteria during the blood phase and suggest that it could be a universal mechanism shared by blood-borne infection-causing bacteria. The *de novo* biosynthetic pathway of purines has been shown to be essential in virulence of *B. anthracis*. The *purH* mutant was characterized in a guinea pig infection model [238] and was attenuated in the blood, in concordance to the phenotype of other mutants of the same pathway (see above) [234]. Random mutagenesis and functional genomics have provided a major contribution in the identification of *de novo* nucleotide synthesis genes required during bacteremia. By performing a dual approach of RNA-seq analysis and Tn-seq screening of *E. faecium* growth in human serum pyrimidine metabolism genes *pyrK_2* and *pyrF* and purine metabolism genes *purD* and *purH* were shown to be important for growth in serum, using a vancomycin resistance clinical isolate

[214]. The *pyrK_2* deletion mutant was shown to be attenuated in an intravenous zebrafish infection model [214]. The *S. pneumoniae* gene *purK* involved in purine biosynthesis identified by STM is important for virulence in a septicemic mouse model [226]. In *S. pyogenes* a TRASH screening identified *guaB* whose mutant growth is attenuated in human blood [209]. In *S. aureus*, a screening of mutants in human serum identified *purA* and *purB* purine biosynthesis genes and showed their importance for growth and in a zebrafish model of infection. The precursor of pyrimidines PabA also contributes to survival in human blood and zebrafish [239]. These multiple examples points to the importance of *de novo* nucleotide biosynthesis for survival of bacteria during the blood phase and suggest that it could be a universal mechanism shared by blood-borne infection-causing bacteria.

4.2.3 Metal uptake

Cobalt. In *S. sanguinis* a screening in human serum of individual mutants of energy coupling factor (ECF) family of transporter genes, *ecfA2*, *ecfT*, and *stpA* mutants and the triple mutant had decreased survival in human serum [240]. These genes were annotated as cobalt transporters. Growth of the triple mutant was also reduced in rabbit serum and in a rabbit endocarditis model of infection.

Iron. Iron has been identified as one of the key elements in regulating virulence in pathogens reaching the bloodstream. Bacterial pathogens have evolved to develop highly efficient systems to capture free iron by high affinity binding proteins. In Gram-negative bacteria for example, avian *E. coli* (APEC) *sitABCD* encoding an ABC transporter that mediates uptake of manganese and iron was shown to contribute to virulence in chicken infection models and is attenuated in blood in a competitive infection model [241]. For *S. enterica* the role of the iron transporters *sitABCD* and *feoB* has been shown to be important for virulence when testing both mutants in the mouse model of infection when injected intravenously [242]. In *S. enterica* serovar Typhimurium deletion of the transporter *sitA* demonstrated the role during infection using a mouse model [243]. For the case of *S. marcescens*, a mutant deficient in siderophore serratiochelin production is attenuated in human serum and required for bacteremia [244]. In *N. meningitidis* TbpBA and HpuAB are main mediators of iron acquisition during the early stages of infection, due to their capacity to bind and acquire iron from transferrin and haemoglobin complexes [245]. TbpA is essential for virulence in a mouse model of bacteremia [246]. In *A. baumannii* a TRaDIS screening using a leukopenic mouse model of bloodstream infection allowed to identify *feoB* encoding ferrous iron transporter subunit) and *fepA* encoding ferric enterobactin receptor as important genes for survival in human serum and within macrophages, as well as resistance to antimicrobial peptides [247].

Similarly, Gram-positive bacteria causing bacteremia have developed systems for capture and uptake of iron when they reach the bloodstream. In *S. pyogenes* the streptococcal hemoprotein receptor protein Shr involved in iron uptake, has been demonstrated to be important for iron uptake in a human blood and for virulence in models of skin and systemic infection [248]. A specific mechanism to lyse erythrocytes and obtain iron from the host has been described in *S. aureus*. This has been linked to the leukocidins LukED and HlgAB bicomponent toxins, whose activity is mediated by the Duffy antigen receptor for chemokines (DARC) on erythrocytes. These toxins promote growth of *S. aureus* in a hemoglobin-acquisition-dependent manner and contribute to infection in mice [249].

Magnesium. Magnesium is a divalent cation that has several biological functions, including as an enzymatic cofactor and a neutralizer of negatively charged macromolecules. In Gram-negative bacteria, the role of the magnesium transporter MgtB was identified in *S. marcescens* by an Inseq screening in a murine model of bloodstream infection. The *mgtB* mutant

exhibited decreased growth in defined medium containing low concentrations of magnesium and was attenuated in virulence [217].

Manganese. Manganese is a required cofactor for all forms of life. The bloodstream is a low-manganese environment. Bacteria encode several broadly conserved classes of importers. One major family of Mn importers is the NRAMP (Natural Resistance-Associated Macrophage Protein) family of metal cation transporters. The NRAMP family of proton-powered Mn importers is conserved across all domains of life and is usually named MntH in bacteria (manganese transporter, H⁺-dependent). In Gram-negative bacteria, *N. meningitidis* exports Mn²⁺ via MntX to regulate the intracellular Mn/Fe ratio and prevent manganese toxicity that is exacerbated in low iron conditions. MntX was shown to be important for *N. meningitidis* to resist killing by human serum and for survival in mice blood in a septicemia mouse model following intraperitoneal inoculation [250]. For Gram-positive bacteria, in *S. agalactiae*, a TRaDIS approach allowed to identify the *mtsA* gene encoding a substrate-binding lipoprotein of manganese transporter involved in bacterial growth in both human blood and plasma [229]. The role of Mn²⁺ in the virulence of *B. abortus* has been linked to the MntH protein, since an *mntH* deletion mutant exhibited extreme attenuation in both cultured murine macrophages and infected mice [251]. In *S. sanguinis*, the manganese transporter SsaB has been shown to be important for growth in rabbit serum. A connection with the manganese-dependent superoxide dismutase (SodA) was proposed to be important for *S. sanguinis* response to oxidative stress and in virulence [252]. Additionally, a screening in human serum of *S. sanguinis* mutants identified *ssaA*, *ssaB* and *ssaC* genes which were important for growth in human serum [240]. A previous study failed to demonstrate a role of MntH in *Salmonella* virulence following intravenous infection of congenic 129/Sv Nramp1D169 mice [242]. In contrast, both the MntH and Sit transport systems have been shown to play an important role in *Salmonella* virulence following intraperitoneal infection of C57BL/6-derived mice expressing a functional Nramp1 locus [243].

In *E. faecalis* the ABC-type permease EfaCBA and two Nramp-type transporters, named MntH1 and MntH2, work collectively to promote cell growth under Mn-restricted conditions. The simultaneous inactivation of *efaCBA*, *mntH1* and *mntH2* led to severe growth defects in serum and urine *ex vivo*, significant loss of virulence in *Galleria mellonella*, and virtually complete loss of virulence in rabbit endocarditis and murine catheter-associated urinary tract infection (CAUTI) models. Interestingly, EfaCBA appears to play a prominent role during systemic infection, whereas MntH2 was more important during CAUTI [253]. In *Y. pseudotuberculosis* MntH promotes survival in *G. mellonella* protecting bacteria from the antimicrobial products released during the respiratory burst. [254]. In *S. aureus* deletion of *mntE* triggers accumulation of intracellular Mn, leading reduced tolerance to oxidative stress and decreased virulence during systemic infection suggesting an essential role of MntE in Mn detoxification [255]. In *S. suis* the TroA lipoprotein is required for growth in porcine serum in a manganese dependent manner, counteracting oxidative stress, and is also required for fully virulence in mice [256]. Another study using Tn-seq in *S. suis* also identified the gene SSU1869/TroA showing its importance during septicemia using piglets as model [257].

Zinc. In Gram-negative bacteria, the conserved outer-membrane zinc transporter zinc-uptake component D ZnuD of *N. meningitidis* has been described to be required for efficient systemic infections in a mouse model [258]. This may link ZnuD to a mechanism to overcome nutritional restriction imposed by the host organism during infection. In *Y. pestis*, *irp2*, a gene encoding the synthetase HMWP2 involved in synthesis of yersiniabactin Ybt is required for growth in Zn²⁺-deficient conditions in a *znuABC* mutant. It has been suggested that Ybt may serve as a “zincophore” for Zn²⁺ acquisition and this may depend on the presence of

YbtX [259]. The ZnuABC system and the Ybt synthetase HMWP2 both contribute to the development of a lethal infection in murine septicaemic plague [259].

For Gram-positive bacteria, the role of zinc metabolism seems to play an important role in blood survival. This is the case for *S. pneumoniae* where deletion of two genes *adcA* or *adcAll* reduced *S. pneumoniae* zinc uptake, and a double deletion further decreases zinc import and impairs growth in human serum. Both genes are required for proper cell division and *S. pneumoniae* survival during infection [260]. *S. pyogenes* zinc import genes (Δ *adcA* Δ *adcAll*) and export gene (Δ *czcD*) contribute to growth *in vitro*, *in vivo* virulence models and in human blood [261]. A TRASH screening in human blood allowed to identify genes important for *S. pyogenes* fitness in this clinically relevant environment such as the gene involved in zinc uptake *adcC* [209]. The deletion mutant of *adcC* showed decreased growth in human blood [209]. A screen of mutants in human serum identified *czcD* to have an impact in growth of *S. sanguinis* in human serum [240].

Calcium. In *S. pneumoniae* the gene *caxP* has been shown to be important for survival in a mouse infection model. The *caxP* mutant accumulated intracellular calcium and was attenuated in sheep blood, human plasma and human serum [262].

Sodium. It has been reported that sodium pumps may play a role in the pathogenesis of bacteria surviving in the bloodstream. This is the case for *Y. pestis* Na⁺/H⁺ antiporters NhaA and NhaB whose inactivation abolishes *Y. pestis* virulence, possibly by protecting *Y. pestis* from Na⁺ toxicity in blood [263].

Nickel. Transcriptomics of porcine ExPEC in infected animal bloodstream and in swine blood *in vitro* highlighted upregulation of the nickel transporter NikABCD and its importance for bacterial growth in swine blood and in mice [218].

5 Antimicrobial peptide resistance factors

Antimicrobial peptides (AMPs) are defense components of all living organisms. They are generally broad-spectrum antimicrobials that kill not only bacteria, but also non-enveloped viruses, parasites and fungi. Resistance to AMPs contributes to the subversion of the immune system by bacteria during the blood phase of infection. In many bacteria, AMP toxicity is prevented by the action of efflux pumps. For instance, polymyxin B sensitivity screening of a library of mariner transposon mutants of *N. meningitidis* identified MtrCDE, a multidrug efflux pump that contributes to the intrinsic high resistance to CAMPs [264]. In the highly virulent serotype V CNCTC 10/84 strain of *S. agalactiae*, a TRaDIS approach identified the gene W903_1820 encoding a multidrug export family protein involved in survival in whole blood [229]. It was suggested W903_1820 may confer resistance to killing by human neutrophils and neutrophil-derived antimicrobial compounds, such as α -defensin-1, LL-37, and cathepsin G. Another mechanism of AMP resistance widely used by bacteria is reduction of the negative charge of their surface that prevents electrostatic attraction of cationic defense molecules. This is in part mediated by the *dltABCD* operon and the *mprF* gene responsible for D-alanylation of teichoic acids and/or lysinylation of membrane phosphatidylglycerol, respectively, in bacteria such as *S. agalactiae*, *S. pneumoniae*, *B. anthracis*, *S. aureus* and *L. monocytogenes* [265–271]. In *S. aureus*, this surface charge modification is associated with increased resistance to a number of endogenous cationic antimicrobial peptides, such as α -defensins, and to thrombin-induced platelet microbicidal protein 1 (tPMP-1) and virulence in a rabbit endocarditis model [267]. In *S. agalactiae*, AMPs resistance also relies on the

penicillin binding protein 1a (PBP1a) gene *ponA* as a PBP1a mutant is more sensitive to killing by LL-37, CRAMP and HNP-1 [272]. In *P. gingivalis* OmpA-like proteins were shown to contribute to serum resistance [273] and were later shown to protect against the bactericidal activity of LL-37 but not human β -defensin (hBD). However, LL-37 activity had a positive synergistically effect on hBD bactericidal activity [274].

Reduction in the negative charge of the LPS or LOS lipid A is a common mechanism of AMP resistance among Gram-negative bacteria. The mechanism by which certain strains of *N. gonorrhoeae* resist normal human serum is not fully understood, but alterations in LOS structure can affect such resistance. During an investigation of the biological significance of phosphoethanolamine (PEA) extensions from LOS, it was found that loss of PEA substitution from the lipid A of LOS, due to insertional inactivation of the *lptA* gene encoding a PEA transferase, resulted in increased gonococcal susceptibility to polymyxin B and suggested that serum killing of the *lptA* mutant may occur through the classical complement pathway [275]. In *N. meningitidis*, fHBP is involved in resistance to killing by the antimicrobial peptide LL-37 [276] besides its aforementioned main role in complement inhibition. Two hypothetical genes in *N. meningitidis* serogroup B (NMB0741 and NMB1828) were identified to play a role in resistance to AMPs such as CRAMP and LL37 *in vitro* and also affected the capacity to cause bacteremia in an *in vivo* mouse model [277]. In *V. vulnificus* the *trkA* potassium transport gene was shown to be involved in resistance to AMPs such as protamine or polymyxin B, serum and important for virulence in mouse models of infection [278]. In *S. enterica* Typhimurium also the *sapG* potassium transport gene contributes to protamine resistance [279] and virulence in a mouse model of infection [280]. Interestingly, *Salmonella* exposure to sublethal doses of AMPs caused mutations in the genes *pmrB*, *waaY* and *phoP*. AMP resistance elicited by these mutants was not associated with reduced fitness and questions the therapeutic use of AMPs in clinical settings that might select more virulent mutants that are cross-resistant to host defense peptides [281]. In *A. baumannii* a TRaDIS screen using a leukopenic mouse model identified a mutant in the gene *pntB* encoding a subunit of the pyridine nucleotide transhydrogenase which had increased sensitivity to human serum, macrophages, and antimicrobial peptides killing [247]. Another sensitive mutant identified by this study is the gene *ddc* encoding a d-Ala-d-Ala-carboxypeptidase involved in peptidoglycan biogenesis. AMP resistance mechanisms also include AMP trapping, proteolytic AMP degradation, regulation of host AMP production and involve regulators of bacterial determinants (see following sections).

6 Bacterial factors contributing to bloodstream infection through unknown mechanisms

There are still many genes in the bacterial world without known functions or that are considered as encoding hypothetical proteins. Some screens in bacteria have identified some genes of this type to be essential for survival in the bloodstream during the bacteremic phase of infection. Although their functions are not well known these proteins may represent important candidates for further investigation of mechanisms involved in contributing to blood survival. Here we introduce genes encoding both hypothetical proteins and proteins of unknown functions for which targeted deletion mutants have been produced and functional experiments have been performed in *ex vivo* and *in vivo* models. In *E. coli* by using an IVET screening *in vivo*, different genes were identified to be induced during the septicemic phase. Mutants of the open reading frame (ORF) of unknown function *o761*, the *ivi817* (with no similarities to sequences deposited in Genbank) and the gene *ycjF* that encodes a hypothetical protein were attenuated in a mouse model of septicemia using a competitive infection model [211]. Additionally, the mutant of ORF V encoding a protein similar to ser-

ine threonine protein phosphatase was also attenuated in an *in vivo* model of septicemia but without a mechanism described [211]. Later, in UPEC, the repeat-in-toxin (RTX) protein TosA has been linked to lethality during sepsis. A *tosA* deletion mutant was shown to be attenuated in a mouse bacteremia model [282]. A microarray study of APEC in blood isolated from infected chicken identified the gene *sodA* encoding a superoxide dismutase, which was necessary for virulence in the chicken infection model [283].

In the case of Gram-positive bacteria, a microarray study analyzing *S. aureus* transcriptome in response to human serum and whole blood allowed the identification of a gamma-hemolysin as an important factor for survival in blood. The deletion mutant of the three genes coding for gamma-hemolysin subunits ($\Delta hlgABC$) was less virulent compared to the wild type in a bacteremia model of mice and the mutant strain had reduced survival in human blood [180]. In *S. sanguinis* a screening of individual mutants in human serum has allowed to identify two genes, ΔSSA_0048 and ΔSSA_2241 , that were defective in growth in human serum and in the endocarditis mouse model [240]. Both genes are annotated as encoding hypothetical proteins and further studies will be required to determine their specific roles for survival in blood. This group of genes, encoding proteins of unknown functions and hypothetical proteins, needs further investigation to dissect the molecular mechanisms involved in the attenuated phenotype during the bacteremic phase of infection.

6.1 Cell surface

Regarding the role of proteins involved in stability and functionality of the cell surface, some genes and their potential mechanisms in blood survival have been described. In Gram-negative bacteria, for *S. enterica* serovar Typhimurium the deletion of the gene *pbgA* makes *Salmonella* more sensitive in the mouse bacteremia model. The role of this protein seems to be related to enhancing OM integrity while promoting bacteremia in a mice model. This effect is suggested to be done by influencing the LPS assembly to survive during stress conditions such as facing the bloodstream [284]. In *N. meningitidis* the hybrid protein peroxiredoxin Prx5-grX is a surface exposed protein containing domains involved in antioxidant response. This protein has been shown to interact with plasminogen and this interaction was affected by a single residue substitution in the C-terminal domain. The mutant was more resistant to hydrogen peroxide. The deletion mutant of *pxn5* and *grx* has a defective growth in human blood and indicating a potential role in bacteremia [285]. The mechanism is not clear since it is not explained by plasminogen binding and higher sensitivity to hydrogen peroxide [285]. In the case of Gram positive bacteria, in *S. aureus* a STM screening allowed to identify genes required for virulence in a murine model of bacteremia [210]. Mutations in *femA* and *femB* are involved in the formation of cell wall peptidoglycan pentaglycine cross-bridges which are critical for the survival and replication of this pathogen in blood [210]. The gene *lsp* encoding the *S. aureus* prolipoprotein signal peptidase was identified to be important for virulence in a bacteremia model. The role of this protein may be related to the maturation process of membrane lipoproteins [210]. In the same screening another gene P9B66 encoding the MsrA-peptide methionine sulfoxide reductase, was shown to be important in the maintenance of adhesins on the bacterial surface and in virulence in a mouse bacteremia model [210]. In *S. suis* *penA* (also known as PBP2B), a gene involved in peptidoglycan synthesis, was shown to be important for growth in porcine sera. The deletion of *penA* may affect the function and/or exposure of virulence determinants attached to the cell wall to be important during septicemia [257]. The *S. suis* protein SspB is a surface protein dependent on the YSIRK-G/S directed translocation and is upregulated during the bloodstream infection in the mouse model. The deletion mutant of this gene was attenuated in *in vivo* and its survival in blood was compromised. The clear mechanism is not well understood but may not be linked to complement resistance, since initial studies demonstrated no role in

cleaving C5a [194].

6.2 5.2. Pilus

The pilus is a filamentous structure formed by protein subunits with a dynamic mechanism whose main function is adhesion to host surfaces and bacteria-bacteria interaction. Pili are mainly present in Gram-negative bacteria but are also present in some Gram-positive bacteria and its role in bacteremia are discussed in the following lines. In Gram-negative, a TraDIS screening of *E. coli* mutants in human serum identified the gene *traL*, involved in pilus assembly, to be necessary to resist human serum and virulence in the mouse model [154]. Another example of the role of pilus in bacteremia is the case of *N. meningitidis*, in which the genes involved in the type IV pili (TFP), *pilU* and *pilT*, were shown to be important for blood survival in the mouse model [286]. Contrary to the *in vivo* phenotype, the loss of *pilU* significantly increases bacterial survival in normal human serum and as stated by the authors the ability to control *pilU* expression may be important during the invasion of the bloodstream [286]. Also in *N. meningitidis*, a comparative proteomic analysis of bacteria isolated from different infected niches of mice identified *pilQ* encoding an inner membrane protein dehydrogenase, a type IV pili gene, whose deletion mutant was shown to be defective in growth in blood of mice [172]. More recently, in *N. meningitidis* the role of type IV pili was evaluated in a humanized mouse model of bacteremia. It was reported that the functional retraction of TFP is essential to promote sustained bacteremia [287].

In Gram-positive, in non-encapsulated strains of *S. pyogenes*, the pilus promotes survival in human blood and increased virulence in murine models of invasive infection [288]. In *S. agalactiae*, the contribution of a specific pilus type, type 2b in a ST-17, shown to contribute in survival in the bloodstream in an *in vivo* mouse model. This contribution was not correlated with opsonophagocytosis resistance [289]. In *S. pneumoniae*, pilated strains and mutants are more virulent and induce a stronger host inflammatory response in murine bacteremic infection model [290]. In *S. agalactiae* the role of pilus subunit PilB was evaluated for the role in pathogenesis and bacteremia [291]. The *pilB* deletion mutant is shown to be more susceptible to killing by macrophages and neutrophils. Also the deletion of *pilB* affected survival in the bloodstream and virulence in a mouse model of infection [291]. Additionally, the role of *pilB* in resistance to antimicrobial peptides such as mCRAMP and LL-37 has been also reported. Although the role of pilus in contributing to bacteremia is not shown to be widespread in bacteria infecting the bloodstream, a combination of mechanical/functional as well as molecular interactions of pilus with components of the innate immune response are occurring and additional research is needed to extend the knowledge of this bacterial structure in the bacteremic phase.

6.3 Biofilms

Biofilms are microbial communities that are organized in a specific manner and structured with extracellular material released by bacteria in order to form a support for the development of the bacterial community. There are not many bacterial factors linked to biofilm formation reported to play a role in bloodstream infection. A few examples are represented for Gram-negative bacteria. *Haemophilus parasuis* genes *galU* and *galE* were shown to be involved in serum resistance in porcine sera. A *galU* mutant is unable to form biofilm and auto-agglutinate, but a *galE* mutant produces more biofilm. GalU plays a role in autoagglutination and biofilm formation but the role of GalE may be affecting biofilm formation in an indirect way [292]. For Gram-positive bacteria, in *E. faecalis* the analysis of the gene *bgsA* (biofilm-associated glycolipid synthesis A) encoding a putative glucosyltransferase whose mutation affects structure of cell membrane and cell wall. The deletion of this gene affected

biofilm formation and was also affected in survival in the mouse model of bacteremia [293]. Further investigation of bacterial factors playing a role in biofilm formation during the bacteremic phase is needed.

7 Bacterial regulatory mechanisms involved in bloodstream infection

7.1 Two component systems

Two Component Systems (TCS) play an important role in sensing the environment that bacteria face during the infection process and help to modulate its response to it. As bacteria reach the bloodstream, they sense signals to adapt rapidly by deploying mechanisms to block the different components of the immune response and adapt their metabolism. Thus, TCS activate expression of virulence factors important for immune evasion and modulate biosynthetic pathways. TCS are normally composed of one sensor histidine kinase (SHK) anchored to the membrane and a transcriptional regulator activated by the SHK and acts as a transcriptional activator or repressor of target genes. Among the Gram-negative bacteria, some examples of the role of the TCS in adapting to the bloodstream have been described. For instance, in the case of *P. aeruginosa*, the PhoP/PhoQ TCS that senses Mg²⁺ concentration is shown to be involved in the regulation of the expression of OprH, a protein that binds complement factor C3 inhibiting humoral response. By regulating the level of expression of this protein, PhoP/PhoQ can impact the response to opsonophagocytosis, promoting survival in blood and consequently having a positive impact on virulence [294]. Also, in *P. aeruginosa* the transcriptional regulator SoxR, part of the SoxRS TCS, acts as autorepressor that was identified in a screening based on the IVET expression system in a burned mouse model. The deletion mutant of *soxR* is shown to have a delay in causing infectivity and systemic infection. This mutant was also more sensitive to killing by macrophages [295]. In *H. influenzae* the *arcA* mutant, part of the TCS ArcAB involved in oxygen-dependent regulation, showed markedly reduced survival compared to its parental strain in human blood or serum [296]. Also this mutant was impaired in the capacity to cause disease in the mouse septicemia model [296]. Later, the role of ArcA has been related to complement resistance since ArcA can modulate the expression of *lic2B*, a gene encoding a glycosyltransferase required for addition of a galactose residue to the outer core of LOS. The deletion of *lic2B* affects survival in bacteremia mouse models and also resistance to the classical pathway from the complement in serum [297]. In the case of *N. meningitidis* serogroup C, the deletion of PhoP, the regulator of the TCS PhoP/PhoQ, impairs the capacity to grow in mouse serum but not sensitivity in human serum and is not attenuated in the mouse model. A *phoP* mutant in *N. meningitidis* is hypersensitive to human defensin HNP-1 [298]. Another study using *N. meningitidis* serogroup C, showed that the *phoP* mutant was attenuated in the mouse model of meningococcal infection and had increased sensitivity to polymyxin B [299]. Later, the possible explanation for the role of this TCS in *N. meningitidis* serogroup B was established since the deletion of the TCS *misR/misS* (homolog to PhoP/PhoQ) increases the level of capsule production and also the resistance to bactericidal activity in normal human serum [300]. Later, up-regulation of this system in adaptation to bacteremia phase was confirmed in human blood [77]. For the case of extra-intestinal *E. coli* (ExPEC) the TCS Rcs has been shown to mediate serum resistance through regulation of the EPS colanic acid production. This is a mechanism by which ExPEC may get protection while cell wall damage caused by serum components is repaired [27]. For the TCS EnvZ/OmpR in *Y. enterocolitica* (serotype O:9) the strain lacking OmpR exhibits extremely high resistance to the bactericidal activity of normal human serum (NHS) compared with the wild-type strain. This

effect was reported to be linked to the regulatory action of OmpR on Ail and OmpX, two homologous outer membrane proteins (OMPs) of *Y. enterocolitica*. It was proposed that OmpR might alter the susceptibility of *Y. enterocolitica* O:9 to complement-mediated killing through remodeling of the outer membrane [301]. In *A. baumannii*, the hyperproduction of capsular EPS is induced by exposure to low concentrations of antibiotics. This hyperproduction was mediated by the locus K (capsule) and regulated by the TCS BfmRS. This hyperproduction of the capsule promotes resistance to killing by complement and is translated into a higher virulence in a mouse infection model [302].

For Gram positive bacteria, the role of TCS in blood survival has been well characterized in *S. aureus*. SaeR/S TCS has been identified by a DNA microarray study and the mutant shown to play a role in resistance to human blood survival and virulence in an in vivo model [303]. In a later study, the genes encoding the TCS were shown to be upregulated in a transcriptome analysis of *S. aureus* grown in human blood and human serum [180]. More recently, it has been described the role of this TCS in the regulation of coagulase Coa, a protein able to convert host prothrombin to staphylothrombin, leading to activate the protease activity of thrombin and causing localized clotting, which is hypothesized to protect *S. aureus* from host immune response, as a consequence impacting the survival of *S. aureus* in the bloodstream [304]. This TCS was only upregulated in the blood condition, which is in accordance with the role of this TCS in opsonophagocytosis previously reported. AirS/R, another TCS in *S. aureus*, has been involved in blood survival possibly through the regulation of virulence factors such as SspA, SppB and SspC [305]. These proteases are involved in the inhibition of *S. aureus* killing by professional phagocytes. AirS/R has been also linked to the regulation of staphyloxanthin, which confers antioxidant properties and survival in human blood [190]. Also the role of the TCS AgrAC in regulating the expression of the operon *agr* in response to human serum was studied. The downregulation was linked to the response to a quorum sensing (QS) signaling molecule called AIP (autoinducing peptide). The downregulation process seems to be mediated by a component of human serum such as apolipoprotein B, which could represent a mechanism of the innate immune response [306]. This downregulation could be inhibited mainly by the constitutive expression of the AgrC sensor. The relevance of this observation is to show the possibility of natural occurring mutants in the component of the AgrAC TCS that could lead to constitutive expression of the *agr* operon and consequently lead to hypervirulent strains [306]. Also, the AgrAC TCS seems to play a role in modulation of the adaptation of *S. aureus* in the autophagosome influencing the bacterial response to phagocytic activity and promoting bacterial dissemination in a model of systemic infection [307]. It may also play a role in the regulation of capsule expression impacting the survival during the bacteremia phase [307]. Another TCS in *S. aureus*, ArlRS, is shown to be involved in the regulation of the agglutination mechanism during exposure to human plasma or fibrinogen. The action of this TCS was reported to be related to the *ebh* gene, encoding the giant staphylococcal surface protein (GSSP), acting as a negative regulator whose expression is increased in the TCS deletion mutant [308]. By using a rabbit combined model of sepsis and endocarditis it was shown to have an important role in the agglutination affecting the pathogenesis during the bacteremia phase [308]. In *S. pneumoniae* serotype 2 by a transcriptomic analysis, the TCS 09 ZmpRS has been recently linked to the regulation of carbon metabolism and consequently modulating capsule expression indirectly [309]. Later, it was demonstrated that TCS09 enhances robustness during dissemination in the host by maintaining bacterial fitness in a *S. pneumoniae* serotype 4 strain. This was demonstrated by deleting the genes and using a mouse model of co-infection suggesting the role in keeping metabolic fitness and resistance under *in vivo* conditions [309]. In the two previous reports studying different serotypes this indicates that TC09 could have a regulatory role in a serotype specific manner. For *S. pyogenes*, the TCS CovR/S has been also shown to be involved in blood survival. The deletion of *covS* has an

impact in the capacity of *S. pyogenes* to survive in blood in a strain-dependent manner [310]. It seems that CovR/S modulates the expression of capsule and virulence factors involved in complement resistance [310]. Also, CovR has been shown to be important for survival in human blood in *S. mutans*. The deletion of *covR* reduces susceptibility to C3b deposition [311]. This susceptibility seems to be mediated by the interaction with glucans from EPS and also decreases phagocytosis and killing by neutrophils. The deletion increases bacteremia in a rat model of bacteremia and infective endocarditis [311]. In *S. mutans* the role of the two-component systems VicRK and CovR has been linked to the regulation of the protein PepO, protein involved in immune evasion and affects resistance in the human whole blood [312]. For *S. agalactiae*, the response regulator CiaR, part of TCS CiaRH, has been shown to have an impact in blood survival most likely through a role in intracellular survival within neutrophils and murine macrophages [313]. Also the mutant of *ciaR* showed an increased susceptibility to killing by antimicrobial peptides, lysozyme, and reactive oxygen species [313]. In *S. agalactiae* a single eukaryotic-type serine/threonine kinase (Stk1) is reported to play a role in adaptive response of these bacteria to the bloodstream. The *stk1* mutant is shown to be more sensitive to human whole blood, phagocytic mediated killing by neutrophils and oxidative stress. It has been shown that this effect may be due to the positive regulation of Stk1 on β -haemolysin expression (β -H/C). This effect on β -H/C by Stk1 may be regulated also by the transcriptional regulator CovR, which is part of the TCS CovR/S [314]. In *S. suis* a screening of mutants in mouse macrophages identified WalR, the transcriptional regulator of the TCS WalRK, involved in resistance to phagocytosis. The *walR* mutant was shown to have an attenuated phenotype of virulence in a mouse model, and the effect may be related to the regulation of a target gene (HP1065) that shares some degree of homology with PspA from *S. pneumoniae* which has a role in complement resistance [315]. More recently in *S. suis*, the role of the Stk (eukaryotic-like serine/threonine kinases) and Stp1 (eukaryotic-like serine/threonine phosphatases) has been studied. Stk and Stp1 have been shown to regulate capsule production and the translocation of virulence factors [316]. Mutants of these two genes were easily phagocytosed by murine macrophages, *stk* mutant showed reduced survival in macrophages compared to *stp1* mutant that showed increased survival. This may be due to the increase of capsule thickness, *stk* deletion showing increased secretion of suilysin. Although showing differences in survival in phagocytes, both mutants showed reduced survival in pig whole blood and also were attenuated in the mouse model [316]. More research is needed to complete the role of other TCSs in bacteremia causing infections and in particular the cross talks between TCS. In relation with signal transduction, in *L. interrogans* a Tn-seq approach of infected hamsters identified a putative adenylate/guanylate cyclase gene (*lic12327*), whose deletion affected the survival in blood indicating that cyclic nucleotides may play a role during the bacteremia phase [317]. The mechanism on the factors affected by this mutation need further investigation.

7.2 Transcriptional regulators

Transcriptional regulators control the gene expression of virulence determinants. The role of transcriptional regulators that play a role in survival in the bloodstream are described in the following section. In Gram-negative bacteria different transcriptional regulators playing a role in the bacteremia phase have been identified. In *E. coli* K1 strains, *rfaH* was identified in a TRaDIS screening *in vivo*, and showed to prevent capsule expression [154]. The loss of this gene seems to have a more profound effect on the surface topography of *E. coli*, as this transcriptional antiterminator is required for the expression of operons that direct the synthesis, assembly, and export of LPS core components, pili, and toxins in addition to the capsule. The interruption of *rfaH* impaired the growth in normal human serum and also in the neonatal rat model [154]. For another *E. coli* K1, UPEC, a TRaDIS screening has allowed to identify

regulatory mechanisms for expression of genes involved in capsule synthesis, such as the transcriptional regulators MrpA and LrhA. These can directly impact the capsule production and survival in human whole blood without affecting the production of LPS [318]. The deletion of *mprA* decreases the production of the capsule, while the overexpression of *LrhA* has the same effect. These effects on regulation of MprA and LrhA on capsule production seem to be conserved among different strains and are not dependent on the type of capsule [318]. Another experimental strategy, as is the TRADISort (based on gradient centrifugation and TRADIS) has revealed the complexity of regulation of capsule expression in *K. pneumoniae* [319]. By this approach MprA is described as a regulator of capsule since the *mprA* mutation increases its production [319]. In this case, the *mprA* deletion has an opposite effect compared to what is described for its homologous gene in *E. coli* (UPEC), since *mprA* deletion increases rather than decreases capsule production [318]. Additionally, in *K. pneumoniae* the mutation of the transcriptional regulator/antiterminator RfaH showed a defect in capsule biosynthesis and the incubation of the *rfaH* mutant in serum demonstrated a significant loss of viability [227]. It seems that RfaH mediates resistance to complement-mediated serum killing and is also important for maximal growth in iron-limited serum [227]. Also in *K. pneumoniae*, the regulator KbvR seems to be involved in the modulation of defense against macrophages. A transcriptome analysis shows that KbvR may modulate the capsule production and some outer membrane proteins. The KbvR mutant is more susceptible to killing in human serum and also sensitive to antimicrobial peptide LL-37 anti phagocytosis assay and in animal infection [320]. Other Gram-negative bacteria such as *V. vulnificus* undergo phase variation among colonies, including a virulent opaque form which produces capsular polysaccharide (CPS) and a translucent phenotype that produces little or no CPS [321]. The mutant defective for RfaH antitermination control showed a diminished capacity to undergo phase variation and displayed significantly reduced gene expression of the CPS operon. Moreover, the *rfaH* mutant produced negligible CPS and was highly sensitive to killing by normal human serum, thus suggesting that *rfaH* is likely to be essential for virulence [321]. For the regulation of iron uptake, some insight has been made for heme uptake by the IscR transcriptional regulator in *Y. pseudotuberculosis* during the blood phase. The *Y. pseudotuberculosis* Δ *iscR* mutant has a survival defect when incubated in whole blood, in which iron is sequestered by heme-containing proteins [322]. This phenotype was independent of the Hmu system, the type III secretion system, complement, and the ability of *Yersinia* to replicate intracellularly. This suggests that IscR regulates multiple virulence factors important for *Y. pseudotuberculosis* survival and growth in mammalian tissues eliciting a complexity of heme uptake expression and function under different iron conditions. In *E. coli* (ExPEC) the transcriptional regulator Fur, controlling iron uptake, seems to be the central regulator for serum resistance. This was confirmed by a transcriptome analysis, proteomic analysis and functional growth of mutants in human serum showing that this response to serum is most likely through the regulation of iron metabolism [323]. In swine ExPEC a the FNR deletion mutant as important for survival in the bloodstream, indicating that the central carbon metabolism and anaerobic respiratory chain are important for fitness in the bloodstream [ma](Ma et al., 2020). In porcine ExPEC a transposon mutagenesis screening identified important genes for survival in swine serum. The role of regulators such as Fur, FNR, HyxA and HyxR was tested in a mouse model of infection [162]. HyxA and HyxR contribute to porcine ExPEC fitness in swine serum and full virulence in mice. This may be related to modulation of O-antigen chain length as has been reported in UPEC [157] and may be linked to the response against the innate immunity [162]. In the case of FNR, it was required for bacterial fitness both in active and inactive swine serum suggesting that the role of FNR may be more involved in response to nutritional limitations. On the contrary Fur was only required for growth in active serum suggesting that Fur may be involved only against the innate immunity from complement system. For *V. vulnificus* by using the IVIAT technology

using convalescent-phase human serum, the transcriptional regulator HlyU was identified to be one of the master regulators of *in vivo* virulence expression [235]. HlyU is a transcriptional regulator and seems to control the production of a potent hemolysin/cytolysin (VvhA) and also the elastolytic protease, another exotoxin produced by *V. vulnificus*, was also significantly decreased in the mutant [235]. The identification of the HlyU regulator by the IVIAT approach could indicate the importance of this gene in the bloodstream phase. Also in *V. vulnificus*, the mutant of the transcriptional regulator Lrp is defective for growth in mouse serum and in the mouse model. This effect does not compromise its antiphagocytic ability [324]. It is suggested that Lrp could mediate the phenotype of serum resistance through the regulation of the iron acquisition and virulence by modulating chemotaxis [324]. In *A. actinomycetemcomitans* an RNA-seq analysis and functional reporter assay identified rpoE (σ E), a sigma factor, as potential regulator of an unknown factor that interacts with a host protein ApoA1. This interaction must be linked to a non-identified factor that could potentially have a role in complement resistance [325]. Later by another transcriptomic analysis *ex vivo* the role of Fur for survival of *N. meningitidis* in human blood was established since the mutant was impaired [77]. Also the transcriptomic response to glucose identified the role of HexR in response to glucose. Glucose is a carbon source abundant in the bloodstream. The study identified the HexR regulator as a repressor that can affect the expression of central carbon metabolism. The mutant *hexR* was not be able to establish bacteremia in an infant rat model [326]. In Gram-positive bacteria transcriptional regulators also play an important role in adapting the bacterial mechanisms to survive in the blood . Recently *S. aureus* Rsp has been shown to play a role in the transition between colonizing stage to bacteremia. This regulator modulates the transcriptional regulator Agr and consequently have an impact in the transition of *S. aureus* from a colonizing isolate to one that causes bacteremia [327]. Agr modulates the production of traditional virulence determinants with opposite consequences for antibiotic tolerance and its ability to survive immune attack and cause disease. Also in *S. aureus* a transcriptional regulator responsible for Mn homeostasis plays an important role in virulence through the control of transcriptional repression of the operon *mntABC* and induction of *mntE*. The deletion of *mntR* has been shown to be critical for the *S. aureus* pathogenesis in a model of systemic infection [255]. In *S. aureus* a LysR-type transcriptional regulator (LTTR) was identified by a Tn-seq analysis in a metastatic bloodstream infection model [328]. Under induction control of the LTTR regulator, it was possible to identify the target genes. This regulator targets branched-chain amino acid biosynthesis, a methionine sulfoxide reductase, and a copper transporter as well as decreases transcription of genes encoding urease and components of pyrimidine nucleotides. This regulator seems to be repressed by glucose and depends on copper ions and additional *in vivo* data is needed to confirm the role in bacteremia [328]. For *S. pneumoniae* the role of IDTR (iron-dependent transcriptional regulator) in virulence has been described. The *idtr* mutant was significantly attenuated in a mouse model of sepsis induced by either intranasal or intravenous infection. The lack of *idtr* markedly attenuates the ability of *S. pneumoniae* to invade and cause fatal bacteremia from the nasopharyngeal epithelial surface suggesting modulation of pneumonia virulence [329]. For *S. agalactiae* a Tn-seq approach in the presence of human amniotic fluid allowed to identify a GntR-class transcription factor, MrvR, that conferred a significant fitness benefit to *S. agalactiae* in amniotic fluid. In a sepsis model the *mrvR* deletion mutant showed significantly decreased lethality. Furthermore RNA-seq on wild type and *mrvR* deletion strains in *S. agalactiae*, revealed that the transcription factor affects the expression of genes involved in nucleotide biosynthesis and salvage pathways that were highly represented among the set of differentially expressed genes. This suggests that MrvR may be involved in regulating nucleotide availability thus promoting virulence *in vivo* [330]. Also in *S. agalactiae*, the XtgS transcriptional regulator has been reported to play a role as a negative regulator. The mutation of this regulator increases bacterial survival in host blood

and animal challenge tests. The action of this transcriptional regulator may be through the repression of the gene *pseP*, encoding a SEC10/PgrA surface exclusion domain-containing protein with an LPXTG motif that needs further investigation [331]. In this study the phenotype was analyzed in a zebrafish model and in mice. The mutant survived more in the mouse blood and zebrafish blood ex vivo [331]. In the case of *S. pyogenes* Ralp3 (RofA-like protein regulator type 3) central regulator in the ERES pathogenicity island, contributed to survival in human blood and serum and to hyaluronic acid capsule production. SpeB (cysteine protease) shown to decrease in the *ralp3* mutant. Transcriptomics of wild type versus *ralp3* mutant showed the differential use of carbon sources in the *ralp3* mutant and showed that the effect of this mutant is a serotype-specific transcriptional regulator [332]. The effect of *ralp3* may be connected to regulation of proteins that mediate antiphagocytic resistance and capsule synthesis. In *S. pyogenes* a TRASH analysis in human blood approach has allowed the identification of the transcriptional regulator from the LysR family, CpsY [209]. Deletion of *cpsY* gene is important for *S. pyogenes* fitness in a clinically relevant environment since it has been attenuated in human blood [209]. Also CpsY was identified in *S. aniae* to be important in survival in a human blood. The contribution of CpsY could be mediating by resistance to neutrophils [333]. In *E. faecalis*, BopD, a sugar binding transcriptional regulator, seems to be important for biofilm formation and deletion mutant of this gene was impaired in the capacity to survive in the bloodstream in a mouse model when injecting the mice intravenously [334]. Clearly, the mechanisms of control of gene regulation in bacteria to adapt to the bloodstream are variable and each regulator can target different specific bacterial factors or have pleiotropic effects. More investigation is needed to completely dissect the common and specific mechanisms among the bacteria during the bacteremia phase of infection.

7.3 Phase variation

Phase variation refers to the mechanism by which bacterial organisms regulate the expression of certain groups of genes rapidly and in a reversible manner, either on-off switching or modulating the expression of multiple allelic variants. The presence of phase-variable genes allows a population of bacteria to generate a number of phenotypic variants, some of which may be better suited to either colonizing certain host niches, surviving a particular environmental condition and/or evading the immune response. Genes under phase-variable control typically encode bacterial surface structures, such as adhesins, pili, capsule and lipooligosaccharide (LOS). These structures can potentially have a role in blood survival of pathogenic bacteria. An example of phase variation impacting resistance to innate immune response in the bloodstream is the case of the regulation of the modification of LOS by PCho (phosphorylcholine) in *H. influenzae*. PCho is acquired from the host through the *lic* operon, which is controlled by phase variation. It has been suggested that by regulating the LOS modification of PCho to lower levels, this modification decreases the amount of the complement factor C3 that can be deposited on the bacterial surface, thus increasing survival in serum [335]. For the case of non-typeable *H. influenzae* (NTHi) the gene *lpsA* encoding glycosyltransferase has been reported as phase variable. This is due to the truncation of the gene that translates into a phase off. This modification has an impact by decreasing resistance to serum survival [336]. In NTHi the phase variable DNA methyltransferase ModA10 gain or loss of repeats can lead to on or off state. The mutant of *modA10* was tested in vivo and the mouse had less bacteria in blood but the fatality rate was greater. Potentially this phase variable gene can modulate genes that can have an impact in the increase of virulence of NTHi [337]. For the case of *N. meningitidis*, the most frequent change in serogroups B strains is phase variation in the gene *siaD*, which encodes the sialyl transferase involved in capsule synthesis. Other genes in sialic acid biosynthesis or export of the capsule can

be inactivated by an insertion sequence IS1301 (transposon) [338]. Recently, it has been shown in *N. meningitidis* serogroup C that the insertion of IS1301 into the *sia/ctr* IGR (intergenic region) leads to upregulation of capsule expression and enhanced resistance against complement mediated lysis [339]. Insertion and excision of IS1301 into *siaA* causes phase-variation of capsule biosynthesis and this is most likely occurring *in vivo* during bacteremia [339]. In *N. gonorrhoeae* the regulation of *lptA*, involved in Phosphoethanolamine (PEA) decoration of the lipid A in LOS, has been proposed to go through phase variation by the identification of high-frequency mutations in a polynucleotide repeat within *lptA*. This can translate into a stop codon and consequently shift between an state off and on and then influencing gonococcal resistance to cationic antimicrobial peptides (CAMPs) [340]. In the case of *S. enterica* serovar Typhi the O-antigen side chain of the LPS can be modified by the activity of the glycosyltransferase *gtr* operons. The glucosylated form of the O-antigen enhanced survival in human serum by decreased complement binding. It has been described that a single nucleotide deviation from an epigenetic phase variation signature sequence rendered the expression of the *gtr* operon uniform in the population. In contrast, the expression of the acetylating *gtrC* gene is controlled by epigenetic phase variation [341]. For Gram positive bacteria, the role of phase variation in controlling factors important for blood survival have been described in *S. pneumoniae*. The level of capsule polysaccharide and teichoic acid can be regulated through phase variation [342], where a phenotype with more capsular polysaccharide and less teichoic acid could translate into a more virulent phenotype. In this context survival in the bloodstream during the septic phase may be promoted [342]. Furthermore, the modulation of the capsule in *S. pneumoniae* has been seen through the regulation of tandem duplications within the *cap3A* gene of the type 3 capsule locus. The transition between the off (duplication) and on (no-duplication) state depends on the reversion of the duplication [343]. Although this phase variation mechanism has not been demonstrated *in vivo*, it is possible that this mechanism can be activated during the blood phase of infection. These represent examples of genes regulated by phase variation, but since many other genes implicated in combat the host immune response have been described, it is more likely that some of them use this mechanism to obtain plasticity and adapt better to resist and proliferate in the bloodstream.

7.4 Small RNAs

Small RNAs are ubiquitous regulators in all three domains of life. Bacteria employ small RNAs ranging from 50 to 500 nucleotides for posttranscriptional regulation. These sRNAs fold into diverse structures and act on downstream gene targets with different molecular mechanisms. One of the major mechanisms of sRNA-mediated regulation in bacteria is direct binding of the sRNA via base pairing to a target mRNA. A bacterial single sRNA can play a central regulatory role in controlling multiple gene targets leading to a global regulation effect. By this way, bacteria adapt to environmental stress quickly by regulating post-transcriptional responses. Recently a sRNA, sRNA-17, has been identified in *E. coli* K1 to have an impact in genes related to blood survival. This sRNA is linked to the transcriptional regulator ArcA (component of the TCS ArcAB) which downregulates the sRNA-17 expression to benefit bacterial survival in blood and penetration of the blood–brain barrier. The functional analysis of the deletion of sRNA-17 using a bacteremia mouse model showed that this deletion promotes survival in the blood. Thus, the loss of this sRNA explains the mechanism of this phenotype by increasing the regulation of genes involved in amino acid transport and metabolism that promote the growth in blood [344]. For *N. meningitidis*, a tiling microarray approach of bacteria incubated in whole human whole blood allowed the identification of several sRNA differentially regulated in response to this condition. Four sRNAs shown to be important to cause bacteremia when tested in an infant rat model of bacteremia

[345]. One sRNAs denominated Bns1 is linked to a GntR-like regulator and seems to be part of a common network that responds to carbon source availability and energy metabolism and as consequence having an impact in blood survival [345].

In Gram-positive bacteria, *S. pyogenes* sRNA MarS' for Mga-activating regulatory sRNA regulates the expression of Mga (a transcriptional regulator) that regulates positively capsule expression and negatively the antiphagocytic M protein [346]. Deletion of this small RNA is shown to have a negative impact on survival in human blood that may be related to the lack of M protein and susceptibility to neutrophil clearance [346]. On the opposite side the virulence in a sepsis model *in vivo* is increased. This contradictory observation may be explained by the differential regulation of adhesion molecules such as M protein and fibronectin binding proteins (SfbX49 and Sof) thus decreasing adherence to keratinocytes but can promote dissemination *in vivo*. This sRNA seems to be conserved in many streptococci and could be a shared mechanism of gene regulation among different *Streptococcus* species [346]. A combination of RNA-seq and Tn-seq analysis in *S. pneumoniae* [347] has allowed the identification of several sRNAs important for virulence. The sRNAs named F41, R12 and F25 shown to be important specifically for survival in blood using an infection model of sepsis [347]. The F41 sRNA seems to have an effect on the regulation of an putative ABC transporter involved in carbohydrate transport but functional data is necessary to confirm this link. In *S. pyogenes* the small RNA FasX regulates the expression of pili and the thrombolytic agent streptokinase. The mutation of the small RNA FasX decreases the expression of pili and also regulates the expression of streptokinase that catalyzes the activation of human plasminogen into the protease plasmin that can process several enzymes to degrade blood clots and activate metalloproteinases and collagenases. The FasX regulates the virulence since it was observed in the bacteremia model of mice expressing human plasminogen. The effect of the small RNA FasX on regulation of pili and streptokinase is serotype dependent [348]. FasX regulates negatively the expression of pilus but acts as a positive regulator of streptokinase. Although these sRNAs seem to play an important role in virulence and survival in the blood, the precise mechanism of regulation and the complete map of gene targets still need to be revealed.

7.5 Thermosensors

The definition of thermosensors includes protein, DNA and RNA that can be potential controllers of gene expression in different bacterial pathogens in response to changes in environmental temperature. Regarding thermosensors in controlling gene expression of bacteria to adapt during the bacteremia phase of infection, some RNA thermosensors (RNAT) have been described. In Gram-negative bacteria, it has been shown that *N. meningitidis* regulates the expression of capsule (*cssA*), fHbp and the sialylation (*Ist*) of LPS by RNATs. These three factors are important for evasion of the immune killing, consequently contributing to proliferation in the bloodstream [349]. For the specific case of fHbp expression, a recent report based on comparative analysis of the promoter regions of fHbp suggest that not all fHbp alleles undergo thermoregulation [350] and additionally that the levels of expression of fHbp may be regulated also by the variation in the coding sequence of the ORF by itself [350]. It has also been identified, one RNAT in the 5' untranslated region (UTR) of the *tviA* gene encoded by the typhoid fever-causing bacterium *S. enterica* serovar Typhi (*S. Typhi*). *TviA* is a transcriptional regulator of the critical virulence factors Vi capsule, flagellin, and Type III Secretion System-1. The inhibition of the RNAT in *S. enterica* Typhi causes aberrant virulence factor expression, leading to enhanced innate immune responses during infection [351]. Another example is the role of RNATs in regulation of expression of capsule and Factor H binding proteins in *S. pneumoniae* and *H. influenzae* [352]. Both pathogens have RNATs that impact the regulation of fHbp and capsule expression and as consequence

impact the resistance to complement. It is clear that many other mechanisms of thermosensors important in adaptation to the bloodstream playing a role in metabolic adaptation or response to the immune system still need to be described among the bacterial pathogens that cause bacteremia.

7.6 Stringent response, DNA replication, recombination, and repair

Facing the bloodstream can represent a harsh environment to allow survival of bacteria. In this context the activation of bacterial systems to face stress conditions must be activated. Stringent response (SR) is defined by global changes in bacterial gene expression associated with nutritional deprivation. It is triggered by intracellular accumulation of two small, hyperphosphorylated GTP-/GDP-derived molecules, namely, pppGpp and ppGpp, collectively called (p)ppGpp. In Gram-negative bacteria, the role of a stringent response (SR) system is *S. enterica* serovar Typhi has been reported to be mediated by (p)ppGpp. The deletion of two genes *spoT* and *relA* regulate Vi capsule expression affecting the resistance to complement and also survival in macrophages [353]. The double mutant was phenotypically (p)ppGpp⁰ and attenuated in human serum and also *in vivo*. It is highly probable that this SR system may play a role in the blood phase when *S. typhi* causes septicemia [353]. More recently, in *S. typhimurium* the stringent response with SpoT and PpnN was shown to impact the O antigen and the mutation of these genes affect the resistance to the complement and also was shown to be important for survival in human serum [354]. In the case of *Y. pestis* the effect of the SR system on causing systemic disease was evaluated and the deletion of the genes *relA* and *spoT* resulted in reduced synthesis and secretion of LcrV and a number of Yops, including YopD. YopD (an effector of the T3SS) is essential for several steps during infection and its reduced expression may affect other Yops. The double mutant of $\Delta relA \Delta spoT$ was attenuated in a mouse model when injecting *Y. pestis* subcutaneously, suggesting a relevant role of SR in the development of a systemic disease [355].

In the case of Gram-positive bacteria, a Tn-seq approach in whole blood and RNA-seq analysis help to identify the *S. agalactiae relA* gene involved in the SR. The *relA* mutant was shown to be important for the survival in blood [356]. For *S. aureus* (MRSA) a study comparing strains causing persistent bacteremia and resolving bacteremia helped to dissect the role of SR in bacteremia. Strains causing persistent bacteremia (defined by [357] as more or equal to 7 days of positive blood cultures despite appropriate antibiotic therapy), show a connection between the purine biosynthesis pathways and SR. The molecule (p)ppGpp is synthesized from two nucleobases GDP and GTP and MRSA causing persistent bacteremia has significantly higher (p)ppGpp production, higher lysis of polymorphonuclear leukocytes and survival compared to the clinical isolates in which bacteremia was resolved between 2 to 4 days of antibiotic treatment (resolving bacteremia). Higher levels of (p)ppGpp may be related to the elevated GDP and GTP in the case of the persistent bacteremia strains and this also produced more phenol soluble modulins (PSM) which lyse PMN affecting the host immune response. Expression of Psm α 1–4 was higher in the persistent bacteremia compared to the resolving bacteremia. The purine biosynthesis pathway was linked to this phenotype since the *purF* deletion mutant produced less (p)ppGpp, GDP, and GTP. Also the *relP* (an alarmone synthetase) mutant was studied and exhibited multiple phenotypes associated with acute bacteria: (1) significantly decreased Psm α 1–4 and psm β 1,2 expression, reduced PMN lysis and less survival in PMNs exposure. The role of the *relP*-mediated SR with respect to the persistent bacteremia outcome was studied in the rabbit model by testing the *relP* mutant tested in the infective endocarditis model [357]. The *relP* gene has been demonstrated to be necessary to overcome antibiotic treatment in the strains of persistent bacteremia [357]. Another mechanism of adaptation to stress conditions can be the activation of repair systems inside bacteria. In *S. pyogenes*, a TRASH screening in whole

blood, allowed to identify genes related to DNA replication, recombination, and repair (*tatD*, *spy0221* and *spy0414*) that were attenuated in human blood [209]. In a closely related species *S. pneumoniae* two genes, *mutX* involved in degradation of 8-oxo-dGTP) and *recJ* involved in methylation-directed mismatch repair were identified by a STM screening and deletion mutant of these genes were attenuated in a septicemia mouse model [226]. In *S. aureus*, an STM screening *in vivo* allowed to identify the gene *recA*, which is involved in DNA repair and response to environmental stress to be attenuated in a mouse model [210]. In the same screening a gene associated with a ATP-dependent Clp protease ATP-binding subunit of *E. coli* was identified. This gene is part of a stress response system and its mutant was attenuated in a bacteremia murine model [210]. In *N. meningitidis* a screening using proteomics of bacteria isolated from different niches in a mouse infection model identified the gene *groEL* encoding a chaperone responsible for protein folding under stressful conditions to be more expressed during infection in the CSF compared to the blood [172]. The mutant of *groEL* was more resistant to phagocytosis but interestingly it was more susceptible to growth in human serum compared to the wild type. The role of the mechanisms of stress response for bacteria causing bacteremia needs further investigation to gain a better understanding of this process.

8 Conclusion

Bacterial infections of the bloodstream has become a serious threat in the context of antibiotic resistance. Thus, understanding of the bacterial factors and mechanisms involved in survival and proliferation in the bloodstream are essential for the development of alternative therapeutic strategies to combat bloodstream infections. The genomic revolution has brought the opportunity to explore the bacterial mechanisms on a large scale, first with sequencing of genomes and later with the application of functional approaches based on transcriptomics, proteomics and more recently transposon mutagenesis and high throughput sequencing. Application of functional genomics allowed identification of a wealth of bacterial factors and mechanisms important for blood survival. Application of early technologies, such as microarray and IVIAT, and more recent ones such as RNA-seq, Tn-seq, comparative proteomics and dual proteomics,; have brought to light new molecular mechanisms involved in bloodstream infections. In addition, combination of current high-throughput approaches with relevant experimental models *ex vivo* and *in vivo* led to a more comprehensive understanding of the bacteremic phase of diseases. An overview of research work performed using many different blood-borne pathogenic bacteria highlight a clear scenario. While a vast number of mechanisms are shared by different bacteria, such is the case for bacterial proteins targeting the complement factors, other mechanisms have been evolved specifically by some species. Importantly, there are also variations between strains of the same bacterial species, which can explain unique pathogenic properties of some clinical isolates compared to others. Expectedly, the multiple regulatory mechanisms used by pathogenic bacteria to subvert host immunity and adapt to nutritional restrictions in the bloodstream are extremely complex systems whose activation signals and crosstalks remain to be fully understood. Ultimately, technological innovations and advances in blood infection biology will help design new diagnostic methods and develop improved preventive and therapeutic strategies.

Table 1. Bacterial factors interacting with the complement components, increasing serum or blood survival. Exp: experiment. +: bacterial survival was assessed *in vivo* or *ex vivo*. -: only factor interactions were demonstrated.

Pathway	Complement component	Bacterial species	Bacterial factor	Ref.	Exp.			
General	C3	<i>E. coli</i>	EspP (EHEC)	[358]	-			
			Pic (protease)	[57, 359]	+			
		<i>H. influenzae</i>	Capsule	[96]	+			
			HtrA (protease)	[360]	+			
		<i>K. pneumoniae</i>	Capsule	[97]	+			
			RfaH (capsule regulator)	[227, 361]	+			
		<i>L. interrogans</i>	Thermolysin (protease)	[85, 86]	+			
		<i>N. meningitidis</i>	NalP (protease)	[87]	+			
		<i>P. gingivalis</i>	Prth (protease)	[170]	-			
		<i>P. aeruginosa</i>	PaAp (protease)	[54]	-			
			PaE (elastase)	[54]	-			
		<i>Salmonella</i> spp	Psl (polysaccharide)	[100]	+			
			SpoT/RelA (Vi capsule regulator)	[353]	+			
		<i>S. aureus</i>	Vi capsule	[94, 95]	+			
			Aureolysin	[362]	+			
		<i>Streptococcus</i> spp	Efb (secreted)	[63, 363]	+			
			Ehp (secreted)	[364]	-			
			Sbi/Efb	[104, 365]	-			
			NanA/BgaA/StrH	[88]	+			
			ScpA (protease)	[123]	+			
		C3a	<i>S. aureus</i>	SpeB (protease)	[83, 122]	+		
				Sbi / Efb	[104]	-		
		C3b	<i>Streptococcus</i> Spp	ScpA (protease)	[123]	+		
				<i>A. baumannii</i>	Capsule structure	[106]	+	
		<i>B. anthracis</i>	<i>B. anthracis</i>	Capsule	[98]	+		
				Enolase (moonlighting)	[91]	+		
				Tu (elongation factor)	[91]	+		
				<i>E. coli</i>	EspP (EHEC)	[358]	+	
					Pic (protease)	[57, 359]	+	
				<i>F. tularensis</i>	O-antigen	[101]	+	
				<i>H. influenzae</i>	Protein E	[366]	+	
				<i>K. pneumoniae</i>	Smooth LPS	[115]	+	
				<i>L. interrogans</i>	Lsa23 (adhesin)	[367]	+	
				<i>P. aeruginosa</i>	Tu (elongation factor)	[90]	+	
				<i>Salmonella</i> spp	PgtE (protease)	[92]	+	
				<i>S. aureus</i>	Sbi/Efb	[104]	-	
					Staphylokinase	[93]	+	
				<i>Streptococcus</i> spp	<i>Streptococcus</i> spp	Capsule	[47]	+
						M protein	[368]	+
						Pgk	[110]	-
						Sfb1/PrtF1	[369]	+
						SpeB (protease)	[122]	+
				C5	<i>P. aeruginosa</i>	Psl (polysaccharide)	[100]	+
						<i>Salmonella</i> spp	PgtE (protease)	[92]
		C5a	<i>S. aureus</i>	SSL7	[103]	+		
				<i>P. aeruginosa</i>	AprA (protease)	[53]	+	
		<i>S. aureus</i>	<i>S. aureus</i>	CHIPS	[105, 370]	+		
				<i>Serratia marescens</i>	56kDa protease	[371]	+	
				<i>Streptococcus</i> spp	ScpA (protease)	[372]	-	
					SpeB (protease)	[107]	-	
Factor I	<i>S. aureus</i>			ClfA (clumping factor)	[102]	-		
Fibrinogen	<i>Streptococcus</i> spp	M protein	[373, 374]	+				
Heparin	<i>Neisseria</i> spp	Msf (fibril)	[375]	+				
		NHBA	[376]	+				
iC3b	<i>S. pneumoniae</i>	Capsule	[47]	+				
Plasmin/PLG	<i>B. anthracis</i>	Enolase (moonlighting)	[91]	+				
		Tu (elongation factor)	[91]	+				
		<i>Borrelia</i> spp	HcpA	[377]	+			
			<i>H. influenzae</i>	Protein E	[366]	+		
		<i>L. interrogans</i>	Enolase (moonlighting)	[134]	-			
			LIC11711	[378]	+			
		<i>P. aeruginosa</i>	Lsa23 (adhesin)	[367]	+			
			Lsa30 (adhesin)	[379]	-			
		<i>P. aeruginosa</i>	Tuf (elongation factor)	[90]	+			
		<i>Salmonella</i> spp	PgtE (protease)	[92]	+			
			<i>S. aureus</i>	Sbi/Efb	[104]	-		
		<i>Streptococcus</i> spp	<i>Streptococcus</i> spp	Staphylokinase	[93]	+		
				Enolase (moonlighting)	[380]	-		
				M protein	[368]	+		
				Pgk	[110]	-		

CP/LP	C1q	<i>P. aeruginosa</i>	PaAp (protease) PaE (elastase)	Hong 1992 [54]	
	C1q/CRP	<i>Streptococcus</i> spp	Capsule LytA PspA	[47] [381] [382]	-
	C1q & Ig	<i>H. influenzae</i>	Oligosaccharide SiaPQM (sialic acid) VacJ/Yrb (mla homolog)	[50] [383] [384]	+ +
		<i>P. gingivalis</i> <i>Neisseria</i> spp <i>S. aureus</i>	PrtH (protease) Cps capsule Sbi SpA SSL-10	[170] [45, 46] [42] [43] [197]	
		<i>Streptococcus</i> spp	Staphylokinase EndoS Capsule IdeS (protease) Mac-2 SpG PepO (Pneumolysin	[93] [385] [47] [386] [387] [388] [389] [390]	+ + +
	C1r	<i>Vibrio cholerae</i> <i>B. burgdorferi</i> <i>S. aureus</i>	OMV harboring OmpU BBK32 Cna	[150] [55, 56] [391]	+ +
	C1s	<i>P. aeruginosa</i>	AprA (protease)	[53]	+
	C1-INH	<i>B. pertussis</i> <i>E. coli</i>	OMV harboring Vag8 StcE	[64] [65]	
		<i>Serratia marescens</i> <i>Streptococcus</i> spp	56kDa protease SpeB (protease)	[392] [107]	- +
	C2	<i>B. burgdorferi</i> <i>E. coli</i> <i>P. aeruginosa</i> <i>Streptococcus</i> spp	OspC Pic AprA (protease) SpeB (protease)	[59] [57, 359] [53] [107]	+ + +
	C4	<i>B. pertussis</i> <i>E. coli</i> <i>Streptococcus</i> spp	BrkA Pic (protease) SpeB (protease)	[60] [57, 359] [107]	+ + +
	C4b	<i>E. coli</i> <i>H. influenzae</i> <i>Salmonella</i> spp	Pic (protease) LgtC (LOS biosynthesis) PgtE (protease)	[57, 359] [51] [92]	+ + +
	C4b2b (C4b2a)	<i>S. aureus</i>	Eap SCIN SCIN-B, SCIN-C efb/ecb	[393] [61] [62] [62, 63]	+ + +
	C4b2bC3b	<i>S. aureus</i>		[62, 63]	+
	C4BP	<i>A. actinomycet-</i> <i>emcomitans</i> <i>B. pertussis</i> <i>Borrelia</i> spp <i>E. coli</i> <i>H. influenzae</i> <i>L. interrogans</i>	OmpA1 (more sensitive to AP) Filamentous hemagglutinin P43 Nlpl OmpA Unknown Enolase (moonlighting) LcpA LigAB Lsa23 (adhesin) Lsa30 (adhesin) UspA1/UspA2 PorB1 (porin) PorA (porin) Rck SrdE/Bbp BibA Enolase (moonlighting) M protein Protein H PspA PspC Ail YadA (adhesin) O-antigen O-antigen	[394] [395] [396] [68] [69] [397] [134] [398] [127] [367] [379] [399] [70] [71] [139] [126] [400] [380] [67, 401] [66] [382] [133] [135, 141, 143, 146] [135] [49] [49]	+ - - + + - - + - + + + - - + + + - - + +
	unknown	<i>M. catarrhalis</i> <i>N. meningitidis</i> <i>Salmonella</i> spp. <i>S. aureus</i> <i>Streptococcus</i> spp	UspA1/UspA2 PorB1 (porin) PorA (porin) Rck SrdE/Bbp BibA Enolase (moonlighting) M protein Protein H PspA PspC Ail YadA (adhesin) O-antigen O-antigen	[399] [70] [71] [139] [126] [400] [380] [67, 401] [66] [382] [133] [135, 141, 143, 146] [135] [49] [49]	+ + + + + + - + - - + +
AP	C3bBbP	<i>S. aureus</i>	Efb/Ecb SCIN SCIN-B, SCIN-C Efb/Ecb PgtE (protease)	[62, 63] [61] [62] [62, 63] [81]	+ + + + +
	C3bBbC3b (C3b2Bb) Factor B	<i>S. aureus</i> <i>Salmonella</i> spp			+ +

Factor H, FHL-1, FHR-1		<i>A. baumannii</i>	OmpA	[73]	+	
		<i>A. actinomycet-</i> <i>emcomitans</i>	Omp100	[74]	+	
		<i>B. pertussis</i>	<i>pertussis</i> toxins	[404]		
		<i>Borrelia</i> spp	CRASP	[405]		
			CspA (CRASP-1)	[406, 407]	+	
			CspZ (CRASP-2)	[408]	+	
			Erp/OspE	[409]	-	
			HcpA	[377]	+	
		<i>E. coli</i>	OmpW	[75]		
			Stx2 (EHEC not invasive)	[410]		
		<i>H. influenzae</i>	P5	[50, 411]		
			Protein H	[412]		
		<i>L. interrogans</i>	Tu	[413]		
			Enolase (moonlighting)	[134]	-	
			LcpA	[414]	-	
			LenAB/LfhA	[415, 416]	+	
			LigAB	[417]	+	
			Lsa23 (adhesin)	[367]	+	
		<i>Neisseria</i> spp	NspA	[79, 80]	+	
			FHbp	[418]	+	
			LPS/LOS/LNT sialiation	[78, 419, 420]	+	
			PorB2	[421]	+	
			PorB3	[80]	+	
		<i>P. aeruginosa</i>	Tu (elongation factor)	[90]	+	
		<i>Salmonella</i> spp	PgtE (protease)	[81]	+	
			Rck	[140]	+	
		<i>S. aureus</i>	Sbi	[365]	-	
			SrdE/Bbp	[126]	+	
		<i>Streptococcus</i> spp	Bac/Beta	[422]		
			PspC	[133]	+	
			Tu	[423]		
			Scl1 (collagen like)	[424]		
			Hic	[425]	+	
			M protein	[426]	+	
			Fhb	[427]	+	
		<i>Yersinia</i> spp	Ail	[137, 141, 142, 146, 147]	+	
			YadA	[137, 428]	+	
		Properdin	<i>Streptococcus</i> spp	SpeB (protease)	[83]	+
		Unknown	<i>Bordetella</i> spp	LPS	[429]	+
			<i>B. pseudomallei</i>	O-antigen	[84]	+
	TP	C5b	<i>Streptococcus</i> spp	SpeB (protease)	[107]	-
		C5b/C6/ C7/C8/C9 components	<i>Borrelia</i> spp	BGA66; BGA71	[109]	+
				CspA (CRASP-1)	[430]	+
			<i>E. coli</i>	TraT	[108]	+
			<i>L. interrogans</i>	LIC12587	[378]	+
				Lsa23 (adhesin)	[431]	+
				Thermolysin (protease)	[432]	+
	<i>P. aeruginosa</i>		PsI (polysaccharide)	[100]	+	
	<i>Salmonella</i> spp		Rck (omp)	[138]	+	
			TraT	[108, 433]	+	
	<i>Streptococcus</i> spp		Pgk	[110]	-	
			SIC	[434, 435]	+	
			SpeB (protease)	[107]	-	
	MAC efficacy	<i>A. baumannii</i>	MlaACDEF	[436]	+	
			Prc/Tsp	[437]	+	
		<i>Neisseria</i> spp	Capsule	[36]		
			Nhha	[438]	+	
		<i>P. gingivalis</i>	A-LPS	[111]	+	
		<i>Salmonella</i> spp	O-antigen	[113, 114, 439, 440]	+	
			SpoT (LPS regulator)	[354]	+	
	CD-59	<i>Borrelia</i> spp	CD-59 like	[120]		
		<i>E. coli</i>	Unknown	[441]		
	Clusterin	<i>P. aeruginosa</i>	Lpd (moonlighting)	[118]	+	
	COMP	<i>M. catarrhalis</i>	UspA2	[119]	+	
	Vitronectin	<i>H. influenzae</i>	Hsf	[442]		
			P4	[443]		
			Protein E	[444]	-	
			Protein F	[116]	+	
			protein H	[117]	+	
			OMV	[445]	+	
		<i>L. interrogans</i>	Enolase (moonlighting)	[134]	-	
			LcpA	[414]	-	
			LIC11711 / 12587	[378]	-	
			LIC13259	[446]	-	
		<i>M. catarrhalis</i>	USPA1/USPA2	[447, 448]	+	

	<i>Neisseria</i> spp	OpaA	[449]	
		Msf (fibril)	[375]	+
		Opc	[450] not in serum	
	<i>P. aeruginosa</i>	Lpd (moonlighting)	[118]	+
		Porin D	[451]	+
	<i>Streptococcus</i> spp	PspC	[133]	+
		VnBP	[448]	
		Hic	[452]	+
	<i>Yersinia</i> spp	Ail	[144, 145]	+
		YadA	[136]	+
Comp. exhaust.	<i>A. actinomycetemcomitans</i>	OMV	[151]	
	<i>B. pertussis</i>	OMV (Vag8)	[64]	
	<i>Neisseria</i> spp	OMV	[148]	+
	<i>P. gingivalis</i>	OMV (LPS)	[149]	+
	<i>Streptococcus</i> spp	NanA	[152]	+
	<i>Vibrio cholerae</i>	OMV (OmpU)	[150]	+
Unknown	<i>A. actinomycetemcomitans</i>	rpoE	[325]	+
	<i>A. baumannii</i>	DedA	[436]	+
		L-lysine permease	[436]	+
		LPS	[453]	+
		PBP-7/8	[454]	+
		PKF	[455]	+
		PLD	[456]	+
		RelA	[436]	+
		Wza/Wzi/QhbA/Wzy (capsule)	[436]	+
	<i>B. pertussis</i>	BpsA-D locus	[457]	+
	<i>E. coli</i>	Capsule	[153, 458–460]	+
		LPS	[154–157, 162]	+
		Murein lipoprotein	[157]	
	<i>K. pneumoniae</i>	MagA	[461]	+
		O-antigen	[159, 462]	+
		Pal/ LppA	[463]	
	<i>P. aeruginosa</i>	LPS	[464]	
		O-antigen	[465]	
	<i>Salmonella</i> spp	PagC	[466]	
		O-antigen	[158, 467]	
	<i>Streptococcus</i> spp	Sof4	[173]	
	<i>V. vulnificus</i>	Capsule	[468]	+
		Tad123 (pili)	[161]	+

References

1. Lockhart, P. B. *et al.* Bacteremia associated With toothbrushing and dental extraction. *Circulation* **117**, 3118–3125 (June 2008).
2. Hotchkiss, R. S. *et al.* Sepsis and septic shock. *Nature Reviews Disease Primers* **2**, 16045 (June 2016).
3. Fleischmann, C. *et al.* Assessment of global incidence and mortality of hospital-treated sepsis. Current estimates and limitations. *American Journal of Respiratory and Critical Care Medicine* **193**, 259–272 (Feb. 2016).
4. Reinhart, K. *et al.* Recognizing sepsis as a global health priority — A WHO resolution. *New England Journal of Medicine* **377**, 414–417 (Aug. 2017).
5. Goto, M. & Al-Hasan, M. N. Overall burden of bloodstream infection and nosocomial bloodstream infection in North America and Europe. *Clinical Microbiology and Infection* **19**, 501–509 (2013).
6. Diekema, D. J. *et al.* The microbiology of bloodstream infection: 20-Year trends from the SENTRY antimicrobial surveillance program. *Antimicrobial Agents and Chemotherapy* **63**, 00355–19 (2019).
7. Bonten, M. *et al.* Epidemiology of *Escherichia coli* bacteremia: a systematic literature review. *Clinical Infectious Diseases* **72**, 1211–1219 (Apr. 2021).
8. Stewardson, A. J. *et al.* The health and economic burden of bloodstream infections caused by antimicrobial-susceptible and non-susceptible *Enterobacteriaceae* and *Staphylococcus aureus* in European hospitals, 2010 and 2011: a multicentre retrospective cohort study. *Eurosurveillance* **21**, 30319 (Aug. 2016).
9. Barnett, A. G. *et al.* The increased risks of death and extra lengths of hospital and ICU stay from hospital-acquired bloodstream infections: a case–control study. *BMJ Open* **3**, e003587 (Oct. 2013).
10. Reddy, E. A., Shaw, A. V. & Crump, J. A. Community-acquired bloodstream infections in Africa: a systematic review and meta-analysis. *The Lancet. Infectious diseases* **10**, 417–432 (June 2010).
11. Deen, J. *et al.* Community-acquired bacterial bloodstream infections in developing countries in south and southeast Asia: a systematic review. *The Lancet Infectious Diseases* **12**, 480–487 (June 2012).
12. Nabera, C. K. *Staphylococcus aureus* bacteremia: epidemiology, pathophysiology, and management strategies. *Clinical Infectious Diseases* **48**, S231–S237 (May 2009).
13. Brunelli, S. M., Turenne, W., Sibbel, S., Hunt, A. & Pffaffe, A. Clinical and economic burden of bloodstream infections in critical care patients with central venous catheters. *Journal of Critical Care* **35**, 69–74 (Oct. 2016).
14. Wang, Y. C., Shih, S. M., Chen, Y. T., Hsiung, C. A. & Kuo, S. C. Clinical and economic impact of intensive care unit-acquired bloodstream infections in Taiwan: a nationwide population-based retrospective cohort study. *BMJ Open* **10**, e037484 (Nov. 2020).
15. Hattori, H. *et al.* Epidemiology and risk factors for mortality in bloodstream infections: a single-center retrospective study in Japan. *American Journal of Infection Control* **46**, e75–e79 (Dec. 2018).
16. MacKinnon, M. C. *et al.* Mortality in *Escherichia coli* bloodstream infections: a multinational population-based cohort study. *BMC Infectious Diseases* **21**, 606 (Dec. 2021).
17. Kern, W. V. & Rieg, S. Burden of bacterial bloodstream infection—a brief update on epidemiology and significance of multidrug-resistant pathogens. *Clinical Microbiology and Infection* **26**, 151–157 (Feb. 2020).
18. Iwashyna, T. J., Ely, E. W., Smith, D. M. & Langa, K. M. Long-term cognitive impairment and functional disability among survivors of severe sepsis. *JAMA* **304**, 1787–1794 (Oct. 2010).
19. Nathan, C. Neutrophils and immunity: challenges and opportunities. *Nature Reviews Immunology* **6**, 173–182 (Feb. 2006).
20. Sheldon, J. R. & Skaar, E. P. Metals as phagocyte antimicrobial effectors. *Current Opinion in Immunology* **60**, 1–9 (Oct. 2019).
21. Ricklin, D., Hajishengallis, G., Yang, K. & Lambris, J. D. Complement: a key system for immune surveillance and homeostasis. *Nature immunology* **11**, 785–797 (Sept. 2010).
22. Hood, M. I. & Skaar, E. P. Nutritional immunity: transition metals at the pathogen–host interface. *Nature Reviews Microbiology* **10**, 525–537 (July 2012).
23. Yeaman, M. R. Platelets: at the nexus of antimicrobial defence. *Nature reviews Microbiology* **12**, 426–437 (2014).
24. Larochette, V. *et al.* IL-26, a cytokine with roles in extracellular DNA-induced inflammation and microbial defense. *Frontiers in Immunology* **10**, 204 (Feb. 2019).
25. Walport, M. J. Complement. First of two parts. *The New England journal of medicine* **344**, 1058–66 (Apr. 2001).
26. Pietrocola, G., Nobile, G., Rindi, S. & Speziale, P. *Staphylococcus aureus* manipulates innate immunity through own and host-expressed proteases. *Frontiers in Cellular and Infection Microbiology* **7**, 166 (May 2017).

27. Miajlovic, H. & Smith, S. G. Bacterial self-defence: how *Escherichia coli* evades serum killing. *FEMS Microbiology Letters* **354**, 1–9 (May 2014).
28. Abreu, A. G. & Barbosa, A. S. How *Escherichia coli* circumvent complement-mediated killing. *Frontiers in Immunology* **8**, 452 (Apr. 2017).
29. Doorduyn, D. J., Rooijackers, S. H., van Schaik, W. & Bardoel, B. W. Complement resistance mechanisms of *Klebsiella pneumoniae*. *Immunobiology* **221**, 1102–1109 (Oct. 2016).
30. Riesbeck, K. Complement evasion by the human respiratory tract pathogens *Haemophilus influenzae* and *Moraxella catarrhalis*. *FEBS Letters* **594**, 2586–2597 (Aug. 2020).
31. Dulipati, V., Meri, S. & Panelius, J. Complement evasion strategies of *Borrelia burgdorferi sensu lato*. *FEBS Letters* **594**, 2645–2656 (Aug. 2020).
32. Barbosa, A. S. & Isaac, L. Complement immune evasion by spirochetes. *Current Topics in Microbiology and Immunology* **415**, 215–238 (2018).
33. Laabei, M. & Ermert, D. Catch me if you can: *Streptococcus pyogenes* complement evasion strategies. *Journal of Innate Immunity* **11**, 3–12 (Dec. 2019).
34. Syed, S., Viazmina, L., Mager, R., Meri, S. & Haapasalo, K. Streptococci and the complement system: interplay during infection, inflammation and autoimmunity. *FEBS Letters* **594**, 2570–2585 (Aug. 2020).
35. Krukonis, E. S. & Thomson, J. J. Complement evasion mechanisms of the systemic pathogens *Yersiniae* and *Salmonellae*. *FEBS Letters* **594**, 2598–2620 (Aug. 2020).
36. Schneider, M. C., Exley, R. M., Ram, S., Sim, R. B. & Tang, C. M. Interactions between *Neisseria meningitidis* and the complement system. *Trends in Microbiology* **15**, 233–240 (May 2007).
37. Lewis, L. A. & Ram, S. Complement interactions with the pathogenic *Neisseriae*: clinical features, deficiency states, and evasion mechanisms. *FEBS Letters* **594**, 2670–2694 (Aug. 2020).
38. Zipfel, P. F., Würzner, R. & Skerka, C. Complement evasion of pathogens: common strategies are shared by diverse organisms. *Molecular Immunology* **44**, 3850–3857 (Sept. 2007).
39. Hovingh, E. S., van den Broek, B. & Jongerius, I. Hijacking complement regulatory proteins for bacterial immune evasion. *Frontiers in Microbiology* **7**, 2004 (Dec. 2016).
40. Ermert, D., Ram, S. & Laabei, M. The hijackers guide to escaping complement: lessons learned from pathogens. *Molecular Immunology* **114**, 49–61 (Oct. 2019).
41. Holmes, C. L., Anderson, M. T., Mobley, H. L. & Bachman, M. A. Pathogenesis of gram-negative bacteremia. *Clinical Microbiology Reviews* **34**, 00234–20 (2021).
42. Zhang, L., Jacobsson, K., Vasi, J., Lindberg, M. & Frykberg, L. A second IgG-binding protein in *Staphylococcus aureus*. *Microbiology* **144**, 985–991 (Apr. 1998).
43. Kronvall, G. & Gewurz, H. Activation and inhibition of IgG mediated complement fixation by staphylococcal protein A. *Clinical and Experimental Immunology* **7**, 211–220 (1970).
44. Kim, H. K., Falugi, F., Thomer, L., Missiakas, D. M. & Schneewind, O. Protein A suppresses immune responses during *Staphylococcus aureus* bloodstream infection in guinea pigs. *mBio* **6**, 02369–14 (Jan. 2015).
45. Agarwal, S., Vasudhev, S., DeOliveira, R. B. & Ram, S. Inhibition of the classical pathway of complement by meningococcal capsular polysaccharides. *The Journal of Immunology* **193**, 1855–1863 (Aug. 2014).
46. Hammerschmidt, S. *et al.* Contribution of genes from the capsule gene complex (cps) to lipooligosaccharide biosynthesis and serum resistance in *Neisseria meningitidis*. *Molecular Microbiology* **11**, 885–896 (Mar. 1994).
47. Hyams, C., Camberlein, E., Cohen, J. M., Bax, K. & Brown, J. S. The *Streptococcus pneumoniae* capsule inhibits complement activity and neutrophil phagocytosis by multiple mechanisms. *Infection and Immunity* **78**, 704–715 (Feb. 2010).
48. Muñoz, V. L., Porsch, E. A. & Geme, J. W. *Kingella kingae* surface polysaccharides promote resistance to human serum and virulence in a juvenile rat model. *Infection and Immunity* **86**, 00100–18 (June 2018).
49. Devyatyarova-Johnson, M. *et al.* The lipopolysaccharide structures of *Salmonella enterica* serovar typhimurium and *Neisseria gonorrhoeae* determine the attachment of human mannose-binding lectin to intact organisms. *Infection and Immunity* **68**, 3894–3899 (July 2000).
50. Langereis, J. D. & Weiser, J. N. Shielding of a lipooligosaccharide IgM epitope allows evasion of neutrophil-mediated killing of an invasive strain of nontypeable *Haemophilus influenzae*. *mBio* **5**, 1–10 (Aug. 2014).
51. Ho, D. K., Ram, S., Nelson, K. L., Bonthuis, P. J. & Smith, A. L. IgtC expression modulates resistance to C4b deposition on an invasive nontypeable *Haemophilus influenzae*. *Journal of Immunology* **178**, 1002–1012 (Jan. 2007).
52. Lewis, L. A., Shafer, W. M., Ray, T. D., Ram, S. & Rice, P. A. Phosphoethanolamine residues on the lipid moiety of *Neisseria gonorrhoeae* lipooligosaccharide modulate binding of complement inhibitors and resistance to complement killing. *Infection and Immunity* **81**, 33–42 (Jan. 2013).

53. Laarman, A. J. *et al.* *Pseudomonas aeruginosa* alkaline protease blocks complement activation via the classical and lectin pathways. *The Journal of Immunology* **188**, 386–393 (Jan. 2012).
54. Hong, Y. & Ghebrehiwet, B. Effect of *Pseudomonas aeruginosa* elastase and alkaline protease on serum complement and isolated components C1q and C3. *Clinical Immunology and Immunopathology* **62**, 133–138 (Feb. 1992).
55. Garcia, B. L., Zhi, H., Wager, B., Höök, M. & Skare, J. T. *Borrelia burgdorferi* BBK32 inhibits the classical pathway by blocking activation of the C1 complement complex. *PLoS Pathogens* **12**, e1005404 (2016).
56. Caine, J. A. & Coburn, J. A short-term *Borrelia burgdorferi* infection model identifies tissue tropisms and bloodstream survival conferred by adhesion proteins. *Infection and Immunity* **83**, 3184–3194 (Aug. 2015).
57. Abreu, A. G. *et al.* The serine protease Pic from enteroaggregative *Escherichia coli* mediates immune evasion by the direct cleavage of complement proteins. *The Journal of Infectious Diseases* **212**, 106–115 (July 2015).
58. Tokarz, R., Anderton, J. M., Katona, L. I. & Benach, J. L. Combined effects of blood and temperature shift on *Borrelia burgdorferi* gene expression as determined by whole genome DNA array. *Infection and Immunity* **72**, 5419–5432 (Sept. 2004).
59. Caine, J. A. *et al.* *Borrelia burgdorferi* outer surface protein C (OspC) binds complement component C4b and confers bloodstream survival. *Cellular Microbiology* **19**, e12786 (Dec. 2017).
60. Barnes, M. G. & Weiss, A. A. BrkA protein of *Bordetella pertussis* inhibits the classical pathway of complement after C1 deposition. *Infection and Immunity* **69**, 3067–3072 (2001).
61. Rooijackers, S. H. M. *et al.* Immune evasion by a staphylococcal complement inhibitor that acts on C3 convertases. *Nature Immunology* **6**, 920–927 (Aug. 2005).
62. Jongerius, I. *et al.* Staphylococcal complement evasion by various convertase-blocking molecules. *Journal of Experimental Medicine* **204**, 2461–2471 (Oct. 2007).
63. Jongerius, I. *et al.* *Staphylococcus aureus* virulence is enhanced by secreted factors that block innate immune defenses. *Journal of Innate Immunity* **4**, 301–311 (Apr. 2012).
64. Hovingh, E. S. *et al.* Acquisition of C1 inhibitor by *Bordetella pertussis* virulence associated gene 8 results in C2 and C4 consumption away from the bacterial surface. *PLoS Pathogens* **13** (July 2017).
65. Lathem, W. W., Bergsbaken, T. & Welch, R. A. Potentiation of C1 esterase inhibitor by StcE, a metalloprotease secreted by *Escherichia coli* O157:H7. *The Journal of Experimental Medicine* **199**, 1077–1087 (Apr. 2004).
66. Ermert, D. *et al.* Human IgG increases virulence of *Streptococcus pyogenes* through complement evasion. *Journal of Immunology* **200**, 3495–3505 (May 2018).
67. Carlsson, F., Berggård, K., Stålhammar-Carlemalm, M. & Lindahl, G. Evasion of phagocytosis through cooperation between two ligand-binding regions in *Streptococcus pyogenes* M protein. *Journal of Experimental Medicine* **198**, 1057–1068 (Oct. 2003).
68. Tseng, Y. T. *et al.* NlpI facilitates deposition of C4bp on *Escherichia coli* by blocking classical complement-mediated killing, which results in high-level bacteremia. *Infection and Immunity* **80**, 3669–3678 (Oct. 2012).
69. Wooster, D. G., Maruvada, R., Blom, A. M. & Prasadarao, N. V. Logarithmic phase *Escherichia coli* K1 efficiently avoids serum killing by promoting C4bp-mediated C3b and C4b degradation. *Immunology* **117**, 482–493 (Apr. 2006).
70. Ram, S. *et al.* Binding of C4b-binding protein to PorinA molecular mechanism of serum resistance of *Neisseria gonorrhoeae*. *Journal of Experimental Medicine* **193**, 281–296 (Feb. 2001).
71. Jarva, H., Ram, S., Vogel, U., Blom, A. M. & Meri, S. Binding of the complement inhibitor C4bp to serogroup B *Neisseria meningitidis*. *The Journal of Immunology* **174**, 6299–6307 (May 2005).
72. Ferreira, V. P., Pangburn, M. K. & Cortés, C. *Complement control protein factor H: the good, the bad, and the inadequate* Aug. 2010.
73. Kim, S. W. *et al.* Serum resistance of *Acinetobacter baumannii* through the binding of factor H to outer membrane proteins. *FEMS Microbiology Letters* **301**, 224–231 (Dec. 2009).
74. Asakawa, R. *et al.* Outer membrane protein 100, a versatile virulence factor of *Actinobacillus actinomycescomitans*. *Molecular Microbiology* **50**, 1125–1139 (Nov. 2003).
75. Li, W. *et al.* Contribution of the outer membrane protein OmpW in *Escherichia coli* to complement resistance from binding to factor H. *Microbial Pathogenesis* **98**, 57–62 (Sept. 2016).
76. Madico, G. *et al.* The meningococcal vaccine candidate GNA1870 binds the complement regulatory protein factor H and enhances serum resistance. *Journal of Immunology* **177**, 501–510 (July 2006).
77. Echenique-Rivera, H. *et al.* Transcriptome analysis of *Neisseria meningitidis* in human whole blood and mutagenesis studies identify virulence factors involved in blood survival. *PLoS Pathogens* **7** (May 2011).

78. Lewis, L. A., Carter, M. & Ram, S. The relative roles of Factor H Binding protein, neisserial surface protein A, and lipooligosaccharide sialylation in regulation of the alternative pathway of complement on meningococci. *The Journal of Immunology* **188**, 5063–5072 (May 2012).
79. Lewis, L. A., Rice, P. A. & Ram, S. Role of gonococcal neisserial surface protein A (NSpA) in serum resistance and comparison of its factor H binding properties with those of its meningococcal counterpart. *Infection and Immunity* **87** (Feb. 2019).
80. Giuntini, S., Pajon, R., Ram, S. & Granoff, D. M. Binding of complement factor H to PorB3 and NspA enhances resistance of *Neisseria meningitidis* to anti-factor H binding protein bactericidal activity. *Infection and Immunity* **83**, 1536–1545 (2015).
81. Riva, R., Korhonen, T. K. & Meri, S. The outer membrane protease PgtE of *Salmonella enterica* interferes with the alternative complement pathway by cleaving factors B and H. *Frontiers in Microbiology* **0**, 63 (2015).
82. Askarian, F. *et al.* The lytic polysaccharide monoxygenase CbpD promotes *Pseudomonas aeruginosa* virulence in systemic infection. *Nature Communications* **12**, 1–19 (Dec. 2021).
83. Tsao, N. *et al.* Streptococcal pyrogenic exotoxin B cleaves properdin and inhibits complement-mediated opsonophagocytosis. *Biochemical and Biophysical Research Communications* **339**, 779–784 (Jan. 2006).
84. DeShazer, D., Brett, P. J. & Woods, D. E. The type II O-antigenic polysaccharide moiety of *Burkholderia pseudomallei* lipopolysaccharide is required for serum resistance and virulence. *Molecular Microbiology* **30**, 1081–1100 (1998).
85. Fraga, T. R. *et al.* Immune evasion by pathogenic *Leptospira* strains: the secretion of proteases that directly cleave complement proteins. *The Journal of Infectious Diseases* **209**, 876–886 (Mar. 2014).
86. Chura-Chambi, R. M. *et al.* *Leptospira interrogans* thermolysin refolded at high pressure and alkaline pH displays proteolytic activity against complement C3. *Biotechnology Reports* **19**, e00266 (Sept. 2018).
87. Del Tordello, E., Vacca, I., Ram, S., Rappuoli, R. & Serruto, D. *Neisseria meningitidis* NalP cleaves human complement C3, facilitating degradation of C3b and survival in human serum. *Proceedings of the National Academy of Sciences of the United States of America* **111**, 427–432 (2014).
88. Dalia, A. B., Standish, A. J. & Weiser, J. N. Three surface exoglycosidases from *Streptococcus pneumoniae*, NanA, BgaA, and StrH, promote resistance to opsonophagocytic killing by human neutrophils. *Infection and Immunity* **78**, 2108–2116 (May 2010).
89. Koenigs, A., Zipfel, P. F. & Kraiczy, P. Translation elongation factor Tuf of *Acinetobacter baumannii* is a plasminogen-binding protein. *PLoS One* **10** (ed Brissette, C. A.) e0134418 (July 2015).
90. Kunert, A. *et al.* Immune evasion of the human pathogen *Pseudomonas aeruginosa*: elongation factor Tuf is a Factor H and plasminogen binding protein. *The Journal of Immunology* **179**, 2979–2988 (Sept. 2007).
91. Chung, M. C. *et al.* *Bacillus anthracis* interacts with plasmin(ogen) to evade C3b-dependent innate immunity. *PLoS One* **6**, e18119 (2011).
92. Ramu, P. *et al.* The surface protease PgtE of *Salmonella enterica* affects complement activity by proteolytically cleaving C3b, C4b and C5. *FEBS Letters* **581**, 1716–1720 (May 2007).
93. Rooijackers, S. H., Van Wamel, W. J., Ruyken, M., Van Kessel, K. P. & Van Strijp, J. A. Anti-opsonic properties of staphylokinase. *Microbes and Infection* **7**, 476–484 (Mar. 2005).
94. Wilson, R. P. *et al.* The Vi capsular polysaccharide prevents complement receptor 3-mediated clearance of *Salmonella enterica* serotype Typhi. *Infection and Immunity* **79**, 830–837 (Feb. 2011).
95. Hart, P. J. *et al.* Differential killing of *Salmonella enterica* serovar Typhi by antibodies targeting Vi and Lipopolysaccharide O:9 antigen. *PLoS One* **11**, e0145945 (Jan. 2016).
96. Noel, G. J., Brittingham, A., Granato, A. A. & Mosser, D. M. Effect of amplification of the Cap b locus on complement-mediated bacteriolysis and opsonization of type b *Haemophilus influenzae*. *Infection and Immunity* **64**, 4769–4775 (1996).
97. Álvarez, D., Merino, S., Tomás, J. M., Benedí, V. J. & Albertí, S. Capsular polysaccharide is a major complement resistance factor in lipopolysaccharide O side chain-deficient *Klebsiella pneumoniae* clinical isolates. *Infection and Immunity* **68**, 953–955 (Feb. 2000).
98. Sharma, S., Bhatnagar, R. & Gaur, D. *Bacillus anthracis* Poly- γ -D-glutamate capsule inhibits opsonic phagocytosis by impeding complement activation. *Frontiers in Immunology* **11**, 462 (Mar. 2020).
99. Reckseidler-Zenteno, S. L., DeVinney, R. & Woods, D. E. The capsular polysaccharide of *Burkholderia pseudomallei* contributes to survival in serum by reducing complement factor C3b deposition. *Infection and Immunity* **73**, 1106–1115 (Feb. 2005).
100. Mishra, M. *et al.* *Pseudomonas aeruginosa* Psl polysaccharide reduces neutrophil phagocytosis and the oxidative response by limiting complement-mediated opsonization. *Cellular Microbiology* **14**, 95–106 (Jan. 2012).
101. Clay, C. D., Soni, S., Gunn, J. S. & Schlesinger, L. S. Evasion of complement-mediated lysis and complement C3 deposition are regulated by *Francisella tularensis* lipopolysaccharide O antigen. *The Journal of Immunology* **181**, 5568–5578 (Oct. 2008).

102. Hair, P. S., Ward, M. D., Semmes, O. J., Foster, T. J. & Cunnion, K. M. *Staphylococcus aureus* clumping Factor A binds to complement regulator Factor I and increases Factor I cleavage of C3b. *The Journal of Infectious Diseases* **198**, 125–133 (July 2008).
103. Bestebroer, J. *et al.* Functional basis for complement evasion by staphylococcal superantigen-like 7. *Cellular Microbiology* **12**, 1506–1516 (Oct. 2010).
104. Koch, T. K. *et al.* *Staphylococcus aureus* proteins Sbi and Efb recruit human plasmin to degrade complement C3 and C3b. *PLoS One* **7**, e47638 (Oct. 2012).
105. De Haas, C. J. *et al.* Chemotaxis inhibitory protein of *Staphylococcus aureus*, a bacterial antiinflammatory agent. *The Journal of Experimental Medicine* **199**, 687–695 (Mar. 2004).
106. Talyansky, Y. *et al.* Capsule carbohydrate structure determines virulence in *Acinetobacter baumannii*. *PLoS Pathogens* **17**, e1009291 (Feb. 2021).
107. Honda-Ogawa, M. *et al.* Cysteine proteinase from *Streptococcus pyogenes* enables evasion of innate immunity via degradation of complement factors. *The Journal of Biological Chemistry* **288**, 15854–15864 (May 2013).
108. Pramoongjago, P. *et al.* Role of TraT protein, an anticomplementary protein produced in *Escherichia coli* by R100 factor, in serum resistance. *The Journal of Immunology* **148** (1992).
109. Hammerschmidt, C. *et al.* BGA66 and BGA71 facilitate complement resistance of *Borrelia bavariensis* by inhibiting assembly of the membrane attack complex. *Molecular Microbiology* **99**, 407–424 (2016).
110. Blom, A. M., Bergmann, S., Fulde, M., Riesbeck, K. & Agarwal, V. *Streptococcus pneumoniae* phosphoglycerate kinase is a novel complement inhibitor affecting the membrane attack complex formation. *The Journal of Biological Chemistry* **289**, 32499 (Nov. 2014).
111. Slaney, J. M., Gallagher, A., Aduse-Opoku, J., Pell, K. & Curtis, M. A. Mechanisms of resistance of *Porphyromonas gingivalis* to killing by serum complement. *Infection and Immunity* **74**, 5352–5361 (Sept. 2006).
112. Taylor, P. W. Bactericidal and bacteriolytic activity of serum against gram-negative bacteria. *Microbiological Reviews* **47**, 46–83 (Mar. 1983).
113. Joiner, K. A., Hammer, C. H., Brown, E. J., Cole, R. J. & Frank, M. M. Studies on the mechanism of bacterial resistance to complement-mediated killing. I. Terminal complement components are deposited and released from *Salmonella minnesota* S218 without causing bacterial death. *Journal of Experimental Medicine* **155**, 797–808 (1982).
114. Joiner, K., Grossman, N., Schmetz, M. & Leive, L. C3 binds preferentially to long-chain lipopolysaccharide during alternative pathway activation by *Salmonella montevideo*. *Journal of Immunology* **136**, 710–715 (1986).
115. Merino, S., Camprubi, S., Alberti, S., Benedi, V. J. & Tomas, J. M. Mechanisms of *Klebsiella pneumoniae* resistance to complement-mediated killing. *Infection and Immunity* **60**, 2529–2535 (1992).
116. Su, Y. C. *et al.* *Haemophilus influenzae* acquires vitronectin via the ubiquitous Protein F to subvert host innate immunity. *Molecular microbiology* **87**, 1245–1266 (Mar. 2013).
117. Al-Jubair, T. *et al.* *Haemophilus influenzae* type f hijacks Vitronectin using protein H to resist host innate immunity and adhere to pulmonary epithelial cells. *Journal of Immunology* **195**, 5688–5695 (Dec. 2015).
118. Hallström, T. *et al.* *Pseudomonas aeruginosa* uses dihydrolipoamide dehydrogenase (Lpd) to bind to the human terminal pathway regulators vitronectin and clusterin to inhibit terminal pathway complement attack. *PLoS ONE* **10**, e0137630 (Sept. 2015).
119. Liu, G. *et al.* *Moraxella catarrhalis* evades host innate immunity via targeting cartilage oligomeric matrix protein. *The Journal of Immunology* **196**, 1249–1258 (Feb. 2016).
120. Pausa, M. *et al.* Serum-resistant strains of *Borrelia burgdorferi* evade complement-mediated killing by expressing a CD59-like complement inhibitory molecule. *The Journal of Immunology* **170**, 3214–3222 (Mar. 2003).
121. Kuo, C. F., Lin, Y. S., Chuang, W. J., Wu, J. J. & Tsao, N. Degradation of complement 3 by streptococcal pyrogenic exotoxin B inhibits complement activation and neutrophil opsonophagocytosis. *Infection and Immunity* **76**, 1163–1169 (Mar. 2008).
122. Terao, Y. *et al.* Group A streptococcal cysteine protease degrades C3 (C3b) and contributes to evasion of innate immunity. *The Journal of Biological Chemistry* **283**, 6253–6260 (Mar. 2008).
123. Lynskey, N. N. *et al.* Multi-functional mechanisms of immune evasion by the streptococcal complement inhibitor C5a peptidase. *PLoS Pathogens* **13**, e1006493 (Aug. 2017).
124. Sebbane, F., Jarrett, C. O., Gardner, D., Long, D. & Hinnebusch, B. J. Role of the *Yersinia pestis* plasminogen activator in the incidence of distinct septicemic and bubonic forms of flea-borne plague. *Proceedings of the National Academy of Sciences of the United States of America* **103**, 5526–30 (Apr. 2006).
125. Sebbane, F., Uversky, V. N. & Anisimov, A. P. *Yersinia pestis* plasminogen activator. *Biomolecules* **10**, 1554 (Nov. 2020).

126. Sharp, J. A. *et al.* *Staphylococcus aureus* surface protein SdrE binds complement regulator factor H as an immune evasion tactic. *PLoS One* **7**, e38407 (May 2012).
127. Breda, L. C. D. *et al.* Fine mapping of the interaction between C4b-binding protein and outer membrane proteins LigA and LigB of pathogenic *Leptospira interrogans*. *PLoS Neglected Tropical Diseases* **9**, e0004192 (Oct. 2015).
128. Angel, C. S., Ruzek, M. & Hostetter, M. K. Degradation of C3 by *Streptococcus pneumoniae*. *The Journal of Infectious Diseases* **170**, 600–608 (1994).
129. Qi, C., Finkel, D. & Hostetter, M. K. Novel purification scheme and functions for a C3-binding protein from *Streptococcus pneumoniae*. *Biochemistry* **39**, 5450–5457 (May 2000).
130. Dave, S., Brooks-Walter, A., Pangburn, M. K. & McDaniel, L. S. PspC, a pneumococcal surface protein, binds human factor H. *Infection and Immunity* **69**, 3435–3437 (2001).
131. Kerr, A. R. *et al.* The contribution of PspC to pneumococcal virulence varies between strains and is accomplished by both complement evasion and complement-independent mechanisms. *Infection and Immunity* **74**, 5319–5324 (Sept. 2006).
132. Herbert, J. *et al.* Antibody-mediated complement C3b/iC3b binding to group B streptococcus in paired mother and baby serum samples in a refugee population on the Thailand-Myanmar border. *Clinical and Vaccine Immunology* **22**, 319–326 (Mar. 2015).
133. Pathak, A. *et al.* Factor H binding proteins protect division septa on encapsulated *Streptococcus pneumoniae* against complement C3b deposition and amplification. *Nature Communications* **9**, 1–16 (Aug. 2018).
134. Salazar, N., Souza, M. C. L. d., Biasioli, A. G., Silva, L. B. d. & Barbosa, A. S. The multifaceted roles of *Leptospira* enolase. *Research in Microbiology* **168**, 157–164 (Feb. 2017).
135. Kirjavainen, V. *et al.* *Yersinia enterocolitica* serum resistance proteins YadA and ail bind the complement regulator C4b-binding protein. *PLoS Pathogens* **4**, e1000140 (Aug. 2008).
136. Mühlenkamp, M. C. *et al.* Vitronectin binds to a specific stretch within the head region of *Yersinia* adhesin A and thereby modulates *Yersinia enterocolitica* host interaction. *Journal of Innate Immunity* **9**, 33–51 (Jan. 2017).
137. Biedzka-Sarek, M., Jarva, H., Hyytiäinen, H., Meri, S. & Skurnik, M. Characterization of complement factor H binding to *Yersinia enterocolitica* serotype O:3. *Infection and Immunity* **76**, 4100–4109 (Sept. 2008).
138. Heffernan, E. J. *et al.* Mechanism of resistance to complement-mediated killing of bacteria encoded by the *Salmonella typhimurium* virulence plasmid gene rck. *The Journal of Clinical Investigation* **90**, 953–964 (Sept. 1992).
139. Ho, D. K. *et al.* Functional recruitment of human complement inhibitor C4b-binding protein to outer membrane protein Rck of *Salmonella*. *PLoS One* **6**, e27546 (Nov. 2011).
140. Ho, D. K., Jarva, H. & Meri, S. Human complement Factor H binds to outer membrane protein Rck of *Salmonella*. *The Journal of Immunology* **185**, 1763–1769 (Aug. 2010).
141. Bartra, S. S. *et al.* Resistance of *Yersinia pestis* to complement-dependent killing is mediated by the Ail outer membrane protein. *Infection and Immunity* **76**, 612–622 (Feb. 2008).
142. Thomson, J. J., Plecha, S. C. & Krukoniš, E. S. Ail provides multiple mechanisms of serum resistance to *Yersinia pestis*. *Molecular Microbiology* **111**, 82–95 (2019).
143. Ho, D. K., Skurnik, M., Blom, A. M. & Meri, S. *Yersinia pestis* Ail recruitment of C4b-binding protein leads to factor I-mediated inactivation of covalently and noncovalently bound C4b. *European Journal of Immunology* **44**, 742–751 (Mar. 2014).
144. Bartra, S. S. *et al.* *Yersinia pestis* uses the Ail outer membrane protein to recruit vitronectin. *Microbiology* **161**, 2174 (Nov. 2015).
145. Shin, K. *et al.* Structure of human Vitronectin C-terminal domain and interaction with *Yersinia pestis* outer membrane protein Ail. *Science Advances* **5**, eaax5068 (Sept. 2019).
146. Bliska, J. B. & Falkow, S. Bacterial resistance to complement killing mediated by the Ail protein of *Yersinia enterocolitica*. *Proceedings of the National Academy of Sciences of the United States of America* **89**, 3561–3565 (1992).
147. Ho, D. K., Riva, R., Skurnik, M. & Meri, S. The *Yersinia pseudotuberculosis* outer membrane protein Ail recruits the human complement regulatory protein factor H. *Journal of Immunology* **189**, 3593–3599 (Oct. 2012).
148. Pettit, R. K. & Judd, R. C. The interaction of naturally elaborated blebs from serum-susceptible and serum-resistant strains of *Neisseria gonorrhoeae* with normal human serum. *Molecular Microbiology* **6**, 729–734 (Mar. 1992).
149. Grenier, D. & Belanger, M. Protective effect of *Porphyromonas gingivalis* outer membrane vesicles against bactericidal activity of human serum. *Infection and Immunity* **59**, 3004–3008 (1991).
150. Aung, K. M. *et al.* Naturally occurring IgG antibodies provide innate protection against *Vibrio cholerae* bacteremia by recognition of the outer membrane protein U. *Journal of Innate Immunity* **8**, 269–283 (2016).

151. Lindholm, M., Metsäniitty, M., Granström, E. & Oscarsson, J. Outer membrane vesicle-mediated serum protection in *Aggregatibacter actinomycetemcomitans*. *Journal of Oral Microbiology* **12**, 1747857 (Jan. 2020).
152. Syed, S. *et al.* Role of pneumococcal NanA neuraminidase activity in peripheral blood. *Frontiers in Cellular and Infection Microbiology* **9**, 218 (2019).
153. Horwitz, M. A. & Silverstein, S. C. Influence of the *Escherichia coli* capsule on complement fixation and on phagocytosis and killing by human phagocytes. *The Journal of Clinical Investigation* **65**, 82–94 (1980).
154. McCarthy, A. J., Stabler, R. A. & Taylor, P. W. Genome-wide identification by transposon insertion sequencing of *Escherichia coli* K1 genes essential for in vitro growth, gastrointestinal colonizing capacity, and survival in serum. *Journal of Bacteriology* **200** (Apr. 2018).
155. Tomas, J. M., Ciurana, B., Benedi, V. J. & Juarez, A. Role of lipopolysaccharide and complement in susceptibility of *Escherichia coli* and *Salmonella typhimurium* to non-immune serum. *Journal of General Microbiology* **134**, 1009–1016 (Apr. 1988).
156. Grozdanov, L. *et al.* A single nucleotide exchange in the *wzy* gene is responsible for the semirough O6 lipopolysaccharide phenotype and serum sensitivity of *Escherichia coli* strain Nissle 1917. *Journal of Bacteriology* **184**, 5912–5925 (Nov. 2002).
157. Phan, M.-D. *et al.* The serum resistome of a globally disseminated multidrug resistant uropathogenic *Escherichia coli* clone. *PLoS Genetics* **9**, e1003834 (Oct. 2013).
158. Kintz, E. *et al.* *Salmonella enterica* serovar Typhi lipopolysaccharide O-antigen modification impact on serum resistance and antibody recognition. *Infection and Immunity* **85**, 01021–16 (Apr. 2017).
159. Shankar-Sinha, S. *et al.* The *Klebsiella pneumoniae* O antigen contributes to bacteremia and lethality during murine pneumonia. *Infection and Immunity* **72**, 1423–1430 (Mar. 2004).
160. Sarkar, S., Ulett, G. C., Totsika, M., Phan, M. D. & Schembri, M. A. Role of capsule and O antigen in the virulence of uropathogenic *Escherichia coli*. *PloS One* **9**, e94786 (Apr. 2014).
161. Duong-Nu, T. M. *et al.* A stealth adhesion factor contributes to *Vibrio vulnificus* pathogenicity: Flp pili play roles in host invasion, survival in the blood stream and resistance to complement activation. *PLoS Pathogens* **15**, e1007767 (2019).
162. Ma, J. *et al.* Screening virulence factors of porcine extraintestinal pathogenic *Escherichia coli* (an emerging pathotype) required for optimal growth in swine blood. *Transboundary and Emerging Diseases* **68**, 2005–2016 (July 2021).
163. Putrinš, M. *et al.* Phenotypic heterogeneity enables uropathogenic *Escherichia coli* to evade killing by antibiotics and serum complement. *Infection and Immunity* **83**, 1056–1067 (2015).
164. Thakker, M., Park, J. S., Carey, V. & Lee, J. C. *Staphylococcus aureus* serotype 5 capsular polysaccharide is antiphagocytic and enhances bacterial virulence in a murine bacteremia model. *Infection and Immunity* **66**, 5183–5189 (1998).
165. Watts, A. *et al.* *Staphylococcus aureus* strains that express serotype 5 or serotype 8 capsular polysaccharides differ in virulence. *Infection and Immunity* **73**, 3502–3511 (June 2005).
166. Locke, J. B. *et al.* *Streptococcus iniae* capsule impairs phagocytic clearance and contributes to virulence in fish. *Journal of Bacteriology* **189**, 1279–1287 (Feb. 2007).
167. Thurlow, L. R., Thomas, V. C., Fleming, S. D. & Hancock, L. E. *Enterococcus faecalis* capsular polysaccharide serotypes C and D and their contributions to host innate immune evasion. *Infection and Immunity* **77**, 5551–5557 (Dec. 2009).
168. Smith, R. E. *et al.* Decoration of the enterococcal polysaccharide antigen EPA is essential for virulence, cell surface charge and interaction with effectors of the innate immune system. *PLoS Pathogens* **15**, e1007730 (May 2019).
169. Xu, Y., Singh, K. V., Qin, X., Murray, B. E. & Weinstock, G. M. Analysis of a gene cluster of *Enterococcus faecalis* involved in polysaccharide biosynthesis. *Infection and Immunity* **68**, 815–823 (Feb. 2000).
170. Schenkein, H. A., Fletcher, H. M., Bodnar, M. & Macrina, F. L. Increased opsonization of a prtH-defective mutant of *Porphyromonas gingivalis* W83 is caused by reduced degradation of complement-derived opsonins. *The Journal of Immunology* **154**, 5331–5337 (May 1995).
171. Cortes-Perez, N. G. *et al.* Overexpression of *Enterococcus faecalis* *elr* operon protects from phagocytosis microbe-host interactions and microbial pathogenicity. *BMC Microbiology* **15**, 112 (May 2015).
172. Liu, Y. *et al.* Dynamic niche-specific adaptations in *Neisseria meningitidis* during infection. *Microbes and Infection* **18**, 109–117 (Feb. 2016).
173. Courtney, H. S., Hasty, D. L. & Dale, J. B. Anti-phagocytic mechanisms of *Streptococcus pyogenes*: binding of fibrinogen to M-related protein. *Molecular Microbiology* **59**, 936–947 (Feb. 2006).
174. Thammavongsa, V., Kern, J. W., Missiakas, D. M. & Schneewind, O. *Staphylococcus aureus* synthesizes adenosine to escape host immune responses. *Journal of Experimental Medicine* **206**, 2417–2427 (Oct. 2009).
175. Brekke, O. L. *et al.* *Neisseria meningitidis* and *Escherichia coli* are protected from leukocyte phagocytosis by binding to erythrocyte complement receptor 1 in human blood. *Molecular Immunology* **48**, 2159–2169 (Sept. 2011).

176. Jung, C. J., Zheng, Q. H., Shieh, Y. H., Lin, C. S. & Chia, J. S. *Streptococcus mutans* autolysin AtlA is a fibronectin-binding protein and contributes to bacterial survival in the bloodstream and virulence for infective endocarditis. *Molecular Microbiology* **74**, 888–902 (Nov. 2009).
177. Hirakata, Y., Furuya, N., Tateda, K., Kaku, M. & Yamaguchi, K. *In vivo* production of exotoxin A and its role in endogenous *Pseudomonas aeruginosa* septicemia in mice. *Infection and Immunity* **61**, 2468–2473 (1993).
178. Weiner, Z. P. *et al.* Circulating lethal toxin decreases the ability of neutrophils to respond to *Bacillus anthracis*. *Cellular Microbiology* **16**, 504–518 (Apr. 2014).
179. Patel, V. I., Booth, J. L., Dozmorov, M., Brown, B. R. & Metcalf, J. P. Anthrax edema and lethal toxins differentially target human lung and blood phagocytes. *Toxins* **12**, 464 (July 2020).
180. Malachowa, N. *et al.* Global changes in *Staphylococcus aureus* gene expression in human blood. *PLoS One* **6**, 18617 (2011).
181. Malachowa, N. & DeLeo, F. R. *Staphylococcus aureus* survival in human blood. *Virulence* **2**, 567–569 (2011).
182. Alonzo, F. *et al.* *Staphylococcus aureus* leucocidin ED contributes to systemic infection by targeting neutrophils and promoting bacterial growth *in vivo*. *Molecular Microbiology* **83**, 423–435 (2012).
183. Collins, M. M. *et al.* The accessory gene *saeP* of the SaeR/S two-component gene regulatory system impacts *Staphylococcus aureus* virulence during neutrophil interaction. *Frontiers in Microbiology* **11**, 561 (Apr. 2020).
184. Liu, G. Y. *et al.* Sword and shield: linked group B streptococcal β -hemolysin/cytolysin and carotenoid pigment function to subvert host phagocyte defense. *Proceedings of the National Academy of Sciences of the United States of America* **101**, 14491–14496 (Oct. 2004).
185. Pian, Y. *et al.* Binding of human fibrinogen to MRP enhances *Streptococcus suis* survival in host blood in a α x β 2 integrin-dependent manner. *Scientific Reports* **6**, 1–14 (May 2016).
186. Nomura, R., Nakano, K. & Ooshima, T. Contribution of glucan-binding protein C of *Streptococcus mutans* to bacteremia occurrence. *Archives of Oral Biology* **49**, 783–788 (Oct. 2004).
187. Nakano, K., Tsuji, M., Nishimura, K., Nomura, R. & Ooshima, T. Contribution of cell surface protein antigen PAc of *Streptococcus mutans* to bacteremia. *Microbes and Infection* **8**, 114–121 (Jan. 2006).
188. Abdullah, M. R. *et al.* Structure of the pneumococcal l,d-carboxypeptidase DacB and pathophysiological effects of disabled cell wall hydrolases DacA and DacB. *Molecular Microbiology* **93**, 1183–1206 (Sept. 2014).
189. Hu, Q. *et al.* A novel aquaporin subfamily imports oxygen and contributes to pneumococcal virulence by controlling the production and release of virulence factors. *mBio* **12**, 01309–21 (Aug. 2021).
190. Hall, J. W., Yang, J., Guo, H. & Ji, Y. The *Staphylococcus aureus* AirSR two-component system mediates reactive oxygen species resistance via transcriptional regulation of staphyloxanthin production. *Infection and Immunity* **85**, 00838–16 (2017).
191. Grifantini, R. *et al.* Characterization of a novel *Neisseria meningitidis* Fur and iron-regulated operon required for protection from oxidative stress: utility of DNA microarray in the assignment of the biological role of hypothetical genes. *Molecular Microbiology* **54**, 962–979 (Nov. 2004).
192. Vorobjeva, N. V. & Chernyak, B. V. NETosis: molecular mechanisms, role in physiology and pathology. *Biochemistry* **85**, 1178–1190 (Oct. 2020).
193. Buchanan, J. T. *et al.* DNase expression allows the pathogen group A *Streptococcus* to escape killing in neutrophil extracellular traps. *Current Biology* **16**, 396–400 (Feb. 2006).
194. Bai, Q. *et al.* YSIRK-G/S-directed translocation is required for *Streptococcus suis* to deliver diverse cell wall anchoring effectors contributing to bacterial pathogenicity. *Virulence* **11**, 1539–1556 (Jan. 2020).
195. Leung, K. Y., Reisner, B. S. & Straley, S. C. YopM inhibits platelet aggregation and is necessary for virulence of *Yersinia pestis* in mice. *Infection and Immunity* **58**, 3262–3271 (1990).
196. Palace, S. G. *et al.* *Yersinia pestis* escapes entrapment in thrombi by targeting platelet function. *Journal of Thrombosis and Haemostasis* **18**, 3236–3248 (Dec. 2020).
197. Itoh, S. *et al.* Staphylococcal superantigen-like protein 10 (SSL10) binds to human immunoglobulin G (IgG) and inhibits complement activation via the classical pathway. *Molecular Immunology* **47**, 932–938 (Jan. 2010).
198. Itoh, S. *et al.* Staphylococcal superantigen-like protein 10 (SSL10) inhibits blood coagulation by binding to prothrombin and factor Xa via their γ -carboxyglutamic acid (Gla) domain. *Journal of Biological Chemistry* **288**, 21569–21580 (July 2013).
199. Ko, Y. P. *et al.* Phagocytosis escape by a *Staphylococcus aureus* protein that connects complement and coagulation proteins at the bacterial surface. *PLoS Pathogens* **9**, 1–13 (2013).
200. McAdow, M. *et al.* Preventing *Staphylococcus aureus* sepsis through the inhibition of its agglutination in blood. *PLoS pathogens* **7**, e1002307 (Oct. 2011).
201. Higgins, J., Loughman, A., Van Kessel, K. P., Van Strijp, J. A. & Foster, T. J. Clumping factor A of *Staphylococcus aureus* inhibits phagocytosis by human polymorphonuclear leucocytes. *FEMS Microbiology Letters* **258**, 290–296 (May 2006).

202. De Haas, C. J. *et al.* Staphylococcal superantigen-like 5 activates platelets and supports platelet adhesion under flow conditions, which involves glycoprotein Ib α and α IIb β 3. *Journal of Thrombosis and Haemostasis* **7**, 1867–1874 (2009).
203. Sun, D. *et al.* *Bacillus anthracis* peptidoglycan activates human platelets through Fc γ RII and complement. *Blood* **122**, 571–579 (July 2013).
204. Qiu, P. *et al.* *Bacillus anthracis* cell wall peptidoglycan but not lethal or edema toxins produces changes consistent with disseminated intravascular coagulation in a rat model. *The Journal of Infectious Diseases* **208**, 978–989 (Sept. 2013).
205. Palm, F., Sjöholm, K., Malmström, J. & Shannon, O. Complement activation occurs at the surface of platelets activated by streptococcal M1 protein and this results in phagocytosis of platelets. *The Journal of Immunology* **202**, 503–513 (Jan. 2019).
206. Frick, I. M. *et al.* Antibacterial activity of the contact and complement systems is blocked by SIC, a protein secreted by *Streptococcus pyogenes*. *Journal of Biological Chemistry* **286**, 1331–1340 (Jan. 2011).
207. Frick, I. M. *et al.* Streptococcal inhibitor of complement (SIC) modulates fibrinolysis and enhances bacterial survival within fibrin clots. *Journal of Biological Chemistry* **293**, 13578–13591 (Aug. 2018).
208. Uchiyama, S. *et al.* Dual actions of group B *Streptococcus* capsular sialic acid provide resistance to platelet-mediated antimicrobial killing. *Proceedings of the National Academy of Sciences* **116**, 7465–7470 (Apr. 2019).
209. Le Breton, Y. *et al.* Genome-wide identification of genes required for fitness of group A streptococcus in human blood. *Infection and Immunity* **81**, 862–875 (Mar. 2013).
210. Mei, J. M., Nourbakhsh, F., Ford, C. W. & Holden, D. W. Identification of *Staphylococcus aureus* virulence genes in a murine model of bacteraemia using signature-tagged mutagenesis. *Molecular Microbiology* **26**, 399–407 (1997).
211. Khan, M. A. & Isaacson, R. E. Identification of *Escherichia coli* genes that are specifically expressed in a murine model of septicemic infection. *Infection and Immunity* **70**, 3404–3412 (2002).
212. Antunes, A. *et al.* The phosphocarrier protein HPr contributes to meningococcal survival during infection. *PLoS One* **11**, e0162434 (Sept. 2016).
213. Valdes, K. M. *et al.* The *fruRBA* operon is necessary for group A streptococcal growth in fructose and for resistance to neutrophil killing during growth in whole human blood. *Infection and Immunity* **84**, 1016–1031 (Apr. 2016).
214. Zhang, X. *et al.* RNA-seq and Tn-seq reveal fitness determinants of vancomycin-resistant *Enterococcus faecium* during growth in human serum. *BMC Genomics* **18**, 1–12 (Nov. 2017).
215. Sundar, G. S. *et al.* Route of glucose uptake in the group a *streptococcus* impacts SLS-mediated hemolysis and survival in human blood. *Frontiers in Cellular and Infection Microbiology* **8**, 71 (Mar. 2018).
216. Exley, R. M. *et al.* Available carbon source influences the resistance of *Neisseria meningitidis* against complement. *Journal of Experimental Medicine* **201**, 1637–1645 (May 2005).
217. Anderson, M. T., Mitchell, L. A., Zhao, L. & Mogleya, H. L. Capsule production and glucose metabolism dictate fitness during *Serratia marcescens* bacteremia. *mBio* **8**, 740–757 (May 2017).
218. Ma, J. *et al.* Preferential use of carbon central metabolism and anaerobic respiratory chains in porcine extraintestinal pathogenic *Escherichia coli* during bloodstream infection. *Veterinary Microbiology* **249**, 108830 (Oct. 2020).
219. Brauer, A. L., White, A. N., Learman, B. S., Johnson, A. O. & Armbruster, C. E. d-Serine degradation by *Proteus mirabilis* contributes to fitness during single-species and polymicrobial catheter-associated urinary tract infection. *mSphere* **4**, 00020–19 (Feb. 2019).
220. Gaspar, P., Al-Bayati, F. A., Andrew, P. W., Neves, A. R. & Yesilkaya, H. Lactate dehydrogenase is the key enzyme for pneumococcal pyruvate metabolism and pneumococcal survival in blood. *Infection and Immunity* **82**, 5099–5109 (2014).
221. Echlin, H., Frank, M., Rock, C. & Rosch, J. W. Role of the pyruvate metabolic network on carbohydrate metabolism and virulence in *Streptococcus pneumoniae*. *Molecular Microbiology* **114**, 536–552 (Oct. 2020).
222. Painter, K. L., Hall, A., Ha, K. P. & Edwards, A. M. The electron transport chain sensitizes *Staphylococcus aureus* and *Enterococcus faecalis* to the oxidative burst. *Infection and Immunity* **85**, 00659–17 (Dec. 2017).
223. Armbruster, C. E. *et al.* Twin arginine translocation, ammonia incorporation, and polyamine biosynthesis are crucial for *Proteus mirabilis* fitness during bloodstream infection. *PLoS Pathogens* **15**, e1007653 (Apr. 2019).
224. Terwilliger, A. *et al.* *Bacillus anthracis* overcomes an amino acid auxotrophy by cleaving host serum proteins. *Journal of Bacteriology* **197**, 2400–2411 (2015).
225. Carlson, P. E., Bourgis, A. E., Hagan, A. K. & Hanna, P. C. Global gene expression by *Bacillus anthracis* during growth in mammalian blood. *Pathogens and Disease* **73**, ftv061 (Nov. 2015).

226. Polissi, A. *et al.* Large-scale identification of virulence genes from *Streptococcus pneumoniae*. *Infection and Immunity* **66**, 5620–5629 (1998).
227. Bachman, M. A. *et al.* Genome-wide identification of *Klebsiella pneumoniae* fitness genes during lung infection. *mBio* **6**, e00775 (June 2015).
228. Sebkova, A., Karasova, D., Crhanova, M., Budinska, E. & Rychlik, I. *aro* mutations in *Salmonella enterica* cause defects in cell wall and outer membrane integrity. *Journal of Bacteriology* **190**, 3155–3160 (May 2008).
229. Zhu, L. *et al.* Genome-wide assessment of *Streptococcus agalactiae* genes required for survival in human whole blood and plasma. *Infection and Immunity* **88**, 1–14 (Oct. 2020).
230. Günel-Özcan, A., Brown, K. A., Allen, A. G. & Maskell, D. J. *Salmonella typhimurium aroB* mutants are attenuated in BALB/c mice. *Microbial Pathogenesis* **23**, 311–316 (Nov. 1997).
231. Li, M. S. *et al.* A *Neisseria meningitidis* NMB1966 mutant is impaired for invasion of respiratory epithelial cells, survival in human blood and for virulence *in vivo*. *Medical Microbiology and Immunology* **198**, 57–67 (Feb. 2009).
232. Oogai, Y. *et al.* Lysine and threonine biosynthesis from aspartate contributes to *Staphylococcus aureus* growth in calf serum. *Applied and Environmental Microbiology* **82**, 6150–6157 (2016).
233. McFarland, W. C. & Stocker, B. A. Effect of different purine auxotrophic mutations on mouse-virulence of a Vi-positive strain of *Salmonella dublin* and of two strains of *Salmonella typhimurium*. *Microbial Pathogenesis* **3**, 129–141 (Aug. 1987).
234. Samant, S. *et al.* Nucleotide biosynthesis is critical for growth of bacteria in human blood. *PLoS Pathogens* **4**, e37 (Feb. 2008).
235. Kim, Y. R. *et al.* Characterization and pathogenic significance of *Vibrio vulnificus* antigens preferentially expressed in septicemic patients. *Infection and Immunity* **71**, 5461–5471 (Oct. 2003).
236. Brubaker, R. R. Interconversion of purine mononucleotides in *Pasteurella pestis*. *Infection and Immunity* **1**, 446–454 (May 1970).
237. Chauvaux, S. *et al.* Transcriptome analysis of *Yersinia pestis* in human plasma: an approach for discovering bacterial genes involved in septicemic plague. *Microbiology* **153**, 3112–3124 (Sept. 2007).
238. Jenkins, A. *et al.* Role of purine biosynthesis in *Bacillus anthracis* pathogenesis and virulence. *Infection and Immunity* **79**, 153–166 (Jan. 2011).
239. Connolly, J. *et al.* Identification of *Staphylococcus aureus* factors required for pathogenicity and growth in human blood. *Infection and Immunity* **85**, 00337–17 (Nov. 2017).
240. Zhu, B. *et al.* Genome-wide identification of *Streptococcus sanguinis* fitness genes in human serum and discovery of potential selective drug targets. *Molecular Microbiology* **115**, 658–671 (Apr. 2021).
241. Sabri, M. *et al.* Contribution of the SitABCD, MntH, and FeoB metal transporters to the virulence of avian pathogenic *Escherichia coli* O78 strain χ 7122. *Infection and Immunity* **76**, 601–611 (Feb. 2008).
242. Boyer, E., Bergevin, I., Malo, D., Gros, P. & Cellier, M. F. M. Acquisition of Mn(II) in addition to Fe(II) is required for full virulence of *Salmonella enterica* serovar *Typhimurium*. *Infection and Immunity* **70**, 6032–6042 (2002).
243. Zaharik, M. L. *et al.* The *Salmonella enterica* serovar *Typhimurium* divalent cation transport systems *MntH* and *SitABCD* are essential for virulence in an *Nramp1G169* murine typhoid model. *Infection and Immunity* **72**, 5522–5525 (Sept. 2004).
244. Weakland, D. R., Smith, S. N., Bell, B., Tripathi, A. & Mobley, H. L. The *Serratia marcescens* siderophore serratiochelin is necessary for full virulence during bloodstream infection. *Infection and Immunity* **88**, 00117–20 (Aug. 2020).
245. Bidmos, F. A. *et al.* Investigation into the antigenic properties and contributions to growth in blood of the meningococcal haemoglobin receptors, HpuAB and HmbR. *PLoS One* **10** (ed Chang, Y.-F.) e0133855 (July 2015).
246. Renauld-Mongénie, G. *et al.* Role of transferrin receptor from a *Neisseria meningitidis* *tbpB* isotype II strain in human transferrin binding and virulence. *Infection and Immunity* **72**, 3461 (June 2004).
247. Subashchandra, S. *et al.* *Acinetobacter baumannii* genes required for bacterial survival during bloodstream infection. *mSphere* **1**, 00013–15 (Feb. 2016).
248. Dahesh, S., Nizet, V. & Cole, J. N. Study of streptococcal hemoprotein receptor (Shr) in iron acquisition and virulence of M1T1 group A *Streptococcus*. *Virulence* **3**, 566–575 (2012).
249. Spaan, A. N. *et al.* *Staphylococcus aureus* targets the Duffy antigen receptor for chemokines (DARC) to lyse erythrocytes. *Cell Host & Microbe* **18**, 363–370 (Sept. 2015).
250. Veyrier, F. J., Boneca, I. G., Cellier, M. F. & Taha, M. K. A novel metal transporter mediating manganese export (*mntx*) regulates the mn to fe intracellular ratio and *Neisseria meningitidis* virulence. *PLoS Pathogens* **7**, 1002261 (Sept. 2011).
251. Anderson, E. S. *et al.* The manganese transporter *MntH* is a critical virulence determinant for *Brucella abortus* 2308 in experimentally infected mice. *Infection and Immunity* **77**, 3466–3474 (2009).

252. Crump, K. E. *et al.* The relationship of the lipoprotein SsaB, manganese and superoxide dismutase in *Streptococcus sanguinis* virulence for endocarditis. *Molecular Microbiology* **92**, 1243–1259 (June 2014).
253. Colomer-Winter, C. *et al.* Manganese acquisition is essential for virulence of *Enterococcus faecalis*. *PLoS Pathogens* **14**, e1007102 (Sept. 2018).
254. Champion, O. L. *et al.* *Yersinia pseudotuberculosis* mntH functions in intracellular manganese accumulation, which is essential for virulence and survival in cells expressing functional Nramp1. *Microbiology* **157**, 1115–1122 (Apr. 2011).
255. Grunenwald, C. M. *et al.* Manganese detoxification by MntE is critical for resistance to oxidative stress and virulence of *Staphylococcus aureus*. *mBio* **10**, 02915–18 (Jan. 2019).
256. Wichgers Schreur, P. J., Rebel, J. M., Smits, M. A., van Putten, J. P. & Smith, H. E. Troa of *Streptococcus suis* is required for manganese acquisition and full virulence. *Journal of Bacteriology* **193**, 5073–5080 (Oct. 2011).
257. Arenas, J. *et al.* Identification of conditionally essential genes for *Streptococcus suis* infection in pigs. *Virulence* **11**, 446–464 (Jan. 2020).
258. Calmettes, C. *et al.* The molecular mechanism of Zinc acquisition by the neisserial outer-membrane transporter ZnuD. *Nature Communications* **6**, 1–11 (Aug. 2015).
259. Bobrov, A. G. *et al.* The *Yersinia pestis* siderophore, yersiniabactin, and the ZnuABC system both contribute to zinc acquisition and the development of lethal septicaemic plague in mice. *Molecular Microbiology* **93**, 759–775 (Aug. 2014).
260. Bayle, L. *et al.* Zinc uptake by *Streptococcus pneumoniae* depends on both AdcA and AdcAll and is essential for normal bacterial morphology and virulence. *Molecular Microbiology* **82**, 904–916 (Nov. 2011).
261. Ong, C. L. Y., Berking, O., Walker, M. J. & McEwan, A. G. New insights into the role of zinc acquisition and zinc tolerance in group A streptococcal infection. *Infection and Immunity* **86**, 00048–18 (June 2018).
262. Rosch, J. W., Sublett, J., Gao, G., Wang, Y. D. & Tuomanen, E. I. Calcium efflux is essential for bacterial survival in the eukaryotic host. *Molecular microbiology* **70**, 435–444 (Oct. 2008).
263. Minato, Y. *et al.* Na⁺/H⁺ antiport is essential for *Yersinia pestis* virulence. *Infection and Immunity* **81**, 3163–3172 (2013).
264. Tzeng, Y. L. *et al.* Cationic antimicrobial peptide resistance in *Neisseria meningitidis*. *Journal of Bacteriology* **187**, 5387–5396 (Aug. 2005).
265. Poyart, C., Lamy, M. C., Boumaila, C., Fiedler, F. & Trieu-Cuot, P. Regulation of D-alanyl-lipoteichoic acid biosynthesis in *Streptococcus agalactiae* involves a novel two-component regulatory system. *Journal of Bacteriology* **183**, 6324–6334 (2001).
266. Abachin, E. *et al.* Formation of D-alanyl-lipoteichoic acid is required for adhesion and virulence of *Listeria monocytogenes*. *Molecular Microbiology* **43**, 1–14 (Jan. 2002).
267. Weidenmaier, C. *et al.* DltABCD- and MprF-mediated cell envelope modifications of *Staphylococcus aureus* confer resistance to platelet microbicidal proteins and contribute to virulence in a rabbit endocarditis model. *Infection and Immunity* **73**, 8033–8038 (Dec. 2005).
268. Fisher, N. *et al.* The *dltABCD* operon of *Bacillus anthracis* Sterne is required for virulence and resistance to peptide, enzymatic, and cellular mediators of innate immunity. *Journal of Bacteriology* **188**, 1301–1309 (Feb. 2006).
269. Kovács, M. *et al.* A functional *dlt* operon, encoding proteins required for incorporation of D-alanine in teichoic acids in gram-positive bacteria, confers resistance to cationic antimicrobial peptides in *Streptococcus pneumoniae*. *Journal of Bacteriology* **188**, 5797–5805 (Aug. 2006).
270. Thedieck, K. *et al.* The MprF protein is required for lysinylation of phospholipids in listerial membranes and confers resistance to cationic antimicrobial peptides (CAMPs) on *Listeria monocytogenes*. *Molecular Microbiology* **62**, 1325–1339 (Dec. 2006).
271. Samant, S., Hsu, F. F., Neyfakh, A. A. & Lee, H. The *Bacillus anthracis* protein MprF is required for synthesis of lysylphosphatidylglycerols and for resistance to cationic antimicrobial peptides. *Journal of Bacteriology* **191**, 1311–1319 (Feb. 2009).
272. Hamilton, A. *et al.* Penicillin-binding protein 1a promotes resistance of group B *Streptococcus* to antimicrobial peptides. *Infection and Immunity* **74**, 6179–6187 (Nov. 2006).
273. Inomata, M., Horie, T. & Into, T. OmpA-like proteins of *Porphyromonas gingivalis* contribute to serum resistance and prevent Toll-like receptor 4-mediated host cell activation. *PLoS One* **13**, e0202791 (Aug. 2018).
274. Horie, T., Inomata, M. & Into, T. OmpA-like proteins of *Porphyromonas gingivalis* mediate resistance to the antimicrobial peptide LL-37. *Journal of Pathogens* **2018**, 2068435 (Dec. 2018).
275. Lewis, L. A. *et al.* Phosphoethanolamine substitution of lipid A and resistance of *Neisseria gonorrhoeae* to cationic antimicrobial peptides and complement-mediated killing by normal human serum. *Infection and Immunity* **77**, 1112–1120 (2009).

276. Seib, K. L. *et al.* Factor H-binding protein is important for meningococcal survival in human whole blood and serum and in the presence of the antimicrobial peptide LL-37. *Infection and Immunity* **77**, 292–299 (Jan. 2009).
277. Frigimelica, E., Bartolini, E., Galli, G., Grandi, G. & Grifantini, R. Identification of 2 hypothetical genes involved in *Neisseria meningitidis* cathelicidin resistance. *The Journal of Infectious Diseases* **197**, 1124–1132 (Apr. 2008).
278. Chen, Y. C., Chuang, Y. C., Chang, C. C., Jeang, C. L. & Chang, M. C. A K⁺ uptake protein, TrkA, is required for serum, protamine, and polymyxin B resistance in *Vibrio vulnificus*. *Infection and Immunity* **72**, 629–636 (Feb. 2004).
279. Parra-Lopez, C., Lin, R., Aspedon, A. & Groisman, E. A. A *Salmonella* protein that is required for resistance to antimicrobial peptides and transport of potassium. *The EMBO Journal* **13**, 3964–3972 (Sept. 1994).
280. Groisman, E. A., Parra-Lopez, C., Salcedo, M., Lipps, C. J. & Heffron, F. Resistance to host antimicrobial peptides is necessary for *Salmonella* virulence. *Proceedings of the National Academy of Sciences* **89**, 11939–11943 (Dec. 1992).
281. Lofton, H., Anwar, N., Rhen, M. & Andersson, D. I. Fitness of *Salmonella* mutants resistant to antimicrobial peptides. *Journal of Antimicrobial Chemotherapy* **70**, 432–440 (Feb. 2015).
282. Vigil, P. D. *et al.* The repeat-in-toxin family member TosA mediates adherence of uropathogenic *Escherichia coli* and survival during bacteremia. *Infection and Immunity* **80**, 493–505 (Feb. 2012).
283. Gao, Q. *et al.* DNA microarray-mediated transcriptional profiling of avian pathogenic *Escherichia coli* O2 strain E058 during its infection of chicken. *Microbial Pathogenesis* **100**, 1–9 (Nov. 2016).
284. Cian, M. B., Giordano, N. P., Masilamani, R., Minor, K. E. & Dalebroux, Z. D. *Salmonella enterica* serovar typhimurium uses PbgA/YejM to regulate lipopolysaccharide assembly during bacteremia. *Infection and Immunity* **88**, 00758–19 (Jan. 2020).
285. Aljannat, M. A. *et al.* The moonlighting peroxiredoxin-glutaredoxin in *Neisseria meningitidis* binds plasminogen via a C-terminal lysine residue and contributes to survival in a whole blood model. *Microbial Pathogenesis* **139**, 103890 (Feb. 2020).
286. Eriksson, J., Eriksson, O. S. & Jonsson, A. B. Loss of meningococcal PilU delays microcolony formation and attenuates virulence *in vivo*. *Infection and Immunity* **80**, 2538–2547 (July 2012).
287. Barnier, J. P. *et al.* Type IV pilus retraction enables sustained bacteremia and plays a key role in the outcome of meningococcal sepsis in a humanized mouse model. *PLoS Pathogens* **17**, e1009299 (Feb. 2021).
288. Chen, Y. H. *et al.* T4 pili promote colonization and immune evasion phenotypes of nonencapsulated M4 *Streptococcus pyogenes*. *mBio* **11**, 01580–20 (July 2020).
289. Lazzarin, M. *et al.* Contribution of pilus type 2b to invasive disease caused by a *Streptococcus agalactiae* ST-17 strain. *BMC Microbiology* **17**, 148 (July 2017).
290. Barocchi, M. A. *et al.* A pneumococcal pilus influences virulence and host inflammatory responses. *Proceedings of the National Academy of Sciences* **103**, 2857–2862 (Feb. 2006).
291. Maisey, H. C. *et al.* A group B streptococcal pilus protein promotes phagocyte resistance and systemic virulence. *The FASEB Journal* **22**, 1715–1724 (June 2008).
292. Zou, Y. *et al.* The role of *galU* and *galE* of *Haemophilus parasuis* SC096 in serum resistance and biofilm formation. *Veterinary Microbiology* **162**, 278–284 (Feb. 2013).
293. Theilacker, C. *et al.* Glycolipids are involved in biofilm accumulation and prolonged bacteraemia in *Enterococcus faecalis*. *Molecular Microbiology* **71**, 1055–1069 (Feb. 2009).
294. Qadi, M. *et al.* Sensing Mg²⁺ contributes to the resistance of *Pseudomonas aeruginosa* to complement-mediated opsonophagocytosis. *Environmental Microbiology* **19**, 4278–4286 (2017).
295. Ha, U. & Jin, S. Expression of the *soxR* gene of *Pseudomonas aeruginosa* is inducible during infection of burn wounds in mice and is required to cause efficient bacteremia. *Infection and Immunity* **67**, 5324–5331 (1999).
296. De Souza-Hart, J. A., Blackstock, W., Di Modugno, V., Holland, I. B. & Kok, M. Two-component systems in *Haemophilus influenzae*: a regulatory role for *arcA* in serum resistance. *Infection and Immunity* **71**, 163–172 (Jan. 2003).
297. Wong, S. M., St. Michael, F., Cox, A., Ram, S. & Akerley, B. J. ArcA-regulated glycosyltransferase Lic2B promotes complement evasion and pathogenesis of nontypeable *Haemophilus influenzae*. *Infection and Immunity* **79**, 1971–1983 (May 2011).
298. Johnson, C. R. *et al.* Generation and characterization of a PhoP homologue mutant of *Neisseria meningitidis*. *Molecular Microbiology* **39**, 1345–1355 (Mar. 2001).
299. Newcombe, J. *et al.* Infection with an avirulent *phoP* mutant of *Neisseria meningitidis* confers broad cross-reactive immunity. *Infection and Immunity* **72**, 338–344 (Jan. 2004).
300. Tzeng, Y. L., Kahler, C. M., Zhang, X. & Stephens, D. S. MisR/MisS two-component regulon in *Neisseria meningitidis*. *Infection and Immunity* **76**, 704–716 (Feb. 2008).

301. Skorek, K. *et al.* Regulatory protein OmpR influences the serum resistance of *Yersinia enterocolitica* O:9 by modifying the structure of the outer membrane. *PLoS One* **8**, e79525 (Nov. 2013).
302. Geisinger, E. & Isberg, R. R. Antibiotic modulation of capsular exopolysaccharide and virulence in *Acinetobacter baumannii*. *PLOS Pathogens* **11**, e1004691 (2015).
303. Voyich, J. M. *et al.* The SaeR/S gene regulatory system is essential for innate immune evasion by *Staphylococcus aureus*. *Journal of Infectious Diseases* **199**, 1698–1706 (June 2009).
304. Guo, H., Hall, J. W., Yang, J. & Ji, Y. The SaeRS two-component system controls survival of *Staphylococcus aureus* in human blood through regulation of coagulase. *Frontiers in Cellular and Infection Microbiology* **7**, 204 (May 2017).
305. Hall, J. W., Yang, J., Guo, H. & Ji, Y. The AirSR two-component system contributes to *Staphylococcus aureus* survival in human blood and transcriptionally regulates *sspABC* operon. *Frontiers in Microbiology* **6**, 1–12 (2015).
306. James, E. H., Edwards, A. M. & Wigneshweraraj, S. Transcriptional downregulation of *agr* expression in *Staphylococcus aureus* during growth in human serum can be overcome by constitutively active mutant forms of the sensor kinase AgrC. *FEMS Microbiology Letters* **349**, 153–162 (Dec. 2013).
307. O’Keeffe, K. M. *et al.* Manipulation of autophagy in phagocytes facilitates *Staphylococcus aureus* bloodstream infection. *Infection and Immunity* **83**, 3445–3457 (Sept. 2015).
308. Walker, J. N. *et al.* The *Staphylococcus aureus* ArIRS Two-Component System Is a Novel Regulator of Agglutination and Pathogenesis. *PLOS Pathogens* **9**, e1003819 (2013).
309. Hirschmann, S. *et al.* The two-component system O9 regulates pneumococcal carbohydrate metabolism and capsule expression. *Microorganisms* **9**, 468 (Feb. 2021).
310. Sugareva, V. *et al.* Serotype- and strain- dependent contribution of the sensor kinase CovS of the CovRS two-component system to *Streptococcus pyogenes* pathogenesis. *BMC Microbiology* **10**, 34 (Feb. 2010).
311. Alves, L. A. *et al.* CovR regulates *Streptococcus mutans* susceptibility to complement immunity and survival in blood. *Infection and Immunity* **84**, 3206–3219 (2016).
312. Alves, L. A. *et al.* The two-component system VicRK regulates functions associated with *Streptococcus mutans* resistance to complement immunity. *Molecular Oral Microbiology* **32**, 419–431 (Oct. 2017).
313. Quach, D. *et al.* The CiaR response regulator in group B *Streptococcus* promotes intracellular survival and resistance to innate immune defenses. *Journal of Bacteriology* **191**, 2023–2032 (Apr. 2009).
314. Rajagopal, L., Vo, A., Silvestroni, A. & Rubens, C. E. Regulation of cytotoxin expression by converging eukaryotic-type and two-component signalling mechanisms in *Streptococcus agalactiae*. *Molecular Microbiology* **62**, 941–957 (Nov. 2006).
315. Pei, X., Liu, M., Zhou, H. & Fan, H. Screening for phagocytosis resistance-related genes via a transposon mutant library of *Streptococcus suis* serotype 2. *Virulence* **11**, 825–838 (Jan. 2020).
316. Liu, H. *et al.* Stk and Stp1 participate in *Streptococcus suis* serotype 2 pathogenesis by regulating capsule thickness and translocation of certain virulence factors. *Microbial Pathogenesis* **152**, 104607 (Mar. 2021).
317. Lourdault, K., Matsunaga, J. & Haake, D. A. High-Throughput parallel sequencing to measure fitness of *Leptospira interrogans* transposon insertion mutants during acute infection. *PLoS Neglected Tropical Diseases* **10**, e0005117 (Nov. 2016).
318. Goh, K. G. *et al.* Genome-wide discovery of genes required for capsule production by uropathogenic *Escherichia coli*. *mBio* **8**, 1558–1575 (Sept. 2017).
319. Dorman, M. J., Feltwell, T., Goulding, D. A., Parkhill, J. & Short, F. L. The capsule regulatory network of *Klebsiella pneumoniae* defined by density-TraDISort. *mBio* **9**, 01863–18 (Nov. 2018).
320. Xu, L. *et al.* The KbvR regulator contributes to capsule production, outer membrane protein biosynthesis, antiphagocytosis, and virulence in *Klebsiella pneumoniae*. *Infection and Immunity* **89**, 00016–21 (May 2021).
321. Garrett, S. B., Garrison-Schilling, K. L., Cooke, J. T. & Pettis, G. S. Capsular polysaccharide production and serum survival of *Vibrio vulnificus* are dependent on antitermination control by RfaH. *FEBS Letters* **590**, 4564–4572 (Dec. 2016).
322. Schwiesow, L. *et al.* Control of *hmu* heme uptake genes in *Yersinia pseudotuberculosis* in response to iron sources. *Frontiers in Cellular and Infection Microbiology* **8**, 47 (Feb. 2018).
323. Huja, S. *et al.* Fur is the master regulator of the extraintestinal pathogenic *Escherichia coli* response to serum. *mBio* **5**, 01460–14 (Aug. 2014).
324. Ho, Y. C. *et al.* Lrp, a global regulator, regulates the virulence of *Vibrio vulnificus*. *Journal of Biomedical Science* **24**, 54 (Aug. 2017).
325. Tang-Siegel, G. *et al.* Human serum-specific activation of alternative sigma factors, the stress responders in *Aggregatibacter actinomycetemcomitans*. *PLoS One* **11**, e0160018 (Aug. 2016).
326. Antunes, A. *et al.* HexR controls glucose-responsive genes and central carbon metabolism in *Neisseria meningitidis*. *Journal of Bacteriology* **198**, 644–654 (2016).

327. Krishna, A., Holde, M. T., Peacock, S. J., Edwards, A. M. & Wigneshweraraj, S. Naturally occurring polymorphisms in the virulence regulator Rsp modulate *Staphylococcus aureus* survival in blood and antibiotic susceptibility. *Microbiology* **164**, 1189 (Sept. 2018).
328. Groma, M. *et al.* Identification of a novel LysR-type transcriptional regulator in *Staphylococcus aureus* that is crucial for secondary tissue colonization during metastatic bloodstream infection. *mBio* **11**, 01646–20 (2020).
329. Gupta, R., Bhatti, M., Swiatlo, E. & Nanduri, B. Role of an iron-dependent transcriptional regulator in the pathogenesis and host response to infection with *Streptococcus pneumoniae*. *PLoS One* **8**, e55157 (Feb. 2013).
330. Dammann, A. N. *et al.* Genome-Wide fitness analysis of group B Streptococcus in human amniotic fluid reveals a transcription factor that controls multiple virulence traits. *PLoS Pathogens* **17**, e1009116 (Mar. 2021).
331. Liu, G. *et al.* The novel streptococcal transcriptional regulator XtgS negatively regulates bacterial virulence and directly represses PseP transcription. *Infection and Immunity* **88**, 00035–20 (Oct. 2020).
332. Siemens, N. *et al.* Effects of the ERES pathogenicity region regulator Ralp3 on *Streptococcus pyogenes* serotype M49 virulence factor expression. *Journal of Bacteriology* **194**, 3618–3626 (July 2012).
333. Allen, J. P. & Neely, M. N. The *Streptococcus iniae* transcriptional regulator CpsY is required for protection from neutrophil-mediated killing and proper growth *in vitro*. *Infection and Immunity* **79**, 4638–4648 (Nov. 2011).
334. Hufnagel, M., Koch, S., Creti, R., Baldassarri, L. & Huebner, J. A putative sugar-binding transcriptional regulator in a novel gene locus in *Enterococcus faecalis* contributes to production of biofilm and prolonged bacteremia in mice. *Journal of Infectious Diseases* **189**, 420–430 (Feb. 2004).
335. Langereis, J. D. *et al.* Nontypeable *Haemophilus influenzae* invasive blood isolates are mainly phosphorylcholine negative and show decreased complement-mediated killing that is associated with lower binding of IgM and CRP in comparison to colonizing isolates from the oropharynx. *Infection and Immunity* **87**, 00604–18 (Feb. 2019).
336. Lichtenegger, S. *et al.* Serum resistance and phase variation of a nasopharyngeal non-typeable *Haemophilus influenzae* isolate. *International Journal of Medical Microbiology* **307**, 139–146 (Feb. 2017).
337. VanWagoner, T. M. *et al.* The *modA10* phasevarion of nontypeable *Haemophilus influenzae* R2866 regulates multiple virulence-associated traits. *Microbial Pathogenesis* **92**, 60–67 (Mar. 2016).
338. Hammerschmidt, S. *et al.* Modulation of cell surface sialic acid expression in *Neisseria meningitidis* via a transposable genetic element. *The EMBO Journal* **15**, 192–198 (Jan. 1996).
339. Uria, M. J. *et al.* A generic mechanism in *Neisseria meningitidis* for enhanced resistance against bactericidal antibodies. *Journal of Experimental Medicine* **205**, 1423–1434 (June 2008).
340. Kandler, J. L. *et al.* Phase-variable expression of *lptA* modulates the resistance of *Neisseria gonorrhoeae* to cationic antimicrobial peptides. *Antimicrobial Agents and Chemotherapy* **58**, 4230–4233 (2014).
341. Broadbent, S. E., Davies, M. R. & Van Der Woude, M. W. Phase variation controls expression of *Salmonella* lipopolysaccharide modification genes by a DNA methylation-dependent mechanism. *Molecular Microbiology* **77**, 337–353 (July 2010).
342. Kim, J. O. & Weiser, J. N. Association of intrastrain phase variation in quantity of capsular polysaccharide and teichoic acid with the virulence of *Streptococcus pneumoniae*. *The Journal of Infectious Diseases* **177**, 368–377 (Feb. 1998).
343. Waite, R. D., Struthers, J. K. & Dowson, C. G. Spontaneous sequence duplication within an open reading frame of the pneumococcal type 3 capsule locus causes high-frequency phase variation. *Molecular Microbiology* **42**, 1223–1232 (Dec. 2001).
344. Sun, H. *et al.* An ArcA-Modulated Small RNA in Pathogenic *Escherichia coli* K1. *Frontiers in Microbiology* **11**, 574833 (Nov. 2020).
345. Fagnocchi, L. *et al.* Global transcriptome analysis reveals small RNAs affecting *Neisseria meningitidis* bacteremia. *PLoS One* **10**, 126325 (May 2015).
346. Pappesch, R. *et al.* The regulatory small RNA MarS supports virulence of *Streptococcus pyogenes*. *Scientific Reports* **7**, 12241 (Sept. 2017).
347. Mann, B. *et al.* Control of virulence by small RNAs in *Streptococcus pneumoniae*. *PLoS Pathogens* **8**, 34 (July 2012).
348. Danger, J. L. *et al.* The small regulatory RNA FasX enhances group A *Streptococcus* virulence and inhibits pilus expression via serotype-specific targets. *Molecular Microbiology* **96**, 249–262 (Apr. 2015).
349. Loh, E. *et al.* Temperature triggers immune evasion by *Neisseria meningitidis*. *Nature* **502**, 237–240 (Sept. 2013).
350. Spinsanti, M. *et al.* Deconvolution of intergenic polymorphisms determining high expression of Factor H binding protein in meningococcus and their association with invasive disease. *PLoS Pathogens* **17**, e1009461 (Mar. 2021).

351. Brewer, S. M. *et al.* A *Salmonella Typhi* RNA thermosensor regulates virulence factors and innate immune evasion in response to host temperature. *PLoS Pathogens* **17**, e1009345 (Mar. 2021).
352. Eichner, H. *et al.* RNA thermosensors facilitate *Streptococcus pneumoniae* and *Haemophilus influenzae* immune evasion. *PLoS Pathogens* **17** (ed Mitchell, T. J.) e1009513 (Apr. 2021).
353. Dasgupta, S., Das, S., Biswas, A., Bhadra, R. K. & Das, S. Small alarmones (p)ppGpp regulate virulence associated traits and pathogenesis of *Salmonella enterica* serovar Typhi. *Cellular Microbiology* **21**, e13034 (Aug. 2019).
354. Chau, N. Y. *et al.* (p)ppGpp-dependent regulation of the nucleotide hydrolase PpnN confers complement resistance in *Salmonella enterica* serovar typhimurium. *Infection and Immunity* **89** (Feb. 2021).
355. Sun, W., Roland, K. L., Branger, C. G., Kuang, X. & Curtiss, R. The role of *relA* and *spoT* in *Yersinia pestis* KIM5+ pathogenicity. *PLoS One* **4**, e6720 (Aug. 2009).
356. Hooven, T. A. *et al.* The *Streptococcus agalactiae* stringent response enhances virulence and persistence in human blood. *Infection and Immunity* **86**, 00612–17 (Jan. 2018).
357. Li, L. *et al.* The stringent response contributes to persistent methicillin-resistant *Staphylococcus aureus* endovascular infection through the purine biosynthetic pathway. *The Journal of Infectious Diseases* **222**, 1188–1198 (Sept. 2020).
358. Orth, D. *et al.* EspP, a serine protease of enterohemorrhagic *Escherichia coli*, impairs complement activation by cleaving complement factors C3/C3b and C5. *Infection and Immunity* **78**, 4294–4301 (Oct. 2010).
359. Henderson, I. R., Czeczulin, J., Eslava, C., Noriega, F. & Nataro, J. P. Characterization of Pic, a secreted protease of *Shigella flexneri* and enteroaggregative *Escherichia coli*. *Infection and Immunity* **67**, 5587–5596 (1999).
360. Cortés, G., De Astorza, B., Benedí, V. J. & Albertí, S. Role of the *htrA* gene in *Klebsiella pneumoniae* virulence. *Infection and Immunity* **70**, 4772–4776 (Sept. 2002).
361. Short, F. L. *et al.* Genomic profiling reveals distinct routes to complement resistance in *Klebsiella pneumoniae*. *Infection and Immunity* **88**, 00043–20 (Aug. 2020).
362. Laarman, A. J. *et al.* *Staphylococcus aureus* metalloprotease aureolysin cleaves complement C3 to mediate immune evasion. *Journal of Immunology* **186**, 6445–6453 (June 2011).
363. Lee, L. Y. *et al.* Inhibition of complement activation by a secreted *Staphylococcus aureus* protein. *Journal of Infectious Diseases* **190**, 571–579 (Aug. 2004).
364. Hammel, M. *et al.* Characterization of Ehp, a secreted complement inhibitory protein from *Staphylococcus aureus*. *Journal of Biological Chemistry* **282**, 30051–30061 (Oct. 2007).
365. Haupt, K. *et al.* The *Staphylococcus aureus* protein Sbi acts as a complement inhibitor and forms a tripartite complex with host complement factor H and C3b. *PLoS Pathogens* **4**, e1000250 (Dec. 2008).
366. Barthel, D., Singh, B., Riesbeck, K. & Zipfel, P. F. *Haemophilus influenzae* uses the surface protein E to acquire human plasminogen and to evade innate immunity. *Journal of Immunology* **188**, 379–385 (Jan. 2012).
367. Siqueira, G. H., Atzingen, M. V., de Souza, G. O., Vasconcellos, S. A. & Nascimento, A. L. *Leptospira interrogans* Lsa23 protein recruits plasminogen, factor H and C4BP from normal human serum and mediates C3B and C4B degradation. *Microbiology* **162**, 295–308 (Feb. 2016).
368. Ly, D. *et al.* Plasmin(ogen) acquisition by group A *Streptococcus* protects against C3b-Mediated neutrophil killing. *Journal of Innate Immunity* **6**, 240–250 (2014).
369. Hyland, K. A., Wang, B. & Cleary, P. P. Protein F1 and *Streptococcus pyogenes* resistance to phagocytosis. *Infection and Immunity* **75**, 3188–3191 (June 2007).
370. Rooijackers, S. H. M. *et al.* Early expression of SCIN and CHIPS drives instant immune evasion by *Staphylococcus aureus*. *Cellular Microbiology* **8**, 1282–1293 (Aug. 2006).
371. Oda, T. *et al.* Inactivation of chemotactic activity of C5a by the serratial 56-kilodalton protease. *Infection and Immunity* **58**, 1269–1272 (1990).
372. Wexler, D. E., Chenoweth, D. E. & Cleary, P. P. Mechanism of action of the group A streptococcal C5a inactivator. *Proceedings of the National Academy of Sciences of the United States of America* **82**, 8144–8148 (1985).
373. Whitnack, E. & Beachey, E. H. Antipsonic activity of fibrinogen bound to M protein on the surface of group A streptococci. *Journal of Clinical Investigation* **69**, 1042–1045 (Apr. 1982).
374. MacHeboeuf, P. *et al.* Streptococcal M1 protein constructs a pathological host fibrinogen network. *Nature* **472**, 64–70 (Apr. 2011).
375. Griffiths, N. J. *et al.* Meningococcal surface fibril (Msf) binds to activated vitronectin and inhibits the terminal complement pathway to increase serum resistance. *Molecular Microbiology* **82**, 1129–1149 (Dec. 2011).
376. Serruto, D. *et al.* *Neisseria meningitidis* GNA2132, a heparin-binding protein that induces protective immunity in humans. *Proceedings of the National Academy of Sciences* **107**, 3770–3775 (Feb. 2010).

377. Grosskinsky, S. *et al.* *Borrelia recurrentis* employs a novel multifunctional surface protein with anti-complement, anti-opsonic and invasive potential to escape innate immunity. *PLoS One* **4** (Mar. 2009).
378. Kochi, L. T. *et al.* The interaction of two novel putative proteins of *Leptospira interrogans* with E-cadherin, plasminogen and complement components with potential role in bacterial infection. *Virulence* **10**, 734–753 (2019).
379. Souza, N. M. *et al.* Lsa30, a novel adhesin of *Leptospira interrogans* binds human plasminogen and the complement regulator C4bp. *Microbial Pathogenesis* **53**, 125–134 (Sept. 2012).
380. Agarwal, V. *et al.* Enolase of *Streptococcus pneumoniae* binds human complement inhibitor C4b-binding protein and contributes to complement evasion. *The Journal of Immunology* **189**, 3575–3584 (Oct. 2012).
381. Ramos-Sevillano, E. *et al.* Pleiotropic effects of cell wall amidase LytA on *Streptococcus pneumoniae* sensitivity to the host immune response. *Infection and Immunity* **83**, 591–603 (2015).
382. Mukerji, R. *et al.* Pneumococcal surface protein A inhibits complement deposition on the pneumococcal surface by competing with the binding of C-reactive protein to cell-surface phosphocholine. *Journal of Immunology* **189**, 5327–5335 (Dec. 2012).
383. Severi, E. *et al.* Sialic acid transport in *Haemophilus influenzae* is essential for lipopolysaccharide sialylation and serum resistance and is dependent on a novel tripartite ATP-independent periplasmic transporter. *Molecular Microbiology* **58**, 1173–1185 (Nov. 2005).
384. Nakamura, S. *et al.* Molecular basis of increased serum resistance among pulmonary isolates of nontypeable *Haemophilus influenzae*. *PLoS Pathogens* **7**, 1001247 (Jan. 2011).
385. Collin, M. & Olsén, A. Effect of SpeB and EndoS from *Streptococcus pyogenes* on human immunoglobulins. *Infection and Immunity* **69**, 7187–7189 (2001).
386. Von Pawel-Rammingen, U., Johansson, B. P. & Björck, L. IdeS, a novel streptococcal cysteine proteinase with unique specificity for immunoglobulin G. *The EMBO journal* **21**, 1607–1615 (Apr. 2002).
387. Söderberg, J. J., Engström, P. & Von Pawel-Rammingen, U. The intrinsic immunoglobulin g endopeptidase activity of streptococcal Mac-2 proteins implies a unique role for the enzymatically impaired Mac-2 protein of M28 serotype strains. *Infection and Immunity* **76**, 2183–2188 (May 2008).
388. Björck, L. & Kronvall, G. Purification and some properties of streptococcal protein G, a novel IgG-binding reagent. *The Journal of Immunology* **133**, 969–74 (1984).
389. Honda-Ogawa, M. *et al.* *Streptococcus pyogenes* endopeptidase O contributes to evasion from complement-mediated bacteriolysis via binding to human complement factor C1q. *The Journal of Biological Chemistry* **292**, 4244–4254 (Mar. 2017).
390. Paton, J. C., Rowan Kelly, B. & Ferrante, A. Activation of human complement by the pneumococcal toxin pneumolysin. *Infection and Immunity* **43**, 1085–1087 (1984).
391. Kang, M. *et al.* Collagen-binding microbial surface components recognizing adhesive matrix molecule (MSCRAMM) of Gram-positive bacteria inhibit complement activation via the classical pathway. *The Journal of Biological Chemistry* **288**, 20520–20531 (July 2013).
392. Molla, A., Akaike, T. & Maeda, H. Inactivation of various proteinase inhibitors and the complement system in human plasma by the 56-kilodalton proteinase from *Serratia marcescens*. *Infection and Immunity* **57**, 1868–1871 (1989).
393. Woehl, J. L. *et al.* The extracellular adherence protein from *Staphylococcus aureus* inhibits the classical and lectin pathways of complement by blocking formation of the C3 proconvertase. *Journal of Immunology* **193**, 6161–6171 (Dec. 2014).
394. Lindholm, M., Min Aung, K., Nyunt Wai, S. & Oscarsson, J. Role of OmpA1 and OmpA2 in *Aggregatibacter actinomycetemcomitans* and *Aggregatibacter aphrophilus* serum resistance. *Journal of Oral Microbiology* **11**, 1536192 (2019).
395. Berggård, K., Johnsson, E., Mooi, F. R. & Lindahl, G. *Bordetella pertussis* binds the human complement regulator C4BP: role of filamentous hemagglutinin. *Infection and Immunity* **65**, 3638–3643 (1997).
396. Pietikäinen, J., Meri, T., Blom, A. M. & Meri, S. Binding of the complement inhibitor C4b-binding protein to Lyme disease *borreliae*. *Molecular Immunology* **47**, 1299–1305 (Mar. 2010).
397. Hallström, T., Jarva, H., Riesbeck, K. & Blom, A. M. Interaction with C4b-binding protein contributes to nontypeable *Haemophilus influenzae* serum resistance. *Journal of Immunology* **178**, 6359–6366 (May 2007).
398. Barbosa, A. S. *et al.* Functional characterization of LcpA, a surface-exposed protein of *Leptospira* spp. that binds the human complement regulator C4BP. *Infection and Immunity* **78**, 3207–3216 (July 2010).
399. Nordström, T., Blom, A. M., Forsgren, A. & Riesbeck, K. The emerging pathogen *Moraxella catarrhalis* interacts with complement inhibitor C4b binding protein through ubiquitous surface proteins A1 and A2. *The Journal of Immunology* **173**, 4598–4606 (Oct. 2004).
400. Santi, I. *et al.* BibA: a novel immunogenic bacterial adhesin contributing to group B *Streptococcus* survival in human blood. *Molecular Microbiology* **63**, 754–767 (Feb. 2007).

401. Thern, A., Stenberg, L., Dahlbäck, B. & Lindahl, G. Ig-binding surface proteins of *Streptococcus pyogenes* also bind human C4b-binding protein (C4BP), a regulatory component of the complement system. *The Journal of Immunology* **154**, 375–86 (1995).
402. Noofeli, M. *et al.* BapC autotransporter protein is a virulence determinant of *Bordetella pertussis*. *Microbial Pathogenesis* **51**, 169–177 (Sept. 2011).
403. Mil-Homens, D., Leç, M. I., Fernandes, F., Pinto, S. N. & Fialho, A. M. Characterization of BCAM0224, a multifunctional trimeric autotransporter from the human pathogen *Burkholderia cenocepacia*. *Journal of Bacteriology* **196**, 1968–1979 (2014).
404. Amdahl, H. *et al.* Interactions between *Bordetella pertussis* and the complement inhibitor factor H. *Molecular Immunology* **48**, 697–705 (Jan. 2011).
405. Kraicy, P., Skerka, C., Brade, V. & Zipfel, P. F. Further characterization of complement regulator-acquiring surface proteins of *Borrelia burgdorferi*. *Infection and Immunity* **69**, 7800–7809 (2001).
406. Kenedy, M. R., Vuppala, S. R., Siegel, C., Kraicy, P. & Akins, D. R. CspA-mediated binding of human factor H inhibits complement deposition and confers serum resistance in *Borrelia burgdorferi*. *Infection and Immunity* **77**, 2773–2782 (July 2009).
407. Hart, T. *et al.* Polymorphic factor H-binding activity of CspA protects Lyme *borreliae* from the host complement in feeding ticks to facilitate tick-to-host transmission. *PLoS Pathogens* **14**, e1007106 (May 2018).
408. Marcinkiewicz, A. L. *et al.* Blood treatment of Lyme *borreliae* demonstrates the mechanism of CspZ-mediated complement evasion to promote systemic infection in vertebrate hosts. *Cellular Microbiology* **21**, e12998 (Feb. 2019).
409. Hellwege, J. *et al.* The complement regulator Factor H binds to the surface protein OspE of *Borrelia burgdorferi*. *Journal of Biological Chemistry* **276**, 8427–8435 (Mar. 2001).
410. Poolpol, K. *et al.* Interaction of Shiga toxin 2 with complement regulators of the factor H protein family. *Molecular Immunology* **58**, 77–84 (Mar. 2014).
411. Rosadini, C. V., Ram, S. & Akerleya, B. J. Outer membrane protein P5 is required for resistance of nontypeable *Haemophilus influenzae* to both the classical and alternative complement pathways. *Infection and Immunity* **82**, 640–649 (Feb. 2014).
412. Hallström, T. *et al.* *Haemophilus influenzae* interacts with the human complement inhibitor factor H. *Journal of Immunology* **181**, 537–545 (July 2008).
413. Wolff, D. G. *et al.* Interaction of *Leptospira* elongation factor Tu with plasminogen and complement Factor H: a metabolic leptospiral protein with moonlighting activities. *PLOS ONE* **8**, e81818 (Nov. 2013).
414. Da Silva, L. B. *et al.* Pathogenic *Leptospira* species acquire factor H and vitronectin via the surface protein LcpA. *Infection and Immunity* **83**, 888–897 (2015).
415. Stevenson, B. *et al.* *Leptospira interrogans* endostatin-like outer membrane proteins bind host fibronectin, laminin and regulators of complement. *PLoS One* **2**, e1188 (Nov. 2007).
416. Verma, A. *et al.* LfhA, a novel factor H-binding protein of *Leptospira interrogans*. *Infection and Immunity* **74**, 2659–2666 (May 2006).
417. Castiblanco-Valencia, M. M. *et al.* Leptospiral immunoglobulin-like proteins interact with human complement regulators Factor H, FHL-1, FHR-1, and C4BP. *The Journal of Infectious Diseases* **205**, 995–1004 (Mar. 2012).
418. Schneider, M. C. *et al.* Functional Significance of Factor H Binding to *Neisseria meningitidis*. *The Journal of Immunology* **176**, 7566–7575 (June 2006).
419. Ram, S. *et al.* A novel sialic acid binding site on factor H mediates serum resistance of sialylated *Neisseria gonorrhoeae*. *Journal of Experimental Medicine* **187**, 743–752 (Mar. 1998).
420. Estabrook, M. M., McLeod Griffiss, J. & Jarvis, G. A. Sialylation of *Neisseria meningitidis* lipooligosaccharide inhibits serum bactericidal activity by masking lacto-N-neotetraose. *Infection and Immunity* **65**, 4436–4444 (1997).
421. Lewis, L. A. *et al.* Factor h-dependent alternative pathway inhibition mediated by porin B contributes to virulence of *Neisseria meningitidis*. *mBio* **4**, 00339–13 (Oct. 2013).
422. Areschoug, T., Stålhammar-Carlemalm, M., Karlsson, I. & Lindahl, G. Streptococcal beta protein has separate binding sites for human factor H and IgA-Fc. *The Journal of Biological Chemistry* **277**, 12642–12648 (Apr. 2002).
423. Mohan, S. *et al.* Tuf of *Streptococcus pneumoniae* is a surface displayed human complement regulator binding protein. *Molecular Immunology* **62**, 249–264 (2014).
424. Caswell, C. C. *et al.* The Scl1 protein of M6-type group A *Streptococcus* binds the human complement regulatory protein, factor H, and inhibits the alternative pathway of complement. *Molecular Microbiology* **67**, 584–596 (Feb. 2008).
425. Janulczyk, R., Iannelli, F., Sjöholm, A. G., Pozzi, G. & Björck, L. Hic, a novel surface protein of *Streptococcus pneumoniae* that interferes with complement function. *The Journal of Biological Chemistry* **275**, 37257–37263 (Nov. 2000).

426. Horstmann, R. D., Sievertsen, H. J., Knobloch, J. & Fischetti, V. A. Antiphagocytic activity of streptococcal M protein: selective binding of complement control protein factor H. *Proceedings of the National Academy of Sciences of the United States of America* **85**, 1657–1661 (1988).
427. Pian, Y. *et al.* Fhb, a novel factor H-binding surface protein, contributes to the antiphagocytic ability and virulence of *Streptococcus suis*. *Infection and Immunity* **80**, 2402–2413 (July 2012).
428. China, B., Sory, M. P., N'Guyen, B. T., De Bruyere, M. & Cornelis, G. R. Role of the YadA protein in prevention of opsonization of *Yersinia enterocolitica* by C3b molecules. *Infection and Immunity* **61**, 3129–3136 (1993).
429. Harvill, E. T. *et al.* Multiple roles for Bordetella lipopolysaccharide molecules during respiratory tract infection. *Infection and Immunity* **68**, 6720–6728 (2000).
430. Hallström, T. *et al.* CspA from *Borrelia burgdorferi* inhibits the terminal complement pathway. *mBio* **4**, 481–494 (Aug. 2013).
431. Siqueira, G. H., de Souza, G. O., Heinemann, M. B., Vasconcellos, S. A. & Nascimento, A. L. The role of Lsa23 to mediate the interaction of *Leptospira interrogans* with the terminal complement components pathway. *Microbial pathogenesis* **112**, 182–189 (Nov. 2017).
432. Amamura, T. A., Fraga, T. R., Vasconcellos, S. A., Barbosa, A. S. & Isaac, L. Pathogenic *Leptospira* secreted proteases target the membrane attack complex: a potential role for Thermolysin in complement inhibition. *Frontiers in Microbiology* **0**, 958 (May 2017).
433. Rhen, M. & Sukupolvi, S. The role of the traT gene of the *Salmonella typhimurium* virulence plasmid for serum resistance and growth within liver macrophages. *Microbial Pathogenesis* **5**, 275–285 (Oct. 1988).
434. Åkesson, P., Sjöholm, A. G. & Björck, L. Protein SIC, a novel extracellular protein of *Streptococcus pyogenes* interfering with complement function. *The Journal of Biological Chemistry* **271**, 1081–1088 (Jan. 1996).
435. Fernie-King, B. A. *et al.* Streptococcal inhibitor of complement (SIC) inhibits the membrane attack complex by preventing uptake of C567 onto cell membranes. *Immunology* **103**, 390–398 (2001).
436. Sanchez-Larrayoz, A. F. *et al.* Complexity of complement resistance factors expressed by *Acinetobacter baumannii* needed for survival in human serum. *The Journal of Immunology* **199**, 2803–2814 (Oct. 2017).
437. Wang, C. Y. *et al.* Prc contributes to *Escherichia coli* evasion of classical complement-mediated serum killing. *Infection and Immunity* **80**, 3399–3409 (Oct. 2012).
438. Sjölander, H., Eriksson, J., Maudsdotter, L., Aro, H. & Jonsson, A. B. Meningococcal outer membrane protein NhhA is essential for colonization and disease by preventing phagocytosis and complement attack. *Infection and Immunity* **76**, 5412–5420 (Nov. 2008).
439. Reynolds, B. L. & Pruul, H. Protective role of smooth lipopolysaccharide in the serum bactericidal reaction. *Infection and Immunity* **4**, 764–771 (Dec. 1971).
440. Grossman, N. *et al.* Lipopolysaccharide size and distribution determine serum resistance in *Salmonella montevideo*. *Journal of Bacteriology* **169**, 856–863 (1987).
441. Rautemaa, R., Jarvis, G. A., Marnila, P. & Meri, S. Acquired resistance of *Escherichia coli* to complement lysis by binding of glycoposphoinositol-anchored protectin (CD59). *Infection and Immunity* **66**, 1928–1933 (1998).
442. Singh, B. *et al.* A fine-tuned interaction between trimeric autotransporter *Haemophilus* surface fibrils and vitronectin leads to serum resistance and adherence to respiratory epithelial cells. *Infection and Immunity* **82**, 2378–2389 (2014).
443. Su, Y.-C. *et al.* *Haemophilus influenzae* P4 interacts with extracellular matrix proteins promoting adhesion and serum resistance. *The Journal of Infectious Diseases* **213**, 314–323 (Jan. 2016).
444. Singh, B., Al-Jubair, T., Mörgelin, M., Thunnissen, M. M. & Riesbeck, K. The unique structure of *Haemophilus influenzae* protein E reveals multiple binding sites for host factors. *Infection and Immunity* **81**, 801–814 (Mar. 2013).
445. Paulsson, M. *et al.* Bacterial outer membrane vesicles induce vitronectin release into the bronchoalveolar space conferring protection from complement-mediated killing. *Frontiers in Microbiology* **9** (July 2018).
446. Cavenague, M. F. *et al.* Characterization of a novel protein of *Leptospira interrogans* exhibiting plasminogen, vitronectin and complement binding properties. *International Journal of Medical Microbiology* **309**, 116–129 (Mar. 2019).
447. Singh, B. *et al.* Vitronectin binds to the head region of *Moraxella catarrhalis* ubiquitous surface protein A2 and confers complement-inhibitory activity. *Molecular Microbiology* **75**, 1426–1444 (Mar. 2010).
448. Singh, B., Su, Y. C. & Riesbeck, K. Vitronectin in bacterial pathogenesis: a host protein used in complement escape and cellular invasion. *Molecular Microbiology* **78**, 545–560 (2010).
449. Duensing, T. D. & Van Putten, J. P. Vitronectin binds to the gonococcal adhesin OpaA through a glycosaminoglycan molecular bridge. *The Biochemical Journal* **334** (Pt 1), 133–139 (Aug. 1998).

450. Cunha, C. S. E., Griffiths, N. J. & Virji, M. *Neisseria meningitidis* Opc invasin binds to the sulphated tyrosines of activated vitronectin to attach to and invade human brain endothelial cells. *PLoS Pathogens* **6**, e1000911 (May 2010).
451. Paulsson, M. *et al.* Identification of outer membrane Porin D as a vitronectin-binding factor in cystic fibrosis clinical isolates of *Pseudomonas aeruginosa*. *Journal of Cystic Fibrosis* **14**, 600–607 (Sept. 2015).
452. Kohler, S. *et al.* Binding of vitronectin and Factor H to Hic contributes to immune evasion of *Streptococcus pneumoniae* serotype 3. *Thrombosis and Haemostasis* **113**, 125–142 (2015).
453. Garcia, A., Solar, H., Gonzalez, C. & Zemelman, R. Effect of EDTA on the resistance of clinical isolates of *Acinetobacter baumannii* to the bactericidal activity of normal human serum. *Journal of Medical Microbiology* **49**, 1047–1050 (Nov. 2000).
454. Russo, T. A. *et al.* Penicillin-binding protein 7/8 contributes to the survival of *Acinetobacter baumannii* *in vitro* and *in vivo*. *Journal of Infectious Diseases* **199**, 513–521 (Feb. 2009).
455. King, L. B., Pangburn, M. K. & McDaniel, L. S. Serine protease PKF of *Acinetobacter baumannii* results in serum resistance and suppression of biofilm formation. *Journal of Infectious Diseases* **207**, 1128–1134 (Apr. 2013).
456. Jacobs, A. C. *et al.* Inactivation of phospholipase D diminishes *Acinetobacter baumannii* pathogenesis. *Infection and Immunity* **78**, 1952–1962 (May 2010).
457. Ganguly, T., Johnson, J. B., Kock, N. D., Parks, G. D. & Deora, R. The *Bordetella pertussis* Bps polysaccharide enhances lung colonization by conferring protection from complement-mediated killing. *Cellular Microbiology* **16**, 1105–1118 (2014).
458. Howard, C. J. & Glynn, A. A. The virulence for mice of strains of *Escherichia coli* related to the effects of K antigens on their resistance to phagocytosis and killing by complement. *Immunology* **20**, 767–777 (May 1971).
459. Russo, T. A., Moffitt, M. C., Hammer, C. H. & Frank, M. M. TnpA-mediated disruption of K54 capsular polysaccharide genes in *Escherichia coli* confers serum sensitivity. *Infection and Immunity* **61**, 3578–3582 (1993).
460. Buckles, E. L. *et al.* Role of the K2 capsule in *Escherichia coli* urinary tract infection and serum resistance. *Journal of Infectious Diseases* **199**, 1689–1697 (June 2009).
461. Fang, C.-T., Chuang, Y.-P., Shun, C.-T., Chang, S.-C. & Wang, J.-T. A novel virulence gene in *Klebsiella pneumoniae* strains causing primary liver abscess and septic metastatic complications. *Journal of Experimental Medicine* **199**, 697–705 (Mar. 2004).
462. Szijártó, V. *et al.* Both clades of the epidemic KPC-producing *Klebsiella pneumoniae* clone ST258 share a modified galactan O-antigen type. *International Journal of Medical Microbiology* **306**, 89–98 (Feb. 2016).
463. Hsieh, P.-F. *et al.* *Klebsiella pneumoniae* peptidoglycan-associated lipoprotein and murein lipoprotein contribute to serum resistance, antiphagocytosis, and proinflammatory cytokine stimulation. *The Journal of Infectious Diseases* **208**, 1580–1589 (Nov. 2013).
464. Schiller, N. L. & Joiner, K. A. Interaction of complement with serum-sensitive and serum-resistant strains of *Pseudomonas aeruginosa*. *Infection and Immunity* **54**, 689–694 (1986).
465. Kintz, E. & Goldberg, J. B. Regulation of lipopolysaccharide O antigen expression in *Pseudomonas aeruginosa*. *Future Microbiology* **3**, 191–203 (Apr. 2008).
466. Nishio, M., Okada, N., Miki, T., Haneda, T. & Danbara, H. Identification of the outer-membrane protein PagC required for the serum resistance phenotype in *Salmonella enterica* serovar Choleraesuis. *Microbiology* **151**, 863–873 (Mar. 2005).
467. Marshall, J. M. & Gunn, J. S. The O-antigen capsule of *Salmonella enterica* serovar Typhimurium facilitates serum resistance and surface expression of FliC. *Infection and Immunity* **83**, 3946–3959 (2015).
468. Williams, T. C., Ayrapetyan, M., Ryan, H. & Oliver, J. D. Serum survival of *Vibrio vulnificus*: role of genotype, capsule, complement, clinical origin, and *in situ* incubation. *Pathogens* **3**, 822–832 (Oct. 2014).

Appendix E

Original article: Within-host evolution of *Yersinia enterocolitica* during a chronic human infection

In this study, clinicians followed over more than ten years a case of chronic infection with *Y. enterocolitica* causing recurring bacteremia despite antibiotic treatments. Several strains were collected and characterized by the National Reference Center hosted in our laboratory. A mutation involved in antibiotic resistance was identified and genomic analysis revealed a massive loss of genes in strains isolated in late infections compared to strains isolated initially in the patient. My first role in this project was to characterize mutated and lost genes *in silico*, depicted in the discussion of the following article submitted for publication.

In addition to the information described in this manuscript, growth curves of the clinical strains were analyzed to better characterize the slow growth of the strains isolated in late infections. I also took advantage of the proteomics pipeline developed in chapter 5 to analyze the proteomes of the strains. A first examination confirmed the good correlation with genomic analysis, and further proteome-based analysis is ongoing to better describe metabolic and virulence differences between strains responsible for early and late infections.

1 **In-host evolution of *Yersinia enterocolitica* during a chronic human infection**

2

3

4 **Authors:**

5 Cyril Savin^{*1,2,3,4}, Pierre Lê-Bury^{1,4}, Julien Guglielmini⁵, Rodolphe Buzelé^{¶6,7}, Cécile Le Brun⁶, Frédéric

6 Bastides⁷, Maud François⁸, Béatrice Birmelé⁸, Nicolas Cabanel^{1,2,3}, Liliane Martin^{1,2,3}, Olivier

7 Dussurget^{1,4}, Elisabeth Carniel^{§1,2,3}, Philippe Lanotte^{#6,9}, Javier Pizarro-Cerdá^{*#1,2,3}

8

9 **Affiliations:**

10 ¹*Yersinia* Research Unit, Institut Pasteur, F-75724, Paris, France

11 ²*Yersinia* National Reference Laboratory, Institut Pasteur, F-75724, Paris, France

12 ³WHO Collaborative Reference & Research Center for *Yersinia*, Institut Pasteur, F-75724, Paris,

13 France

14 ⁴Université de Paris, F-75013, Paris, France

15 ⁵Hub de Bioinformatique et Biostatistique – Département Biologie Computationnelle, USR 3756

16 CNRS, Institut Pasteur, F-75724, Paris, France

17 ⁶Service de Bactériologie-Virologie, CHRU de Tours, F-37044 Tours, France

18 ⁷Service de Médecine Interne et des Maladies Infectieuses, CHRU de Tours, F-37044 Tours, France

19 ⁸Service d'Hémodialyse, CHRU de Tours, F-37044 Tours, France

20 ⁹ISP, INRA, Université de Tours, UMR1282, F-37380 Nouzilly, France

21

22 [¶] Present address: Service de Médecine interne, CH Yves Le Foll, 22000 Saint Briec, France

23 [§] Present address: General Director, Centre Pasteur du Cameroun, Yaoundé, Cameroon

24 [#] Authors contributed equally to this work

25

26 ***Corresponding authors:**

27 Cyril Savin and Javier Pizarro-Cerdá

28 Unité de Recherche *Yersinia*

29 Institut Pasteur

30 28 rue du Dr Roux

31 75724 Paris cedex 15, France

32 Phone: 00-33-1-40-61-37-67

33 e-mail: cyril.savin@pasteur.fr ; javier.pizarro-cerda@pasteur.fr

34 **ABSTRACT**

35 Following a pacemaker implantation, a 75-years-old patient suffered from five successive bacteremia
36 episodes between in 1999 and 2013, during which five bacterial strains were isolated. Phenotypic
37 and whole-genome sequencing analysis of four isolates identified the strains as *Yersinia*
38 *enterocolitica* bioserotype 4/O:3. Phylogenetic reconstruction showed that the patient was
39 chronically infected by the same strain, which evolved within the host for 14 years. Single-nucleotide
40 polymorphism (SNP) analysis indicates that the last two isolates, which displayed severe growth
41 defects *in vitro* and acquired resistance to quinolones, evolved in parallel and formed two
42 independent lineages within the host. Pan-genome analysis and genome comparison showed that
43 their common evolution was characterized by 41 small insertion/deletion events and loss of three
44 large DNA fragments. These mutations, which may account for the observed growth defect and for
45 the appearance of vegetations on the pacemaker, support antibiotics tolerance. Quinolone
46 resistance was acquired through a so far undescribed deletion in the *gyrA* gene. 140 genes
47 containing mutations vertically acquired from a common ancestor were also identified in the two
48 lineages. A phylogenetic analysis by maximum likelihood identified two genes presenting a positive
49 selection signal, suggesting that these mutations provided a survival advantage to bacteria during
50 chronic infection. This is the first report allowing identification of genetic changes associated to
51 within-host adaptation of a pathogenic *Yersinia* species.

52

53

54 **MAIN**

55 Bacterial exposure to a novel environment in a host creates conditions where evolution might take
56 place. As observed for cancer cells, a bacterial clone can experience selection for an accumulation of
57 genetic variants that promote long-term survival and clonal expansion¹. This scenario has been
58 observed in cystic fibrosis patients who can be chronically infected with pathogenic bacteria. In a
59 study from a single patient infected for 20 years with *Burkholderia multivorans*, bacterial adaptation
60 to respiratory airways was associated with mutations affecting metabolism, cell envelope, and
61 biofilm formation². In a different study concerning 474 *P. aeruginosa* isolates from 34 cystic fibrosis
62 patients, convergent evolution of 52 genes involved in antibiotic resistance, motility, and biofilm
63 formation was observed³. Host-adaptation through rapid evolution of a *Salmonella enterica* serotype
64 Enteridis causing a chronic systemic infection was documented in an immunocompromised patient⁴.
65 Genetic diversification of *Staphylococcus epidermidis* has also been described during a 16-week
66 pacemaker-associated endocarditis, leading to increased biofilm formation, reduced growth rate,
67 and antibiotic tolerance⁵.
68 In-host evolution has not been reported for infections associated with *Yersinia* spp. Yersinioses
69 include fulminant infections such as plague caused by *Yersinia pestis*, as well as mild or severe
70 enteritis caused by *Yersinia pseudotuberculosis* or *Yersinia enterocolitica* (*Ye*)^{6,7}. The latter represents
71 the fourth most common cause of diarrhea from bacterial origin in temperate and cold countries⁸.
72 Systemic *Ye* infections occur mostly in elderly patients with underlying disorders such as diabetes,
73 iron overload, or cirrhosis⁹.
74 Persistent *Y. enterocolitica* infections in patients causing relapses for several years have been
75 reported¹⁰, but the potential genetic relationships between the isolated strains was not determined.
76 This study is the first report of long-term, in-host evolution of a pathogenic *Yersinia* species in a
77 patient presenting iterative episodes of bacteremia over 14 years.

78

79 RESULTS

80 Case description

81 A 75-year-old woman presented with an atrioventricular block that led to a pacemaker implantation
82 in September 1998. In December 1999, the patient had a first septicemic episode resulting in the
83 isolation of a *Ye* strain (Ye.1) (Table 1). She received ceftriaxone and netilmicin treatment for 4 weeks
84 and recovered. In January 2000, the patient experienced a second episode of bacteremia with
85 isolation of another *Ye* strain (Ye.2). She was treated with the same antibiotics for four weeks,
86 followed by 18 months of ciprofloxacin therapy (until July 2001). A third bacteremia occurred in
87 August 2001 with isolation of a third *Ye* (Ye.X, not kept in collection) that was resistant to nalidixic
88 acid but susceptible to ciprofloxacin, which had been used for treatment. The patient received a
89 long-term ceftriaxone therapy until July 2005. In June 2006, the patient was hospitalized for a sepsis
90 but had a negative blood culture. For the first time, echocardiography evidenced vegetations on the
91 pacemaker atrial lead, suggesting endocarditis due to bacterial growth on the cardiac device (Figure
92 S1). A 6-year ceftriaxone treatment was administered, leading to vegetation disappearance. In
93 December 2012, the patient suffered from pneumonia, and ceftriaxone treatment was replaced by
94 spiramycin. In January 2013, she presented with another bacteremia with isolation of a fourth *Ye*
95 strain (Ye.3) and vegetations reappeared on the pacemaker atrial lead. Strain Ye.3, like Ye.X, was
96 resistant to nalidixic acid. The patient was treated with piperacillin/tazobactam/amikacin for one
97 week, followed by a 9-month ceftriaxone therapy. The patient had a last bacteremia in October 2013,
98 during which a fifth *Ye* strain (Ye.4) was isolated. Minimum inhibitory concentration (MIC) of
99 ceftriaxone increased from 0.19 mg/l (Ye.3) to 2 mg/l (Ye.4) leading to antimicrobial treatment
100 modification with cotrimoxazole. Three months later, the patient died of heart failure.

101 *Yersinia enterocolitica* strains were associated with the bacteremia

102 The five strains isolated during the iterative bacteremia were initially identified as *Ye* (Table 1) using a
103 VITEK2 GN card. Except for Ye.X, which was not kept in collection, strains were subjected to

104 phenotypical characterization: Ye.1 and Ye.2 were identified as *Ye* bioserotype 4/O:3; due to a severe
105 growth defect, Ye.3 and Ye.4 could not be characterized by phenotypic methods. We obtained
106 taxonomic assignment based on a core-genome multilocus sequence typing (cgMLST) with 500 core
107 genes using whole-genome *de novo* sequence, confirming that strains Ye.1 to Ye.4 belong to the *Ye*
108 genotype 4, corresponding to bioserotype 4/O:3.

109 **Chronic infection caused the multiple episodes of bacteremia**

110 To investigate whether the multiple infection episodes were independent or due to a chronic
111 colonization by a unique evolving bacterial strain, we studied the genetic relatedness of strains Ye.1
112 to Ye.4 by a core-genome single-nucleotide polymorphism analysis, with inclusion of 259 additional
113 *Ye* biotype 4 strains. The phylogenetic tree reconstruction based on analysis of 4,738 SNPs showed
114 that Ye.1 to Ye.4 were closely related and formed a unique clade separated from other *Ye* strains
115 (Figure 1.A). This result strongly suggests that the patient suffered from a chronic infection due to a
116 unique evolving *Ye* 4/O:3 strain.

117 **In-host evolution of *Y. enterocolitica* led to antibiotic tolerance**

118 We next analyzed the molecular events that characterized the in-host evolution of Ye.1 to Ye.4.
119 Genomic comparison and pan-genome phylogenetic analysis did not evidence any gene acquisition
120 or small insertion/deletion events that were common and specific to the four *Ye* isolates.
121 Ye.1 (isolated in December 1999) and Ye.2 (isolated in January 2000) were identical except for the
122 loss in Ye.1 of a 1.5 kb region (between nucleotides 4,282,424 and 4,283,952 from the Y11 reference
123 genome), indicating that evolution had already started within the first months of infection (Figure
124 1.A). The use of the least-squares dating tool (<https://lsdating.pasteur.fr>) estimated the closest
125 internal node for Ye.1 and Ye.2 in October 1999, suggesting that the patient was contaminated at
126 least two months before the first bacteremic episode (Figure 1.B). The closest internal node for Ye.3
127 (isolated in January 2013) and Ye.4 (isolated in October 2013) was January 2011 (Figure 1.B). Their
128 common ancestor had therefore evolved in the patient for 11 years and had accumulated 195 SNPs

129 before diverging into Ye.3 and Ye.4, which since accumulated an additional 25 and 40 SNPs,
130 respectively. 140 genes containing mutations vertically acquired from their common ancestor
131 (synapomorphies) were identified in the Ye.3 and Ye.4 genomes, including the *gyrA* gene (see below
132 and Table S2).

133 Ye.3 and Ye.4 shared three identical large deletions: a 2-gene deletion of 2.5 kb, a 9-gene deletion of
134 9.9 kb, and a 28-gene deletion of 32.7 kb (Table 2). These strains also shared 41 small
135 insertions/deletions (Table 3). Whereas 6 genes did not exhibit any frameshift, 35 genes displayed a
136 mutation leading to a truncated form of the product, and thus to loss-of-function. Truncated genes
137 and deleted regions were found to be involved in essential physiological functions such as
138 transcription, translation, replication, respiration, division, and carbohydrate and iron metabolism
139 (Figure 2, Tables S3 and S4). The loss of these essential functions accounts for the severe growth
140 defect displayed by Ye.3 and Ye.4, and probably contributes to antibiotic tolerance. Mutations
141 favoring biofilm formation and loss of planktonic life were also detected in these strains (Figure 2,
142 Tables S3 and S4), accounting for the appearance of vegetations on the pacemaker atrial lead, which
143 should also contribute to antibiotic tolerance.

144 Interestingly, a positive selection signal was detected in the acyl-CoA thioesterase II in all isolated
145 strains, and in a phosphate transporter in strains Ye.3 and Ye.4 (Table S5). Therefore, these
146 mutations likely provide an advantage to the strains for their survival and multiplication in the host.

147 **In-host evolution of *Y. enterocolitica* led to quinolone resistance**

148 We tested antimicrobial susceptibility for strains Ye.1, Ye.2 and Ye.3. Ye.4 could not be tested due to
149 a severe growth defect *in vitro*. The first two strains were resistant to amoxicillin,
150 amoxicillin/clavulanic acid, and first-generation cephalosporin, and they were susceptible to all other
151 tested antibiotics, as usually observed for *Ye* bioserotype 4/O:3. Ye.X and Ye.3 had the same
152 antibiotic susceptibility profile as Ye.1 and Ye.2, except that they were resistant to nalidixic acid, a
153 quinolone (Table 1). Resistance to quinolones in *Ye* O:3 is associated with a substitution in the

154 quinolone resistance-determining region (QRDR) of the *gyrA* gene at glycine 81, serine 83, or
155 asparagine 87^{11,12}. Comparison of *gyrA* sequences of Ye.1 to Ye.4 with those of the reference strain
156 Y11 and strain IP38477, which are susceptible to nalidixic acid, showed that Ye.3 and Ye.4 displayed
157 the same 3-nucleotide deletion at positions 245 to 247 in the QRDR of *gyrA* (Figure S2.A). This so far
158 undescribed deletion leads to replacement of aspartic acid 82 and serine 83 with a unique glycine
159 without any frameshift, explaining the genetic basis of the resistance to quinolones in Ye.3 and Ye.4
160 (Table 3, Figure S2.B). As mentioned, the ceftriaxone MIC increased for Ye.4 (2 mg/l) in comparison
161 to Ye.3 (0.19 mg/l). Genomic analyses did not reveal any mutation leading to ceftriaxone resistance,
162 suggesting that the increase in MIC was due to antibiotic tolerance, probably associated with the
163 mutations perturbing essential physiological functions.

164

165 **DISCUSSION**

166 This is the first report of a chronic *Ye* infection case due to a strain evolving in the same patient.
167 Between December 1999 and October 2013, antibiotics were apparently successful in the treatment
168 of five independent *Ye* bacteremia episodes; however, discontinuation of antibiotics was always
169 followed by a new bacteremia. The appearance of vegetations observed by echocardiography in
170 2006, and their disappearance during therapy, argue for *Ye* growth on the atrial lead of the
171 pacemaker and release into the bloodstream during the antibiotic discontinuation periods.
172 Genomic analyses of four *Ye* strains (Ye.1 to Ye.4) isolated from the patient allowed us to identify two
173 major mechanisms that explain the persistent bacterial infection: antibiotic resistance and antibiotic
174 tolerance. Concerning the first mechanism, resistance to nalidixic acid was already observed from
175 August 2001. Resistance to quinolones usually involves mutations in the QRDR of the *gyrA* gene,
176 leading either to (i) a change of glycine 81 into cysteine, (ii) a change of serine 83 into arginine,
177 isoleucine, or cysteine, or (ii) a change of aspartic acid 87 into a tyrosine, asparagine, or glycine¹¹⁻¹³.
178 In Ye.3, we observed a previously undescribed deletion of 3 nucleotides in the *gyrA* QRDR, leading to

179 substitution of aspartic acid 82 and serine 83 by a unique glycine. Our work thus identifies a novel
180 mutation in *gyrA* likely leading to quinolone resistance. The presence of the same mutation in Ye.4
181 suggests that this strain was also quinolone resistant.

182 Despite prolonged ceftriaxone treatment, no resistance to this antibiotic was identified through
183 phenotypic or genomic analyses in the *Ye* isolates. However, antibiotic tolerance could explain
184 bacterial survival to this treatment. Two major biological processes contribute to antibiotic tolerance:
185 biofilm formation^{14,15} and slow growth and/or metabolic dormancy^{16,17}. Vegetations detected in the
186 pacemaker argue for the formation of a biofilm by the *Ye* strains. *Ye* biofilm production has been
187 reported on medical devices such as catheters or feeding tubes^{15,18}. We identified several mutations
188 in Ye.3 and Ye.4 which can be associated with loss of motility and planktonic growth, favoring biofilm
189 formation: for example, mutation of the flagellar genes *flgD* in both Ye.3 and Ye.4, and *flgG* and *flgA*
190 in Ye.4. Of note, loss-of-function mutations associated with decreased motility have been identified
191 in *Burkholderia spp.* and *P. aeruginosa* isolates from cystic fibrosis patients^{2,3}. In addition, flagellar
192 assembly is repressed in adverse and nutrient-poor environments owing to its energetic cost¹⁹. We
193 also identified mutations in the pppGpp pyrophosphatase *gppA* gene and the RNA polymerase-
194 binding transcription factor *dksA* gene, both involved in the stringent response to nutrient
195 starvation²⁰, and associated with biofilm formation and growth²¹. Along these lines, stringent
196 response regulates biofilm formation in *Pseudomonas putida*²¹.

197 Ye.3 and Ye.4 displayed a severe growth defect *in vitro*. In these strains, we identified mutations in
198 genes involved in metabolism or growth in several gene clusters. Mutations in a large gene cluster
199 encoding the RNA polymerase subunits RpoC and RpoD, the DNA topoisomerase ParE, and the 50S
200 ribosomal protein RplF could account for slow growth, as seen in *Escherichia coli*²²⁻²⁴ and
201 *Staphylococcus aureus*^{25,26}. We also observed mutations in genes encoding electron (*rsxABCDEG*) and
202 ABC (*sapABCDF*) transporters required for optimal growth. Interestingly, mutations in a putative
203 toxin ABC transporter operon (*YE1998-YE2000*) as well as loss of the pore-forming toxin YaxAB

204 (YE1984-YE1985) suggest that bacteria defective for pathogenic functions that carry a fitness cost can
205 be selected to favor host adaptation. The strain Ye.4 displayed a more severe growth defect than
206 Ye.3, which can be associated with mutations in important metabolic genes such as genes involved in
207 amino-acid biosynthesis (*mtnA*, *metF*, *carA*), carbon metabolism (*serA*, *metF*), transcriptional
208 regulation (*putA*, *phnF*), and DNA replication (*gyrA*, *gyrB*) (Table S6).

209 In all isolated strains, a positive selection signal was detected in the acyl-CoA thioesterase II, which
210 regulates levels of acyl-CoAs, free fatty acids, and coenzyme A. In position 280 of this enzyme, a
211 glycine is normally conserved in diverse eukaryotic and bacterial species²⁷, while in Ye.1 to Ye.4 a
212 serine was present. Position 280 is located next to important residues involved in two catalytic triads
213 (Q278 together with N204 and T228, as well as E279 together with H58 and S107) and a dimer
214 interface (V277 and V281). We hypothesize that a S280 mutation promoted important adaptive
215 changes in the catalytic and functional activities of the acyl-CoA thioesterase II that were rapidly
216 selected at the onset of the chronic infection, since this mutation was conserved in all the strains
217 isolated from the patient. Another positive selection signal was present in a phosphate transporter,
218 for which the C-terminal region displayed a deletion observed only in Ye.3 and Ye.4 that affects two
219 cytoplasmic and two transmembrane domains. While we did not investigate the specific contribution
220 of this deletion to the functionality of the phosphate transporter, the positive selection signal
221 suggests that the promoted changes provided a survival advantage.

222 In conclusion, we report the unusual clinical case of a patient with iterative bacteremia and
223 endocarditis due to a *Ye* bioserotype 4/O:3 strain evolving over a period of 14 years. The last two
224 isolates, which were simultaneously evolving in the patient, accumulated mutations that allowed
225 antibiotic resistance (a previously unknown substitution conferring resistance to quinolones) and
226 antibiotic tolerance. The latter phenotype was associated with a reduction in genome size and loss of
227 essential functions for growth *in vitro*, while retaining the ability to survive in the host. The last
228 isolated strains caused bacteremia despite the continuity of the antibiotic treatment, highlighting the

229 transition occurring between early onset tolerance and resistance, a critical problem in antibiotic
230 treatment that should urgently be addressed²⁸⁻³⁰. Our findings have implications in case
231 management, as they reinforce the need for early pacemaker removal in addition to
232 antibiotherapy³¹. They may also guide future design of more effective treatments for chronic and
233 biofilm-associated bacterial infections. If the infected material cannot be removed as it was the case
234 in our study, the choice of the right antibiotic is crucial. It must be well tolerated by the patient, be
235 active on the biofilm and should not promote the emergence of resistance nor tolerance. It appears
236 here that long-term ceftriaxone has been well tolerated and did not generate resistance, however it
237 induced tolerance to this antibiotic. Investigation of the mechanisms modulating antibiotic tolerance
238 is therefore a critical issue for the treatment of long-term infections.

239

240 **METHODS**

241 **Phenotypic characterization**

242 Bacterial strains were identified using the VITEK2 GN card (bioMérieux) and were sent to the *Yersinia*
243 National Reference Laboratory (Institut Pasteur) for species confirmation/characterization as
244 described³².

245 **Antibiotic resistance profiling**

246 Antibiotic resistance profile of the bacterial strains was determined using VITEK2 (bioMérieux) and by
247 disk diffusion method on Mueller-Hinton agar supplemented with 5% horse blood (bioMérieux) for
248 growth deficient isolates. Interpretation was performed according to the recommendations of the
249 Antibiogram Committee of the French Society for Microbiology.

250 **Whole genome sequencing and analysis**

251 Bacterial genomes were sequenced as previously described³³. Genome sequences are available in the
252 European Nucleotide Archive under BioProject PRJEB19854 (sample ID starting with ERS and
253 accession numbers starting with FWC) for *Y. enterocolitica* 1 (Ye.1) (ERS1580350, FWCF02000001-

254 FWCF02000181), Ye.2 (ERS1580351, FWCE02000001-FWCE02000227), Ye.3 (ERS1580352,
255 FWCB02000001-FWCB02000195), and Ye.4 (ERS1580353, FWCD02000001-FWCD02000173). Whole
256 genome-based taxonomic assignment was obtained as described³³.

257 259 epidemiologically unrelated *Ye 4/O:3* strains isolated between 1982 and 2016 were also
258 sequenced and public genomes of 34 additional strains were used for subsequent analysis (Table S1).
259 Paired-end FASTQ files were used for variant calling using the Y11 reference strain (accession
260 number: NC_017564) with Snippy version 4.1.0³⁴. Putative recombinogenic regions were detected
261 and masked with Gubbins version 2.3.4³⁵. A maximum-likelihood phylogenetic tree was built from an
262 alignment of 4,738 chromosomal SNPs with RAxML version 8.2.8³⁶. Tree visualization was created
263 with iTOL³⁷.

264 **Pan-genome phylogenetic analysis**

265 A total of 96 additional *Ye* strains were randomly selected together with the *Ye.1-4* for Phylogenetic
266 Analysis by Maximum Likelihood (PAML)³⁸. A pan-genome was constructed using PPanGGOLiN³⁹.
267 Each gene of the pan-genome (3,824 genes) was translated to proteins and aligned using MAFFT
268 v7.407⁴⁰, allowing to search for genes specific to *Ye* isolates. Back translation to nucleotide was
269 performed to obtain codon alignment, and a phylogenetic tree was built for each gene using IQ-TREE
270 v1.6.7.2⁴¹. IQ-TREE's ModelFinder⁴² was used to estimate the best variant of the General Time
271 Reversible (GTR) model. The 3,612 genes for which the strains *Ye.3* and *Ye.4* are not sisters in the
272 tree were removed. Synapomorphies were analyzed using a dedicated script
273 (<https://gitlab.pasteur.fr/GIPhy/findSynapomorphies/>). PAML tests detected genes under positive
274 selection pressure.

275

276 **REFERENCES**

- 277 1. Didelot, X., Walker, A.S., Peto, T.E., Crook, D.W. & Wilson, D.J. Within-host evolution of
278 bacterial pathogens. *Nat Rev Microbiol* **14**, 150-162 (2016).
- 279 2. Silva, I.N., *et al.* Long-term evolution of *Burkholderia multivorans* during a chronic cystic
280 fibrosis infection reveals shifting forces of selection. *mSystems* **1**(2016).
- 281 3. Marvig, R.L., Sommer, L.M., Molin, S. & Johansen, H.K. Convergent evolution and adaptation
282 of *Pseudomonas aeruginosa* within patients with cystic fibrosis. *Nat Genet* **47**, 57-64 (2015).
- 283 4. Klemm, E.J., *et al.* Emergence of host-adapted *Salmonella* Enteritidis through rapid evolution
284 in an immunocompromised host. *Nat Microbiol* **1**, 15023 (2016).
- 285 5. Dengler Haunreiter, V., *et al.* In-host evolution of *Staphylococcus epidermidis* in a pacemaker-
286 associated endocarditis resulting in increased antibiotic tolerance. *Nat Commun* **10**, 1149
287 (2019).
- 288 6. Carniel, E., *et al.* *Y. enterocolitica* and *Y. pseudotuberculosis*. *The Prokaryotes* (Springer New
289 York, 2006).
- 290 7. Perry, R.D. & Fetherston, J.D. *Yersinia pestis*--etiologic agent of plague. *Clin Microbiol Rev* **10**,
291 35-66 (1997).
- 292 8. European Food Safety Authority and European Centre for Disease Prevention and Control
293 (EFSA and ECDC). The European Union One Health 2018 Zoonoses Report. *EFSA Journal*
294 **17**(2019).
- 295 9. Bottone, E.J. *Yersinia enterocolitica*: the charisma continues. *Clin Microbiol Rev* **10**, 257-276
296 (1997).
- 297 10. Hoogkamp-Korstanje, J.A., de Koning, J. & Heesemann, J. Persistence of *Yersinia*
298 *enterocolitica* in man. *Infection* **16**, 81-85 (1988).
- 299 11. Capilla, S., *et al.* Characterization of the molecular mechanisms of quinolone resistance in
300 *Yersinia enterocolitica* O:3 clinical isolates. *J Antimicrob Chemother* **53**, 1068-1071 (2004).

- 301 12. Drummond, N., Stephan, R., Haughton, P., Murphy, B.P. & Fanning, S. Further
302 characterization of three *Yersinia enterocolitica* strains with a nalidixic acid-resistant
303 phenotype isolated from humans with diarrhea. *Foodborne Pathog Dis* **10**, 744-746 (2013).
- 304 13. Sanchez-Cespedes, J., *et al.* Clonal dissemination of *Yersinia enterocolitica* strains with
305 various susceptibilities to nalidixic acid. *J Clin Microbiol* **41**, 1769-1771 (2003).
- 306 14. Girard, L.P., Ceri, H., Gibb, A.P., Olson, M. & Sepandj, F. MIC versus MBEC to determine the
307 antibiotic sensitivity of *Staphylococcus aureus* in peritoneal dialysis peritonitis. *Perit Dial Int*
308 **30**, 652-656 (2010).
- 309 15. Ioannidis, A., Kyratsa, A., Ioannidou, V., Bersimis, S. & Chatzipanagiotou, S. Detection of
310 biofilm production of *Yersinia enterocolitica* strains isolated from infected children and
311 comparative antimicrobial susceptibility of biofilm versus planktonic forms. *Molecular*
312 *diagnosis & therapy* **18**, 309-314 (2014).
- 313 16. Brauner, A., Fridman, O., Gefen, O. & Balaban, N.Q. Distinguishing between resistance,
314 tolerance and persistence to antibiotic treatment. *Nat Rev Microbiol* **14**, 320-330 (2016).
- 315 17. Fridman, O., Goldberg, A., Ronin, I., Shores, N. & Balaban, N.Q. Optimization of lag time
316 underlies antibiotic tolerance in evolved bacterial populations. *Nature* **513**, 418-421 (2014).
- 317 18. Hurrell, E., *et al.* Neonatal enteral feeding tubes as loci for colonisation by members of the
318 *Enterobacteriaceae*. *BMC Infect Dis* **9**, 146 (2009).
- 319 19. Zhao, K., Liu, M. & Burgess, R.R. Adaptation in bacterial flagellar and motility systems: from
320 regulon members to 'foraging'-like behavior in *E. coli*. *Nucleic Acids Res* **35**, 4441-4452
321 (2007).
- 322 20. Song, H., *et al.* Structure and activity of PPX/GppA homologs from *Escherichia coli* and
323 *Helicobacter pylori*. *FEBS J* **287**, 1865-1885 (2020).
- 324 21. Diaz-Salazar, C., *et al.* The stringent response promotes biofilm dispersal in *Pseudomonas*
325 *putida*. *Sci Rep* **7**, 18055 (2017).

- 326 22. Nandy, P., Chib, S. & Seshasayee, A. A mutant RNA polymerase activates the general stress
327 response, enabling *Escherichia coli* adaptation to late prolonged stationary phase. *mSphere*
328 **5**(2020).
- 329 23. Maciag, A., *et al.* *In vitro* transcription profiling of the sigmaS subunit of bacterial RNA
330 polymerase: re-definition of the sigmaS regulon and identification of sigmaS-specific
331 promoter sequence elements. *Nucleic Acids Res* **39**, 5338-5355 (2011).
- 332 24. Harms, A., *et al.* Adenylation of Gyrase and Topo IV by FicT Toxins Disrupts Bacterial DNA
333 Topology. *Cell Rep* **12**, 1497-1507 (2015).
- 334 25. Norstrom, T., Lannergard, J. & Hughes, D. Genetic and phenotypic identification of fusidic
335 acid-resistant mutants with the small-colony-variant phenotype in *Staphylococcus aureus*.
336 *Antimicrob Agents Chemother* **51**, 4438-4446 (2007).
- 337 26. Proctor, R.A., *et al.* *Staphylococcus aureus* Small Colony Variants (SCVs): a road map for the
338 metabolic pathways involved in persistent infections. *Front Cell Infect Microbiol* **4**, 99 (2014).
- 339 27. Li, J., Derewenda, U., Dauter, Z., Smith, S. & Derewenda, Z.S. Crystal structure of the
340 *Escherichia coli* thioesterase II, a homolog of the human Nef binding enzyme. *Nat Struct Biol*
341 **7**, 555-559 (2000).
- 342 28. Levin-Reisman, I., Brauner, A., Ronin, I. & Balaban, N.Q. Epistasis between antibiotic
343 tolerance, persistence, and resistance mutations. *Proc Natl Acad Sci U S A* **116**, 14734-14739
344 (2019).
- 345 29. Levin-Reisman, I., *et al.* Antibiotic tolerance facilitates the evolution of resistance. *Science*
346 **355**, 826-830 (2017).
- 347 30. Windels, E.M., *et al.* Bacterial persistence promotes the evolution of antibiotic resistance by
348 increasing survival and mutation rates. *ISME J* **13**, 1239-1251 (2019).
- 349 31. De Silva, K., Fife, A., Murgatroyd, F. & Gall, N. Pacemaker endocarditis: an important clinical
350 entity. *BMJ Case Rep* **2009**(2009).

- 351 32. Le Guern, A.S., Martin, L., Savin, C. & Carniel, E. Yersiniosis in France: overview and potential
352 sources of infection. *Int J Infect Dis* **46**, 1-7 (2016).
- 353 33. Savin, C., *et al.* Genus-wide *Yersinia* core-genome multilocus sequence typing for species
354 identification and strain characterization. *Microb Genom* **5**(2019).
- 355 34. Seemann, T. Snippy: Rapid haploid variant calling and core genome alignment.
356 <https://github.com/tseemann/snippy> (2015).
- 357 35. Croucher, N.J., *et al.* Rapid phylogenetic analysis of large samples of recombinant bacterial
358 whole genome sequences using Gubbins. *Nucleic Acids Res* **43**, e15 (2015).
- 359 36. Stamatakis, A. RAxML version 8: a tool for phylogenetic analysis and post-analysis of large
360 phylogenies. *Bioinformatics* **30**, 1312-1313 (2014).
- 361 37. Letunic, I. & Bork, P. Interactive Tree Of Life (iTOL) v4: recent updates and new
362 developments. *Nucleic Acids Res* (2019).
- 363 38. Yang, Z. PAML 4: phylogenetic analysis by maximum likelihood. *Mol Biol Evol* **24**, 1586-1591
364 (2007).
- 365 39. Gautreau, G., *et al.* PPanGGOLiN: Depicting microbial diversity via a partitioned pangenome
366 graph. *PLoS Comput Biol* **16**, e1007732 (2020).
- 367 40. Katoh, K. & Standley, D.M. MAFFT multiple sequence alignment software version 7:
368 improvements in performance and usability. *Mol Biol Evol* **30**, 772-780 (2013).
- 369 41. Nguyen, L.T., Schmidt, H.A., von Haeseler, A. & Minh, B.Q. IQ-TREE: a fast and effective
370 stochastic algorithm for estimating maximum-likelihood phylogenies. *Mol Biol Evol* **32**, 268-
371 274 (2015).
- 372 42. Kalyaanamoorthy, S., Minh, B.Q., Wong, T.K.F., von Haeseler, A. & Jermin, L.S. ModelFinder:
373 fast model selection for accurate phylogenetic estimates. *Nat Methods* **14**, 587-589 (2017).

374

375

376 **ACKNOWLEDGMENTS**

377 This work was funded by Santé Publique France (SpF, Saint-Maurice, France), Institut Pasteur,
378 Direction Générale de l'Armement, Agence Innovation Défense, and Université de Paris. The *Yersinia*
379 Research Unit is a member of the LabEX IBEID (ANR LBX-62 IBEID). We thank Vincent Enouf and
380 Andreea Alexandru (P2M platform, Institut Pasteur, Paris, France) for the sequencing of the strains,
381 Daniel Boury (SID'COM, University of Tours) for transesophageal echocardiography image processing,
382 and Pr. Frédéric Patat (University Hospital of Tours) for transesophageal echocardiography image
383 interpretation. We thank Life Science Editors for editorial assistance.

384

385 **AUTHOR CONTRIBUTIONS**

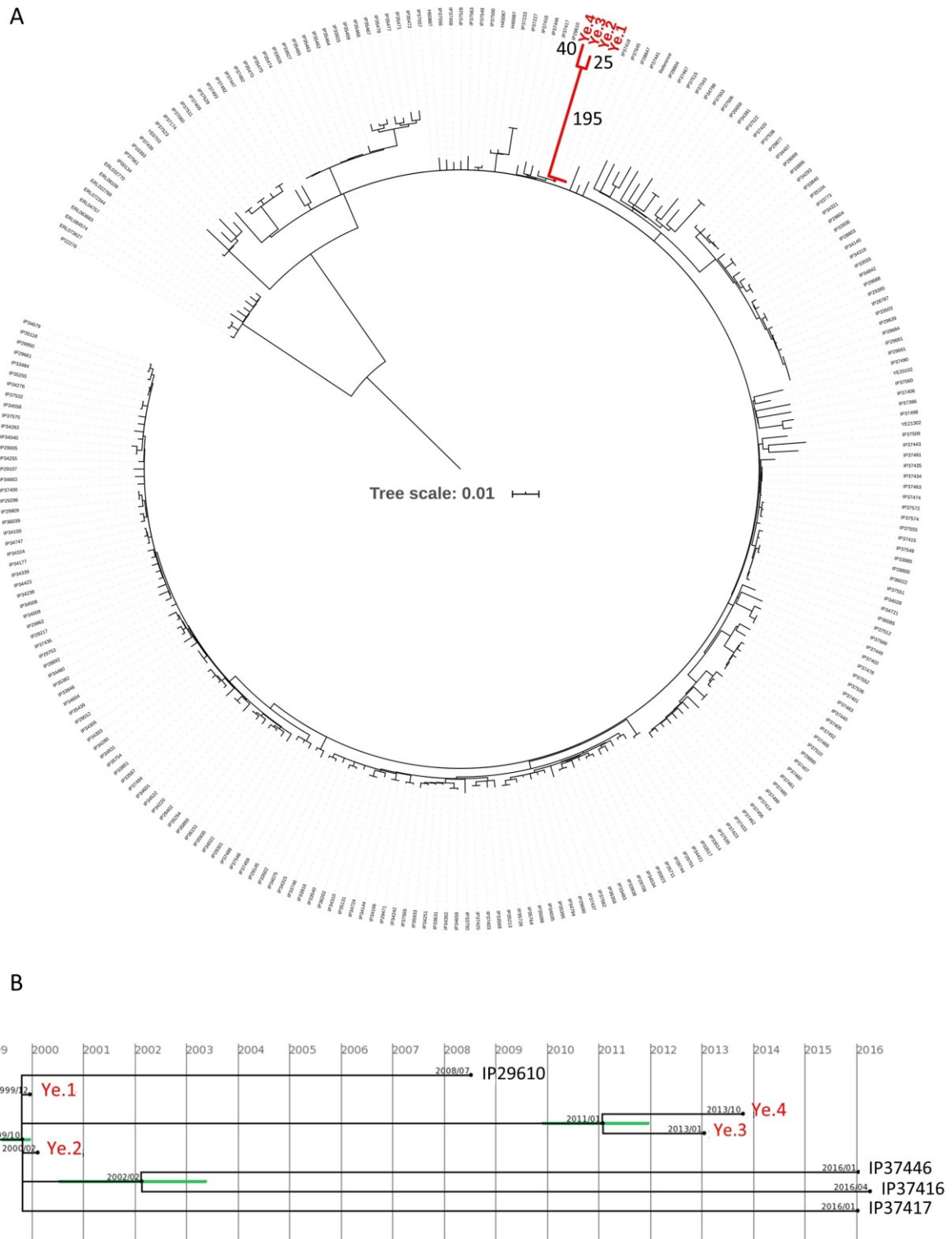
386 C.S. planned, performed and analyzed experiments with the help of L.M. and N.C. J.G. set up and
387 performed pan-genome together with PAML analysis. R.B., C.L.-B., F.B., M.F. and B.M. are the
388 physicians who took care of the patient and shared all the clinico-epidemiological data. P.L.-B. and
389 O.D. were involved in protein interaction analysis and identification of antibiotic tolerance
390 mechanism. C.S. and J.P.-C. interpreted data and wrote the manuscript. E.C., O.D., P.L. and J.P.-C.
391 supervised the work. P.L. and J.P.-C. are shared last authors.

392

393 **COMPETING INTERESTS**

394 The authors declare no competing interests.

395



397

398 **Figure 1**

399

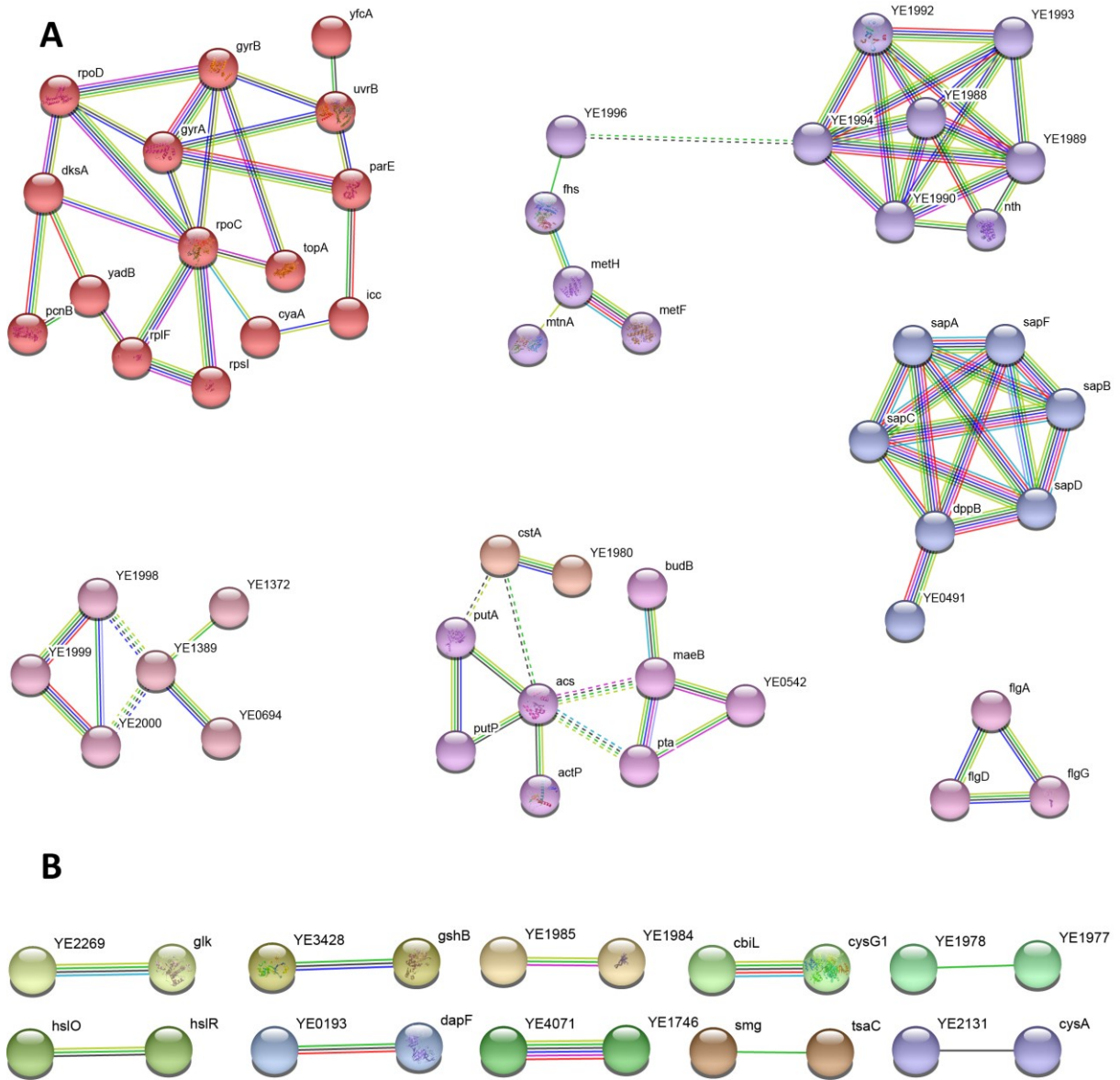


Figure 2

402 **FIGURE LEGENDS**

403 **Figure 1: Phylogenetic reconstruction.** (A) Maximum likelihood phylogeny reconstructed with
404 RAxML under GTR model with 100 bootstraps based on 4,738 SNPs identified in 262 strains.
405 The genome of the Y11 strain (NC_017564) was used as reference for variant calling.
406 Numbers close to the branches indicate SNPs numbers. (B) Estimation of the date of internal
407 nodes using least-squares dating (<https://lsdating.pasteur.fr>) among the 4 strains isolated
408 from the patient. Green bars represent the standard deviation of the estimated date.

409

410 **Figure 2. STRING network** (<https://string-db.org/>) of known interactions between genes or proteins
411 including deleted genes, genes with synapomorphies, as well as common and distinct SNPs in Ye.3
412 and Ye.4 strains. Network is based on *Yersinia enterocolitica* 8081 strain database. Locus equivalence
413 between strains Y11 and 8081 are in Supplementary Table S4. Confidence is set on 0.6. Clustering is
414 done with MCL algorithm using an inflation parameter of 2. The links are inferred with *Y.*
415 *enterocolitica* 8081 proteins or homologous proteins in other species. The pink links are
416 experimentally determined interactions; the green, red and blue links represent predicted
417 interactions based respectively on gene neighborhood, fusions and co-occurrence across genomes;
418 the yellow links stand for textmining; the black links are co-expression; the light purple links
419 represent protein homology. A. The purple cluster (YE1989-YE1994-nth, up right) represents the Rsx
420 transporter operon; the blue cluster (middle right) is the Sap transporter; the pink cluster (YE1998-
421 YE2000, bottom left) is a putative toxin ABC transporter; the red cluster includes genes involved in
422 DNA replication, transcription and repair; the middle bottom pink cluster (acs, maeB) as well as the
423 upper middle purple cluster (meth-metF) contain metabolic genes; the pink cluster in the (bottom
424 right) is involved in flagellar assembly. B. Two-genes links.

425

426 TABLES

427 Table 1: Chronology of bacteremia and clinical case

Episode of bacteremia	Dec 1999	Jan 2000	Aug 2001	Jun 2006	Jan 2013	Oct 2013
Strain's characteristics	- <i>Y. enterocolitica</i> 4/O:3 - genotype 4 → Ye.1	- <i>Y. enterocolitica</i> 4/O:3 - genotype 4 → Ye.2	- <i>Y. enterocolitica</i> - Severe growth defect → Ye.X	Sepsis but blood culture negative	- <i>Y. enterocolitica</i> - Severe growth defect - genotype 4 → Ye.3	- <i>Y. enterocolitica</i> - Severe growth defect - genotype 4 → Ye.4
Abnormal antibiotic resistance	No	No	Nalidixic acid resistance	NA	Nalidixic acid resistance	NA
Sign of infection on pacemaker lead	No	No	No	Yes (vegetation)	Yes (vegetation)	NA
Treatment	ceftriaxone + netilmicin → 4 weeks	- ceftriaxone + netilmicin (4 weeks) - ciprofloxacin (18 months)	long-term ceftriaxone (until July 2005)	long-term ceftriaxone	- piperacillin, tazobactam, amikacin (1 week) - long-term ceftriaxone	cotrimoxazole
Disease evolution	Recovery	- Recovery - Blood culture negative (monthly)	- Recovery - Blood culture negative (monthly)	- Recovery - Disappearance of vegetation during therapy	- Recovery - Disappearance of vegetation during therapy	- Death due to heart failure in Jan 2014

428 NA: Non-Assessed

429 **Table 2:** list of CDS absent in Ye.3 and Ye.4 strain genomes

Genbank_id	Product	Size (bp)
Large deletion of 9,919 bp (positions 887742 to 897661) - 9 genes		
WP_072076553.1	dipeptide/tripeptide permease DtpA	1,472
WP_005166379.1	LysR family transcriptional regulator	905
WP_005166377.1	hypothetical protein	1,211
WP_005178982.1	hypothetical protein	224
WP_005166373.1	peptide ABC transporter ATP-binding protein SapF	815
WP_005166371.1	peptide ABC transporter ATP-binding protein SapD	992
WP_005166369.1	peptide ABC transporter permease SapC	890
WP_005169521.1	peptide ABC transporter permease SapB	965
WP_005166365.1	peptide ABC transporter substrate-binding protein SapA	1,673
Large deletion of 32,673 bp (positions 1039738 to 1072411) - 28 genes		
WP_005164789.1	DUF2813 domain-containing protein	1,178
YP_001006252.1	type I secretion system permease/ATPase	2,118
WP_005164791.1	HlyD family type I secretion periplasmic adaptor subunit	473
WP_005164793.1	peptidase C39	1,943
WP_023161026.1	formate--tetrahydrofolate ligase	1,805
WP_005164796.1	DUF2569 domain-containing protein	443
WP_005164797.1	electron transport complex subunit RxA	581
WP_005164800.1	electron transport complex subunit RxB	623
WP_014608949.1	electron transport complex subunit RxC	1,856
WP_005164805.1	hypothetical protein	491
WP_005164807.1	right oriC-binding transcriptional activator	911
WP_020283189.1	electron transport complex subunit RxD	1,055
WP_005164811.1	electron transport complex subunit RxE	629
WP_005164813.1	electron transport complex subunit RxF	701
WP_005164815.1	endonuclease III	641
WP_016266185.1	hypothetical protein (YaxB)	1,037
WP_005164820.1	hypothetical protein (YaxA)	1,235
WP_005166280.1	oxidoreductase	2,321
WP_005178976.1	hypothetical protein	179
WP_005166281.1	exoribonuclease II	1,934
WP_005166282.1	carbon starvation protein A	2,066
WP_005166289.1	DUF466 domain-containing protein	332
WP_005166294.1	fructose-6-phosphate aldolase	665
WP_005166295.1	DeoR/GlpR transcriptional regulator	746
WP_005166298.1	DUF2164 domain-containing protein	248
WP_005166300.1	L-ribulose-5-phosphate 4-epimerase	695
WP_005166303.1	glycine zipper 2TM domain-containing protein	212
WP_002224869.1	gluconate 5-dehydrogenase	83
Large deletion of 2,533 bp (positions 4134104 to 4136637) - 2 genes		
WP_002228219.1	polynucleotide adenylyltransferase	1,541
WP_005156770.1	tRNA glutamyl-Q(34) synthetase GluQRS	929

430 Positions are expressed on Y11 reference genome (accession number NC_017564).

431 **Table 3:** List of the 41 genes with small insertions/deletions in the Ye.3 and Ye.4 strains

Genbank id	Status	Product
KGA74145.1	complete	hypothetical protein DJ62_2388
WP_005156285.1	truncated	23S rRNA (uridine(2552)-2'-O)-methyltransferase RlmE
WP_005156732.1	truncated	acetate--CoA ligase
WP_005156737.1	truncated	cation/acetate symporter ActP
WP_005156764.1	truncated	RNA polymerase-binding protein DksA
WP_005157750.1	truncated	APC family permease
WP_005158003.1	truncated	transcription-repair coupling factor
WP_005158842.1	truncated	urea ABC transporter ATP-binding subunit UrtE
WP_005161086.1	truncated	DUF3748 domain-containing protein
WP_005163313.1	truncated	Aminopeptidase
WP_005164830.1	truncated	Glucokinase
WP_005165635.1	truncated	MATE family efflux transporter
WP_005166113.1	truncated	DUF484 domain-containing protein
WP_005167417.1	truncated	MFS transporter
WP_005181075.1	truncated	guanosine pentaphosphate phosphohydrolase/exopolyphosphatase GppA
WP_011815289.1	truncated	class II fructose-bisphosphatase
WP_011815418.1	truncated	miniconductance mechanosensitive channel MscM
WP_013649985.1	truncated	MFS transporter
WP_014609301.1	truncated	DUF494 domain-containing protein
WP_016266722.1	truncated	toxin subunit
WP_019250468.1	truncated	inorganic phosphate transporter PitA
WP_023160195.1	truncated	dihydroxyacetone kinase subunit DhaM
WP_049530647.1	truncated	TonB-dependent siderophore receptor
WP_049679210.1	truncated	dipeptide transporter permease DppB
WP_050344735.1	truncated	RNA chaperone ProQ
WP_050879682.1	truncated	amino acid ABC transporter permease
WP_076706727.1	truncated	MFS transporter
WP_085910232.1	truncated	MFS transporter
WP_112999146.1	truncated	sensor domain-containing diguanylate cyclase
WP_145531626.1	truncated	two-component system sensor histidine kinase KdbD
WP_145535939.1	truncated	type I DNA topoisomerase
WP_005165697.1	complete	NADP-dependent oxaloacetate-decarboxylating malate dehydrogenase
WP_013650157.1	complete	DNA topoisomerase (ATP-hydrolyzing) subunit A (GyrA)
WP_005162896.1	complete	HAAAP family serine/threonine permease
WP_001534187.1	truncated	hypothetical protein
WP_005163236.1	truncated	beta-ketoacyl-[acyl-carrier-protein] synthase family protein
WP_005160711.1	truncated	hypothetical protein
WP_005180337.1	truncated	3',5'-cyclic-AMP phosphodiesterase - CpdA
WP_005157438.1	truncated	MurR/RpiR family transcriptional regulator
WP_005165794.1	complete	DNA-directed RNA polymerase subunit beta' - RpoC
WP_004706052.1	complete	two-component system response regulator - ArcA

432

433

Annexe F

Résumé substantiel en français

Yersinia pestis est le bacille hautement virulent responsable de la peste, une zoonose ré-émergente généralement transmise par les puces se nourrissant sur des mammifères bactériémiques, et agent majeur du risque biologique militaire à transmission interhumaine. Il existe trois principales formes cliniques de la peste. La peste bubonique, la forme la plus fréquente, résulte de la piqûre par une puce infectée dans le derme. La bactérie peut ensuite migrer et se multiplier dans les ganglions lymphatiques, formant un ganglion gonflé caractéristique nommé bubon. Si le système immunitaire ne parvient pas à contrôler l'infection, la bactérie dissémine dans l'organisme par voie hématogène, colonisant le foie et la rate et provoquant une peste septicémique dite secondaire. L'introduction directe de la bactérie dans la circulation sanguine par la piqûre de la puce ou par contact d'une blessure avec un élément contaminé résulte quant à elle en une peste septicémique dite primaire. Lors de la dissémination, la bactérie peut atteindre les poumons qu'elle va ensuite coloniser, induisant une peste pulmonaire secondaire transmise par voie aérienne entre individus. Un individu sain contaminé par la toux ou par l'inhalation de gouttelettes contaminées peut contracter une peste pulmonaire dite primaire. Cette forme est caractérisée par la multiplication de la bactérie dans les poumons passant inaperçue auprès du système immunitaire lors d'une phase pré-inflammatoire, suivie d'une phase pro-inflammatoire résultant en une pneumonie, une destruction des poumons et en une dissémination systémique de la bactérie par le sang. Dans les trois formes, les bactéries atteignent la circulation sanguine. Malgré l'importance de la phase bactériémique pour la transmission dans le réservoir animal et pour la progression de la maladie chez l'homme, celle-ci est restée très peu étudiée jusqu'à aujourd'hui. L'objectif de nos travaux est double : en nous reposant sur des méthodes avancées d'analyse à haut-débit et de biologie des systèmes, nous souhaitons d'une part caractériser cette phase bactériémique de façon plus approfondie, et développer d'autre part de nouveaux outils de diagnostic précoce de la peste, notamment de la peste pulmonaire.

Nous avons tout d'abord mis au point des protocoles d'extraction de protéines afin de réaliser des analyses protéomiques par spectrométrie de masse avec les contraintes imposées par l'expérimentation en laboratoire confiné de niveau de sécurité biologique 3. Nous avons comparé trois méthodes d'extraction de protéines, les deux premières basées sur une lyse par billes en urée 8M ou par sonication en SDS 4%, suivies du protocole FASP (*Filter-Aided Sample Preparation*), ainsi qu'une troisième méthode récemment publiée utilisant l'acide trifluoro-acétique comme lyse chimique, nommée SPEED (*Sample Preparation by Easy Extraction and Digestion*). Cette dernière étant rapide, robuste, simple à mettre en place et possédant des performances équivalentes aux deux autres méthodes, nous l'avons sélectionnée et nous avons validé son utilisation en laboratoire de niveau de sécurité biologique 3. Cette méthode inactive efficacement les bactéries et détruit les acides nucléiques, nous permettant de sortir les échantillons en toute sécurité du laboratoire de niveau 3 et de respecter la réglementation française sur les « Micro-Organismes et Toxines » (MOT). Nous

avons ensuite mis au point les conditions de culture de *Y. pestis* dans le plasma humain afin de générer un atlas protéique dans ce milieu et dans deux milieux de culture de laboratoire, un milieu riche et un milieu minimum chimiquement défini. Cette analyse nous a permis d'observer un changement métabolique important de la bactérie, notamment une abondance des protéines impliquées dans la capture du fer et la biosynthèse de la méthionine, lors de la croissance en plasma. Afin de compléter les données plasmatiques, nous avons mis au point un protocole original d'analyse protéomique après croissance des bactéries dans le sang total, un milieu complexe par la très grande quantité de cellules et de protéines humaines empêchant la bonne discrimination des protéines bactériennes. Une librairie spectrale a donc été générée grâce à l'enrichissement non spécifique par billes magnétiques (Nanotrap) de la bactérie après incubation dans le sang humain, ainsi qu'avec une culture pure en milieu de laboratoire, nous permettant d'obtenir le protéome de *Y. pestis* le plus complet à ce jour, couvrant plus de 2800 protéines. Afin d'obtenir des mesures semi-quantitative des protéines bactériennes dans nos conditions, nous avons dû diminuer la complexité de l'échantillon de sang à analyser. Après incubation de la bactérie dans le sang total, nous avons choisi d'enrichir spécifiquement par immunocapture les polynucléaires neutrophiles et les monocytes, cellules du système immunitaire avec lesquels *Y. pestis* interagit de façon privilégiée. Nous avons pu identifier plus de 5000 protéines dont près de 1500 provenant des bactéries dans ces deux fractions cellulaires. Nous avons observé une injection d'effecteurs bactériens plus importantes dans les monocytes que dans les polynucléaires neutrophiles, suggérant une plus grande affinité lors de l'interaction entre *Y. pestis* et les monocytes ou une mortalité plus réduite en comparaison des polynucléaires neutrophiles. L'analyse des protéomes humains nous a permis de valider la spécificité de l'enrichissement des deux fractions cellulaires, grâce à l'enrichissement de protéines spécifiques des polynucléaires neutrophiles ainsi que des voies de dégranulation et de métabolisme des sucres. Concernant les monocytes, outre la spécificité de certaines protéines et du complexe d'histocompatibilité de classe 2, nous avons observé un enrichissement des protéines impliquées dans la respiration mitochondriale, en accord avec les différences de métabolisme connues entre les polynucléaires neutrophiles et les monocytes. Notre protocole nous a permis d'obtenir le premier protéome mixte d'une bactérie et de l'hôte dans un échantillon aussi complexe que le sang décrit à ce jour, qui plus est appliqué en laboratoire de niveau de sécurité biologique 3. Ces résultats permettent d'ouvrir la voie à l'étude protéomique des interactions hôte-pathogène dans des conditions expérimentales plus complexes qu'auparavant.

En parallèle, nous avons développé un site internet – Yersiniomics – afin d'analyser et visualiser ces données. Nous avons collecté les 200 génomes complets disponible pour l'espèce *Yersinia* ainsi que les expériences transcriptomiques et protéomiques publiées, représentant plus de 300 conditions biologiques *in vitro* et *in vivo* intégrées dans la base de données. Ce site unique permet d'accéder à la collection de données de l'espèce *Yersinia* la plus complète actuellement, grâce à un navigateur génomique interactif intégrant l'ensemble des expériences au niveau de chaque gène. Une visualisation des données de couverture de séquençage des ARNs, le contrôle de la qualité de ces séquençages, ainsi que des plages de couleur représentant les analyses différentielles des données transcriptomiques et protéomiques ont été implémentées. Chaque gène des génomes de référence est dynamiquement lié à des bases de données externes tels que GenBank, Kyoto Encyclopedia of Genes and Genomes (KEGG), UniProt, InterPro, IntAct ou *Search Tool for the Retrieval of Interacting Genes/Proteins* (STRING), permettant ainsi un accès simplifié à l'ensemble des annotations depuis les génomes de *Yersinia*. Cet outil, grandement apprécié par la communauté scientifique travaillant sur les *Yersinia*, pourra être facilement transposable à d'autres organismes pour lesquels il n'existe pas encore à ce jour de base de données dédiée.

Grâce à cet outil, combiné à nos données protéomiques, nous avons sélectionné 47 protéines dont l'expression était modulée lors de la croissance bactérienne dans le plasma

humain et/ou présentant un profil intéressant dans notre base de données, puis nous avons inactivé les gènes correspondants par recombinaison et insertion d'une cassette de résistance à un antibiotique. Nous avons caractérisé la survie de ces souches mutantes après incubation dans du sang total humain, ainsi que leur virulence dans un modèle murin de peste septicémique, après injection intraveineuse. L'étude des souches mutantes nous a permis d'identifier plusieurs protéines impliquées dans l'homéostasie du cuivre, une subtilase, une protéase et des lipoprotéines nécessaires à la survie de *Y. pestis* dans le sang humain et/ou à la virulence chez la souris. Nous avons notamment démontré que la lipoprotéine SlyB joue un rôle critique pour la virulence dans les trois formes de peste, après injection intradermique imitant la piqûre de la puce et menant à une peste bubonique, après instillation intranasale causant une peste pulmonaire, ou après injection intraveineuse menant à une peste septicémique. Le mutant de délétion *slyB* montre une croissance affectée dans le sérum et le sang humain ainsi qu'une survie réduite dans des macrophages humains. Nous avons également démontré que l'inactivation de *slyB* conduit à une sensibilité accrue des bactéries mutantes à des éléments majeurs de la réponse immunitaire innée, tels que le complément, les *neutrophil extracellular traps* (NET) et les *proteoglycophili* (PGF) relâchés par les polynucléaires neutrophiles, ainsi que les protéases et peptides anti-microbiens décorant ces NET et PGF. Une analyse protéomique du mutant de délétion *slyB* a dévoilé une abondance plus faible pour nombre de protéines périplasmiques dont certaines ont été détectées dans le surnageant de culture, suggérant une plus grande fragilité et/ou perméabilité de la membrane externe de la bactérie. La répression du système de sécrétion de type 3 et du régulateur de virulence RovA, couplée à une augmentation de la quantité de protéines du système à deux composants Cpx dans le mutant *slyB* suggère l'activation des réponses aux stress de membrane. L'observation d'un changement métabolique avec notamment l'activation des voies d'import du soufre pourrait découler de la réponse aux stress d'enveloppe et de la fuite périplasmique précédemment décrite. SlyB, largement répandu chez les bactéries Gram-négatives et notamment chez certaines bactéries pathogènes, a précédemment été décrit comme nécessaire pour résister aux agents ciblant la membrane tels que les détergents ou les peptides anti-microbiens chez *Pseudomonas* ou *Burkholderia*. Notre étude met en lumière pour la première fois le rôle de SlyB dans la pathogenèse bactérienne en permettant une plus grande résistance des bactéries à l'immunité innée.

Enfin, nous avons exploité nos modèles expérimentaux pour découvrir de nouveaux biomarqueurs de la peste. L'un des enjeux majeurs, que ce soit pour les forces armées ou pour les cliniciens des pays touchés par la peste, est le diagnostic rapide de la maladie. Bien que l'antibiothérapie soit efficace contre *Y. pestis*, celle-ci doit être administrée très rapidement. En effet, en cas de peste pulmonaire ou septicémique, la mort peut survenir en moins de 48 heures après la survenue des premiers symptômes qui par ailleurs sont non spécifiques. Des tests de diagnostic rapide (TDR) ont été mis au point dès le début des années 2000. Ils se basent sur la détection de l'antigène F1, composant de la pseudocapsule de *Y. pestis*. Une modélisation récente, tirant partie de l'épidémie de peste de 2017 à Madagascar, a démontré une sensibilité des TDR de seulement 28% et une spécificité de 82% en cas de peste pulmonaire, et une sensibilité de seulement 7% pour la culture bactériologique. La détection basée sur des techniques de biologie moléculaire possède quant à elle une sensibilité de 80% et une spécificité de 100%, mais n'est réalisée qu'en laboratoire par du personnel formé avec des équipements spécialisés, contrairement aux TDR réalisés au chevet des patients. Au-delà de l'absence de tests rapides et fiables pour le diagnostic de patients symptomatiques, un manque total existe en ce qui concerne le diagnostic présymptomatique. Nous souhaitons donc élaborer de nouvelles approches diagnostiques fondées sur la détection des biomarqueurs de l'hôte. Pour cela, nous avons choisi d'étudier les microARNs systémiques de l'hôte différenciellement exprimés lors de l'infection par *Y. pestis*, potentiellement utilisables comme biomarqueurs pour le diagnostic précoce de la maladie.

Nous avons implémenté un modèle murin de peste pulmonaire bien caractérisé dans la littérature et nous avons criblé par PCR quantitative 179 microARNs circulant dans le sang. Nous avons pu établir la preuve de concept de cette approche en identifiant trois candidats prometteurs surexprimés à un stade précoce de la maladie, seulement 24 heures après infection. Nous avons ensuite optimisé notre méthodologie afin de prélever le sang des souris de façon plus reproductible et de minimiser l'hémolyse, facteur majeur de contamination de microARNs. Nous développons maintenant une approche de criblage non biaisée, basée sur le séquençage des microARNs totaux appliquée aux différents stades de la maladie, à 6 heures, 24 heures et 48 heures après infection.